GEOLOGICAL SURVEY RESEARCH 1970

Chapter D

GEOLOGICAL SURVEY PROFESSIONAL PAPER 700–D

Scientific notes and summaries of investigations in geology, hydrology, and related fields

UNITED STATES GOVERNMENT PRINTING OFFICE, WASHINGTON: 1970

UNITED STATES DEPARTMENT OF THE INTERIOR

WALTER J. HICKEL, Secretary

GEOLOGICAL SURVEY

William T. Pecora, Director

For sale by the Superintendent of Documents, U.S. Government Printing Office
Washington, D.C. 20402 – Price $3.75

CONTENTS

GEOLOGIC STUDIES

GEOLOGICAL SURVEY RESEARCH 1970

This collection of 45 short papers is the third published chapter of "Geological Survey Research 1970." The papers report on scientific and economic results of current work by members of the Geologic, Water Resources, and Topographic Divisions of the U.S. Geological Survey.

Chapter A, to be published later in the year, will present a summary of significant results of work done in fiscal year 1970, together with lists of investigations in progress, reports published, cooperating agencies, and Geological Survey offices.

"Geological Survey Research 1970" is the eleventh volume of the annual series Geological Survey Research. The ten volumes already published are listed below, with their series designations.

Geological Survey Research	*Prof. Paper*
1960	400
1961	424
1962	450
1963	475
1964	501
1965	525
1966	550
1967	575
1968	600
1969	650

LATERAL DISPLACEMENT ON THE GARLOCK FAULT, SOUTHEASTERN CALIFORNIA, SUGGESTED BY OFFSET SECTIONS OF SIMILAR METASEDIMENTARY ROCKS

By GEORGE I. SMITH and KEITH B. KETNER,
Menlo Park, Calif., Denver, Colo.

Abstract.—Similar sections of homoclinal east-dipping eugeosynclinal metasedimentary rocks on opposite sides of the Garlock fault and 30 to 40 miles apart suggest this amount of left-lateral displacement. The metasedimentary rocks on the north side belong to the Garlock Formation, in part of Permian age; the undated rocks on the south side, in Pilot Knob Valley, consist largely of chert with lesser amounts of slate, quartzite, sandstone, limestone, and stretched chert conglomerate.

The Garlock fault is a major left-lateral fault in southeastern California (fig. 1). About 40 miles of displacement on it has been suggested on the basis of a dike swarm that appears offset by this amount along the fault (Smith, 1962). The suites of pre-Tertiary rocks on the north and south sides of the fault also change along zones normal to the fault trace, and the transitional zones also appear to be offset about 40 miles along the fault (Smith, 1962, p. 102; Smith, 1963). Fractured metamorphic rocks in the Lava Mountains south of the fault (Smith, 1964, p. 10) are thought by Dibblee (1967, p. 115) to be possible offset equivalents of the Garlock Formation in the El Paso Mountains north of the fault and at least 17 miles to the west. The Rand Schist in the Rand Mountains south of the fault is also considered by Dibblee (1967, p. 115) to be possibly an offset segment of the Pelona Schist in the Tehachapi Mountains north of the fault and 30 miles west. About 40 miles of displacement was proposed by Michael (1966) on the basis of the distance between similar tectonic discontinuities inferred by him in blocks north and south of the Garlock fault.

In view of these estimates of displacement, we decided to compare the eugeosynclinal metasedimentary rocks of the Garlock Formation, which crop out north of the Garlock fault in the El Paso Mountains (Dibblee, 1952, p. 15–19; 1967, p. 27–32), with eugeosynclinal metasedimentary rocks which crop out south of the Garlock fault in Pilot Knob Valley and 30 to 40 miles east of the El Paso Mountains (Smith and others, 1968, p. 9). Correlative sequences of sedimentary rocks are inherently less reliable than dike swarms for determining the lateral displacement on a fault (Smith, 1962, p. 90), but they can supply supplementary evidence. Furthermore, an offset extension of the Garlock Formation would provide better evidence than most formations because the Garlock is so distinct from other formations in this region.

The Garlock Formation, described by Dibblee (1952, p. 15–19; 1967, p. 27–32), consists of a great thickness of phyllite, hornfels, chert, greenstone, limestone, quartzite, and chert conglomerate. Fusulinids about 12,000 feet up from the base indicate that this part of the Garlock Formation is Permian; crinoid stems occur in the overlying 14,000 feet. The lithologic similarity of the eugeosynclinal deposits that constitute the entire formation suggests that all of it is about the same age, but the thickness of deposits is so great that a significant part of the Paleozoic and early Mesozoic could be represented. Although Dibblee includes about 35,000 feet of rocks in the formation, 4,000 feet of the described section is intrusive(?) andesite, and folding and faulting of the type mapped by Christiansen (1961) may have thickened individual units and repeated parts of the section. The Garlock Formation is broadly homoclinal; dips are mostly 50° to 70° to the northeast, and strikes average about N. 30° W.

U.S. GEOL. SURVEY PROF. PAPER 700-D, PAGES D1–D9

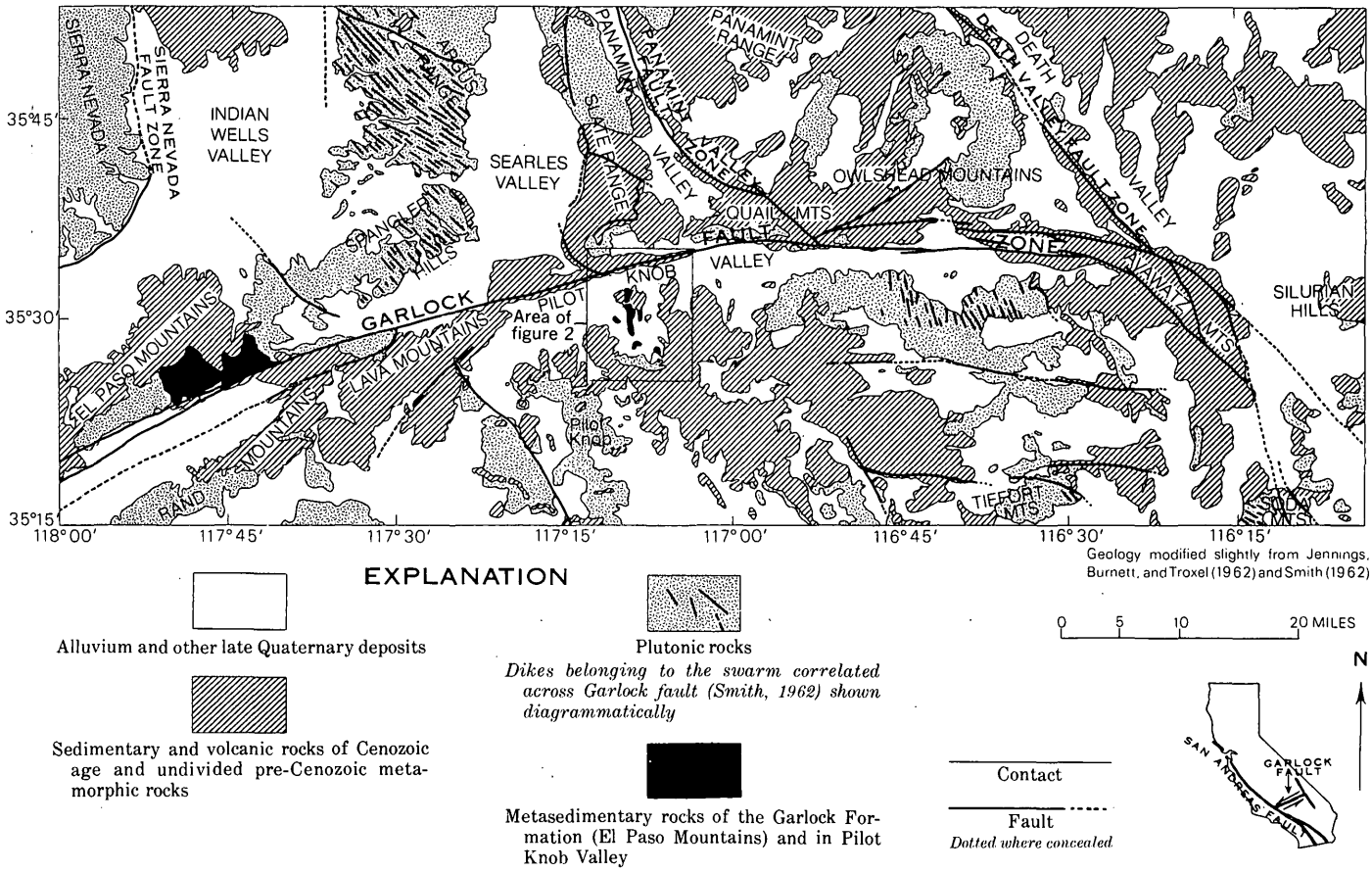

FIGURE 1.—Generalized geology of the east half of the Garlock fault, showing location of metasedimentary rocks discussed in this report, and area included in figure 2.

Both areas of eugeosynclinal rocks were visited by us in the spring of 1966. A brief reconnaissance of the Garlock Formation had been made previously by Ketner, using Dibblee's (1952) map and lithologic data. The rocks in Pilot Knob Valley had been noted during earlier reconnaissance mapping by Smith (*in* Jennings, Burnett, and Troxel, 1962). A striking similarity between the two statigraphic sections was evident, and subsequent work was aimed at testing the degree of similarity. Data on the Garlock Formation presented here are chiefly from the reports by Dibblee (1952, p. 15–19; 1967, p. 27–28 and 34–35) and Christiansen (1961), supplemented by results of the short inspection described above and a few later visits for study of specific rock units. Data on the metasedimentary rocks in Pilot Knob Valley presented in this paper were collected by Smith during 6 days' additional geologic fieldwork and subsequent study of about 40 specimens in the laboratory.

The metasedimentary rocks in Pilot Knob Valley crop out 2 to 8 miles south of the Garlock fault as isolated small hills, 150 to 400 feet high, that project through the alluvium. Because the outcrops lie within a U.S. Navy testing range, fieldwork was minimal and had to be done on weekends, sometimes with a military escort. The work consisted of delineating the extent of metasedimentary rocks and traversing the best-exposed sections. On each traverse, the planimetric width of each separable lithologic unit was measured by pace, and the pace distance and lithologic description of each recorded on a portable tape recorder to be transcribed later. The traverses totaled about 16,000 feet. The pace distances were obviously approximate, and most rock descriptions are based only on criteria that could be applied in the field. The measured traverses described in table 1 and shown on figure 3 are not stratigraphic sections in the conventional sense. Not enough time was available to make reliable geologic maps of the areas composed of these rocks; and the many faults and small-scale folds observed along the traverse lines, though not shown on figure 2, plus the large areas of poor exposure, limit the confidence one could have in stratigraphic sections made without geologic maps. Furthermore, the

extensive areas of alluvial cover between hills make it impossible to trace any part of a stratigraphic section in one hill into the section exposed in another. The data obtained are therefore analogous to Rosiwal analyses, as the percentages and lithologic characteristics of the metasedimentary rocks in this assemblage have been approximated by making traverses across representative segments of the outcrops.

DESCRIPTION OF METASEDIMENTARY ROCKS IN PILOT KNOB VALLEY

The distribution of metasedimentary rocks in Pilot Knob Valley is shown on figure 2. The rocks consist of thick sequences of fine-grained to very fine grained siliceous deposits such as chert, siliceous slate, slate, and quartzite separated by thinner sequences of sandy limestone and conglomerate. In the southern third of the outcrop area, near the intrusive contact of these rocks with plutonic rocks, many of the metasediments are metamorphosed to hornfels and calc-silicate rocks and are cut by numerous veins of massive quartz. The lithologies of rocks along the seven traverses are shown diagrammatically in figure 3; rocks along three traverses are described in table 1. These data are based on field descriptions and later laboratory study of about 40 selected specimens. The total thickness of the sequence is unknown, but if the average dip is assumed to be 70°, the measured traverses shown on figure 3 represent about 15,000 feet of metasediments if no part of the section is repeated.

Most of the metasedimentary rocks have a thick coating of very dark gray or brown desert varnish; some are lighter on fresh surfaces. The section is broadly homoclinal, although small tight folds were observed; beds generally strike within 20° of north and dip east at 65° or more (the few dips toward the west shown on figure 2 are thought to be on overturned sections). Massive rock units are well exposed along ridges, but thin-bedded chert and slate units tend to be concealed by loose regolith composed of their own fragments.

Many of the chert units have beds that are only a few inches thick; others are massive. Colors on fresh surfaces range from black through shades of brown, purple, red, or tan to nearly white; some units have banded sequences of alternating colors, with bands mostly 2 inches wide or less. Interbeds of limestone or stretched chert-pebble conglomerate are fairly common. Thin-section study of rocks identified in the field as chert shows that they are composed chiefly of quartz with some sericite and opaque minerals. Quartz crystals range from submicroscopic to sand size, and many of them have shapes and size distributions suggesting that many rocks called chert are actually pure to impure quartzites. Many of the fine-grained massive beds called chert have mineral assemblages that are more characteristic of hornfels. Some of the light-colored units may be metamorphosed tuff or rhyolite, although relict igneous textures were not seen. Near the western end of traverse E, one dark chert zone about 10 feet thick and at least 1,000 feet long contains abundant bedding-surface concentrations of elongate diamond-shaped molds that are filled with sericite and are of uncertain origin (fig. 4). They may represent altered metacrysts of a mineral such as andalusite. It is possible, however, that they represent deformed and replaced fusulinids, although they now are not of the shape or size, nor do they have any internal characteristics, of the *Schwagerina* found in the Garlock Formation (C. W. Merriam, oral commun., March 1969). Rocks designated in the field as chert therefore include a wide variety of siliceous sediments. Their compositions probably overlap those designated as siliceous slate, slate, sandstone, and quartzite, and may include rocks that are hornfels and siliceous metavolcanics.

The slates and siliceous slates are mostly thin bedded. Their colors are similar to those of the cherts, although the darkest colors are less common. Many of the slates are calcareous. Interbeds of chert and limestone are found. Microscopic study reveals extensive recrystallization with the formation of muscovite, and many of the rocks are phyllitic.

Most beds identified in the field as sandstone and quartzite are dark brown to black. The quartzite beds are mostly resistant and massive; the sandstones are less resistant, calcareous, and faintly to well bedded. The medium to very fine sand grains are fairly well sorted, subangular to round, and nearly all quartz. The quartzite and quartz-rich rocks are extensively recrystallized, and the quartz grains in many have developed sutured boundaries that obscure the distinction between grains and matrix.

Limestone zones mostly weather dark brown and are thin bedded. They generally contain conspicuous amounts of well-rounded sand, both in beds and disseminated, and some grade into calcareous sandstone. Interbeds of both sandstone and chert are found. The calcite grains are recrystallized but, with sporadic exceptions, have not grown to sizes that characterize marble. The boundaries of the

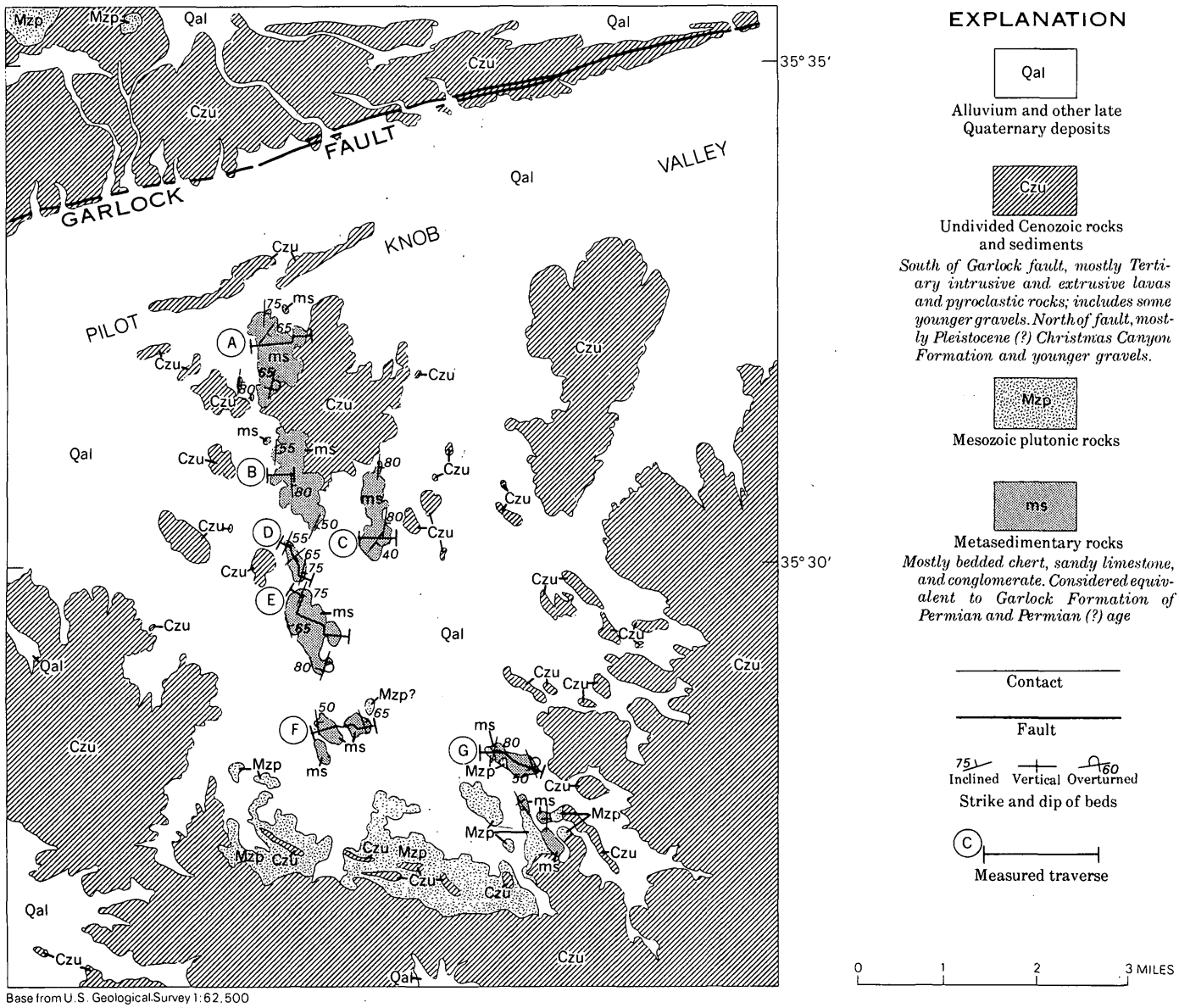

FIGURE 2.—Map of Pilot Knob Valley area, showing location and attitudes of metasedimentary rocks, their position relative to the Garlock fault, and location of traverses A through G.

quartz sand grains are generally sharp. Near the west ends of traverses E and G, some of the limestones are altered to wollastonite or wollastonite-diopside mixtures.

The conglomerates consist of fragments of chert, quartzite, and sandy limestone in a matrix of chert, impure sandstone, or quartzite. Chert fragments are most common; granitic fragments were not seen. The pebble- to granule-size fragments are angular to subround and are flattened parallel to bedding with the long dimension commonly three to five times the short dimension. In many exposures, fragments make up 50 to 75 percent of the rock and are of nearly uniform size.

AGE AND CORRELATION OF METASEDIMENTARY ROCKS IN PILOT KNOB VALLEY

Identifiable fossils were not found in the metasedimentary rocks in Pilot Knob Valley, and stratigraphic evidence restricts the age only within broad limits. Near the southeast limit of their outcrop area, the metasedimentary rocks are intruded by plutonic rocks (along and near traverse *G*, fig. 2). Radiometric dates are not available for plutonic

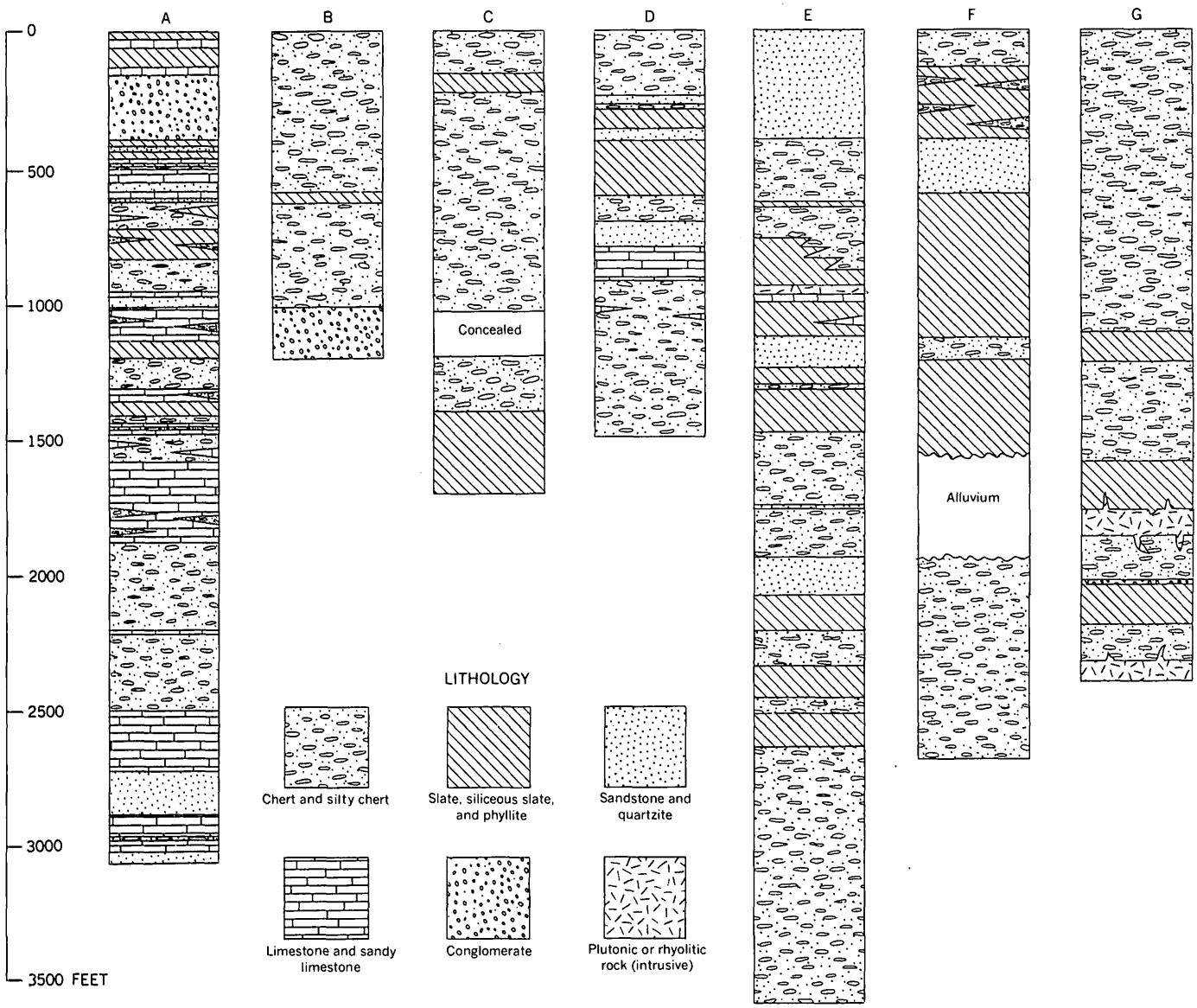

FIGURE 3.—Lithologies of rocks along traverses A through G, Pilot Knob Valley (fig. 2). Measured west to east and plotted with west end at base of column.

rocks of this immediate area, but lead-alpha dates on similar rocks in the southwest Basin and Range province and Mojave Desert are mostly between 85 and 130 million years (Jaffe and others, 1959, p. 87–90; Smith and others, 1968, p. 12). Plutonic rocks in the Mojave Desert area intrude metasedimentary rocks of probable Triassic or Jurassic age and are found as fragments in rocks of Paleocene age (McCulloh, 1954, p. 21; Smith, 1962, p. 101). It is reasonable to conclude that the metasedimentary rocks in Pilot Knob Valley are older than late Mesozoic, but the lower limit of their possible age is less definite. Rocks in southeastern California having the deformational and metamorphic characteristics of this assemblage may range in age from late Precambrian to late Mesozoic. However, all that contain diagnostic fossils are of late Paleozoic (or possible early Mesozoic) age (Hewett, 1954, p. 7–15; McCulloh, 1954, p. 13–18; Dibblee, 1967, p. 14–28), and the ages of many unfossiliferous sections as well may lie within this range. If the elongate molds found in one of the chert beds in Pilot Knob Valley represent fusulinids, a late Paleozoic age is indicated for these rocks.

The metasedimentary rocks in Pilot Knob Valley cannot be correlated on the basis of lithology with rocks of other sections described from areas south of the Garlock fault. Most of the thick sections that

TABLE 1.—*Measured traverses of metasedimentary rocks in Pilot Knob Valley, Calif.*

[Units listed from west to east; traverse lengths are estimated by pace and are approximately normal to strike; see fig. 2 for locations of traverses]

Traverse A

	Feet
Sandstone, fine-grained, dark-gray	40
Limestone, sandy, gray; beds 2 to 10 in. thick	40
Chert, black	10
Limestone, sandy, tan, massive	80
Sandstone, black, calcareous; weathers with blocky fractures; dark-rusty-brown; indistinct beds of finer grained limestone	160
Limestone, sandy, grayish to tan; locally thin-bedded with streaks of sand or silt; lithologies persistent in layers 3 to 5 ft thick; bedding within layers very indistinct except on weathered surfaces	220
Chert, thinly bedded, black to tan; forms poor outcrops	80
Chert, massive to thin-bedded, white, tan, or black	210
Limestone, thinly bedded, gray	10
Chert, banded, thinly bedded; beds ¼ to 1 in. thick, tan, brown	340
Limestone; beds 1 in. to 1 ft. thick; 2 percent black chert beds	160
Limestone, tan, thin-bedded, sandy, poorly exposed	140
Chert, banded, black, brown, or tan; forms resistant outcrops; 1 percent interbedded fine-grained limestone	80
Limestone and chert, thinly bedded	50
Chert, black, bedded	40
Slate, thin-bedded, pink to gray, calcareous	60
Limestone, slightly sandy, tan, fine-grained; black chert interbeds	40
Chert, black, orange or red, greenish; indistinct zones of stretched pebbles or boudinage structures	120
Slate, calcareous, thin-bedded, gray	60
Limestone; about 15 percent sand; beds thin in lower part and as much as 1 in. thick in upper part; interbeds of black chert as much as 1 ft thick	130
Quartzite, tan to dark-brown, noncalcareous, massive	30
Chert, black to tan; massive near top and bottom; beds about 1 in. thick near middle; quartz veins common, especially in upper part	120
Slate or phyllite, noncalcareous, gray to pinkish-gray, thin-bedded, poorly exposed; interbeds of chert	120
Chert and thinly bedded slate; about 25 percent brown sandy limestone	80
Quartzite, black, slightly calcareous, resistant	20
Limestone, sandy, tan	30
Quartzite, tan to orange; weathers black; massive	20
Limestone, sandy, brown	60
Chert, black	10
Slate, gray to pink; 20 percent sandy limestone	40
Quartzite, black	20
Slate, pink, tan, and purple; paper-thin beds; forms poor outcrops	30
Conglomerate; pebbles form 50 to 70 percent of rock, mostly ½ in. or less, sheared and flattened parallel to bedding, composed of multicolored chert; small percentage of sandstone and sandy limestone fragments; matrix is chert and sandstone; a few 1- to 6-in. thick beds of silty limestone in upper part of unit	250
Limestone, sandy; darker and more sandy near base	20
Slate, gray to pink, poorly exposed	80
Limestone, sandy, gray to tan	30
Slate, light-purple; paper-thin beds	10
[End of section]	

Traverse D

Chert, black; massive in lower part and faintly bedded in upper part; orange beds near top	180
Chert, thinly bedded, black, poorly exposed; beds 1 in. thick (avg)	80
Chert or siliceous slate; dark gray in lower part, light gray in upper part; beds indistinct, 1 in. thick (avg)	120
Chert; beds 1 in. thick (avg); some ½-in. white layers; sporadic sandy limestone partings 1 in. thick or less	120
Chert, black; bedding indistinct to massive	70
Limestone, sandy; weathers brown	120
Sandstone, locally slightly calcareous; weathers brown; massive to faintly bedded	100
Chert, black; beds 1 to 6 in. thick; several orange or red-purple zones near top	100
Slate, dark-gray; lighter gray and brown in upper part; fractures into beds a few inches thick; weathers to duller surface than chert	210
Sandstone, gray, medium- to fine-grained; uniform with thin bedding-plane layers of sand forming ridges about 1 in. apart on weathered surfaces	40
Slate or siliceous slate, dark-gray to brown, poorly exposed, thin-bedded	70
Chert, black, faintly bedded	10
Sandstone, calcareous; bedding indistinct	40
Chert, black, thin-bedded; several 1-in. thick interbeds of white chert in lower part	50
Chert, massive, black; some thin interbeds	100
Chert, black; beds 1 in. thick (avg); unit forms east slope of southeast end of traverse	80
[End of section]	

Traverse E

Chert, massive to thickly bedded, possibly silty, black to dark-brown; some zones (5 ft thick) more red or brown	270
Chert, gray to dark-brown; beds 2 in. thick	50
Chert, black; beds 6 in. to 1 ft. thick; forms prominent outcrop; at east edge of unit is zone of gray elongate diamond-shaped casts at least 10 ft. thick, with about 2 percent of beds containing conspicuous percentages of casts (fig. 4); zone extends at least 2,000 ft. south	30
Chert, like that below	50
Chert, light-brown to tan, faintly bedded; beds 1 to 2 in. thick	10
Chert, dark-brown; beds 1 to 2 in. thick	30
Chert, mostly black, well-bedded; some beds 1 to 2 in. thick; others 1 to 2 ft. thick	100
Chert, orange-brown; beds 1 in. to 1 ft. thick	120
Chert, orange-brown; beds 1 in. to 1 ft. thick	120
Chert, dark; beds as much as 1 ft thick	50
Chert, light- to dark-brown, thin-bedded	240

TABLE 1.—*Measured traverses of metasedimentary rocks in Pilot Knob Valley, Calif.*—(continued)

[Units listed from west to east; traverse lengths are estimated by pace and are approximately normal to strike; see fig. 2 for locations of traverses]

Traverse E (cont.)

	Feet
Slate, light-tan to orange-tan, flaggy; color bands 1 to 5 mm thick	120
Chert, black; beds 1 in. thick	70
Slate, flaggy, tan to orange	40
Zone of secondary white opaline material	10
Slate, tan to orange	50
Chert, black, thin-bedded	130
Slate or siliceous slate, thin-bedded; weathers to bluish-gray hues except top 10 ft which is orange	150
Sandstone, calcareous; weathers brown; medium to fine grained; grains are well rounded and well sorted	130
Chert, black; thin-bedded except top 10 ft	170
Sandstone, like that below	10
Chert, tan, orange, or brown; beds 1 to 2 in. thick	160
Chert, silty, black, massive	50
Chert or siliceous slate; beds ½ to 2 in. thick	50
Slate, siliceous; weathers red brown; laminated to thinly bedded	30
Slate or siliceous slate; weathers to grayish or smokey blue hue; fissile	130
Chert, black	10
Slate or siliceous slate, grayish to bluish, fissile	70
Calcareous sandstone or sandy limestone; weathers gray to tan; uniform with thin beds of sand forming streaks about 1 in. or less apart	120
Siliceous slate, black, dark-brown, or orange, poorly exposed, thinly bedded; 6-in.-thick limestone bed occurs in middle	150
Limestone; appears free of sand; weathers to bluish gray	30
Rhyolite, white, fine-grained; intruded as sill(?) into section; 1 or 2 percent phenocrysts of quartz and feldspar; streaks of biotite(?); probably Tertiary in age	50
Slate and siliceous slate grading up to black chert; slate and siliceous slate are black, fissile near base of unit; beds 1 in. thick near top	190
Chert, yellow to white, poorly exposed; may be thin bedded	50
Slate, bluish-weathering, fissile	20
Chert, yellowish to orange	160
Chert, interbedded black and gray	80
Quartzite, white to light-gray; indistinct color bands 1 in. to 1 ft thick	400
[End of section]	

have been studied are described by Hewett (1954, p. 7–15), McCulloh (1954, p. 13–18), Grose (1959, p. 1519–1523), and Dibblee (1967, p. 14–28); relative to the section in Pilot Knob Valley, the rocks in them generally include more dolomite and marble but less chert, and their conglomerates contain plutonic rock fragments but few or no chert fragments.

North of the Garlock fault, outcrops of metasedimentary rocks of comparable grade are scarce. Except for the Garlock Formation, published descriptions cite only three: quartzite-pebble metaconglomerates, hornfelsic metavolcanic rocks, and other metasedimentary rocks in the western El Paso Mountains (Dibblee, 1952, p. 19; Christiansen, 1961, p. 42–48; and Dibblee, 1967, p. 14–19); schist and marble as isolated pendants in the southern Sierra Nevada and northern Tehachapi Mountains (Dibblee, 1967, p. 19); and schist, hornfels, phyllite, and marble in the Slate Range (Smith and others, 1968, p. 9). Metasedimentary rocks not described in the literature occur in a strip that may be less than a mile wide along the northeastern end of the Spangler Hills (fig. 1); they are mostly massive hornfels but include a few zones of hornfels-fragment breccia and stretched breccia or conglomerate. Only the rocks in the Garlock Formation and in the western El Paso Mountains 8 miles west of the Garlock Formation have lithologies that are comparable to any of the rocks described here from Pilot Knob Valley.

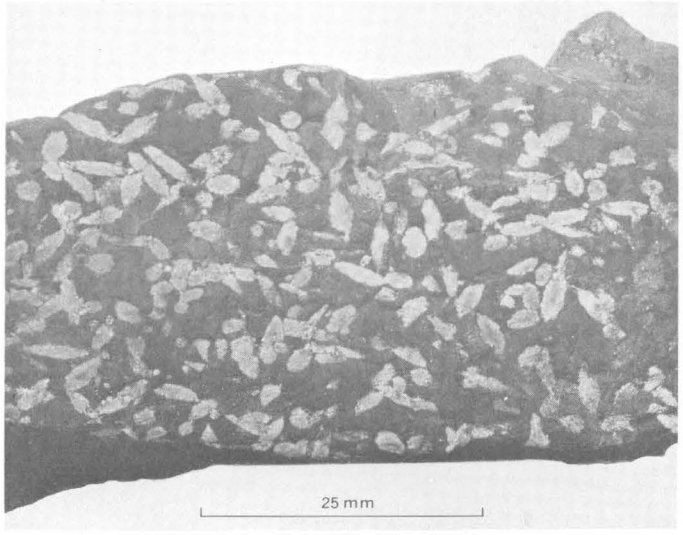

FIGURE 4.—Sericite-filled molds on bedding surfaces of chert samples. See table 1, traverse E, for rock description.

Strata that are much less metamorphosed but do have similarities to those of the Garlock Formation occur in the southern Inyo Mountains, about 75 miles north of the El Paso Mountains. They are of Permian age and constitute the Owens Valley Formation (Merriam and Hall, 1957). Rocks of this formation may also occur in the northern Slate Range (Smith and others, 1968, p. 11). In addition to limestone, shale, siltstone, and sandstone, the formation contains sandy limestone, chert, and chert or limestone conglomerate. The Owens Valley Forma-

TABLE 2.—*Estimated percentages of rock types in metasedimentary sequences in Pilot Knob Valley and in the Garlock Formation in the El Paso Mountains*

Rock types (field identifications)	Pilot Knob Valley								Garlock Formation (El Paso Mountains) (Dibblee, 1967, p. 27–28)
	Traverse							Weighted average	
	A	B	C	D	E	F	G		
Phyllite, slate, and siliceous slate	13	3	4	19	25	46	25	20	46
Hornfels (includes tactite)	0	0	0	0	0	0	0	0	22
Chert	35	80	96	62	56	46	74	56	13
(Sum of siliceous fine-grained rock percentages)	(48)	(83)	(100)	(81)	(81)	(92)	(99)	(76)	(81)
Quartzite and sandstone	10	0	0	11	18	8	0	10	5
Limestone and marble	34	0	0	8	1	0	0	10	6
Conglomerate	8	17	0	0	0	0	1	4	2
Greenstone	0	0	0	0	0	0	0	0	[1]6

[1] Estimate of rock-type percentages in the Garlock Formation excludes 4,300 feet of andesite and related rocks considered by Dibblee (1967, p. 28; oral commun. 1969) to be probably intrusive into the section.

tion is partly equivalent in age to the eugeosynclinal Garlock Formation, and represents an assemblage that is transitional between eugeosynclinal and miogeosynclinal facies. Permian rocks composed of interbedded limestone and chert that are transitional between eugeosynclinal and miogeosynclinal assemblages also crop out in the Soda Mountains, 60 miles east of Pilot Knob Valley (Grose, 1959, p. 1519–1523). If the Pilot Knob Valley rocks are of the same age, they bear about the same facies and areal relations to the Soda Mountains assemblage as does the Garlock Formation to the Owens Valley Formation.

There is more similarity between the metasedimentary rocks in Pilot Knob Valley and the Garlock Formation than between any other known sequences in this part of California. Both are thick eugeosynclinal sections that contain similar rock types. The conglomerates containing abundant chert and sandy limestone fragments but no plutonic fragments are especially similar and differ from all other described sections in the area.

Table 2 summarizes the estimated percentages of the different rock types found in the Pilot Knob Valley area and in the Garlock Formation in the El Paso Mountains area. The differences between the percentages of the siliceous fine-grained rock types —phyllite, slate, siliceous slate, hornfels, and chert —could be real, but quite possibly they reflect differences in the criteria used for field identifications; it is worth noting that the sums of the percentages of such rocks are similar, 76 and 81 percent, respectively. The percentages of quartzite plus sandstone in the two areas are 10 and 5 percent. Limestone and marble account for 10 and 6 percent of the rocks in the two sections. Chert-pebble conglomerates account for an estimated 4 and 2 percent of each assemblage. No altered basalt (greenstone) was found in the Pilot Knob Valley area, although some units may represent siliceous volcanic rocks.

CONCLUSIONS

The Garlock Formation in the El Paso Mountains and the rocks in Pilot Knob Valley represent very thick and distinctly eugeosynclinal facies. There is a notable similarity in both the percentages of various rock types and the petrography of the component rock types, especially the stretched conglomerates. Furthermore, the two sequences may lie about the same distances west or southwest from assemblages that are transitional between eugeosynclinal and miogeosynclinal facies.

The structural setting of the two sections is also similar. Both the Garlock Formation and the metasedimentary rocks in Pilot Knob Valley are pendants with generally homoclinal steep easterly dips. Although their strikes differ by 30° to 40°, a 20° to 45° clockwise rotation of rocks in the block south of the Garlock fault, suggested by differences in the orientation of the correlated dikes (Smith, 1962, p. 95), would account for this difference.

Inasmuch as there are no other exposed sections of metasedimentary rocks of these types exposed in the area just north or south of the Garlock fault, the best possible correlation is between the Garlock Formation and the rocks in Pilot Knob Valley described in this paper. It is therefore reasonable to suggest that after emplacement of plutonic rocks in late Mesozoic time, there was a north-trending pendant containing homoclinally dipping late Paleozoic eugeosynclinal rocks in the area later cut by the Garlock fault, and that it was subsequently offset left laterally 30 to 40 miles by that fault.

REFERENCES

Christiansen, R. L., 1961, Structure, metamorphism, and plutonism in the El Paso Mountains, Mojave Desert, California: Stanford Univ., Ph.D. thesis, 180 p.

Dibblee, T. W., Jr., 1952, Geology of the Saltdale quadrangle, California: California Div. Mines Bull. 160, 66 p.

——— 1967, Areal geology of the western Mojave Desert, California: U.S. Geol. Survey Prof. Paper 522, 153 p.

Grose, L. T., 1959, Structure and petrology of the northeast part of the Soda Mountains, San Bernardino County, California: Geol. Soc. America Bull., v. 70, no. 12, p. 1509–1547.

Hewett, D. F., 1954, General geology of the Mojave Desert region, California, [pt.] 1 *in* chap. 2 *of* Jahns, R. H., ed., Geology of southern California: California Div. Mines Bull. 170, p. 5–20.

Jaffe, H. W., Gottfried, David, Waring, C. L., and Worthing, H. W., 1959, Lead-alpha age determinations of accessory minerals of igneous rocks (1953–1957): U.S. Geol. Survey Bull. 1097-B, p. 65–148.

Jennings, C. W., Burnett, J. L., and Troxel, B. W., 1962, Geologic map of California, Olaf P. Jenkins edition, Trona sheet: California Div. Mines, scale 1:250,000.

McCulloh, T. H., 1954, Problems of the metamorphic and igneous rocks of the Mojave Desert, [pt.] 2 *in* chap. 7 *of* Jahns, R. H., ed., Geology of southern California: California Div. Mines Bull. 170, p. 13–24.

Merriam, C. W., and Hall, W. E., 1957, Pennsylvanian and Permian rocks of the southern Inyo Mountains, California: U.S. Geol. Survey Bull. 1061-A, 15 p.

Michael, E. D., 1966, Large lateral displacement of Garlock fault, California, as measured from offset fault system: Geol. Soc. America Bull., v. 77, no. 1, p. 11–113.

Smith, G. I., 1962, Large lateral displacement on Garlock fault, California, as measured from offset dike swarm: Am. Assoc. Petroleum Geologists Bull., v. 46, no. 1, p. 85–104.

——— 1963, Possible large left-lateral displacement on the Garlock fault: Am. Assoc. Petroleum Geologists News Letter, Pacific Section, v. 17, no. 2, p. 2.

——— 1964, Geology and volcanic petrology of the Lava Mountains, San Bernardino County, California: U.S. Geol. Survey Prof. Paper 457, 97 p.

Smith, G. I., Troxel, B. W., Gray, C. H., Jr., and von Huene, R. E., 1968, Geologic reconnaissance of the Slate Range, San Bernardino and Inyo Counties, California: California Div. Mines and Geology Spec. Rept. 96, 33 p.

APOLLO 7 PHOTOGRAPHY IN ANTOFAGASTA PROVINCE, CHILE—AN INTERPRETATION

BY KENNETH SEGERSTROM, Denver, Colo.

Abstract.—As a result of 1969 field checking of Apollo 7 (October 1968) color photography of northern Chile, photographic tonal values were correlated with the natural colors of surficial deposits and rock of the Salar de Atacama area. An est-west linear feature on Apollo 7 photographs of the Taltal-Salar de Gorbea area defies field identification because it is largely concealed by sedimentary and volcanic deposits. This feature is interpreted as a transverse fracture which has been inactive since Jurassic time. Fragmental evidence from Peru and central Chile indicates that despite its poor visibility on the ground and on conventional aerial photographs, an ancient structural trend transverse to the modern circum-Pacific trend is real, and its distribution is broader than has hitherto been recognized.

Several oblique color photographs of northern Chile (fig. 1) taken by 70-mm cameras during the Apollo 7 mission were examined in the field by the author and several colleagues of the Instituto de Investigaciones Geológicas. The loan of vehicles and camping facilities by the Instituto, and fruitful discussions with the Director, Carlos Ruiz F., and the Regional Geologist, Aldo Moraga B., are gratefully acknowledged. In turn, Ruiz and Moraga have acknowledged the timeliness of AS 7–7–1593, a fine color print of the Salar de Atacama (Atacama Salt Pan) made available to them early in the course of their high-priority economic study of the salar in June-August, 1969. This study was also supported, in part, by the National Aeronautics and Space Administration. Walter M. Schirra, Jr., Don F. Eisele, and R. Walter Cunningham, the Apollo 7 crew, took the photographs.

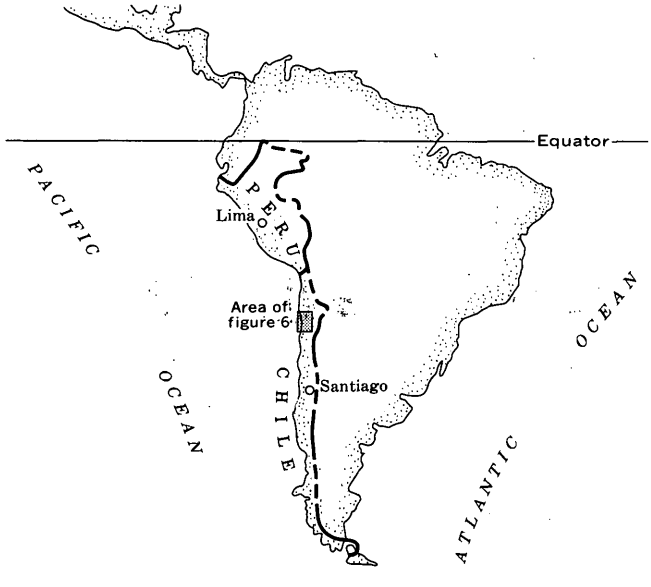

FIGURE 1.—Index map of South America, showing Chile, Peru, and the location of figure 6.

The photographs were also valued by resident geologists of the International Telephone and Telegraph Co. and Texas Gulf Sulphur Co., in Antofagasta, for use in exploration for porphyry copper deposits. Some of the photographs are particularly helpful to structural geologists from the California Institute of Technology who are studying the displacement along the great Atacama fault (fig. 5), in an area near the port of Taltal, some 200 km south of Antofagasta.

The objectives of this study were (1) to attempt to correlate the color rendition displayed in Apollo 7 photographs with the natural colors of rock and surficial materials observed in the field; and (2) to field-check and, if possible, assess the relationship of major linear features observed in space photographs to the regional geologic structure of the Atacama Desert, Chile.

TONAL VALUES IN THE SALAR DE ATACAMA

A high-angle oblique color photograph, AS 7–7–1593, was taken October 21, 1968, at 19^h01^m G.m.t.[1] (or 3:01 p.m. local time) from an altitude of 175 nautical miles. A black-and-white print of that color photograph is shown as figure 3. It depicts an

[1] Times are given in hours and minutes, Greenwich mean time.

area of the Atacama Desert where Argentina, Bolivia, and Chile join. Figure 2 shows 1969 field observations by Aldo Moraga B. and colleagues of the Instituto de Investigaciones Geológicas; Segerstrom accompanied the field party for a few days. Color portrayal in the original space photograph is close to that observed in the field; the human eye automatically corrects for a bluish cast which is noted only in distant parts of the oblique view. The area shown is that of the Salar de Atacama, a large closed basin between the Cordillera de Domeyko, to the west, and the Chile-Argentina boundary, to the southeast. The original scale of the color photograph was approximately 1: 1,200,000 in the Chilean sector, and progressively smaller in the Bolivian and Argentine sectors.

Table 1 shows the colors corresponding to the classification of surficial materials made in the field and shown by number in figure 2.

A lake in Bolivia, which was not visited because of its inaccessibility from the Chilean side, is rightly named "Laguna Colorada"—its color is brownish red (possibly because of the surrounding ignimbrite). The lake is labeled on figure 3.

POSSIBLE TRANSVERSE FAULT NEAR TALTAL

A low-angle oblique color photograph, AS 7–7–1826, was taken October 16, 1968, at 22^h14^m G.m.t. (6:14 p.m. local time) from an altitude of 117 nautical miles. A black-and-white print of that color photograph is shown as figure 4. It depicts much of the southern Atacama Desert and part of the distant Argentine Pampa. The sun is low—about 10° above the western horizon—producing shadows which enhance a strong north-south topographic and structural grain. The view is southeastward, from off the shore of the Península de Mejillones where the scale is nearly 1 : 1,000,000—almost the same as that of the new edition of the geologic map of Chile (Instituto de Investigaciones Geológicas, 1968). Another oblique color photograph, also from Apollo 7, is represented as a black-and-white print in figure 5. The serial number and date and time taken have been lost. This photograph shows the coast from about 75 km north of the Península de Mejillones southward nearly to the Rio Copiapó.

On figure 6, a segment of the geologic map of Chile, the approximate southwest limit of the area covered by photograph AS 7–7–1826 (fig. 4) is shown by a straight line. Figure 5 coverage extends farther along the coast, but not as far inland as that in figure 4. Looking at the map (fig. 6) of these areas is like looking at the photographs, as the same circum-Pacific fractures, generally parallel to the coast, are evident. Major features on the map and photographs are (1) the Salar del Carmen fault, which extends from slightly north of lat 21°00′ S. to slightly south of lat 25°00′ S., and (2) the Atacama fault, which extends from just south of lat 27°00′ S. northward through El Salado nearly to Taltal. The Pacific Ocean conveniently covers a gap in the mapping of the two faults. Recent unpublished work by Walter Arabasz (written commun., Aug. 6, 1969), of the California Institute of Technology, indicates that the Atacama fault zone is displaced left laterally by a northwest-trending fault at Taltal.

One major feature which is apparent on the photographs but not heretofore mapped is a strong lineament that runs westward from near the Salar de Gorbea (fig. 4) to the coast near Taltal (fig. 5). This is shown, for the first time on a geologic map, at about lat 25°30′ S. (fig. 5). The alinement exhibits a decided flexure south-southeast of Taltal, near where the feature crosses the Atacama fault.

The author field-checked parts of the lineament with Carl Ulrichsen, a geologist assigned to map the Taltal quadrangle for the Instituto de Investigaciones Geológicas. The field observations were supplemented by study of vertical aerial photographs which provided stereo image coverage at 1:60,000 scale. The only field evidence that was found for fault displacement along the lineament was along Quebrada Cifuncho, near the coast, where Paleozoic granite and Lower Jurassic (Lias) marine sedimentary rocks appear to be displaced right laterally about 10 km. A little farther east, however, bedding in volcanic and continental sedimentary rocks of the La Negra Formation (Upper Jurassic) continues without interruption across the lineament. Elsewhere, no evidence for faulting along the lineament was seen either in outcrop or in stereo photograph image. Where other watercourses (such as the Quebrada de la Peineta) follow the lineament, the rocks on both sides are the same. Nevertheless, disseminated sulfide minerals in the rocks seem to extend farther east on the north side of the lineament than on the south side (Nelson Aliste, International Telephone and Telegraph Co., oral commun., June 1969).

According to Arabasz (written commun., Aug. 6, 1969),

> The age of the lineament may be difficult to judge * * * older granitic rocks of the Mesozoic batholithic sequence (Jurassic?) * * * are affected by mineralization and alteration along east-west fractures, especially between Taltal and Paposo. Younger post-orogenic granodiorites don't seem to be similarly affected.

The right-lateral displacements of Paleozoic granite and Lias sedimentary rocks near the coast suggest a post-Lias, Jurassic age for the lineament.

It seems worth considering, therefore, that the lineament may represent an ancient fracture or zone of crustal weakness along which no displacement of blocks has occurred since La Negra (Late Jurassic) time.

Farther to the south, outside the area of Apollo 7 photograph coverage, evidence of other right-lateral displacement of similar magnitude along ancient transverse faults lends support to this consideration. Two Chilean Coast Range localities may present such evidence: (1) At Quebrada Flamenco (about lat 26°30′ S.) no transverse structure has been mapped, but right-lateral displacement of Paleozoic granite seems to have taken place in an east-southeast direction (fig. 6). (2) At San Antonio-Melipilla (about lat 33°35′ S.), 65 km west-southwest of Santiago, right-lateral displacement of Paleozoic granite has taken place along a mapped east-southeast-trending fault; Lower Cretaceous sedimentary rocks crop out south of this fault, but are absent immediately north of it. Both localities are in areas of the massive Cretaceous "Andean batholith," which seems to be unaffected by the transverse faulting.

Much farther to the north, in southern Peru, evidence for concealed east-southeast-trending frac-

TABLE 1.—*Color, color-chart designation, and description of surficial materials of the Salar de Atacama area, Chile, determined in the field*

Color	Color-chart designation [1]	Geologic material
White	*N* 9	Relatively pure salt precipitated from brine.
Light browish gray	5*YR* 6/1	Impure salt (deposited in playa; forms hard, rough surface).
Moderate brown	5*YR* 3/4	Saline silt (in playa).
Pale brown	5*YR* 5/2	Saline silt (in delta).
Moderate brown	5*YR* 4/4	Sandstone, shale, and bedrock salt of the San Pedro Formation (lower Tertiary).
Medium gray and medium light gray.	*N* 5 and *N* 6	Alluvium and piedmont deposits (lighter are recent streambeds).
Dusky blue	5*PB* 3/2	Sandstone and conglomerate of the Purilactis Formation (Cretaceous), and alluvium derived therefrom.
Pale red	10*R* 6/2	Ignimbrite (partly covered with somewhat darker lahars).
Between browish gray and brownish black.	5*YR* 3/1	Andesite volcanoes and lahars (modern).
Dark gray	*N* 3	Andesites (Jurassic).

[1] Goddard and others (1948).

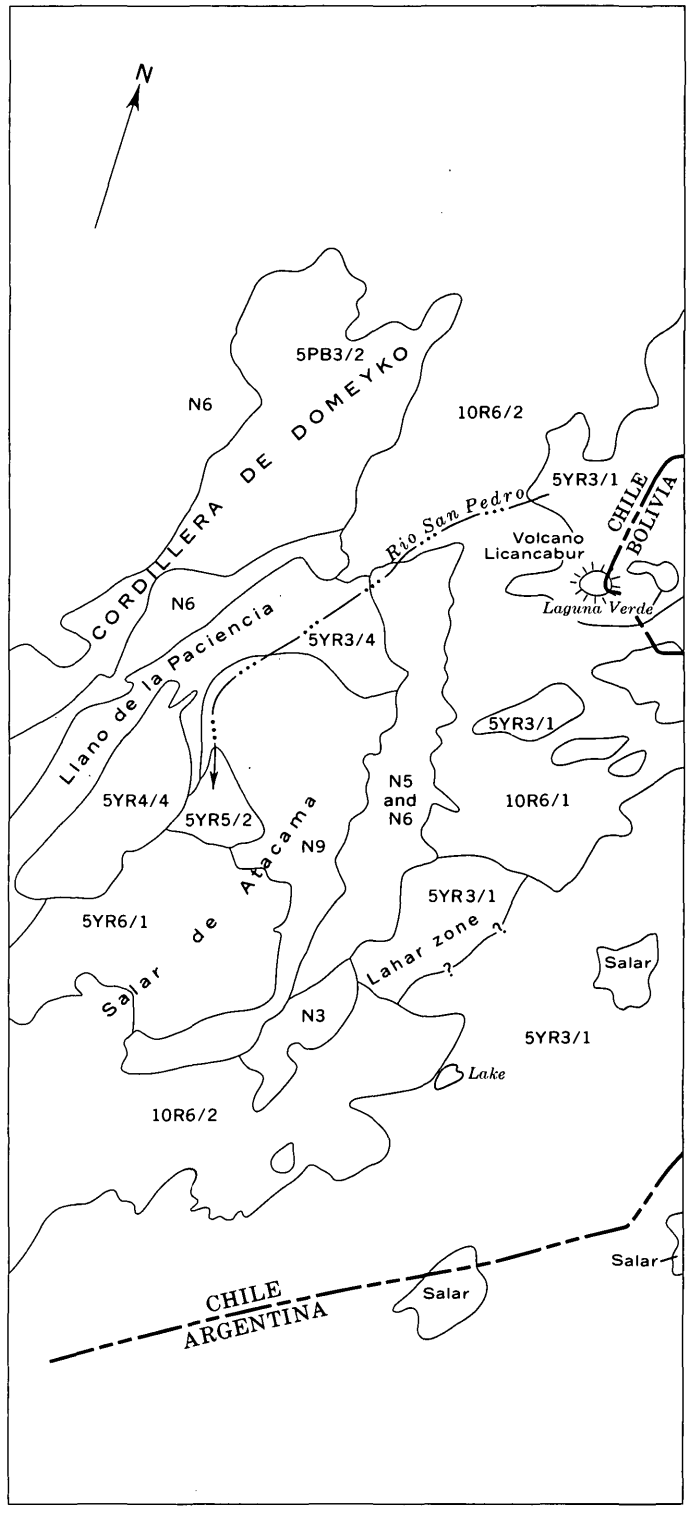

FIGURE 2.—Map of western part of area of photograph AS 7-7-1593, showing color-chart values (Goddard and others, 1948) observed in the field. Scale variable: north-south distance across mapped area is approximately 140 km. Source of data: unpublished map by Aldo Moraga B. and associates of the Instituto de Investigaciones Geológicas.

FIGURE 3.—Black-and-white print of Apollo 7 color photograph AS 7–7–1593. Scale variable.

FIGURE 4.—Black-and-white print of Apollo 7 color photograph AS 7–7–1826, looking southeastward across the southern Atacama Desert toward the Argentine Pampa. Arrows indicate lineament referred to in text.

FIGURE 5.—Black-and-white print of an Apollo 7 photograph (serial number unknown), showing faults north and south of Antofagasta. Arrows indicate lineament referred to in text.

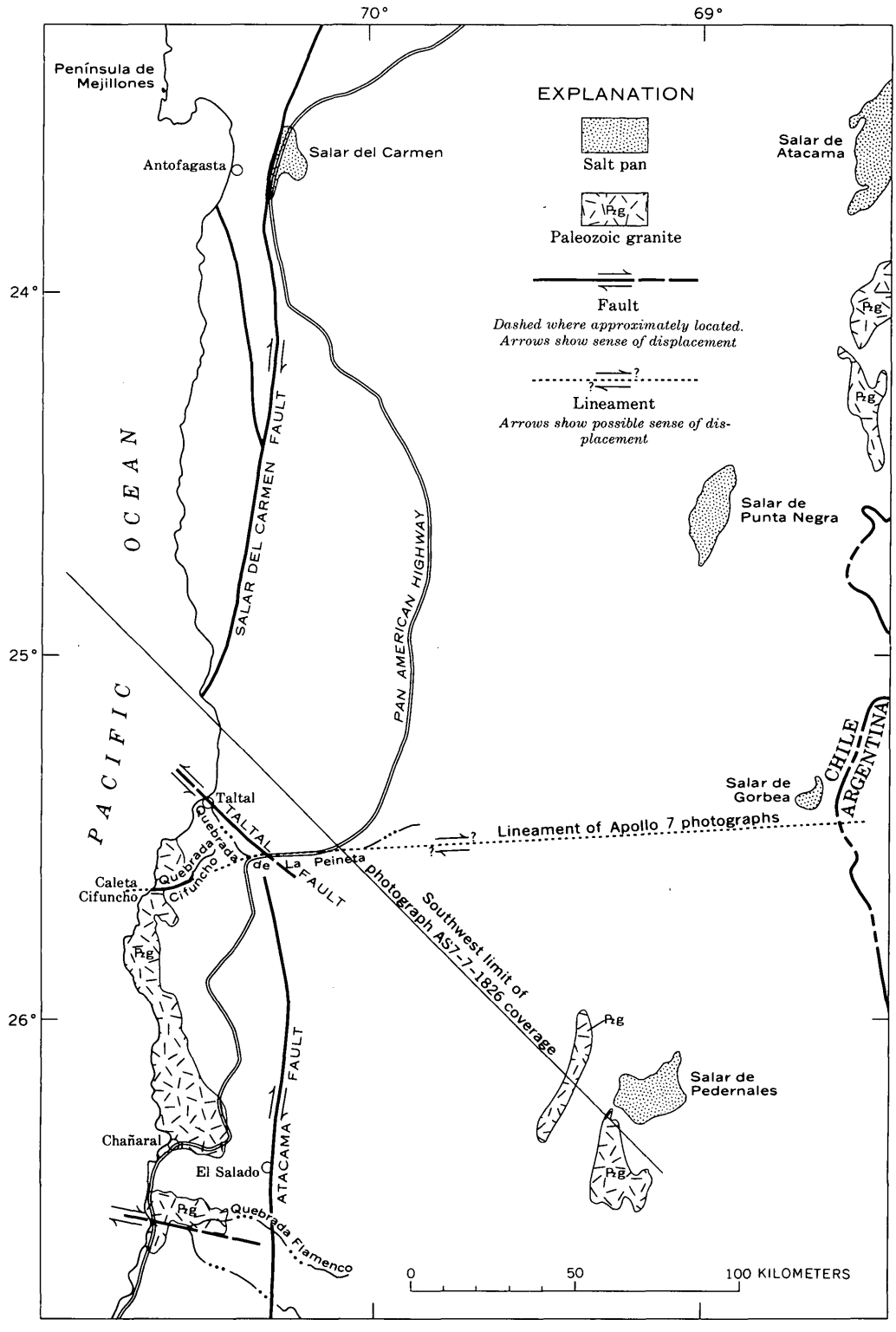

FIGURE 6.—Map of Chile between Antofagasta and Chañaral, showing faults and lineament referred to in text, and distribution of Paleozoic granite. Sources: Instituto de Investigaciones Geológicas (1968); Walter Arabasz (written commun., 1969); Aldo Moraga B. (oral commun., 1969); and observations by the author.

tures was described by E. A. Stephens, Photogeological Unit, Institute of Geological Sciences, London (written commun. to W. A. Fisher, U.S. Geological Survey, June 20, 1969), after he examined Gemini IX photograph C38, the coverage of which extends from Lima southward:

> This photograph shows a dominant negative lineament direction trending ESE. Rivers near the coast follow this direction, and some of the lineaments can be traced for many miles across the whole width of the satellite photograph. This direction, however, does not correspond with prominent geological features. The main Andean trend shows up well in the sediments and is roughly parallel to the coast, and the main faults in this area trend NE.
>
> It would seem that the main ESE-trending lineaments are not faults. They do correspond, however, with internal contacts within the coastal batholith. For instance, the contact of diorite and tonalite follows this direction. Movements at a much larger scale have occurred along this trend to the south of the area covered by the satellite photographs. The Excelsior Series (metamorphic rocks) and the granitic rocks of the batholith are displaced eastwards. The displacement is not by faulting but by a very large-scale kinking of the structures along the ESE trend.
>
> It seems likely that the satellite photographs are showing major fractures of deep-seated origin which do not displace the sediments and are, therefore, not picked up in normal photogeological or field mapping.

In order to give an objective analysis of the east-west lineament at about lat 25°30′ S., the considerable evidence which invalidates it as a throughgoing structure should be stated. Most, if not all, of the field evidence for a fault along the lineament is confined to the coastal area; inland, the observer cannot see the lineament either from the earth's surface or, in effect, from 30,000 feet up, where the 1:60,000 aerial photographs were taken. Although in figure 4 most of the lineament is a ruler-straight line and looks like a fault, it is somewhat less straight in figure 5 and, there, could be interpreted as accidental alinement of small playa lakes and dry watercourses. The apparent lack of displacement where the lineament is crossed by the Atacama and Taltal faults suggests that the lineament represents two accidentally alined structures, rather than a single throughgoing one. Displacement along the lineament, though right lateral like that of Quebrada Flamenco and San Antonio-Melipilla, is counter to the left-lateral displacement along most of the known transverse faults in the circum-Pacific belt; for example, the "transverse" (northwest-striking) Taltal fault has left laterally displaced the north-striking, right-lateral Atacama fault by as much as 10 km (Walter Arabasz, written commun., Aug. 6, 1969).

Despite the counter arguments that can be marshalled, the conclusion that the lineament has major structural significance is almost inescapable. A strong argument can thus be made for two epochs of transverse faulting—one producing right-lateral displacement which ended in Jurassic time, and the other producing left-lateral displacement which is Cenozoic. It may be difficult or impossible to perceive the lineament at the altitude of the earth's surface or from 30,000 feet above the surface, but from the altitude of a satellite a single field of vision can encompass features of subcontinental, continental, or even planetary scale. The lineament at about lat 25°30′ S. in the Atacama Desert can thus be compared to ancient Indian pictographs in the California desert which were first reported in 1932 by George Palmer, a private pilot, and described by Deuel (1969, p. 248):

> Some eighteen miles from Blythe, flying at an altitude of five thousand feet, he suddenly saw a huge human figure lying spread-eagled on the desert flats as if basking in the sun. Palmer swung his plane over, took a closer look, and a four-legged creature beside the giant swam into his view. Both figures appeared to him about one hundred feet long.

Curiously, although these figures were scraped into the ground, they were only visible from the air.

In summary, there is mounting evidence, some of it inconclusive, of the existence of major east-to-southeast-striking faults in western South America from about Lima, Peru (lat 12°S.), to Santiago, Chile (lat 33°30′ S.). These faults were active during the Mesozoic Era, but they have been inactive since. They are difficult to trace; hence, most of them have not been mapped. There seems to be no continuity between these faults and known structural features of the floor of the Pacific.

REFERENCES

Deuel, Leo, 1969, Flights into yesterday, the story of aerial archaeology: New York. St. Martin's Press, Inc., 332p.

Goddard, E. N., chmn., and others, 1948, Rock-color chart: Washington, Natl. Research Council, 6 p.

Instituto de Investigaciones Geológicas, 1968, Mapa geológico de Chile (scale 1:1,000,000): Santiago, in 7 sheets.

LIMESTONE TURBIDITE OF KINDERHOOK AGE AND ITS TECTONIC SIGNIFICANCE, ELKO COUNTY, NEVADA

By KEITH B. KETNER, Denver, Colo.

Abstract.—A limestone unit of Kinderhook (early Early Mississippian) age is exposed in the Swales Mountain quadrangle, southern Independence Range, Nev. This unit, here termed the Camp Creek sequence, is underlain concordantly by the Roberts Mountains Formation and is overlain by thrust plates composed of Ordovician and Devonian rocks. Sedimentary features of the Camp Creek indicate that it was deposited by turbidity currents which flowed from the miogeosyncline toward the eugeosyncline. All thrust faults in the area are younger than the Camp Creek sequence and, therefore, younger than the Roberts Mountains thrust as dated in the neighboring Piñon Range.

The rocks of central Elko County, Nev., like those of the Piñon Range (Smith and Ketner, 1968), record a middle Paleozoic revolution of the Cordilleran geosyncline. This event, widely known as the Antler orogeny (Roberts and others, 1958), involved both uplift of eugeosynclinal rocks and thrusting of these rocks over contemporaneous rocks of the miogeosyncline. Paleozoic sediments laid down after the beginning of the Antler orogeny characteristically contain recognizable debris derived from uplifted eugeosynclinal rocks, and the time of initial exposure to erosion of provenance terranes can be determined by the age of the oldest beds that contain such debris.

In the Piñon Range (fig. 1) the oldest formation that contains eugeosynclinal debris is the Webb Formation of Kinderhook (early Early Mississippian) age. The minimum age of the oldest thrust in the Piñon Range, termed the "Roberts Mountains thrust" (Smith and Ketner, 1968), is fixed by the Webb Formation which overlaps the thrust and lies with depositional contacts on both the upper and the lower plates. Thus, the Webb Formation is a key to dating both the uplift and the thrust phases of the Antler orogeny in the latitude of the Piñon Range. Although beds similar to the Webb Formation have not been found in the area north of the Piñon Range, a correlative unit of different lithology was found in the Swales Mountain quadrangle of the southern Independence Range. This unit, which is the subject of the present report, is here informally termed the Camp Creek sequence. It is exposed in a window below thrust plates composed of parautochthonous Devonian limestone and allochthonous Ordovician chert and shale (fig. 2). The Swales Mountain area was studied by the author and J. G. Evans at intervals during 1966–68.

ROBERTS MOUNTAINS FORMATION

Carbonate rocks in the Camp Creek area regarded as autochthonous, or nearly so, comprise two concordant stratigraphic units—the Roberts Mountains Formation and the Camp Creek sequence. Upper beds of the Roberts Mountains

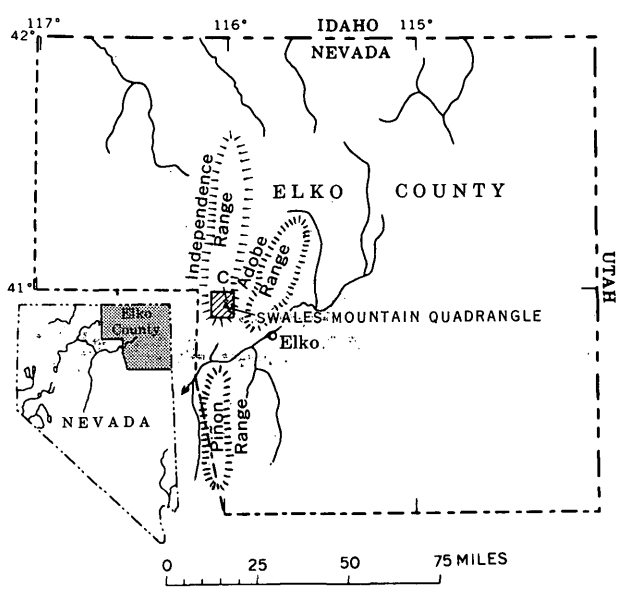

FIGURE 1.—Index map of Elko County, Nev., showing location of the Camp Creek sequence in the Swales Mountain quadrangle (C).

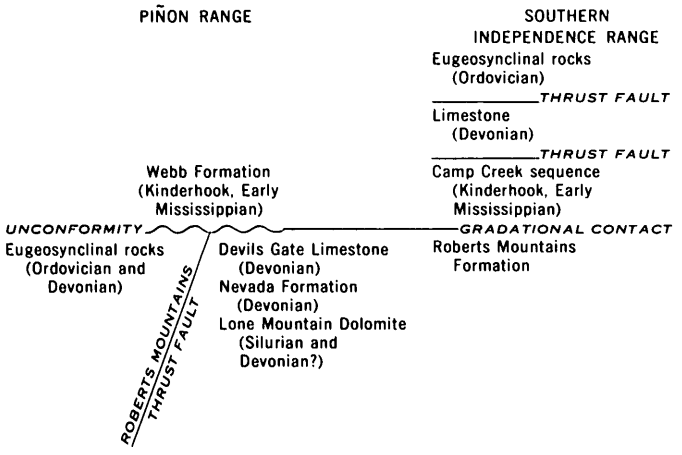

FIGURE 2.—Contrasting structural and stratigraphic setting of the correlative Webb Formation and Camp Creek sequence in the Piñon Range (modified from Smith and Ketner, 1968) and the southern Independence Range, respectively.

Formation crop out along Camp Creek, but the lower beds are known only from core drilling. The lithology of the Roberts Mountains Formation, which is very uniform throughout its observable thickness, is predominantly black calcilutite and subordinately gray calcarenite. Noncalcareous constituents are illite, quartz silt, and carbon. The base of the Roberts Mountains Formation was not reached by drilling, but the minimum thickness is 2,700 feet.

The Roberts Mountains Formation in the type locality is regarded as Silurian (Merriam, 1940), but recent data indicate an age span that includes a significant part of the Devonian in the area of the type locality (Murphy, 1969; Johnson and Murphy, 1969). North of the type locality the Roberts Mountains Formation may represent a more significant part of the Devonian (T. E. Mullens, oral commun., 1969). Graptolites collected by J. G. Evans from the Roberts Mountains Formation in the southern Independence Range 12 miles southwest of Camp Creek include the Early Devonian form *Monograptus hercynicus* Perner, identified by W. B. N. Berry (USGS colln. D269SD). In the author's opinion the Roberts Mountains Formation of the Camp Creek area could represent the entire Devonian Period, as well as the Silurian, because it seems to be gradational with the overlying Camp Creek sequence of Mississippian age. Alternatively, the contact is inconspicuously disconformable.

CAMP CREEK SEQUENCE

The Camp Creek sequence crops out on both banks of Camp Creek in sec. 4, T. 35 N., R. 53 E., in the Swales Mountain quadrangle (fig. 1).

The Camp Creek consists almost entirely of repeated graded cycles of quartz-sandy bioclastic calcarenite and argillaceous calcisiltite and calcilutite. The graded cycles are from 1 to 5 feet thick. Commonly, the basal beds of each cycle are composed of well-sorted sand-sized grains. Most of the grains are angular to rounded calcite, but well-rounded quartz grains constitute a small part of the rock. Basal beds in some graded cycles include small chips eroded from the upper surfaces of earlier formed cycles. A very few of the basal beds are edgewise conglomerates composed of large plates of earlier formed consolidated material. Convolute lamination and crossbedding are common in the coarser grained parts of graded cycles. Upper beds of graded cycles are composed of silt- to clay-sized carbonate, less commonly of clay-shale. The fine-grained uppermost beds of graded cycles are marked by differential pressure pits, flute marks, tool marks, and worm trails (figs. 3, 4). Although some of these markings are preserved as positive molds of calcilutite, most are preserved as negative casts in the overlying calcarenite. Load casts and fluting are the most common types of sole marks. Many forms of fluting are directional in plan, and the few directional measurements which could be made on outcrops indicate a current direction from the northeast quadrant.

The thickness of the unit from the base, arbitrarily fixed among the transitional beds between the typical Roberts Mountains lithology and the first distinctly graded cycle to the overthrust parautochthonous Devonian carbonate, is about 650 feet.

The Camp Creek sequence is of Kinderhook (early Early Mississippian) age as indicated by the following collection of conodonts from the middle part:

Field No. 2593 (USGS 22702–PC), Swales Mountain quadrangle, T. 35 N., R. 53 E., east edge of SE¼NW¼ sec. 4, on south-facing slope. Identified by J. W. Huddle.

	Number of specimens
Bryantodus sp	1
Gnathodus sp	1
Polygnathus inornatus Branson	1
P. communis Branson and Mehl	3
Pseudopolygnathus sp	1
Siphonodella obsoleta Hass	10
Spathognathodus	1

According to J. W. Huddle (written commun., 1968), a comparison of this fauna with that of the Webb Formation (Smith and Ketner, 1968) fails to indicate a significant age difference. Referring to collections from both units, Huddle stated, "Both collections could be as old as the upper Hannibal Shale or as young as uppermost Chouteau Lime-

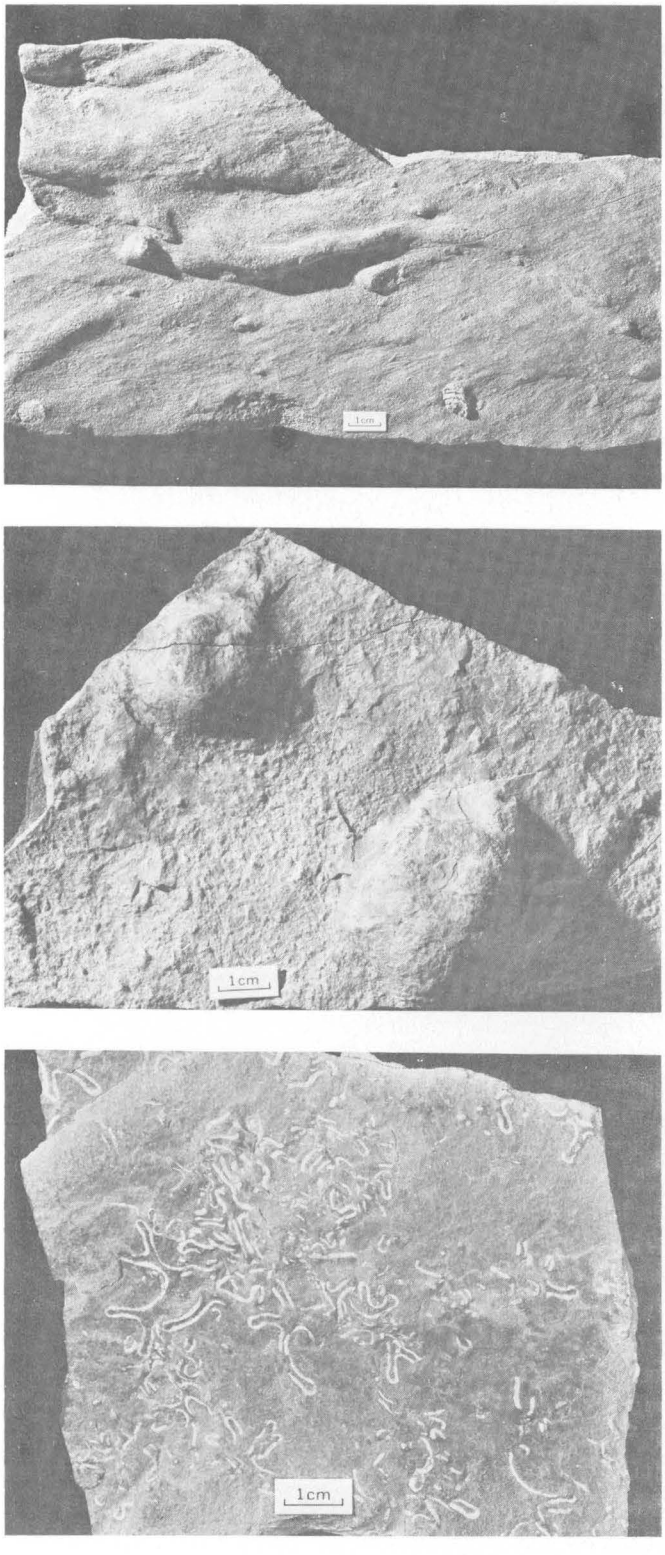

FIGURE 3.—Bedding surface features, Camp Creek sequence. Top, obstacle scour casts on underside of basal calcarenite of graded cycle. Middle, load structures on underside of calcarenite probably formed by load pressure of sand on underlying soft calcareous clay. Bottom, worm(?) trails common only at top of graded cycles.

stone in the upper Mississippi Valley. The presence of an advanced species of *Gnathodus* in both collections suggests that they are both equivalent to some part of the Chouteau Limestone."

The Kinderhook age of the Camp Creek sequence was confirmed by C. G. Tillman, of Virginia Polytechnic Institute, Blacksburg, Va., who identified the genus *Siphonodella* in eight samples taken from the base to the top of the sequence. Tillman identified the following species from the Camp Creek:

Siphonodella obsoleta—common
S. isosticha—common
S. cooperi
S. duplicata(?)
Gnathodus delicatus
Polygnathus communis

ORIGIN AND SIGNIFICANCE OF THE CAMP CREEK SEQUENCE

Conspicuous lithologic features of the Camp Creek sequence, such as graded bedding, sole marks, and convolute lamination, suggest that the sequence was deposited by turbidity currents. The northeastern provenance of the Camp Creek indicated by directional sole marks and the location of the sequence between the miogeosyncline and the eugeosyncline suggest that the sequence was deposited by currents flowing from the edge of the miogeosyncline toward the eugeosyncline.

Because the Camp Creek sequence is a deposit derived from the east and is free from detritus of eugeosynclinal rocks, its deposition must have preceded the first local emergence of the eugeosynclinal rocks. However, the evident instability of sediments near the edge of the miogeosyncline, which is suggested by turbidity currents, may have resulted from early pulses of the Antler orogenic episode. The Mississippian Chainman Shale (Waterpipe Canyon Formation of Kerr, 1962) in the northern Independence Range and in the neighboring Adobe Range (Ketner, 1970) contains abundant debris of eugeosynclinal rocks. Therefore, the initial local emergence of eugeosynclinal rocks must have occurred shortly after the Camp Creek sequence was deposited.

If the Webb Formation of the Piñon Range and the Camp Creek sequence of the southern Independence Range are precisely contemporaneous, as their conodont faunas indicate, then the initial uplift and erosion of eugeosynclinal rocks in the latitude of the southern Independence Range lagged behind the corresponding events in the latitude of the Piñon Range. A presentation of all the evidence bearing on the date of earliest thrusting in central Elko

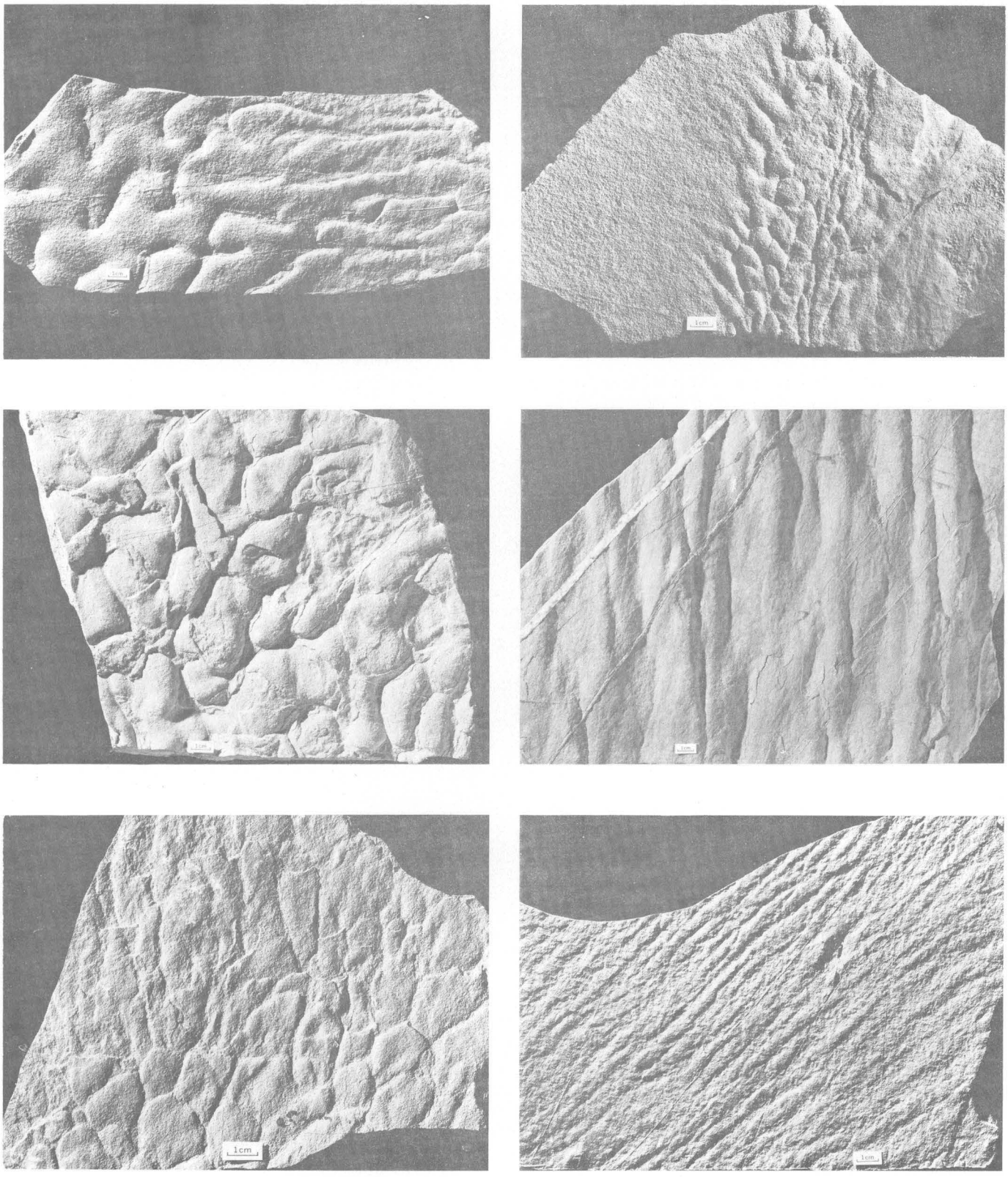

FIGURE 4.—Bedding surface features, Camp Creek sequence, showing flute casts displayed on undersides of basal calcarenite beds of graded cycles. Evidently these were formed where calcareous sand filled current-scoured depressions at the top of previously deposited graded cycles. These depressions are strikingly similar to those figured by Dzulyński and Walton (1965, p. 44, 64, 67, 78).

County is beyond the scope of this report, but one thing is clear from the relations in the southern Independence Range. The earliest thrusting in that area postdates the deposition of the Camp Creek sequence, and again, if the Webb Formation and the Camp Creek are precisely contemporaneous, the oldest thrust fault in the latitude of the southern Independence Range is distinctly younger than the oldest thrust fault in the latitude of the Piñon Range. This is consistent with evidence from the northern Independence Range (Kerr, 1962) which indicates that the earliest thrust faulting in that more northern latitude is younger than the Chainman Shale of Mississippian age.

REFERENCES

Dzulyński, Stanislaw, and Walton, E. K., 1965, Sedimentary features of flysch and greywackes: New York, Elsevier Publishing Co., 274 p.

Johnson, J. G., and Murphy, M. A., 1969, Age and position of Lower Devonian graptolite zones relative to the Appalachian standard succession: Geol. Soc. America Bull., v. 80, no. 7, p. 1275–1282.

Kerr, J. W., 1962, Paleozoic sequences and thrust slices of the Seetoya Mountains, Independence Range, Elko County, Nevada: Geol. Soc. America Bull., v. 73, no. 4, p. 439–460.

Ketner, K. B., 1970, Geology and mineral potential of the Adobe Range, Elko Hills, and adjacent areas, Elko County, Nevada *in* Geological Survey Research 1970: U.S. Geol. Survey Prof. Paper 700-B, p. B105–B108.

Merriam, C. W., 1940, Devonian stratigraphy and paleontology of the Roberts Mountains region, Nevada: Geol. Soc. America Spec. Paper 25, 114 p.

Murphy, M. A., 1969, Stratigraphy of the Roberts Mountains Formation in the type region, *in* Abstracts for 1968: Geol. Soc. America Spec. Paper 121, p. 535.

Roberts, R. J., Hotz, P. E., Gilluly, James, and Ferguson, H. G., 1958, Paleozoic rocks of north-central Nevada: Am. Assoc. Petroleum Geologists Bull., v. 42, no. 12, p. 2813–2857.

Smith, J. F., Jr., and Ketner, K. B., 1968, Devonian and Mississippian rocks and the date of the Roberts Mountains thrust in the Carlin-Piñon Range area, Nevada: U.S. Geol. Survey Bull. 1251–I, 18 p.

STRATIGRAPHY AND GEOCHRONOLOGY OF MIOCENE VOLCANIC ROCKS IN NORTHWESTERN NEVADA

By DONALD C. NOBLE[1]; EDWIN H. McKEE, JAMES G. SMITH;
and MARJORIE K. KORRINGA[2], Cambridge, Mass.;
Menlo Park, Calif.; Stanford, Calif.

Abstract.—A thick succession of ash-flow and air-fall tuff and mafic, intermediate, and silicic lavas in western Humboldt and northern Washoe Counties, Nev., has been subdivided, using widespread ash-flow sheets, four of which are named herein, as key stratigraphic markers. The approximate original areal extent and definite or probable source areas have been determined for many of the ash-flow sheets. Potassium-argon age determinations show that most of the volcanic rocks were erupted between 14.5 and 16 million years ago, but that the lowest ash-flow unit described in this paper is about 24 million years old. These ages indicate a Miocene age for the volcanism.

A stratigraphically complex and chemically diverse succession of pyroclastic rocks and lavas of Miocene age that is well exposed by pervasive normal faulting in western Humboldt and northern Washoe Counties, Nev. (fig. 1), was studied in reconnaissance. The purposes of this preliminary paper are: (1) to outline the Tertiary stratigraphy of northwestern Nevada, with particular attention to the major ash-flow sheets; (2) to present K-Ar age data on certain of the volcanic units; and (3) to report certain preliminary petrographic and chemical observations on the tuffs and lavas.

The ash-flow sheets in northwestern Nevada range from relatively thin "high-energy" (Noble, 1969) sheets of great areal extent to "low-energy" sheets of very limited original distribution. Each of the ash-flow sheets constitutes a single cooling unit; no evidence for the existence of a composite sheet has yet been recognized. (Terminology descriptive of ash-flow units—for example, "cooling unit", "sheet", and related terms—follows Smith, 1960, as supplemented by Noble, Bath, Christiansen, and Orkild, 1968, p. C61.) With several notable exceptions, the various sheets are lithologically distinctive and readily identified in isolated outcrop.

Acknowledgments.—Part of the fieldwork was carried out under the U.S. Geological Survey's Nevada State geologic mapping project in cooperation with the Nevada Bureau of Mines. The K-Ar dating was done in the isotope laboratory of the U.S. Geological Survey, Menlo Park, Calif.

Preparation of mineral and glass concentrates for analysis, other laboratory and photographic work, and part of the fieldwork were supported by National Science Foundation grant GA–1546 and National Aeronautics and Space Administration grant NGR–22–007–103 to D. C. Noble. Work of M. K. Korringa was supported by Geological Society of America grant 1296–69. J. W. Creasy and D. W. Chipman assisted during parts of the fieldwork.

LOWER MIOCENE OR OLDER TERTIARY VOLCANIC ROCKS

The oldest rocks exposed in the area include a sequence of olivine basalt flows that underlie the unit herein named the Ashdown Tuff in the central part of the Black Rock Range, and a thick sequence of locally altered lavas and subordinate pyroclastic rocks that form the southern part of the Calico Mountains. A K–Ar age of 31.3 ± 1.2 million years has been obtained on an intermediate rock from west of the Calico Mountains (Bonham, 1969). These rocks may in part correlate with minor air-fall, ash-flow, and reworked tuffs along the western and southern flanks of the Pine Forest Range and perhaps with certain of the rocks included in the Oligocene (?) and Miocene Pike Creek Formation in southeastern Oregon (Walker and Repenning, 1965).

[1] Department of Geological Sciences, Harvard University.
[2] Department of Geology, Stanford University.

U.S. GEOL. SURVEY PROF. PAPER 700–D, PAGES D23–D32

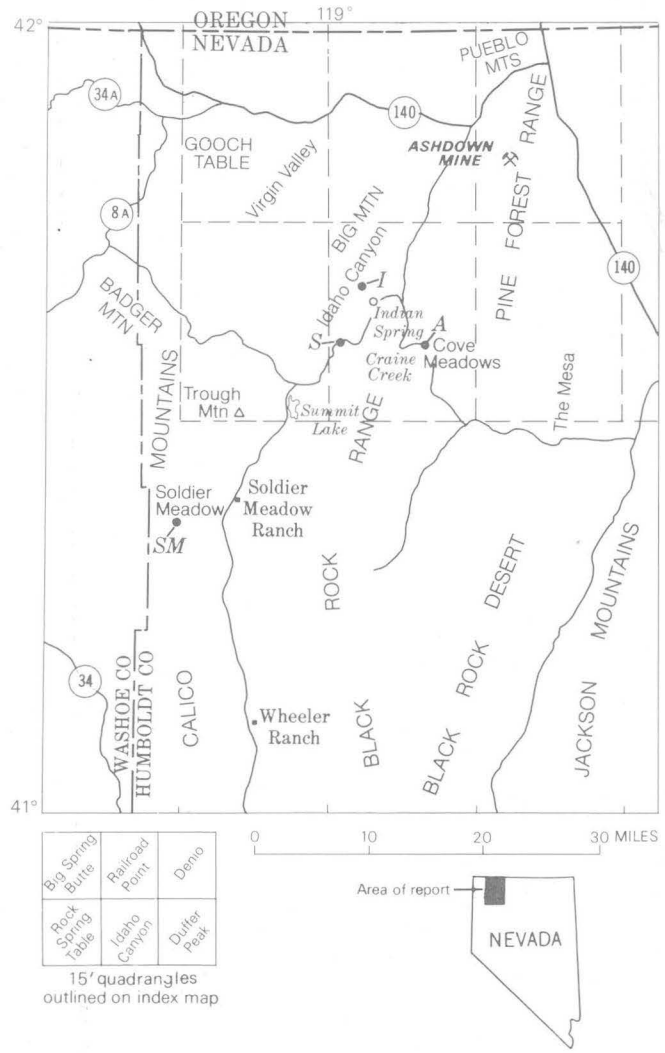

FIGURE 1.—Index map of part of northwestern Nevada. *A*, type locality of the Ashdown Tuff; *I*, type locality of the Idaho Canyon Tuff; *S*, type locality of the Summit Lake Tuff; *SM*, type section of the Soldier Meadow Tuff. Light dashed lines show the boundaries of published U.S. Geological Survey 15-minute quadrangle maps, which should be referred to for exact locations. For other locations, refer to the Vya 1:250,000-scale map.

Ashdown Tuff

The Ashdown Tuff is here named for the Ashdown mine on the west side of the Pine Forest Range (fig. 1), where the unit forms a conspicuous west-dipping hogback. The formation is also exposed along the western and southern flanks of the Pine Forest Range and in scattered localities in the northern, central, and southern parts of the Black Rock Range. In the northwesternmost and southeasternmost parts of the Pine Forest Range, the unit underlies mafic lavas that are the southern extension of the Steens Basalt exposed on Steens Mountain in southeastern Oregon (Fuller, 1931; Williams and Compton, 1953; Baldwin, 1964; Walker and Repenning, 1965; G. W. Walker, oral commun., 1969). The Ashdown Tuff forms the thickest cooling unit exposed in the canyon walls of Cove Creek (NE¼ sec. 2, T. 42 N., R. 27 E.), designated its type locality (fig. 2) directly northwest of Cove Meadows. It also forms the thickest cooling unit on the west face of the Black Rock Range southeast of Summit Lake. Maximum observed thickness is about 200 feet. The thickness and persistence of the formation suggests that it is also present beneath the northern part of the Calico Mountains, Big Mountain, and the Black Rock Desert and in intervening areas. The original volume probably was approximately 30 to 60 cubic miles.

In most localities the Ashdown Tuff forms a dark-tan- to reddish-brown-weathering cliff that is densely welded and devitrified throughout most of its vertical extent. Discontinuous horizontal jointing is present in most exposures, but vertical columnar jointing generally is poorly developed. Partial cooling breaks are present locally. The basal glassy zone is thin in most places.

In most places the tuff contains 15 to 25 percent phenocrysts; a few ash flows within the unit contain as few as 5 percent. Most of the phenocrysts are unzoned and sparsely twinned phenocrysts of anorthoclase (table 1) as large as 1 cm in greatest dimension. Biotite, typically highly oxidized, and uncommon grains of clinopyroxene make up 1 percent or less of the rock. Lithic fragments of fine-grained tan, pink, or gray lava of intermediate

FIGURE 2.—The Ashdown Tuff (dark rock at top of cliff) in its type locality, the canyon of Cove Creek directly northwest of Cove Meadows.

TABLE 1.—*Partial chemical analyses and molecular ab/ab+or ratios of alkali feldspar phenocrysts*

[Na_2O and K_2O analyses by L. B. Schlocker using flame-photometer methods; Sr analyses by M. K. Korringa using X ray fluorescence methods]

Rock unit	Ashdown Tuff	Tuff of Craine Creek	Summit Lake Tuff	Soldier Meadow Tuff
Sample No.	N9-150-S	N-42-S	N-25-S	NR-11-S
Na_2O (wt percent)	7.47	6.65	7.44	----
K_2O (wt percent)	5.84	6.88	5.64	7.54
ab/ab+or	0.685	0.595	0.692	----
Sr (ppm)	13.	7.	35.	≤2.

composition make up from several percent to about 10 percent of the rock. In addition to the large anorthoclase phenocrysts, the Ashdown Tuff contains a second generation of distinctive lath-shaped sanidine microphenocrysts (fig. 3). The presence of these microphenocrysts and the uncommon twinning in the larger anorthoclase phenocrysts serve in thin section to readily distinguish rocks of the Ashdown Tuff from rocks of the megascopically similar Summit Lake Tuff, described in a later section.

Two K–Ar age determinations on anorthoclase gave an approximate age of 24 m.y., which suggests that the formation is early Miocene.

Local unnamed ash-flow units

At least five unnamed ash-flow cooling units which appear to be genetically related to the Ashdown Tuff are locally present in the northern part of the Black Rock Range and in the southern Pine Forest Range (fig. 4). Although lithologically very similar to the Ashdown, these units can be distinguished in megascopic and microscopic examination by small differences in petrology.

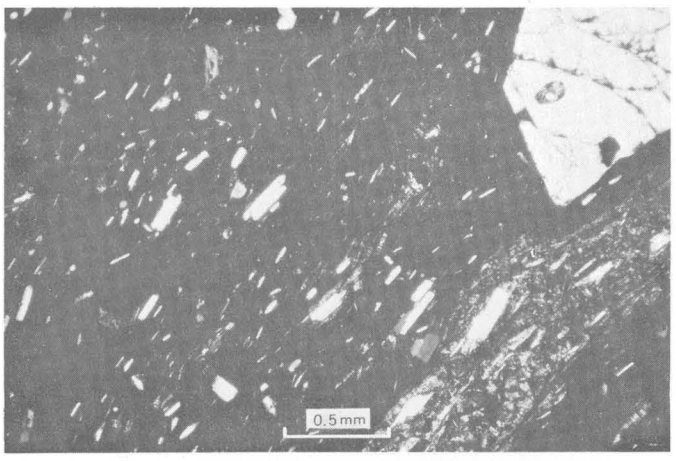

FIGURE 3.—Photomicrograph (crossed polarizers) of thin section of the Ashdown Tuff, showing abundant lath-shaped sanidine microphenocrysts characteristic of the unit. Anorthoclase phenocryst in upper right-hand corner.

Source of Ashdown Tuff

Reconnaissance study suggests that the Ashdown Tuff was erupted from a vent area centered about 5 miles east of Summit Lake in the northern part of the Black Rock Range. Evidence for this location is the distribution pattern and thickness variation of the formation and the presence of the local ash-flow units and thick intercalated air-fall tuffs and silicic lavas in the area (compare Christiansen and others, 1968).

UPPER MIOCENE VOLCANIC ROCKS

Tuff of Craine Creek

Near Craine Creek (fig.1) an ash-flow unit, here informally called the tuff of Craine Creek , is separated from the underlying Ashdown Tuff by small unnamed ash-flow sheets, and locally by silicic lavas. In the vicinity of Idaho Canyon, along the southern and western flanks of the Pine Forest Range, and in the southern Pueblo Mountains, the unit overlies mafic lavas.

The tuff of Craine Creek consists of a simple cooling unit, less than 100 feet thick, having a relatively thick basal zone of platy-weathering, partly to densely welded, grayish-green to gray glassy tuff. Crystallized tuff is generally light to medium tan. Phenocrysts of sodic sanidine, quartz, and distinctive phenocrysts of micrographically intergrown quartz and sanidine make up about 10 percent of the rock. Altered mafic phenocrysts are present in trace amounts. Fine-grained vapor-phase and groundmass arfvedsonite is present in the crystallized tuffs, indicating that the rock is peralkaline. A K-Ar age determination on sanidine gave an approximate age of 16 m.y., which suggests late Miocene.

Stratigraphic relations (fig. 2), similar distribution pattern, and close similarity in phenocryst mineralogy suggest that the tuff of Craine Creek may be genetically related to the Idaho Canyon Tuff, described later in this report.

Tuff of The Mesa

In the southeastern part of the Pine Forest Range and locally along the eastern flank of the Black Rock Range, mafic lavas petrographically resembling the Steens Basalt overlying the Ashdown Tuff are in turn overlain by a thin cooling unit of moderately phenocryst-poor comendite ash-flow tuff. A lithologically identical unit of tuff is

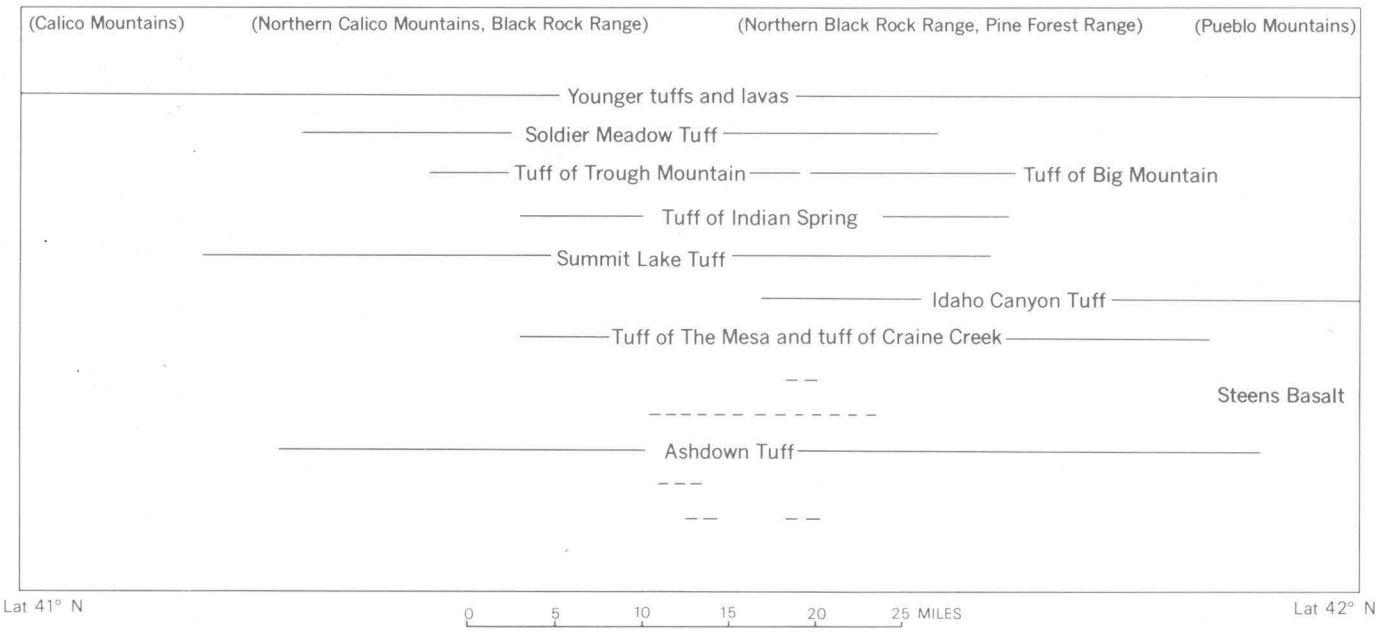

FIGURE 4.—Diagrammatic cross section extending from the southern part of Calico Mountains north-northeast to the southern part of the Pueblo Mountains, showing stratigraphic relations of ash-flow units. Some rock units are projected into the section. Local unnamed ash-flow units which may be genetically related to the Ashdown Tuff are shown by dashed lines.

locally intercalated with the lavas in the southeastern Pine Forest Range. These tuffs, informally designated tuff of The Mesa, are megascopically and microscopically very similar to the tuff of Craine Creek except that they contain considerably more, approximately 1 percent total, mafic phenocrysts—iron-rich clinopyroxene, fayalite, and magnetite. The units probably are of restricted areal extent and very small original volume.

Idaho Canyon Tuff

The Idaho Canyon Tuff is here named for exposures at Idaho Canyon, Big Mountain (figs. 1, 5). At the type locality, in the center of sec. 1, T. 43 N., R. 26 E., the formation directly overlies the tuff of Craine Creek, forming the upper part of the north-trending ridge east of Idaho Canyon and directly south of the mouth of the canyon. North of the type locality, the Idaho Canyon Tuff forms a prominent dark-colored cliff low on the eastern flank of Big Mountain. From a maximum thickness of about 400 feet at the type locality, the formation thins east, south, and southeastward and pinches out in the Pine Forest Range and the northern part of the Black Rock Range. Thick and extensive exposures of the formation north and northeast of Gooch Table (for example, at lat 41°54′00″ N.; long 119°17′20″ W.) in northwestern Humboldt County, and northeastern Washoe County, Nev. (fig. 1), thin northward into Oregon, where the Idaho Canyon Tuff is stratigraphically above the Steens Basalt (Walker and Repenning, 1965).

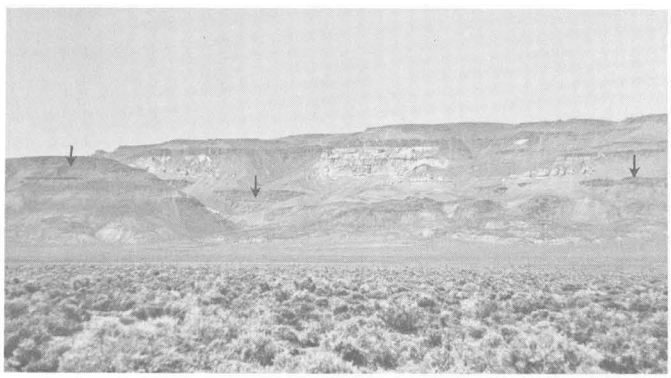

FIGURE 5.—Exposures of Idaho Canyon Tuff (arrows) near the mouth of Idaho Canyon. Ash-flow tuffs of the tuff of Big Mountain are on the skyline. View west.

In most localities the Idaho Canyon Tuff is densely welded and granophyrically crystallized throughout nearly all of its vertical extent. The rock is grayish green, gray, or tan, weathering to a very dark brown. Highly flattened lenticular gas cavities, localized by pumice fragments (Noble, 1968b), are present in the central part of the unit; and in many places one or more zones of spherical to somewhat flattened lithophysal cavities are found near the top of the formation. Phenocrysts of soda-rich sanidine, quartz, and rare micrographically

intergrown quartz and sanidine constitute several percent of the tuff in most places, and near the top of the unit they are commonly as much as 5 to 15 percent. Lithic fragments are rare. In composition the tuff is comendite, the peralkaline character of the rock being shown by the presence of vapor-phase arfvedsonite in the gas cavities and fine-grained sodic amphibole and pyroxene in the groundmass. The Idaho Canyon Tuff is remarkably similar in physical appearance to the Grouse Canyon Member of the Belted Range Tuff in southern Nevada (Sargent and others, 1965; Noble, Sargent, and others, 1968; Noble, 1970).

The Idaho Canyon Tuff thickens from the southeast and northwest toward Virgin Valley (fig. 1), which is in the approximate center of the distribution of the formation. Although these thickness relations suggest that the source is in the general vicinity of Virgin Valley, no exposures of the Idaho Canyon Tuff have yet been recognized in the area. The Idaho Canyon presumably is present at depth beneath the upper Miocene vertebrate-bearing strata (Merriam, 1910) exposed in the Virgin Valley area.

No K–Ar dates were obtained on the Idaho Canyon Tuff. However, the stratigraphic relations indicate that it is younger than the tuff of Craine Creek and older than the Summit Lake Tuff (fig. 4). Thus the age of the Idaho Canyon is considered to be late Miocene (about 15.5 m.y.).

Summit Lake Tuff

The Summit Lake Tuff is here named for exposures in the vicinity of Summit Lake, Rock Spring Table quadrangle. The type locality is in the SW¼NW¼ sec. 35, T. 43 N., R. 26 E., Idaho Canyon quadrangle, in the northwestern part of the Black Rock Range, where the formation directly overlies the Idaho Canyon Tuff. An easily reached section in the southeastern part of the Calico Mountains is at lat 41°10′00″ N., long 119°09′15″ W. The formation has been traced from the west-central part of the Pine Forest Range to the southernmost part of the Black Rock Range and to lat 41°08′ in the southern part of the Calico Mountains. Extensive exposures of the Summit Lake Tuff are present in the general vicinity of Massacre Lake in northernmost Washoe County, Nev., and the formation also has been recognized at several locations farther to the south in Washoe County. The original areal extent of the Summit Lake Tuff exceeds 3,000 square miles. Only in a few places, however, does the formation exceed 100 feet in thickness, and its original volume probably was no greater than 50 cubic miles. Based on the presently known distribution pattern, the source of the Summit Lake Tuff would appear to be located in westernmost Humbolt County at a latitude of about 41°25′ N.

The Summit Lake Tuff typically forms a single well-defined, though somewhat rounded, cliff of densely welded very dark brown to dark-reddish-brown-weathering tuff. Discontinuous horizontal jointing is conspicuous in most exposures, and lenticular gas cavities are well developed in many outcrops. Densely welded devitrified tuff tends to disintegrate into equant blocks averaging 3 to 10 mm in diameter. A relatively thin basal vitrophyre is present locally.

Rocks of the formation contain about 20 to 25 percent total phenocrysts, mainly anorthoclase with distinctive polysynthetic twinning (fig. 6, table 1). Biotite, strongly oxidized in devitrified rocks, clinopyroxene, and amphibole compose 1 to 2 percent of the rock, and generally light-colored lithic fragments of intermediate volcanic rock compose from 2 to about 10 percent of the rock.

K–Ar determinations on anorthoclase give an approximate age of 15.5 m.y., which suggests a late Miocene age for the unit.

Tuff of Indian Spring

A cooling unit of light-gray- to tan-weathering, phenocryst-poor ash-flow tuff, ranging in thickness from 10 to approximately 100 feet, locally overlies the Summit Lake Tuff in the northern Black Rock Range, south of Big Mountain, in the western Pine Forest Range, and along the east flank of the Black Rock Range. In most places the unit has an unusually thick, partly welded basal glassy zone. Phenocrysts consist mainly of soda-rich alkali feldspar. Presently available data do not indicate whether these exposures belong to one or to more than one ash-flow sheet.

Tuff of Big Mountain

A partly welded, subalkaline ash-flow tuff, 300 feet thick, caps the eastern edge of Big Mountain near the mouth of Idaho Canyon (fig. 5). The unit, designated the tuff of Big Mountain, thins markedly to the north, south, and west, and probably originally covered an area of less than 100 square miles. The tuff is tan to gray, contains 10 to 15 percent phenocrysts of sanidine and quartz, and exhibits well-developed vapor-phase crystallization, particularly of the pumice fragments. North of Big Mountain, the unit overlies the Summit Lake Tuff and a

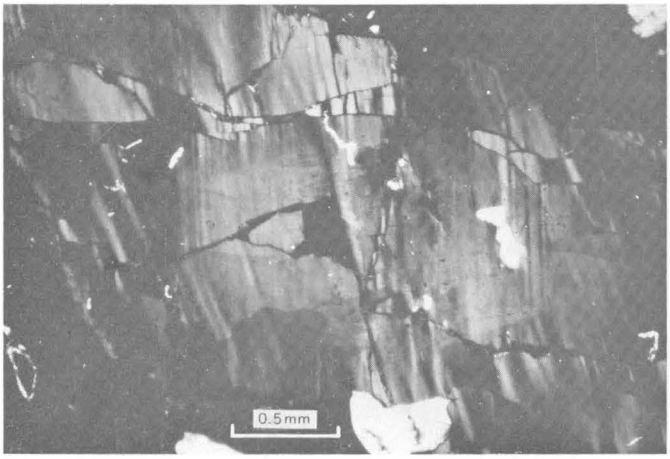

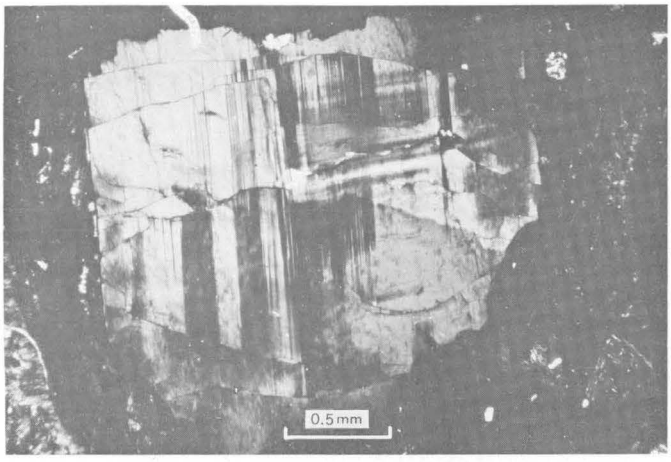

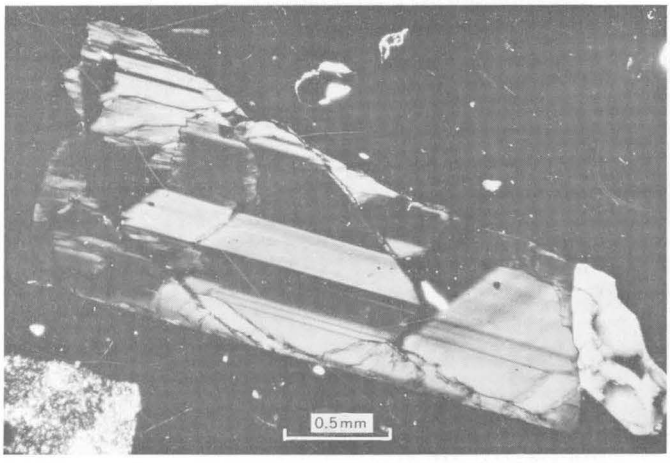

FIGURE 6.—Photomicrographs (crossed polarizers) of anorthoclase phenocrysts from the Summit Lake Tuff, showing characteristic coarse twinning.

cooling unit here assigned to the tuff of Indian Spring, and in turn is overlain by the Soldier Meadow Tuff.

Tuff of Trough Mountain

A thick sequence, locally exceeding 1,000 feet, of air-fall tuff, nonwelded ash-flow tuff, and numerous cooling units of partly to densely welded tan, gray, or greenish- or bluish-gray ash-flow tuff overlies the Summit Lake Tuff in the vicinity of Trough Mountain (fig. 1). Most of the tuffs are aphyric or phenocryst-poor, but a few units contain as much as 10 percent sanidine phenocrysts. In most places the welded tuffs are granophyrically crystallized. Sodic amphibole is present in most of the primarily crystallized rocks, showing that the tuff of Trough Mountain is of peralkaline chemical character. The tuff of Trough Mountain overlies and is intruded by aphyric to phenocryst-poor peralkaline lavas which may prove to be genetically related to the tuffs.

The unit thins in all directions from Trough Mountain; original areal extent probably did not exceed 400 square miles. Welded airfall tuffs are present within the tuff of Trough Mountain between the western flank of Trough Mountain and the Soldier Meadow Ranch (fig. 1), suggesting that the unit was erupted from a north-south-trending series of small vents.

Soldier Meadow Tuff

The Soldier Meadow Tuff is here named for exposures west of Soldier Meadow (fig. 1). The type section is located in the northern part of the Calico Mountains, 5 miles west-southwest of the Soldier Meadow Ranch, at lat 41°22′30″ N., long 119°15′40″ W. (fig. 7). A good reference section for the formation in the northern part of its areal

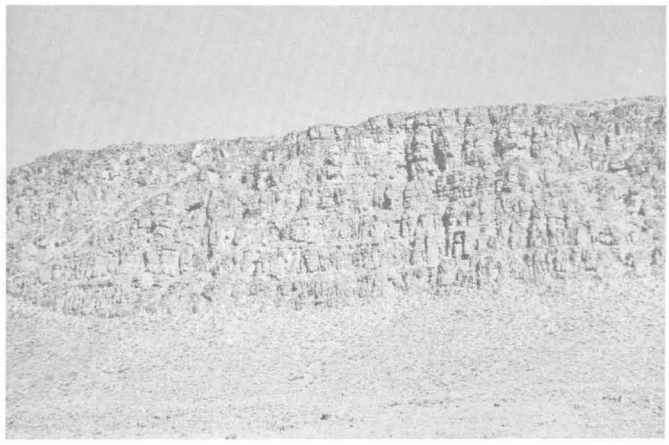

FIGURE 7.—Type section of Soldier Meadow Tuff, 390 feet thick, exposed west of Soldier Meadow.

extent is located at lat 41°34′30″ N., long 119°11′30″ W. The ash-flow sheet has been traced from the Calico Mountains at lat 41°12′ N. for nearly 40 miles to points directly south of Big Mountain and west and northeast of Badger Mountain (fig. 1). Erosional remnants of the Soldier Meadow Tuff cap the central part of the Black Rock Range. Very large lithic fragments of Soldier Meadow Tuff in local air-fall tuffs, thickness variations in the unit, and the location of the vent area (see below) suggest that the formation is also present at depth over perhaps 500 square miles in northeastern Washoe County.

The Soldier Meadow Tuff typically shows very regular and well-developed vertical columnar jointing and conspicuous, laterally persistent horizontal jointing. In the type locality and in other localities, the multiple ash-flow character of the sheet is clearly shown by numerous partial cooling breaks and partings and by minor lithologic differences between successive depositional units.

Rocks of the Soldier Meadow Tuff are bluish gray, tan, and, in a few localities, grayish green, very light gray, or medium orange brown; in most localities they weather to a very deep brown. Phenocrysts of smoky quartz and soda-rich sanidine make up 20 to 25 percent of the rock, arfvedsonite and iron-rich clinopyroxene less than 1 percent each. Most rocks are granophyrically crystallized. Well-developed vapor-phase arfvedsonite and groundmass sodic amphibole and clinopyroxene clearly demonstrate the peralkaline character of the unit, and preliminary chemical data (Noble, Chipman, and Giles, 1968; M. K. Korringa, unpub. data) show that the rock is comendite rather than pantellerite. Cognate lithic fragments composed of earlier formed, welded Soldier Meadow Tuff are present in certain ash flows and locally constitute as much as 50 percent of the flow.

Detailed field study shows that the Soldier Meadow Tuff was erupted from a north-south-trending series of vents centered 5 miles north of the Soldier Meadow Ranch (Korringa and Noble, 1970). The vents are defined by fluidal-flow patterns in very fluid comendite lavas that were erupted immediately after the Soldier Meadow Tuff and by the local presence of abundant welded air-fall tuff in the upper part of the Soldier Meadow Tuff. The lavas are identical with the Soldier Meadow Tuff petrographically, chemically, and in general megascopic appearance and in most places cooled and crystallized in continuum with the underlying tuff as shown by the absence of a complete cooling break. No discernible subsidence followed eruption.

Two K-Ar age determinations, one on sanidine and one on nonhydrated glass from the Soldier Meadow Tuff, gave an approximate age of 15 m.y., which suggests that the unit is late Miocene.

Younger tuffs and lavas

In northeastern Washoe County and westernmost Humboldt County, the Soldier Meadow Tuff is overlain by a distinctive unit of nonwelded, phenocryst-poor, glassy air-fall tuff and by reworked tuff. These tuffs are intruded and overlain by dikes, domes, and flows of comendite lava (Noble, Chipman, and Giles, 1968; Bonham, 1969). Most of these lavas are aphyric, but some contain as much as 10 percent sanidine phenocrysts. Biotite-bearing silicic lavas, presumably subalkaline, locally are abundant north of Gooch Table, Virgin Valley, and Big Mountain (fig. 1). The silicic lavas in turn are overlain by intermediate and mafic lavas that appear to become progressively more abundant westward towards the Nevada-California border. The youngest igneous rock recognized in northwestern Nevada is the Mesa Basalt of Merriam (1910), which has a K–Ar age of 1.2 m.y. (Walker and Swanson, 1969).

PRELIMINARY PETROCHEMISTRY

The silicic tuffs and lavas in northwestern Nevada include both subalkaline and peralkaline types (Noble, Chipman and Giles, 1968; Noble, McKee and Creasy, 1969). The subalkaline rocks include the Ashdown and Summit Lake Tuffs, the tuff of Big Mountain, rhyolite lavas which overlie the Ashdown Tuff througout the Black Rock Range, and late Miocene rhyolites in northwestern Humboldt County. The peralkaline rocks all contain less than 4 weight percent iron as FeO and thus should be termed comendites (Noble, 1968c). The close association in space and time of peralkaline and subalkaline silicic volcanic rocks is similar to that observed in late Miocene and Pliocene volcanic terranes in southern Nevada (Noble and others, 1965; Noble, 1968a). The peralkaline and many of the subalkaline rocks are very highly differentiated. This is shown most obviously by the persistent absence of plagioclase phenocrysts and is corroborated by the very low Sr content of sanidine phenocrysts (table 1) and of whole rocks and groundmass material (Noble, Haffty, and Hedge, 1969; M. K. Korringa and D.C. Noble, unpub. data).

Intermediate rocks include aphyric and phenocryst-poor high-potash andesite that is petrographically and chemically similar to rocks from south-

eastern Oregon and northwestern Nevada described by Fuller (1931) and LeMasurier (1968) and, in the southern part of the Calico Mountains, phenocryst-rich calc-alkalic rocks which appear to be similar to rocks described from other parts of the Great Basin (see, for example, Thompson and White, 1964; Anderson and Ekren, 1968). The mafic rocks are mainly diktytaxitic lavas, some containing large blade-shaped plagioclase phenocrysts, presumably chemically similiar to the high-alumina and somewhat low-magnesia basalts found in southeastern Oregon (Fuller, 1931; Walker, 1970).

The eruption of silicic volcanic rocks with and immediately after voluminous mafic lavas, which themselves appear to have undergone appreciable differentiation (Gunn and Watkins, 1970), is of considerable petrogenetic interest, suggesting as it does that the silicic melts may have been produced by extreme fractional crystallization of mafic magma. Also notable is the intimate association in space and time of these rocks (which comprise a bimodal basalt-rhyolite association similiar in many ways to those, for example, of Yellowstone National Park, Wyoming, and Iceland) with high-potash andesites and quartz latites of the calc-alkalic suite which do not appear to be differentiation products of the basaltic magma.

K-Ar AGE DETERMINATIONS

Ages were determined on six sanidine separates and three specimens of nonhydrated glass using standard isotope dilution procedures on a Nier-type, 6-inch-radius, 60°-sector mass spectrometer (table 2). A K-Ar age of 15.6 m.y. has been determined by Evernden, Savage, Curtis, and James (1964, p. 189 Bonham, 1969, p. 18) on sanidine from a pumicite from near Massacre Lake in northern Washoe County. This sample was probably from the Summit Lake Tuff, which is the only conspicuous ash-flow unit exposed in the area.

The isotope data show that most of the Tertiary volcanic rocks in northwestern Nevada were erupted during the late Miocene, about 15 or 16 m.y. ago. Following this intense pulse of igneous activity, there was a hiatus of several million years before the reinception of mafic volcanism in the Pliocene. The Ashdown Tuff represents an earlier volcanic episode, perhaps the same episode that produced the voluminous subalkaline silicic lavas in the Black Rock Range. Basalt very similar to the Steens Basalt was erupted at a number of places in northwestern Nevada during a restricted interval of time. In the southern Pueblo Mountains, along the west flank and southeastern portion of the Pine Forest Range, in the Idaho Canyon area, in the southern Calico Mountains, and in various places in the Black Rock Range, basaltic volcanism postdates the deposition of the Ashdown Tuff. In most of these areas, the basalts are overlain by the tuff of Craine Creek, the tuff of The Mesa, or the Idaho Canyon Tuff. In the southern part of the area, however, where the tuff of Craine Creek and the Idaho Canyon Tuff are not present, the basalts are overlain by the Summit Lake Tuff. No K-Ar determinations have been made on the mafic or intermediate lavas. However, comparison with the Steens Basalt, for which numerous age determinations of approximately 15 m.y. have been obtained (Evernden and others, 1964; Baski and others, 1967), suggests that most of the mafic lavas in northwestern Nevada belong to the late Miocene period of volcanic activity. The absence of K-Ar ages in the 16–24-m.y. interval reflects the marked decrease in volcanic activity in the Great Basin during the middle Mio-

TABLE 2.—*Potassium-argon age determinations on rocks from northwestern Nevada*

Unit	Field No.[1]	Latitude (N.)	Longitude (W.)	K_2O (weight percent)[2]	Radiogenic Ar^{40} (moles/g)	Radiogenic Ar (percent)	Age (m.y.)
Young comendite lava	NN–21B–NG	41°18′20″	119°35′00″	4.52	1.016×10^{-10}	79.95	15.1±0.5
	N–13A–NG	41°21′40″	119°21′55″	4.55	1.038×10^{-10}	66.28	15.3± .5
Soldier Meadow Tuff	NR–11–S	41°21′25″	119°04′40″	7.54	1.651×10^{-10}	12.51	14.7± .5
Soldier Meadow Tuff[3]	M–90–NG	41°27′00″	119°09′15″	4.60	1.061×10^{-10}	16.	15.6±1.7
Summit Lake Tuff	N–25–S	41°34′10″	119°01′15″	5.64	1.264×10^{-10}	72.25	15.1± .5
Tuff of Craine Creek	N–42–S	41°35′15″	118°55′00″	6.88	1.598×10^{-10}	52.68	15.7± .5
Ashdown Tuff	N9–150–S	41°35′40″	118°51′10″	5.84	[4]2.198×10^{-10}	60.25	25.3± .9
					[4]2.054×10^{-10}	54.31	23.7± .7
	N–SL–C3–S	41°30′00″	119°01′00″	5.96	2.117×10^{-10}	51.48	23.9± .7

K^{40} decay constants: $\lambda\varepsilon = 0.585 \times 10^{-10}$ yr^{-1}
$\lambda\beta = 4.72 \times 10^{-10}$ yr^{-1}
Abundance ratio: $K^{40}/K = 1.19 \times 10^{-4}$ atom per atom

[1] NG, nonhydrated glass; S, sanidine.
[2] Determined by flame photometer methods with lithium internal standard, L. B. Schlocker, analyst.
[3] From Marvin and others (1970).
[4] Two-argon analysis from the same sanidine separate.

cene (McKee and others, 1970) before resumption of volcanism toward the margin of the Great Basin (Armstrong and others, 1969).

RELATIONSHIP OF BASIN-RANGE FAULTING AND VOLCANISM

The Tertiary structure in northwestern Nevada is dominated by closely spaced north-, northwest-, and northeast-trending high-angle faults. The faults define a complex pattern of intimately related horst-and-graben structure, major tilted fault blocks, and relatively undeformed plates characterized by the presence of two systems of high-angle faults intersecting at a high angle (compare Donath, 1962). Faulting is particularly intense in the vicinity of through-going grabens that appear to be the principal loci of late Cenozoic deformation (compare Stewart, 1969).

A major fault bounds the west side of the Black Rock Range, where the Soldier Meadow Tuff has been offset more than 3,000 feet; more than 3,000 feet of displacement has been recognized by Willden (1964) in the Pine Forest Range.

Faulting has continued from the late Miocene through the Quaternary. The oldest faulting so far recognized was contemporaneous with the deposition of the late Miocene ash-flow sheets. This is well shown in the southwestern Pine Forest Range by angular discordance and progressive offlap relations between the Ashdown Tuff, the tuff of Craine Creek, the Idaho Canyon Tuff, and the Summit Lake Tuff. Comparable relations in lava flows have been observed by G. W. Walker (oral commun., 1969) at Steens Mountain and adjacent areas in southeastern Oregon. Major late Quaternary faulting is demonstrated by numerous vertical offsets of as much as several hundred feet in the Mesa Basalt of Merriam (1910) between Idaho Canyon and Summit Lake (fig. 1); Willden (1964) reports faults that offset alluvium along the west side of the Jackson Mountains (fig. 1). The long duration of high-angle faulting is similar to that observed in south-central Nevada, where faulting continued through much of the Miocene and Pliocene (for example, Ekren and others, 1968). Such evidence as (1) the remarkable lack of erosion of most of the fault blocks, (2) the presence of major nondissected landslides along the western side of the Black Rock Range, the eastern Flank of Big Mountain, the southern part of the Pine Forest Range, and elsewhere, and (3) the ubiquitous tectonic control of drainage (see, for example, Willden, 1964, p. 77–78) shows that much of the major high-angle faulting in the area was very recent.

REFERENCES

Anderson, R. E., and Ekren, E. B., 1968, Widespread Miocene igneous rocks of intermediate composition, southern Nye County, Nevada, *in* Eckel, E. B., ed., Nevada Test Site: Geol. Soc. America Mem. 110, p. 57–63.

Armstrong, R. L., Ekren, E. B., McKee, E. H., and Noble, D. C., 1968, Space-time relations of Cenozoic silicic volcanism in the Great Basin of the western United States: Am. Jour. Sci., v. 267, p. 478–490.

Baksi, A. K., York, D., and Watkins, N. D., 1967, Age of the Steens Mountain geomagnetic polarity transition: Jour. Geophys. Research, v. 72, p. 6299–6308.

Baldwin, E. M., 1964, Geology of Oregon: Eugene, Oreg., Univ. Oregon Coop. Book Store, 165 p.

Bonham, H. F., 1969, Geology and mineral deposits of Washoe and Storey, Counties, Nevada, with a section on industrial minerals by K. G. Papke: Nevada Bur. Mines Bull. 70, 140 p.

Christiansen, R. L., Noble, D. C., Orkild, P. P., and Sargent, K. A., 1968, Cogenetic sequences and source areas in silicic volcanic terranes [abs.]: Geol. Soc. America Spec. Paper 101, p. 435–436.

Donath, F. A., 1962, Analysis of Basin-Range structure, south-central Oregon: Geol. Soc. America Bull., v. 73, p. 1–16.

Ekren, E. B., Rogers, C. L., Anderson, R. E., and Orkild, P. P., 1968, Age of Basin and Range normal faults in Nevada Test Site and Nellis Air Force Range, Nevada, *in* Eckel, E. B., ed., Nevada Test Site: Geol. Soc. America Mem. 110, p. 247–250.

Evernden, J. F., Savage, D. E., Curtis, G. H., and James, G. T., 1964, Potassium-argon dates and the Cenozoic mammalian chronology of North America: Am. Jour. Sci., v. 262, p. 145–198.

Fuller, R. E., 1931, The geomorphology and volcanic sequence of Steens Mountain in southeastern Oregon: Washington Univ. Pubs. Geology, v. 3, no. 1.

Gunn, B. M., and Watkins, N. D., 1970, Geochemistry of the Steens Mountain basalts, Oregon: Geol. Soc. America Bull., v. 81, p. 1497–1516.

Korringa, M. K., and Noble, D. C., 1970, Ash-flow eruption from a linear vent area without caldera collapse [abs.]: Geol. Soc. America Abstracts with programs, v. 2, p. 108–109.

LeMasurier, W. E., 1968, Crystallization behavior of basalt magma, Santa Rosa Range, Nevada: Geol. Soc. America Bull., v. 79, p. 949–972.

Marvin, R. F., Mehnert, H. H., and Noble, D. C., 1970, Use of Ar^{36} to evaluate the incorporation of air by ash flows: Geol. Soc. America Bull., v. 81. [In press]

McKee, E. H., Noble, D. C., and Silberman, M. L., 1970, Middle Miocene hiatus in volcanic activity in the Great Basin of the western United States: Earth and Planetary Sci. Letters, v. 8, p. 93–96.

Merriam, J. C., 1910, Tertiary mammal beds of Virgin Valley and Thousand Creek in northwestern Nevada—Pt. 1, Geologic history: California Univ. Pubs. Geol. Sci., Dept. Geology Bull., v. 6, no. 2, p. 21–53.

Noble, D. C., 1968a, Kane Springs Wash volcanic center,

Lincoln County, Nevada, *in* Eckel, E. B., ed., Nevada Test Site: Geol. Soc. America Mem. 110, p. 109–116.

——— 1968b, Laminar viscous flowage structures in ash-flow tuff from Gran Canaria, Canary Islands—A discussion: Jour. Geology, v. 76, p. 721–723.

——— 1968c, Systematic variation of major elements in comendite and pantellerite glasses: Earth and Planetary Sci. Letters, v. 4, p. 167–172.

——— 1969, Energy of eruption, timing of subsidence, and the distribution and form of welded pyroclastic deposits [abs.]: Geol. Soc. America Abstracts with programs for 1969, pt. 3, p. 48.

——— 1970, Loss of sodium from crystallized comendite welded tuffs of the Miocene Grouse Canyon Member of the Belted Range Tuff: Geol. Soc. America Bull., v. 81, p. 2677–2687.

Noble, D. C., Bath, G. D., Christiansen, R. L., and Orkild, P. P., 1968, Zonal relations and paleomagnetism of the Spearhead and Rocket Wash Members of the Thirsty Canyon Tuff, southern Nevada, *in* Geological Survey Research, 1968: U.S. Geol. Survey Prof. Paper 600–C, p. C61–C65.

Noble, D. C., Chipman, D. W., and Giles, D. L., 1968, Peralkaline silicic volcanic rocks in northwestern Nevada: Science, v. 160, p. 1337–1338.

Noble, D. C., Haffty, Joseph, and Hedge, C. E., 1969, Strontium and magnesium contents of some natural peralkaline silicic glasses and their petrogenetic significance: Am. Jour. Sci., v. 267, p. 598–608.

Noble, D. C., Kistler, R. W., Christiansen, R. L., Lipman, P. W., and Poole, F. G., 1965, Close association in space and time of alkalic, calc-alkalic, and calcic volcanism in southern Nevada [abs.]: Geol. Soc. America Spec. Paper 82, p. 143.

Noble, D. C., McKee, E. H., and Creasey, J. W., 1969, Late Tertiary peralkaline volcanism in north-central Humboldt County, Nevada [abs.]: Geol. Soc. America Abstracts with programs for 1969, pt. 3, p. 48–49.

Noble, D. C., Sargent, K. A., Mehnert, H. H., Ekren, E. B., and Byers, F. M., Jr., 1968, Silent Canyon volcanic center, Nye County, Nevada, *in* Eckel, E. B., ed., Nevada Test Site: Geol. Soc. America Mem. 110, p. 65–75.

Sargent, K. A., Noble, D. C., and Ekren, E. B., 1965, Belted Range Tuff of Nye and Lincoln Counties, Nevada, *in* Cohee, G. W., and West, W. S., Changes in stratigraphic nomenclature by the U.S. Geological Survey 1964: U.S. Geol. Survey Bull. 1224–A, p. A32–A36.

Smith, R. L., 1960, Zones and zonal variations in welded ash flows: U.S. Geol. Survey Prof. Paper 354–F, p. 149–159.

Stewart, J. H., 1969, Systematic pattern of tensional failure producing Basin and Range structure in Nevada and Utah [abs.]: Geol. Soc. America Abstracts with programs for 1969, pt. 5, p. 78–79.

Thompson, G. A., and White, D. E., 1964, Regional geology of the Steamboat Springs area, Washoe County, Nevada: U.S. Geol. Survey Prof. Paper 458–A, p. A1–A52.

Walker, G. W., 1970, Some comparisons of basalts of southeast Oregon with those of the Columbia River Group: Columbia River Basalts Symposium, Northwest Sci. Assoc. mtg., Eastern Washington State College, Cheney, Wash. [In press]

Walker, G. W., and Repenning, C. A., 1965, Reconnaissance geologic map of the Adel quadrangle, Lake, Harney, and Malheur Countries, Oregon: U.S. Geol. Survey Misc. Geol. Inv. Map I–446, scale 1:250,000.

Walker, G. W., and Swanson, D. A., 1969, Discussion of paper by H. E. Wheeler and H. A. Coombs, "Late Cenozoic Mesa Basalt sheet in northwestern United States": Bull. Volcanologique, v. 1, p. 581–582.

Willden, Ronald, 1964, Geology and mineral deposits of Humboldt County, Nevada: Nevada Bur. Mines Bull. 59, 154 p.

Williams, Howel, and Compton, R. R., 1953, Quicksilver deposits of Steens Mountain and Pueblo Mountains, southeast Oregon: U.S. Geol. Survey Bull. 995–B, p. 19–77.

OUTLIER OF CASEYVILLE SANDSTONE NEAR PRINCETON, KENTUCKY, MAY BE BETHEL SANDSTONE

By J. J. CONNOR and R. D. TRACE,
Denver, Colo., Princeton, Ky.

Abstract.—Geochemical studies indicate that an isolated outcrop mapped as Caseyville Sandstone (Lower Pennsylvanian) near Princeton, Ky., is more closely allied in its composition to sandstones of Mississippian age. Recent regional geologic studies suggest that it may in fact be part of the Bethel Sandstone of Late Mississippian age.

Recent studies have shed light on the stratigraphic relation of an isolated outcrop of sandstone northwest of Princeton, Ky. (fig. 1). The sandstone crops out in a narrow northeast-trending graben in limestones of the Renault Formation and Ste. Genevieve and St. Louis Limestones (Upper Mississippian). Most of the sandstone in this outlier has been mapped as part of the Caseyville Sandstone of Early Pennsylvanian age (Sample, 1965; see also Jillson, 1927), although its true stratigraphic position has long been uncertain. The purpose of this report is to present evidence suggesting that the sandstone is in fact an outlier of the Bethel Sandstone of Late Mississippian age.

The outcrop lies near the southeastern edge of the extensively faulted western Kentucky fluorspar district. Discontinuous outcrops of sandstone are common throughout the fluorspar district, but the outcrop near Princeton is unusual in that its stratigraphic isolation and lack of diagnostic fossils made stratigraphic assignment difficult. Assignment of the sandstone in this outcrop to the Caseyville Sandstone is justified principally because of the presence of locally contained conglomeratic and coarse-grained sandstone. Such sandstone is generally considered to be diagnostic of a Pennsylvanian age in this part of Kentucky.

Two lines of evidence, however, suggest that the sandstone in question is not part of the Caseyville Sandstone. Connor (1969, p. 30), in a study of geochemical differences between Mississippian and Pennsylvanian sandstones in Kentucky, concluded that the sandstone in this outcrop is more closely allied in its chemical composition to sandstones of Mississippian age. This study made use of a discriminant function based on relative content of Al_2O_3, MgO, H_2O+, TiO_2, and Cr, which correctly assigned (in a preliminary study) 133 out of 159 hand specimens of Mississippian and Pennsylvanian rocks collected from outcrops across the State. Applied to four hand specimens from the outcrop in the Princeton West quadrangle, this function classified three as Mississippian and one as Pennsylvanian by composition.

The second line of evidence is structural. If sandstone in the graben is in fact part of the Caseyville, the total throw on the bounding faults seems excessive. If a normal stratigraphic sequence of Chester and Meramec rocks underlies the outcrop, displacement here must exceed 1,300 feet; faults with throws of this magnitude are not unknown in this part of the State (indeed, there is just such a fault in the southeast corner of the Olney quadrangle), but they are uncommon. Moreover, the particular fault zone bounding the outcrop has been traced nearly 25 miles to the southwest (Sample, 1965; Rogers, 1963; Hays, 1964; Fox and Olive, 1966) and stratigraphic offset elsewhere does not exceed 600 feet. Thus, 1,300 feet of throw near Princeton seems unrealistic, particularly for a graben of such narrow proportions.

If one provisionally accepts the fact that the sandstone in question is not Pennsylvanian, then the sandstone most likely is Late Mississippian (Chester) because it lacks the abundant gravel content and weak cementation of the Tuscaloosa Formation (Cretaceous) which constitutes the only realistic alternative in the immediate area. Chester

U.S. GEOL. SURVEY PROF. PAPER 700-D, PAGES D33-D35

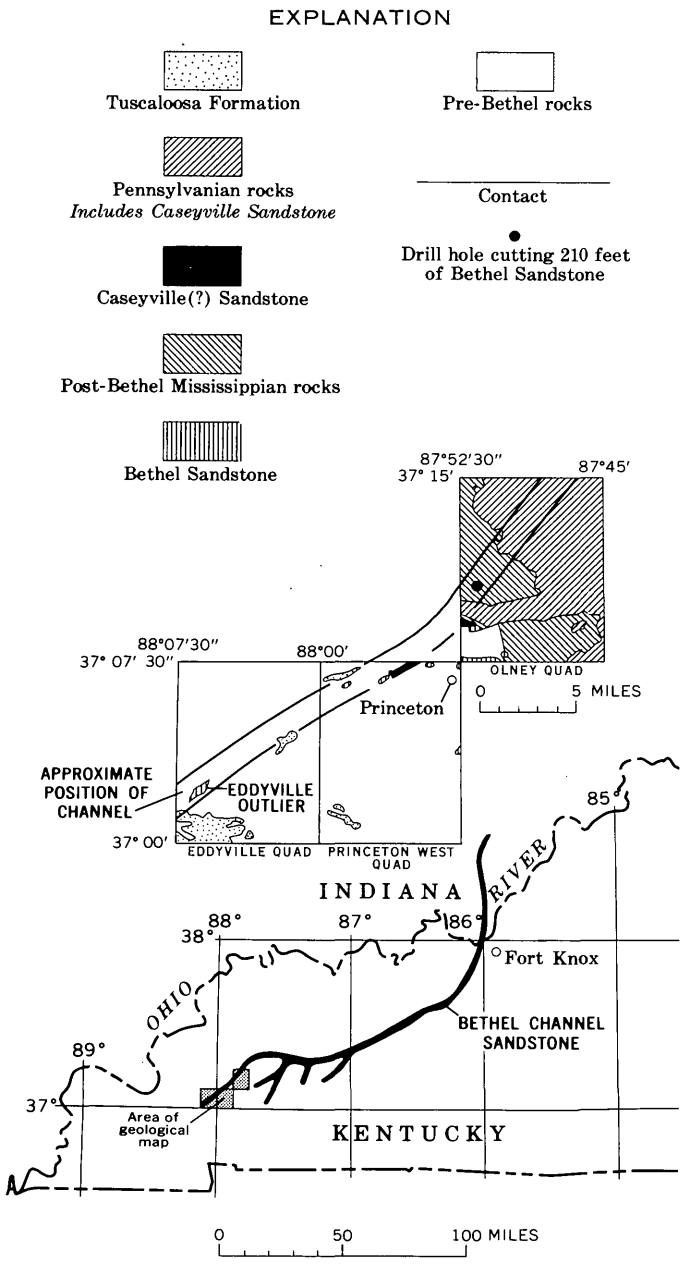

FIGURE 1.—Map showing relation of Caseyville(?) Sandstone outcrops to Bethel channel. Modified from Rogers (1963), Sample (1965), Reynolds and Vincent (1967), Trace and Kehn (1968), and Sedimentation Seminar (1969).

rocks of the fluorspar district include at least seven named sandstones (Trace, 1962), and it seems highly probable that this sandstone is one of them. Figure 1 demonstrates that the outcrop lies on a line with a sinuous channel sandstone that has been traced (partly in subsurface) for more than 200 miles to the northeast (Reynolds and Vincent, 1967). This sandstone has been identified as a channel facies of the Bethel (Mooretown) Sandstone. Near the Ohio River the sandstone ranges in thickness from 150 to 200 feet and rests in a steep-sided channel, more than a half mile wide, which has been cut into the underlying Paoli, Ste. Genevieve, and St. Louis Limestones (Sedimentation Seminar, 1969, p. 9). In the subsurface north of Princeton, the same channel is cut at least 50 feet into the Ste. Genevieve Limestone (Trace and Kehn, 1968) and is filled with as much as 210 feet of sandstone. In view of the location of the outcrop in the Princeton West quadrangle and its juxtaposition with the Ste. Genevieve and St. Louis Limestones, it is here proposed that the outcrop of mapped Caseyville Sandstone northwest of Princeton, Ky., is in fact a part of the channel facies of the Bethel Sandstone of Late Mississippian age.

The presence of coarse or conglomeratic sandstone in the outcrop in the Princeton West quadrangle is consistent with assignment to either the Caseyville or the channel facies of the Bethel Sandstone. Near Fort Knox, Ky., the lower part of the channel fill contains some quartz granules and pebbles (Sedimentation Seminar, 1969, p. 11). As an area of higher than average environmental energy, the channel might be expected to serve as a conduit and resting place for coarser than average sediments.

Finally, it may be noted that Trace and Kehn (1968) have mapped an additional ambiguous outcrop of Caseyville(?) Sandstone in the southwest corner of the Olney quadrangle. This outcrop also lies near the edge of the Bethel channel, and although the temptation to assign the outcrop to the channel facies of the Bethel Sandstone is strong, its proximity to known Caseyville and lack of corroborative evidence (such as geochemical affinity) preclude such a proposal here.

REFERENCES

Connor, J. J., 1969, A geochemical discriminant for sandstones of Mississippian and Pennsylvanian age in Kentucky: Colorado School Mines Quart., v. 64, no. 3, p. 17–34.

Fox, K. F., Jr., and Olive, W. W., 1966, Geologic map of the Birmingham Point quadrangle, western Kentucky: U.S. Geol. Survey Geol. Quad. Map GQ–471.

Hays, W. H., 1964, Geology of the Grand Rivers quadrangle, Kentucky: U.S. Geol. Survey Geol. Quad. Map GQ–328.

Jillson, W. R., 1927, Geologic map of Kentucky showing oil and gas pools and pipelines, fluorspar and rock asphalt deposits, and the eastern and western coal fields: Kentucky Geol. Survey, ser. 6.

Reynolds, D. W., and Vincent, J. K., 1967, Western Kentucky's Bethel channel—the largest continuous reservoir in the Illinois basin: Kentucky Geol. Survey, ser. 10, Spec. Pub. 14, 19 p.

Rogers, W. B., 1963, Geology of the Eddyville quadrangle, Kentucky: U.S. Geol. Survey Geol. Quad. Map GQ–255.

Sample, R. D., 1965, Geology of the Princeton West quadrangle, Kentucky: U.S. Geol. Survey Geol. Quad. Map GQ–385.

Sedimentation Seminar, 1969, Bethel Sandstone (Mississippian) of western Kentucky and south-central Indiana, a submarine-channel fill: Kentucky Geol. Survey, ser. 10, Rept. Inv. 11, 24 p.

Trace, R. D., 1962, Geology of the Salem quadrangle, Kentucky: U.S. Geol. Survey Geol. Quad. Map GQ–206.

Trace, R. D., and Kehn, T. M., 1968, Geologic map of the Olney quadrangle, Caldwell and Hopkins Counties, Kentucky: U.S. Geol. Survey Geol. Quad. Map GQ–742.

PLEISTOCENE STRATIGRAPHY OBSERVED IN A PIPELINE TRENCH IN EAST-CENTRAL CONNECTICUT AND ITS BEARING ON THE TWO-TILL PROBLEM

By MAURICE H. PEASE, JR., Boston, Mass.

Abstract.—Four lithostratigraphic units—bedrock, lower till, upper till, and glaciofluvial deposits—were exposed in a 17-mile-long pipeline trench in east-central Connecticut during 1966. Bedrock is generally overlain by till in the uplands and by glaciofluvial deposits in valleys. The lower till, most extensive in uplands between bedrock highs, is oxidized, olive brown, and compact. The upper till, which forms a thin veneer above bedrock and lower till almost everywhere in the uplands, is less oxidized, olive gray, and friable. Glaciofluvial deposits consist of crudely stratified gravel and sand having few fine-grained constituents. At many localities in New England the presence of an oxidation profile as much as 40 feet deep beneath an upper unoxidized till and the occurrence of contorted and truncated structures in the underlying till indicate that an older till probably was deposited during an early ice advance and was overridden by a later ice sheet. Such evidence for two ice advances was not apparent in the trench, but the lower and upper tills in the trench have been correlated with the older and younger tills on the basis of lithology, texture, and stratigraphic position.

A 17-mile-long, nearly continuous, shallow cross section of the Pleistocene deposits of east-central Connecticut was exposed for a few weeks during the summer of 1966 in a trench excavated for a pipeline by the Algonquin Gas Co. The writer had an opportunity to examine the geology of the trench during the brief period that it was open. During this same summer, the Connecticut State Highway Department provided a rotary drill rig to investigate the distribution of bedrock formations beneath Pleistocene deposits along the Spring Hill-Hampton quadrangle border south of the trench. Seven holes were drilled to a maximum depth of 72 feet into bedrock (fig. 1*A*), and Pleistocene material and bedrock were examined. The report that follows is a description and interpretation of the Pleistocene deposits. Thomas F. McGuire assisted in the field.

The trench was excavated for a gas transmission line from New York across Connecticut to Boston. The segment of the trench open in 1966 extended from Spring Hill on State Route 195 in the southwest part of the Spring Hill quadrangle, northeast through the Hampton and Danielson quadrangles, to the southwest corner of the Putnam quadrangle, Connecticut (fig. 1*A*). The average width of the trench was 5 feet; its average depth was 8 feet, but locally it reached depths of 15 feet.

The nearly continuous profile of Pleistocene deposits provided an unusual opportunity to examine their distribution relative to bedrock and topographic relief and to study the lateral configuration of stratigraphic contacts. The vertical dimension of this profile, however, is limited by the shallow depth of the trench. The Highway Department drill holes and water wells in the vicinity of the trench provided additional data on depth to bedrock and thickness of surficial deposits.

Low rounded hills dissected by southward-flowing streams characterize the topography of the area. Major streams are the Fenton and Mount Hope Rivers in the Spring Hill quadrangle and the Natchaug River in the Hampton quadrangle. The lowest altitude along the trench is 240 feet in the Fenton River valley; the highest is 710 feet about 1½ miles east of the Natchaug River. Local relief is generally slight; a maximum slope of about 16° is traversed on the west side of the Fenton River valley.

Exposures in the trench have been assigned to four principal lithostratigraphic units: bedrock, lower till, upper till, and glaciofluvial deposits. Bedrock was exposed in about 12 percent of the trench, including a 1¼-mile stretch of continuous outcrop in the Hampton quadrangle. Outcrops as much as ¼ mile long were exposed on a few steep slopes, but most were only 50 to 100 feet long. Rock

U.S. GEOL. SURVEY PROF. PAPER 700–D, PAGES D36–D48

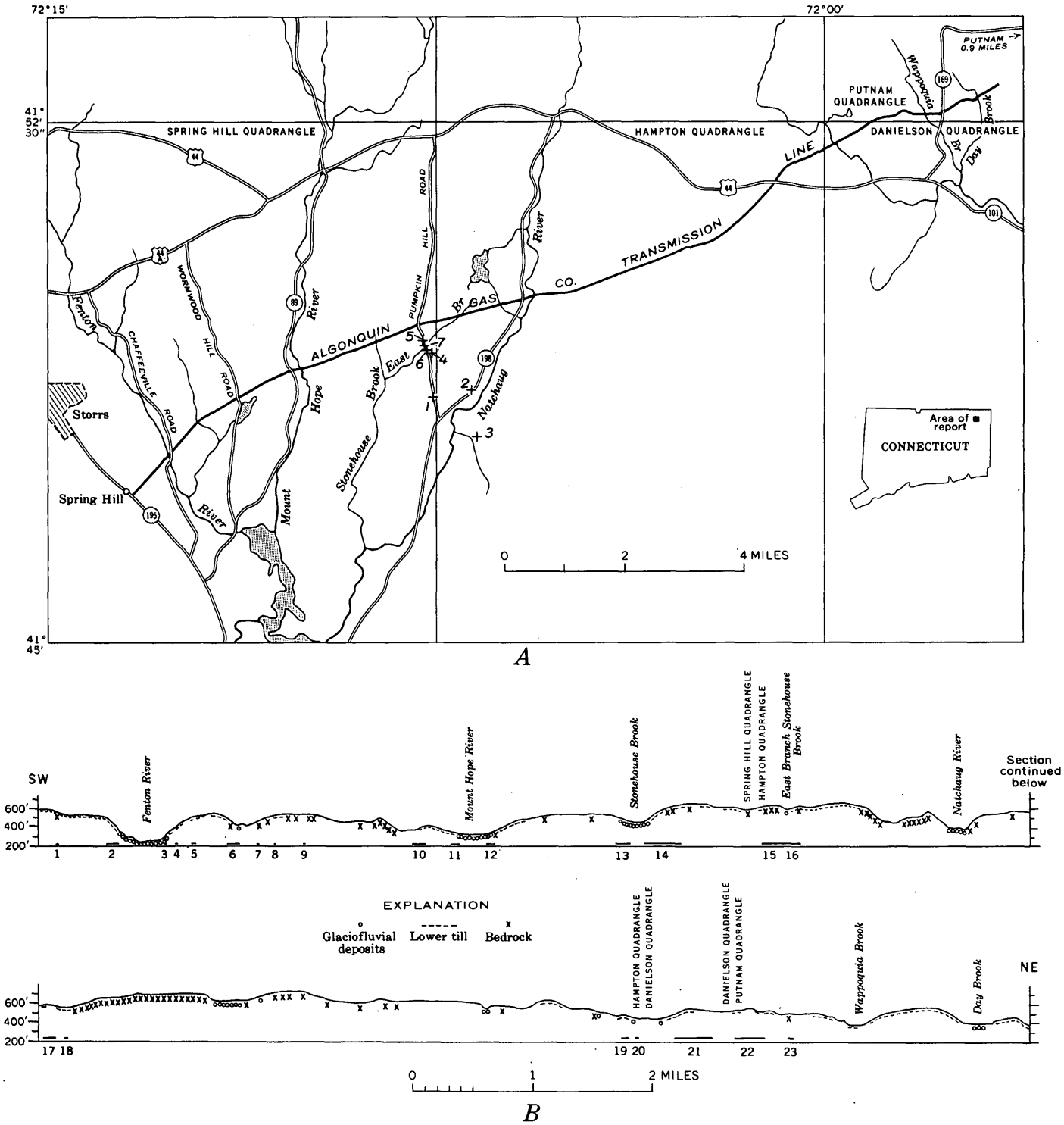

FIGURE 1.—Index map, *A*, showing location of trench. Numbered localities indicate Connecticut Highway Department drill holes. *B*, Topographic profile of trench. Numbered localities projected from surface to baseline of section (line shows approximate length of locality). Symbols indicate deepest lithostratigraphic unit (see text) exposed in trench. Distribution of upper till not shown, but it is generally present except in major stream valleys and on largest rock exposures.

rarely crops out above trench level, and no bedrock was observed in the major stream valleys. Till was exposed along 90 percent of the trench, and commonly both tills were present. Glaciofluvial deposits, present in less than 5 percent of the trench, include ice-contact deposits, preserved along the principal valley margins above present stream level, and small isolated deposits in the uplands. Recent allu-

vium and swamp deposits were poorly preserved in the trench because they were either disturbed by excavation or covered by water.

LITHOSTRATIGRAPHIC UNITS

Bedrock

Exposures west of the Mount Hope River in the Spring Hill quadrangle are interlayered medium-grained quartzofeldspathic gneiss and biotite schist and minor gneissoid pegmatite. Pegmatite is rarely exposed east of the Mount Hope River. Nonlayered felsic gneissoid quartz monzonite occurs east of the Mount Hope River and the East Branch of Stonehouse Brook. From this brook to the end of the trench in the Putnam quadrangle, the rock is mostly schist except for the 1¼-mile exposure in the center of the Hampton quadrangle which is gneissoid quartz monzonite. Two types of schist are present west of the long quartz monzonite exposure: strongly foliated biotite-muscovite (staurolite) schist and granular biotite schist containing layers rich in calc-silicate minerals. East of the gneissoid quartz monzonite, thin-layered to laminated fine-grained biotite schist containing trace amounts of muscovite predominates.

The hard, competent, and felsic quartzofeldspathic rocks are resistant to weathering and to abrasion and erosion by overriding ice. They commonly form bedrock highs. The schists readily weather to brown micaceous saprolite and silty clayey soil and were readily quarried by ice.

Lower till

The lower till is homogeneous, olive brown, massive, very poorly sorted, and stony. Anastomosing joints containing hard dark-brown platy deposits of iron and manganese are characteristic. Most are roughly parallel to the local topography and are so closely spaced as to form a crude fissility in the till. The matrix of the till is hard compact sand, silt, and clay having a pronounced olive-brown iron oxidation; subangular to subrounded pebbles, cobbles, and boulders generally amount to less than 25 percent by volume. Most are from local bedrock, but glacial erratics account for as much as 10 percent of the volume. Resistant quartzofeldspathic stones are most common; schist apparently is so readily ground up that schist slabs are present only directly above schist bedrock. No systematic vertical or horizontal variation in the color or texture of the lower till was observed, but it is locally mottled light and dark olive brown. No deposits of Pleistocene age were observed in the trench below the olive-brown lower till.

Upper till

The upper till is olive gray to light gray, massive to crudely stratified, and stony. It is characteristically sandier and more friable than the lower till. The matrix is chiefly sand mixed with silt and clay showing little or no evidence of oxidation; stones compose 25 percent or more of the till and are mostly resistant little-weathered quartzofeldspathic pebbles, cobbles, and boulders of gneiss and igneous rock. Less resistant schist fragments are rarely incorporated in the till more than 2 feet above schist bedrock. Rock types typically reflect a more varied source than that of the lower till. Lenses of pebble gravel and sand bearing almost no silt or clay are common within the upper till. Most are a few feet long and less than 6 inches thick, but several as much as 3 feet thick were observed. The upper till locally is mottled by streaks rich in olive-brown clay or yellowish-gray sand. Sand forms yellow- to orange-gray halos around a few rusty weathered stones. The maximum thickness of upper till exposed in the trench is about 8 feet, and in most exposures it is less than 4 feet. Weak oxidation is apparent in the upper part of this till in some exposures.

Glaciofluvial deposits

Glaciofluvial deposists consist of interstratified sand and gavel containing little or no clay, silt, or fine sand. Crudely stratified gravel predominates in most exposures; it is poorly sorted and contains well-rounded pebbles, cobbles, and boulders and 10 to 60 percent medium- to coarse-grained sand. Stones are a heterogeneous assortment of hard, resistant quartz-rich metamorphic and igneous rock. Distinct layers and lenses of moderately well sorted, fine- to coarse-grained sand a few inches to several feet thick are interlayered with the gravel. The sand consists chiefly of quartz and feldspar but contains minor mica and garnet; it is stained shades of yellowish orange. High-angle crossbedding and channeling are common.

DESCRIPTIVE GEOLOGY

Bedrock

Distribution of outcrops in the trench (fig. 1*B*) shows that bedrock is near the surface and overlain mostly by till in the upland areas and is deeper and overlain mostly by sand and gravel in the major stream valleys. Data supporting this were provided

by the seven holes of the Connecticut State Highway Department and by wells near the trench. Two holes were drilled on each side of the East Branch of Stonehouse Brook where it is crossed by Pumpkin Hill road, and except for about 10 feet of sand and gravel and a few inches of possible till in hole 6 nearest the stream, weathered bedrock was reached in these four holes within a few feet of the surface. Hole 1, (fig. 1*A*) however, which is on a south-facing slope on Pumpkin Hill road about 1¼ miles south of the trench, penetrated about 50 feet of till before bedrock was reached. In the Hampton quadrangle, hole 2 at the south end of a drumlin-shaped hill on the north side of State Route 198 penetrated 50 feet of till above bedrock, and hole 3 at the base of a steep west-facing slope penetrated 18 feet of till. Water test wells in the Fenton River valley, on the other hand, bottomed in bedrock at about 60 feet 2 miles north of the trench and at about 130 feet 1½ miles south of the trench, both wells having penetrated sand and gravel but no till.

The shape of rock exposures is controlled by the orientation of joint surfaces and foliation and bedding planes. No rounded waterworn surfaces were observed, but circulation of considerable water at the bedrock-till interface was evident from the local presence of a thin layer of yellowish-gray well-sorted sand and gravel. This water-washed material is 2 to 4 inches thick and follows irregularities in the bedrock surface, thickening in the pockets (loc. 7, fig. 1*B* and fig. 2). At locality 9 (fig. 1*B*), a 2 foot-thick deposit of sand grading upward into pebble gravel rests against a vertical bedrock face and grades upward into upper till.

Most bedrock exposed in the trench is overlain by sandy olive-gray upper till and shows little evidence of weathering except for rust stains along joints and oxidation of micaceous foliation surfaces. At a few localities, however, lower till rests on bedrock,

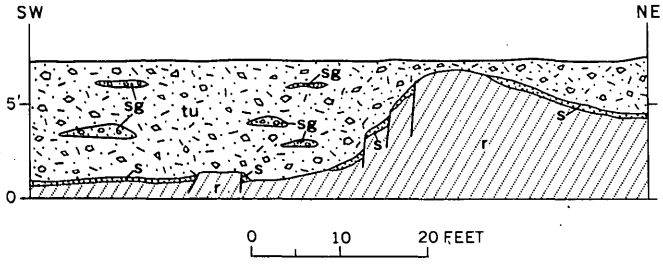

FIGURE 2.—Section of northwest wall of trench at locality 7 (fig. 1*B*). Upper till overlies layered biotite gneiss. Well-sorted sand 2 to 4 inches thick at interface is joint controlled. Lenses of sand and gravel common in till. Lithology: s, sand; sg, sand and gravel; tu, upper till; r, bedrock. Vertical exaggeration × 2.

and in some exposures till was observed to rest on weathered bedrock or saprolite. Representative examples of bedrock exposures in the trench are described below in order from southwest to northeast.

Olive-brown friable sandy saprolite rests on dark-gray layered quartzofeldspathic biotite gneiss at the western end of the trench (loc., fig. 1*B*). Relic foliation in the saprolite, parallel to bedrock foliation, is shown by dark and light banding and by preferred orientation of abundant bleached golden-brown biotite. The transition from fresh gneiss to saprolite takes place across a single parting parallel to foliation. Evidently the saprolite represents a less weather resistant, more biotite rich schist resting on the gneiss. The saprolite grades upward into olive-brown lower till containing 1- to 3-inch slabs of schist 6–18 inches long.

At locality 12, partly weathered, gneissoid quartz monzonite is overlain by olive-brown lower till having irregular platy jointing. It is sandier than typical lower till because of sandy detritus from the quartz monzonite, but it appears to be lower till in place, not upper till or flowtill.

Saprolite of the gneissoid quartz monzonite is exposed for almost 100 feet in the trench on the west bank of the East Branch of Stonehouse Brook at locality 15 (fig. 3). The saprolite is a light-gray to yellowish-gray, friable, and coarse-grained biotitic quartzofeldspathic sand; it grades into hard but still weathered bedrock through a thickness of several feet. Foliation in the saprolite is accentuated by staining along foliation planes. The overlying upper till is light gray, sandy, and friable, and is composed entirely of quart monzonite detritus. It is difficult to distinguish the till from saprolite except that the till is generally fresher; perhaps the till was derived from a fresher bedrock nearby.

On the east bank of the East Branch of Stonehouse Brook, at locality 16 (fig. 3) lower till rests on bedrock. Here olive-brown compact till overlies leucocratic quartz monzonite but contains few quartz monzonite fragments, although the overlapping upper till is composed mostly of quartz monzonite.

Bedrock exposed in the trench in the Putnam quadrangle is weathered but not to saprolite. At locality 23, fine-grained friable biotite schist grades upward from medium gray to brownish gray, and the overlying till is a rubble of brown schist fragments in silty sand.

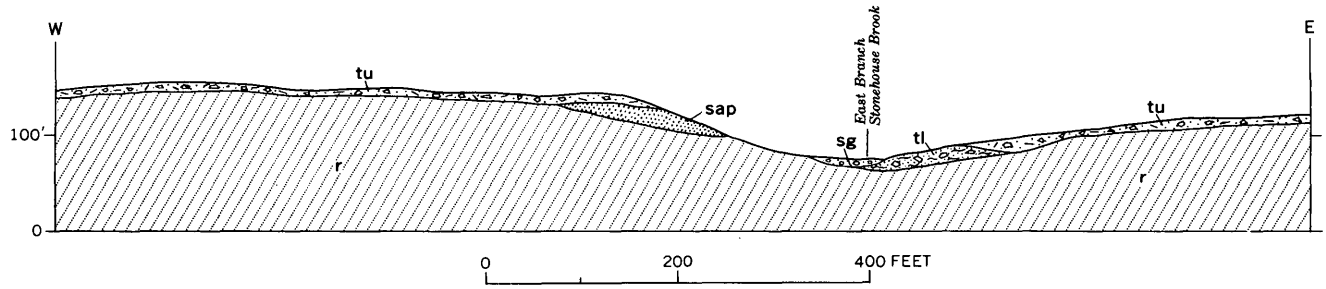

FIGURE 3.—Section of north wall of trench across the East Branch of Stonehouse Brook at localities 15 and 16. Thickness of surficial deposits exaggerated. At locality 15, upper till composed of nonweathered quartz monzonite debris rests on quartz monzonite saprolite. On east side of valley at locality 16, oxidized olive-brown lower till rests on leucocratic quartz monzonite and is overlapped by upper till composed mostly of nonweathered quartz monzonite debris. Lithology: sg, sand and gravel; tu, upper till; tl, lower till; sap, saprolite; and r, bedrock.

The two tills

Exposures of the lower till in the trench are most extensive on steep valley walls, but scattered exposures on hillcrests and gentle slopes suggest that the lower till is present in the upland areas at or just below the bottom of the trench throughout much of its length. The thickness of the lower till generally could not be determined because the trench bottoms in lower till. At locality 12, however, where the trench is 15 feet deep and bedrock is exposed in the bottom, the lower till is about 8 feet thick and grades upward into sandy upper till.

The lower till generally is overlain by upper till or glaciofluvial deposits. Only rarely is lower till exposed at the surface. The upper till is 8 to 10 feet thick were it extends the full depth of the trench, but in most exposures it is restricted to the upper 2 to 5 feet and is underlain by lower till or bedrock. Till-bedrock contacts have been described above. The contact between upper and lower till is exposed in the trench throughout much of the upland area.

Most of the till collected from the holes drilled by the Connecticut State Highway Department (fig. 1*A*) has the texture and compactness of the lower till exposed in the trench. In hole 1, till collected from a depth of 46 feet is olive brown, compact, and indistinguishable from the lower till in the trench. At 56 feet, friable saprolitic quartz monzonite shows little evidence of oxidation discoloration, and black biotite appears unweathered. Apparently oxidized till rests on weathered but only slightly oxidized quartz monzonite gneiss. In hole 2, drilled at the down-ice end of a northeast-trending streamline hill, four samples of till were recovered at 10-foot intervals to a depth of 40 feet. These show a gradational color change with depth from olive brown to olive gray that strongly suggests a weathering profile. The olive-brown oxidized till near the top could not be distinguished from samples of lower till exposed in the trench.

The only till that might be correlated with upper till was yellowish-gray sandy friable till recovered from hole 3. No lower till lithology was identified from this hole. Evidently the upper till was generally either absent or too friable to recover by coring. As stated above, virtually no till was recovered from holes drilled in the upland at the East Branch of Stonehouse Brook.

The contact between upper and lower till in the trench is generally irregular and poorly defined by an indistinct zone of lateral and vertical gradation. This mixed zone commonly is 2 or 3 feet thick. In many exposures, however, the contact is in part sharp and clearly defined by an abrupt subhorizontal change in color and texture from olive brown to olive gray and from compact to friable. Lenses and layers, or streaks, of olive-brown compact till similar to lower till are found in the upper till, and lenses of olive-gray to yellowish-gray friable sand and silt characteristic of the upper till occur in the lower till. This interlayering is most common in the mixed zone or within 2 feet of an abrupt contact.

At locality 2 (fig. 1*B*) the contact is poorly exposed on the steep northeast-facing slope of Spring Hill, from the crest of the hill almost to the glaciofluvial deposits in the Fenton River. In general, olive-gray friable sandy till overlies olive-brown compact clayey till, but the contact is extremely irregular, and diffuse. Near its base the upper till is mottled olive gray to olive brown. The brown material appears more clayey. Also near the contact in the upper till are lenses of brown clayey material. The upper till grades downward into typical olive-brown compact lower till with conspicuous iron and manganese-stained platy jointing parallel to the slope of the hill.

An abrupt change from olive-brown compact till to olive-gray friable till defines the contact between lower and upper till at locality 4 (fig. 4) on the east side of the Fenton River valley. This sharp contact follows the contour of the hill in the trench for several tens of feet, but the contact then becomes obscure and gradational over a vertical distance of about a foot for at least 1,000 feet. Stones in the upper till are generally more rounded than in the lower till; sand lenses a few inches thick are common. The lower till appears more clayey than the upper till, and irregular iron- and manganese-stained platy joints subparallel to the hill are common. Lenses with color and texture like the upper till occur as much as 2 feet below the contact in the lower till, and at least one irregular "dike" of upper till extends down into the lower till locality 4 (fig. 4).

Locality 5 on the same slope has a sharply defined color change at the contact from olive gray above to deep olive brown below. Pebbles and cobbles in the upper till are rounded resistant rock types that show little evidence of weathering, whereas the lower till contains slabs of rotted biotite schist, and the more resistant rock types are subangular. The

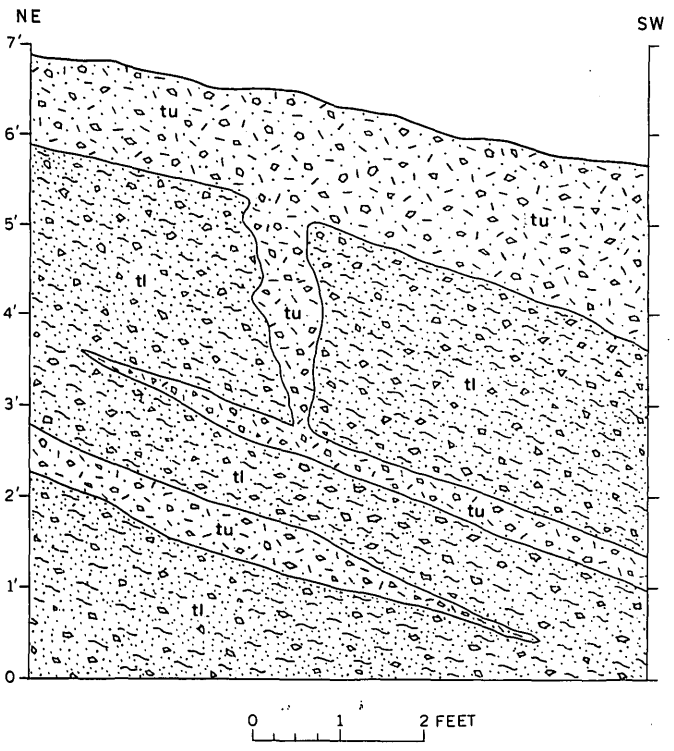

FIGURE 4.—Section of southeast wall of trench at locality 4, showing well-defined contact between upper and lower till. "Dike" of upper till extends into lower till, and tongues of upper till are subparallel to contact and platy jointing in lower till. Lithology: tu, upper till; tl, lower till.

contact between the two tills becomes diffuse in both directions along the trench as the color contrast is lost.

Only upper till is exposed in the trench on the west slope of the hill west of Wormwood Hill Road, but at locality 8 near the crest of the hill the olive-gray friable till becomes browner and more compact with depth. It lacks the platy structures and appears sandier than the lower till, but a lens of dark-brown compact till with platy structures is present near the bottom of the trench. Possibly the lower till is not far below.

Exposures on the west slope of the hill just west of State Route 89 (loc. 10) showed a sharp color and textural change from upper to lower till, 2 to 4 feet down in the trench. Near the crest of the hill, however, the lower till gradually becomes more friable, although subhorizontal platy structures are still apparent. At this locality a lens of olive-gray sandy material occurs in the olive-brown compact lower till. The lens grades laterally into typical lower till with no evidence of shearing or squeezing.

Intertonguing of the two tills is clearly apparent at locality 14 (fig. 5, *C* and *D*) on the west slope of the hill west of Pumpkin Hill Road. At *C* the upper till interfingers northeastward into lower till over a lateral distance of about 15 feet. At *D* the reverse is true. The olive-brown, hard, and compact lower till progressively is more mottled and changes northeastward into light-olive-gray friable upper till.

Both tills were exposed at localities 17 and 18 on a small knoll near the center of the Hampton quadrangle. On the west side of the knoll, color and textural changes define a sharp contact, but toward the crest and on the east slope these changes become gradational over a vertical distance of about 2 feet. On the west side the contact is 2 to 3 feet from the top of the trench, but it slopes eastward toward the base of the trench. The lower till is olive brown, compact, and has typical iron-stained platy surfaces. A few weathered schist pebbles as well as the more quartzofeldspathic stones are present. The upper till is light olive gray, streaked rusty yellowish gray; it is exceptionally sandy and friable, and stones are mostly pebble to small cobble size, hard, quartzose, and well rounded. Six-inch lenses and ½-inch-thick streaks in the upper till that have the color and compactness of the lower till occur above the contact.

In the northeast corner of the Hampton quadrangle at locality 19, a mottled friable sandy till shows a gradational decrease in chroma (olive gray to light gray) upward from the bottom of the trench.

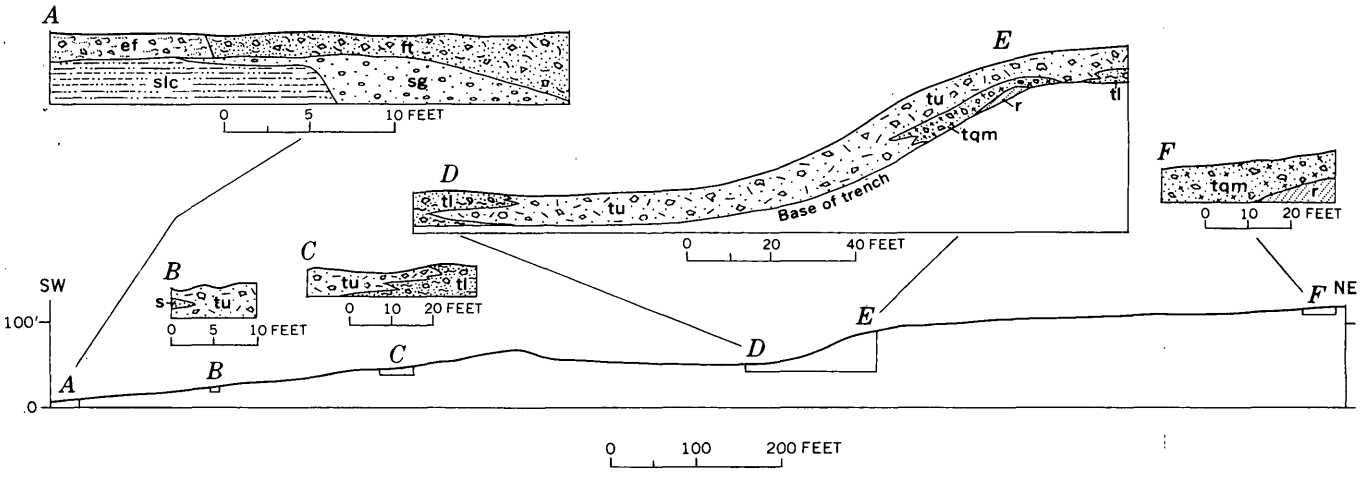

FIGURE 5.—Sections in north wall of trench on east bank of Stonehouse Brook at locality 14.
A. Flowtill and earth-flow deposits overlie glaciofluvial deposits of iron-stained sand and gravel that abut downslope against silty clay.
B. Tongue of glaciofluvial sand in upper till.
C. Lower till intertongues westward with upper till; contact is diffuse; lower till mottled brown and light gray.
D. Lower till intertongues eastward with upper till.
E. Quartz monzonite overlain by till composed almost entirely of quartz monzonite debris with streaks of brown clayey material; till grades upward into normal sandy upper till that grades eastward into olive-brown lower till.
F. Yellowish-olive-gray sandy till with abundant quartz monzonite clasts resting on quartz monzonite bedrock.
Lithology: ef, earth-flow deposits; ft, flowtill; s, sand; slc, silt and clay; sg, sand and gravel; tu, upper till; tqm, till of quartz monzonite debris; tl, lower till; r, quartz monzonite bedrock.

This is the reverse of a weathering profile and suggests that the upper part has been leached of iron. This sandy upper till appears to grade laterally eastward by diffuse intertonguing into the olive-brown compact lower till having platy iron- and manganese-stained surfaces.

Both tills are well exposed at localities 21 and 22 near the Danielson and Putnam quadrangle boundary. The contact is 2 to 5 feet deep and is sharp to gradational. At locality 21 the upper 2 feet of olive-brown lower till is mottled by neutral-gray patches with rusty-brown iron-stained halos.

Glaciofluvial and younger deposits

Glaciofluvial deposits in the trench consist chiefly of sand and gravel in terraces along the margins of major stream valleys. Sand and gravel, overlain by silt and clay, are also present at higher levels perched in topographic lows of the uplands. The glaciofluvial-terrace deposits in the major stream valleys mostly overlie or interfinger with the upper till. The contact is commonly covered by earth-flow deposits at the break in slope between the steep valley wall and glaciofluvial terrace. These earth-flow deposits are composed mostly of sandy upper till and a jumble of large blocks of rock 2 to 5 feet in diameter. Tongues of flowtill (Hartshorn, 1958) interfinger with and overlie stratified sand and gravel (fig. 5). Large blocks of rock in a matrix of eolian silt and sandy till rest on terrace surfaces.

Eolian deposits as much as 2 feet thick are preserved locally in topographic lows. They may be more extensive but probably are thin and were largely destroyed during excavation. In valley bottoms and upland swamps most surficial deposits are either under water or were disturbed beyond recognition during excavation. Well data indicate that glaciofluvial sand and gravel deposits resting directly on bedrock are more than a hundred feet thick beneath the trench in the major stream valleys.

Glaciofluvial terraces in the Fenton and Mount Hope River valleys occur at altitudes of 300 to 310 feet and 350 to 360 feet. Two levels mapped by Pessl (Dixon and Pessl, 1966) in the Natchaug River valley in the Hampton quadrangle are considerably higher, at 400 to 450 feet. Deposits in the valley at Stonehouse Brook are at about 450 feet. A high-level glaciofluvial deposit, not mapped by Pessl, is exposed in the trench at 520 feet on the east wall of the Natchaug River valley. It evidently is only sparsely preserved on this steep slope. Detailed descriptions of glaciofluvial and younger deposits and contact relationships are given below.

On the west side of the Fenton River valley (loc. 2), poorly stratified, poorly sorted glaciofluvial deposits at an altitude of 360 feet are overridden by earth-flow deposits. This incoherent material is exposed in the trench on the steep slope of the hill, and at the break in slope it is mixed with and has

flowed out over sand and gravel; it is exposed intermittently in the trench down to the lower 300-foot terrace where thicker more extensive well-stratified glaciofluvial deposits butt against the earth-flow material. Evidently the colluvial slump that formed these earth-flow deposits was active during deposition of glaciofluvial deposits.

On the east side of this valley (loc. 3, fig. 6) well-stratified sand and gravel rests unconformably on olive-brown lower till in the trench at an altitude of 280 feet; the contact slopes 20° downhill, and uphill it flattens and disappears below trench level. At an altitude of 300 feet, near the top of the glaciofluvial terrace, sand and gravel intertongue with the sandy upper till. Tongues of sandy friable flowtill are underlain and overlain by subhorizontal stratified sand and gravel. Unlike the west side of the valley, no glaciofluvial deposits are exposed in the trench at the 350- to 360-foot level on this side of the valley.

A very similar relationship exists in the Mount Hope River valley. An incoherent earth-flow deposit of sandy till containing abundant angular biotite gneiss blocks several feet in diameter is exposed on the west side of the valley (loc. 11) at an altitude of about 350 feet. It overlies and is in part mixed with poorly sorted deposits of sand and gravel at the break in slope. Deposits of a lower glaciofluvial terrace at 310 feet appear to rest on earth-flow material. On the east side of the valley (loc. 12), earth-flow material underlies sand and gravel at 300 feet. This material is mostly gneissoid quartz monzonite derived from bedrock exposed in the trench a few tens of feet uphill. No glaciofluvial deposits are exposed at the 350-foot level on the east side of the valley.

A 6-foot-thick deposit of unevenly stratified sand and gravel is exposed on both sides of the swamp along Stonehouse Brook (locs. 13 and 14). This glaciofluvial deposit is at 460 feet in the trench, an altitude comparable to the altitude of a glaciofluvial deposit in the Natchaug River valley. On the west side of the swamp (loc. 13, fig. 7) the sand and gravel rest on sandy upper till and contain several large blocks of gneiss that apparently slumped from till upslope. The contact between till and glaciofluvial deposits is irregular; the till is exposed only locally in the bottom of the trench. Brown eolian silt about 2 feet thick is exposed in a sag upslope of the sand and gravel in contact with till.

On the east side of the valley, at locality 14, stratigraphic relations are more complex. At about swamp level in the trench (fig. 5*A*), clean sand and gravel are overlain by sandy flowtill which grades southwestward into an incoherent earth-flow mixture of brown eolian silt, sandy till, and large blocks. This earth-flow material rests on ponded deposits of sandy, clayey silt. The contact between silt and sand and gravel is sharp and nearly vertical except for a thin tongue of rusty sand that extends part way over the silt beneath the flowtill and earth-flow material. The ponded material and sand and gravel are essentially contemporaneous glaciofluvial deposits laid down before colluvial slump from uphill. About 200 feet northeast in the trench (fig. 5*B*), sandy upper till is exposed the full depth of the trench except for a thin wedge of well-sorted sand and gravel.

The upper till exposed in the trench on the broad hill northeast of the Fenton River contains numerous lenses of clean yellow sand as much as 3 feet thick. The sand is well sorted but contains sparse

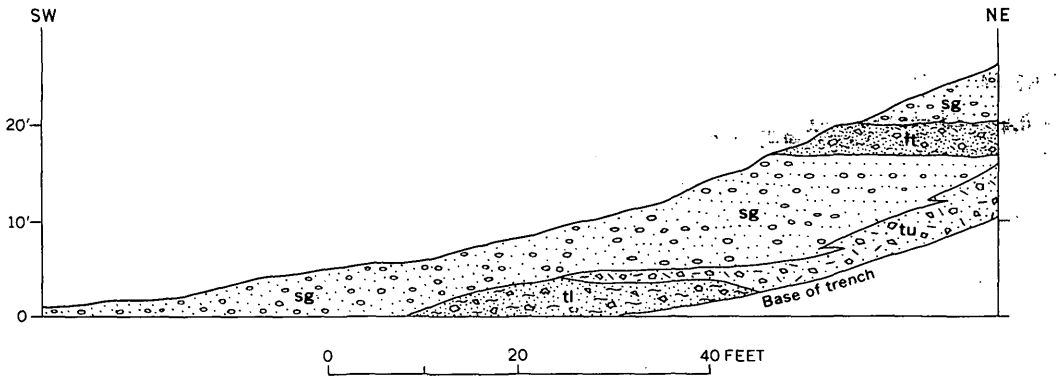

FIGURE 6.—Section of northwest side of trench on east bank of the Fenton River at locality 3. Glaciofluvial sand and gravel overlie and intertongue with upper till and contain tongues of flowtill. Farther downhill, sand and gravel rest on a 20° slope in lower till. Lithology: sg, sand and gravel; ft, flowtill; tu, upper till; tl, lower till. No vertical exaggeration.

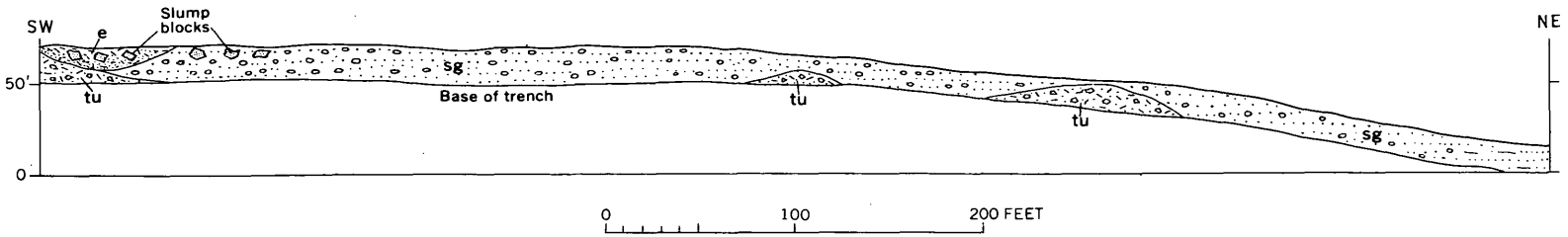

FIGURE 7.—Section of northwest side of trench on west bank of Stonehouse Brook at locality 13. Glaciofluvial sand and gravel rest on irregular surface of upper till. Sag on upslope side of glaciofluvial deposit is filled with brown eolian silt. Large gneiss blocks from upslope till mixed with eolian debris and upper sand and gravel beds. Lithology: e, eolian debris; sg, sand and gravel; tu, upper till.

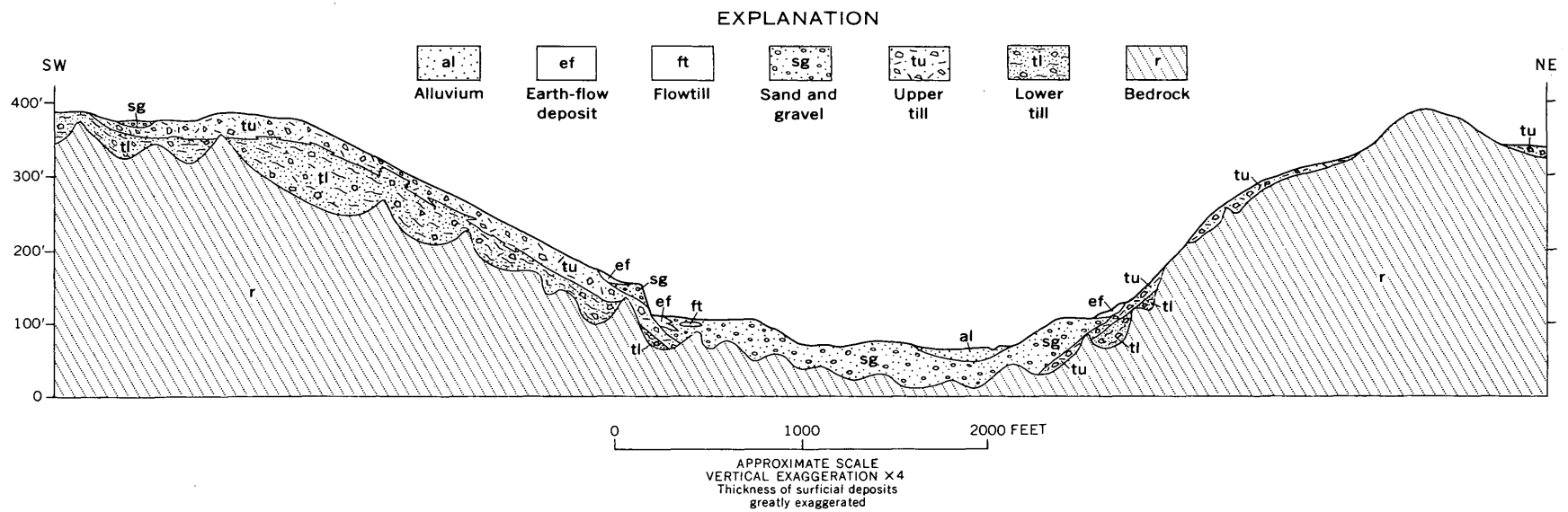

FIGURE 8.—Schematic section across major stream valley in east-central Connecticut.

RELATIONSHIPS DEMONSTRATED

Bedrock surface, irregular in detail, conforms generally to present topography.

Lower till fills irregularities of bedrock surface; thickest on sides of valleys.

Upper till blankets upland surfaces and valley walls.

Contact between the two tills locally sharp but generally diffuse with intertonguing relations.

Flow till interstratified with glaciofluvial sand and gravel.

Colluvial slump from upland till forms earth-flow deposits at break in slope between uplands and glaciofluvial valley fill. Deposits overlie and intertongue with sand and gravel.

Glaciofluvial deposits of sand and gravel thickest in valley where they rest directly on bedrock. Thin glaciofluvial deposits also present in upland rest on till.

More than one glaciofluvial terrace in valley. Recent alluvium generally restricted to narrow band along present stream.

pebbles and cobbles. Pebble gravel and lenses of clayey silt are also present. Deposits in the small high-level valley on the eastern side of this hill are mostly glaciofluvial material. At locality 6, coarse sand and minor gravel are overlain by fine-grained sand and silt. At the break in slope to the southwest, earth-flow deposits consist of gneiss blocks 2 to 6 feet in diameter mixed with sand and gravel but little silt or clay. The small hill on the northeast side of the stream consists of very sandy unsorted unstratified olive-gray to yellowish-gray till with little silt or clay. This till evidently was flushed of its fines by melt water without appreciable sorting or stratification.

Small isolated high-level deposits of sand and gravel were exposed at several other localities in the trench, as for example, at altitudes of 520 feet (loc. 21) and 460 feet (loc. 20) in the northwest corner of the Danielson quadrangle.

DISCUSSION

General

A composite of the stratigraphic relations of Pleistocene and younger deposits observed in the trench is illustrated by figure 8. This is a schematic cross section of a major stream valley in which the vertical scale is four times the horizontal and the thickness of the surficial deposits is further exaggerated to demonstrate the relationships.

Bedrock in the trench is generally within a few tens of feet of the surface as indicated by the distribution of bedrock exposures. The Connecticut State Highway drill holes south of the trench, however, show as much as 50 feet of till on slopes of these upland surfaces, and in major stream valleys sand and gravel deposits are known to be as much as 100 feet thick.

The lower till is most extensively exposed and probably thickest on hillsides where bedrock is not exposed; it rarely was observed resting on bedrock in the trench. The lower till generally smooths out irregularities in the bedrock topography. The upper till forms a thin veneer on bedrock and lower till. It intertongues with lower till, and the contacts, both lateral and vertical, appear gradational, particularly on steep slopes. Till apparently is absent in the major stream valleys because water wells show sand and gravel resting directly on bedrock. Either till never was deposited in these valleys or it was removed by streams that subsequently deposited the gravels.

Most glaciofluvial deposits in the trench are ice-contact terraces laid down when ice remained in the major valleys but was absent or very thin in the uplands. Two terrace levels at 300–310 and 350–360 feet in both the Fenton and Mount Hope Rivers suggest that during ice wasting both streams responded to the same outlets at two slightly different base levels. Higher levels in the Natchaug River valley at 400 and 450 feet suggest that melt water in this valley also responded to two base levels, perhaps to the same outlets or to higher level outlets when the lower reaches of the three rivers were still buried by ice. Deposits in Stonehouse Brook may be related to the latter sequence. There may have been a still earlier, higher outlet represented by the sand and gravel at 520 feet in the Natchaug valley.

Earth flow and flowtill mixed with glaciofluvial deposits at most till-terrace breaks in slope suggest that during deposition of the glaciofluvial deposits melt-water runoff caused large-scale colluvial slump along valley walls. Eolian deposits are thin or spotty and were recognized only where mixed with the colluvial material or in shallow swales against the break in slope. Alluvium and alluvial-terrace deposits in major stream valleys record deposition of post-Pleistocene sediments after the disappearance of ice. Swamp deposits commonly drained by small streams now fill irregularities in the upland till surface.

Origin of the two tills

The two tills recognized in the trench are distinguished by stratigraphic position, color and degree of oxidation, composition, texture, and internal structures. They are correlated with two superposed tills with similar distinguishing features recognized at many localities elsewhere in southern New England (White, 1947; Flint, 1961; Oldale, 1962, 1964; and Koteff, 1964), and particularly in the upland areas of southern Connecticut (Pessl, 1966; Pessl and Schafer, 1968).

Exposures in the trench suggest that the lower till is lodgement till and that the upper is ablation till, both of which were deposited by a single ice sheet. Extensive deep cross sections of the two tills, however, have been exposed at several localities in New England (Pessl and Schafer, 1968), and these indicate that the upper till must have been deposited by a later ice sheet after deep weathering of the lower till.

The lower till in the trench appears to be a lodgement till deposited in lows between local resistant bedrock highs, and it could be considerably thicker than the depth of the trench. It is hard and com-

monly has a strong subhorizontal fissility probably caused by compaction and shearing beneath an overriding ice sheet. The olive-brown oxidation color of the lower till persists with little variation throughout the length of the trench.

Many features of the upper till are indicative of ablation till. It is sandy, friable, and shows little evidence of compaction. Pervasive circulation of melt water in this till is demonstrated by winnowing of fines, crude stratification, and numerous lenses and layers of clean well-sorted sand and gravel. The common occurrence of well-sorted sand and gravel at the base of upper till on bedrock is evidence for considerable melt-water circulation at this interface. The near absence of oxidation suggests that the upper till was derived mostly from unweathered resistant bedrock.

In the trench there is no evidence of unoxidized or weakly oxidized lower till that might indicate the postdepositional weathering profile that has been noted in deep cuts elsewhere in New England. The difference in color between the two tills, though generally distinct, is not great. It could readily be attributed to a slightly greater content of brown clayey material in the lower till. At locality 1 the lower till rests on saprolite of biotite schist, and the color of the till and saprolite is about the same. This color is indistinguishable from the olive-brown color of typical lower till. Thus, the color difference might be attributed in part to differences in the source material of the two tills.

Contact relations between the two tills observed in the trench do not clearly support either the hypothesis that both tills were deposited during a single ice advance or the hypothesis that each till represents deposition from a separate ice sheet with a nonglacial period represented by weathering of the lower till. No evidence was observed in the trench for significant tectonic disturbance at the contact, as might be expected beneath an overriding ice sheet; such disturbance has been found elsewhere in New England (Schafer, 1969).

It is also difficult to explain by either hypothesis the formation of the mixed zone so typical of most contacts between upper and lower till. The contact zone is extremely irregular through several feet, and the two lithologic types grade into one another both laterally and vertically. Moreover, lenses of each lithologic type are found in the other, and although these are clearly distinguishable, their contacts are typically diffuse, particularly where they feather out laterally.

This mixed zone might either represent a blend of subglacial and superglacial till from a single ice sheet or incorporation of the upper part of an old till in younger till by an overriding ice sheet. The mixed zone can be attributed at least in part to colluvial creep after deposition. Pessl and Schafer (1968) use the presence of angular blocks of lower till in the upper till as one argument for a second ice advance. No such discrete inclusions were observed in the trench.

The writer has examined many of the two-till localities in Connecticut, including several deep cuts showing an oxidation profile, and he has mapped both tills in the Eastford quadrangle north of the trench. The striking similarity between the oxidized lower till of the Eastford and Hampton quadrangles (Dixon and Pessl, 1966) and that in the trench strongly suggests that they are correlative. Cores from the Connecticut State Highway Department drill holes not far south of the trench, moreover, are distinctly less oxidized at depth than near the surface, which suggests that unoxidized lower till may be present below trench level.

Pessl and Schafer (1968) show that the two tills must represent deposits from separate ice advances even though the lower till is predominantly lodgement till and the the upper till predominantly ablation till. Although they use the terms lower and upper till for the early or late ice advance, I have called them old and young tills to distinguish them from the lower and upper tills in the trench.

Their argument for two ice advances is summarized below:

1. The old till commonly is browner and more strongly colored than the olive-gray young till at the contact. The color contrast is attributed to oxidation of the old till before deposition of the young till. The oxidized zone evidently is very thick because neutral gray nonoxidized old till is found only in a few deep exposures. Oxidation of the old till before young till deposition is also indicated by the presence of strongly oxidized dark-brown inclusions of old till in young till that shows no evidence of oxidation.
2. Truncation and contortion of the old till at the contact and inclusions of old till in young till suggest that the old till was overridden by ice.
3. The young till probably includes subglacial as well as superglacial facies, as indicated by strongly developed fabric lineation and

almost massive structure in some exposures of the young till. (See Pessl, 1971).

4. Differences between orientations of till fabrics, striations, and streamline hill axes suggest differences in directions of ice movement for the young and old tills. The validity of this as an argument for two ice advances is weakened by evidence for an upward change in the fabric lineation within the young till, which suggests that such changes can occur during a single ice advance.

Further analysis, however, reveals several drawbacks to the two-ice-advance hypothesis. There is a persistent distinctive, though slight, textural difference between the old and young till. According to Pessl and Schafer (1968) the old till generally is more compact, less sandy, and contains fewer stones than the young till. If not attributed to a difference between subglacial and superglacial modes of deposition, then possibly it can be attributed to a difference in source material or physical conditions during the two ice advances.

It is preferable to assume, as apparently do Pessl and Schafer (1968), that the old till is subglacial and the young till is chiefly superglacial. This assumption, however, leads to the question of why no superglacial till or glaciofluvial deposits related to the early ice advance have been recognized in Connecticut. Could erosion cut so deep into subglacial till that no trace of the overlying superglacial till and associated sand and gravel deposits was left? If such erosion did take place after formation of the deep weathering profile in the old till, a younger ice sheet would be the logical agent of this erosion.

Considering the total evidence, however, particularly the superposition of nonweathered upper till over deeply weathered lower till and structural truncation of the older till, one must assume that the two tills represent deposits from two separate ice sheets.

SUMMARY

The Algonquin Gas Co. trench in east-central Connecticut exposed Pleistocene deposits and various bedrock and Holocene deposits. Bedrock is everywhere near the surface in the upland area; there are few drumlins. The Pleistocene cover is probably less than a few tens of feet thick in the uplands. Bedrock in the major valleys is overlain by as much as 130 feet of glaciofluvial and alluvial sand and gravel of Pleistocene to Holocene age. The lower of the two tills exposed in the trench appears to fill bedrock lows, rounding the contours of a somewhat more rugged bedrock topography. The upper till forms a thin skin draped across bedrock and lower till, mostly in the uplands. The lower till is a lodgement till; it is hard, compact, olive brown, and has a characteristic platy texture. The upper till is an ablation till; it is sandy and contains numerous lenses of sand and gravel.

The depositional history of the two tills could not be determined from observations in the trench alone. Exposures in the trench did not provide conclusive evidence whether the olive-brown compact lower till was derived from an early ice advance that underwent deep erosion and weathering during a nonglacial period before a later ice sheet deposited the upper till, or whether both tills were deposited by the same ice sheet and the lower till is simply a subglacial till containing relatively more oxidized material than the superglacial till.

Exposures elsewhere in New England, however, have provided evidence that an older till does exist. On the basis of striking lithologic and textural similarities and the relative stratigraphic position of the lower till in the trench to the old till, it seems probable that the lower till in the trench was deposited by an early ice sheet. The geologist mapping till in eastern Connecticut, therefore, should be aware that an old till, which is a recognizable lithostratigraphic unit, probably does exist and that the evidence for the early age of this till may not be apparent in shallow exposures, particularly in areas underlain by iron-bearing schist.

REFERENCES

Dixon, H. R., and Pessl, Fred, Jr., 1966, Geologic map of the Hampton quadrangle, Windham County, Connecticut: U.S. Geol. Survey Geol. Quad. Map GQ–468.

Flint, R. F., 1961, Two tills in southern Connecticut: Geol. Soc. America Bull., v. 72, no. 11, p. 1687–1692.

Hartshorn, J. H., 1958, Flowtill in southeastern Massachusetts: Geol. Soc. America Bull., v. 69, no. 4, p. 477–482.

Koteff, Carl, 1964, Surficial geology of the Concord quadrangle, Massachusetts: U.S. Geol. Survey Geol. Quad. Map GQ–331.

Oldale, R. N., 1962, Surficial geology of the Reading quadrangle, Massachusetts: U.S. Geol. Survey Geol. Quad. Map GQ–168.

——— 1964, Surficial geology of the Salem quadrangle, Massachusetts: U.S. Geol. Survey Geol. Quad. Map GQ–271.

Pessl, Fred, Jr., 1966, A two-till locality in northeastern Connecticut: U.S. Geol. Survey Prof. Paper 550–D, p. D89–D93.

——— 1971, Till fabrics and till stratigraphy in western Connecticut, *in* Goldthwait, R. P., Forsyth, J. L., Gross, D. L., and Pessl, Fred, eds., Till, a symposium: Columbus, Ohio, Ohio State Univ. Press. [In press]

Pessl, Fred, Jr., and Schafer, J. P., 1968, Two-till problem in Naugatuck-Torrington area, western Connecticut, Trip B–1, *in* New England Intercollegiate Geol. Conf., 60th Ann. Mtg., Oct. 25–27, 1968, Guidebook for field-trips in Connecticut: Connecticut State Geol. and Nat. History Survey Guidebook 2, p. 1–12.

Schafer, J. P., 1969, Structural relationships of tills in western Connecticut: Geol. Soc. America, North-Central Sec., Ann. Mtg., Abs. with programs for 1969, [v. 1], pt. 6, p. 42.

White, S. E., 1947, Two tills and the development of glacial drainage in the vicinity of Stafford Springs, Connecticut: Am. Jour. Sci., v. 245, no. 12, p. 754–778.

DELTAIC DEPOSITS OF THE BORDEN FORMATION IN CENTRAL KENTUCKY

By WARREN L. PETERSON and ROY C. KEPFERLE,
Lexington, Ky., Cincinnati, Ohio

Prepared in cooperation with the Kentucky Geological Survey

Abstract.—The Borden Formation (Lower Mississippian) in central Kentucky is a deltaic deposit consisting of three main sedimentary units, in which most beds seem to have had initial southwestward dips. These units are the Muldraugh Member and the underlying shale member, which has two parts. The top of the shale member preserves a relatively steep southwest-facing, northwest-trending slope which is interpreted to be an ancient delta front. To the northwest, the front is continuous with a front on Borden deltaic sediments in the Indiana and Illinois subsurface. It continues southeastward to at least a few miles southeast of Campbellsville, Ky.; beyond there it probably coincides with a southeasterly trending line of lithologic change across which the carbonate-poor Borden Formation passes laterally southwestward into the stratigraphically equivalent, and carbonate-rich, Fort Payne Formation.

Geologic mapping since 1960 by members of the U.S. Geological Survey in cooperation with the Kentucky Geological Survey has shown in detail the distribution of lithologies in the Borden Formation over many 7½-minute quadrangles in Kentucky. The purpose of this report is to summarize the deltaic aspects of the Borden Formation in central Kentucky. Part of the information on which this report is based has appeared in published geologic maps (Peterson, 1966a, b, 1967, 1968; Kepferle, 1966a, b, 1967a; Moore, 1968). The deltaic origin of Lower Mississippian strata in the subsurface of Illinois and Indiana has been described by Swann, Lineback, and Frund (1965) and Lineback (1966, 1969).

BORDEN FORMATION

The Borden Formation, particularly the upper two-thirds, is well exposed in the east-facing Muldraughs Hill escarpment (fig. 1) and the hills, or "knobs," east of it. Good exposures and the sharp conformable contact at the base of the Borden have

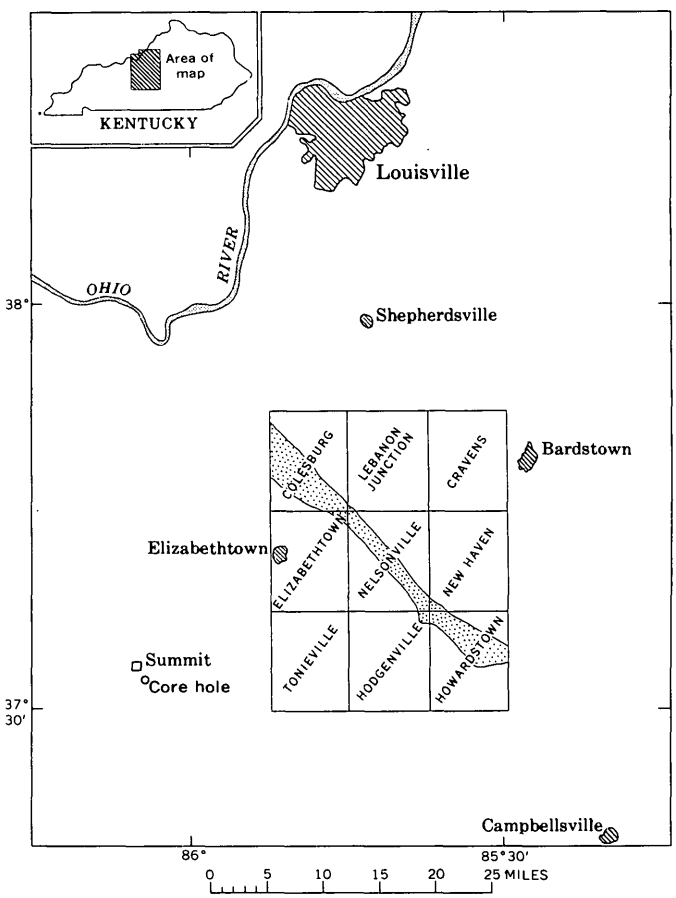

FIGURE 1.—Index map of central Kentucky and adjacent areas, showing location of towns, quadrangles, a core hole, and position of the area of abrupt thinning of the shale member of the Borden Formation (stippled area). Muldraughs Hill escarpment coincides approximately with the area of abrupt thinning.

made it possible to determine the thicknesses and the stratigraphic relations of units making up the Borden.

In central Kentucky the Borden Formation is between the New Albany Shale of Devonian age and the Harrodsburg Limestone of Mississippian age. It consists of a lower shale member, which is divided into two units, and the Muldraugh Member, which is composed of siltstone and carbonate (figs. 2 and 3). These three units correspond approximately to the New Providence, Brodhead, and Muldraugh Formations of Stockdale (1939).

The Borden Formation thins southwestward from more than 400 feet to 280 feet across the area of outcrop considered here (figs. 2, 3, and 4*A*).

Shale member

The shale member consists of a lower clay shale unit and an upper silt shale unit. It thins southwestward, abruptly across a northwest trending belt 1–6 miles wide, shown on the index map (fig. 1) and the isopach map (fig. 4*B*). The shale member is very thin or missing in the subsurface to the west; it is not present in a core hole drilled at Summit (Moore, 1964).

The lower unit of the shale member consists of soft, gray, greenish-weathering silty clay shale and subordinate amounts of siltstone and crinoidal and bryozoan limestone. It thins irregularly southwestward as shown by the isopach map (fig. 4*C*). Large ironstone concretions are locally abundant, and a persistent layer of phosphatic nodules occurs at the base of the unit (fig. 3).

Siltstone occurs in well-defined tabular beds in a zone 4–8 feet thick, which is as much as 40 feet thick locally. The zone descends southwestward about 14 feet per mile relative to the base of the unit, as shown in the cross section (fig. 2) and the isopach map (fig. 4*D*). The siltstone beds are generally megascopically structureless, although faint lamination parallel to bedding, crossbeds, ripple marks, and faint upward decrease in grain size have been observed. The bottoms of the beds have abundant flow and load casts. Origin of the siltstone beds has been ascribed to southwest-flowing turbidity currents by Kepferle (1967b).

The upper unit of the shale member is silt shale containing lesser amounts of siltstone and minor amounts of crinoidal and bryozoan limestone. The silt shale is gray, weathers greenish gray, and is composed mostly of quartz silt. Coarser grain size, distinct lamination or thin bedding, and lack of ironstone concretions distinguish it from the clay shale of the lower unit. Siltstone occurs in a large body in the upper part of the unit in the northern part of the Lebanon Junction quadrangle and north of there. It differs in many aspects from siltstone in the lower unit of the shale member, primarily in that it is not in well-defined beds intercalated with shale and does not show current structures. Limestone occurs in discontinuous beds in silt shale, mainly in the upper 20 feet of the unit; many of the crinoidal limestones are crossbedded.

At the close of shale member deposition, an abrupt southwest-facing, northwest-trending slope interpreted to be a delta front had formed on the sea bottom (figs. 2, 3, 4*B*). This slope is apparent in the field and on published geologic maps but is probably nowhere steeper than 2° and nearly everywhere less than 1°.

Glauconitic zone

A conspicuous glauconitic zone occurs in the upper few inches of the shale member and in places in the lower few inches of the Muldraugh Member; locally, it is missing. The zone consists of shale, siltstone, limestone, or dolomite containing abundant glauconite. It is the more abundantly glauconitic part of the Floyds Knob Formation of Stockdale (1939). In the Howardstown quadrangle, it rises northeastward from 60 feet above the base of the Borden Formation to 260 feet above the base within about 6 miles (figs. 3, 4*B*). It is the presence of this glauconitic zone which has made possible the confident tracing of the delta front on the shale member.

Glauconite is scattered throughout the Borden Formation, and its concentration presumably occurred when little land-derived sediment was being deposited. Its local absence is probably the result of removal by scour currents.

Muldraugh Member

The Muldraugh Member is composed of siltstone, dolomite, limestone, and chert that thickens abruptly southwestward across the same narrow northwesterly trending belt where the shale member thins (figs. 2, 3). The dominant rock type is a strongly indurated greenish-gray to olive-gray siltstone composed of quartz, dolomite, calcite, chert, and minor silicate minerals; voids between the silt grains are filled with a very fine grained matrix of silica and carbonate. Silicification is variable but present in every thin section. Insoluble residues commonly make up 70 to 85 percent of the rock, but much of this is secondary silica in silt-sized or smaller grains. Because of the silicification, dolomitization, and fine-grained matrix, the original composition of the rock is difficult to determine, but

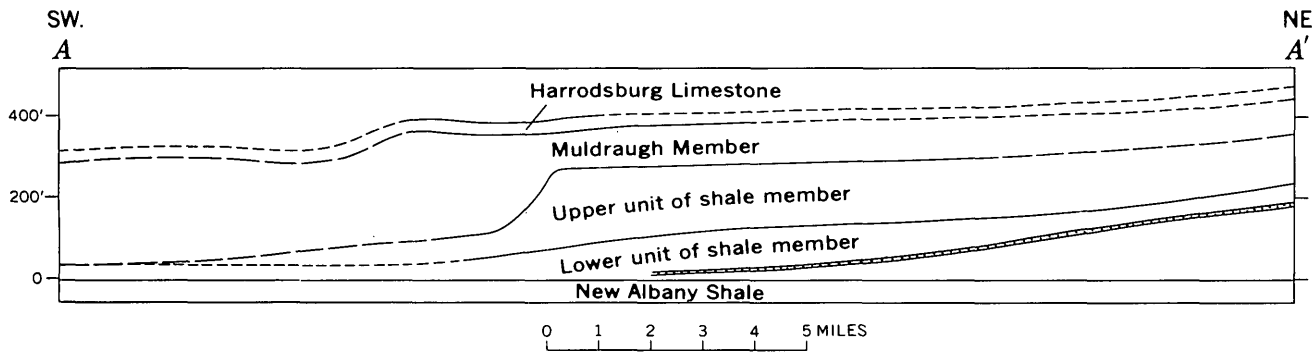

FIGURE 2.—Diagrammatic restored cross section along line *A–A'* shown on figure A*B*. Stippled pattern represents zone of abundant siltstones (turbidites) in the lower unit of the shale member of the Borden Formation. Contacts long dashed where based on wide-spaced and subsurface information, short dashed where inferred. Vertical exaggeration × 44.

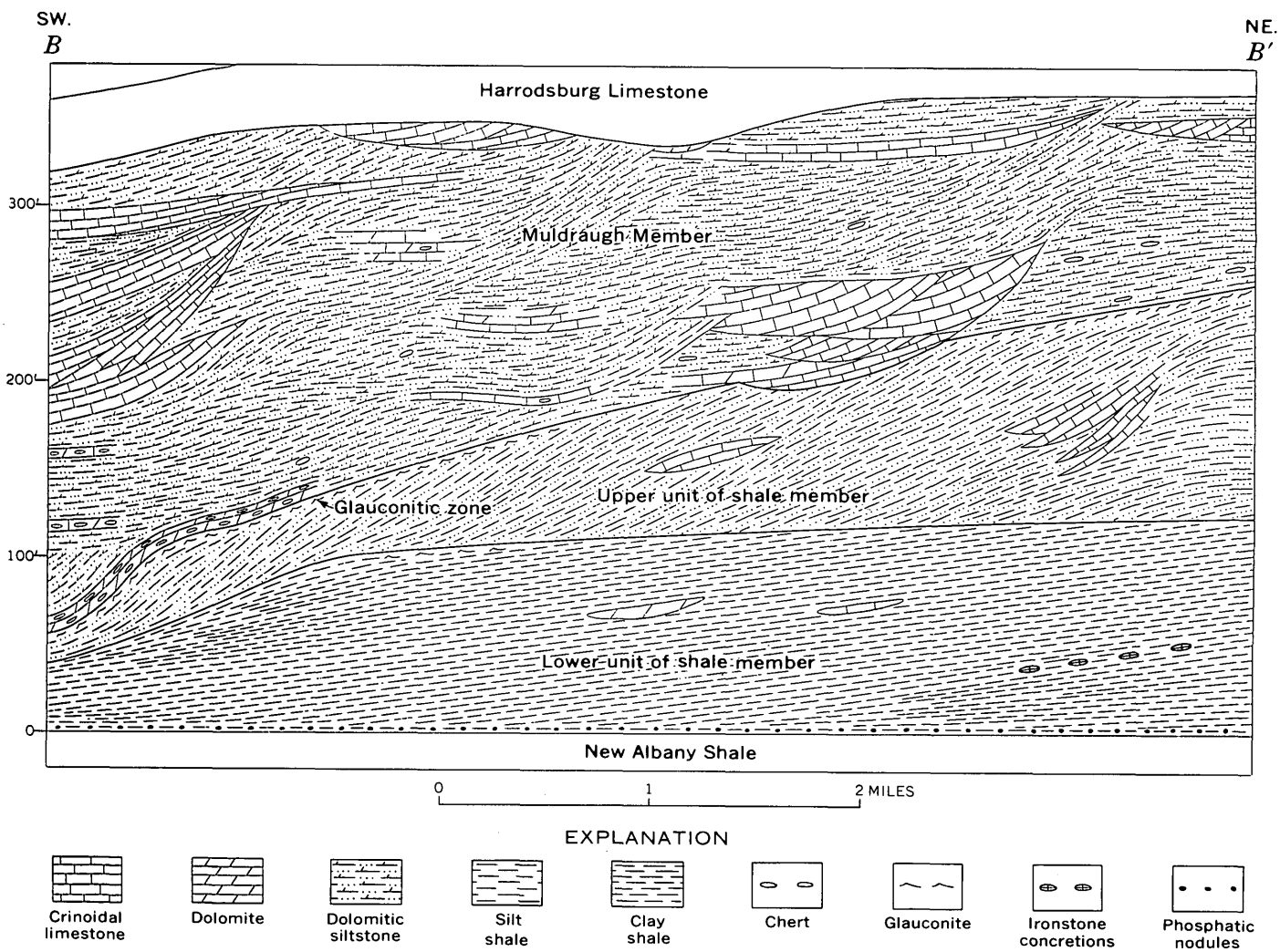

FIGURE 3.—Diagrammatic restored cross section along line *B–B'* shown on figure 4*B*. Southwestward dip of bedding planes in clay shale and silt shale and southwestward dip of layers of ironstone concretions inferred. Slope of contact between Muldraugh Member and shale member about 90 feet per mile in steepest part. Vertical exaggeration × 44.

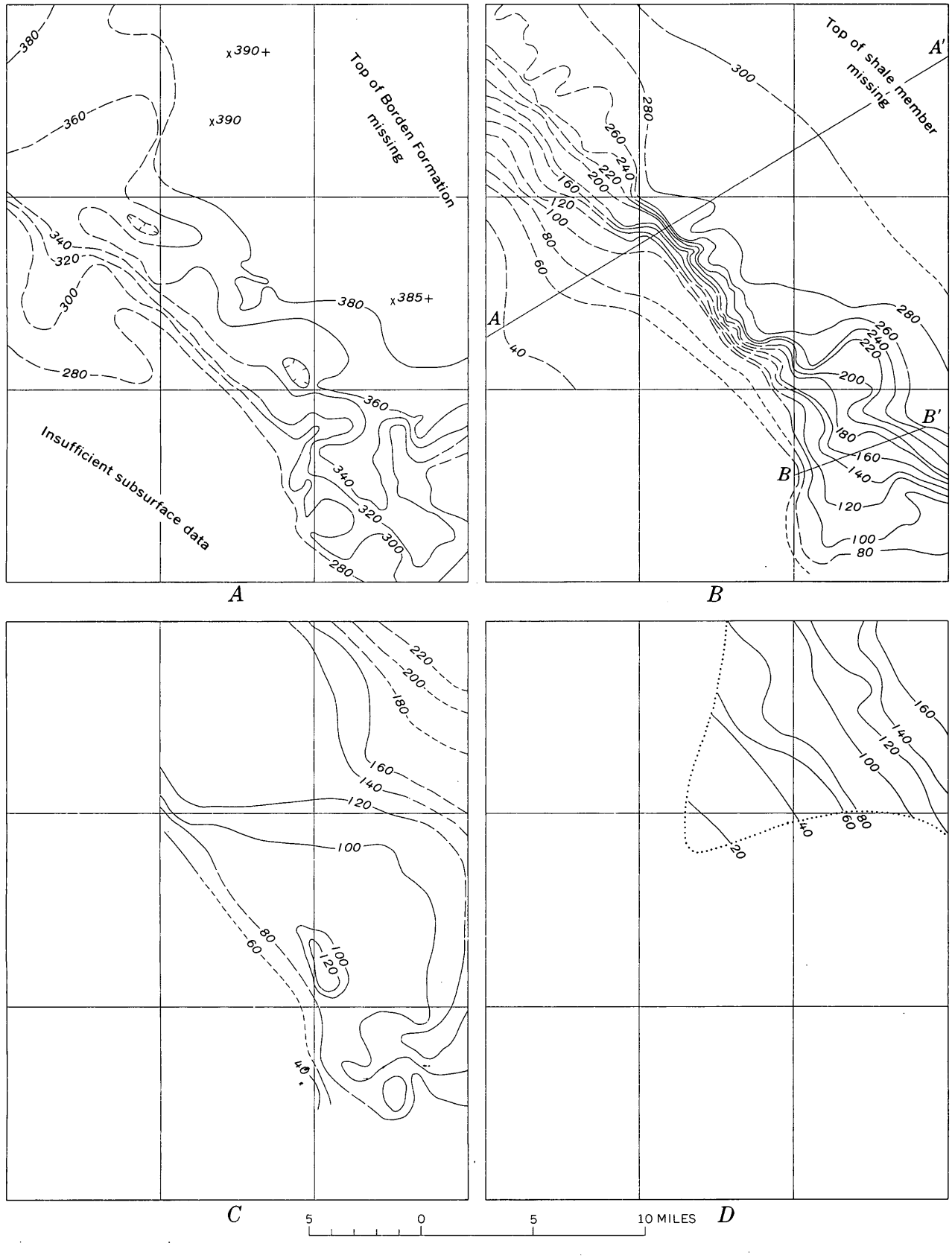
Top of Borden Formation missing
Insufficient subsurface data
Top of shale member missing
A
B
C
D
A'
B'
5 0 5 10 MILES

FIGURE 4.

probably nearly half the original sediment was calcitic (or aragonitic) skeletal debris.

Limestone occurs in lenses, beds, and large bodies in the Muldraugh Member and is interstratified with the siltstone. Much of it is nearly free of terrigenous clastic materials, but it also grades into siltstone. The limestone is dominantly calcirudite composed mainly of whole or fragmental crinoid columnals; lesser amounts are calcarenite composed largely of crinoidal skeletal fragments. Large whole fossils are rare.

The coarser grained limestones of the Muldraugh are generally crossbedded. Cut-and-fill structures are common in the limestones and siltstones. These current structures are mainly in the upper one-third of the Muldraugh where the member is thick and in the entire Muldraugh where it is thin. Crossbeds dip generally southwest.

SEDIMENTARY HISTORY

After deposition of the organically rich muds which are now the New Albany Shale, a thin widespread layer of fine clastic sediments containing phosphatic nodules accumulated on the sea bottom. This layer was overridden by clay-rich prodelta sediments of the lower unit of the shale member, coming from the northeast. The prodelta deposit advanced toward the southwest with gentle (5–20 feet per mile) southwest-facing slopes on which silt-laden turbidity currents came to rest. As sedimentation, mainly silt, continued, the upper unit of the shale member was deposited. This deposit advanced with somewhat steeper foreset slopes (½°–2°) toward the southwest across the older sediments, at the same time contributing clay to the prodelta deposits. The silt and clay shales are interpreted to be comparable with the delta front silty clay and prodelta clay of a modern delta (Fisk and others, 1954). At the close of deposition of the shale member, a distinct southwest-facing front on the accumulated sediments trended northwestward across the area. An episode of light sedimentation ensued, during which the glauconitic zone accumulated.

A pronounced change in conditions followed. Terrigenous sediments and shell debris from abundant organisms, which lived in shallower waters to the northeast, were swept southwestward across the earlier sediments. Strong currents are indicated by cut-and-fill structures and crossbedded limestones. The glauconitic zone was probably scoured away from some areas. The Muldraugh Member was built southwestward across the deltaic front on the shale member.

The Harrodsburg Limestone (Sable and others, 1966) later blanketed the upper surface of the Borden Formation. Its relatively even thickness and generally pure composition indicate that deltaic infilling by terrigenous clastic material had ceased and that the calcitic skeletal debris was deposited on a nearly even surface in shallow water.

REGIONAL RELATIONSHIPS

The deltaic front defined by the contact between the carbonate-poor rocks of the shale member and the carbonate-rich rocks of the Muldraugh Member of the Borden Formation in central Kentucky is continuous with a similar front in the subsurface of Indiana and Illinois delineated by Swann, Lineback, and Frund (1965) and Lineback (1966, 1969). The front in the Indiana and Illinois subsurface, however, is not reported to be marked by a glauconitic zone.

The deltaic front continues southeastward from central Kentucky to at least a few miles southeast of Campbellsville, Ky., where roadcuts along Kentucky Highways 70 and 76 expose the glauconitic zone and show that it drops stratigraphically to the southwest. The front probably continues farther southeast and coincides with a southeasterly trending line of lithologic change across which the carbonate-poor Borden Formation on the northeast passes laterally into the stratigraphically equivalent, and carbonate-rich, Fort Payne Formation on the southwest.

FIGURE 4.—Isopach maps of total Borden Formation and units within Borden; each map shows same area as quadrangle group shown on figure 1. *A*, isopach of total Borden Formation. *B*, isopach of the shale member of the Borden formation; *A*–*A'* is line of cross section shown on figure 2; *B*–*B'* is line of cross section shown on figure 3. *C*, isopach of the lower unit of the shale member of the Borden Formation. *D*, isopach of the interval between the top of the New Albany Shale and the top of the zone of abundant siltstone beds in the lower unit of the shale member of the Borden Formation; dotted line shows areal limit of well-defined zone containing abundant siltstone beds. Isopachs long dashed where data are widely spaced, short dashed where inferred from established trends. Isopach interval 20 feet.

REFERENCES

Fisk, H. N., McFarlan, E., Jr., Kolb, C. R., and Wilbert, L. J., Jr., 1954, Sedimentary framework of the modern Mississippi delta: Jour. Sed. Petrology, v. 24, no. 2, p. 76–99.

Kepferle, R. C., 1966a, Geologic map of the Howardstown quadrangle, central Kentucky: U.S. Geol. Survey Geol. Quad. Map GQ–505.

Kepferle, R. C., 1966b, Geologic map of the Elizabethtown quadrangle, Hardin and Larue Counties, Kentucky: U.S. Geol. Survey Geol. Quad. Map GQ–559.

——— 1967, Geologic map of the Colesburg quadrangle, Hardin and Bullitt Counties, Kentucky: U.S. Geol. Survey Geol. Quad. Map GQ–602.

——— 1967b, Turbidites in the Lower Mississippian Borden Formation of central Kentucky [abs.]: Geol. Soc. America, North-Central Sec., 1st Ann. Mtg., Program, p. 15.

Lineback, J. A., 1966, Deep-water sediments adjacent to the Borden Siltstone (Mississippian) delta in southern Illinois: Illinois Geol. Survey Circ. 401, 48 p.

——— 1969, Illinois basin—sediment-starved during Mississippian: Am. Assoc. Petroleum Geologists Bull., v. 53, no. 1, p. 112–126.

Moore, F. B., 1964, Lithologic and radioactivity log of Summit area drill hole, Hardin County, Ky.: U.S. Geol. Survey open-file report.

——— 1968, Geologic map of the Hodgenville quadrangle, Larue and Nelson Counties, Kentucky: U.S. Geol. Survey Geol. Quad. Map GQ–749.

Peterson, W. L., 1966a, Geologic map of the New Haven quadrangle, Nelson and Larue Counties, Kentucky: U.S. Geol. Survey Geol. Quad. map GQ–506.

——— 1966b, Geologic map of the Nelsonville quadrangle, central Kentucky: U.S. Geol. Survey Geol. Quad. Map GQ–564.

——— 1967, Geologic map of the Lebanon Junction quadrangle, central Kentucky: U.S. Geol. Survey Geol. Quad. Map. GQ–603.

——— 1968, Geologic map of the Cravens quadrangle, Bullitt and Nelson Counties, Kentucky: U.S. Geol. Survey Geol. Quad. Map GQ–737.

Sable, E. G., Kepferle, R. C., and Peterson, W. L., 1966, Harrodsburg limestone in Kentucky: U.S. Geol. Survey Bull. 1224–I, 12 p.

Stockdale, P. B., 1939, Lower Mississippian rocks of the east-central interior: Geol. Soc. America, Spec. Paper 22, 248 p.

Swann, D. H., Lineback, J. A., and Frund, Eugene, 1965, The Borden Siltstone (Mississippian) delta in southwestern Illinois: Illinois Geol. Survey Circ. 386, 20 p.

LOCAL STRATIGRAPHIC AND TECTONIC SIGNIFICANCE OF *LEPTOCERATOPS*, A CRETACEOUS DINOSAUR IN THE PINYON CONGLOMERATE, NORTHWESTERN WYOMING

By MALCOLM C. McKENNA[1] and J. D. LOVE,
New York, N.Y., Laramie, Wyo.

Abstract.—An unabraded tooth of *Leptoceratops*, a small hornless dinosaur of latest Cretaceous age, was found in place 150 feet above the base of the Pinyon Conglomerate in its principal reference section on the east side of Pinyon Peak, northwestern Wyoming. This discovery necessitates a reevaluation of the age of at least part of the Pinyon Conglomerate, because 30 miles to the southeast of Pinyon Peak the Pinyon contains Paleocene fossils at its base and top. The lack of abrasion of the specimen and the absence of dinosaurs from rocks of undisputed Paleocene age suggest that at least the basal 150 feet of the 3,700-foot-thick Pinyon Conglomerate in the type locality is of Cretaceous age. The angularity of the unconformity at the base of the Pinyon ranges from very little at the dinosaur locality to 90° about 3 miles southeast. It thus seems probable that the tectonic activity that produced the Washakie Range and the Buffalo Fork thrust fault began as early as latest Cretaceous time.

The Pinyon Conglomerate was named and first described by W. H. Weed (in Hague, 1896) from exposures on Pinyon Peak (fig. 1), 5 miles south of Yellowstone National Park, northwestern Wyoming. The conglomerate has, in recent years, been considered to be of Paleocene age on the basis of Paleocene pollen and mollusks in underlying strata and Paleocene vertebrate fossils in overlying strata (Love, 1947, and unpub. data; Love and others, 1948; M. C. McKenna, unpub. data). These Paleocene fossils bracketing the Pinyon Conglomerate, however, occur in the southeastern part of Jackson Hole, 30–40 miles south of Pinyon Peak. Between these two localities is a 10-mile gap from which the conglomerate has been removed by erosion. No fossils had been found previous to this study in the conglomerate in the Pinyon Peak area, and the strata were correlated across the gap entirely on the basis of lithology and structural relations with older rocks, which range in age from Mississippian to Late Cretaceous.

A principal reference section of the Pinyon Conglomerate on Pinyon Peak (no type section was designated by Weed or by later workers) was measured in 1966 by Love and, although no fossils were observed, a limestone pellet conglomerate closely resembling those that yielded abundant fossil mammals in the strata overlying the Pinyon Conglomerate in southern Jackson Hole was noted in the lower part of the reference section. This unit was searched by the field party of the American Museum of Natural History in the summer of 1969. Embedded in the conglomerate were one 2-inch clam, unidentifiable as to genus, one lizard? scute, and one tooth of *Leptoceratops*, a small hornless dinosaur.

The presence of this dinosaur tooth in the type locality of a formation previously thought to be of Paleocene age is considered of sufficient stratigraphic and tectonic significance to warrant the brief discussion presented here.

Acknowledgments.—We wish to thank Dr. Donald Baird, Department of Geology, Princeton University, for his suggestion that the tooth might belong to *Leptoceratops*, and we are grateful to Dr. Baird, Dr. Dale A. Russell, National Museum of Canada, Ottawa, and Dr. Nicholas Hotton 3d, U.S. National Museum, Washington, for their improvements of the manuscript. Dr. Russell kindly provided unpublished data concerning the upper dentition of a skull of *Leptoceratops*, NMC (National Museum of Canada) collection 8889.

[1] Department of Vertebrate Paleontology, American Museum of Natural History.

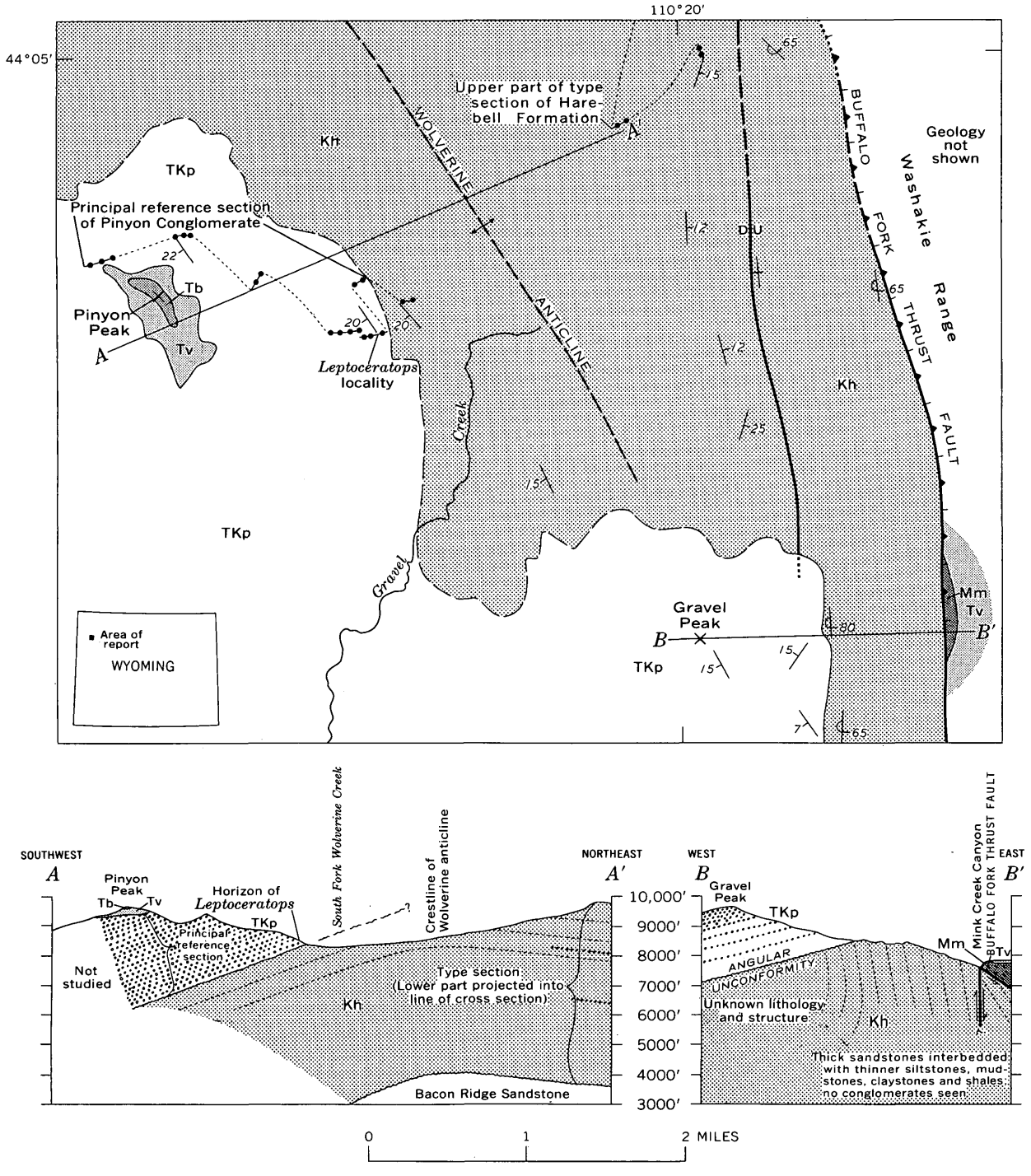

FIGURE 1.—Geologic map and sections showing location of principal reference section of Pinyon Conglomerate, collection site and position in section of *Leptoceratops*, angular unconformity between Pinyon Conglomerate and Harebell Formation, and upper part of type section of Harebell Formation. Base from U.S. Geological Survey, Mount Hancock quadrangle, 1959.

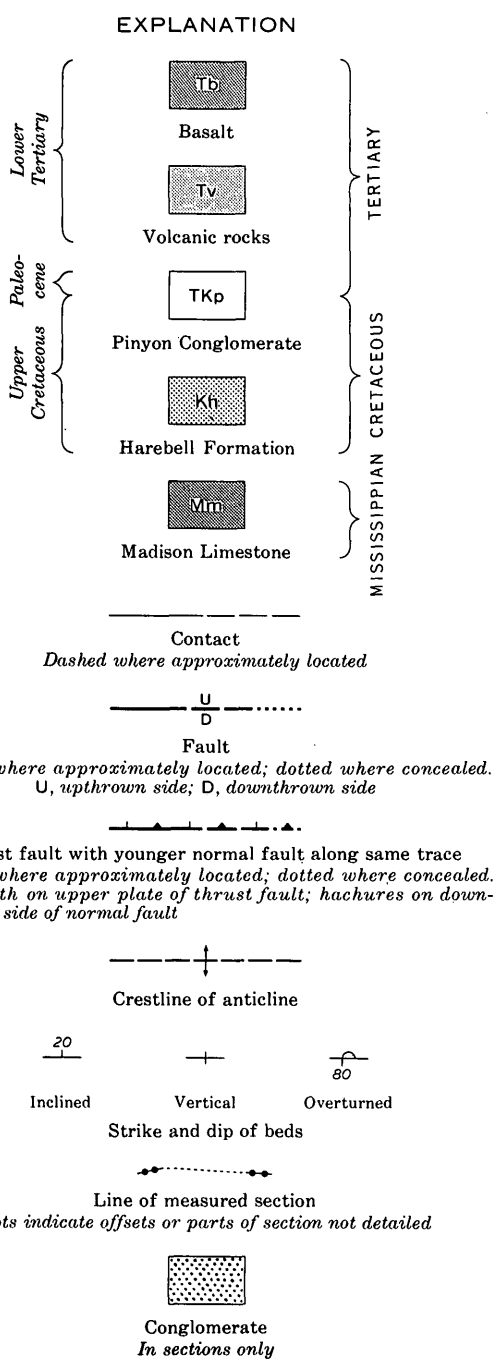

FIGURE 1.

STRATIGRAPHY

Figure 1 shows the distribution of the Pinyon Conglomerate and Harebell Formation (Love, 1956) in the vicinity of Pinyon Peak, the location of the principal reference section of the Pinyon Conglomerate, and the locality where *Leptoceratops* was discovered. Unconformably overlying the Pinyon at the principal reference section are lower Tertiary volcanic rocks. Cross section *A–A′* crosses the reference section. The fossil horizon is projected onto section *A–A′*. The Pinyon Conglomerate is more than 3,700 feet thick on Pinyon Peak and consists almost entirely of quartzite pebble, cobble, and boulder conglomerate. Only the lower part of the principal reference section, which is pertinent to this discussion, is presented here.

Lower part of principal reference section of Pinyon Conglomerate and upper part of Harebell Formation, Pinyon Peak, Wyoming

	Thickness (feet)
Pinyon Conglomerate (lower part):	
8. Conglomerate, tan; chiefly red and gray quartzite roundstones 2-4 in. in diameter in a coarse-grained light-brown sandstone matrix	25
7. Sandstone, gray to tan, coarse-grained, massive to crossbedded; forms upper part of relatively smooth bare slope and in places a cliff; some gray claystone lenses and pellets; sparse quartzite pebbles near base	50
6. Limestone pellet conglomerate, greenish-brown; weathers dark brown; lenticular; crops out in ragged ledge with very uneven top and bottom; angular to rounded fragments of gray silty dense limestone, as much as 3 in. in diameter but commonly ¼ to 1 in., embedded in an olive-drab hard tightly cemented medium-grained sandstone matrix; sparse angular to rounded quartzite pebbles and granules; some brown dense fine-grained brittle hard claystone pebbles; yielded one poorly preserved clam shell 2 in. long and 1¼ in. from umbo to margin, one small lizard? scute, and one tooth of *Leptoceratops*	0-3
5. Sandstone, gray to tan, coarse-grained, massive to crossbedded; forms lower part of relatively smooth bare slope that merges with a cliff; contains sporadic highly rounded quartzite pebbles; lenses of lead-gray soft blocky claystone	47
Offset 1,800 ft. north-northwest on base of unit 5 to bare northeast-facing exposure for underlying units.	
4. Conglomerate, tan; with red and gray quartzite roundstones most abundant; a few as much as 1 ft in diameter; lens of conglomerate near base and between sandstone layers thins from 10 to 2 ft in a horizontal distance of 10 ft, and underlying sandstone thickens from 1 ft where conglomerate is thickest to 5 ft where conglomerate is thinnest; this lowest conglomerate tongue grades into sandstone of underlying unit 3 about 25 ft south of line of section; uppermost 5 ft of unit is about half sandstone and half conglomerate	67
3. Sandstone, brown, crossbedded; with black grains concentrated along bedding planes; forms smooth bare face	37
Lower part of Pinyon Conglomerate	226–229

Approximate contact between Pinyon Conglomerate and Harebell Formation. Areal relations indicate that this contact is marked by an unconformity, but the underlying Harebell Formation is so badly slumped here that the contact is nowhere exposed. It is put at the top of the covered interval because in this general area the Pinyon Conglomerate is commonly more resistant, is better exposed, and consists almost entirely of conglomerate except for the basal sandstones, whereas the Harebell Formation here contains very few and very thin conglomerates (major conglomerates begin to appear, however, short distances to the west and southwest). Large slump areas develop characteristically on the soft claystones of the Harebell but only a few develop on the Pinyon. Offset 1,500 ft southeast for underlying beds.	
Harebell Formation (upper part):	
2. Covered interval; probably underlain by soft drab claystone and siltstone and lesser amounts of sandstone	200±
1. Claystone, dark-greenish-gray, hard, blocky; bare of vegetation; sparse but varied mollusk fauna of high- and low-spired gastropods and small ribbed pelecypods; contains fresh-water clams *Eupera* and *Sphaerium*; fresh-water snails *Valvata?*, *Bellamya*, *Reesidella*, *Cleopatra tenuicarinata* (Meek and Hayden), *Micropyrgus?*, and *Bulinus?*; and the land snails *Grangerella?* and an indeterminate form (USGS colln. M2889; D. W. Taylor, written commun., Jan. 11, 1967)	4
Thickness of measured part of Harebell Formation	204±

AGE OF PINYON CONGLOMERATE ON PINYON PEAK AND TIMING OF ADJACENT TECTONIC EVENTS

The presence of *Leptoceratops* in the lower part of the Pinyon Conglomerate forces a review of the Paleocene age that was previously assigned to the formation in the area of its principal reference section. Three possible interpretations are: (1) the strata are post-Cretaceous in age, but the dinosaur tooth was redeposited from older rocks; (2) the specimen represents a dinosaur that survived from Cretaceous into Paleocene time; and (3) the specimen is truly indicative of a Late Cretaceous age for at least the lower part of the Pinyon Conglomerate at the locality of the principal reference section.

The interpretation that *Leptoceratops* was redeposited from older rocks can be dismissed as invalid, because redeposited bones and teeth that have traveled more than a mile are invariably rounded and worn, especially in an environment of conglomerate deposition. Sharp cutting edges such as those on the specimen discussed here are never preserved, and the flat surface of the crown surely would not have survived without damage (the observed imperfection was incurred in the process of collection) had the tooth been reworked.

There is no evidence that the tooth was transported in a protecting fragment of sandstone reworked from the Harebell. Other sandstone fragments of similar type would be expected, and none was observed. Such relatively soft material could not have survived long in the high-energy environment that transported the quartzite roundstones to this area. Furthermore, paleocurrent directions that are indicated in the lower part of the Pinyon Conglomerate show that streams flowed east-northeasterly in this area (Lindsey, 1970). Had *Leptoceratops* been derived from older Cretaceous rocks, the only likely source within several miles would have been the west flank of the Washakie Range (fig. 1), and streams from it would have had to flow westward toward Pinyon Peak. No data are available, at present, to indicate a westward flow.

The possibility of the dinosaur being of Paleocene age appears unlikely because no evidence is conclusive as yet for the existence of Paleocene dinosaurs anywhere in the world. All examples so far suspected as being of Paleocene age have been explained satisfactorily as reworked specimens, misidentifications, or occurrences in strata that have been miscorrelated.

It seems most likely that the strata containing the *Leptoceratops* tooth are of latest Cretaceous age. This means, therefore, that the unconformity between the Pinyon Conglomerate and Harebell Formation (fig. 1; Love, 1956, and unpub. data) in the Pinyon Peak area is not synchronous with the Tertiary-Cretaceous time boundary but is somewhat older and reflects an intra-Cretaceous episode of tectonism and erosion.

The unconformity is important, because it documents the first major uplift of the Washakie Range and the development of the Buffalo Fork thrust fault along the west margin of the range. The magnitude of the unconformity is illustrated by sections *A–A′* and *B–B′* (fig. 1), located 3 miles apart. Section *A–A′* shows near parallelism of the Pinyon and Harebell. Section *B–B′* shows gently dipping Pinyon resting on slightly overturned Harebell. Regional mapping (J. D. Love, unpub. data) demonstrates that this relationship is an unconformity rather than a fault contact. Thus, between deposi-

tion of the Harebell Formation and that of the Pinyon Conglomerate, the Washakie Range rose, was shoved westward along the Buffalo Fork thrust fault, and the core was deeply eroded. In places where the Buffalo Fork thrust fault was not subsequently modified, the dip of the fault plane is 25°–30° E. In post-Miocene time the Washakie Range subsided several thousand feet along a normal fault whose trace is parallel to, and in places coincident with, that of the thrust fault (J. D. Love, unpub. data).

SYSTEMATIC DESCRIPTION

Class REPTILIA

Order ORNITHISCHIA

Suborder CERATOPSIA

Family PROTOCERATOPSIDAE

Genus LEPTOCERATOPS Brown, 1914

Material.—AMNH (American Museum Natural History) collection 2571, a right upper posterior cheek tooth (fig. 2).

Locality and stratigraphic position.—The locality is approximately 7,500 feet east-southeast of VABM triangulation station 9705 on Pinyon Peak, Mount Hancock 15-minute quadrangle, Teton County, Wyo. The stratigraphic position is approximately 150 feet above the base of the Pinyon Conglomerate. This horizon is shown graphically on figure 1, and the lithology is described in unit 6 of the principal reference section of the Pinyon Conglomerate.

Description.—Single-rooted ceratopsian right upper posterior cheek tooth with shearing surface inclined, not vertical. Basal lingual enamel remnant well developed and must have served as a stop against which the lower cheek teeth wore. Buccal enamel wall curved, finely crenulated, exhibiting prominent posterior and posterobuccal crests which tended to both strengthen the tooth and also increase its shearing efficiency. Faint indications of wear grooves for reception of adjacent cheek teeth. Replacement not of the battery type. Maximum height, root to crown apex, 24.6 mm. Anteroposterior length at right angles to axis of root, 11.3 mm. Width, at base of crown, 11.0 mm. These measurements are somewhat smaller than those of most cheek teeth of the type specimen of *Leptoceratops gracilis,* but in protoceratopsids the size of cheek teeth increases with the age of the individual. If referred to *Montanoceratops,* whose teeth have still not been found, this specimen would probably have to be an immature individual.

Remarks.—AMNH specimen 2571 has been compared with teeth of all the ceratopsians from which teeth are known in the American Museum of Natural History collections. Generally, descriptions of dinosaur teeth in the literature either have been sketchy or tooth orientations were confused, or upper teeth were misidentified as lower teeth and vice versa (for example, Brown, 1914). Also, good illustrations of excellent material have been reproduced at scales inadequate for the portrayal of dental details (for example, Sternberg, 1951). Of all the ceratopsians, the Pinyon specimen most closely resembles, in morphology, the American protoceratopsids, in particular *Leptoceratops gracilis. Montanoceratops* is excluded from the comparisons because its teeth are unknown. *Protoceratops* (Granger and Gregory, 1923) and *Microceratops* (Bohlin, 1953) represent the Protoceratopsidae in the Late Cretaceous of Asia. *Montanoceratops* (Sternberg, 1951), from the lower part of the early Maestrichtian St. Mary River Formation near Buffalo Lake, Mont. (Gilmore, 1939, p. 2; Brown and Schlaikjer, 1942), and the small hornless genus *Leptoceratops,* from the late Maestrichtian upper part of the Edmonton Formation of Alberta and from other Maestrichtian localities, represent North American lineages of the same family. A third, little-known American protoceratopsid occurs in the Campanian Two Medicine Formation of Montana (Gilmore, 1939, p. 1; Sternberg, 1951, p. 228). *Montanoceratops* is somewhat similar to *Protoceratops* but may have had teeth more like those of *Leptoceratops.*

Leptoceratops is only distantly related to *Triceratops* and its allies (Sternberg, 1951; Ostrom, 1966), and in several ways is more primitive than either *Protoceratops* (perhaps Cenomanian to Santonian) or *Montanoceratops* (early Maestrichtian), yet *Leptoceratops* occurs in the upper part of the Edmonton Formation of Alberta, above the Kneehills Tuff (Sternberg, 1947, 1951; D. A. Russell, 1967, p. 7–8; L. S. Russell, 1964). Undescribed *Leptoceratops*-like material from the Maestrichtian Lance Formation of Park County, Wyo., is currently under study by J. H. Ostrom at Yale University. Brown's (1914) original statement that the type specimen of *L. gracilis* came from 400 feet above the base of the Edmonton Formation has been refuted by Sternberg (1947, 1951), who documented the position of the type in the upper beds of the Edmonton.

The Kneehills Tuff was originally dated (Ritchie, 1960) by the potassium-argon method as 70 x 10^6 years B.P. (Before Present), but this has been revised to 66 x 10^6 years B.P. by Shafiqullah (manuscript, quoted in Srivastava, 1966, p. 499). In

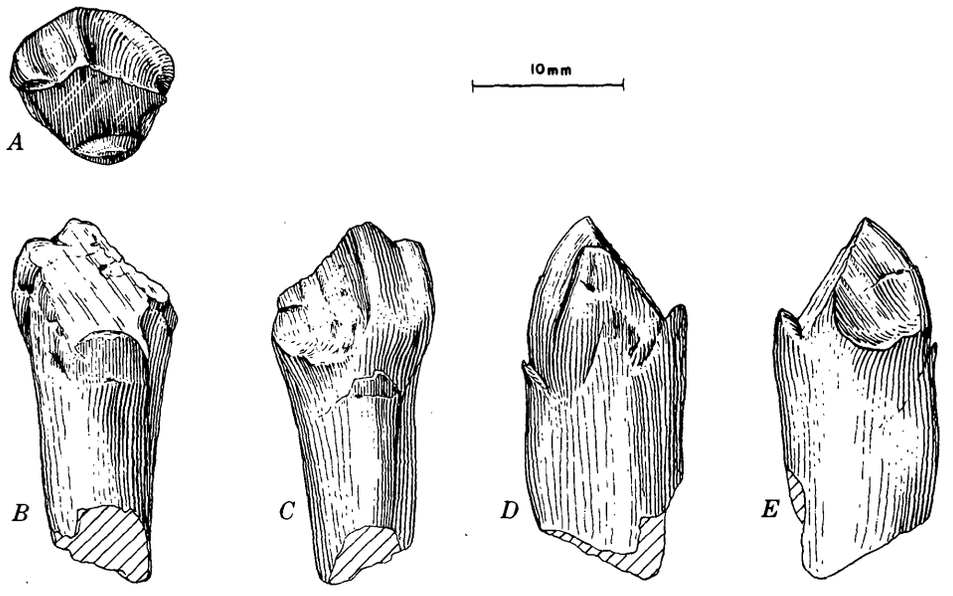

FIGURE 2.—Right upper cheek tooth of *Leptoceratops* sp., AMNH 2571, from an intraformational limestone pebble conglomerate bed 150 feet above the base of the Pinyon Conglomerate, Pinyon Peak, Teton County, Wyo. *A*, occlusal view; *B*, lingual view; *C*, buccal view; *D*, posterior view; *E*, anterior view. Although damaged during collection, the specimen shows no evidence of rounding abrasion that would be characteristic of rolled specimens reworked from older deposits.

Alberta, therefore, the known occurrence of *Leptoceratops* seems to be confined to the late Maestrichitian, just prior to the early Paleocene.

American protoceratopsids that have teeth closely similar to those of *Leptoceratops* are now known to range from the Campanian (Gilmore, 1939) to the end of the Maestrichtian, but in the American Campanian form, which is unnamed, the crenulations of cheek teeth are crude as in *Protoceratops*, not fine as in the present specimen.

As noted by Sternberg (1951) and especially by Ostrom (1966), *Leptoceratops* chewed in a manner different from that of its better known contemporary, *Triceratops*. Chewing by *Triceratops* was confined to shearing action in a vertical plane, but by *Leptoceratops* it involved grinding as well as shearing action. The posterior lower cheek teeth of *Leptoceratops* possess a small buccal enamel remnant at about the level of the mandible; posterior upper cheek teeth have a similar enamel remnant lingually, and the wear surfaces are oblique. Medial and anterior cheek teeth have vertical wear (D. A. Russell, oral commun., 1970). The action of the upper upon the lower cheek teeth was quite complex, owing in part to the effects of replacement processes, but would presumably have permitted a more varied diet for *Leptoceratops* than that attributed to *Triceratops*. This, coupled with the smaller size of adults and the lack of horns, implies a habitat on relatively higher ground than was true for *Triceratops* (Sternberg, 1951, p. 226; D. A. Russell, 1967, p. 7–9). The area in Teton County, Wyo., bounded by the uplifted Washakie Range to the east, the Targhee uplift (Love and Reed, 1968) and the ancestral Teton Range to the west, and the Basin Creek uplift (Love and Keefer, 1969) 15 miles to the north-northwest in southern Yellowstone National Park, may well have been a favorable environment for the *Leptoceratops* described in this report.

REFERENCES

Bohlin, Birger, 1953, Fossil reptiles from Mongolia and Kansu: Sci. Exped. Northwest. Provinces China (Sino-Swedish Exped. Pub. 37), VI, Vertebrate Palaeont. 6, 113 p.

Brown, Barnum, 1914, *Leptoceratops*, a new genus of Ceratopsia from the Edmonton Cretaceous of Alberta: Am. Mus. Nat. History Bull., v. 33, art. 36, p. 567–580.

Brown, Barnum, and Schlaikjer, E. M., 1942, The skeleton of *Leptoceratops* with the description of a new species: Am. Mus. Novitates, no. 1169, 15 p.

Gilmore, C. W., 1939, Ceratopsian dinosaurs from the Two Medicine formation, Upper Cretaceous, of Montana: U.S. Natl. Mus. Proc., v. 87, p. 1–18.

Granger, Walter, and Gregory, W. K., 1923, *Protoceratops andrewsi*, a pre-ceratopsian dinosaur from Mongolia: Am. Mus. Novitates, no. 72, 9 p.

Hague, Arnold, 1896, Yellowstone National Park: U.S. Geol. Survey Geol. Atlas, Folio 30, 4 sheets.

Lindsey, D. A., 1970, Lithofacies and paleocurrents in conglomerates of the Harebell Formation and Pinyon Conglomerate of northwestern Wyoming: Geol. Soc. America Abs. with Programs, v. 2, no. 5, p. 341.

Love, J. D., 1947, The Tertiary stratigraphy of the Jackson Hole area, northwestern Wyoming: U.S. Geol. Survey Oil and Gas Inv. Prelim. Chart 27.

——— 1956, New geologic formation names in Jackson Hole, Teton County, northwestern Wyoming: Am. Assoc. Petroleum Geologists Bull., v. 40, no. 8, p. 1899–1914.

Love, J. D., Duncan, D. C., Bergquist, H. R., and Hose, R. K., 1948, Stratigraphic sections of Jurassic and Cretaceous rocks in the Jackson Hole area, northwestern Wyoming: Wyoming Geol. Survey Bull. 40, 48 p.

Love, J. D., and Keefer, W. R., 1969, Basin Creek uplift and Heart Lake Conglomerate, southern Yellowstone National Park, Wyoming, *in* Geological Survey Research 1969: U.S. Geol. Survey Prof. Paper 650–D, p. D122–D130.

Love, J. D., and Reed, J. C., Jr., 1968, Creation of the Teton Landscape—The geologic story of Grand Teton National Park: Moose, Wyo., Grand Teton Nat. History Assoc., 120 p.

Ostrom, J. H., 1966, Functional morphology and evolution of the ceratopsian dinosaurs: Evolution, v. 20, no. 3, p. 290–308.

Ritchie, W. D., 1960, The Kneehills Tuff: Alberta Soc. Petroleum Geologists Jour., v. 8, no. 11, p. 339–341.

Russell, D. A., 1967, A census of dinosaur specimens collected in western Canada: Canada Natl. Mus. Nat. History Papers, no. 36, p. 1–13.

Russell, L. S., 1964, Cretaceous non-marine faunas of northwestern North America: Royal Ontario Mus. Life Sci. Contr. 61, 24 p.

Srivastava, S. K., 1966, Upper Cretaceous microflora (Maestrichtian) from Scollard, Alberta, Canada: Pollen et Spores, v. 8, no. 3, p. 497–552.

Sternberg, C. M., 1947, The upper part of the Edmonton formation of Red Deer Valley, Alberta: Canada Geol. Survey Paper 47–1, 11 p.

——— 1951, Complete skeleton of *Leptoceratops gracilis* Brown from the Upper Edmonton member on Red Deer River, Alberta: Canada Natl. Mus. Bull. 123, p. 225–255.

PENDENT DIDYMOGRAPTIDS FROM NORTHERN ARKANSAS

By WILLIAM B. N. BERRY[1], Berkeley, Calif.

Abstract.—Pendent didymograptids from two localities near Smithville, Ark., include *Didymograptus artus*, *D. bifidus*, *D.* cf. *D. bifidus*, and *D. smithvillensis* n. sp. These graptolites are indicative of the *Didymograptus bifidus* zone. Shelly fossils associated with the graptolites at one locality are indicative of a latest Early Ordovician age and suggest that the *D. bifidus* zone ranges in age into the latest Early Ordovician from the earliest Middle Ordovician, with which it had previously been correlated. The pendent didymograptids from the Smithville area reveal a relatively wide range in morphologic variation that is comparable to morphologic variation observed among similar pendent didymograptids from most other localities in North America and western Europe at which they are abundant.

Pendent didymograptids have long posed difficult taxonomic problems because the range in variation among them commonly is relatively great, and at many localities many individual rhabdosomes are present that are closely similar to a group of pendent didymograptids concluded to be of a certain species yet slightly different from the species (see Decker, 1944; Berry, 1962a; Berry, 1964). Collections of pendent didymograptids from the Early Ordovician carbonate succession in the southern Ozarks near Smithville, Ark., contribute to this long-standing problem; they also contribute toward precision in correlation of Ordovician graptolite zones with series and stages based on shelly fossils.

Collections of pendent didymograptids from near Smithville, Ark., have been made over a number of years by several geologists, among them, E. O. Ulrich and C. L. Dake. In the past few years, B. F. Clardy and O. A. Wise, Jr., of the Arkansas Geological Commission, and E. L. Yochelson and the late H. D. Miser, of the U.S. Geological Survey, have examined the stratigraphic relations of the fossil-bearing beds in the area about Smithville and have collected fossils from old as well as new localities. Their collections and most of the older material obtained from the area have been examined by the author and constitute the basic data for this report. The older collections were studied by Ruedemann (1947) and also were examined by Decker (1944).

The author is indebted to O. A. Wise, Jr., and E. L. Yochelson for loaning him their graptolite collections from the Smithville area and for providing him with the results of their stratigraphic study in the area. The author thanks G. A. Cooper and E. L. Yochelson for loaning him older graptolite collections from the Smithville area and for their interpretations of the age of the shelly faunas from the area.

THE SMITHVILLE, ARK., DIDYMOGRAPTID OCCURRENCES

Wise, Yochelson, Clardy, and W. V. Bush obtained graptolites from two localities in the Smithville area. One of them is the dump of the Graceland mine, abandoned nearly half a century ago. Wise (written commun., 1970) has contributed the following information concerning this locality:

> The graptolites at the Graceland Mine locality, NW1/4 sec. 24, T. 17 N., R. 4 W., are found in the scrap forming a conical shaped dump 20± feet high and 30 to 35 feet in diameter at the base. The dump is in the center of Pine Creek Valley. Pine Creek has, during high water, cut channels at a number of places across the valley alluvium. While dumps and some ore piles are still present, the shaft of the Graceland mine has been completely obscured by gravel and debris. This situation was previously reported by E. T. McKnight in U.S.G.S. Bulletin 853, 1935.
>
> Because of this filling and lack of data on the number and depths of shafts, there is no way (other than another shaft) to determine the true stratigraphic position of the graptolite occurrence.
>
> The host rock is a very light gray to white dolomite which occurred in beds up to at least two feet in thickness as evidenced by blocks on the dump. The outcrops in the area are scanty and mostly covered by a heavy growth of brush and timber. They are chiefly in the bottom of the present stream channel and immediate banks.

[1] U.S. Geological Survey and Department of Paleontology, University of California (Berkeley).

The graptolite-bearing dolomite is considered to belong in the Smithville Formation. The following graptolites have been identified in the collections from the Graceland mine dump: *Didymograptus artus, D. bifidus, D.* cf. *D. bifidus, D. bifidus* var. *latus, D. smithvillensis, D.* sp., and *Phyllograptus* sp. (fragments similar to *P. ilicifolius*). Yochelson (written communs., 1969) indicated that graptolite collections from the Graceland mine dump have received several U.S. Geological Survey collection numbers over the years; among them are 235-CO, 6772-CO, 212B-CO, and 104P1.

Wise (written commun., 1970) has contributed the following information concerning the second locality from which he, Yochelson, Clardy, and Bush collected graptolites:

> The graptolite occurrence east of Smithville, in the NW1/4 of sec. 34, T. 17 N., R. 3 W., is in the road cut on the south side of the road at the west end of a massive sponge-bearing gray-blue limestone which weathers yellow or buff. The shale (which bears the graptolites) is siliceous and ranges in thickness up to 3 inches. For all practical purposes, the graptolites occur on a single bedding surface. On drying, the shale appears to be more of a siltstone. Parting planes disappear and the rock breaks with a subconchoidal fracture.
>
> The shale occurs between the massive sponge-bearing limestone and a tan to buff colored dolomite which overlies the shale and limestone. The shale appears to be very limited in occurrence, extending along the road cut for a lateral distance of less than fifty feet.

Yochelson (written commun., 1969) has indicated that the graptolite locality has been given U.S. Geological Survey locality number 6760-CO.

The graptolites identified in the collections from this second locality are: *Didymograptus bifidus, D.* cf. *D. bifidus, D. smithvillensis,* and fragments of a pendent didymograptid that may be proximal ends of *D. artus*. The rock unit from which these collections were obtained is the Black Rock Formation (Yochelson, written commun., 1969; Wise, written commun., 1970). Carbonates above and below the graptolite-bearing shale contain poorly preserved shelly fossils, including *Ceratopea,* that Yochelson has concluded indicate a latest Early Ordovician age (Yochelson, written commun., 1969).

Wise (written commun., 1970) has stated in regard to the stratigraphic relation between the two localities that:

> The occurrence east of Smithville is at an elevation of 350 feet while the elevation of the Pine Creek Valley at the Graceland Mine dump is 325–30 feet; and while it is not possible to follow continuous contacts from one outcrop to the other, there are no obvious structural complications. Therefore, considering the regional dip and elevation difference and the fact that the rocks at the Graceland locality came from a mine shaft of at least some depth, the two graptolite occurrences might well be separated by as much as a 200 to 300 foot stratigraphic interval, with the Smithville location being the higher of the two, and in the uppermost part of the Black Rock sequence.

The most abundant species found in the Ordovician sequence near Smithville is the pendent didymograptid *D. bifidus*. The association there of *D. artus* with *D. bifidus* is indicative of the North American *Didymograptus bifidus* zone as recognized by Berry (1960, 1967). Presently available data concerning the ranges of *D. artus* and *D. bifidus* in North America indicate that these species are restricted to the *D. bifidus* zone. That zone has been demonstrated to be present in the Marathon region, Texas (Berry, 1960), the Deepkill Shale in eastern New York (Ruedemann, 1947; Berry, 1962b), the Levis Shale near Quebec City (Hall, 1865; Ruedemann, 1947), the Garden City and Swan Peak Formations in Utah (Ross, 1951; Ross and Berry, 1963), and the Joins Formation in the Arbuckle Mountains, Okla. (Decker, 1944). Decker (1944) and Ruedemann (1947) both noted the presence of *D. artus* and *D. bifidus* near Black Rock, Ark.

Correlation of the *D. bifidus* zone in North America with the series and stages of the Ordovician based on shelly fossils is still being documented. Whittington (1968) has most recently discussed these correlations and indicated that the *D. bifidus* zone may be correlated with trilobite zone M of Ross (1951) and Hintze (1953). This correlation has been established on the presence of *D. artus* in the Swan Peak Formation in rocks bearing zone M trilobites, as well as brachiopods indicative of the Whiterock Stage of Cooper (1956), and on the presence of *D. artus* and *D. bifidus* in the Joins Formation, which also bears brachiopods indicative of correlation with trilobite zone M and the Whiterock Stage. Whittington (1968) indicated that the Ross-Hintze trilobite zones L and M are early Whiterock and thus early Middle Ordovician in age. Ross-Hintze trilobite zones J and K were concluded by Whittington (1968) to be latest Early Ordovician.

Wise and Yochelson (Yochelson, written commun., 1969) have concluded that the Smithville and Black Rock Formations are at least in part lateral equivalents. The graptolite data indicate that at least parts of both fall within the *Didymograptus bifidus* graptolite zone. The late Early Ordovician age suggested by Yochelson on the basis of the *Ceratopea* from limestones above and below graptolites indicative of the *D. bifidus* zone at the second locality cited above suggests that the *D. bifidus* zone

may range in age from latest Early Ordovician to earliest Middle Ordovician. This new evidence indicates that the Early-Middle Ordovician boundary, which is recognized on the basis of shelly fossils, may be within the *Didymograptus bifidus* graptolite zone.

NOTES ON THE DIDYMOGRAPTUS BIFIDUS GROUP

Examination of the thecal form in *Didymograptus bifidus* and specimens closely related to it and in *Didymograptus murchisoni* and subspecies of it reveals that all possess closely similar thecae. The thecae in all are curving tubes that are inclined for the greater part of their length to the stipe axis at an angle of approximately 45°. The initial parts of the thecae are inclined to the stipe axis at approximately 30°–35°, and the thecae curve markedly near their apertures to enclose a 60°–70° angle with the stipe axis. The apertural margins are straight and horizontal. Thecal overlap in mature thecae in the distal parts of the rhabdosomes is three-fourths their length or slightly more. All the rhabdosomes are pendent, and the angle ultimately enclosed by the stipes is commonly within the range 15°–50°, although the stipes become subparallel in some. These characteristics relate many pendent didymograptids which have been grouped into at least a dozen species. These species may be separated one from the other by stipe width, rate of stipe widening, thecal spacing, and size of the angle that the stipes ultimately enclose.

Many individuals and groups of individuals have been recorded (for example, the specimens cited herein as *D.* cf. *D. bifidus*) which clearly belong to this general group but which have not been specifically designated. These individual variants may be discrete phyletic entities, or they may be local variants of described species which reflect some sort of unique environmental conditions at a particular place and time. Further analysis of them is needed. The entire plexus of species, subspecies, and local variants with the characteristics described may be considered a distinct group of pendent didymograptids which may be a distinct phyletic entity itself, as phylogeny among dichograptids, including didymograptids, is unknown. Similar groups of morphologically similar species are present among didymograptids, including pendent didymograptids, suggesting that phyletic units (perhaps genera) may be distinguishable within the genus *Didymograptus* as currently used.

SYSTEMATIC DESCRIPTIONS

GLASS GRAPTOLITHINA Bronn, 1846
ORDER GRAPTOLOIDEA Lapworth, 1875
Family DICHOGRAPTIDAE Lapworth, 1873
Genus DIDYMOGRAPTUS M'Coy in Sedgwick and M'Coy, 1851

Didymograptus artus Elles and Wood

Figure 1, *d*

Didymograptus artus Elles and Wood, 1901, p. 48–49, pl. 4, figs. 6*a–d*, text fig. 30.
Didymograptus artus Elles and Wood. Berry, 1960, p. 58–59, pl. 10, figs. 2, 5, 6.
Didymograptus artus Elles and Wood. Ross and Berry, 1963, p. 85, pl. 4, figs. 10, 11.

Description.—Only broken rhabdosomes were found, the longest of which is 7 mm. The stipes diverge initially to enclose an angle of 125°–130°. They curve markedly in the proximal 2–3 mm to become subparallel. The stipes are 0.4 mm wide at the first theca on each, and they widen to 0.8–0.9 mm at 5 mm from that tneca.

The thecae number 8½ to 9 in the proximal 5 mm. They are inclined to the axis of the stipe at angles of 47°–55°. They are 2½ to 3 times as long as they are wide and they overlap one-half to three-fifths their length. The apertural margins are concave and approximately horizontal. The thecal walls curve slightly near the apertures to give the thecae a moderately mucronate appearance.

The siculae are 1.1–1.2 mm long and 0.4–0.5 mm wide at their apertures. The first theca originates from the sicula a short distance above the aperture, and the crossing-canal part of the second theca is nearly horizontal.

Discussion.—Although only broken specimens were found, the tenuity of the stipes, the close spacing of the thecae, the slight thecal curvature, and the subparallel aspect of the stipes make these Arkansas specimens closely similar to typical specimens of *D. artus*.

Figured specimen.—USNM (U.S. National Museum) 166593.

Didymograptus bifidus (J. Hall)

Figures 1, *b*, *c*, *f*; 2, *c*

Graptolithus bifidus J. Hall, 1865, p. 73–74 (in part), pl. I, figs. 16–18 (*not* pl. III, figs. 9, 10).
Didymograptus bifidus (J. Hall). Ruedemann, 1904, p. 689–692 (in part), text figs. 86, 87, pl. 15, figs. 1–3.
Didymograptus bifidus (J. Hall). Berry, 1962a.

Description.—The longest rhabdosome among the Arkansas specimens studied has stipes that are 24 mm long. The stipes diverge initially from the sicula to enclose an angle of 110°–130°, but they curve

markedly in the proximal 3–5 mm to a pendent position and to ultimately enclose an angle of 18°–25°. The stipes in the majority of the Arkansas specimens enclose an angle of approximately 20°. The dorsal margins of the stipes, after they have curved to the pendent position, are straight.

The stipes are 0.4–0.6 mm wide at the aperture of the first theca on each. They widen gradually through widths of 1.0–1.4 mm at 5 mm from the first theca to 1.6–1.8 mm at 10 mm from that theca to 2.0–2.4 mm at 15 mm from that theca. Stipe width diminishes in the distal portions after attainment of maximum width as a result of the presence of only partly grown thecae in the distal part of the rhabdosome.

Thecae number 7–7½ in the proximal 5 mm and 14–15 in 10 mm throughout the stipe. The thecae are long, slender, curving tubes which at maturity are 3½–4 times as long as they are wide. They are free nearly one-half their length in the proximal parts of the rhabdosome but are free only about one-fourth their length in the distal parts of the rhabdosome. The mature thecae in the distal part of the rhabdosome are inclined for the greater part of their length at an angle of 43°–50° to the stipe axis. The thecae are curved such that in their initial parts they are inclined to the stipe axis at an angle of 30°–35°; close to their apertures, they curve sharply to become inclined to the stipe axis at an angle of 57°–75°. The rapid thecal curvature in the apertural region gives a moderately mucronate appearance to the thecae. The apertural margins are straight and horizontal.

Siculae are 1.0–1.5 mm long and approximately 0.4–0.5 mm wide at their apertures. The first theca (Th 1^1) appears to have originated slightly above the sicula aperture and to have grown outward and slightly downward. The crossing canal appears to be approximately horizontal because the second theca (Th 1^2) appears to be at about the same level as the first (Th 1^1).

Discussion.—The Arkansas specimens of *D. bifidus* are closely similar to the types of the species as described by Hall (1865) and redescribed by Berry (1962a) from Levis, Quebec. The Arkansas specimens widen more rapidly to achieve greater stipe widths at 10 and 15 mm from the first theca than do the Levis specimens, but maximum stipe width falls within the range in variation of stipe width in the Levis specimens. The ultimate angle enclosed by the stipes in the Arkansas specimens is slightly greater in most specimens than it is in most Levis specimens, but the range in variation in this angle is similar (15°–21° in the Levis specimens, 18°–25° in the Arkansas specimens). Range in variation in other characters of the Levis and Arkansas specimens is even more closely similar.

At the Arkansas localities, as at nearly all other localities in North America and in England where *D. bifidus* has been found, a number of specimens are present that are closely similar but differ significantly in one or more characters. Specimens are present in the Arkansas collections that have thecae spaced as closely as 16–18 within 10 mm. Commonly, these specimens also have slightly greater angles between the stipes than do the specimens concluded to be *D. bifidus*. A few of the Arkansas specimens closely similar to *D. bifidus* have not only more closely spaced thecae but also slightly wider stipes. Specimens closely similar but yet not fully identical with those concluded to be *D. bifidus* have been identified as *D. cf. D. bifidus* (see fig. 2, *e, f*).

Figured specimen.—USNM 60659.

Didymograptus bifidus var. latus Ruedemann

Figure 2, d

Didymograptus bifidus (J. Hall) var. *latus* Ruedemann, 1947, p. 328, pl. 54, fig. 17.

Description.—The stipes are broken, but the longer is approximately 3 cm. The stipes diverge from the sicula initially to enclose an angle of at least 100°. They curve within the proximal 2–3 mm to become pendent and to enclose an angle of about 45°. As they appear to curve toward each other at about 16 mm from their origin, the ultimate angle enclosed by them would be less than 45°. The dorsal margins of these stipes are thus curved for a significant part of their length. The stipes widen from 0.7 mm at the first theca on each to 1.5 mm at 5 mm from that theca and to 2.8 mm at 10 mm, 3.5 mm at 15 mm, and to 3.8 mm at 20 mm from that theca.

The thecae number 14 in 10 mm. They are long, slender, curving tubes which at maturity are five times as long as they are wide. They overlap about one-half their length in the proximal part of the rhabdosome but fully seven-eighths of their length in the distal part of the rhabdosome. The mature thecae are inclined to the rhabdosome axis at a 40°–45° angle for the greater part of their length. The thecae are curved such that their initial parts make a 30°–35° angle with the stipe axis; they curve markedly close to the apertures to make a 60°–65° angle with the stipe axis. Marked thecal curvature in the apertural part gives the thecae a

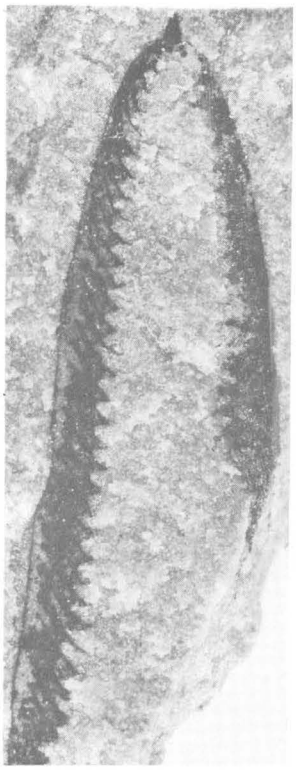

a

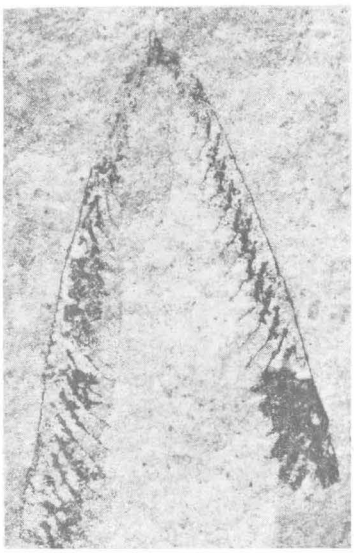

b

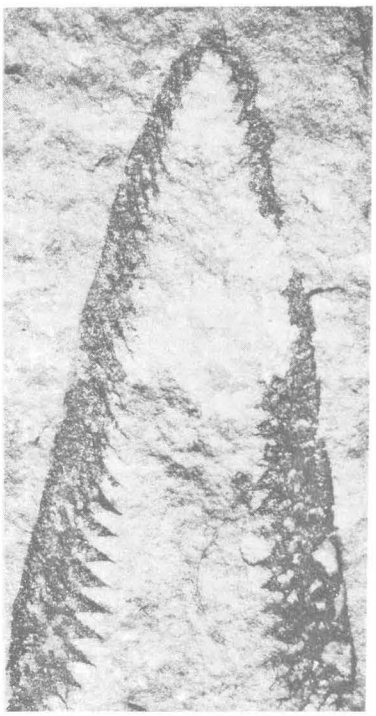

c

d

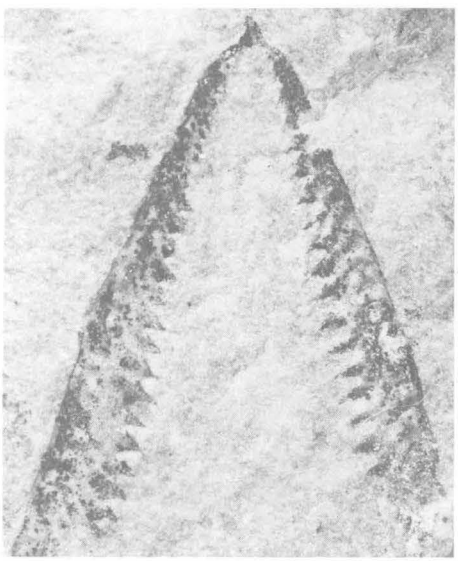

e

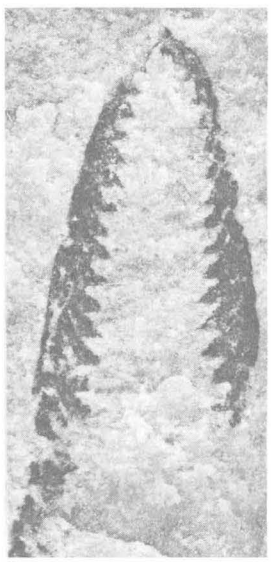

f

g

FIGURE 1.

moderately mucronate aspect. The apertural margins are straight and horizontal.

Discussion.—Only one rhabdosome has been found; it is broken at both its proximal and distal extremities, but it is unique in being relatively similar to *D. bifidus* yet more robust than any other specimen recorded that is so similar to *D. bifidus*. This specimen is similar to *D. bifidus* in thecal characteristics and spacing. The specimen differs by having a greater stipe width and in curvature of the stipes. This single specimen may represent a colony that for some reason, as for example an unusual food supply for its members, achieved a greater size than any of its relatives and so became a giant form. If it does, it probably should not be given subspecific rank. A number of stipe fragments are present in the collections from both localities cited that have size dimensions suggesting that they could have been part of rhabdosomes similar to this specimen. If a plexus of specimens similar to this did exist, then perhaps retention of the subspecific designation is warranted. Fragmentary preservation of numbers of stipes precludes reaching a definite decision concerning the taxonomic status of this individual.

The rhabdosome found is somewhat similar to *Didymograptus turneri* Decker in size and shape and in thecal shape. It differs from that species by having more closely spaced thecae and a slightly lesser angle enclosed between the stipes.

Figured specimen.—USNM 102785.

Didymograptus smithvillensis n. sp.

Figure 1, *e*, *g*; 2, *a*, *b*

Description.—The longest rhabdosomes are 15–16 mm. The stipes diverge initially from the sicula to enclose a 100°–130° angle, but they curve markedly in the proximal 4–5 mm to become straight and to enclose an angle of 35°–42°. Most commonly, the stipes enclose a 40° angle.

The stipes are 0.7–1.2 mm wide at the aperture of the first theca on each. They widen to 1.4–1.6 mm at 5 mm from that theca and to their maximum width, 2.0–2.2 mm, within 7 to 9 mm from the first theca. They maintain that width throughout most of the remainder of their extent in most specimens. The stipes in some specimens widen slightly to a maximum of 2.2–2.5 mm by 15 mm from the first theca. The stipes in the majority of the specimens studied are 1.6 mm wide at 5 mm from the first theca and 2.0 mm at 8 mm from the first theca. The stipes diminish slightly in width in their most distal parts as a result of only partially grown thecae there.

The thecae number 7–8½ in the proximal 5 mm and 14–16 in 10 mm throughout the remainder of the stipe. The thecae are slender, curving tubes. They are inclined to the stipe axis at a 40°–45° angle for the greater part of their length, but their initial parts form a 30°–33° angle with the stipe axis and their apertural parts form a 55°–65° angle with the stipe axis. The thecae in the proximal part of the rhabdosome overlap one-half their length, and those in the distal part overlap three-fourths their length. The thecae are 3½–4 times as long as they are wide. The thecal apertures are straight and horizontal.

The siculae are 1.3–1.6 mm long and 0.5–0.6 mm wide at their apertures. The first theca appears to have originated near the sicula aperture.

Discussion.—*Didymograptus smithvillensis* is similar to *D. bifidus* in general rhabdosome size and thecal characteristics. It differs from *D. bifidus* by having a slightly greater angle enclosed by the stipes and a greater rate of widening of the stipes. The stipes are not only slightly wider at the first theca than in *D. bifidus* but they achieve maximum width in only 7–9 mm from the first theca, whereas maximum stipe width in *D. bifidus* is attained no earlier than 10 mm from the first theca, and more commonly 15–20 mm from that theca. The species may be distinguished from *D. bifidus* relatively easily by the greater angle between the stipes and the more robust appearance of the proximal parts of the stipes.

The species is also similar to *D. murchisoni* var. *geminus* (Hisinger) in rhabdosome form and thecal characteristics. The ultimate angle enclosed by the stipes in this species is slightly greater than in *D. murchisoni* var. *geminus*, and the thecae are more closely spaced. Thecal overlap is also slightly greater in this species than in *D. murchisoni* var.

FIGURE 1.—Pendent didymograptids from the vicinity of Smithville, Ark. All figures × 5.
a. *Didymograptus* sp. Smithville Formation, Graceland mine dump. USNM 166590.
b, *c*, *f*. *Didymograptus bifidus* (J. Hall) Smithville Formation, Graceland mine dump.
b. USNM 166591.
c. USNM 166592.
f. USNM 60659.
d. *Didymograptus artus* Elles and Wood. Smithville Formation, Graceland mine dump. USNM 166593.
e. *Didymograptus smithvillensis* n. sp. Smithville Formation, Graceland mine dump. Paratype, USNM 166594.
g. *Didymograptus smithvillensis* n. sp. Black Rock Formation, roadcut east of Smithville. Paratype, USNM 166595.

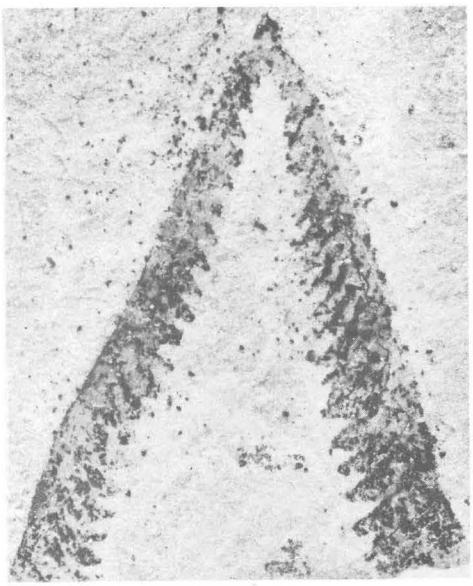

a

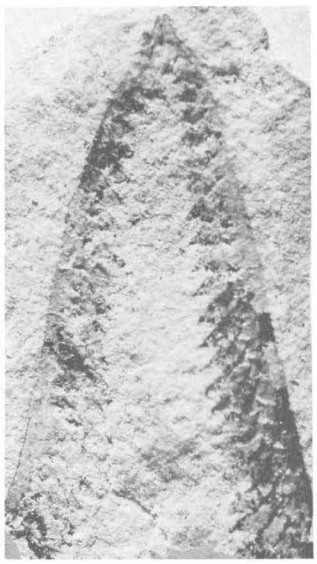

b

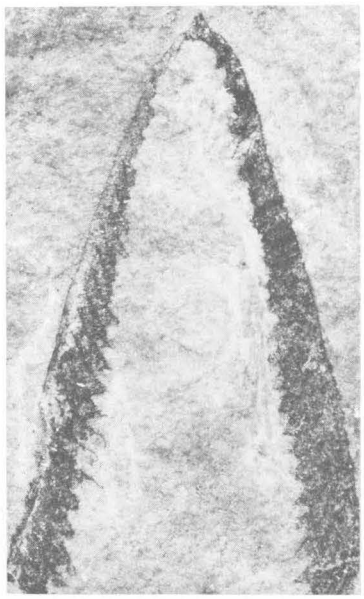

c

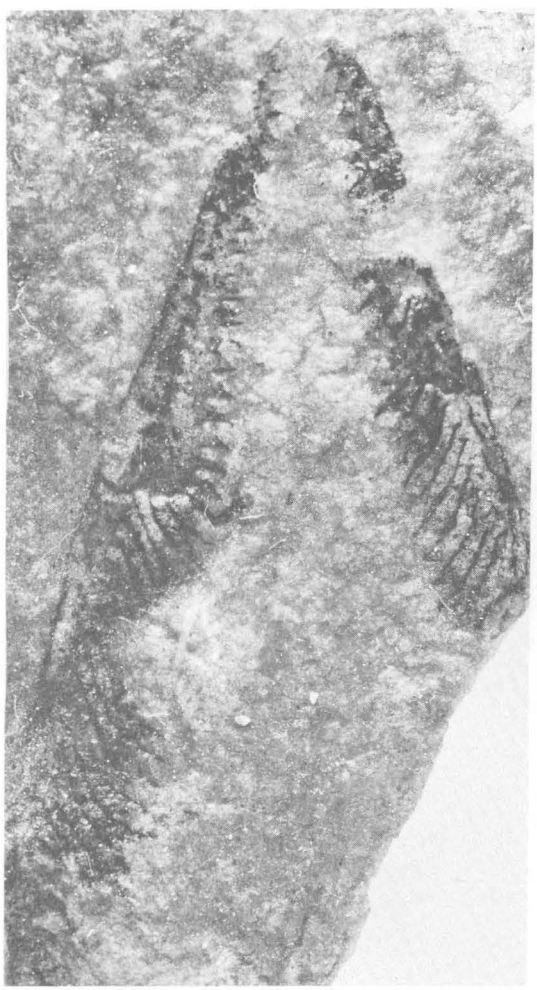

d

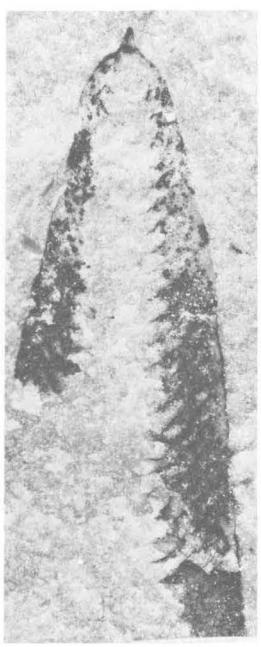

e

f

FIGURE 2.

geminus. The two are closely similar in rate of stipe widening and in maximum stipe width.

Didymograptus smithvillensis is similar in general rhabdosome form and thecal characteristics to *D. protogeminus* Decker, but it differs by having slightly narrower stipes (the stipes in *D. protogeminus* are a maximum of 2.5 mm wide) and by having stipes with straight dorsal margins that enclose a greater angle than do the slightly curving stipes of *D. protogeminus*.

The species may be separated from other pendent didymograptids described by Decker (1944), such as *D. turneri* and *D. protomurchisoni*, by its narrower stipes and more closely spaced thecae. The thecal characteristics of this species are closely similar to these characteristics in both *D. turneri* and *D. protomurchisoni*.

Holotype.—USNM 166596.

Figured paratypes.—USNM 166594, 166595, 166597.

Didymograptus sp.

Figure 1, *a*

Description.—One specimen in the collection from the Graceland mine dump has stipes that diverge initially from the sicula to enclose a 125° angle and then curve in the proximal 4–5 mm to become subparallel. The longer stipe is 20 mm. The stipes are 0.5–0.6 mm wide at the first theca, and they widen to 1.4 mm at 5 mm from that theca and to 1.5 mm at 7 mm from that theca. They remain that width throughout the remainder of their extent.

The thecae number 16 in 10 mm. They are long, curving tubes that are 3½ times as long as they are wide. They overlap one-half to three-fifths their length. They are inclined to the stipe axis at 35°–40° angles for the greater part of their length, but their initial parts make a 30°–35° angle with the stipe axis, and their distal parts form a 65°–70° angle with the stipe axis. The marked curvature of the thecae near their apertures gives them a moderately mucronate aspect. The apertural margins are straight and horizontal.

The sicula is approximately 1 mm long and 0.4 mm wide at its aperture. The first theca originated just above the sicula aperture.

Discussion.—This specimen is similar to *D. bifidus* in thecal characteristics. It differs from that species in possessing subparallel stipes, more closely spaced thecae, narrower stipes, and stipes that achieve maximum stipe width relatively quickly and then remain that width throughout the remainder of their extent. The specimen appears to be related to the *D. bifidus–D. murchisoni* group of pendent didymograptids by its thecal characteristics, but it differs from any recorded member of that group in stipe width and rate of widening.

Figured specimen.—USNM 166590.

Genus PHYLLOGRAPTUS J. Hall, 1858

Phyllograptus sp.

Description.—A few fragmentary specimens of phyllograptids have been found at the Graceland mine dump. The most complete of these indicate that the rhabdosome was at least 18 mm long and 5 mm wide. Other fragments suggest rhabdosome lengths of 13–14 mm and widths of about 4 mm.

The thecae are in contact throughout their length, and they number 14–16 in 10 mm. The thecae are curved in all but the most distal parts of the rhabdosomes studied. The thecae in all but the distal parts of the rhabdosomes form an acute angle with the rhabdosome axis initially, but they curve to become horizontal and then curve slightly downward at their apertures. The apertural margins are slightly concave. The curvature of both the thecal walls and the apertural margins gives the thecae a mucronate appearance.

Discussion.—Only a few rhabdosome fragments of phyllograptids were found. Their thecal characteristics and apparent rhabdosome size and form indicates that they are most nearly similar to *Phyllograptus ilicifolius* J. Hall. These rhabdosomes appear to have been somewhat thinner in proportion to their length than typical *P. ilicifolius*. Also, the thecae are more closely spaced than in typical *P. ilicifolius*.

Ruedemann (1947, p. 319) described *P. ilicifolius* var. *ozarkianus* from collections he had at hand from the Graceland mine dump. Ruedemann (1947, p. 319 and pl. 53, fig. 20) indicated that the thecae

---

FIGURE 2.—Pendent didymograptids from the vicinity of Smithville, Ark. All figures × 5.

a, b. Didymograptus smithvillensis n. sp Black Rock Formation, roadcut east of Smithville.
- *a*. Holotype, USNM 166596.
- *b*. Paratype, USNM 166597.

c. Didymograptus bifidus (J. Hall). Distorted specimen in which stipes show effect of being twisted from normal position. Smithville Formation, Graceland mine dump. USNM 166598.

d. Didymograptus bifidus var. *latus* Ruedemann. The only rhabdosome found of this form. Smithville Formation, Graceland mine dump. USNM 102785.

e, f, Didymograptus cf. *D. bifidus* (J. Hall).
- *e*. Smithville Formation, Graceland mine dump. USNM 166599.
- *f*. Black Rock Formation, roadcut east of Smithville. USNM 166600.

in P. *ilicifolius* var. *ozarkianus* were more closely spaced than in typical *P. ilicifolius* and that the variety was a considerably larger form. The specimens studied by the author are neither as long nor as wide as Ruedemann (1947. pl. 53, fig. 20) indicated *P. ilicifolius* var. *ozarkianus* to be. None of the rhabdosome fragments found suggest the presence of rhabdosomes as large as Ruedemann (1947, pl. 53, fig. 20) indicated for the variety *ozarkianus*.

REFERENCES

Berry, W. B. N., 1960, Graptolite faunas of the Marathon region, west Texas: Texas Univ. Pub. 6005, 179 p., 20 pls.

——— 1962a, *Didymograptus bifidus* (J. Hall)—Its lectotype, description, and occurrence: Jour. Paleontology, v. 36, p. 294–299, 2 figs.

——— 1962b, Stratigraphy, zonation, and age of Schaghticoke, Deepkill, and Normanskill shales, eastern New York: Geol. Soc. America Bull., v. 73, p. 695–718, 3 figs., 2 pls.

——— 1964, The Middle Ordovician of the Oslo region, Norway. no. 16, Graptolites of the *Ogygiocaris* Series: Norsk Geol. Tidsskr., v. 44, p. 61–170, 16 pls.

——— 1967, Comments on correlation of the North America and British Lower Ordovician: Geol. Soc. America Bull., v. 78, p. 419–428, 2 figs.

Cooper, G. A., 1956, Chazyan and related brachiopods: Smithsonian Misc. Colln., v. 127, pts. 1 and 2, 1,245 p., 269 pls.

Decker, C. E., 1944, Pendent graptolites of Arkansas, Oklahoma, and Texas: Jour. Paleontology, v. 18, p. 378–386, 1 fig.

Elles, G. L., and Wood, E. M. R., 1901–1918, A monograph of British graptolites, pts. 1–11: London, Palaeontographical Soc. 539 p., 52 pls.

Hall, James, 1865, Graptolites of the Quebec Group, *in* Figures and descriptions of Canadian organic remains, decade 2: Canada Geol. Survey, p. 1–147, pls. A, B, I–XXI.

Hintze, L. F., 1953, Lower Ordovician trilobites from western Utah and eastern Nevada: Utah Geol. Mineral. Survey Bull. 48, 249 p., 28 pls.

Ross, R. J., Jr., 1951, Stratigraphy of the Garden City Formation in northeastern Utah, and its trilobite faunas: Yale Univ. Peabody Mus. Nat. History Bull. 6, 161 p., 36 pls.

Ross, R. J., Jr., and Berry, W. B. N., 1963, Ordovician graptolites of the Basin Ranges in California, Nevada, Utah, and Idaho: U.S. Geol. Survey Bull. 1134, 177 p., 14 pls.

Ruedemann, Rudolf, 1904, Graptolites of New York. pt. 1, Graptolites of the lower beds: New York State Mus. Mem. 7, p. 457–803, 17 pls.

——— 1947, Graptolites of North America: Geol. Soc. America Mem. 19, 652 p., 92 pls.

Whittington, H. B., 1968, Zonation and correlation of Canadian and Early Mohawkian Series, *in* Zen, E-an, White, W. S., Hadley, J. B., and Thompson, J. B., Jr., eds., Studies of Appalachian geology, Northern and maritime: New York, John Wiley & Sons, p. 49–60, 2 figs.

OCCURRENCE OF THE LATE CRETACEOUS AMMONITES *DIDYMOCERAS STEVENSONI* (WHITFIELD) AND *EXITELOCERAS JENNEYI* (WHITFIELD) IN DELAWARE

By W. A. COBBAN, Denver, Colo.

Abstract.—The heteromorphic ammonites, *Didymoceras stevensoni* (Whitfield) and *Exiteloceras jenneyi* (Whitfield), are known from many localities in the western interior of the United States, but they have not been recorded outside that region. *Didymoceras stevensoni* is a helical ammonite easily identified from fragments by its sparse ribbing and an impressed area on one or two whorls. *Exiteloceras jenneyi* is loosely coiled in a plane with most or all of its whorls not in contact. This characteristic and the presence of a pair of tubercles on each rib readily identify fragments of this species. Recently five fragments of heteromorphs referable to these species were found as float by members of the Monmouth Amateur Paleontologists Society near the east end of the Chesapeake and Delaware Canal in New Castle County, Del. The fragments of *D. stevensoni* are possibly from the Marshalltown Formation, and the pieces of *E. jenneyi* may be from the Mount Laurel Sand.

Didymoceras stevensoni (Whitfield) and *Exiteloceras jenneyi* (Whitfield) are heteromorphic ammonites known previously only from the western interior of the United States. Fragments referable to these species were discovered recently in Delaware by members of the Monmouth Amateur Paleontologists Society (West Long Branch, N.J.). Why these species have not been reported elsewhere in the Cretaceous outcrops along the Atlantic and gulf coast areas is puzzling. Perhaps by drawing attention to this important discovery in Delaware, other specimens will come to light from other localities.

The present collection, consisting of two examples of *Didymoceras stevensoni* and three of *Exiteloceras jenneyi,* was kindly made available to me for study by Mr. Harold Mendryk, North Arlington, N.J. The specimens were collected by Mr. Henry Curlett, Saint Georges, Del., Mr. William Beck, Bridgeton, N.J., and Mr. Richard Heinz, River Plaza, N.J. Present plans call for the specimens to be placed in the Monmouth County Museum. Plaster casts are in the U.S. National Museum (Washington, D.C.) and in the U.S. Geological Survey's fossil collections at the Federal Center (Denver, Colo.).

Genus DIDYMOCERAS Hyatt, 1894

Hyatt (1894, p. 573) defined *Didymoceras* to include "* * * a series of forms having loose helicoid spirals, two rows of more or less irregular ventral tubercles and irregularly bifurcated costae, which also have, or appear to have, a gerontic stage with a retroversal volution, as in Nostoceras." The genotype is *Ancyloceras? nebrascensis* Meek and Hayden (1856a, p. 71), a species based on a fragment of a whorl from the Pierre Shale of South Dakota. Meek and Hayden had considerable doubt as to the proper generic placement of this fragment inasmuch as they soon assigned it to *Turrilites* (1856b, p. 280), and later Meek (1864, p. 25) assigned it questionably to *Helicoceras* and finally with doubt to *Heteroceras* (Meek, 1876, p. 480). The type specimen is in the United States National Museum (USNM 469).

Hyatt (1894, pl. 14, figs. 13, 14) illustrated a very fine specimen from the Pierre Shale of South Dakota that he considered as the "type form" of his genus *Didymoceras.* The specimen, which is in the Yale University Peabody Museum of Natural History (YPM 6093), consists of a complete adult body chamber and half of the last septate whorl. It is part of a helical spire in which the body chamber bends down and then curves back so that the aperture faces the septate coil. Ribs and tubercles are

strong on most of the body chamber, but on the phragmocone, the tubercles are very weak and the ribs are fine and numerous.

At the time *Didymoceras* was proposed, Hyatt (1894, p. 575) defined *Emperoceras* as another new genus on the basis of a very well preserved helical spire that he described as the new species *E. beecheri*. The type (YPM 6131), which came from the Pierre Shale at or near the locality of Hyatt's "type form" of *D. nebrascense*, consists of a hamitid whorl followed by two helical whorls. Ribs are numerous and every third or fourth bears two ventral tubercles of equal size. Large collections of heteromorphs from the Pierre Shale collected since the publication of Hyatt's paper reveal that Hyatt's specimens of *D. nebrascense* and *E. beecheri* represent different parts of the same species and that *Emperoceras* should be considered a synonym of *Didymoceras*. These large collections show a considerable range in variation within *D. nebrascense*. Juvenile stages are hamitid, and these hamitid whorls may lie in a plane at right angles to the axis of the helical spire (Hyatt, 1894, pl. 14, fig. 17) or at some angle to it (Scott and Cobban, 1965). The helical spire ordinarily has the whorls well separated (Hyatt, 1894, pl. 14, fig. 15; Scott and Cobban, 1965), but the spire may be depressed to such a degree that adjoining whorls may be almost in contact or actually touch each other without forming an impressed area. The drawing shown on a map by Scott and Cobban (1965) is based on many fragments of *D. nebrascense* and represents the form that most specimens tend to follow.

Didymoceras has been considered a synonym of *Cirroceras* Conrad (1868, p. 730). Conrad proposed his genus for a specimen from Arneytown, N.J., that had been described as *Ammonceratites conradi* Morton (1841, p. 109). Morton's specimen consisted of an entire crushed whorl of a helicoid ammonite. The specimen is apparently lost, but several casts were made of it before its disappearance. These casts, which are at the Academy of Natural Sciences of Philadelphia, at the National Museum (Washington, D.C.), and at the Federal Center (Denver), suggest that the original specimen was badly worn. The two rows of tubercles are barely discernible, but one row seems to have larger and fewer tubercles than the other—a condition quite unlike that of *D. nebrascense*. However, in the Late Cretaceous of the gulf coast and western interior, helicoid ammonites are present that have this asymmetric tubercle arrangement, and *Cirroceras* can perhaps be applied to them.

Didymoceras stevensoni (Whitfield)

Figures 1, *a–f, l, m;* 2

1877. *Helicoceras stevensoni* Whitfield, Preliminary report on the paleontology of the Black Hills, U.S. Geog. and Geol. Survey Rocky Mtn. Region (Powell), p. 39.
1880. *Helicoceras stevensoni* Whitfield. Whitfield, Paleontology of the Black Hills of Dakota, *in* Newton, Henry, and Jenney, W. P., Report on the geology and resources of the Black Hills of Dakota, U.S. Geog. and Geol. Survey Rocky Mtn. Region (Powell), p. 447, pl. 14, figs. 5–8.
1880. *Heteroceras? nebrascense* (Meek and Hayden). Whitfield, Paleontology of the Black Hills of Dakota, *in* Newton, Henry, and Jenney, W. P., Report on the geology and resources of the Black Hills of Dakota, U.S. Geog. and Geol. Survey Rocky Mtn. Region (Powell), p. 451, pl. 14, fig. 9; pl. 15, fig. 6.
1894. *Helicoceras stevensoni* Whitfield. Hyatt, Am. Philos. Soc. Proc., v. 32, no. 143, p. 568.
1896. *Heteroceras nebrascense* (Meek and Hayden). Gilbert, U.S. Geol. Survey 17th Ann. Rept., pt. 2, pl. 64.
1901. *Helicoceras stevensoni* Whitfield. Whitfield, Am. Mus. Nat. History Bull., v. 14, art. 16, p. 219, pls. 29, 30.
1907. *Helicoceras stevensoni* Whitfield. Chamberlin and Salisbury, Geology, v. 3, Earth history, 2d ed., text fig. 417e, f.
1910. *Helicoceras stevensoni* Whitfield. Grabau and Shimer, North American index fossils, v. 2, p. 203, text figs. 1470, 1471.
1921. *Helicoceras stevensoni* Whitfield. Grabau, A textbook of geology, pt. 2, Historical geology, text fig. 1754d.
1921. *Didymoceras? stevensoni* (Whitfield). Spath, South African Mus. Annals, v. 12, pt. 7, no. 16, p. 250.
1965. *Didymoceras stevensoni* (Whitfield). Scott and Cobban, U.S. Geol. Survey Misc. Geol. Inv. Map I–439.
1966. *Didymoceras stevensoni* (Whitfield). Gill and Cobban, U.S. Geol. Survey Prof. Paper 393–A, p. A31–A32.

The type specimen (USNM 12307) of Whitfield (1877, p. 39; 1880, p. 447, pl. 14, figs. 5–8) consists of three helical whorls that almost touch one another. Ribs and tubercles are strong and conspicuous. The spire is narrower than that of *D. nebrascense*, and the ribbing is much sparser. The retroversal body chamber of this species was illustrated by Gilbert (1896, pl. 64), as an example of *"Heteroceras nebrascense."* Whitfield (1901, pls. 29, 30) has also illustrated the body chamber. Large collections of *D. stevensoni* show that the juvenile stages consist of hamitid whorls followed by very loose helical whorls. The typical form of the species is shown in a drawing on a map by Scott and Cobban (1965). This illustration, based on many specimens, does not include the juvenile hamitid stage. The helical spire of *D. stevensoni* becomes rather tightly coiled just before the body chamber makes its downward bend, and this tightening results in an impressed area on the last one or two whorls of the spire.

Didymoceras stevensoni is known from many localities in the Great Plains region from northeastern Montana (Jensen and Varnes, 1964, p. F10) to southern Colorado (Gilbert, 1896, pl. 64; Scott, 1964). A few specimens have been found in Colorado, west of the Great Plains province, near Walden (Hail, 1968, p. 40) and near Aspen and Montrose (U.S. Geol. Survey collections).

Each of the two specimens of *D. stevensoni* from Delaware consists of less than half a whorl (fig. 1). Both are septate internal molds that have impressed areas on one side. Whorl sections are broadly rounded and a little wider than high. The specimens have rib densities of about 17 ribs per half whorl compared to the 19 on half a whorl of comparable size on the holotype. Ribs are well rounded and narrower than the interspaces. They cross the flanks and venter obliquely and disappear on the dorsum. Every other rib has one or two blunt nodate tubercles located to one side of the venter. The lack of perfect pairing of tubercles on these specimens is also described by Whitfield (1877, p. 39) for the holotype. The sutures show very clearly on the venter and flanks (fig. 2). The dorsal part of the specimens is too weathered to show the details of the internal (dorsal) lobe. Both specimens have sutures similar in complexity and form to that of the holotype (Whitfield, 1880, pl. 14, fig. 8).

The specimens were found as float on the south side of the Chesapeake and Delaware Canal just east of St. George's bridge, New Castle County, Del. The matrix attached to them is highly glauconitic calcareous clay. The specimens are possibly from the Marshalltown Formation (N. F. Sohl, oral commun., 1969). Carter (1937, p. 259) noted that the Marshalltown in Delaware consisted of very glauconitic, calcareous sandy clay, and that it could be traced in the banks of the Chesapeake and Delaware Canal eastward to one-fourth mile east of St. George's bridge.

Genus EXITELOCERAS Hyatt, 1894

In proposing *Exiteloceras,* Hyatt (1894, p. 576–577) seems to have had in mind a *Didymoceras*-like form that differed from that genus by having two tubercles on every rib. He assigned to *Exiteloceras* fragments of heteromorphs that had been described originally as *Ancyloceras cheyenensis* Meek and Hayden (1856a, p. 71), *Ancyloceras (Hamites) uncus* Meek and Hayden (1858, p. 56), and *Helicoceras angulatum* Meek and Hayden (1860, p. 176). *Ancyloceras jenneyi* Whitfield (1877, p. 42) was also assigned to *Exiteloceras* by Hyatt, who stated that the juvenile part, which was not preserved on the type, was probably helicoidal. Diener (1925, p. 88) designated Whitfield's species as the genotype of *Exiteloceras*. Large collections of *E. jenneyi* made since the publication of Hyatt's paper show that the juvenile whorls are not helical but tend to be hamitid and lie in the plane of the adult whorls (Scott and Cobban, 1965). Regarding the three species proposed by Meek and Hayden and assigned to *Exiteloceras* by Hyatt, studies in progress by G. R. Scott and me reveal that Meek and Hayden's types are parts of the body chambers of a single species readily assignable to *Didymoceras—D. cheyennense.* A restoration of this species has been presented on a map (Scott and Cobban, 1965).

Exiteloceras jenneyi (Whitfield)

Figures 1, *g–k, n–r;* 3

1877. *Ancyloceras jenneyi* Whitfield, Preliminary report on the paleontology of the Black Hills, U.S. Geog. and Geol. Survey Rocky Mtn. Region (Powell), p. 42.
1880. *Ancyloceras jenneyi* Whitfield. Whitfield, Paleontology of the Black Hills of Dakota, *in* Newton, Henry, and Jenney, W. P., Report on the geology and resources of the Black Hills of Dakota, U.S. Geog. and Geol. Survey Rocky Mtn. Region (Powell), p. 452, pl. 15, fig. 5; pl. 16, figs. 7–9.
1887. *Ancyloceras jenneyi* Whitfield. Stanton, Colorado Sci. Soc. Proc., v. 2, pt. 3, p. 185.
1894. *Exiteloceras (Ancyloceras) jenneyi* (Whitfield). Hyatt, Am. Philos. Soc. Proc., v. 32, no. 143, p. 577.
1910. *Exiteloceras jenneyi* (Whitfield). Grabau and Shimer, North American index fossils, v. 2, p. 205, text fig. 1474.
1925. *Exiteloceras jenneyi* (Whitfield). Diener, Fossilium catalogus, I, Animalia, pt. 29, Ammonoidea neocretacea, p. 88.
1957. *Exiteloceras jenneyi* (Whitfield). Wright, *in* Moore, R. C., ed., Treatise on invertebrate paleontology, Part L, Mollusca 4, p. L224, text figs. 251–7a, b, c.
1965. *Exiteloceras jenneyi* (Whitfield). Scott and Cobban, U.S. Geol. Survey Misc. Geol. Inv. Map I–439.
1966. *Exiteloceras jenneyi* (Whitfield). Gill and Cobban, U.S. Geol. Survey Prof. Paper 393–A, p. A32.

A short diagnosis of this species was presented by Gill and Cobban (1966, p. A32) as follows:

Exiteloceras jenneyi is an aberrant ammonite that has juvenile whorls as straight limbs connected by semicircular bends, and later whorls loosely coiled in a plane without contact between adjacent whorls. Ornamentation consists of moderately coarse ribs, each of which terminates in a node at the margin of the venter.

The restoration shown by Scott and Cobban (1965) was based on an examination of many specimens.

Exiteloceras jenneyi occurs at many localities in the Great Plains province from east-central Montana to northeast New Mexico. It has also been

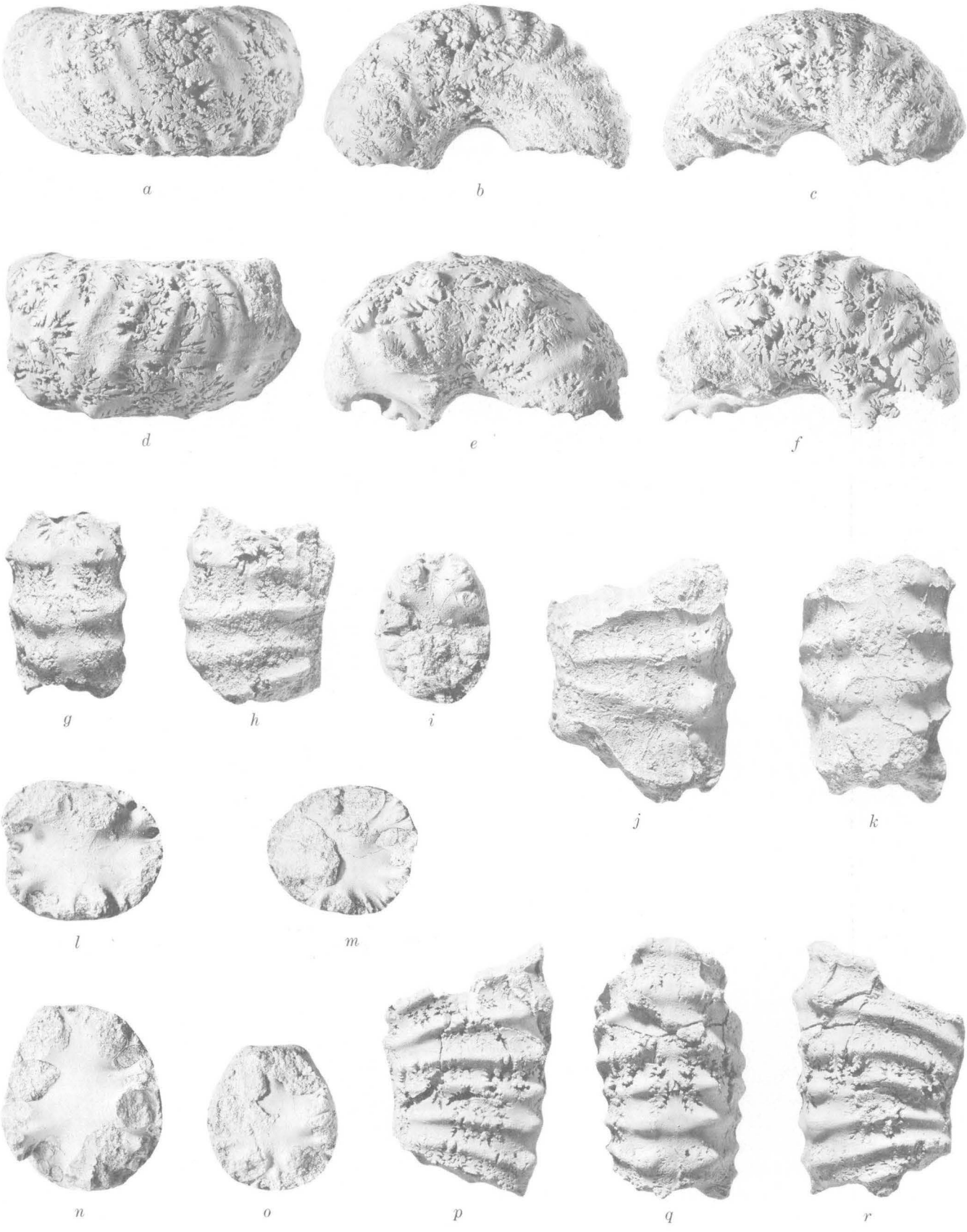

FIGURE 1.

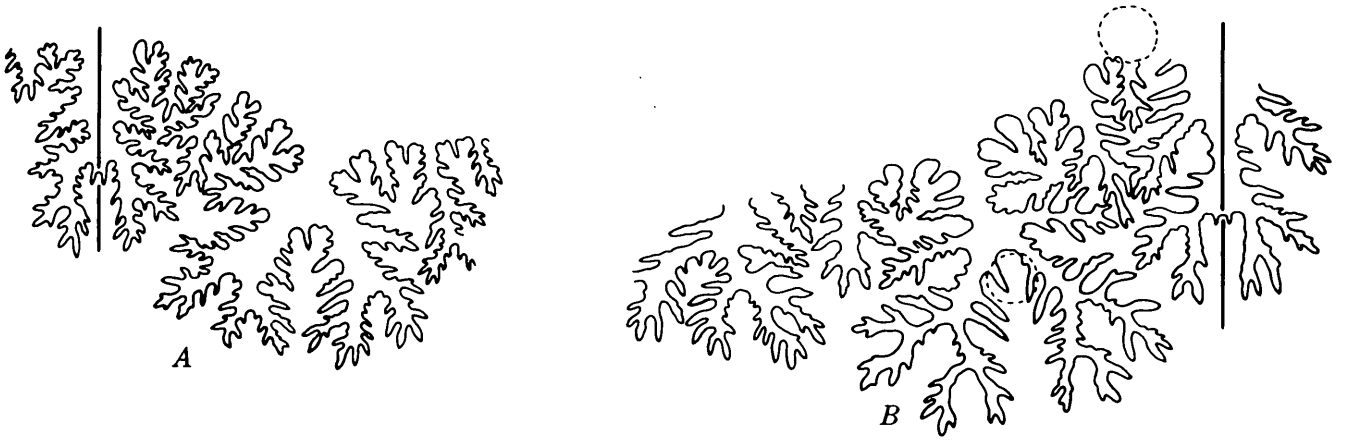

FIGURE 2.—Sutures, × 2, of *Didymoceras stevensoni* (Whitfield). The straight line marks the middle of the venter; the dashed circles show positions of tubercles. *A*, suture of specimen shown on figure 1, *a–c, m*. *B*, suture of specimen shown on figure 1, *d–f, l*.

found farther west at localities near Aspen and Montrose, Colo., and along the east side of the San Juan Basin in northwestern New Mexico.

The three fragments from Delaware are readily assignable to *E. jenneyi*. All are septate internal molds, and each is a short segment. Whorl sections are stout; they are higher than wide, with the greatest width a little below the middle (fig. 1, *i, n, o*). The venter is flattened a little and narrower than the dorsum. Flanks are very broadly rounded. The specimens are ornamented by narrowly rounded slightly rectiradiate ribs that rise into blunt tubercles at the edge of the venter. On the venter the ribs become weak and flat topped and number three to five in a distance equal to the diameter of the shell. They greatly weaken or disappear on the dorsum. The tubercles, which represent bases of spines (Scott and Cobban, 1965), are nodate and conspicuous. The suture (fig. 3) is very digitate and typical of the species (Whitfield, 1880, pl. 15, fig. 5; pl. 16, fig. 9). Lobes greatly expand from narrow bases.

The specimens were found as float on the south side of the Chesapeake and Delaware Canal just east of St. George's bridge in New Castle County, Del. The matrix attached to two of the specimens is sandy, calcareous, slightly glauconitic clay. Coarser sandstone that is noncalcareous and only very slightly glauconitic is attached to the third specimen. All specimens may have come from the Mount Laurel Sand (N. F. Sohl, oral commun., 1969), which is present on the north side of the canal east of St. George's bridge (Carter, 1937, fig. 32).

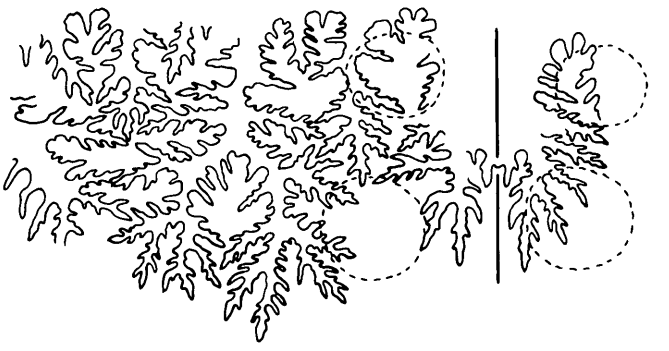

FIGURE 3.—Suture, × 2, of the specimen of *Exiteloceras jenneyi* (Whitfield) shown on figure 1, *j, k, n*.

FIGURE 1.—Specimens of *Didymoceras* and *Exiteloceras* from the south side of the Chesapeake and Delaware Canal, New Castle County, Del. All specimens natural size.
a–f, l, m. Didymoceras stevensoni (Whitfield).
a–c, m. Ventral view, two lateral views, and end view of a specimen.
d–f, l. Ventral view, two lateral views, and end view of a stouter and more sparsely ribbed specimen.
g–k, n–r. Exiteloceras jenneyi (Whitfield).
g–i. Ventral, lateral, and end views of a sparsely ribbed specimen.
j, k, n. Lateral, ventral, and end views of a large septate specimen.
o–r. End, lateral, ventral, and lateral views of a finely ribbed specimen.

REFERENCES

Carter, C. W., 1937, The Upper Cretaceous deposits of the Chesapeake and Delaware Canal of Maryland and Delaware: Maryland Geol. Survey [Rept.], v. 13, pt. 6, p. 237–281, pls. 42–46.

Conrad, T. A., 1868, Synopsis of invertebrate fossils [Cretaceous and Eocene], *in* Cook, G. H., Geology of New Jersey: New Jersey Geol. Survey, Newark, p. 721–732.

Diener, Carl, 1925, Ammonoidea neocretacea, pt. 29 *of* Fossilium Catalogus; I—Animalia, Carl Diener, ed.: Berlin, W. Junk, 244 p.

Gilbert, G. K., 1896, The underground water of the Arkansas Valley in eastern Colorado: U.S. Geol. Survey 17th Ann. Rept., pt. 2, p. 551–601, pls. 56–68.

Gill, J. R., and Cobban, W. A., 1966, The Red Bird section of the Upper Cretaceous Pierre Shale in Wyoming: U.S. Geol. Survey Prof. Paper 393–A, 73 p., 12 pls.

Hail, W. J., Jr., 1968, Geology of southwestern North Park and vicinity, Colorado: U.S. Geol. Survey Bull. 1257, 119 p., illus.

Hyatt, Alpheus, 1894, Phylogeny of an acquired characteristic: Am. Philos. Soc. Proc., v. 32, no. 143, p. 349–647, pls. 1–14.

Jensen, F. S., and Varnes, H. D., 1964, Geology of the Fort Peck area, Garfield, McCone, and Valley Counties, Montana: U.S. Geol. Survey Prof. Paper 414–F, 49 p., illus.

Meek, F. B., 1864, Check list of the invertebrate fossils of North America; Cretaceous and Jurassic: Smithsonian Misc. Colln. 177, 40 p.

——— 1876, A report on the invertebrate Cretaceous and Tertiary fossils of the upper Missouri country: U.S. Geol. Survey Terr. (Hayden) Rept. 9, 629 p., 45 pls.

Meek, F. B., and Hayden, F. V., 1856a, Descriptions of new species of Gastropoda and Cephalopoda from the Cretaceous formations of Nebraska Territory: Acad. Nat. Sci. Philadelphia Proc., v. 8, p. 70–72.

——— 1856b, Descriptions of new fossil species of Mollusca collected by Dr. F. V. Hayden, in Nebraska Territory; together with a complete catalogue of all the remains of Invertebrata hitherto described and identified from the Cretaceous and Tertiary formations of that region: Acad. Nat. Sci. Philadelphia Proc., v. 8, p. 265–286.

——— 1858, Descriptions of new organic remains collected in Nebraska Territory . . . together with some remarks on the geology of the Black Hills and portions of the surrounding country: Acad. Nat. Sci. Philadelphia, Proc. 1858, p. 41–59.

——— 1860, Descriptions of new organic remains from the Tertiary, Cretaceous, and Jurassic rocks of Nebraska: Acad. Nat. Sci. Philadelphia, Proc. 1860, p. 175–185.

Morton, S. G., 1841, Description of several new species of fossil shells from the Cretaceous deposits of the United States: Acad. Nat. Sci. Philadelphia Proc., v. 1, p. 106–110.

Scott, G. R., 1964, Geology of the Northwest and Northeast Pueblo quadrangles, Colorado: U.S. Geol. Survey Misc. Geol. Inv. Map I–408.

Scott, G. R., and Cobban, W. A., 1965, Geologic and biostratigraphic map of the Pierre Shale between Jarre Creek and Loveland, Colorado: U.S. Geol. Survey Misc. Geol. Inv. Map I–439.

Whitfield, R. P., 1877, Preliminary report on the paleontology of the Black Hills, containing descriptions of new species of fossils from the Potsdam, Jurassic, and Cretaceous formations of the Black Hills of Dakota: U.S. Geog. and Geol. Survey Rocky Mtn. Region (Powell), 49 p.

——— 1880, Paleontology of the Black Hills of Dakota, *in* Newton, Henry, and Jenney, W. P., Report on the geology and resources of the Black Hills of Dakota; U.S. Geog. and Geol. Survey Rocky Mtn. Region (Powell), p. 325–468, 16 pls.

——— 1901, Note on a very fine example of *Helicoceras stevensoni* preserving the outer chamber: Am. Mus. Nat. History Bull., v. 14, art. 16, p. 219, pls. 29–30.

PALYNOLOGY OF SOME UPPER QUATERNARY PEAT SAMPLES FROM THE NEW JERSEY COASTAL PLAIN

By LESLIE A. SIRKIN[1]; JAMES P. OWENS; JAMES P. MINARD, and MEYER RUBIN, Garden City, N.Y.; Beltsville, Md.; Washington, D.C.

Abstract.—Upper Quaternary peaty samples from the New Jersey coastal plain were analyzed for radiocarbon age and pollen content. The oldest sample (older than 38,000 years) contains deciduous and coniferous pollen and may have been deposited during the Sangamon Interglaciation. The next oldest sample (26,800 years) has a similar pollen spectrum and may correlate with the Farmdale Stade. Pollen of several other samples may be compared with the late-glacial pollen zones to the north. One sample (16,700 years) has a pollen spectrum that suggests correlation with the herb pollen zone (subzone W). A second sample (13,200 years), and the lower and middle parts of a third sample (13,680 and 12,330 years), contain pollen spectra that may correlate with subzone T3. The upper part of the third sample has pollen that indicates transition to the spruce pollen zone. The fourth sample (10,770 years) contains pollen dominated by pine and spruce which provides a minimum date for the close of the spruce pollen zone (subzone A4). The time-transgressive nature of the pollen zones is suggested by the early age of occurrence of the zones when compared with their counterparts in southern New England. The youngest samples are dated at 5,100, 3,900, and 2,760 years B.P. The pollen spectra represent subzones C1 and C2 of the oak pollen zone.

Comprehensive pollen stratigraphic studies in New England and southern New York (Ogden, 1965; Sirkin, 1967a, b) have provided the basis for reconstruction of late Quaternary environments in the Northeastern United States. Investigation of the region immediately south of the terminal moraines has been limited (see Martin, 1958; Potzger and Otto, 1942; Potzger, 1952). As a result of renewed interest in geological mapping of the area by the U.S. Geological Survey, surface and subsurface samples containing organic matter were obtained largely from the New Jersey coastal plain for radiocarbon dating and pollen analysis. These samples have yielded ages that cover a greater time span during the late Quaternary than has been typical of samples from the region north of the moraine. In addition, the study area lies between the better studied glaciated areas of southern New York and New England and the unglaciated areas of the Southeast in Virginia and North Carolina and thus can yield important information on chronology, rate of forest migrations, and environments during the Pleistocene.

SAMPLE LOCATION, DESCRIPTION, AND AGE

Nine samples were obtained at several localities in the New Jersey coastal plain, mainly in the vicinity of Trenton, N.J. (fig. 1). Five samples were collected from surface bogs and four within stream alluvium.

The sedimentary sections from which the samples were collected range in lithology from deposits containing coarse carbonaceous debris, as in samples CO 49, CO 149, TW 21, BR 12, TE 24, and DC 1, to deposits in which the carbonaceous matter is comminuted, as in samples CA 6, SH 29, and TW 74. Only one sample was collected from each section, except at locality 5 (fig. 1), where channel samples of the bog were taken (sample SH 29).

Radiocarbon analyses were made at the Washington, D.C., laboratory of the U.S. Geological Survey on the carbonaceous matter in each deposit. The ages obtained are listed in figure 2. Most of the deposits yielded finite ages in the range from 2,760 to 26,800 years B.P. (before present, arbitrarily defined as 1950), or from "classical" Wisconsin through Holocene time. One sample (DC 1) yielded an age greater than 38,000 years. Field relations

[1] Adelphi University, Garden City, N.Y.

suggest correlation of this deposit with the Cape May Formation, which is considered to be Sangamon in age (Richards and Judson, 1965). The pollen and spores from this deposit, therefore, provide an opportunity to compare a flora from an interglacial time (Sangamon) with the flora that existed during the Wisconsin Glaciation.

The spatial relations of the sampled deposits near Trenton are shown in figure 3. In this area, carbonaceous matter is associated with a number of lithic units that occur at different elevations. Many of the deposits are surface bogs, and their use in stratigraphic studies is limited. It should be noted that the pollen zones associated with the deposits are based on pollen content, whereas the finite ages for each sample are considered in correlating these zones with those of other areas. Vegetational and climatic trends are suggested within the context of the pollen and radiocarbon data, even though it is acknowledged that such reasoning is tentative where only individual samples are available (Emery and others, 1967). The consistency of the late Quaternary pollen record throughout the region, however, indicates that the palynology of the samples does reflect climatic changes during late-glacial and postglacial time.

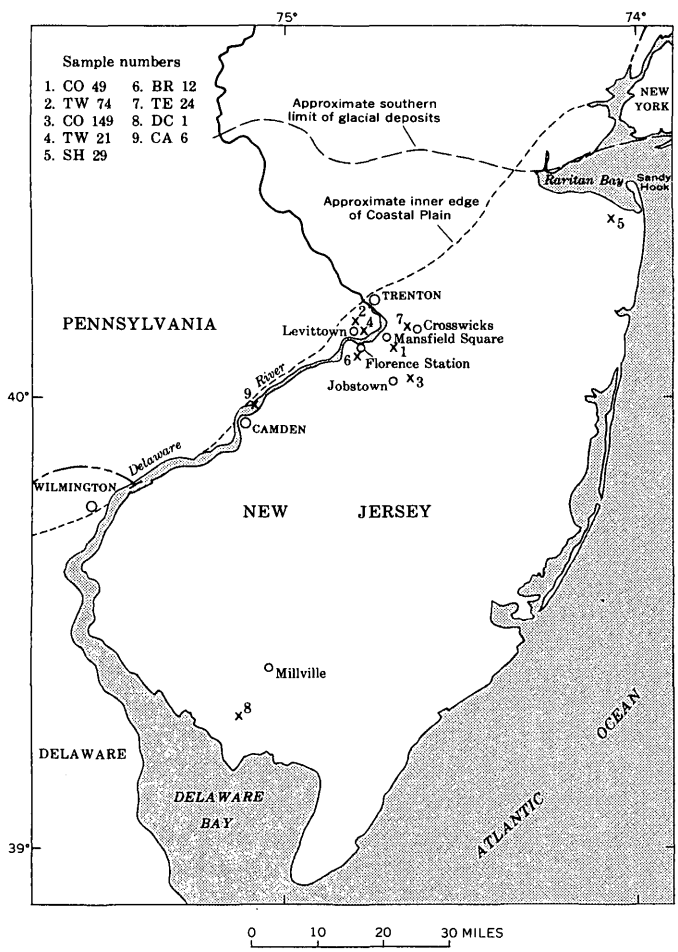

FIGURE 1.—Map showing approximate locations of samples discussed in text.

LABORATORY METHODS

The samples, which were generally of low organic content (that is, 10 percent organic material), were processed by standard laboratory techniques for pollen extraction. Also, the coarse sedimentary fraction was inspected for larger microfossils. Estimates of total pollen were made from the pollen counts of 10-gram sediment samples in order to derive relative pollen frequencies. This provides a rough approximation of pollen sedimentation in the whole sample and an idea of the sedimentary environment. The pollen diagram (fig. 4) was computer generated (Sirkin and Grossman, 1967) and includes arboreal pollen, nonarboreal pollen, and spores. Associated microfossils are mentioned in the text. Percentages of the pollen of the Betulaceae, *Alnus, Salix,* the Ericaceae, Rosaceae, and *Sambucus* are included in the arboreal pollen columns and in the total arboreal pollen percentages in the pollen diagram because the shrubs were not differentiated from the trees in all families. Pollen of nonarboreal, nonwoody, and herbaceous plants are included in the nonarboreal pollen columns. Botanical and common names for the plant taxa appear on the pollen diagram, although only common names are used in the text. The designation "T.J.C." in figure 4 stands for the genera *Thuja, Juniperus,* and *Chamaecyparis.*

For radiocarbon analysis, each sample was pretreated in the conventional manner by boiling in acid and alkali. The washed and dried sample was then combusted and converted to acetylene gas, and its C^{14} activity was counted twice in duplicate gas proportional counters. Dates are reported in years (before present), using the old Libby half-life of 5,570 years with no correction for initial atmospheric variations.

SAMPLE DISCUSSION

Sample CO 49

Sample CO 49, dated at 2,760±300 years B.P. (W–1196),[1] was collected from a bog exposed on the east bank of a small north-flowing creek, 0.1 mile east of State Route 69 and 1.4 miles southeast of Mansfield Square, N.J. (fig. 1). The bog is approximately 5 feet thick and overlies the Englishtown Formation of Late Cretaceous age. The Eng-

[1] Radiocarbon samples throughout this paper are numbered with the prefix "W" denoting that the analyses were made in the radiocarbon laboratory of the U.S. Geological Survey in Washington, D.C.

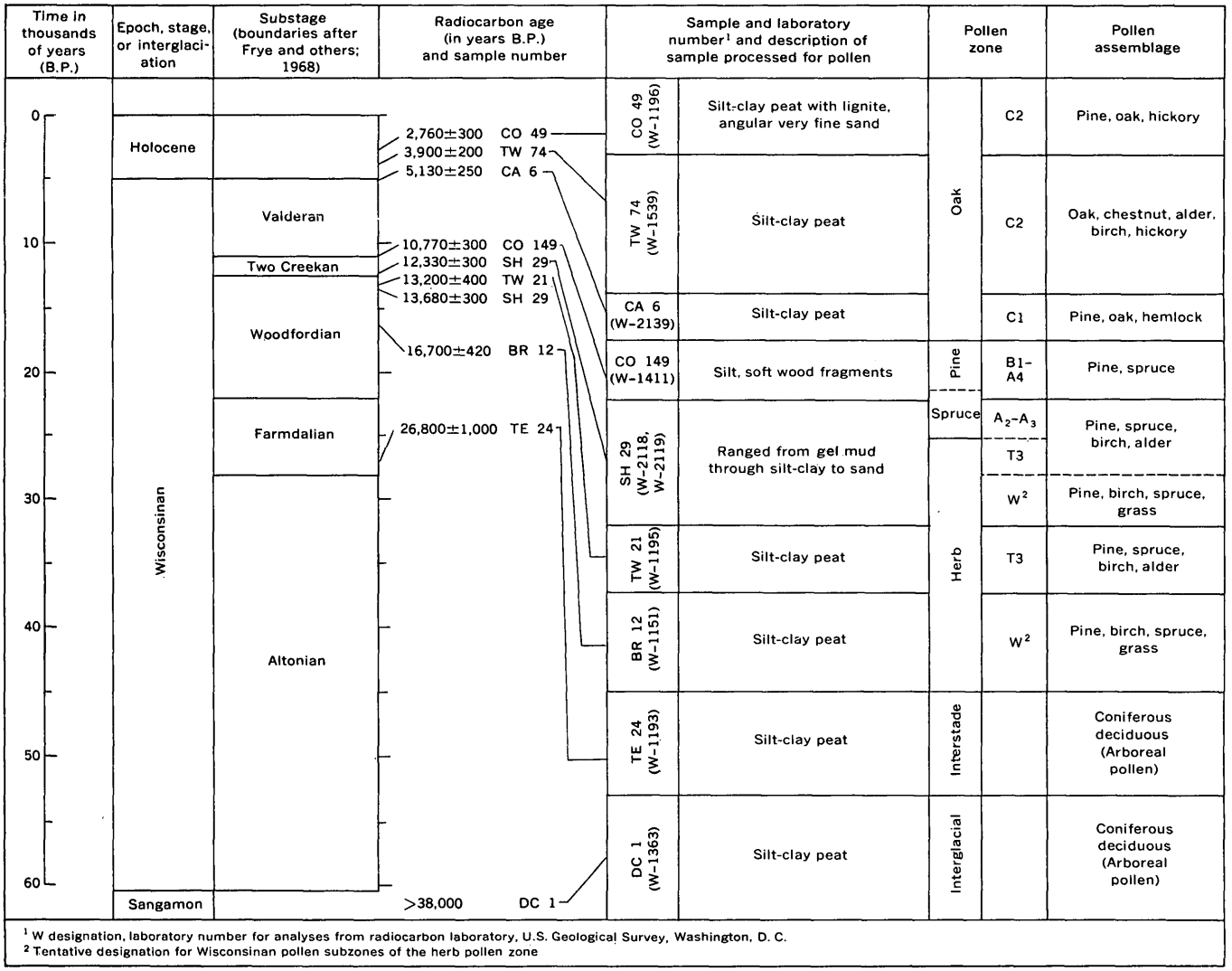

[1] W designation, laboratory number for analyses from radiocarbon laboratory, U.S. Geological Survey, Washington, D. C.
[2] Tentative designation for Wisconsinan pollen subzones of the herb pollen zone

FIGURE 2.—Sample ages and pollen zones and assemblages plotted within the stage-substage scheme proposed by Frye, Willman, Rubin, and Black (1968).

lishtown in this area contains abundant coarse carbonaceous matter, and the lower part of the bog deposits may contain some reworked Englishtown material. For this reason, only the upper 1 foot of the bog was sampled. The sample is an oxidized organic silt-clay peat containing lignite and very fine angular quartz grains. The lignite in this sample was not processed for pollen and spores because it was reworked Cretaceous lignite containing Cretaceous pollen and spores. For radiocarbon analysis, fibrous to granular peat was processed and picked clean of any contaminating lignite. The sediment yielded a total of 91 pollen grains (76 of arboreal pollen, 15 of nonarboreal pollen) and 71 spores, not including fungus spores (fig. 4). The arboreal pollen assemblage accounts for 83 percent of the pollen, and it consists mainly of pine, oak, hickory, alder, birch, and willow pollen. The nonarboreal pollen assemblage consists of grass, sedge, and composite pollen.

The pollen spectrum of pine, oak, and hickory is similar to spectra in the upper part of the pollen diagrams from the Pine Barrens of New Jersey (Potzger, 1952). The pollen assemblage in Sample CO 49 suggests the presence of an oak-pine forest (Braun, 1950) with hickory and other deciduous trees and a climate similar to the present climate in southern New Jersey. The age (2,760 years) of the sample and its geographic location enable correlation with the C2 subzone of the oak pollen zone (fig. 2), a zone characterized by a pollen assemblage of oak and hickory (Deevey, 1958). The high number of *Isoetes* spores (60 of 71 spores recorded) and the fineness of the sediments suggest deposition

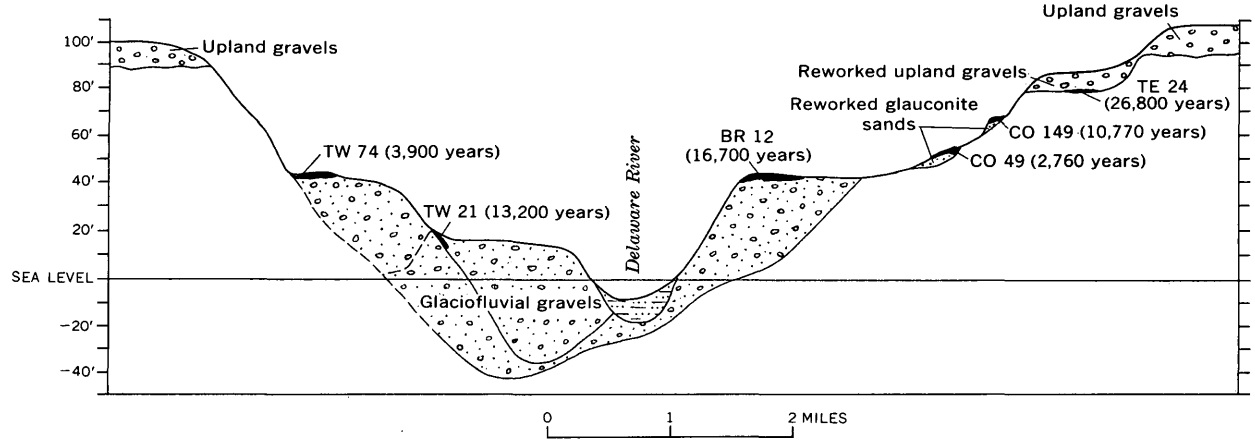

FIGURE 3.—Generalized cross section of Quaternary sediments near Trenton, N.J., showing distribution and age of carbonaceous deposits (black) and the type of alluvium with which each is associated.

in an aqueous environment. The relatively low number of pollen grains per cubic centimeter may indicate a drained marsh rather than a closed bog environment.

Sample TW 74

Sample TW 74, dated at 3,900±200 years B.P. (W–1539), is a borehole sample from the basal part of a 10-foot deep bog near Levittown Parkway in Levittown, Pa. (fig. 1). The boring was made on the east side of the parkway, 0.4 mile north of the junction of the parkway and Mill Creek Road. At this locality, the bog overlies 23 feet of glaciofluvial sands and gravels of Pleistocene age.

The silt-clay peat sediments yielded a pollen spectrum dominated by the arboreal pollen (86 percent) of mainly deciduous trees, including oak, chestnut, birch, hickory, and alder (fig. 4). The nonarboreal pollen is represented mainly by pollen of cattail and grass. Spores of *Sphagnum* and *Isoetes* are numerous.

High proportions of oak and chestnut pollen, along with pollen of birch, hickory, and other deciduous trees, indicate an oak-chestnut forest, similar to the modern forests of the eastern Appalachian region (Braun, 1950; Whitehead, 1965). The age of the dated peat sample (3,900 years) suggests a time correlation with the C2 subzone of the oak pollen zone in areas to the north. Chestnut largely replaces hickory in the pollen spectrum of this sample. The depositional environment is interpreted as a closed or poorly drained bog or an alder thicket on the basis of: (1) a high proportion of alder pollen and the presence of pollen of grass, heath, and cattail, and spores of *Sphagnum* and *Isoetes*; (2) a pollen frequency exceeding 12,000 grains per cubic centimeter; and (3) the high-clay content of the sample.

Sample CA 6

Sample CA 6, dated at 5,130±250 years B.P. (W–2139), is a borehole sample obtained 57 feet below the surface of the Delaware River, and therefore below mean sea level, near Camden, N.J. (fig. 1). The radiocarbon date was run on disseminated fine pieces of wood. The pollen percentages indicate a pollen assemblage slightly different from that of the 3,900-year-old sample (TW 74) and suggest affinities with subzone C1 of the oak pollen zone (figs. 2 and 4).

Sample CO 149

Sample CO 149, dated at 10,770±300 years B.P. (W–1411), was collected from the basal part of a 5-foot-thick bog exposed along the banks of Annaricken Creek, 1.3 miles east of Jobstown, N.J., and 0.1 mile southeast of State Route 537 (fig. 1). The bog overlies the Mount Laurel Sand of Late Cretaceous age. Most of the bog consists of dark, fine-grained sediments, but logs several feet long are present. The radiocarbon date was determined on a piece of log.

The sample is composed of an organic silt with numerous fragments of soft wood, probably pine. It contains a very high proportion of pine pollen (83 percent or 122 grains) and small amounts of pollen of spruce, hemlock, grass, and of *Isoetes* spores (fig. 4). The number of pollen grains and spores concentrated from a 10-gram sample is relatively low: 140 arboreal pollen, 6 nonarboreal pollen, and 17 spores.

The pollen content of sample CO 149 indicates affinities with subzone B1 of the pine pollen zone, and (or) A4 of the spruce pollen zone as suggested by: (1) the age of the sample; (2) the predominance (122) of pine pollen grains, of which

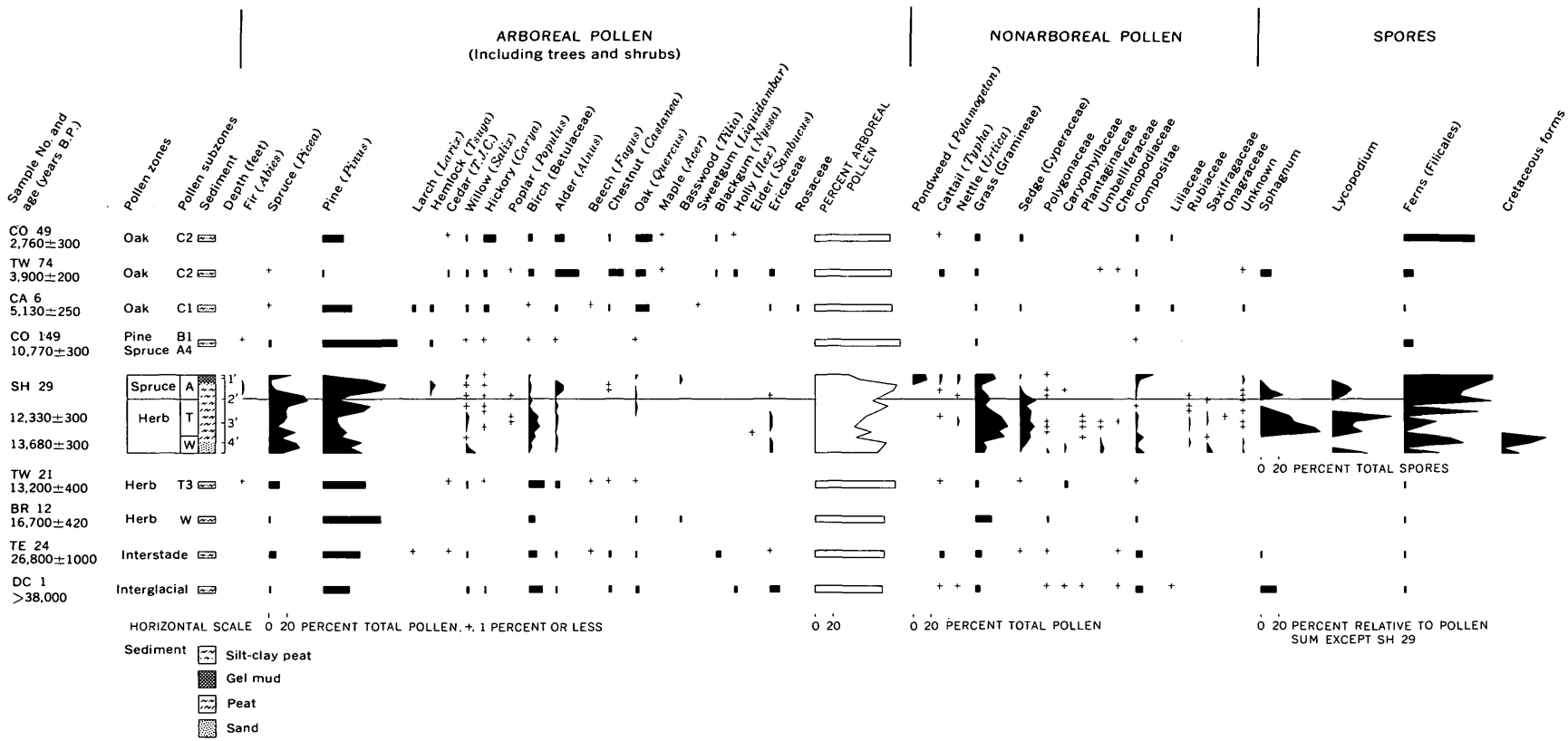

FIGURE 4.—Pollen diagram of samples discussed in text.

110 are mainly large-size pollen grains and only 12 grains are small ($<45\mu$) and of the type associated with jack pine (Davis, 1958; Martin, 1958) and red pine (Whitehead, 1965); (3) the presence of spruce and hemlock pollen, because spruce characteristically decreases, and hemlock increases after subzone A4; and (4) the apparent time-transgressive nature of the forests and the pollen zones during glacial recession (Whitehead, 1965). The pine pollen zone began in southern New England about 8,500 years B.P. (Deevey, 1958), but it has been demonstrated to have begun approximately 9,500 years B.P. in Long Island (Sirkin, 1967a) and in southeastern Pennsylvania (Martin, 1958). The presence of numerous large fragments of soft wood in the organic silt of the sample may indicate (1) a fairly dry or alternately wet and dry environment of deposition such as a drained marsh or a tidal area rather than open water, although indications of saline water are lacking; and (or) (2) a warm dry climatic episode. Because the wood is pine, the subzone B1 (pine pollen zone) designation may be confirmed through the correlation of macrofossil evidence (wood) with the pollen data.

Sample TW 21

Sample TW 21, dated at 13,200±400 years B.P. (W–1195), was collected along a drainage ditch east of the electrical substation on Gable Hill Road in Levittown, Pa. (fig. 1). The peaty bed sampled for pollen analysis is about 1 foot thick and occurs beneath about 8 feet of interbedded glaciofluvial gravels and sands which fill a small abandoned channel. The sample from this bed is mostly a silt in which both comminuted carbonaceous matter and small twigs are present. It contains a pollen spectrum dominated by pine, birch, spruce, and alder (fig. 4) and a high relative pollen frequency (12,000 grains per cubic centimeter). The arboreal pollen represents 90 percent of the pollen, and very few spores are present. The testaceous rhizopod, *Assulina,* was present.

This pollen spectrum is similar in many respects to the birch park-tundra spectrum of subzone T3 of the herb pollen zone of southern New England (Deevey, 1958). Subzone T3 has also been recorded in a pine-spruce-birch pollen spectrum from the Wallkill Valley in southeastern New York (Connally and Sirkin, 1967) and may be present in the basal part of a section in northwestern New Jersey (Niering, 1953). However, the low representation of the nonarboreal pollen, which includes pollen of grass, Caryophyllaceae, and Compositae, may be more typical of environments associated with boreal forests or spruce parklands than a park-tundra. The silty peat of this sample, the high pollen count, the *Isoetes* spores, and the rhizopod, *Assulina,* suggest a closed wet bog as the site of deposition.

Sample SH 29

Samples from the SH 29 section were collected along a drainage ditch cut into a bog 2.0 miles east of Middletown, N.J., and 0.15 mile south of Highlands Road (fig. 1). The bog overlies the Mount Laurel Sand of Late Cretaceous age. Two radiocarbon ages were obtained from peat samples of this bog: one sample, from the base of the section, is dated at 13,680±300 years B.P. (W–2119); the other, from the middle of a 3.5-foot peat bed exposed in the ditch, is dated at 12,330±300 years B.P. (W–2118).

A sedimentary section, approximately 4.5 feet thick and composed of 0.5 foot silt, 3.5 feet mossy peat, and 0.5 foot gel mud from base to top was sampled at 3-inch intervals for pollen analysis. The late-Wisconsin-age (12,330 to 13,680 years) pollen spectra fall into at least three and perhaps four assemblages or zones. In the basal silts, pine and spruce pollen are prevalent, and there is an arboreal pollen maximum of nearly 80 percent. A grass-sedge-shrub pollen assemblage having a nonarboreal pollen maximum of 56 percent typifies the central parts of the peat section. This is overlain by the spruce-pine zone, which is similar to the basal pollen sequence. A pine zone occurs near the top of the bog and is succeeded by a spruce zone (fig. 4). Thus the section illustrates the cyclic character of the flora during this time: spruce-pine zone, followed by the herb pollen zone, then a return to the spruce-pine zone. The two peaks of *Sphagnum* (fig. 4) also suggest two layers of peat growth.

The upper gel mud, which contains pollen of aquatic plants such as pondweed and cattail, may have been deposited in a postglacial lake. The absence of a Holocene oak pollen zone indicates that the section has been truncated.

The pollen spectra in this section (fig. 4) appear to incorporate much of the late-glacial pollen record and can be correlated with the pollen zones in the glaciated region to the north. The spectrum of the basal silts, predominantly spruce-pine but containing lesser amounts of grass, willow, and Ericaceae pollen, is similar to the spectra recorded in subzone W and correlative pollen zones in the end moraines region of eastern North America (Sirkin, 1967b). These zones and the correlative spectra at SH 29

suggest that a park-tundra environment existed in the vicinity of the moraines before 14,000 years B.P. The term "park tundra" is used for the late-glacial botanical setting throughout this region and is based on a high representation of spruce and pine pollen along with pollen of plants that are commonly found in tundra vegetation. It has been shown by Sirkin (1967b) that pollen spectra of this type (having arboreal pollen percentages exceeding 50 percent) are generally found below pollen spectra in which the nonarboreal values exceed 50 percent. Though pollen of true subarctic tundra plants is not consistently found, pollen of related plant families has been identified in both microfossil and macrofossil finds in eastern North America (Ogden, 1965). It should be further noted that although precise models or modern analogs of each biologic community that might have existed during the Pleistocene are as yet not available, those workers who are involved in such problems commonly speculate on possible environments as indicated by the pollen record. Thus, it seems reasonable to believe that very cold climatic conditions were associated with the Pleistocene glaciation in the vicinity of the end moraines in eastern North America, that tundra vegetation existed in that region, and that the pollen record reflects the botanical setting that existed during the Pleistocene when the deposits in question were laid down.

The nonarboreal pollen-dominated pollen spectra of the central part of the peat bed and the corresponding radiocarbon age indicate a correlation with the herb pollen zone. This zone existed in southern New York and New England during recession of the glacier from the end moraines during late Wisconsinan time (Deevey, 1958; Connally and Sirkin, 1967; Sirkin, 1967b).

The upper spruce-pine zone in section SH 29 correlates well with the spruce pollen zone of southern New York, particularly subzones A2–A3. The uppermost pine maximum in the pine profile probably represents the upper A subzone, because the pine peak is succeeded by a spruce return at the top of the spruce profile.

The duration of the herb pollen zone indicates that deposition was concurrent with glacial advance to the terminal moraine position during late Wisconsinan time. If the basal sediments are outwash from this glacial advance, then the variety of nonarboreal pollen in this zone may be the result of tundralike conditions near the glacial front. The spruce and pine pollen was probably derived from nearby stands of these trees to the south and east.

Sample BR 12

Sample BR 12, dated at 16,700±420 years B.P. (W–1151), was collected from the basal part of a surface bog exposed in a small sandpit 1.3 miles southeast of Florence Station, N.J., and 0.15 mile north of U.S. Route 130 (fig. 1). The bog is lens shaped and has a maximum thickness of 3 feet. The bog fill is fine-grained sediment and has carbonaceous matter concentrated in the basal 1 foot. The bog overlies approximately 40 feet of glaciofluvial sands and gravels of Pleistocene age.

This partly oxidized silt-clay-peat sample contained very few pollen grains (35 arboreal pollen and 10 nonarboreal pollen), one pteridophyte spore, two fungus spores, and one Cretaceous spore (fig. 4). Such sparse pollen content may indicate either a lack of vegetation or the destruction of pollen in the sample by oxidation. The former possibility seems more likely because most of the pollen grains counted were well preserved, which indicates that complete oxidation did not take place. The pollen spectrum is dominated by pine and includes grass and birch. This assemblage resembles the basal spectra of the herb pollen zone sediments in section SH 29 (as previously discussed), in Long Island (Sirkin, 1967a), and in southeastern Pennsylvania (the "F" subzones of Martin, 1958). The absolute ages of the Long Island and southeastern Pennsylvania sediments have not been established, but they should be greater than 15,000 years B.P., the radiocarbon ages of the oldest herb pollen zone sediments in southern New England (as listed in Davis, 1965). Differences in pollen representation and relative number may be attributed to the difference in sites of deposition and distance from the ice front. The herb pollen zone sediments in Long Island were deposited in kettle lakes on glacial drift after the recession of the glacier from the Harbor Hill moraine. The relative pollen frequency per cubic centimeter of the Long Island bog samples is two to three times higher than that of sample BR 12, which was probably deposited in more open drainage.

A high representation of the pollen of deciduous trees in the pollen spectrum at BR 12 would be expected because this site is about 20 miles from the nearest drift border. However, it is not uncommon for occasional pollen grains of oak, for example, to appear in herb pollen zone spectra from sites within the glacial margin.

The similarity of the pollen records suggests a correlation of the pollen spectra in sample BR 12

with the herb pollen zone from sites at the glacial margin. The correlation and the radiocarbon age of the sample (16,700±420 years B.P.) help confirm the greater than 17,000 years age postulated for the beginning of the pollen record in Long Island and for the inception of glacial recession from the end moraines (Harbor Hill episode). The pollen spectrum in sample BR 12 also helps to substantiate the existence of glacially controlled environments and associated tundralike vegetation in this region in late Wisconsinan time. Additional support of the presence of tundra near the drift border in New Jersey is the presence of pollen spectra of pine, spruce, and fir from sediments 15,000 to 16,000 years old in Virginia, and small-sized pine pollen, spruce and "northern" ferns in glacial-age sediments from North Carolina (Whitehead, 1965). This data implies cold conditions and boreal forests with "northern" vegetational elements as far south as North Carolina.

Sample TE 24

Sample TE 24, dated at 26,800±1,000 years B.P. (W–1193), was collected in a gravel pit on the north side of the Bordentown-Crosswicks Road, 0.2 mile west of Crosswicks, N.J. (fig. 1). The sample came from a thin lenslike dark carbonaceous deposit that occurred between an overlying yellow gravelly sand and the underlying Woodbury Clay of Late Cretaceous age. The sample is predominantly silty clay with peat colored dark gray by abundant fine-grained carbonaceous matter. The radiocarbon date was determined from pieces of wood, some as much as 1 foot long, which are common in this deposit. This organic matter has a high relative pollen frequency (12,000 grains per cubic centimeter) and a pollen assemblage dominated by arboreal pollen (more than 77 percent). There is also a diverse nonarboreal pollen representation (fig. 4).

The arboreal pollen is represented mainly by pollen of pine (42 percent of the pollen), spruce, birch, alder, and willow, and a variety of deciduous trees such as black gum, chestnut, and oak. The nonarboreal pollen includes that of Compositae, grass, chenopod, and sedge. Spores of *Sphagnum* and the pteridophytes are also present. Two size ranges are present for both pine and birch. Approximately half the pine pollen consists of the small-size ($< 45\mu$) pollen grains. The small-size ($< 20\mu$) birch pollen grains are the most abundant of the birch-type pollen found. These size determinations suggest the presence of cold-climate species of pine and birch (after Davis, 1958; Martin, 1958).

The pollen assemblage in sample TE 24 appears to include a mixture of pollen from quite different vegetational and climatic regimes. The presence of such cold-climate indicators as spruce and the small-size pine and birch pollen in association with willow, alder, Ericaceae, and a variety of nonarboreal pollen might indicate the persistence of glacially controlled environments at that time. However, pollen of the large-size pine and the deciduous hardwoods, particularly black gum, suggests that pine and deciduous hardwood forests may have been close by.

The mixture of such diverse forest elements in the pollen record may be interpreted to mean that both cold-climate and temperate-climate assemblages of plants existed in close proximity. The site of deposition may have been within the ecotone between these forests. This situation implies that a major change was taking place in forest type, which in turn suggests that a major climatic change was taking place. With only one sample available for analysis, it is impossible to tell whether the trend was one of cooling or warming. However, there is close agreement in age between Sample TE 24 (26,800±1,000 years B.P.), the Farmdalian peats (Frye and others, 1968), and the Plum Point interstadial of the Great Lakes region. On the basis of the time correlation with the Farmdalian record, this sample would appear to represent conditions during glacial advance in late Altonian time. Deposition of the reworked upland gravels which overlie the sample may have taken place during fluvial downcutting to a new lower base level associated with glaciation of late Altonian age. Additional time-stratigraphic control may be inferred from the age of a peat underlying the Titusville Till of White and Totten (1965) in western Pennsylvania. That peat, dated at 31,400 ± 2,100 years B.P., indicates a late Altonian age for the Titusville Till.

Sample DC 1

Sample DC 1, dated as older than 38,000 years B.P. (W–1363), was collected in the large sandpits of the National Glass Sand Co. 8.4 miles southwest of Millville, N.J., and 0.5 mile west of State Route 555 (fig. 1). The sample was collected from a surface bog, more than 20 feet thick, which overlies the Cohansey Sand of Miocene(?)-Pliocene(?) age. Most of the section consists of fine carbonaceous matter, but logs several feet long are present in the lower part of the bog. The dated sample, consisting of a stump and the sample that was examined for pollen and spores, came from the lower part of the

bog. Again, no sequence of samples was available for pollen analysis.

The sample is an organic silt-clay peat containing abundant pollen (about 12,000 grains per cubic centimeter). The pollen assemblage is composed of 80 percent arboreal pollen, mainly pine and birch, and a representation of spruce and of the deciduous trees such as oak, chestnut, holly, hickory, willow, and alder (fig. 4). Pollen of the Ericaceae is abundant and is included in the arboreal pollen. The nonarboreal pollen consists mainly of the composites and grasses. Spores of *Sphagnum* are numerous. The presence of two sizes of pine pollen and two sizes of birch pollen in association with spruce, alder, and willow pollen indicates a cold-climate plant assemblage, whereas the pollen of the various hardwoods indicates the temperature of oak-hickory forests.

The mixture of deciduous and coniferous pollen indicates the proximity of two forest types and a climatic change in progress which could have occurred near the beginning or the end of an interstadial or an interglacial episode. Thus, possible correlations with either the Port Talbot and St. Pierre Interstadials (mid-Altonian time) or the Sangamon Interglaciation might be suggested. The proximity of this sample to the type locality of the Cape May Formation suggests a Sangamon age.

Because the sample age is beyond the range of radiocarbon dating, comparison of the pollen content with the existing record is open to some speculation. On the basis of pollen stratigraphy, the DC 1 sample may possibly be correlated with the following samples of early Wisconsinan or greater age:

1. The Port Talbot Interstadial beds, dated at 47,500 years. As interpreted from the pollen evidence, these beds contain a three-part (subarctic, boreal, subarctic) climatic sequence (Dreimanis, 1960).
2. The Don and Scarborough Beds of Toronto, possibly of Sangamon Interglaciation and St. Pierre Interstadial ages, respectively. The Don Beds contain deciduous forest elements indicating the temperate climate of an interglacial, but there are no cold-climate indicators in the sequence preceding this pollen assemblage. The Scarborough Beds contain a pollen assemblage of a boreal forest, mainly conifers with few hardwoods (Terasmae, 1960).
3. The lower Wisconsin peats at Otto, N.Y., bracketed by ages of 52,000 years B.P. (minimum) and 63,000 years B.P. (Muller, 1964). These peats contain spruce-pine forest pollen with some open-meadow (sedge, grass, and composite) pollen. This section predates the Port Talbot, postdates the Sangamon, and may correlate with the Scarborough beds.
4. A peat from Fernbank, near Ithaca, N.Y., dated as older than 52,000 years. The pollen from Fernbank is similar to the pollen of the Don Beds (Bloom, 1966).
5. Magog River Beds, Quebec (Dr. Barry McDonald, oral commun., 1966). The peats (analyzed by Sirkin after collecting samples with McDonald in 1966) contain evidence of a boreal forest and park tundra. This is shown in the pollen spectrum by the arboreal pollen (54 percent of the pollen) which is represented by two sizes of pine pollen, hemlock (hemlock leaves were also found in the peat), spruce, two sizes of birch, willow, and alder, and by the nonarboreal pollen which is represented by grass, sedge, cattail, chenopods, and the Carophyllaceae, and spores of *Sphagnum* and pteridophytes. This sample is dated as older than 41,500 years and is correlated by McDonald (oral commun., 1966) with the St. Pierre peat (61,500 years B.P.).
6. Walker Cypress Swamp deposit from Washington, D.C. (Knox, 1962) which has been cited as an interglacial (Sangamon?) deposit. The pollen spectra, mainly oak, grass, pine, cedar, and hickory, indicate a climate similar to or warmer than that of today. Pollen of all these plants, except cedar, is found in significant quantities in sample DC 1.
7. Gardiners Clay, from eastern Long Island, for which a Sangamon age has been indicated. MacClintock and Richards (1936) suggest correlation of the Gardiners with the Cape May Formation on the basis of faunal evidence, mainly mollusks and Foraminifera. Donner (1964), who also ascribes a Sangamon age to the Gardiners Clay, shows a three-part, cold-warm-cold, alternation of pollen spectra, having a coniferous assemblage in the spectra of the upper and lower parts and a deciduous pollen spectra in the middle part of the Gardiners Clay.

CONCLUSIONS

Pollen analysis of organic silts and peats from surface bogs and alluvium in the New Jersey coastal plain indicates that varied environments existed in this area during the Sangamon Interglaciation and Wisconsinan Stage of the Pleistocene and the succeeding postglacial interval (fig. 2).

Sample DC 1 (>38,000 years B.P.) is from the lower part of an upper Pleistocene bog which developed in a closed depression on an older (Tertiary?) nonglaciated surface. The bog's preserved vegetational record reflects significant climatic changes, such as increased rainfall, as well as higher ground-water levels and subsequent bog development. The formation of a bog 20 feet thick indicates that cool-moist conditions persisted for a long period of time. The pollen spectrum indicates existence of a mixed deciduous and coniferous forest during deposition of the sampled interval. Neither the pollen data nor the >38,000 year date limit the age of this sample. Comparison of its pollen spectrum with existing radiocarbon-dated pollen samples from northeastern North America suggests that the bog developed during the Sangamon Interglaciation or a mid-Wisconsin interstade.

A similar mixed deciduous and coniferous forest was also present at 26,800 years B.P. (sample TE 24), during the major Wisconsinan substage, the Farmdalian. The age of the sample in this case would indicate early Farmdalian time if compared with the record in Illinois. The mixture of deciduous and coniferous pollen in this sample suggests a transition from a park-tundra or boreal forest to a deciduous forest during a mid-Wisconsinan substage. Because the sediments lie well below the level of the high-level gravels (fig. 1), the TE 24 gravels may reflect stream downcutting resulting from a drop in sea level associated with the advance of the Altonian Age ice sheet.

The BR 12 bog near the present Delaware River developed on glaciofluvial sands and gravels about 16,700 years ago. This bog is particularly interesting because it was deposited during the late Wisconsinan maximum low stand of sea level. The low stand of sea level has been correlated with a maximum continental glaciation as interpreted from the sea-level curve of Milliman and Emery (1968). The pollen and spores in the bog indicate possible tundralike vegetation and cold climatic conditions south of the glacial margin in New Jersey at this time.

The pollen spectra of the other younger samples are readily correlated with the established pollen record in the Northeastern United States and indicate a general amelioration of the climate. The late-glacial and postglacial pollen assemblages compare closely with the pollen zones in southern New England (Deevey, 1958) and with the late-glacial pollen zones in southern New York (Sirkin, 1967a). Late-glacial correlations may also be made with the pollen spectra described by Whitehead (1965) in the Chesapeake Bay region particularly with the pine-spruce-birch-alder spectra of Woodfordian Age (fig. 2) and with pollen spectra in the Carolina bays, where full-glacial time is represented by spruce-pine-fir-birch spectra indicative of boreal forests. The transitional nature of the vegetation from New Jersey, which is between the glacial margin to the north and the established forests to the south, is indicated by the mixing of pollen of both deciduous and coniferous assemblages. This relationship, if correctly interpreted, adds support to the concept of broad forest migrations (as reviewed in Whitehead, 1965). The forests have been highly sensitive to the major fluctuations of the ice margins. The data from the New Jersey peat samples provide a link between the known pattern of tundra migration to the north and forest migration to the south. This is particularly well demonstrated by the data from samples SH 29 and BR 12, which have a mixture of tundra and boreal (spruce-pine) vegetal types. The study of these samples confirms the existence of tundralike vegetation prior to 16,700 years ago, and also confirms the minimum age for the Harbor Hill episode at about 17,000 years B.P.

Analysis of the duration of pollen zones, based on radiocarbon-dated zones, indicates the rapidity of forest migration (table 1) and permits an inference as to rate of glacial recession from the glacial terminus into southern New England.

The herb zone plant assemblage indicates that tundralike conditions persisted near the glacial margin, while the ice was in the vicinity of the end moraine. Relative agreement for the duration of this zone indicates the relatively slow retreat of the ice into southern New England. The relatively short duration of the spruce zone in New Jersey may indicate the narrow width of this zone by late-Wisconsinan time and the compression of the zone by the

TABLE 1.—*Duration of pollen zones, in years, in southern New England and in New Jersey*

Pollen zone	*Southern New England*	*Central New Jersey*
Oak (C)	6,000	5,770
Pine (B)	2,500	5,670
Spruce (A)	5,000	1,560 (maximum)
Herb (T, W)	4,000	4,439 (minimum)

rapid advance of the pine and oak forests from the south and east. Because climates were progressively warming at this latitude in the early stages of glacial recession, pine and oak probably invaded the spruce forests rather rapidly. The situation in New York and New England is the subject of current work of G. G. Connally and Sirkin (unpub. data). Thus, in the absence of C^{14} ages for the end-moraine deposits, the duration and rate of migration of the herb and spruce zones provide a scale to which glacial recession may be related.

The pine zone appeared much earlier in New Jersey than in the moraine region of New England and persisted much longer. Again, climatic variations because of latitudinal differences between New Jersey and southern New England are the presumed cause rather than the persistence, or readvance, of the ice sheet. The duration of the spruce, pine, and oak zones in the regions discussed depends on gradual climatic change, the three zones being initially arranged from north to south. The pine zone, however, did not appear in southern New England until the glacial margin was well north of that region. Finally, the oak zone seems to have persisted in equal length of time in both regions.

REFERENCES

Bloom, A. L., 1966, Fernbank—A rediscovered interglacial deposit near Ithaca, N.Y.: New York Glaciogram, v. 1, p. 18.

Braun, E. L., 1950, Deciduous forests of eastern North America: Philadelphia, Blakiston Co., 596 p.

Connally, G. G., and Sirkin, L. A., 1967, The Pleistocene geology of the Wallkill Valley, *in* New York State Geol. Assoc., Guidebook to field trips, 39th Ann. Meeting, New Paltz, N.Y., 1967: New York, New York State Univ., City College, Dept. Geology, p. A1–A21, G1–G3.

Davis, M. B., 1958, Three pollen diagrams from central Massachusetts: Am. Jour. Sci., v. 256, no. 8, p. 540–570.

——— 1965, Phytogeography and palynology of northeastern United States, *in* Wright, H. E., Jr., and Frey, D. G., eds., The Quaternary of the United States: Princeton, N.J., Princeton Univ. Press, p. 377–401.

Deevey, E. S., Jr., 1958, Radiocarbon-dated pollen sequences in eastern North America: Geobot. Inst., Rübel Veröff., no. 34, p. 30–37.

Donner, J. J., 1964, Pleistocene geology of eastern Long Island, New York: Am. Jour. Sci., v. 262, no. 3, p. 355–376.

Dreimanis, Aleksis, 1960, The early Wisconsin in the eastern Great Lakes region, North America: Deut. Akad. Wiss. Berlin Monatsber., v. 3, p. 196–205.

Emery, K. O., Wigley, R. L., Bartlett, A. S., Rubin, Meyer, and Barghoorn, E. S., 1967, Freshwater peat on the continental shelf: Science, v. 158, p. 1301–1307.

Frye, J. C., Willman, H. B., Rubin, Meyer, and Black, R. F., 1968, Definition of Wisconsinan Stage: U.S. Geol. Survey Bull. 1274–E, 22 p.

Knox, A. S., 1962, Pollen from the Pleistocene terrace deposits of Washington, D.C. [abs.]: Pollen et Spores, v. 4, no. 2, p. 357–358.

MacClintock, Paul, and Richards, H. G., 1936, Correlation of late Pleistocene marine and glacial deposits of New Jersey and New York: Geol. Soc. America Bull., v. 47, no. 3, p. 289–338.

Martin, P. S., 1958, Taiga-tundra and the full-glacial period in Chester County, Pennsylvania: Am. Jour. Sci., v. 256, no. 7, p. 470–502.

Milliman, J. D., and Emery, K. O., 1968, Sea levels during the past 35,000 years: Science, v. 162, no. 3858, p. 1121–1123.

Muller, E. H., 1964, Quaternary section at Otto, New York: Am. Jour. Sci., v. 262, no. 4, p. 461–478.

Niering, W. A., 1953, The past and present vegetation of High Point State Park, New Jersey: Ecol. Mon., v. 23, p. 127–148.

Ogden, J. G., 3d, 1965, Pleistocene pollen records from eastern North America: Bot. Rev., v. 31, no. 3, p. 481–504.

Potzger, J. E., 1952, What can be inferred from pollen profiles of bogs in the New Jersey Pine Barrens: Bartonia, v. 56, p. 20–27.

Potzger, J. E., and Otto, J. H., 1942, Post-glacial forest succession in northern New Jersey as shown by the pollen records from five bogs: Am. Jour. Botany, v. 30, no. 2, p. 83–87.

Richards, H. G., and Judson, Sheldon, 1965, The Atlantic Coastal Plain and the Appalachian Highlands in the Quaternary, *in* Wright, H. E., Jr., and Fred, D. G., eds., The Quaternary of the United States: Princeton, N.J., Princeton Univ. Press, p. 129–136.

Sirkin, L. A., 1967a, Late-Pleistocene pollen stratigraphy of western Long Island and eastern Staten Island, New York, *in* Quaternary paleocology—Internat. Assoc. Quaternary Research, 7th Cong., 1965, Proc., v. 7: New Haven, Conn., Yale Univ. Press, p. 249–274.

——— 1967b, Correlation of late glacial pollen stratigraphy and environments in the northeastern United States: Rev. Paleobotany and Palynology, v. 2, nos. 1–4, p. 205–218.

Sirkin, L. A., and Grossman, C. J., 1967, Computer program for graphical presentation of aeropalynologic and pollen stratigraphic data: U.S. Natl. Aeronautics and Space Adm., Sci. Tech. Aerospace Rec. N 68–10065, 8 p.

Terasmae, Jaan, 1960, Contributions to Canadian palynology no. 2, pt. 2, A palynological study of Pleistocene interglacial beds at Toronto, Ontario: Canada Geol. Survey Bull. 56, p. 23–41.

White, G. W., and Totten, S. M., 1965, Wisconsinan age of the Titusville Till (formerly called "Inner Illinoian"), northwestern Pennsylvania: Science, v. 148, no. 3667, p. 234–235.

Whitehead, D. R., 1965, Palynology and Pleistocene phytogeography of unglaciated eastern North America, *in* Wright, H. E., Jr., and Frey, D. G., eds., The Quaternary of the United States: Princeton, N.J., Princeton Univ. Press. p. 417–432.

SOURCE AREAS OF LOWER MISSISSIPPIAN RED BEDS IN EASTERN MIDCONTINENT

By EDWARD G. SABLE, Denver, Colo.

Abstract.—Distribution and facies of red beds of Early Mississippian (early Osage) age in Missouri, Illinois, Indiana, and Michigan suggest that most of their terrigenous detritus was derived from a broad lowland area to the northwest which included the Transcontinental and Wisconsin arches. These sediments were deposited along a southwest-trending shelf which was marginal to deeper water to the east. Red beds in central Indiana and parts of southern Ohio and northeastern Kentucky seem to indicate mild emergence of the Cincinnati arch area during this time.

Features that are generally cited as evidence for the presence of major positive structural elements such as the Transcontinental arch, the Ozark uplift, and the Cincinnati arch during the Paleozoic consist of thinning and overlap of units, increase in degree of hiatus toward the positive feature, and, to a lesser extent, depositional patterns. This paper suggests that the distribution of roughly contemporaneous red-bed strata of Early Mississippian (early Osage) age in several Midwestern States may be additional evidence for the presence of land along the northern part of the Transcontinental arch and along the Cincinnati arch during mild but widespread emergence in the eastern midcontinent.

RED-BED OCCURRENCES

Although the major middle to late Paleozoic unconformities recognized in the midcontinent are Middle Devonian and post-Mississippian–pre-Pennsylvanian, lesser degrees of hiatus are recorded by overlap relationships and faunal gaps in Mississippian rocks. One such hiatus, of early Osage age, is documented largely by overlap relationships of Burlington Limestone strata (middle Osage) with underlying Ordovician to Lower Mississippian rocks in the Ozark Plateau and upper Mississippi River valley areas (Laudon, 1937; Workman and Gillette, 1956). A possibly contemporaneous hiatus along the west side of the Cincinnati arch in Kentucky is indicated by a gap in the conodont succession (Rexroad and Scott, 1964). Units of earliest Osage age older than the Burlington include the Fern Glen Limestone of eastern Missouri and Illinois and the Pierson Formation of the St. Joe Group of Beveridge and Clark (1952) of southwestern Missouri (table 1). These units contain various amounts of basal or near-basal variegated strata such as (1) red, green, and gray claystone, (2) admixtures and interbeds of variegated claystone and carbonate rocks and chert, and (3) pink, green, and white clayey, crinoidal, and cherty carbonate rocks. Strata containing similar red beds are recorded in the basal parts of strata of Osage age in eastern Illinois and in Michigan; red and green mudstones are also present west of the Cincinnati arch in central Indiana and east of the arch in south-central Ohio and northeastern Kentucky (table 1). The mudstones are land-derived detritus; the reddish color in carbonate rocks of the Fern Glen also seems to be related to increase in detrital content (Kissling, 1961, p. 142). Although these strata may not be exact time equivalents, they are broadly contemporaneous, and represent deposition of sediments inferred to contain reddish clay in widely spaced areas. If the reddish coloration results from original red clays of transported red soils, then distribution patterns of these rocks should provide clues to positions of land areas from which they were derived.

Figure 1 shows the distribution of red beds of early Osage age in Missouri, Illinois, Michigan, Indiana, south-central Ohio, and northeastern Kentucky, and the approximate relative abundance of carbonate rock and mudstone in the stratigraphic intervals that contain these red beds. Control-point data were obtained largely from studies of subsurface samples and of well logs from the files of the

TABLE 1.—*Stratigraphic units of Early Mississippian age that contain basal or near-basal red beds in the eastern midcontinent*

[Exact time equivalency of units not implied]

Southwestern Missouri (Beveridge and Clark, 1952)	Illinois and eastern Missouri	Eastern Illinois (Swann and others, 1965)	Indiana	Northeastern Kentucky	Southern Ohio (Hyde, 1915)	Michigan
Upper part of St. Joe Group (Pierson Formation).	Fern Glen Limestone.	Borden Siltstone.	New Providence Shale of Borden Group.	Henley Bed of Farmers Member of Borden Formation.	Henley Shale Member of Cuyahoga Formation.	Coldwater Shale.

State geological surveys of Illinois, Indiana, Missouri, Ohio, Kentucky, and Michigan, the Laboratory of Subsurface Studies at the University of Michigan, and to a lesser extent from published information (Cohee and others, 1951). George V. Cohee and Wallace de Witt, Jr., collected the data for Michigan and for south-central Ohio and northeastern Kentucky, respectively; I thank them for their contributions. All data were collected as part of a larger U.S. Geological Survey investigation in preparation—paleotectonic maps of the Mississippian System.

The stratigraphic intervals used in lithofacies calculations within the units shown in table 1 range from the base of these units to the uppermost occurrence of red beds which are considered to be part of a virtually continuous genetic succession. Thus an interval may include basal beds (generally less than 20 feet thick) that are not red, as well as green and gray mudstones and carbonate rocks interbedded with red beds. All the red beds considered here occur in basal or near-basal parts of the units; higher red beds as much as 900 feet above the base in Michigan and nearly 500 feet above the base in central Illinois are not included in this discussion. Although the distribution of red beds shown in figure 1 is fairly accurate, the determinations of the mudstone-carbonate ratio are more subjective and should be considered as approximations. They nevertheless show generalized trends which are real. In southwestern Missouri the distribution limits shown may be too extensive; there, well logs which refer to "Fern Glen Formation" were assumed to mean that red beds are present, because they have been generally considered to be a lithologic criterion for rocks of the Fern Glen.

Several features are apparent in or suggested by the patterns shown on figure 1: (1) Distribution of strata that contain red beds suggests that the present isolated belts of red-bed occurrence in Michigan, Illinois, and Missouri may be preserved segments of a continuous linear belt that extended from northern Michigan to southwestern Missouri, a distance of about 700 miles. (2) In both Michigan and Illinois, carbonate rocks occur similarly along the western margins of red-bed occurrence, and mudstones are along the eastern margins. The carbonate-mudstone ratio increases westward and southwestward. (3) A digitate pattern of red mudstone distribution in central Indiana and a tonguelike shape in southern Ohio and adjoining Kentucky appear to be spatially unrelated to the linear belt suggested above. (4) Isopach approximations, not shown on figure 1, indicate that the thicker stratigraphic intervals that contain red beds, particularly in Illinois, are associated with southward-pointing lobes along the southern margins of red-bed occurrence.

Terrigenous detritus in the Fern Glen Limestone of eastern Missouri was suggested to have originated in Ozark areas and been swept northeastward by marine currents (Kissling, 1961, p. 147). A northeastward increase in insoluble detrital material shown by Kissling (1961, p. 145), however, in view of the regional portrayal shown here, might be better explained as an increase toward a northern source area, such as the Wisconsin arch. From Missouri across Illinois a decided northeasterly increase in mudstone relative to carbonate occurs in the subsurface.

INTERPRETATIONS

The following provisional interpretations regarding the distribution of Lower Mississippian red beds in this region are based on the assumption that the red clay constituents are erosional products of red soils according to the hypothesis of Van Houten (1948), and that there have been no significant postdepositional color changes. They also take into account the depositional framework of the Illinois basin during Early Mississippian time as described by Workman and Gillette (1956), Swann, Lineback, and Frund (1965), and Lineback (1966, 1969). Tentative conclusions are: (1) Distribution

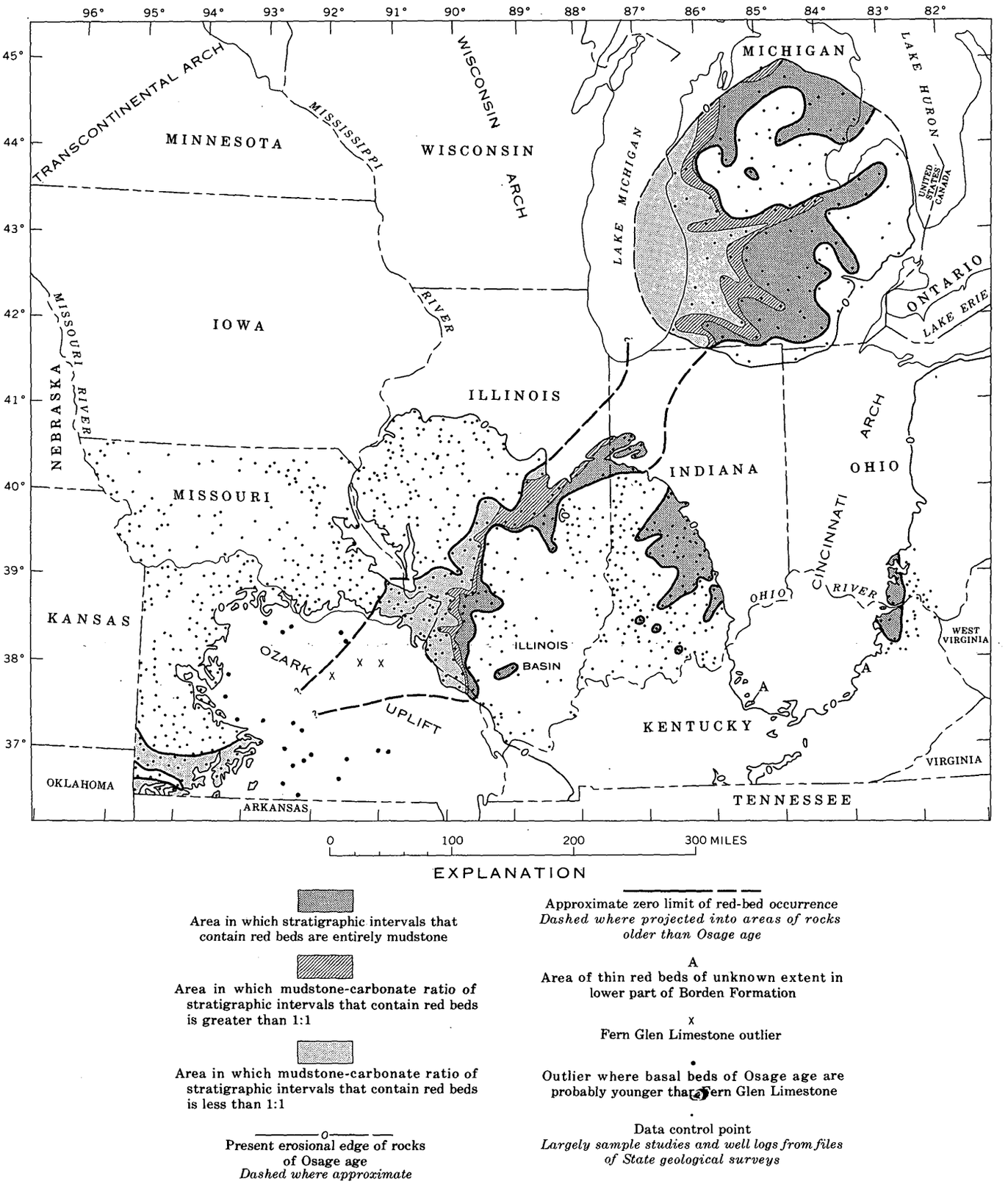

FIGURE 1.—Map showing distribution and generalized lithofacies of red-bed units of early Osage age in Missouri, Illinois, Indiana, Michigan, south-central Ohio, and northeastern Kentucky. (See table 1 for unit names.)

of red rocks of early Osage age indicates the presence of a broad emergent lowland area to the west and northwest on which red soils developed, were eroded, and were transported to the areas shown on figure 1. The lowland lay along the Transcontinental arch and its extension, the Wisconsin arch. (2) The western limits of the belts of red rocks in Illinois and Michigan approximately coincide with an early Osage shoreline. The eastern limits of these red rocks roughly mark the edge of deeper water in troughs and basins. Red sediments accumulated on a shelf between the lowlands and areas of deep water. Fine detrital material may have been transported eastward directly across the shelf, as suggested by lobate patterns and greater thicknesses generally associated with the lobes, or it may have entered largely along the northern part of the shelf and been carried southwestward along the shelf by marine currents. (3) Carbonate rocks with clay interbeds and admixtures formed as banks on the shallow landward portions of the shelf while only silicate clays accumulated in slightly deeper water on the seaward side, where conditions were unfavorable to prolific growth of organisms. These carbonate banks were precursors of the later more extensive bank deposits that formed the Burlington Limestone. (4) The predominance of carbonate rocks in southwestern Missouri indicates that these rocks accumulated on a part of the shelf remote from sources of terrigenous detritus. (5) The patterns of red-bed distribution in central Indiana and southern Ohio–northeastern Kentucky suggest that the source for these sediments was most likely a belt of lowlands along the Cincinnati arch. These rocks, however, may be distal tongues of sediments that originated farther north in the Canadian Shield and were carried down a south- or southwest-dipping paleoslope.

In conclusion, the expression of the Transcontinental arch and adjoining areas as a broad but low-lying landmass during Early Mississippian time is suggested by the above evidence. Terrigenous detritus in the Fern Glen, St. Joe, basal Borden of eastern Illinois and northwestern Indiana, and basal Coldwater of Michigan probably were derived from this landmass. The possibility that parts of other positive elements such as the Cincinnati arch were also subaerially exposed at about this time suggests that an episode of fairly widespread emergence occurred in the eastern midcontinent during early Osage time.

REFERENCES

Beveridge, T. R., and Clark, E. L., 1952, A revision of the Early Mississippian nomenclature in western Missouri, p. 71–79 *in* Clark, E. L., and Beveridge, T. R., Kansas Geol. Soc. guidebook 16th regional field conf., west-central Missouri, 1952: Missouri Geol. Survey and Water Resources Rept. Inv. 13, 93 p.

Cohee, G. V., Macha, Carol, and Holk, Margery, 1951, Thickness and lithology of Upper Devonian and Carboniferous rocks in Michigan: U.S. Geol. Survey Oil and Gas Inv. Chart OC–41, 5 sheets.

Hyde, J. E., 1915, Stratigraphy of the Waverly formations of central and southern Ohio: Jour. Geology, v. 23, p. 655–682, 757–779.

Kissling, D. L., 1961, Lower Osagean stratigraphy of east-central Missouri, *in* Kansas Geol. Soc. guidebook 26th ann. field conf., northeastern Missouri and west-central Illinois, 1961: p. 142–148.

Laudon, L. R., 1937, Stratigraphy of northern extension of Burlington limestone in Missouri and Iowa: Am. Assoc. Petroleum Geologists Bull., v. 21, no. 9, p. 1158–1167.

Lineback, J. A., 1966, Deep-water sediments adjacent to the Borden Siltstone (Mississippian) delta in southern Illinois: Illinois Geol. Survey Circ. 401, 48 p.

——— 1969, Illinois basin—sediment-starved during Mississippian: Am. Assoc. Petroleum Geologists Bull., v. 53, no. 1, p. 112–126.

Rexroad, C. B., and Scott, A. J., 1964, Conodont zones in the Rockford Limestone and the lower part of the New Providence Shale (Mississippian) in Indiana: Indiana Geol. Survey Bull. 30, 54 p.

Swann, D. H., Lineback, J. A., and Frund, Eugene, 1965, The Borden Siltstone (Mississippian) delta in southwestern Illinois: Illinois Geol. Survey Circ. 386, 20 p.

Van Houten, F. B., 1948, Origin of red-banded Early Cenozoic deposits in Rocky Mountain region: Am. Assoc. Petroleum Geologists Bull., v. 32, no. 11, p. 2083–2126.

Workman, L. E., and Gillette, Tracey, 1956, Subsurface stratigraphy of the Kinderhook series in Illinois: Illinois Geol. Survey Rept. Inv. 189, 46 p.

MODIFICATION OF POTASSIUM-ARGON AGES BY TERTIARY THRUSTING IN THE SNAKE RANGE, WHITE PINE COUNTY, NEVADA

By DONALD E. LEE[1], RICHARD F. MARVIN[1],
T. W. STERN[2], and ZELL E. PETERMAN[1],
[1] Denver, Colo., [2] Washington, D.C.

Abstract.—More than 70 radiometric ages have been determined for samples of Jurassic and Tertiary igneous and Precambrian and Cambrian metasedimentary rocks from the southern and central Snake Range of eastern Nevada. The main intrusive activity in the southern Snake Range has been dated as Middle Jurassic by uranium-thorium-lead isotopic work on a zircon sample. Mineralization at the Johnson mine, and mineralization and aplite veining in the Hub mine area were related to the Jurassic igneous event. An Oligocene aplite phase in the southern Snake Range probably was squeezed up by late activity along the Snake Range décollement, and mineralization at the Mount Wheeler mine probably is genetically related to this Oligocene aplite. Potassium-argon ages determined on micas recovered from the Jurassic igneous terrane range from 17.0 to 156 m.y.; ages determined on micas from the Precambrian and Cambrian metasedimentary rocks range from 22.1 to 259 m.y. Generally, the K-Ar age of a mica increases with its distance below the Snake Range décollement. Thus the Tertiary and Cretaceous K-Ar mica ages are interpreted to have resulted from loss of argon due to thermal stresses related to the Tertiary activity along the thrust. The data indicate a late activity along the Snake Range décollement about 17–18 m.y. ago (Miocene).

The general area of study (fig. 1) is about 50 miles southeast of Ely, Nev., in the southern and central parts of the Snake Range of eastern Nevada. The area is east of the Mississippian Antler orogenic belt (Gilluly, 1963, p. 139–140) and just west of the Cretaceous Sevier orogenic belt of Armstrong (1968, p. 436).

This area is well exposed and accessible, and field relations have been defined by previous workers. The area discussed in most detail here (fig. 2) was mapped by Drewes (1958), and by Whitebread, Griggs, Rogers, and Mytton (1962, 1970). Some of the adjoining area to the north (fig. 3) was mapped by Misch and Hazzard (1962). The regional geology is shown on the reconnaissance map of White Pine County, Nev. (Hose and Blake, 1970).

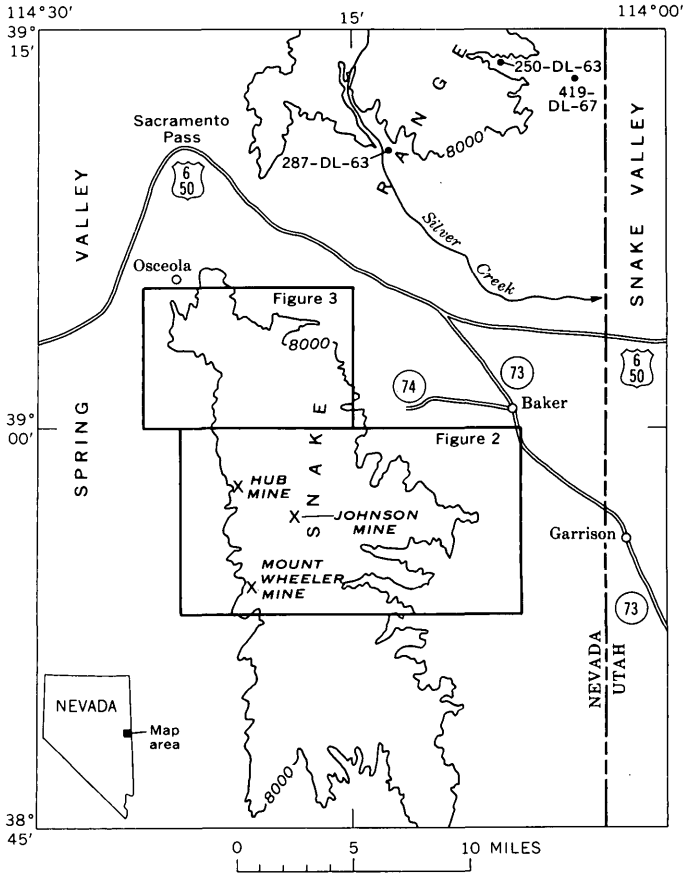

FIGURE 1.—Map of part of eastern Nevada, showing sample localities 250–DL–63, 287–DL–63, and 419–DL–67, and areas of figures 2 and 3.

The present study is the result of an attempt to date the granitoid rocks exposed over an area of about 20 square miles within the Wheeler Peak and Garrison quadrangles (fig. 2). Uranium-thorium-lead isotopic dating shows the main intrusive to be Middle Jurassic in age (Lee and others, 1968; also table 4, this report), but further work has been necessary in order to reconcile some inconsistencies involving mainly K-Ar and Pb-α ages. The purpose of this paper is to report an indicated sequence of events that comprises two periods of intrusive activity, and then Tertiary tectonic (thrust fault) deformation of part of the Middle Jurassic intrusive.

The reader should keep in mind that a thrust plate once covered this area. Erosion has removed all but a small remnant of the upper plate (see fig. 2) and cut deeply into the lower plate. On the basis of the dip of the present-day thrust surface and the topographic heights of the eroded lower plate, one can project the eroded thrust surface upward in a westerly direction. Thus, distance from the thrust surface to the present surface of the lower plate increases westward.

THE GRANITOID ROCKS

The chemical petrology of the 20 square miles of granitoid outcrop referred to in the previous paragraph has been described by Lee and Van Loenen (1970). These granitoid rocks were intruded into part of a miogeosynclinal sequence of predominantly quartzite and carbonate rocks (fig. 2). The rocks exposed in intrusive contact with the granitoid rocks are Prospect Mountain Quartzite, Pioche Shale, and Pole Canyon Limestone, all of Cambrian age. All these granitoid rocks are hybrid, and probably none has been eroded to a depth of more than 1,000 feet. Nonetheless, despite these common characteristics and the relatively small outcrop area involved, these granitoid rocks constitute three separate petrologic and structural study units—the Snake Creek–Williams Canyon area, the Pole Canyon–Can Young Canyon area, and the Young Canyon–Kious Basin area (fig. 2). Bases for distinction among these three areas (Lee and Van Loenen, 1970) are summarized below.

Influence of host-rock type on the chemistry and mineralogy of the granitoid rock is most obvious in the Snake Creek–Williams Canyon area, where the intrusive is well exposed in contact with quartzite, shale, and limestone host rocks. The SiO_2 content of this granitoid rock ranges from 62 to 76 percent, depending upon chemistry of the host rock. Many corresponding and well-defined chemical and mineralogical differences are described elsewhere (Lee and Van Loenen, 1970).

In the Pole Canyon-Can Young Canyon area, granitoid rock is exposed in contact with quartzite, but it is very different from the intrusive seen in contact with quartzite in the Snake Creek–Williams Canyon area. It is distinguished by the presence of large muscovite phenocrysts, many of which contain euhedral crystals of biotite, and also by an almost complete lack of zircon, except for some tiny acicular crystals within the accessory apatite present in the rock. The distinctive nature of this intrusive probably resulted (Lee and Van Loenen, 1970) from assimilation of the Osceola Argillite of Misch and Hazzard (1962) (750–800 feet thick), even though this argillite is not exposed in contact with the granitoid rock.

Of the three areas, the granitoid rock exposed in the Young Canyon–Kious Basin area is most indicative of the regional geology and tectonics, for part of this intrusive outcrop has been cataclastically deformed as a result of movement on the Snake Range décollement. The deformed part of the intrusive is separated from the undeformed part by a fault that probably represents the location of the Pioche Shale before the advent of the intrusive (fig. 2).

The area of intrusive rock referred to as the Osceola stock by Armstrong (1966) is just north of the granitoid rocks described in the previous paragraphs. Although the petrology of this granitoid rock is not yet well known we have made K-Ar age determinations for several samples of the stock (fig. 3) in order to test some of the ideas developed during our detailed study of the area shown in figure 2.

RADIOMETRIC AGES

More than 70 radiometric ages have been determined. Tables 1–3 list K-Ar, Pb-α, and Rb-Sr ages, respectively. Standard techniques for potassium and argon analysis were used (Evernden and Curtis, 1965). Analytical error for individual K-Ar ages was evaluated in the manner described by Cox and Dalrymple (1967) and expressed as two standard deviations. Lead concentration and alpha activity were determined in the manner described by Rose and Stern (1960) and by Gottfried, Jaffe, and Senftle (1959), respectively. Concentrations of rubidium and strontium were determined by isotope-dilution methods (Peterman and others, 1967). Analytical error for an individual Pb-α or Rb-Sr age

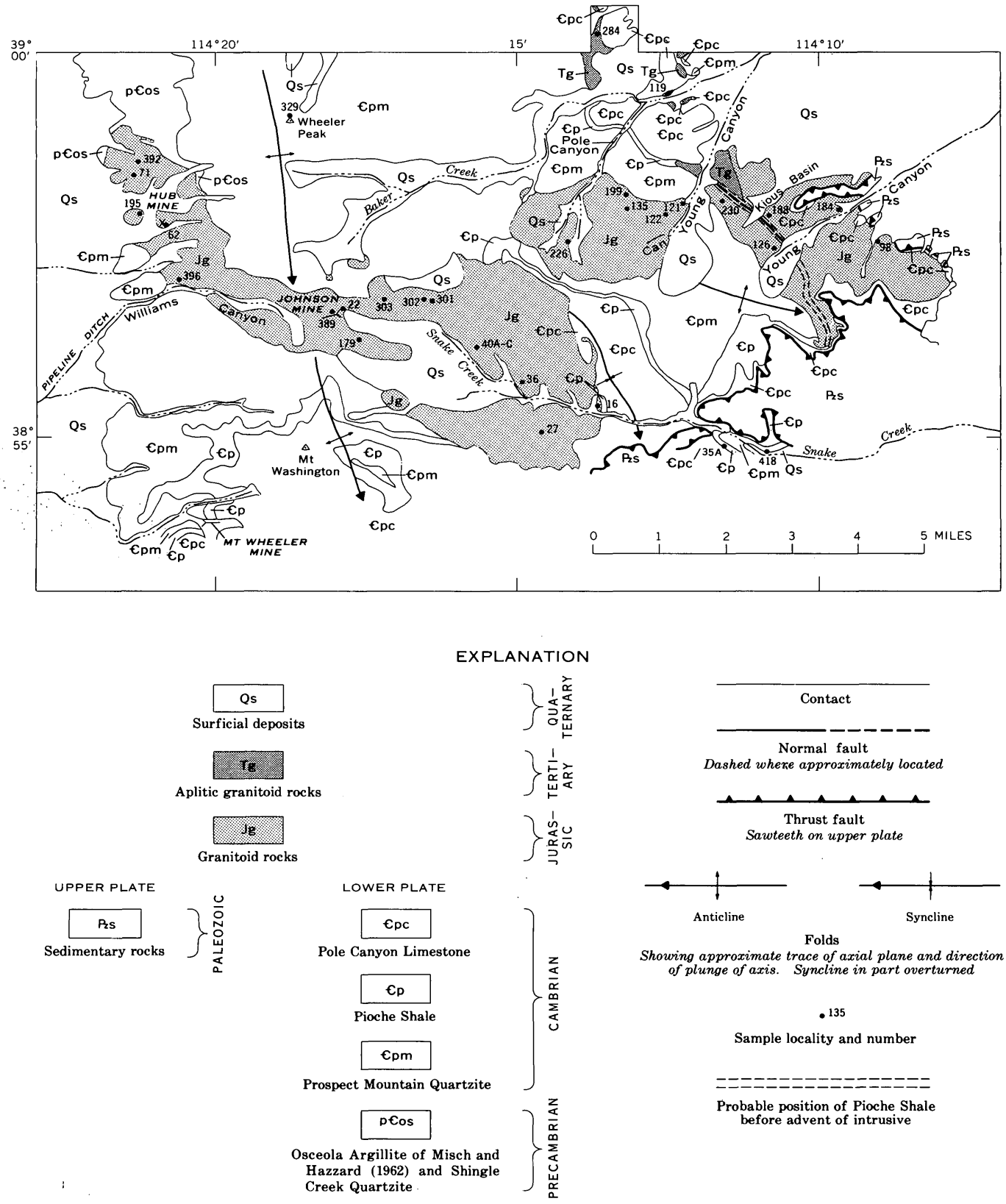

FIGURE 2.—Simplified geologic map showing sample localities in the Snake Creek–Williams Canyon, Pole Canyon–Young Canyon, and Can Young Canyon–Kious Basin areas. Sample localities are identified hereon only by first part of each number; complete field numbers are used in text and tables. Geology from Whitebread, Griggs, Rogers, and Mytton (1970). Features within intrusive from Lee and Van Loenen (1970). Base from U.S. Geological Survey, 1:62,500, Wheeler Peak, 1948, and Garrison, 1949.

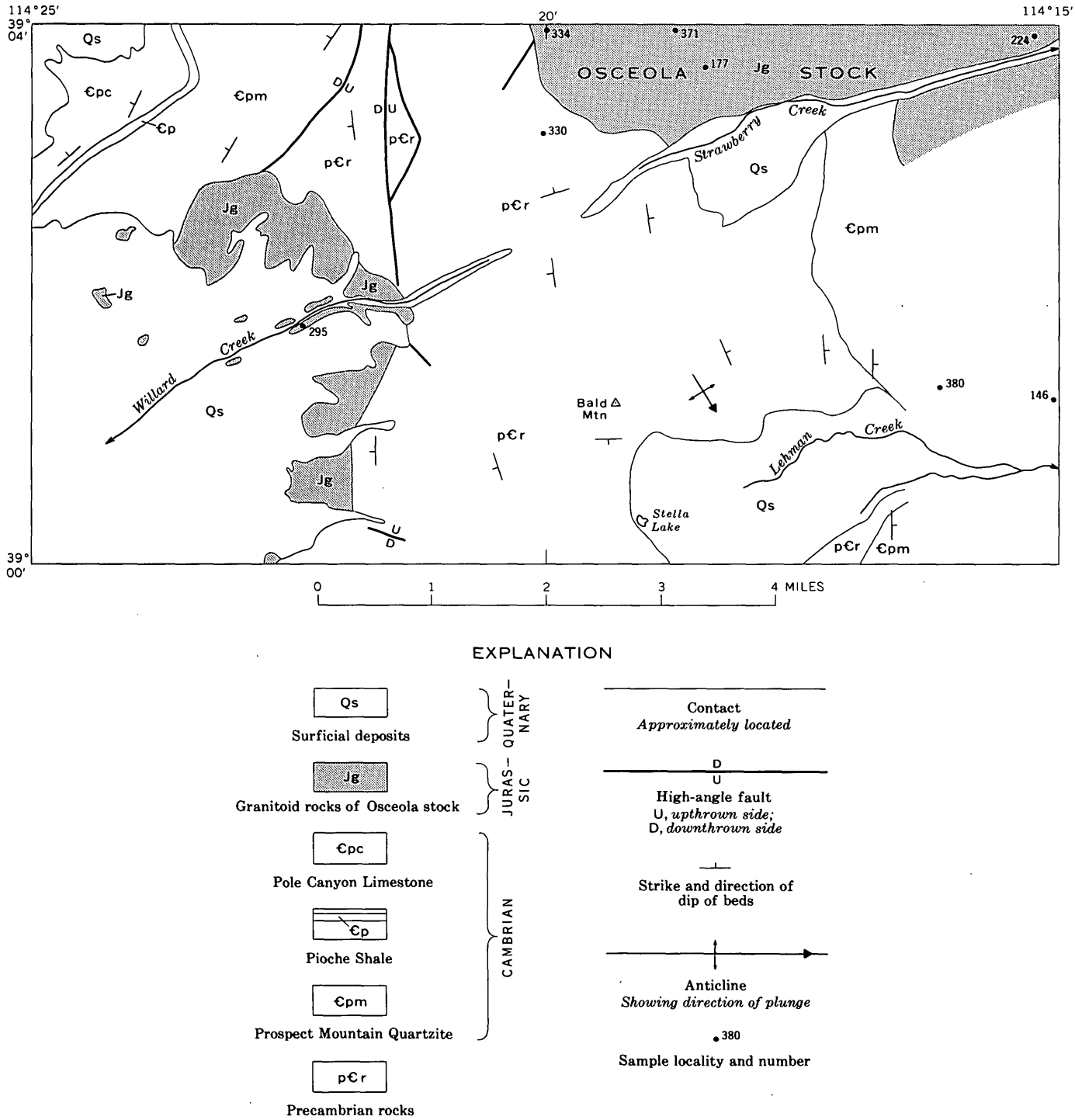

FIGURE 3.—Simplified geologic map showing sample localities in the area of the Osceola stock. Adapted from Misch and Hazzard (1962).

is largely dependent on lead concentration or radiogenic Rb^{87} concentration. Sample localities are shown in figures 1, 2, and 3.

Where more than one method was used to date the same rock, ages from tables 1–3 are compared in table 4. Particularly notable (table 4) is lack of agreement among results for different minerals from a given field sample. This lack of agreement is discussed below.

From geologic relations, the age of the granitoid rocks within the area of our detailed study (fig. 2) can be determined as younger than the Cambrian

TABLE 1.—*Potassium-argon ages of selected minerals from the Snake Range, White Pine County, Nev.*

[Samples within individual area groupings arranged from east to west. Samples 16–MW–60, 35A–MW–60, 62–MW–60, 71–MW–60, and 121–MW–60 analyzed by H. H. Thomas, R. F. Marvin, P. L. D. Elmore, I. H. Barlow, Samuel Botts, and Gillison Chloe. All other samples analyzed by R. F. Marvin, H. H. Mehnert, R. E. Zartman, Viola Merritt, and Wayne Mountjoy except as otherwise noted]

Sample No.	Rock type	Mineral	Mesh size	K_2O (weight percent)	$^{1}Ar^{40}$ (10^{-10} moles/gram)	Radiogenic Ar^{40} (percent)	$^{1}Ar^{40}/K^{40}$	Age (m.y.) $\pm 2\sigma$
Snake Creek–Williams Canyon area (fig. 2)								
16–MW–60	Intrusive	Biotite	−150	8.89	9.83	91	0.00437	73±4
		Muscovite	−150	8.14	9.63	96	.00467	78±4
27–DL–61	Xenolith	Biotite	−100	[2] 9.48	13.56	93	.00566	94.5±4.2
			−80 +100	9.14	13.75	95	.00596	99.3±4.2
		Hornblende	−100	[3].73	1.748	86	.00948	156±5
40A–MW–60	Intrusive	Microline	−150	14.70	9.287	89	.00250	42.3±1.4
		Biotite	−150	8.89	9.519	87	.00424	71.2±3.1
40B–MW–60	Xenolith	do	−60 +150	[2] 9.59	11.82	94	.00488	81.7±3.4
			+60	8.66	10.98	90	.00502	84.0±3.5
22–MW–60	Intrusive	do	−100	8.00	14.40	98	.00713	118±5
		Muscovite	−100	9.50	20.38	96	.00849	140±6
389–DL–67	Quartz vein	do	+60	9.30	19.91	90	.00848	140±5
396–DL–67	do	do	+60	10.88	11.81	94	.00430	72.1±2.2
62–MW–60	Aplite	do	−100	10.08	20.1	98	.00786	130±6
195–DL–62	Quartz vein	do	−50 +100	10.38	22.60	94	.00862	142±4
392–DL–67	do	do	+60	9.44	22.63	90	.00949	156±6
71–MW–60	Intrusive	Biotite	−100	9.03	12.9	89	.00563	94±5
Pole Canyon–Can Young Canyon area (fig. 2)								
121–MW–60	Aplite	Muscovite	−100	10.10	4.65	82	0.00182	31±2
122–DL–62	Intrusive	Biotite	−100	9.14	4.424	84	.00192	32.5±1.4
		Muscovite	−100	10.30	7.989	88	.00307	51.8±1.5
135–DL–62	do	Biotite	−100	8.72	2.919	50	.00132	22.5±1.3
		Muscovite	−100	10.48	11.19	92	.00423	71±2.0
199–MW–61	Aplite	do	−100	10.77	8.687	94	.00319	53.9±1.5
226–MW–61	Intrusive	Biotite	−100	7.32	3.357	38	.00182	30.8±2.1
		Muscovite	−100	10.10	11.82	90	.00463	77.7±2.2
119–MW–60	Aplite	do	−100	10.06	5.096	82	.00200	34±1.0
Young Canyon–Kious Basin area (fig. 2)								
98–DL–62	Xenolith	Biotite	+100	8.50	2.848	66	0.00116	19.7±1.3
184–MW–61	Cataclastic part of intrusive.	Muscovite + quartz.	−100	3.62	.9112	80	.000998	17±0.8
126–MW–61	Xenolith	Biotite	+100	8.52	3.912	84	.00182	30.9±1.5
188–MW–61	Cataclastic part of intrusive.	Muscovite + quartz.	−100	6.14	1.689	86	.00109	18.5±1.0
230–MW–61	Intrusive	Biotite	−100	8.92	3.964	73	.00176	29.9±1.4

Pole Canyon Limestone and older than the most recent movement on the Snake Range décollement. The uranium-thorium-lead isotopic ages of zircon 40A–MW–60 (table 4) date the main intrusive at about 160 m.y., or Middle Jurassic.

The K-Ar age—156 m.y.—of hornblende 27–DL–61 is in good agreement. Hart (1964) has shown that hornblende is vastly superior to muscovite, biotite, or feldspar in retaining radiogenic argon during periods of thermal stress. Hornblende has, however, been of limited use to us in this study because it occurs in these granitoid rocks only where large masses of xenolithic material have been partially assimilated (Lee and Van Loenen, 1970).

K-Ar ages

The K-Ar ages determined for minerals from these Middle Jurassic granitoid rocks (table 1) show a wide range. The two lowest ages (17.0 and 18.5 m.y.) are for muscovite concentrates recovered from the cataclastic part of the intrusive exposed in the Young Canyon–Kious Basin area, and the third lowest age (19.7 m.y.) is for a biotite recovered from one of the few xenoliths found within the cataclastic part. The megascopic and microscopic features of these rocks are described in detail by Lee and Van Loenen (1970). The evidence presented therein indicates that these low age dates result from loss of argon during cataclasis of the intrusive by late movement on the Snake Range décollement.

In the same area, some 400–500 feet southwest of the projected Pioche Shale zone in the intrusive, biotite samples 230–MW–61 and 126–MW–61 give ages of 29.9 and 30.9 m.y., respectively. We ascribe these low ages also to loss of argon as a result of thermal stresses related to late movement on the Snake Range décollement, although the intrusive is not visibly deformed southwest of the projected Pioche Shale. To pursue further this line of reason-

TABLE 1.—*Potassium-argon ages of selected minerals from the Snake Range, White Pine County, Nev.*—(Continued)

[Samples within individual area groupings arranged from east to west. Samples 16–MW–60, 35–MW–60, 62–MW–60, 71–MW–60, and 121–MW–60 analyzed by H. H. Thomas, R. F. Marvin, P. L. D. Elmore, I. H. Barlow, Samuel Botts, and Gillison Chloe. All other samples analyzed by R. F. Marvin, H. H. Mehnert, R. E. Zartman, Viola Merritt, and Wayne Mountjoy except as otherwise noted]

Sample No.	Rock type	Mineral	Mesh size	K_2O (weight percent)	$^{1}Ar^{40}$ (10^{-10} moles/gram)	Radiogenic Ar^{40} (percent)	$^{1}Ar^{40}/K^{40}$	Age (m.y.) $\pm 2\sigma$
Osceola area (fig. 3)								
224–DL–63	Phlogopitic skarn	Phlogopite	−100	9.54	7.127	83	0.00296	50±2.0
177–MW–60	Intrusive	Biotite	+100	9.04	10.36	89	.00454	76.1±2.9
371–DL–66	----do	----do	+ 60	8.48	9.632	84	.00450	75.5±2.9
334–DL–66	----do	----do	−100	9.22	14.47	91	.00621	103±4
		Muscovite	−100	9.24	15.92	90	.00682	113±4
295–DL–64	----do	Biotite	−100	8.76	16.10	96	.00728	121±4
		Muscovite	−100	10.01	23.14	85	.00915	151±4
Silver Creek area (fig. 1)								
287–DL–63	Intrusive	Biotite	−100	9.28	3.511	75	0.00150	25.5±1.3
		Muscovite	−100	10.38	4.798	47	.00183	31.1±1.7
Central and southern Snake Range area (fig. 1–3)								
419–DL–67	Prospect Mountain Quartzite.	Phengite[4]	+ 80	10.58	3.476	61	0.00130	22.1±1.3
250–DL–63	----do	Muscovite + quartz.	− 60	7.76	2.848	47	.00145	24.7±1.7
418–DL–67	----do	Biotite[4]	−100	8.75	3.274	55	.00148	25.2±1.2
		Phengite[4]	−100	10.66	8.637	91	.00321	54.1±1.5
35A–MW–60	Marble in limestone member of Pioche Shale.	Biotite	− 60	9.87	8.88	93	.00359	60±3
146–DL–62	Prospect Mountain Quartzite.	Phengite[4]	−100	[2] 10.80	9.912	91	.00363	61.2±1.8
380–DL–66	----do	----do[4]	−100	10.91	10.59	91	.00384	64.6±1.8
330–DL–66	Strawberry Creek Formation of Misch and Hazzard (1962) of Precambrian age.	Muscovite + quartz.	−100	7.32	13.69	94	.00741	123±5
329–DL–66	Prospect Mountain Quartzite.	----do	−100	6.92	28.38	96	.0162	259±9

Constants: $K^{40}\lambda_e = 0.585\times10^{-10}$/yr, $\lambda_\beta = 4.72\times10^{-10}$/yr. Atomic abundance: $K^{40} = 1.19\times10^{-4}$.

[1] Radiogenic isotope.
[2] Potassium determinations by wet chemistry; Elaine L. Munson and Vertie C. Smith, analysts. Each of the other potassium values is an average of two determinations made with a Perkin-Elmer flame photometer, using a lithium internal standard.
[3] Potassium determination by isotope dilution; Z. E. Peterman, R. A. Hildreth, W. T. Henderson, analysts.
[4] Complete chemical analysis and physical properties of mineral given by Lee and Van Loenen (1969).

ing, we have diagramed (fig. 4) K-Ar ages determined for various minerals from the main (not aplitic) intrusive phase. Data for xenoliths are included, and samples are arranged from east to west. It is apparent that K-Ar ages usually increase toward the west, as distance from (below) the thrust surface tends to increase. Where coexisting muscovite-biotite pairs have been dated, the results for muscovite give the older age—not surprising inasmuch as the muscovite structure retains argon better than the structure of biotite does (Faul, 1966, p. 50). Sample 135–DL–62 was collected from a small area showing shears very similar to those found in the cataclastic part of the intrusive (as described by Lee and Van Loenen, 1970), which relates to the very low K-Ar age (22.5 m.y.) determined for the biotite from this rock.

Judged from their K-Ar ages (table 1), mineralization at the Johnson mine (quartz vein, sample 389–DL–67), and mineralization and aplite dikes in the Hub mine area north of Williams Canyon on the west side of the range (fig. 2) all appear to be related to the Middle Jurassic igneous event. The Jurassic age of one aplite in the Hub mine area (62–MW–60) is confirmed by a whole-rock Rb-Sr age (151 m.y., tables 3 and 4). Muscovite from one of the quartz veins in this area (396–DL–67, table 1) gives an age (72.1 m.y.) notably younger. This young age might result from loss of argon during late slippage along the vein. Slickensides both within and flanking some quartz veins were noted in the Hub mine area.

The aplitic material in the northeastern part of the area shown in figure 2 is believed to have been squeezed up by stresses resulting from relatively late activity on the Snake Range décollement (Lee and Van Loenen, 1970). Whole-rock (284–DL–63) Rb-Sr work shows this aplite to be of Oligocene (28 m.y.) age (table 3). K-Ar data for muscovite from another sample of this aplite (119–MW–60) give a

TABLE 2.—*Lead-alpha ages of some minerals from the Snake Creek-Williams Canyon and the Young Canyon–Kious Basin areas, Snake Range, Nev.*

[Samples arranged from east to west]

Sample No. (fig. 2)	Rock type	Mineral	$\frac{(\alpha/mg)}{hr}$	Pb (ppm)[1]	Calculated age (m.y.)[2]
98–DL–62	Xenolith	Zircon[3]	405	6.7	40±10
126–MW–61	do	do[3]	443	6.8	40±10
16–MW–60	Intrusive	do[3]	302	20.5	170±20
27–DL–16	Xenolith	do[3]	428	29	170±30
36–DL–61	Intrusive	do[3]	584	43	180±20
40C–MW–65	Xenolith	do	637	53	210±20
40B–MW–60	do	do[3]	283	2.0	20±10
301–DL–65	do	do	563	33	150±20
302–DL–65	do	do	513	38.5	190±20
303–DL–65	do	do	738	71	240±20
179–DL–62	do	do	320	24	190±20
62–MW–60	Aplite	Monazite	3,008	236	190±20
71–MW–60	Intrusive	Zircon[3]	647	57.5	220±25
		Monazite[4]	2,537	215	180±20

[1] All lead determinations were made by Harold Westley, except that for 62–MW–60, monazite, which was made by Charles Annell and Harold Westley. Each lead value is an average of duplicate determinations, except that for 27–DL–61, zircon.

[2] For ages < 200 m.y., the following equation was used: $t = C\ Pb/\alpha$, where t is the calculated age in millions of years, C is a constant based upon the Th/U ratio, Pb is the lead content in parts per million, and α is the alpha count per milligram per hour.

For ages > 200 m.y., the following equation was used: $T = t - \frac{1}{2}\ Kt^2$, where T is the age in millions of years corrected for decay of uranium and thorium, and K is a decay constant based upon the Th/U ratio. The assumed Th/U ratio equals 1.0 for zircon and 25 for monazite. Constant C equals 2,485 for zircon and 2,085 for monazite. Constant K equals 1.56×10^{-4} for zircon and 0.65×10^{-4} for monazite. Age is rounded off to nearest 10 m.y. The error quoted is that due only to uncertainties in analytical techniques.

[3] Data from Lee, Stern, Mays, and Van Loenen (1968).

[4] Data from Lee and Bastron (1967).

slightly older Oligocene age (34 m.y.). For geochemical and mineralogical reasons (Lee and Van Loenen, 1970) we consider the numerous aplite dikes within the mass of the intrusive in the Pole Canyon–Can Young Canyon area to be related to the aplitic material shown in the northeastern part of figure 2. Muscovite from a sample of aplite (121–MW–60) in Young Canyon gives a K-Ar age (31 m.y.) that agrees with this idea. However, muscovite from another aplite (199–MW–61) in the same intrusive area gives a K-Ar age of 53.9 m.y. Perhaps sample 199–MW–61 is a border-zone aplite (Lee and Van Loenen, 1970) not genetically related to the younger fault-zone aplites.

Several K-Ar ages (50.0 to 151 m.y.) for micas from the Osceola area (fig. 3) show a general tendency to increase from early Tertiary to Jurassic (from east to west). In this respect, the ages strongly suggest a history similar to that of the Jurassic granitoid phase in figure 2.

Sample 287–DL–63 (fig. 1) was collected from a granitoid mass exposed below the décollement in the central part of the Snake Range. Directional elements within the granitoid mass indicate that it has been affected by movement on the décollement. K-Ar ages determined for muscovite and biotite from this sample (table 1) are 31.1 and 25.5 m.y., respectively. We also interpret these age results to reflect relatively late movement on the décollement.

Micas from seven Cambrian, and one Precambrian, metasedimentary rock samples were recovered for K-Ar age determination. Four of these micas are phengites of almost identical composition, depite the fact that they were recovered from quartzites miles apart, quartzites that themselves show a considerable range of composition (Lee and Van Loenen, 1969). Phengitic micas, being high in silica and low in alumina and containing several percent $MgO + FeO + Fe_2O_3$, represent a solid solution between muscovite and celadonite. Recent studies (cited by Lee and Van Loenen, 1969) have shown that phengites are stable under conditions of high pressure and relatively low temperature which describe the environment for low-grade greenschist facies. Thus the presence of phengites in this area attests to the regional metamorphism in the eastern Great Basin recognized by previous workers, including Drewes (1958, 1967), Misch and Hazzard (1962), and Armstrong and Hansen (1966).

However, K–Ar ages for micas from the metasedimentary rocks listed in table 1 do not date the regional metamorphic event, but reflect Tertiary

TABLE 3.—*Rubidium-strontium ages of selected material from the southern Snake Range, Nev.*

[Analysts: Z. E. Peterman, R. A. Hildreth, and W. T. Henderson]

Sample No. (fig. 2)	Material analyzed	Rb (ppm)	Sr (ppm)	Rb^{87}/Sr^{86}	Sr^{87}/Sr^{86}	Radiogenic Sr^{87} (percent)	Age (m.y.)
284–DL–63	Aplite	529	8.88	173	0.7821	8.7	[1] 28±3
226–MW–61	Muscovite	582	20.04	84.9	.8123	13.1	[2] 90±5
62–MW–60	do	1,671	3.44	1,814	3.670	81	[2] 117±3
62–MW–60	Aplite	348	7.42	136	.9913	28.8	[2] 151±7

Decay constants for Rb^{87}: $\lambda_\beta = 1.39\times10^{-11}$/yr. Isotope abundance: $Rb^{87}/Rb = 0.283$ g/g.

[1] Age calculated with initial Sr^{87}/Sr^{86} ratio equal to 0.714.
[2] Age calculated with initial Sr^{87}/Sr^{86} ratio equal to 0.706.

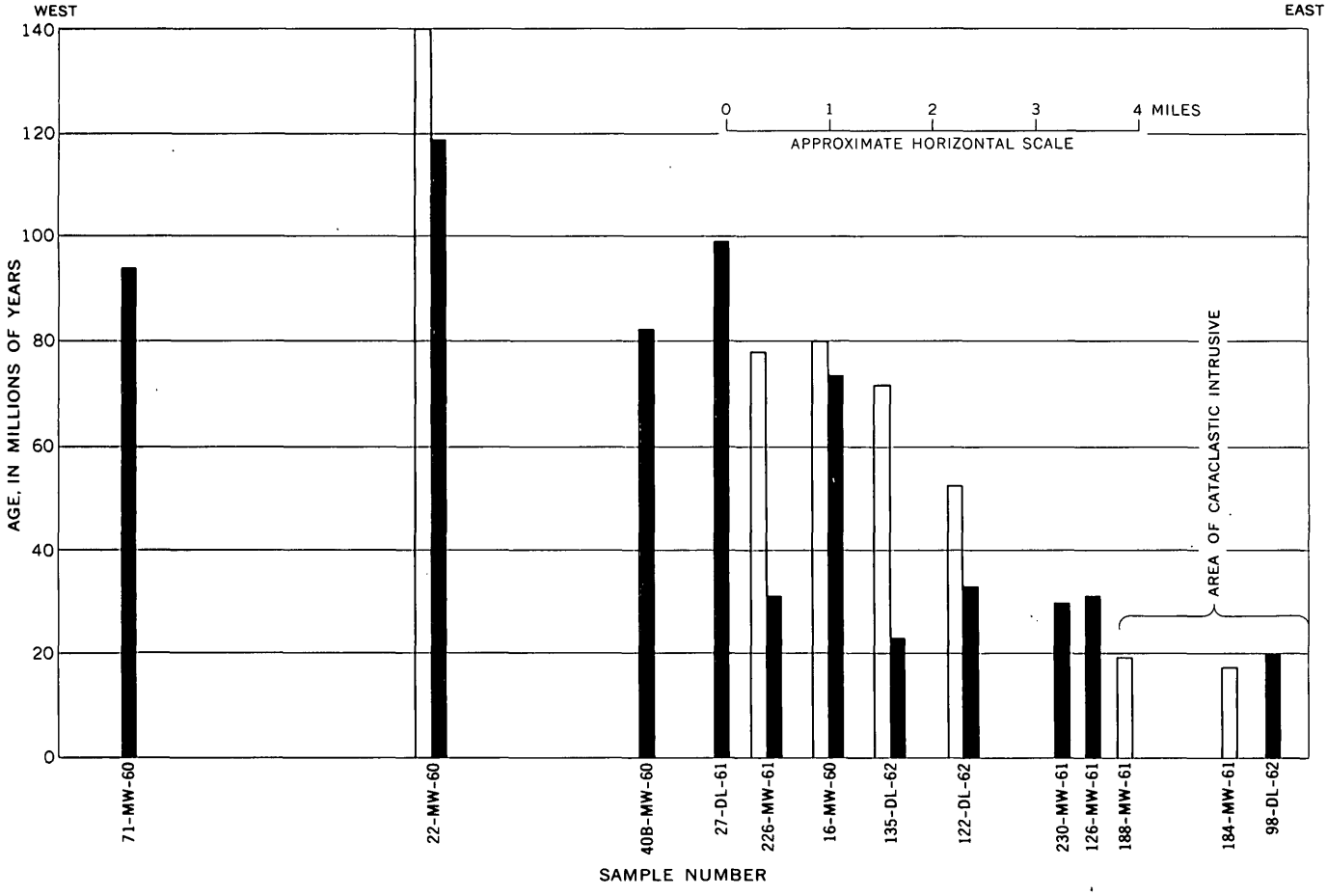

FIGURE 4.—East to-west increase in K-Ar ages determined for muscovite (unshaded) and biotite (black) from the main (Jurassic) intrusive phase shown in figure 2. Total east-west horizontal distance represented is about 12 miles. Age data from table 1.

activity along the Snake Range décollement. The youngest ages (22–28 m.y.) determined for these metamorphic micas approach the ages (17–20 m.y.) for micas from the cataclastic part of the intrusive. From figures 2 and 3 and the White Pine County map (Hose and Blake, 1970), it is apparent that K-Ar age results for these micas tend to increase with increase of distance from the thrust surface, as is true for the igneous micas shown in table 1.

Combining all these data, figure 5 illustrates a hypothetical relation between distance below the thrust surface and K-Ar age results for biotite and muscovite (including phengite) that probably applies to the general area of figure 1. However, we do not suppose that all future age determinations will support the ideas illustrated in figure 5. The age determined for a specific field sample might depend largely on rather localized conditions, such as those already discussed for intrusive sample 135–DL–62 (Can Young Canyon area).

Movement along the Snake Range décollement must have been accompanied by increase in temperature, and no doubt this temperature rise was largely responsible for total to partial argon degassing of almost all the micas listed in table 1. Thus, our explanation of the reset K-Ar ages (Tertiary ages) in table 1 differs from Armstrong and Hansen's (1966, p. 120–121) explanation for Tertiary K-Ar ages in their table 1. We ascribe the temperature rise and degassing of the micas to activity along a thrust fault (as did Kistler and Willden, 1969), whereas Armstrong and Hansen interpreted their Tertiary K-Ar ages to record the time of cooling of the rocks below some critical temperature as Tertiary uplift and erosion proceeded. Neither can we subscribe to the presence of "inherited excess" argon in the minerals as described by Mauger, Damon, and Livingston (1968) to explain certain ages older than a proposed mid-Tertiary uplift and cooling period.

TABLE 4.—*Comparison of selected age data from tables 1–3*

[Samples arranged from east to west. Leaders (---), not applicable or not determined]

Sample No. (fig. 2)	Rock type	Mineral	Age (m.y.) K-Ar	Pb/α	Rb-Sr	$\frac{Pb^{206}}{U^{238}}$	$\frac{Pb^{207}}{U^{235}}$	$\frac{Pb^{208}}{Th^{232}}$
98–DL–62	Xenolith	Biotite	19.7±1.3	---	---	---	---	---
		Zircon	---	40±10	---	---	---	---
126–MW–61	---do	Biotite	30.9±1.5	---	---	---	---	---
		Zircon	---	40±10	---	---	---	---
16–MW–60	Intrusive	Biotite	73±4	---	---	---	---	---
		Muscovite	78±4	---	---	---	---	---
		Zircon	---	170±20	---	---	---	---
27–DL–61	Xenolith	Biotite (−100 mesh)	94.5±4.2	---	---	---	---	---
		Biotite (+100 mesh)	99.3±4.2	---	---	---	---	---
		Hornblende	156±5	---	---	---	---	---
		Zircon	---	170±30	---	---	---	---
226–MW–61	Intrusive	Biotite (−100 mesh)	30.8±2.1	---	---	---	---	---
		Muscovite (−100 mesh)	77.7±2.2	---	90±5	---	---	---
40A–MW–60	---do	Microline	42.3±1.4	---	---	---	---	---
		Biotite	71.2±3.1	---	---	---	---	---
		Zircon	---	---	---	[1] 162	[1] 175	[1] 153
40B–MW–60	Xenolith	Biotite (−60 mesh)	81.7±3.4	---	---	---	---	---
		Biotite (+60 mesh)	84.0±3.5	---	---	---	---	---
		Zircon	---	20±10	---	---	---	---
62–MW–60	Aplite	Muscovite	130±6	---	117±3	---	---	---
		Zircon	---	190±20	---	---	---	---
		Whole rock	---	---	151±7	---	---	---
71–MW–60	Intrusive	Biotite	94±5	---	---	---	---	---
		Zircon	---	220±25	---	---	---	---
		Monazite	---	180±20	---	---	---	---

[1] Data from Lee, Stern, Mays, and Van Loenen (1968).

The idea of cooling with Tertiary uplift and erosion may well apply to parts of the eastern Great Basin, but it does not fit the data in table 1 except for one sample, 330–DL–66 (fig. 3), which was collected near the top of 13,063-foot Wheeler Peak. The muscovite age of 259 m.y. is the oldest K-Ar age determined in this study. By itself, this age could be explained as a result of deep burial followed by uplift. However, in view of the other radiometric ages, together with the geologic intrusive and structural considerations, the age is as easily explained, and in our opinion, more logically explained, by a temperature increase arising from the intrusion of the nearby Jurassic pluton and (or) from movement along the overlying Snake Range décollement.

The age of sample 329–DL–66 is an exception to our general hypothesis that K-Ar ages become younger as one approaches the Snake Range décollement. The age of this sample is much older than would be postulated by our figure 5 according to its probable distance from the décollement, a distance of 1000–2000 feet. However, there may have been local factors that in some way mitigated the thermal effects arising from movement along the décollement.

Pb-α ages

Table 2 lists Pb-α age data for several zircon fractions not previously described. Their ages range from Permain to Jurassic. Most of the Pb-α ages in table 2 can be reconciled with the Jurassic age of the rocks from which the dated minerals were recovered. The presence of xenocrystic zircons and (or) nonradiogenic lead in the zircon concentrates could result in Pb-α ages greater than the age of the host rock (see Stern and others, 1965). However, the mid-Tertiary Pb-α ages cannot be explained in that manner. Each of these low ages was determined on zircons recovered from a xenolith about the size and shape of a coconut. The field settings and physical properties of these zircons are described in some detail by Lee, Stern, Mays, and Van Loenen (1968), who suggested that the low ages for these three zircon fractions resulted from diffusion of lead in the solid state, even though this explanation meets with obvious difficulties. Each new age shown in table 2 was given by a zircon fraction recovered from a xenolith similar to those yielding the zircons with the mid-Tertiary Pb-α ages. Indeed, xenolith 40C–MW–65 (210 m.y.) was collected within a few feet of xenolith 40B–MW–60 (20 m.y.). Our answers to this puzzling age prob-

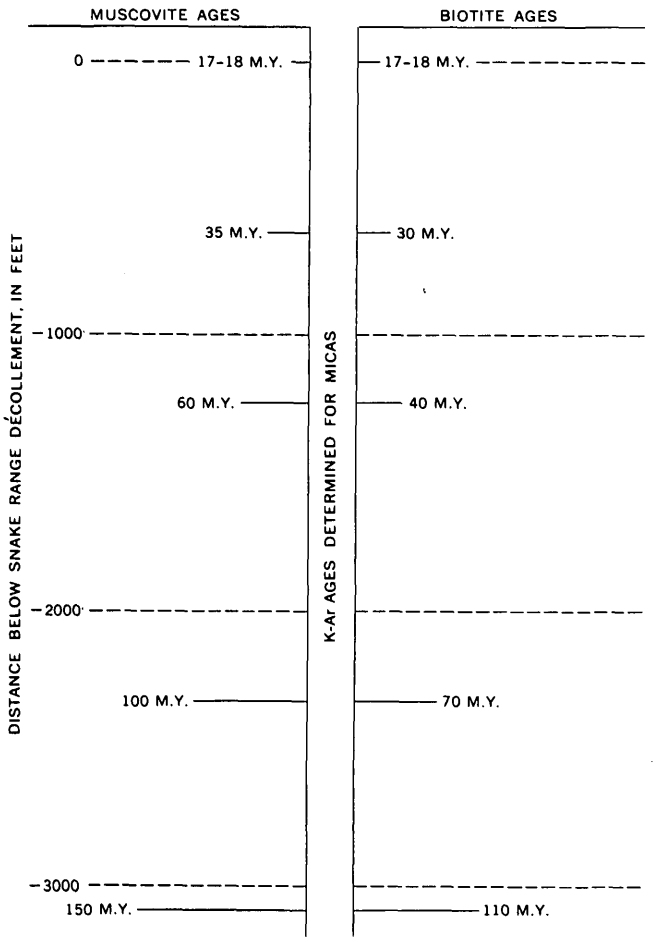

FIGURE 5. Hypothetical relation between distance below Snake Range décollement and K-Ar dates determined for muscovites and biotites in general area of figure 1. Based on age data in table 1 and geologic relations shown in figures 2 and 3 and on the map by Hose and Blake (1970).

lem are all highly speculative and without supportive data, and therefore will not be discussed in this paper.

SUMMARY AND CONCLUSIONS

The main intrusive phase in the area of our detailed study (fig. 2) crystallized during Middle Jurassic time, about 160 m.y. ago. Mineralization at the Johnson mine (scheelite, galena), and in the Hub mine area (wolframite, galena) was related to the Jurassic intrusive activity; aplite dikes in the Hub mine area also were emplaced about the same time. Probably the Osceola stock also crystallized during Middle Jurassic time.

Our data do not conflict with the idea of a regional metamorphic event about mid-Mesozoic, perhaps Late Jurassic (Misch and Hazzard, 1962; Armstrong and Hansen, 1966). This metamorphism was probably of low-grade greenschist facies in the area of our sampling (Lee and Van Loenen, 1969).

The Oligocene aplitic phase shown in the northeastern part of figure 2 (the "fault zone aplite" of Lee and Van Loenen, 1970) was squeezed up by stresses resulting from activity on the Snake Range décollement. Most of the aplite dikes in the Pole Canyon–Can Young Canyon area also are Oligocene. From some rather tenuous geochemical and mineralogical evidence, Lee and Van Loenen (1970) have concluded that the nonpegmatite beryllium mineralization at the Mount Wheeler mine (extreme southwest part of fig. 2) was related to the Oligocene aplitic phase rather than to the Middle Jurassic igneous activity.

Finally, the most recent movement on the Snake Range décollement occurred about 17–18 m.y. ago. This movement could not have been very great, for the geologic relations exposed in the area shown in figure 1 provide no evidence of great movement on the décollement 17–18 m.y. ago (R. K. Hose, oral commun., 1969). Moreover, there is positive evidence in the cataclastic part of the intrusive (fig. 2) that movement along individual shears was no more than a few inches (Lee and Van Loenen, 1970).

Mid-Tertiary K-Ar dates have been reported for metamorphic and igneous terranes in many parts of the eastern Great Basin (Thorman, 1966; Willden and others, 1967; Armstrong, 1966; Armstrong and Hansen, 1966; Armstrong and Hills, 1967; Mauger and others, 1968; Kistler and Willden, 1969; Lee and Marvin, unpub. data). These mid-Tertiary ages have helped direct our attention to previously unrecognized problems in the geologic history of the eastern Great Basin. When these ages are fully understood, they will contribute immeasurably to the understanding of the regional geologic history. We interpret the Tertiary K-Ar dates presented in this study to have resulted from degassing of the micas, as a result either directly or indirectly of activity along the Snake Range décollement.

REFERENCES

Armstrong, R. L., 1966, K-Ar dating using neutron activation for Ar analysis: Geochim. et Cosmochim. Acta, v. 30, no. 5, p. 565–600.

——— 1968, Sevier orogenic belt in Nevada and Utah: Geol. Soc. America Bull., v. 79, no. 4, p. 429–458.

Armstrong, R. L., and Hansen, Edward, 1966, Cordilleran infrastructure in the eastern Great Basin: Am. Jour. Sci., v. 264, no. 2, p. 112–127.

Armstrong, R. L., and Hills, F. A., 1967, Rubidium-strontium and potassium-argon geochronologic studies of mantled gneiss domes, Albion Range, southern Idaho,

U.S.A.: Earth and Planetary Sci. Letters, v. 3, no. 2, p. 114–124.

Cox, Allan, and Dalrymple, G. B., 1967, Statistical analysis of geomagnetic reversal data and the precision of potassium-argon dating: Jour. Geophys. Research, v. 72, no. 10, p. 2603–2604.

Drewes, Harald, 1958, Structural geology of the southern Snake Range, Nevada: Geol. Soc. America Bull., v. 69, no. 2, p. 221–239.

——— 1967, Geology of the Connors Pass quadrangle, Schell Creek Range, east-central Nevada: U.S. Geol. Survey Prof. Paper 557, 93 p.

Evernden, J. F., and Curtis, G. H., 1965, The potassium-argon dating of late Cenozoic rocks in East Africa and Italy: Current Anthropology, v. 6, p. 343–385.

Faul, Henry, 1966, Ages of rocks, planets, and stars: New York, McGraw-Hill Book Co., Inc., 109 p.

Gilluly, James, 1963, The tectonic evolution of the western United States—17th William Smith lecture: Geol. Soc. London Quart. Jour., v. 119, no. 2, p 133–174.

Gottfried, David, Jaffe, H. W., and Senftle, F. E., 1959, Evaluation of the lead-alpha (Larsen) method for determining ages of igneous rocks: U.S. Geol. Survey Bull. 1097–A, p. 1–63.

Hart, S. R., 1964, The petrology and isotope-mineral age relations of a contact zone in the Front Range, Colorado: Jour. Geology, v. 72, no. 5, p. 493–525.

Hose, R. K., and Blake, M. C., Jr., 1970, Geologic map of White Pine County, Nevada: U.S. Geol. Survey open-file map, scale 1:150,000.

Kistler, R. W., and Willden, Ronald, 1969, Age of thrusting in the Ruby Mountains, Nevada, *in* Abstracts with programs for 1969, pt. 5: Geol. Soc. America, p. 40–41.

Lee, D. E., and Bastron, Harry, 1967, Fractionation of rare-earth elements in allanite and monazite as related to geology of the Mt. Wheeler mine area, Nevada: Geochim. et Cosmochim. Acta. v. 31, no. 3, p. 339–356.

Lee, D. E., Stern, T. W., Mays, R. E., and Van Loenen, R. E., 1968, Accessory zircon from granitoid rocks of the Mount Wheeler mine area, Nevada, *in* Geological Survey Research 1968: U.S. Geol. Survey Prof. Paper 600–D, p. D197–D203.

Lee, D. E., and Van Loenen, R. E., 1969, Phengitic micas from the Cambrian Prospect Mountain Quartzite of eastern Nevada, *in* Geological Survey Research 1969: U.S. Geol. Survey Prof. Paper 650–C, p. C45–C48.

——— 1970, Hybrid granitoid rocks of the southern Snake Range, Nevada: U.S. Geol. Survey Prof. Paper 668. [In press]

Mauger, R. L., Damon, P. E., and Livingston, D. E., 1968, Cenozoic argon ages from metamorphic rocks from the Basin and Range province: Am. Jour. Sci., v. 266, no. 7, p. 579–589.

Misch, Peter, and Hazzard, J. C., 1962, Stratigraphy and metamorphism of Late Precambrian rocks in central northeastern Nevada and adjacent Utah: Am. Assoc. Petroleum Geologists Bull., v. 46, no. 3, pt. 1, p. 289–343.

Peterman, Z. E., Doe, B. R., and Bartel, Ardith, 1967, Data on the rock GSP–1 (granodiorite) and the isotope-dilution method of analysis for Rb and Sr, *in* Geological Survey Research 1967: U.S. Geol. Survey Prof. Paper 575–B, p. B181–B186.

Rose, H. J., Jr., and Stern, T. W., 1960, Spectrochemical determination of lead in zircon for lead-alpha age measurements: Am. Mineralogist, v. 45, p. 1243–1256.

Stern, T. W., Newell, M. F., Kistler, R. W., and Shawe, D. R., 1965, Zircon uranium-lead and thorium-lead ages and mineral potassium-argon ages of La Sal Mountains rocks, Utah: Jour. Geophys. Research, v. 70, no. 6, p. 1503–1507.

Thorman, C. H., 1966, Mid-Tertiary K-Ar dates from Late Mesozoic metamorphosed rocks, Wood Hills and Ruby-East Humboldt Range, Elko County, Nevada, *in* Abstracts for 1965: Geol. Soc. America Spec. Paper 87, p. 234–235.

Whitebread, D. H., Griggs, A. B., Rogers, W. B., and Mytton, J. W., 1962, Preliminary geologic map and sections of the Wheeler Peak quadrangle, White Pine County, Nevada: U.S. Geol. Survey Mineral Inv. Field Studies Map MF–244.

——— 1970, Geologic map of the Wheeler Peak and Garrison quadrangles, White Pine County, Nevada, and Milford County, Utah: U.S. Geol. Survey Misc. Geol. Inv. Map I–578. [In press]

Willden, Ronald, Thomas, H. H., and Stern, T. W., 1967, Oligocene or younger thrust faulting in the Ruby Mountains, northeastern Nevada: Geol. Soc. America Bull., v. 78, no. 11, p. 1345–1358.

GAS CHROMATOGRAPHIC DETERMINATION OF CARBONATE CARBON IN ROCKS AND MINERALS

By JOHN MARINENKO and IRVING MAY, Washington, D.C.

Abstract.—A simple, rapid, and direct gas chromatographic method for determining carbonate carbon in rocks and minerals was developed. Powdered samples are heated with phosphoric acid, and evolved gases are separated on a silica-gel column. Carbon dioxide is detected by thermal conductivity using helium as a carrier gas. The method is most applicable for determining carbon dioxide when only a limited quantity of sample is available. As little as 2 micrograms of carbon dioxide can be determined.

Gas chromatographic methods have seldom been used in the analysis of rocks and minerals. The reason for this lies chiefly in the difficulty of quantitatively converting most elements present in rocks and minerals to a reasonably stable and volatile compound suitable for gas chromatographic separation.

Carbonate carbon, however, can easily be released quantitatively from most geologic materials by acid digestion. A gas chromatographic method for determination of carbonate carbon after acid evolution from rocks and minerals was developed by Jeffery and Kipping (1962). They evolve carbon dioxide by digesting the sample with phosphoric acid and then collecting the gases in a reservoir. The collected gases then are swept with hydrogen through a coarse silica-gel column to remove water and then through another silica-gel column to separate carbon dioxide. Carpenter (1962) generated carbon dioxide from carbonates with cold hydrochloric acid and collected the gas in an evacuated chamber. A small fraction of the total carbon dioxide collected was used for its determination by gas chromatography. His detection limit was 6 micrograms of carbon dioxide.

The method developed in this laboratory requires no storage of carbon dioxide prior to its separation and detection. The reaction vessel is a simple, inexpensive, standard sidearm test tube.

REAGENTS

Sodium carbonate (anhydrous powder), dried at 285°C.
Phosphoric acid.
Beeswax (white).

APPARATUS

A schematic of the apparatus is shown in figure 1. A gas chromatograph (Hewlett Packard F and M Model 700) equipped with a tungsten thermal conductivity cell is used. Needle valves *A* and *B* are part of the standard equipment. An auxiliary valve, *C*, is installed to permit rapid switching of carrier gas flow without any adjustment of needle valve *B*. Externally, the carrier gas is controlled by a three-way valve, *D*; an on-off valve, *E*; and a needle valve, *F*. The wheatstone-bridge output voltages are measured with a Minneapolis-Honeywell Electronik 15 recorder.

The chromotagraphic columns are prepared by packing 4-foot lengths of stainless steel tubing (¼-in. OD) with 30- to 60-mesh silica gel (Matheson, Coleman, and Bell). Helium is used as the carrier gas. The reaction vessel is a standard 20- by 150-mm Pyrex sidearm test tube. The test tube is closed with a rubber stopper through which a 6-mm OD Pyrex tube is inserted to introduce the carrier gas. This tube is adjusted so that when the test tube is stoppered, the helium flow is no higher than a few millimeters from the bottom of the test tube. The tip of the tube is fire polished to about a 1-mm opening. All the gas connections are made with rubber tubing (medical grade, 1/16-in. bore and 1/16-in. wall).

The heater is a thin-walled (1.5 mm) quartz tube looped by about four turns of a 36-cm length of platinum wire (0.8 mm diam.). To keep the wire in place the coil is wrapped with a moist asbestos cloth. A 10-volt alternating current is applied across

U.S. GEOL. SURVEY PROF. PAPER 700-D, PAGES D103-D105

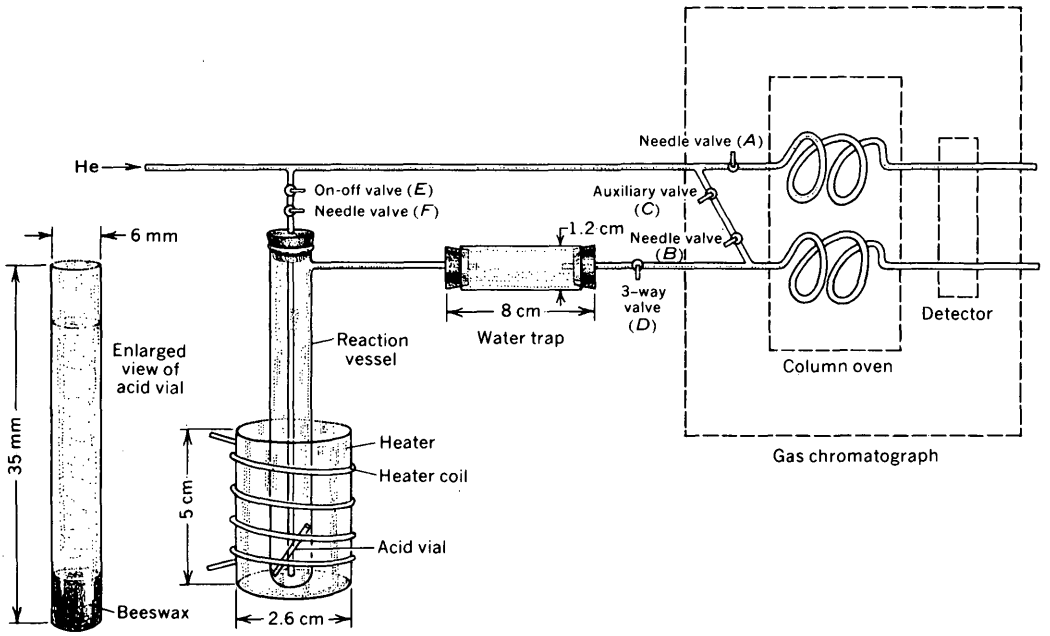

FIGURE 1.—Schematic diagram of apparatus and acid vial. Heater covered by asbestos cloth (not shown).

the two ends of the coil with a 10-amp autotransformer. Several 2-minute heating periods harden the asbestos. The heater is mounted so that it can be easily raised or lowered as needed.

A water trap prevents excessive water from entering the chromatographic column. It is made by inserting a 10- by 50-mm Whatman double-thickness extraction thimble into a Pyrex tube. The extraction thimble should be replaced with a dry one after three or four sample runs.

The acid vials shown in figure 1 are made from Pyrex glass tubing. Enough white beeswax is melted in a petri dish to give a liquid height of 6–8 mm. The pieces of cut tubing are carefully placed upright into the dish, and liquid wax is allowed to enter at the lower end. Upon cooling, the vials are removed by jiggling and then lifting free. Wax is removed or added, as required, with a hot spatula. The tube is then filled with phosphoric acid to about 2 mm from the top, using an elongated eyedropper.

PROCEDURE

Deliver helium carrier gas at 12 psi and a flow rate of 60 ml/min through the sample and the reference chromatographic columns (valve *E* closed, valve *F* open, the reaction vessel open to the atmosphere through valve *D*, and valves *A*, *B*, and *C* open). Set the attenuator control knob on the 64 position for the standards of 1–4 mg of carbon dioxide. Set the recorder speed at 1 in. per min, filament current at 250 ma, the detector temperature at 90°–100°C, and the injection port at 70°C.

Raise the temperature of the column oven to about 150°C prior to running a set of determinations, and then decrease it and maintain it at 60°C. Accurately weigh from 3 to 10 mg of sodium carbonate on a microslide cover, and transfer slide and sample to the reaction vessel, taking care that no sample adheres to the sides. Add just enough water to submerge the slide cover, and then insert an acid vial upright into the reaction vessel with the aid of long straight tweezers. Open valve *E* to permit helium flow through the tube in the stopper. Then stopper the reaction vessel, and break the microslide cover in the process.

The reaction vessel should be free of air in 1 minute. Close valve *C* and open valve *D* to allow carrier gas through the sample column. At this time check the rate of helium flow and, if necessary, adjust to a flow of 60 ml/min through the reference column with valve *A* and through sample column with valve *F*.

Raise the heater so that the bottom of the reaction vessel is about 1 cm above the lower end of the heater. Turn the power on and start the recorder chart. Turn the heat off after 90 seconds. After the peak area is registered on the chart, vent the sample reaction vessel to the atmosphere with valve *D* and open valve *C*. Repeat the procedure described

TABLE 1.—*Carbon dioxide content of selected group of rocks and minerals determined by gas chromatography and other methods*

Sample	Approximate sample weight (grams)	Carbon dioxide (percent)	Coefficient of variation (percent)	Number of determinations	Other methods	
					Carbon dioxide (percent)	Reference
Granite, G–1	0.1	0.063	4	4	0.06	Jeffery and Kipping (1962).
Diabase, W–1	.1	.044	4	4	.044	Do.
Peridotite, PCC–1	.05	.16	9	4	0.02–0.18	Flanagan (1969).[1]
Dunite, DTS–1	.15	.065	8	4	0.03–0.17	Do.
Granite, G–2	.1	.062	13	4	0.04–0.15	Do.
Granodiorite, GSP–1	.1	.098	6	4	0.05–0.33	Do.
Andesite, AGV–1	1	0.0040, 0.0035	—	—	0.01–0.11	Do.
Basalt, BCR–1	1	0.0045, 0.0037	—	—	0.01–0.06	Do.
Fluorspar, NBS No. 79	.01	0.95, 1.02	—	—	.98	National Bureau of Standards certificate value.
Phosphate rock, NBS No. 120a	.01	2.97	5	3	3.18	Do.
Dolomite, NBS No. 88	.008	46.7	[2] 1.2	2	47.25	Do.
Argillaceous limestone, NBS No. 1a	.007	33.3	[2] 1.7	2	33.53	Do.
Dolomite, 1522	.007	44.4	[2] 1.3	2	44.5, 44.1	Grimaldi, Shapiro, and Schnepfe (1966).
Siderite, 2028	.007	30.9	[2] 1.8	2	31.1, 30.5	Do.

[1] Compilation of range in CO_2 values obtained by conventional methods.
[2] Calculated from the standard deviation derived from the formula for a set of duplicate determinations.

above for the samples. Large samples can be weighed directly into the reaction vessel without using cover glasses.

The wheatstone-bridge output voltages received by the recorder can be attenuated to produce an area under the chromatographic peak for the samples which is of the same order of magnitude as that for the standards. Measure the peak area with a planimeter or an integrator and relate it to the peak area of the standards.

DISCUSSION AND RESULTS

To minimize errors, the same carrier-gas flow rate must be used for a set of samples and standards. Column oven temperature and filament current must be held constant.

The coefficient of variation for standards is 1–2 percent. A peak area of 1 square inch corresponds to about 5 μg of carbon dioxide at minimum attenuation if other instrumental parameters are maintained as described above. Hydrogen sulfide and halogen acids do not interfere. No reagent blank can be detected at minimum attenuation. Samples up to 2 g can be analyzed easily for carbonates.

The procedure was tested on a selected group of rocks and minerals. To obtain realistic estimates of precision, replicate determinations were performed at different times over a period of 10 days. Only one determination for any one sample was made each day. Results are tabulated in table 1.

REFERENCES

Carpenter, F. G., 1962, Use of gas chromatography for rapid determination of carbonate at low levels: Anal. Chemistry, v. 34, no. 1, p. 66–67.

Flanagan, F. J., 1969, U.S. Geological Survey standards—[Pt.] II, First compilation of data for the new USGS rocks: Geochim. et Cosmochim. Acta, v. 33, p. 81–119.

Grimaldi, F. S., Shapiro, Leonard, and Schnepfe, M. M., 1966, Determination of carbon dioxide in limestone and dolomite by acid-base titration, *in* Geological Survey Research 1966: U.S. Geol. Survey Prof. Paper 550–B, p. B186–B188.

Jeffery, P. G., and Kipping, P. J., 1962, The determination of constituents of rocks and minerals by gas chromatography: Analyst, v. 87, p. 379–382.

"CATOCTIN SCHIST" ANALYSIS—ITS TRUE IDENTITY

By MARJORIE HOOKER, Washington, D.C.

Abstract.—A chemical analysis, published as that of a schist from South Mountain, Pa., is shown to be, in reality, that of a basalt from Madera County, Calif.

In view of the current revival of exploration for metal-bearing rock formations in the Appalachian region in the eastern part of the United States, it seems appropriate to put on record the facts concerning the published chemical analysis of a rock that is stated to be Catoctin schist from the copper belt of southern Pennsylvania. This rock is really basalt from the base of a lava flow near the head of the San Joaquin River in Madera County, Calif.

In their discussion of the Precambrian volcanic series in Frederick County, Md., Stose and Stose (1946, p. 21) quoted two chemical analyses of metabasalt from South Mountain in adjacent Pennsylvania from earlier publications because, as they say on page 22, "no analyses of the Catoctin metabasalt in Frederick County are available." One of the analyses, by F. A. Genth, is of an epidote rock and is quoted from Persifor Frazer (1880, p. 264). The other analysis, by C. H. Henderson, of a rock called Catoctin schist, is cited as follows: "Idem. p. 307, quoted from Williams, G. H., Trans. Am. Inst. Min. Eng. vol. XII, p. 82."

Philip B. King (written commun., 1962) drew my attention to the fact that the cited article in the AIME volume was not by G. H. Williams and did not contain the schist analysis given by the Stoses. He went on to say,

> Thus, the analysis quoted by the Stoses is an "orphan" without any evidence as to where the rock came from, who made the analysis, or when, but it has been quoted and used in subsequent discussion of the geochemistry of the Catoctin. Regretfully, I threw it out, but it might be worth somebody's while to trace it, to straighten out the records.

The paper in the AIME Transactions volume is by Persifor Frazer rather than G. H. Williams (Frazer, 1884). He does give an analysis of a chlorite schist ($SiO_2 = 41.28$) from near the Bechtel shaft, C. H. Henderson analyst, but it is not the analysis quoted by the Stoses. Neither does a following paper by C. H. Henderson (1884), also on the copper deposits of South Mountain, contain the analysis quoted. Subsequent search of other papers by Frazer and by others on the southern Pennsylvania area turned up no analysis resembling the orphan. The paper by G. H. Williams (1892) on the volcanic rocks of South Mountain quotes the chlorite schist analysis given by Frazer (1884) and the same Bechtel shaft locality given by the Stoses, but there the resemblance ends. A routine check of Pennsylvania and Maryland rock analyses that I had compiled from post-1913 literature drew another blank.

Later, King (written commun., 1962) mentioned that the orphan analysis had the general look of one done in the U.S. Geological Survey laboratory. It then occurred to me that it could just as well be an older analysis, and if it had been made in the Survey, it should appear in one of the bulletins in which the analyses were compiled from time to time. Starting with Clarke (1915) and scanning only silica percentages, it was not long before I found the orphan on page 195 where it is identified as follows:

> Basalt, base of a lava flow, east of the head of San Joaquin River, Madera County [Calif.]. *Andose.* Description supplied by Turner. Contains pyroxene, partly augite, plagioclase, olivine, and iron ores. Analysis by W. F. Hillebrand, record No. 1767.

The analysis is given below. The original place of

SiO_2	51.89	TiO_2	0.91
Al_2O_3	15.28	P_2O_5	0.61
Fe_2O_3	3.10	MnO	0.12
FeO	3.60	ZrO_2	Trace
MgO	8.68	CO_2	None
CaO	7.38	NiO	0.02
Na_2O	3.27	BaO	0.15
K_2O	2.57	SrO	0.09
H_2O+	1.37	Li_2O	Trace
H_2O-	1.17	Total	100.21

U.S. GEOL. SURVEY PROF. PAPER 700-D, PAGES D106-D107

publication is a prior compilation of Geological Survey analyses (Clarke, 1900, p. 218), where the analysis is indicated as hitherto unpublished. It is quoted correctly in both of Henry S. Washington's compilations (1903, 1917), but it is probably fortunate that King decided that it should not be used in his report, for in the quotation by the Stoses, two constituents were omitted and two others (H_2O+, H_2O-) were reversed.

The erroneous insertion of the name of G. H. Williams in the citation given by Stose and Stose can be attributed to careless handling of reference material. In his article on South Mountain, Williams (1892) quotes the analyses given earlier by both Frazer and Henderson in the AIME Transactions, and these three references have obviously been confused. How the California basalt became Catoctin schist can only be surmised. However, reference back to the ledgers in which the work of the Geological Survey chemical laboratory was recorded at that time shows that analyses of a number of Pennsylvania and Maryland rocks (record numbers 1710–1755) and the analysis of the California basalt (record number 1767) were made and recorded at about the same time and by the same analyst. If a group of analyses were later being copied directly from the ledger, hurriedly or carelessly, the basalt from California could easily have been included with those from the other areas.

REFERENCES

Clarke, F. W., 1900, Analyses of rocks from the laboratory of the United States Geological Survey, 1880 to 1899: U.S. Geol. Survey Bull. 168, 308 p.

——— 1915, Analyses of rocks and minerals from the laboratory of the United States Geological Survey, 1880 to 1914: U.S. Geol. Survey Bull. 591, 376 p.

Frazer, Persifor, Jr., 1880, The geology of Lancaster County: Pennsylvania Geol. Survey, 2d, Rept. CCC, 350 p.

——— 1884, An hypothesis of the structure of the copper belt of the South Mountain: Am. Inst. Mining Engineers Trans., v. 12, p. 82–85.

Henderson, C. H., 1884, The copper deposits of the South Mountain: Am. Inst. Mining Engineers Trans., v. 12, p. 85–90.

Stose, A. J., and Stose, G. W., 1946, Geology of Carroll and Frederick Counties: Maryland Dept. Geology, Mines, and Water Resources, Carroll and Frederick Counties Rept., p. 11–131.

Washington, H. S., 1903, Chemical analyses of igneous rocks published from 1884 to 1900 * * *: U.S. Geol. Survey Prof. Paper 14, 495 p.

——— 1917, Chemical analyses of igneous rocks published from 1884 to 1913, inclusive * * *: U.S. Geol. Survey Prof. Paper 99, 1201 p.

Williams, G. H., 1892, The volcanic rocks of South Mountain in Pennsylvania and Maryland: Am. Jour. Sci., 3d ser., v. 44, p. 482–496, map.

POTASSIUM AND RUBIDIUM IN GRANITIC ROCKS OF CENTRAL CALIFORNIA

By F. C. W. DODGE, B. P. FABBI,
and D. C. ROSS, Menlo Park, Calif.

Abstract.—The trends of K–Rb ratios of granitic rocks from two regions of central California differ slightly. Masses near the San Andreas fault yield an average ratio near 230 with some seemingly random variation at all K contents, whereas the Sierra Nevada batholith yields ratios that tend to decrease at higher K contents. The differences in ratios may be related to differences in water pressure during crystallization or possibly to late-stage introduction of K-feldspar into granitic rocks near the San Andreas fault. Both K and Rb contents decrease westward across the Sierra Nevada, but the lack of systematic variation of the K–Rb ratio with distance from the continental margin is inconsistent with the model that relates landward increase of K solely to increasing depths during magma generation. Recent experiments by D. H. Green and A. E. Ringwood lead to the expectation of a landward increase in K–Rb ratio. In addition, crystallization temperatures near 700°C are suggested by K and Rb partition coefficients of several biotite and K-feldspar pairs.

Potassium and rubidium contents of Mesozoic granitic rocks of both the central Sierra Nevada batholith and masses near the San Andreas fault in central California (fig. 1) and of selected constituent minerals have been determined as part of current programs of petrological, mineralogical, and geochemical studies of the two regions. The same samples used in this investigation have been or are now being used in other studies related to these programs (for example, Dodge and others, 1968, 1969; Dodge and Ross, 1970; Hurley and others, 1965; Kistler and others, 1965; Naeser and Dodge, 1969; Piwinskii, 1968a, b). Purposes of this investigation were (1) to evaluate K-Rb ratios as a means of furthering the understanding of processes responsible for batholith generation, and (2) to determine if similar processes were operative in the two different granitic terranes of central California.

The relative behavior of potassium and rubidium during magmatic processes has been the subject of numerous investigations in recent years. The geochemistry of the alkali metals has been comprehensively reviewed by Heier and Adams (1964), and several other workers have extensively discussed the application of K-Rb ratios (for example, Ahrens and others, 1952; Erlank, 1968; Taylor, 1965); hence the underlying basis for use of the ratio is dealt with only briefly in this paper.

PROCEDURES

Samples of rocks from masses near the San Andreas fault were selected from splits of previously analyzed samples (D. C. Ross, unpub. data) to represent as great a range of potassium contents as possible; samples of Sierra Nevada granites also were generally selected from previously analyzed rocks. Mineral separates were prepared by centrifuging carefully sized rock powders in adjusted mixtures of methylene iodide, bromoform, and dimethylformamide and by repeated passes through an electromagnetic separator. Final sample purity invariably exceeded 96 percent and generally was estimated to exceed 99 percent.

Potassium and rubidium in analyzed samples were quantitatively estimated using a General Electric XRD–6 vacuum spectrograph.

For potassium, a Cr target and a PET analyzing crystal were used. Calibration curves for these analyses were prepared using U.S. Geological Survey rock standards G–1, W–1, AGV–1, GSP–1, BCR–1, and G–2, the French rock standards Br, Gr, GA, and GH, and the Canadian and Russian syenite standards. Both standards and unknown rocks were prepared in the same fashion (that is, 0.5 g of sample and 0.5 g of cellulose powder were mixed, ground, and pressed into a pellet).

For mineral analysis, previously analyzed "stand-

ard" minerals and rock standards were fused (fusion consisted of a mixture of 0.1 g of unknown, 0.7 g of $LiBO_2$ flux, and 0.1 g of chromatographic cellulose binder), ground, and pressed into pellets. Unknown minerals were prepared similarly. Calibration curves for potassium were drawn on the basis of the previously analyzed minerals and on the rock standards, and potassium was determined in the unknown minerals. Estimated detection limit for potassium is 0.01 percent, and relative accuracy of the potassium content is 1.5 percent.

A tungsten target and a LiF crystal cut on the 220 plane were used for analysis of rubidium. The same standards as those used for potassium were used to calibrate rubidium in the rock analyses, and the same pellets were used for rubidium determination. The detection limit for rubidium in the rock analyses is 20 ppm.

In addition to the rock and mineral standards used for potassium, an analyzed lepidolite containing 18,190 ppm Rb was used for a high-concentration rubidium standard for mineral analysis. Calibration curves were drawn and used to determine rubidium in the unknowns. Again, the pellets used for potassium analysis were used for rubidium determination. Rubidium detection limit for the minerals is 50 ppm, 30 ppm higher than for the rocks, because of dilution with the $LiBO_2$ flux. Relative accuracy of the rubidium determination is 5 percent.

RESULTS

Contents of potassium and rubidium for plutonic rocks of the central Sierra Nevada batholith are listed in table 1, those for rocks near the San Andreas fault in table 2. The 44 samples from the Sierra Nevada batholith were collected from a strip between lats 36°45′ and 38°00′ N. (fig. 1) across the Sierra Nevada and Inyo Mountains. Analyzed samples were selected as representative of principal rock types of the batholith. Most of them were either collected during geologic mapping or taken from borings made for heat-flow measurements (Lachenbruch, 1968). Where possible, samples are grouped in table 1 according to intrusive sequences proposed by Bateman and Dodge (1970). Rocks of several comagmatic plutonic bodies are included in each sequence. Sequences are listed in the table in chronological order, that is, order of increasing age. Insufficient data on three samples prevent their being assigned to a specific sequence.

The granitic rocks near the San Andreas fault, unlike those of the Sierra Nevada, are generally poorly exposed and crop out over only a small part of the area that they are believed to underlie. Our samples are from four discontinuously exposed areas: the central Coast Ranges, the southern Coast Ranges, the Transverse Ranges, and the Mojave Desert. The rocks from the two areas in the Coast Ranges are similar and probably genetically related (Compton, 1966; Ross, unpub. data); rocks of the other two areas, however, are in separate structural

TABLE 1.—*Potassium and rubidium contents of granitic rocks of the central Sierra Nevada batholith*

Sample No.	K (percent)	Rb (ppm)	K-Rb ratio
John Muir sequence and Tuolumne Intrusive Series			
M–127	1.8	65	277
M–131	2.7	87	310
M–139	2.9	103	282
M–135	3.0	128	234
M–133	2.9	109	266
HC–1; 3.2 m	3.0	155	194
HC–1; 480.2 m	3.1	158	196
MG–1	2.6	106	245
R–99	3.8	220	173
BCa–20	3.1	134	231
BCc–12	2.5	118	211
HL–4	2.7	96	281
FD–13	1.5	61	246
I–397	4.1	205	200
Shaver sequence			
BCc–13	2.1	89	236
SL–18	2.6	109	239
SL–32	2.9	130	223
HL–29	3.3	176	188
SL–1; 9.5 m	1.3	59	220
SL–1; 609.2 m	1.7	69	246
JB–1; 1.9 m	1.9	81	235
JB–1, 489.5 m	1.8	81	222
KPc–138	2.8	159	176
Western foothills and Yosemite rocks			
CL–1	0.42	<20	>210
WV–1	1.9	76	250
FD–20	2.0	74	270
SJ–1; 3.3 m	1.6	55	291
SJ–1; 459.3 m	1.2	57	211
ST–1; 157.1 m	.66	36	183
ST–1; 485.2 m	.56	22	254
FD–12	3.7	186	199
Palisade Crest sequence			
BP–1	2.5	84	298
BP–2	3.4	126	270
FD–2	3.2	136	235
FD–3	3.6	169	213
FD–4	3.5	156	224
MG–3	2.7	111	243
Sheelite sequence			
MT–1	3.2	189	169
MT–3	2.5	105	167
MT–6	1.8	68	265
MG–2	4.0	231	173
Unassigned rocks			
KR	3.1	106	292
MP–568	2.4	101	238
MP–328	3.0	167	180

TABLE 2.—*Potassium and rubidium contents of granitic rocks of masses near the San Andreas fault*

Sample No.	K (percent)	Rb (ppm)	K-Rb ratio
Central Coast Ranges			
DR–510	1.2	52	231
DR–532A	2.8	104	269
DR–518	3.6	182	198
DR66–1	1.1	46	239
Leo–126	1.4	62	226
DR–496A	4.1	127	323
Southern Coast Ranges			
DR–566A	2.4	87	276
G–1A	3.6	117	308
DR–576	3.3	162	204
DR–546	4.5	157	286
P–1	2.3	109	211
SLO–10B	4.0	116	345
DR66–63A	4.1	132	311
DR66–66	3.7	181	204
DR66–109	2.1	83	253
BM–1C	3.3	149	221
DR–589B	.19	<20	>95
DR66–121	.12	<20	>60
Mo–1c	2.8	130	215
Transverse Ranges			
CS–2	2.2	96	229
V–4	2.0	80	250
DR–593	1.6	53	302
DR–590	3.6	92	391
DR–631	2.7	87	310
DR–690	2.8	111	252
DR66–479	1.9	68	279
BBL	3.2	148	216
DR–726	3.6	189	190
Mojave Desert			
DR66–316A	1.9	67	284
DR66–321B	2.2	93	237
DR66–349	3.5	139	252

TABLE 3.—*Potassium and rubidium contents of minerals of analyzed granitic rocks*

Sample No.	K (percent)	Rb (ppm)	K-Rb ratio
Potassium feldspar			
M–139	12.23	320	382
MG–1	11.73	350	335
HL–4	12.07	280	431
FD–13	11.70	200	585
I–397 (groundmass)	12.39	560	221
I–397 (phenocrysts)	11.76	340	346
SL–18	12.26	260	472
HL–29	11.49	490	234
KPc–138 (groundmass)	11.87	370	321
KPc–138 (phenocrysts)	11.11	360	309
FD–20	12.12	260	466
BP–1	11.31	230	492
MG–3	11.52	290	397
MT–1	11.05	460	240
KR	11.80	180	656
Mo–1c	11.32	270	419
Biotite			
M–139	8.01	530	151
MG–1	7.01	600	117
HL–4	7.79	480	162
FD–13	7.84	420	187
SL–18	7.48	620	121
HL–29	7.65	1,210	63
KPc–138	7.65	910	84
CL–1	7.75	540	144
FD–20	7.70	280	275
ST–1; 485.2 m	7.72	240	322
BP–1	7.13	630	113
MG–3	7.08	540	131
MT–1	6.93	1,240	56
KR	7.70	380	203
DR–510	6.73	300	224
Mo–1c	7.26	620	117
Muscovite			
FD–20	8.88	300	296
Mo–1c	8.97	500	179
Hornblende			
MG–1	0.63	<50	>126
SL–18	.81	<50	>162
BP–1	.41	<50	>82

and physiographic provinces. Thirty-one samples were selected, on the basis of a previous study (D. C. Ross, unpub. data), to span as wide a range of potassium contents as possible; thus while individual samples are representative of rocks in the vicinity, the sampling may be biased toward slightly higher potassium contents than are prevalent in the region.

Values of potassium and rubidium contents for selected coexisting constituent minerals of some of the analyzed rocks are presented in table 3. As commonly observed, rubidium is concentrated in biotite to a greater degree than in potassium feldspar, and the average K-Rb ratio for biotite is about half that for potassium feldspar. These two minerals contain the bulk of potassium and rubidium in their host rocks. Two analyses of muscovites are given; however, this mineral is rarely present in significant amounts. Contents of rubidium in analyzed hornblendes are below our detectibility level.

DISCUSSION

Variation of the K-Rb ratios between rocks of the different intrusive sequences of the Sierra Nevada batholith is slight; in fact, the variation appears to be as great within individual sequences as between sequences (table 1). Similarly, systematic differences between rocks of the different groups of masses along the San Andreas fault are undetectable (table 2).

The granitic rocks of central California generally have K-Rb ratios near the commonly accepted "normal" value for igneous rocks of 230 (Shaw, 1968). Constancy of the ratio is particularly well shown by K-Rb relations in rocks from near the San Andreas fault (fig. 2). On the other hand, the ratio tends to decrease from values higher than 230

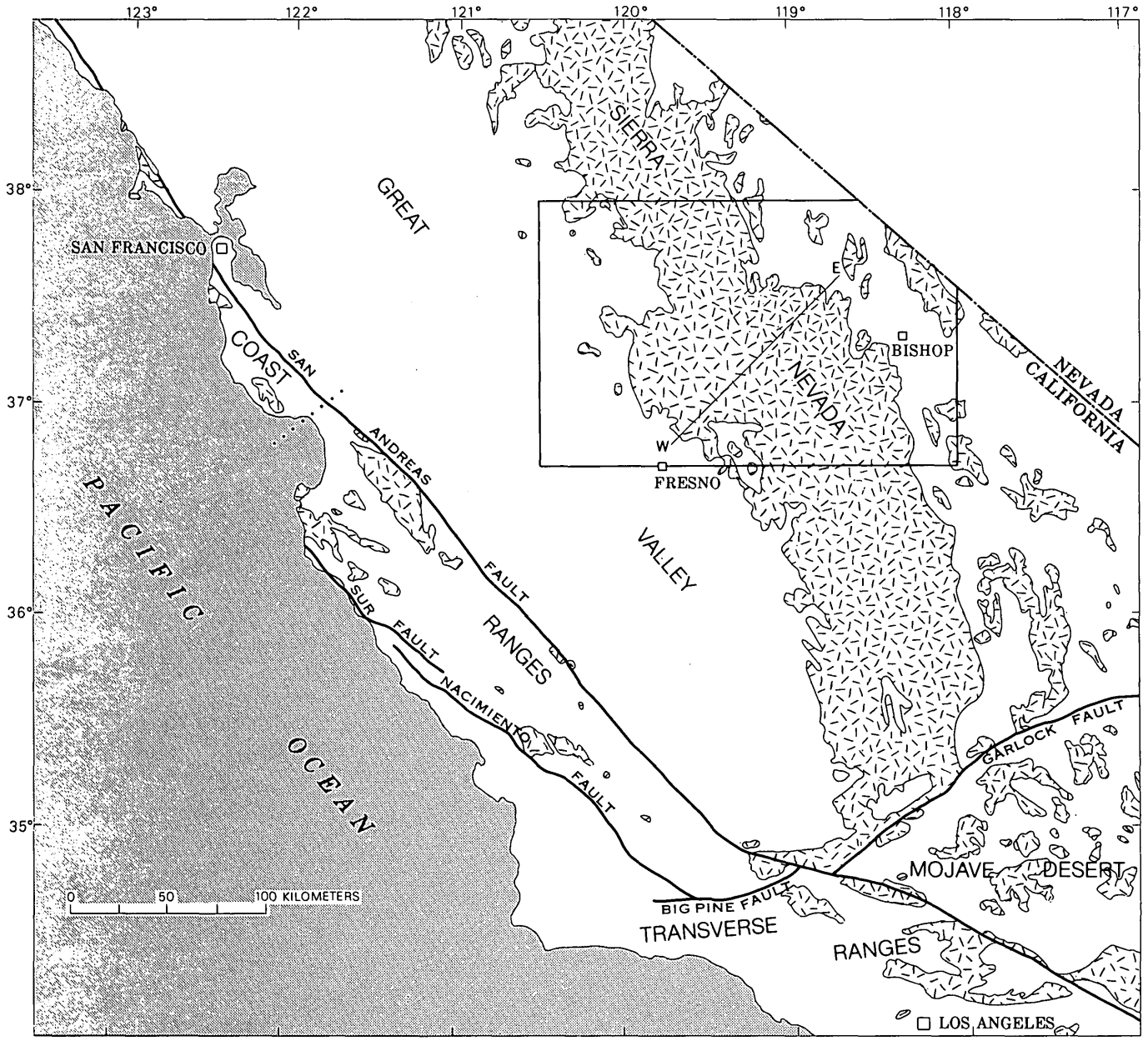

FIGURE 1.—Map of central California, showing distribution of granitic rocks (patterned). Dotted line is the arbitrary boundary between the central and southern Coast Ranges. Area of study in the central Sierra Nevada is outlined. W–E, line of projection of figure 3.

at low potassium contents to values lower than 230 at high potassium contents in rocks from the Sierra Nevada (fig. 2); that is, rubidium is enriched relative to potassium at high potassium contents, although for the greater part of potassium contents these rocks also tend to have ratios near or slightly above 230. K-Rb relations in igneous rocks can take one of three forms (Shaw, 1968, p. 482, fig. 4), referred to as (1) the main trend, which has a linearity of log K–log Rb relations; (2) the oceanic tholeiite trend, which is similar to the main trend but has high K-Rb ratios at low potassium contents; and (3) the pegmatitic-hydrothermal trend, which is similar to the main trend but has low K-Rb ratios at high potassium contents. K-Rb relations of granitic rocks near the San Andreas fault typify Shaw's main trend, whereas Sierra Nevada patterns are more akin to the pegmatitic-hydrothermal trend, although the ratios do not attain the extremely low values figured by Shaw. Actually, the field of the plots of the K-Rb data from masses near the San Andreas fault and those of the central Sierra

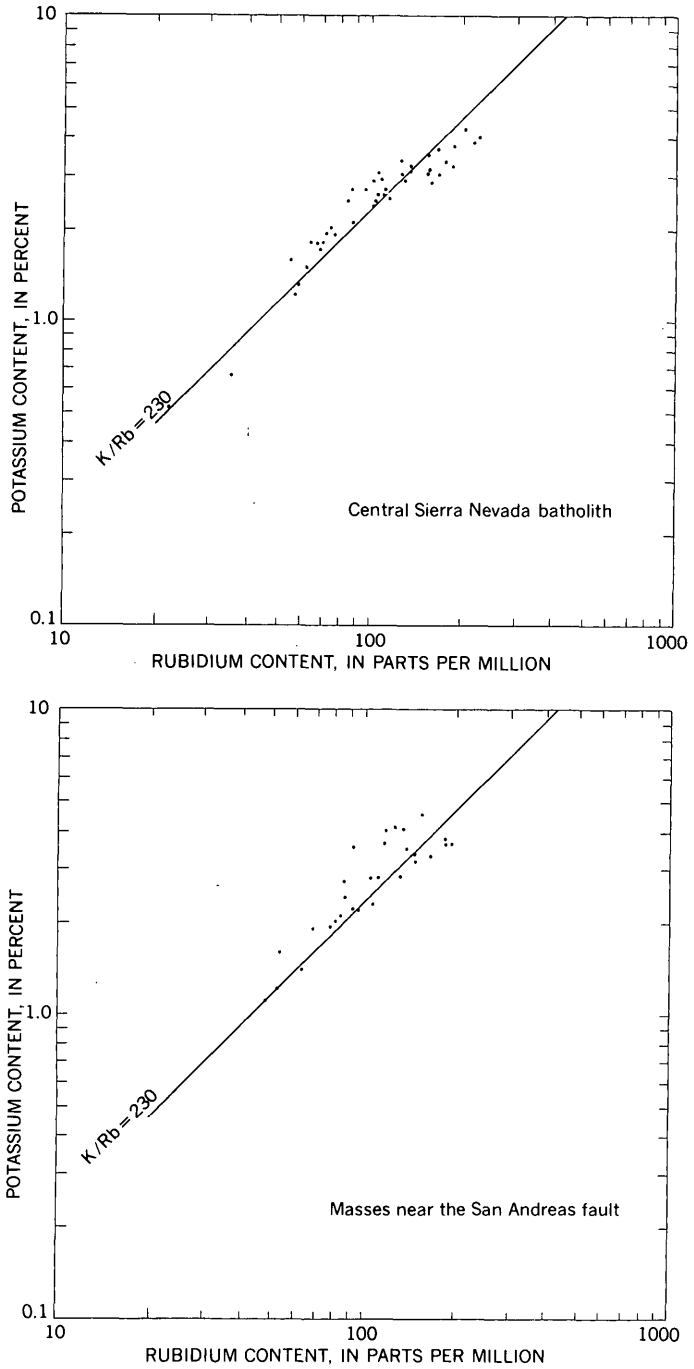

FIGURE 2.—K-Rb relations in granitic rocks of central California. The straight line shows the commonly accepted K-Rb ratio for igneous rocks.

Nevada batholith are virtually identical except for half a dozen points that have relatively high potassium values from the masses near the San Andreas fault. These potassium-enriched specimens detract from, and virtually cancel out, the common late rubidium enrichment in granitic rocks that is exemplified by the central Sierra Nevada rocks.

Pegmatitic rocks are present in both regions; they were not sampled, however. Some of the high potassium Sierra Nevada rocks are miarolitic, indicating presence of a vapor phase during crystallization. This in turn suggests that water pressure during the terminal stages of crystallization of these rocks was the same as total pressure. Miarolitic cavities have not been noted from rocks of the masses along the San Andreas fault. Dodge and Ross (1970) have commented on the "dry" nature (or low water pressure) of formation of rocks from near the fault relative to those of the Sierra Nevada batholith; this may be intimately related to the different K-Rb trends displayed by rocks from the two different areas. Shaw (1968, p. 595) has reviewed the evidence that hydrothermal waters may in fact have low K-Rb ratios that would account for low ratios of minerals being deposited from the waters.

A second possible, but less likely, way of maintaining constancy of the K-Rb ratio rather than enriching rubidium relative to potassium would be by introduction of late potassium feldspar into the rocks. Potassium feldspar has about twice as high a K-Rb ratio as biotite, the other major contributor of potassium and rubidium in felsic plutonic rocks (table 3). Thus late potassium feldspar in place of, or possibly replacing, constituents such as plagioclase or quartz would enrich the rock in potassium relative to rubidium and could account for canceling out of the pegmatitic-hydrothermal rubidium enrichment of late-stage granitic rocks. There is evidence of late potassium feldspar in the masses near the San Andreas fault. Coarse, poikilitic, and sporadically distributed potassium feldspar is indeed visibly late and has replaced plagioclase in many rocks. From the limited number of samples, however, it is difficult to conclude that there is a reaction quantitatively important enough to cause the slightly different K-Rb trend. The sporadic late enrichment in potassium from potassium feldspar also is compatible with the fact that not all K-rich granitic rocks in masses near the San Andreas fault are enriched in potassium; indeed, the K-Rb ratios of some samples lie on the pegmatitic-hydrothermal trend.

Neither the rocks of the Sierra Nevada nor those of the masses near the San Andreas fault have any affinity to the oceanic tholeiite trend; however, rubidium is below our detectibility level in the rock samples with the lowest potassium contents (CL–1, DR–589B, DR66–121), and potassium contents generally are much greater than the potassium contents of oceanic tholeiite basalt.

Bateman and Dodge's recent study (1970) of chemical analyses of plutonic rocks of the central Sierra Nevada and Inyo Mountains has shown that K_2O decreases significantly across the Sierra Nevada batholith, whereas other major-element oxides exhibit less pronounced changes. In figure 3, the potassium, rubidium, and K/Rb values of table 1 are projected onto line *W–E* (of fig. 1), which crosses the batholith approximately normal to its axis. The plot of rubidium as well as potassium clearly shows a westward decrease from an average near 150 ppm in the eastern Sierra Nevada to below 50 ppm in the western Sierran foothills. In contrast, the plot of the K-Rb ratio indicates no significant change across the batholith.

Lateral changes in the potassium content of circum-Pacific island arc andesites, similar to the potassium change across the Sierra Nevada batholith, have been related to the depth to dipping seismic (Benioff) zones beneath volcanoes of the arcs (Dickinson, 1968; Dickinson and Hatherton, 1967; Hatherton, 1969; Hatherton and Dickinson, 1969). Recently it has been proposed that Sierran batholithic magmas were generated along an eastward-dipping Mesozoic subduction zone or zones (Hamilton, 1969a, b). Bateman and Dodge (1970) have noted that progressive decrease of K_2O across the batholith is consistent with magma formation along a subduction zone, but they also point out that the hypothesis encounters several difficulties.

Green and Ringwood (1969), in a report on high-pressure experimental studies on the origin of andesites, have suggested that the K_2O change of various calc-alkaline suites is controlled by a complete continuum of fractionation processes occurring with increasing depth and pressure and decreasing water content. At shallow levels along a seismic zone, amphibole containing small but significant amounts of potassium would be the solid phase in equilibrium with any melt formed by the partial fusion of basalt in the presence of water. The potassium-enriched melts would then in turn be emplaced higher in the earth's crust. With increasing depth and pressure and decreasing water content, amphibole would gradually be replaced by garnet and clinopyroxene as the solid phases in the fractional melting of quartz eclogite, the high-pressure equivalent of basalt. As garnet and pyroxene contain negligible amounts of potassium, the fluid fractionates derived from greater depths should have much higher potassium contents than their shallower counterparts. Green and Ringwood suggest a complete transition from one residuum to the other with increasing depth.

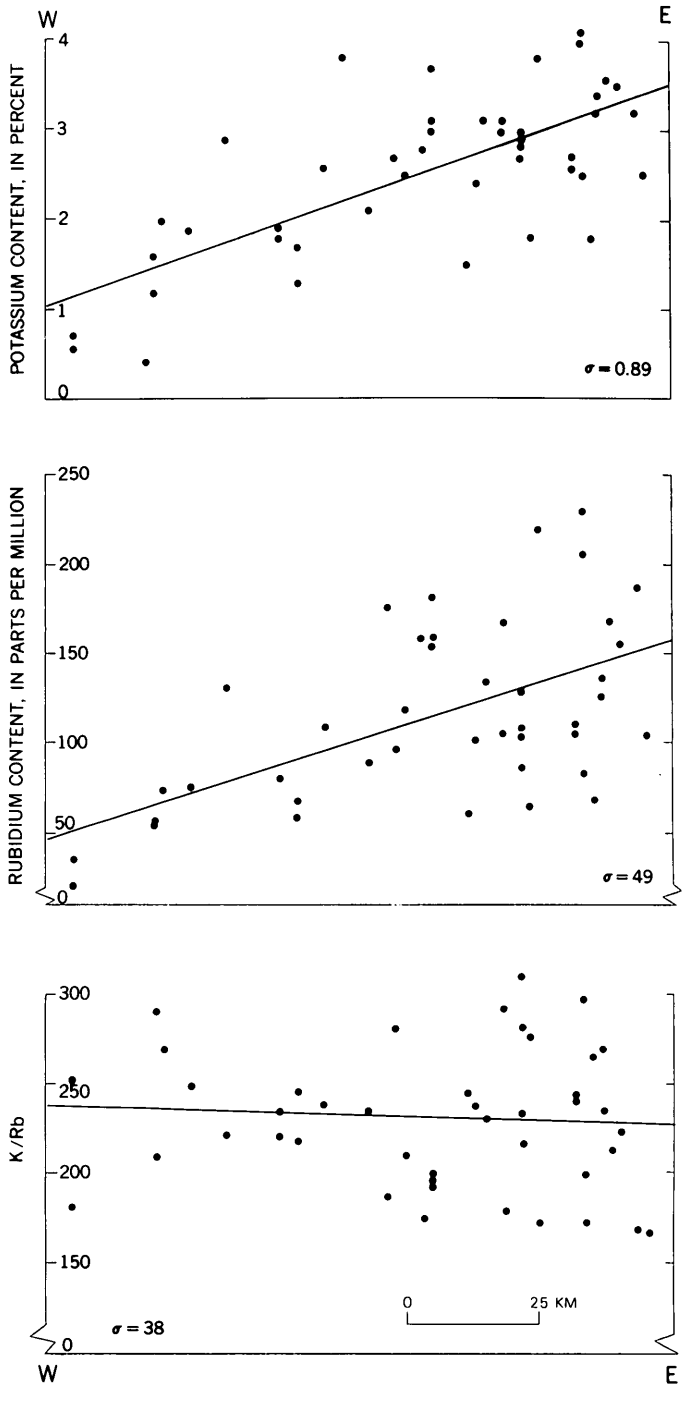

FIGURE 3.—Potassium and rubidium contents and K–Rb ratios of granitic rocks of the central Sierra Nevada batholith projected to line *W–E*. Dashed line represents least-squares approximation to the formula $y = ax + b$, where y is weight percent of a specific oxide and x is the distance along line *W–E*. σ represents one standard deviation from the least-squares line.

Characteristically, amphiboles have high ratios of potassium to rubidium, ratios commonly greater

than 1,000 (Hart and Aldrich, 1966). As a result, fractionation of an amphibole from a melt should cause enrichment of rubidium relative to potassium in the fractionated liquid, whereas fractionation of garnet or pyroxene should cause no change in amount of rubidium relative to amount of potassium. Thus, according to the model set forth by Green and Ringwood, rocks derived from melts fractionated at shallow depths along a seismic zone will not only have low contents of potassium but will also have low K-Rb ratios, whereas rocks derived from melts fractionated at greater depths will not only have higher potassium contents but will also have higher, "normal" K-Rb ratios. The lack of a significant change of the ratio across the Sierra Nevada batholith is inconsistent with the model. Unfortunately, rubidium contents of hornblendes of rocks of the Sierra Nevada batholith are below detectibility levels of the method used in this study.

A stability study of hornblende from one of the samples analyzed in our study (sample BCa–20) by Lambert and Wyllie (1968) indicates that at pressures between 15 and 25 kilobars, that is, at depths roughly from 50 to 80 kilometers, there is a pressure-induced reaction involving breakdown of the amphibole. Thus, if the Sierra Nevada potassium trend is a reflection of magma generation along a subduction zone, depths greater than 45 kilometers, and probably greater than 80, would be required.

Ratios of potassium to rubidium for analyzed minerals vary as much as the ratios for their host rocks; however, potassium feldspar invariably has a ratio higher than its host rock, whereas biotite commonly has a lower ratio. Little difference can be seen between the two K-Rb ratios for biotites from rocks near the San Andreas fault and those for biotites from the Sierra Nevada rocks. Distribution coefficients have been calculated for the 13 analyzed

$$K_D = \frac{(K/Rb)_{K\text{-feldspar}}}{(K/Rb)_{biotite}}$$

mineral pairs (table 4). K_D ranges from 1.69 to 4.35 and has a mean value of 3.15. Comparable values have been calculated from data on mineral pairs from granitic rocks of the southern California batholith (Sen and others, 1959) and on mineral pairs from rocks of several other regions (for example, Barbieri and others, 1968; Lange and others, 1966; Whitney, 1969). The mean value of 3.15 agrees with that of 3.2 experimentally determined by Beswick and Eugster (1968) for the distribution coefficient of synthetic sanidine-phlogopite

TABLE 4.—*Distribution coefficients,* K_D, *of potassium and rubidium in coexisting potassium feldspars and biotites*

$$\left[K_D = \frac{(K/Rb)_{K\text{-feldspar}}}{(K/Rb)_{biotite}} \right]$$

Sample No.	K_D	Sample No.	K_D
M–139	2.53	FD–20	1.69
MG–1	2.86	BP–1	4.35
HL–4	2.66	MG–3	3.03
FD–13	3.13	MT–1	4.29
SL–18	3.90	KR	3.23
HL–29	3.71	Mo–1c	1.85
KPc–138	[1]3.82		

[1] K_D based on groundmass potassium feldspar.

pairs at 700°C (at temperatures of 500 and 800°C, Beswick and Eugster determined values of 4.5 and 2.8, respectively), a temperature that probably rather closely approximates the general original crystallization temperatures of the natural potassium feldspar-biotite pairs of the granitic rocks of central California.

CONCLUSIONS

K-Rb ratios of granitic rocks of central California define two slightly different trends. The ratio is generally constant in rocks from near the San Andreas fault, whereas it tends to decrease slightly at high potassium contents in rocks from the central Sierra Nevada batholith. The ratios may be different due to differences in water pressures that prevailed during formation of the respective rocks. Higher water pressures are thought to have prevailed during the final stages of crystallization of Sierra Nevada rocks, causing greater partial separation of potassium and rubidium between melts and aqueous phases, a process recently discussed by Shaw (1968), and consequent deposition from rubidium-rich fluids during crystallization of late, high-potassium magmas. It is also conceivable that the differing behavior of the ratio may be due to late introduction of potassium feldspar into some rocks near the San Andreas fault.

The lack of systematic variation of the K-Rb ratio across the Sierra Nevada batholith, when compared with Green and Ringwood's (1969) experimentally based model for the origin of andesite, suggests that the westward decrease of potassium and rubidium contents is probably not attributable solely to magma generation along an easterly dipping Mesozoic seismic (subduction) zone, at least at relatively shallow depths.

Partitioning of potassium and rubidium between coexisting potassium feldspar and biotite related to the distribution of the two elements in experimen-

tally produced sanidine and phlogopite (Beswick and Eugster, 1968), suggests a temperature generally near 700°C during crystallization of the natural mineral pair.

REFERENCES

Ahrens, L. H., Pinson, W. H., and Kearns, M. M., 1952, Association of Rb and K in common igneous rocks and meteorites: Geochim. et Cosmochim. Acta, v. 2, p. 229–242.

Barbieri, M., Fornaseri, M., and Penta, A., 1968, Rubidio e potassio nelle vulcanti dei Colli Albani, di Vico del Cimino: Period. Mineralogia, v. 37, p. 243–298.

Beswick, A. E., and Eugster, H. P., 1968, The distribution of potassium and rubidium between sanidine and phlogopite [abs.]: Geol. Soc. America, Program with abstracts, Ann. Mtgs., Mexico City 1968, p. 25–26.

Bateman, P. C., and Dodge, F. C. W., 1970, Variations of major chemical constituents across the central Sierra Nevada batholith: Geol. Soc. America Bull., v. 81, p. 409–420.

Compton, R. R., 1966, Granitic and metamorphic rocks of the Salinian block, California Coast Ranges, *in* Bailey, E. H., ed., Geology of northern California: California Div. Mines Bull. 190, p. 277–288.

Dickinson, W. R., 1968, Circum-Pacific andesite types: Jour. Geophys. Research, v. 73, p. 2261–2269.

Dickinson, W. R., and Hatherton, Trevor, 1967, Andesitic volcanism and seismicity around the Pacific: Science, v. 157, p. 801–803.

Dodge, F. C. W., Papike, J. J., and Mays, R. E., 1968, Hornblendes from granitic rocks of the central Sierra Nevada batholith, California: Jour. Petrology, v. 9, p. 378–410.

Dodge, F. C. W., and Ross, D. C., 1970, Coexisting hornblendes and biotites from granitic rocks near the San Andreas fault, California: Journal of Geology. [In press]

Dodge, F. C. W., Smith, V. C., and Mays, R. E., 1969, Biotites from granitic rocks of the central Sierra Nevada batholith, California: Jour. Petrology, v. 10, p. 250–271.

Erlank, A. J., 1968, The terrestrial abundance relationship between potassium and rubidium, *in* Ahrens, L. H., ed., Origin and distribution of the elements: Oxford and New York, Pergamon Press, p. 871–888.

Green, D. H., and Ringwood, A. E., 1969, High-pressure experimental studies on the origin of andesites, *in* McBirney, A. R., ed., Proceedings of the Andesite Conference: Oregon Dept. Geology and Mineral Industries Bull. 65, p. 21–32.

Hamilton, Warren, 1969a, Mesozoic California and underflow of Pacific mantle: Geol. Soc. America Bull., v. 80, p. 2409–2430.

——— 1969b, The volcanic central Andes—a modern model for the Cretaceous batholiths and tectonics of western North America, *in* McBirney, A. R., ed., Proceedings of the Andesite Conference: Oregon Dept. Geology and Mineral Industries Bull. 65, p. 175–184.

Hart, S. R., and Aldrich, L. T., 1966, Fractionation of K/Rb by amphiboles—implications regarding mantle composition: Science, v. 155, p. 325–327.

Hatherton, Trevor, 1969, The geophysical significance of calc-alkaline andesites in New Zealand: New Zealand Jour. Geology and Geophysics, v. 12, p. 436–459.

Hatherton, Trevor, and Dickinson, W. R., 1969, The relationship between andesitic volcanism and seismicity in Indonesia, the Lesser Antilles, and other island arcs: Jour. Geophys. Research, v. 74, p. 5301–5310.

Heir, K. S., and Adams, J. A. S., 1964, The geochemistry of the alkali metals: Physics and Chemistry Earth, v. 5, p. 253–382.

Hurley, P. M., Bateman, P. C., Fairbairn, H. W., and Pinson, W. H., Jr., 1965, Investigation of initial Sr^{87}/Sr^{86} ratios in the Sierra Nevada plutonic province: Geol. Soc. America Bull., v. 76, p. 165–174.

Kistler, R. W., Bateman, P. C., and Brannock, W. W., 1965, Isotopic ages of minerals from granitic rocks of the central Sierra Nevada and Inyo Mountains, California: Geol. Soc. America Bull., v. 76, p. 155–164.

Lachenbruch, A. H., 1968, Preliminary geothermal model of the Sierra Nevada: Jour. Geophys. Research, v. 73, p. 6977–6989.

Lambert, I. B., and Wyllie, P. J., 1968, Stability of hornblende and a model for the low velocity zone: Nature, v. 219, p. 1240–1241.

Lange, I. M., Reynolds, R. C., and Lyons, J. B., 1966, K/Rb ratios in coexisting K-feldspars and biotites from some New England granites and metasediments: Chem. Geology, v. 1., p. 317–322.

Naeser, C. W., and Dodge, F. C. W., 1969, Fission-track ages of accessory minerals from granitic rocks of the central Sierra Nevada batholith, California: Geol. Soc. America Bull., v. 80, p. 2201–2212.

Piwinskii, A. J., 1968a, Studies of batholithic feldspars—Sierra Nevada, California: Contr. Mineralogy Petrology, v. 17, p. 204–223.

——— 1968b, Experimental studies of igneous rock series, central Sierra Nevada batholith, California: Jour. Geology, v. 76, p. 548–570.

Sen, N., Nockolds, S. R., and Allen, R., 1959, Trace elements in minerals from rocks of the southern California batholith: Geochim. et Cosmochim. Acta, v. 16, p. 58–78.

Shaw, D. M., 1968, A review of K–Rb fractionation trends by covariance analysis: Geochim. et Cosmochim. Acta, v. 32, p. 573–601.

Taylor, S. R., 1965, The application of trace-element data to problems in petrology: Physics and Chemistry Earth, v. 6, p. 133–213.

Whitney, P. R., 1969, Variations of the K/Rb ratio in magmatic paragneisses of the northwestern Adirondacks: Geochim. et Cosmochim. Acta, v. 33, p. 1203–1212.

CHANGING PATTERNS OF THERMAL EMISSION FROM SURTSEY, ICELAND, BETWEEN 1966 AND 1969

By JULES D. FRIEDMAN[1] and RICHARD S. WILLIAMS, JR.[2],
Washington, D.C., Bedford, Mass.

Work done in cooperation with the U.S. Air Force Cambridge Research Laboratories and the Iceland National Energy Authority

Abstract.—Comparison of August 1968 aerial infrared images of Surtsey, Iceland, with 1966 aerial infrared survey data indicates continued but generally diminishing thermal emission following cessation of effusive activity in mid-1967. Emission from most but not all secondary or rootless sources including flow fractures, collapse features, and secondary fumaroles diminished more rapidly than from primary convecting structures, notably ring fractures associated with the Surtur II vent, and linear structures related to faults which controlled various phases of eruptive activity between 1964 and 1967. However, thermal emission increased in 1969 from the Surtur I and II tephra rims. Heat flux from the tephra anomalies is estimated at greater than 1,500 μcal·cm^{-2}·sec^{-1} and is dominantly convective. Heat flux from the primary convecting structures may be an order of magnitude greater, suggesting a total heat transport to the surface of the island of 10^9 to 10^{10} μcal·sec^{-1} in 1969, less than 1 percent of the peak heat transport during the effusive eruption phase.

AUGUST 1966 INFRARED SURVEYS

Infrared imagery obtained in August 1966 by an AFCRL (U.S. Air Force Cambridge Research Laboratories) C-130 aircraft equipped with a thermal infrared scanning system showed areas of thermal emission from Surtsey and Jólnir (fig. 1) (Friedman and others, 1967, 1969; Williams and others, 1968). In 1966, intensity of infrared emission was greatest from the August lava flow on the floor of Surtur I (Friedman and others, 1969, p. C96, fig. 6*B*) and from lava cauldron activity in three craters (figs. 2*A* and *B*) active during the August 23–29 survey. Thermal anomalies of moderate intensity were recorded from the Surtur II vent and from a complex pattern of 1964–65 lava outflow channels and tubes in the Surtur II lava shield (fig. 3). Thermal anomalies which resulted from convective venting to the surface outlined a possible subsurface lava tube leading from the Surtur II vent area to a triangular flow at the toe of the shield on the west side of the island—the last large surface expression of the flows of 1965. Within this flow, convective venting from secondary or rootless fumaroles (Wentworth and MacDonald, 1953, p. 29), circular collapse features, and pressure-ridge fractures was shown as a variegated pattern of thermal anomalies in which point and curvilinear sources are conspicuous. East of the triangular area, somewhat fainter thermal anomalies mark the position of convecting fractures and fumaroles at the surface of flows dating back to 1964.

The 1966 surveys also recorded the last phase of thermal activity of Jólnir. The main tephra crater (Friedman and Williams, 1970, p. 93, fig. 5*A*) contained a lake on August 19, 1966, the temperature of which was estimated by Sigurður Thórarinsson (Science Institute, University of Iceland, Reykjavík) at 40°–50°C. A faint, generalized hydrothermal anomaly within the structural lagoon of Jólnir noted between August 19 and 23 developed into a more distinct localized anomaly by August 29 (Friedman and others, 1969, p. C99, fig. 7*A* and *B*) after parts of the tephra island, including the main crater, were destroyed by wave action.

AUGUST 1968 INFRARED SURVEYS

Several survey flights over Surtsey were made in August 1968 with a modified M1A1 line-scan system

[1] U.S. Geological Survey.
[2] U.S. Air Force Cambridge Research Laboratories, Bedford, Mass.

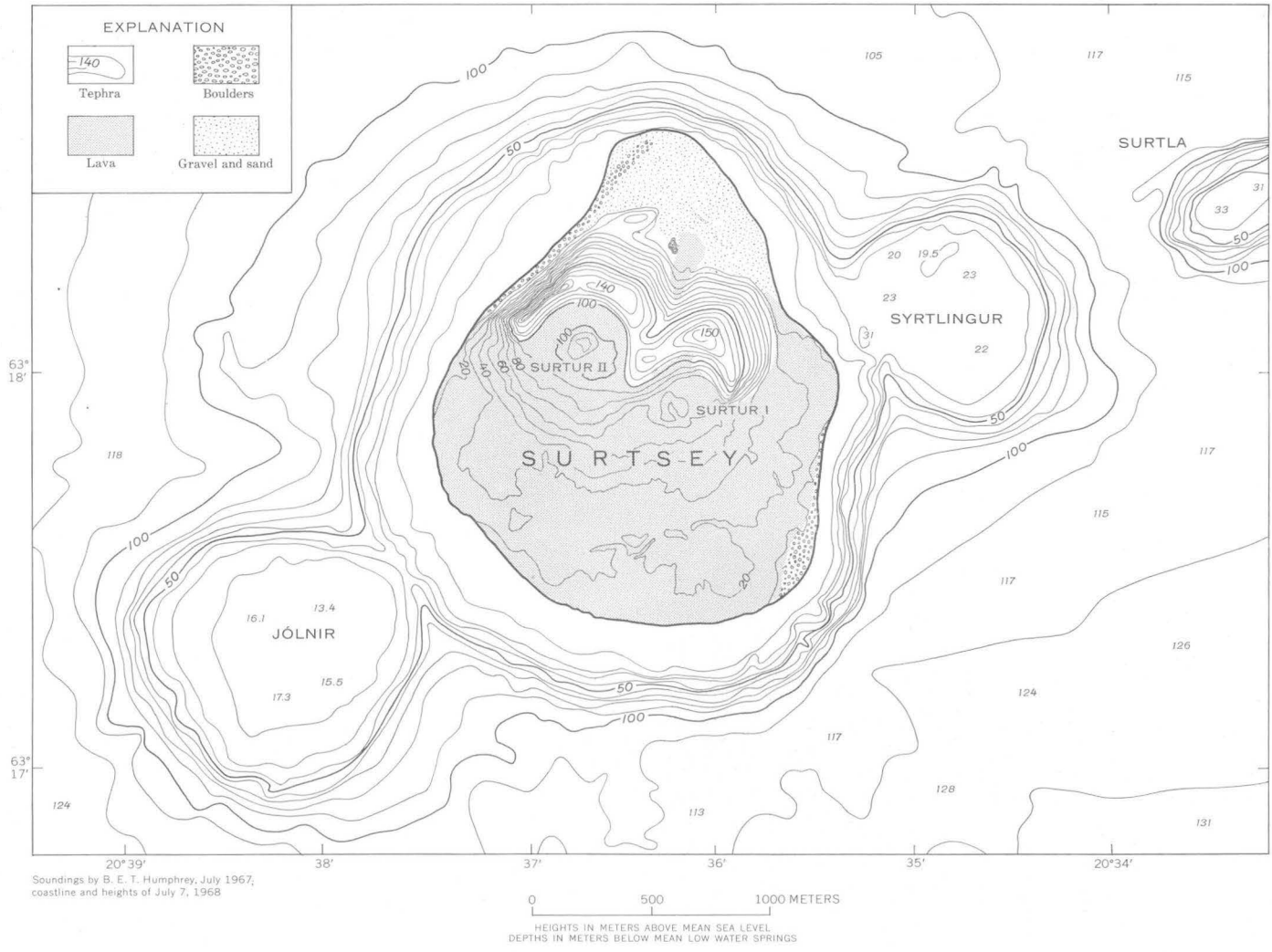

FIGURE 1.—Surtsey shoreline in 1968 in relation to shoal areas representing truncated submarine volcanoes Jólnir, Syrtlingur, and Surtla. Bathymetry suggests a N. 60° E. alinement of eruptive centers. Modified from Norrman (1969, 1970).

to record changes in the thermal pattern since August 1966. Conspicuous features of the imagery recorded in 1968 (fig. 4) can be divided into three categories:

1. *Thermal features of 1966 that have disappeared.*—This category includes: (a) hydrothermal anomalies of the last phase of Jólnir; (b) convection-feature anomalies of the eastern side of Surtsey, marking 1964 flows (now partly covered by the flows of 1966 from Surtur I); (c) the convection anomaly marking a subsurface lava tube connecting the Surtur II vent area with the triangular 1965 flow area (fig. 3); and (d) the triangular configuration of the 1965 flow area itself (fig. 3). The disappearence of these anomalies confirms that they in general represented secondary thermal emission which diminished markedly during the 2 years elapsed between August 1966 and August 1968.

2. *Residual anomalies identified on both 1966 and 1968 imagery.*—This category includes: (a) a bright curvilinear anomaly at the toe of the Surtur II shield (fig. 4). That this feature has persisted since 1966, whereas the thermal emission from the remainder of the triangular area has virtually disappeared, suggests that the thermal source of the anomaly is probably at a depth greater than the base of the cooling surface flows and may be primary in origin rather than secondary. This anomaly may mark a point of emergence of lava from some depth, although it could be a rootless vent (Wentworth and MacDonald, 1953, p. 26). The relationship of this persistent thermal feature to the now-disappeared anomaly representing a lava tube between the main Surtur II vent and the triangular

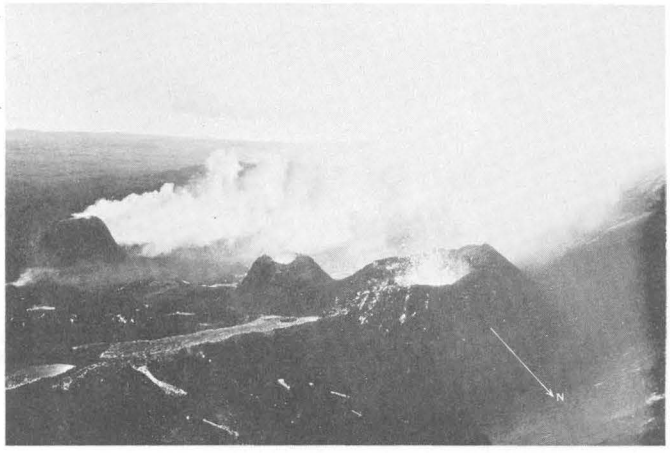

A

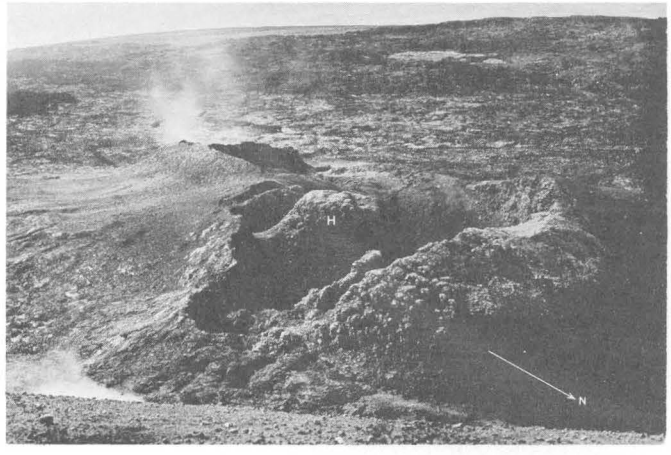

B

FIGURE 2.—Photographs (from color transparencies) of the Surtur I crater row. *A*, August 27, 1966, 1800 Universal Mean Time, during period of lava fountain and flow activity. Distance between the two cones on the north is about 80 m. *B*, July 21, 1967. Hornito (H) in northern crater, one of the last features to form, is 10 m high.

flow area is not entirely clear. Whether the flow occupying the triangular area has a distinctly separate conduit from the main Surtur II vent or was fed by lava tubes in the Surtur II shield is an interesting but unresolved question; (b) a sizable circular anomaly that continues to mark the Surtur II vent area (figs. 4 and 5), suggesting increased primary convective heat flow along a circular fracture pattern parallel to the walls of the vent; the evolution of this anomaly since 1966 suggests increased thermal emission along a developing ring fracture possibly related to subsidence of 0.5 to 1.0 mm per day (Tryggvason, 1970) of this part of the shield since the last eruptive pulse in mid-1967; (c) distinct anomalies that continue to mark subsurface lava outflow courses (tubes) and possible linear fractures high on the Surtur II shield (fig. 4); and (d) continued thermal emission from the 1966 flow emanating from Surtur I; radiant emission from these flows has diminished since 1966 and is secondary in origin.

3. *Thermal anomalies that have appeared since August 1966.*—The most outstanding anomalies of this type are intense linear features, forming two sets striking N. 3° W. and N. 87° E., marking the alinement of primary fumaroles along the eruption fissures of 1966 and 1967 on the Surtur I tephra rim and Surtur I crater floor similar to parallel sets of enhanced linear anomalies on the Surtur II shield. Generalized tephra rim anomalies related to Surtur I are also discernible.

Enhanced linear anomalies of the Surtur II shield and Surtur I mark a northeast trend, related to alinement of the major Surtsey eruptive centers (fig. 1) and northwest-striking anomalies, one of which, at least, is related to the effusive eruption fissure in the floor of Surtur I in 1966.

INCREASE IN HEAT FLOW THROUGH TEPHRA RIMS IN 1969

In 1969, increasing surface temperatures were noted by Icelandic observers in the area of the tephra rim anomalies (figs. 4 and 6). On April 23, 1969, Sigurđur Thórarinsson observed that 5 m west of the 155-m summit of Surtur I, the temperature at a depth of 20 cm was somewhat less than 100°C (Thórarinsson, written commun., Sept. 3, 1969). On August 2, 1969, Thórarinsson recorded a temperature of 80°C at a depth of 40 cm at the same locality, but he reports that the temperature at the surface did not exceed 30°C.

Utilizing the data of Robertson and Dawson (1964), who have shown that in the Wairakei geothermal field, New Zealand, the change from dominantly conductive to dominantly convective heat transport occurs when the mean annual temperature at a depth of 1 m is 25°C greater than the mean annual surface temperature, we may conclude that the heat transport through the tephra pile is dominantly convective. Furthermore, utilizing the relation (Dawson, 1964, p. 160) between convective heat flux and temperatures at depths of less than a meter, we conclude that the heat flux observed by Thórarinsson on August 21, 1969, was greater than 1,500 $\mu cal \cdot cm^{-2} \cdot sec^{-1}$. In mid-August 1969, Ævar Jóhannesson, photographer, observed that nearly the entire semicircular crest of Surtur I was as warm as the summit area. At the end of August 1969, thermal emission from the Surtur II tephra rim was noted 200 to 300 m from the Pálsbaer observatory (Thórarinsson, written commun., 1969). If we assume that the entire tephra pile was involved, the total heat transport through this anomalously warm area is estimated at 10^8 to 10^9 $\mu cal \cdot sec^{-1}$ during August 1969. Thermal emission from this area continued at least through May 1970.

Convective heat transport through the Surtur I and II vents, primary fumaroles, and fractures in the shield and lava flow areas may be an order of magnitude greater, suggesting a total heat transport to the surface of about 10^9 to 10^{10} $\mu cal \cdot sec^{-1}$, less than 1 percent of the peak heat transport during the effusive eruption phase (Friedman and others, 1969, p. C103, table 2).

CONCLUSIONS

Thermal emission from primary volcanic structures associated with effusive activity in 1965, 1966, and 1967 was recorded on infrared imagery in August 1968 and has continued at least through May 1970. Thermal emission from most but not all secondary sources, such as lava flow fractures, collapse features, and secondary fumaroles diminished more rapidly than that from primary convecting structures, including the circular fractures of the Surtur II vent and linear convecting fractures of Surtur I and II. Emission continued from a possible rootless vent at the toe of the Surtur II shield. The fracture pattern of Surtur I associated with the effusive eruptions of December 1966 and January 1967 was also still clearly marked on the images.

Increased thermal emission observed from the tephra rims of Surtur I and II in 1969 is estimated as somewhat greater than 1,500 $\mu cal \cdot cm^{-2} \cdot sec^{-1}$. The heat transport mechanism is dominantly convective and may be the result of closure of heat release outlets at depth following cessation of lava outflow in 1967, but merits continuing observation.

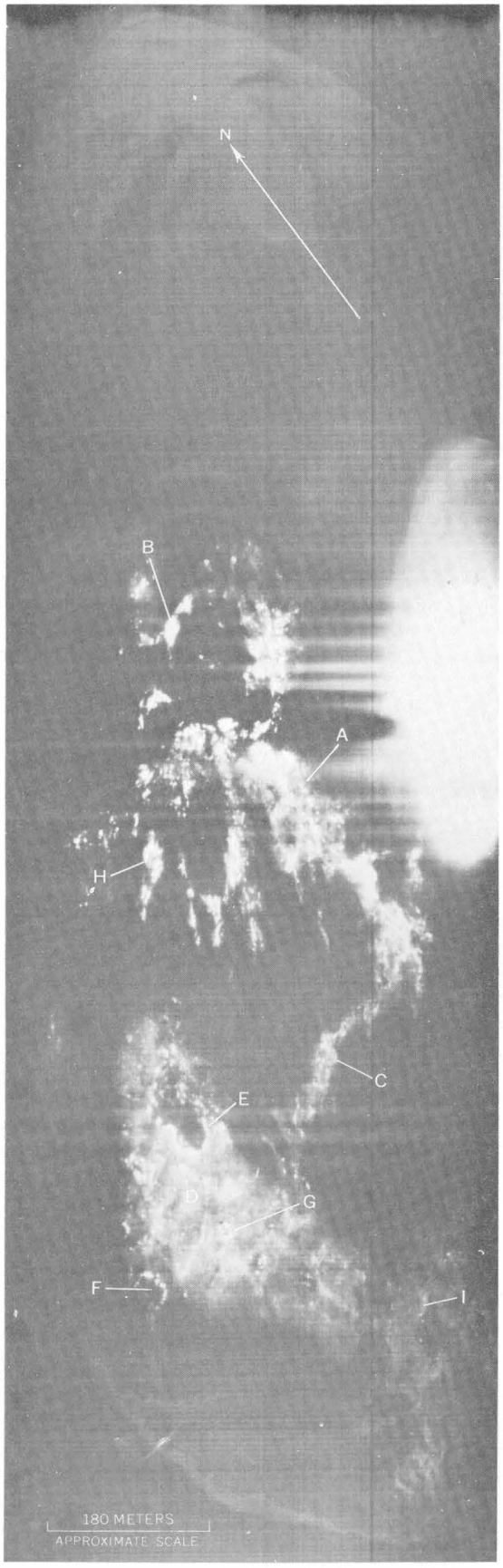

←
FIGURE 3.—Aerial infrared image of western half of Surtsey, August 19, 1966, about 1900 Universal Mean Time, by M1A1 line-scan system utilizing an InSb detector. White areas represent thermal emission. Image shows linear anomalies of Surtur II shield area (A) and circular anomalies of Surtur II vent (B). Large subsurface lava tube (C) connects main vent with triangular flow area (D) of 1965 at toe of shield. Convective venting outlines the fracture pattern of pressure ridge (E). Possible rootless vent (F) appears at apex of 1965 flow, west of circular collapse feature (G). Chimney (H) formed by roof collapse over lava tube in Surtur II shield was used for geochemical gas sampling during eruption of 1965. Convecting fractures (I) of eastern Surtsey, dating back to 1964, appear near margin of image.

→
FIGURE 4.—Aerial infrared image mosaic of Surtsey, August 22, 1968, 2049–2108 Universal Mean Time, made from video tape records obtained by the M1A1 line-scan system utilizing an InSb detector. Features identifiable on figure 3 and on this mosaic are shown by the same letters. Note, in comparison with figure 3, enhancement of linear anomalies of Surtur II shield area (A) and circular anomalies of Surtur II vent (B) on this 1968 image. Several secondary thermal anomalies, including emission from subsurface lava tube in Surtur II shield, (C, fig. 3), triangular flow area of 1965 (D, fig. 3), and pressure ridge fractures (E, fig. 3) have disappeared. Possible rootless vent (F) has persisted since at least 1966. Surtur I anomalies (J) associated with August 1966, December 1966, and January 1967 effusive eruptions outline two fracture sets striking approximately N. 3° W. and N. 87° E., roughly parallel to sets of linear anomalies of Surtur II. Surtur I tephra rim anomalies (K) appear in gray tones on this mosaic. Thermal emission from cooling lava flows of 1966–67 (L) appears in slightly brighter gray tones to the south.

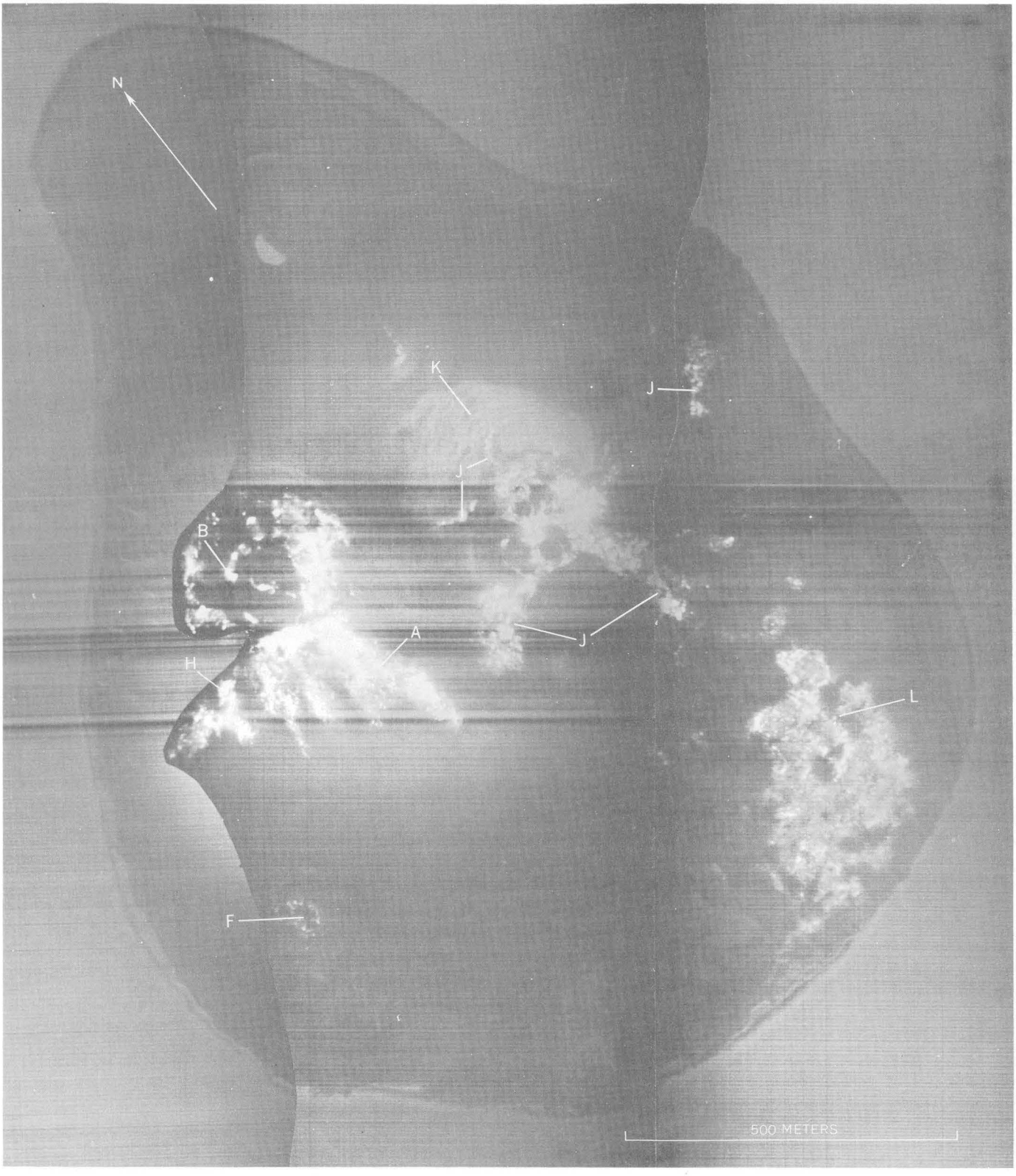

FIGURE 4

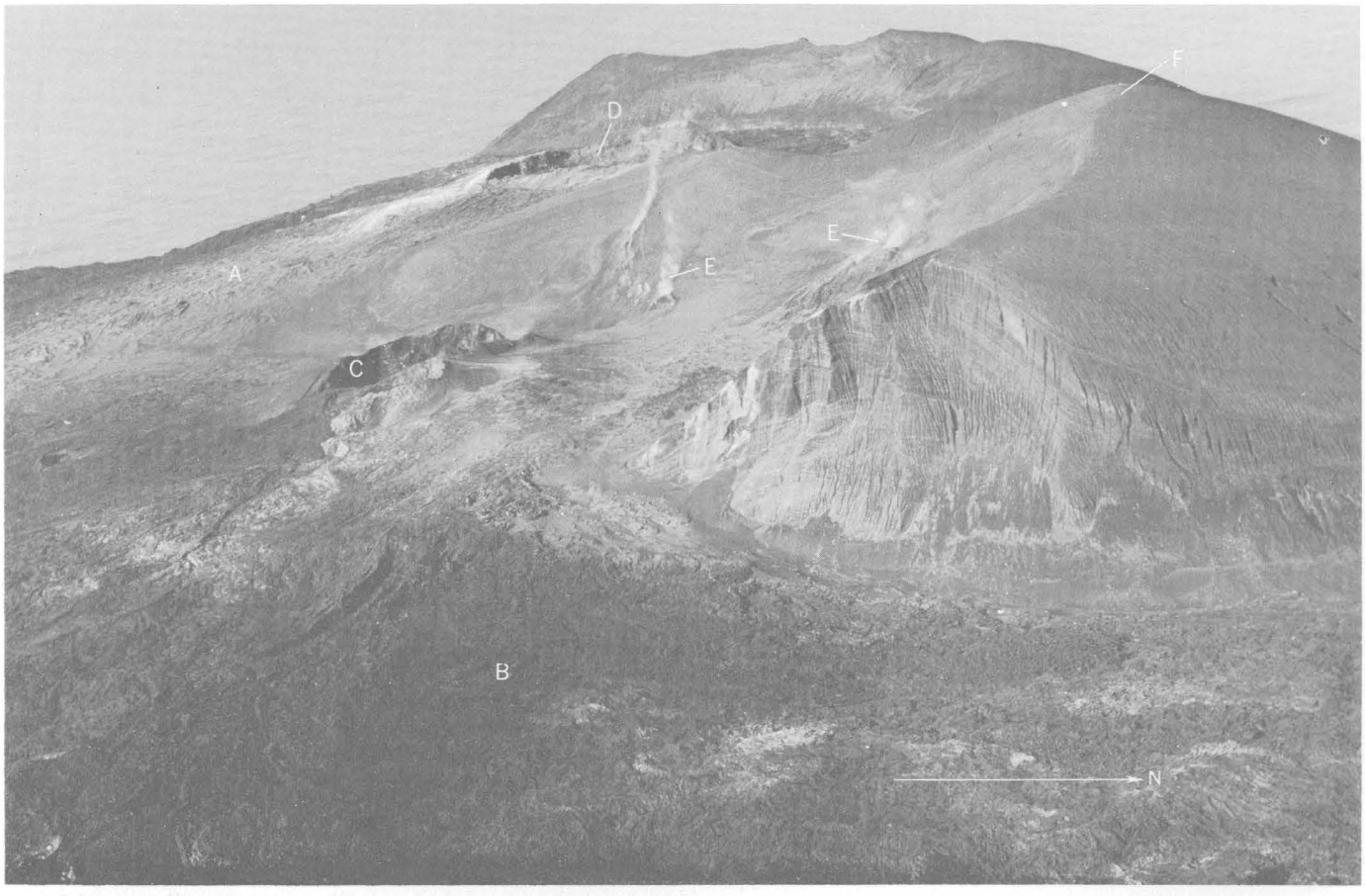

FIGURE 5.—Photograph (from color transparency), September 1969, showing Surtur II lava shield (A), Surtur I flows (B), Surtur I vent (C), and Surtur II vent (D), fumarolic emission (E) along fracture lines shown by the letters J on infrared image mosaic (fig. 4), and 155-m summit of tephra rim (F) where thermal emission was recorded in 1969.

FIGURE 6.—Photograph (from color transparency), September 1969, showing Surtur II vent (A) and part of lava shield; subsidence along walls of vent (B); vapor emission from scoriaceous wall materials of vent (C), also shown as circular anomalies arond vent on infrared images (point B in figures 3 and 4); and chimney (D) formed by roof collapse of lava tube (shown by point H in fig. 4).

REFERENCES

Dawson, G. B., 1964, The nature and assessment of heat flow from hydrothermal areas: New Zealand Jour. Geology and Geophysics, v. 7, p. 158–160.

Friedman, J. D., and Williams, R. S., Jr., 1970, Comparison of 1968 and 1966 infrared imagery of Surtsey: Surtsey Research Soc., Reykjavík, Prog. Rept. 5, 1968 field season, p. 90–94.

Friedman, J. D., Williams, R. S., Jr., Pálmason, Guđmundur, and Miller, C. D., 1967, Infrared surveys in Iceland in 1966: Surtsey Research Soc., Reykjavík, Prog. Rept. 3, p. 99–103.

——— 1969, Infrared surveys in Iceland—Preliminary report, *in* Geological Survey Research 1969: U.S. Geol. Survey Prof. Paper 650–C, p. C89–C105.

Norrman, J. O., 1969, Kustmorfologiska studier på Surtsey: Uppsala Universitets Geografiska Institutioner, Meddelanden, ser. A, no. 239, p. 63.

——— 1970, Trends in postvolcanic development of Surtsey Island. Progress report on geomorphological activities in 1968: Surtsey Research Soc., Reykjavík, Prog. Rept. 5, 1968 field season, p. 97.

Robertson, E. L., and Dawson, G. B., 1964, Geothermal heat flow through the soil at Wairakei, N.Z.: New Zealand Jour. Geology and Geophysics, v. 7, p. 134–143.

Tryggvason, Eysteinn, 1970, Surface deformation on and near three volcanoes in Iceland [abs.]: Am. Geophys. Union Trans., v. 51, no. 4, p. 441.

Wentworth, C. K., and MacDonald, G. A., 1953, Structures and forms of basaltic rocks in Hawaii: U.S. Geol. Survey Bull. 994, 98 p.

Williams, R. S. Jr., Friedman, J. D., Thórarinsson, Sigurđur, Sigurgeirsson, Thorbjörn, and Pálmason, Guđmundur, 1968, Analysis of 1966 infrared imagery of Surtsey, Iceland: Surtsey Research Soc., Reykjavík, Prog. Rept. 4, p. 177–192.

INDUCED POLARIZATION AND RESISTIVITY SURVEYS ON CLEARY SUMMIT, ALASKA

By LENNART A. ANDERSON and GORDON R. JOHNSON,
Denver, Colo.

Abstract.—Induced polarization and resistivity surveys were made on the north flank of Cleary Summit about 16 air miles north-northeast of Fairbanks, Alaska. Data were obtained along three traverses that were positioned to transect some of the known vein structures that have produced gold, silver, and other metallic minerals. Two disseminated sulfide concentrations of possible economic interest, one deep seated and the other about 75–150 feet beneath the surface, were detected.

From 1903 into the mid-1950's lode gold was mined from narrow quartz veins in the Cleary Summit area, which is about 16 air miles north-northeast of Fairbanks, Alaska (fig. 1). Sulfide minerals were also found in the fractures that contained the gold-quartz veins. Stibnite was mined for antimony when the market price for that mineral warranted independent production (Killeen and Mertie, 1943). At the time the present survey was made, mining was being carried on as a one-man operation which involved the extraction of fault gouge primarily for its lead content and secondarily for its small silver content.

The quartz veins strike approximately eastward and generally dip to the south. The mineral-bearing veins are confined to the north slope of Cleary Summit and are thought to be related to igneous rocks that intrude the schistose country rock (Killeen and Mertie, 1943).

To test the area for possible new sources of sulfide minerals, we made induced polarization and resistivity surveys along three traverses that were positioned to transect the trend of two of the known vein structures.

METHOD, RESULTS, AND INTERPRETATION

The dual-frequency method was used to measure induced polarization. In this method, a set of current and potential electrodes placed directly in contact with the earth are used to measure resistivity at two discrete frequencies. If conductive or polarizable minerals are present in disseminated form, the resistivity will decrease as the frequency is increased. This effect can then be considered a measure of induced polarization and is expressed as percent frequency effect (PFE) where $PFE = (\rho_l - \rho_h) \times 10^2 / (\rho_l \rho_h)^{1/2}$; ρ_l and ρ_h are the resistivities measured at the low and high frequencies, respectively. For a detailed discussion of the dual-frequency method, see Keller and Frischknecht (1966).

The induced polarization surveys were made with the pole-dipole or half Schlumberger electrode configuration in which one current electrode is placed at a distance at least 10 times greater than the maximum separation between the near-current electrode and the measuring dipole. A 100-foot dipole was used, and measurements were made at frequencies of 0.05 and 1.0 Hz. Five in-line measurements were made for every current electrode emplacement at distances of 100–500 feet in multiples of 100 feet.

Traverses *A–A′*, *B–B′*, and *C–C′* were made across the major trend of the mineralized zone on Cleary Summit (fig. 1). Traverse *A–A′* was positioned to transect the Jamesonite vein near the site of the old Keystone mine, where fault gouge associated with the vein was mined during 1967–68 for its lead-silver content. The gouge is significantly more conductive, electrically, than the surrounding schist and therefore can be detected easily with the induced polarization method.

The contoured resistivity data obtained along traverse *A–A′* (fig. 2) indicate the presence of a narrow conductive zone which can be associated with the vein gouge. The high resistivity anomaly

U.S. GEOL. SURVEY PROF. PAPER 700-D, PAGES D125–D128

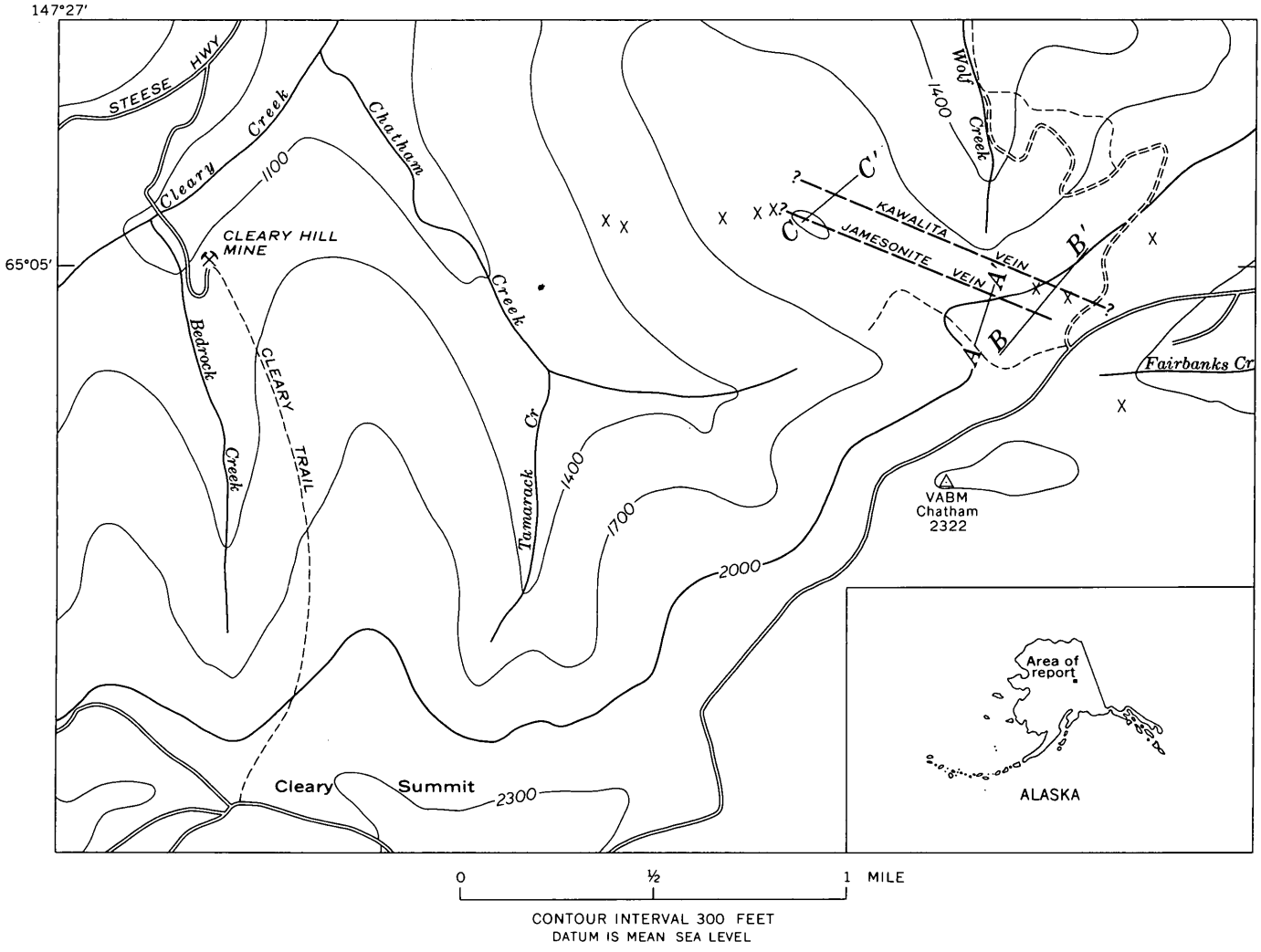

FIGURE 1.—Location of induced polarization-resistivity traverses (*A–A'*, *B–B'*, and *C–C'*) on Cleary Summit. X, mine or prospect. Contour interval, 300 feet. Base from U.S. Geological Survey Livengood A–1 quadrangle, 1951, scale 1 : 63,360.

immediately south of the fault is characteristic of the three-electrode or pole-dipole array when profiling across a near-vertical conductive boundary (Keller and Frischknecht, 1966; Dakhnov, 1959). The lowest apparent resistivities were found in the near-surface rock, indicating that some degree of weathering has occurred in the upper layer.

The contoured induced polarization data taken along traverse *A–A'* do not produce a pattern that can be related directly to the distribution of conductive gouge within the vein. The polarization values obtained over the unaltered schist average about 5.0 PFE near the surface and increase slightly with depth. This increase can be caused by either an increase in the volume fraction of conducting minerals or a subtle variation in clay content.

In the vicinity of the Jamesonite vein, the increase in the polarization values probably is caused by the combined effects of clay and sulfide minerals within the fault zone. These minerals are well concentrated and occupy only a relatively small volume compared with the gross volume taken in by any one field measurement, which may account for the rather minor change in the observed PFE values. The PFE values near the vein increase with depth, possibly because the gouge interval becomes wider or because the polarizing minerals are more disseminated at depth.

Traverse *B–B'*, positioned about 700 feet east of traverse *A–A'*, was carried out to a greater length than traverse *A–A'* in order to test for other mineralized veins on the north flank of Cleary Summit as well as to transect the Jamesonite vein. A resistivity pattern similar to the principal resistivity anomaly noted on the plot of traverse *A–A'* data can be seen beneath field stations 6 and 7 (fig.

2, *B–B′*). Despite the absence of an observable low resistivity zone, the pattern is sufficiently similar to the anomaly of traverse *A–A′* to identify the source as the easterly extension of the Jamesonite vein.

Farther north, in the vicinity of station 12, the resistivity plot shows a low resistivity zone. The cause of the anomaly may be the Kawalita vein, which parallels the Jamesonite vein to the north according to Forbes, Pilkington, and Hawkins (1968). Their description of the Kawalita vein indicates that it is similar to the Jamesonite vein in

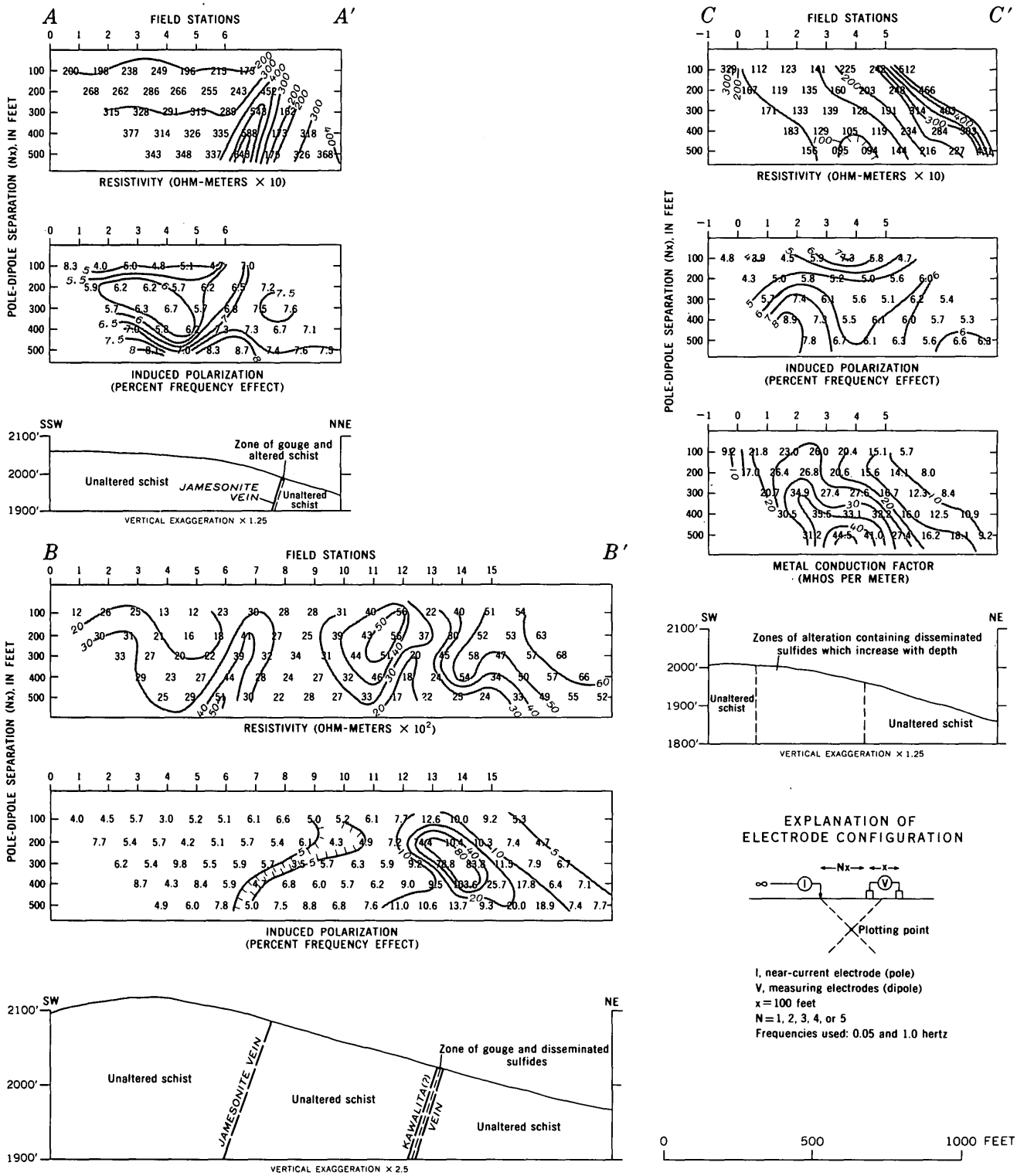

FIGURE 2.—Induced polarization and resistivity data obtained on Cleary Summit. Lines of traverses shown on figure 1.

that it contains quartz veins, gouge, and sulfide nodules. The vein possibly broadens with depth; the most conductive material is estimated to be in excess of 125 feet below the surface.

The corresponding induced polarization data show no polarization anomaly associated with the Jamesonite vein. In contrast, the Kawalita(?) vein produces a fairly strong polarization anomaly with values as much as 20 times the background level. The anomaly possibly is caused by disseminated sulfides within or near the main vein located at an estimated depth of 75–150 feet below the surface.

Traverse *C–C′* (fig. 2) was positioned about 3,000 feet northwest of traverse *A–A′* in the expectation of surveying across the main mineralized zone as determined from the alinement of mine workings and prospect pits on Cleary Summit (fig. 1). The contoured resistivity data indicate that the traverse apparently was well placed, although the southern limit of the low resistivity zone is not well defined. A low resistivity anomaly detected at depth beneath station 4 is the only source of interest on the resistivity plot.

The induced polarization data plotted as percent frequency effect show small variations within the section, but the pattern created by the contours shows no strong evidence of mineral concentrations. To enhance the diagnostic qualities of the induced polarization data, a parameter known as metal factor was calculated by using the formula $2\pi\times10^3$ $(\mathrm{PFE}/(\rho_h\,\rho_l)^{1/2})$ where ρ_h and ρ_l are the high and low resistivities, respectively. Metal factor has the units of conductivity and is shown in contour form below the PFE data (fig. 2, *C–C′*).

The plot of these data indicates a single anomaly which coincides with the low resistivity anomaly detected at depth beneath station 4. The anomaly has a peak metal factor value of 45, which signifies only a small amount of sulfide mineralization within the rock (Keller and Frischknecht, 1966).

How this mineralized zone relates to the recognized mineral veins on Cleary Summit is unknown. The principal source of the resistivity and induced polarization anomalies is buried much deeper than those found along traverses *A–A′* and *B–B′*, and the zone of mineralization or alteration is much broader and better defined than elsewhere. Although the suggested sulfide content is not of economic interest, the apparent increase in the volume fraction of sulfides with depth may possibly lead to significant metal concentration at depths greater than 200 feet.

CONCLUSION

Interpretation of the electrical resistivity and induced polarization surveys obtained on Cleary Summit, Alaska, indicates that narrow zones of conductive minerals exist in conjunction with known vein structures. The economic significance of the conductive zones may be difficult to assess on the basis of these investigations, but the data may be useful for selecting locations at which further study is warranted. It seems that the induced polarization anomaly near the north end of the *B–B′* traverse and the deep-seated mineralized zone beneath the *C–C′* traverse, in particular, may be worthy of additional investigation.

REFERENCES

Dakhnov, V. N., 1959, Promyslovaia geofizika: Moskva, Gostoptekh-Izdat., 692 p. (English translation (part) by G. V. Keller, 1962, Geophysical well logging: Colorado School Mines Quart., v. 57, no. 2, 445 p.)

Forbes, R. B., Pilkington, H. D., and Hawkins, D. B., 1968, Gold gradients and anomalies in the Pedro Dome–Cleary Summit area, Fairbanks district, Alaska: U.S. Geol. Survey open-file report, 49 p.

Keller, G. V., and Frischknecht, F. C., 1966, Electrical methods in geophysical prospecting: London and New York, Pergamon Press, 517 p.

Killeen, P. L., and Mertie, J. B., Jr., 1943, Antimony ore in the Fairbanks district, Alaska: U.S. Geol. Survey open-file report, 43 p. [1951].

GEOLOGIC INTERPRETATION OF A RESIDUAL AEROMAGNETIC MAP OF THE NIXON FORK DISTRICT, ALASKA

By LENNART A. ANDERSON[1], BRUCE L. REED[2], and GORDON R. JOHNSON[1],

[1] Denver, Colo.; [2] Menlo Park Calif.

Abstract.—A residual aeromagnetic map covering approximately 480 square miles was compiled for the Nixon Fork district located about 35 miles northeast of McGrath, Alaska. The aeromagnetic survey was flown in search of concealed intrusive rocks similar to the quartz monzonite stocks that have produced contact metamorphic deposits in limestone, the principal source of gold in the district. Negative magnetic anomalies are associated with quartz monzonite stocks, establishing a useful criterion for locating favorable prospecting areas. Some new localities of possible economic interest in this area are discussed.

In 1968, an aeromagnetic survey was made of a 480-square-mile area lying between Nixon Fork and the North Fork Kuskokwim River in Alaska, in conjunction with mineral-resource investigations by the U.S. Geological Survey (fig. 1). The survey was flown by Lockwood, Kessler, and Bartlett, Inc., and compiled by the U.S. Geological Survey. The objectives were (1) to determine the magnetic characteristics of the intrusive rocks in the vicinity of the Nixon Fork mines, and (2) to delineate other areas where similar concealed intrusive rocks may occur.

The Nixon Fork district, located approximately 35 miles northeast of McGrath, is a region of rugged hills that range in elevation from 400 to 2,800 feet above sea level. Gold placers were discovered in the area in 1917, but lode deposits soon became the chief source of gold. The gold lodes at the Nixon Fork mines occur as small contact metamorphic deposits in limestone, generally within a few hundred feet of the quartz monzonite contact. The chief ore minerals are auriferous pyrite and chalcopyrite. Locally, extensive oxidation has resulted in the release of gold from the sulfide minerals and consequent enrichment in the oxidized zone. Although the data are incomplete, the total production, through 1942, from the several lodes in the area was valued at approximately $1.3 million (Herreid, 1966). The mines have been virtually inactive since 1942, although limited operations were attempted in 1960.

GEOLOGIC SUMMARY

The geology of the Nixon Fork district (fig. 1) and descriptions of the lode and placer deposits are given in reports by Martin (1922), Brown (1926), Mertie (1936), White and Stevens (1953), Jasper (1961), and Herreid (1966). A brief summary, based largely on those reports, follows.

The oldest and most common rock type in the area is complexly folded Paleozoic limestone which forms most of the higher hills between the Nixon Fork and North Fork Kuskokwim River. The limestone, 5,000–7,000 feet thick, is white to dark gray, thin to thick bedded, and contains thin interbeds of shale, chert, and calcareous sandstone. Near contacts with quartz monzonite and granitic stocks the limestone is metamorphosed to a calc-silicate marble.

Cretaceous rocks in the area consist of a monotonous sequence of medium- to dark-gray graywacke, arkosic sandstone, shale, and siltstone, and local beds of conglomerate. These rocks are at least 5,000 feet thick, have a conspicuous slaty cleavage, and are hornfelsic near contacts with intrusive stocks.

Tertiary stocks of quartz monzonite and granite cut the Paleozoic and Cretaceous rocks. Quartz latite porphyry is found within and along the borders of the quartz monzonite stock at the Nixon Fork mines. These porphyry phases are believed to represent chilled border zones (Brown, 1926) or late differentiates of the magma (Herreid, 1966).

Quaternary deposits of unconsolidated gravel, sand, and silt occupy the flat lowlands along the

U.S. GEOL. SURVEY PROF. PAPER 700-D, PAGES D129-D133

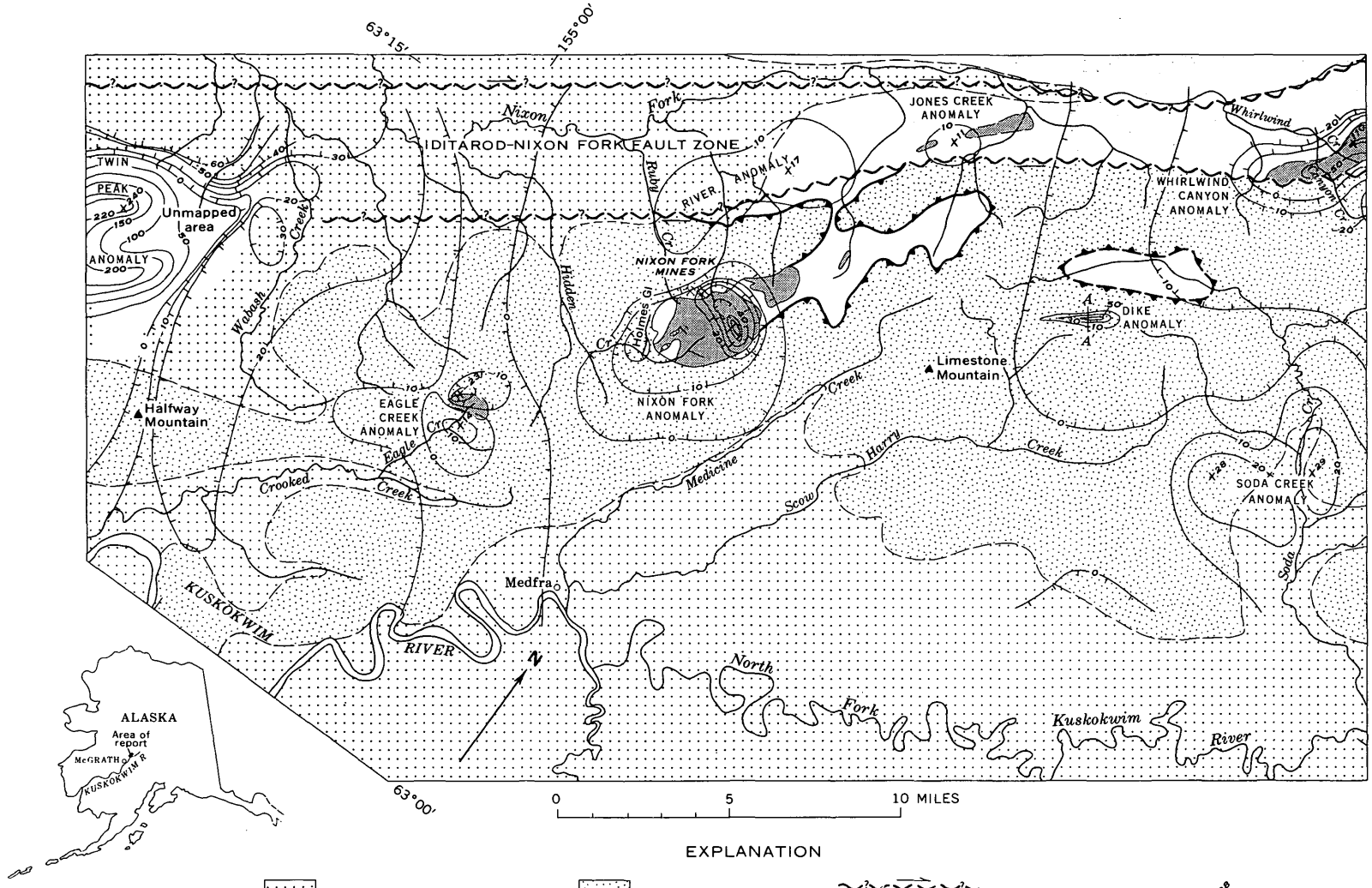

FIGURE 1.—Geologic reconnaissance and residual aeromagnetic map of the Nixon Fork district, Alaska. Geology is based on the early work of Brown (1926) and is supplemented by aerial-photograph interpretation. Base from parts of U.S. Geological Survey quadrangles, scale 1:63,360: Medfra B–4, 1953; A–3, A–4, A–5, 1954; B–3, 1955.

North Fork Kuskokwim River and the Nixon Fork.

The Paleozoic limestones have been thrust northwestward over the Cretaceous rocks (Brown, 1926, p. 120–123). These Paleozoic rocks were subsequently folded and pierced by acidic intrusive stocks, and therefore the possibility that a mineralized thrust plate occurs at the base of the limestone near intrusive contacts should be considered. Subsequent erosion has formed fensters exposing Cretaceous rocks below the thrust plate (fig. 1). To the north, the thrust plate appears to be terminated by the Iditarod-Nixon Fork fault zone—a major fault zone in south-central Alaska with probable right-lateral movement (Grantz, 1966).

AEROMAGNETIC SURVEY

The aeromagnetic survey consisted of 40 northwest-southeast traverses approximately 12 miles long and spaced 1 mile apart. The traverses were flown at a barometric flight elevation of 2,500 feet, except where topography required higher flight elevations. A fluxgate magnetometer was used to obtain a total intensity magnetic profile along each traverse.

The magnetic data in figure 1 are in the form of a residual magnetic map, which was constructed from the total field magnetic map of Anderson, Reed, and Johnson (1969) by removing the earth's normal total magnetic field using a computer technique employing the method of least squares as described by Oldham and Sutherland (1955). There is little difference between the two maps except that some of the magnetic features are somewhat more prominent in the residual magnetic data.

AEROMAGNETIC DATA

The larger known intrusive bodies in the Nixon Fork district can be correlated with either a negative or positive magnetic anomaly. Although each exposed igneous body has been mapped as a "granitic" intrusive, including quartz monzonite, a marked difference in magnetic properties from one body to another is indicated by the variety of magnetic expressions. Other magnetic anomalies shown in figure 1 are produced by intrusives, unknown prior to this survey, which possibly may be identified as to rock type by the polarity of the anomaly.

Negative anomalies

The known gold lodes and prospects in the district are related to a quartz monzonite stock at the Nixon Fork mines and a similar stock located about 7 miles southwest at the headwaters of Eagle Creek (Brown, 1926; White and Stevens, 1953). A negative anomaly, labeled Nixon Fork anomaly on figure 1, delineates the Nixon Fork stock. The reason for the negative signature of the anomaly is unknown, but because the quartz monzonite shows little alteration (Herreid, 1966) and the shape and amplitude of the anomaly do not indicate reversed magnetization of the rock, we believe that the quartz monzonite has no magnetic expression. The negative anomaly is most likely the result of the intruded stock replacing a more magnetic unit at depth, thereby distorting the magnetic field so as to lessen the relative magnetic intensity over the area of the stock.

Within the Nixon Fork anomaly and west of the exposed quartz monzonite, a small negative anomaly lies over the valley of Hidden Creek which is underlain by limestone. This anomaly may correlate with a cupola of the main stock located within the ridge that parallels Holmes Gulch. The depth to the source of the anomaly as determined from the magnetic profile over the proposed cupola is less than 300 feet.

The Eagle Creek stock is also delineated by a negative anomaly that occurs in close association with a positive anomaly to the south, jointly labeled Eagle Creek anomaly on figure 1. The magnetic properties of the quartz monzonite probably are similar to those of the Nixon Fork stock although the magnetic high and low conceivably can be caused by magnetic differences within the exposed quartz monzonite. A depth estimate determined from the profile crossing the stock, however, indicates that the source of the positive magnetic anomaly is approximately 1,500 feet beneath the ground surface. The depth to the source and the location of the magnetic high and low suggest, therefore, either that the stock is more magnetic at depth or that a magnetic rock unit occurs along the south flank of the stock.

Two broad negative magnetic features, not labeled as anomalies on figure 1, are present in the mapped area. One, which is located immediately east of the Twin Peak anomaly and which trends northward, may be caused by a ridge of quartz monzonite that is fairly close to the surface, but it is more likely caused by a structural depression in the magnetic basement rock. The other feature, which is in the northeastern part of the mapped area, possibly indicates the existence of a large intrusive similar to the quartz monzonite at the Nixon Fork mines.

Positive anomalies

The two most prominent positive magnetic features in the mapped area (fig. 1) are the Whirlwind Canyon anomaly, at the northeast corner, and the

Twin Peak anomaly, near the southwest boundary. The Whirlwind Canyon anomaly is caused by an elongate body of exposed granite which forms the southwest extension of Whirlwind Ridge (Brown, 1926, p. 117). The Twin Peak anomaly coincides with a pair of rounded, isolated hills having a relief of about 1,000 feet. The hills are extensively covered by vegetation, and the bedrock geology is not known. The intensity of the Twin Peak anomaly is similar to that of the Whirlwind Canyon anomaly, suggesting the presence of an igneous mass like that found on Whirlwind Ridge.

Within the broad negative anomaly in the northeast section of the map, a small elliptical magnetic high, labeled Dike anomaly on figure 1, occurs over a northeast-trending ridge. The ridge (crossed by section line A–A' on fig. 1) probably consists of steeply dipping limestone as determined from inspection of aerial photographs. The relatively steep gradient of the magnetic anomaly suggests the presence of an intrusive that is not deeply buried. To test this observation, a theoretical magnetic body was constructed using a two-dimensional magnetic-profile computer program. A theoretical model that generates a magnetic anomaly similar to that observed on profile A–A' is shown in figure 2. The theoretical magnetic body is 250 feet wide, dips 70° NW., and extends to an infinite depth. The magnetic susceptibility contrast was chosen to be 6.4×10^{-3} cgs units. A physical counterpart to the model structure having an equivalent magnetic susceptibility would be a mafic body which is dikelike in form. The top of the dike lies near the surface of the limestone ridge. If the dike exists in association with quartz monzonite, then the limestone in the vicinity of the dike provides a favorable environment for lode deposits similar to those found at the Nixon Fork mines (Brown, 1926, p. 135).

North of the Nixon Fork intrusive, two low-intensity positive anomalies, labeled River anomaly and Jones Creek anomaly, possibly correlate with granitic bodies surrounded by Upper Cretaceous rocks. The contacts between Cretaceous sedimentary rocks and Tertiary intrusive bodies, however, are not considered as favorable as contacts with limestone for contact metamorphic deposits, and the intrusives along the Iditarod-Nixon Fork fault zone offer little encouragement to the prospector (Brown, 1926, p. 140). Likewise, the broad double-peaked magnetic feature named Soda Creek anomaly, located near the northeast boundary of the surveyed area, is too deeply buried to be of economic interest.

SUMMARY AND CONCLUSIONS

The intrusives associated with known mineral deposits appear on the map as negative magnetic anomalies. If this observed relation is used as a criterion for locating new prospecting sites, then the area associated with the small negative anomaly within the Nixon Fork anomaly southwest of the Nixon Fork mines and the area in the vicinity of the Dike anomaly may be of interest to the prospector. In the vicinity of the Dike anomaly, in an area possibly underlain by quartz monzonite, a feature that is inferred to be a dike is clearly defined by the magnetic data. This proposed dike is near the surface in a limestone ridge, and the difference in elevation between the top of the ridge and the thrust (mapped from aerial photographs), which has the fenster that exposes Cretaceous rocks to the north (fig. 1), is about 1,000 feet. Thus the depth to the

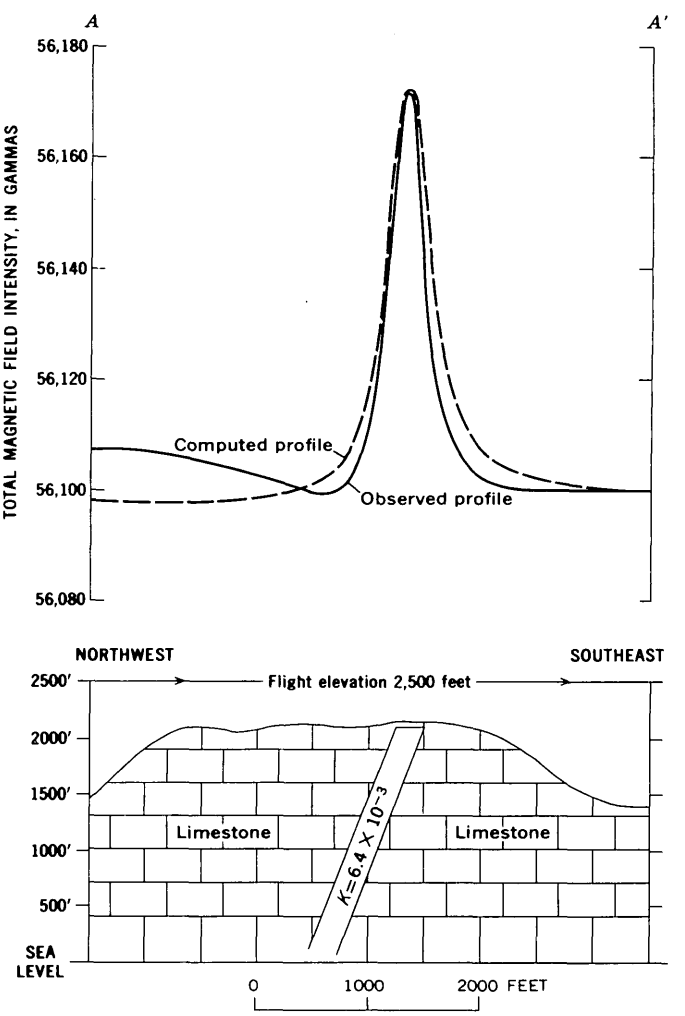

FIGURE 2.—Observed and computed magnetic profiles along line A–A' (fig. 1) over an assumed dike of infinite depth. Magnetic susceptibility (K) in cgs units.

thrust in this area cannot be great, and the thrust probably would have been pierced by the inferred dike and possibly by the inferred body of underlying quartz monzonite.

REFERENCES

Anderson, L. A., Reed, B. L., and Johnson, G. R., 1969, Preliminary geologic interpretation of aeromagnetic data in the Nixon Fork district, Alaska: U.S. Geol. Survey open-file report, 6 p.

Brown, J. S., 1926, The Nixon Fork country [Alaska]: U.S. Geol. Survey Bull. 783–D, p. 97–144.

Grantz, Arthur, 1966, Strike-slip faults in Alaska: U.S. Geol. Survey open-file report, 82 p.

Herreid, Gordon, 1966, Geology and geochemistry of the Nixon Fork area, Medfra quadrangle, Alaska: Alaska Div. Mines and Minerals Geol. Rept. 22, 37 p.

Jasper, M. W., 1961, Report on the Mespelt mine of Strandberg Mines, Inc., Nixon Fork district, Medfra quadrangle, Alaska: Alaska Div. Mines and Minerals Rept. PE 65–1, 9 p.

Martin, G. C., 1922, Gold lodes in the upper Kuskokwim region, Alaska: U.S. Geol. Survey Bull. 722–E, p. 149–161.

Mertie, J. B., Jr., 1936, Mineral deposits of the Ruby-Kuskokwim region, Alaska: U.S. Geol. Survey Bull. 864–C, p. 115–245.

Oldham, C. H. G., and Sutherland, D. B., 1955, Orthogonal polynomials—their use in estimating the regional effect: Geophysics, v. 20, no. 2, p. 295–306.

White, M. G., and Stevens, J. M., 1953, Reconnaissance for radioactive deposits in the Ruby-Poorman and Nixon Fork districts, west-central Alaska, 1949: U.S. Geol. Survey Circ. 279, 19 p.

PLACER GOLD OF UNIQUE FINENESS IN DOUGLAS AND ELBERT COUNTIES, COLORADO

By GEORGE A. DESBOROUGH[1], WILLIAM H. RAYMOND[1]; and COURTNEY SOULE[2], Denver, Colo.; Stanford, Calif.

Abstract.—Electron-microprobe studies show that placer gold from the Russellville placers, Douglas and Elbert Counties, Colo., contains less than 1 percent silver. Gold from the known lodes in Colorado contains at least 10 times this amount of silver. The Russellville placers are in recent alluvium, and their gold is derived from fossil concentrations in the Castle Rock Conglomerate. The lode source of the Russellville gold is unknown, but as shown by sedimentary structural features in the Castle Rock Conglomerate and by the presence of gold of similar purity in mountain gravels east of Woodland Park, the source area lies to the west or southwest.

Gold was discovered in Colorado in 1858 about 35 miles south of Denver in the drainage of Cherry Creek at the Russellville placers in Russellville Gulch. The workings were soon abandoned when richer deposits in the mountains were found, and the Russellville placers are now of historic interest. Old assay reports indicated that the Russellville placer gold contained far less silver in proportion to gold than did gold at any other place in Colorado. This study of the silver content of the gold from the Russellville area, including Cherry and Running Creeks (fig. 1), was directed toward identifying the lode source of this unusually pure gold.

GEOLOGIC SETTING

The gold placers in the Russellville area are in modern streams which transect beds of Paleocene to Oligocene age. These beds dip northeastward about 75 feet per mile (Richardson, 1915, p. 9) and are virtually unbroken by faults. The generalized stratigraphic relations of the rocks are given below:

Age	*Unit*	*Character and thickness*
Early Oligocene	Castle Rock Conglomerate.	Sandstone, conglomeratic sandstone, and conglomerate; 0–300 feet.
Early Oligocene	Unnamed rhyolitic ash-flow tuff.	Pink, gray, maroon (only locally present); 0–40 feet.
Paleocene and Late Cretaceous.	Dawson Arkose	Arkosic sandstone, shales in upper part; 2,000 feet.

Gabriel (1933) demonstrated that the modern stream placers were formed by secondary concentration of gold derived from the Castle Rock Conglomerate. He reported that samples from the Paleocene part of the Dawson Arkose and from the overlying rhyolite ash-flow tuff contained no gold, but that two of three samples from the Castle Rock Conglomerate were gold bearing. Furthermore, no gold has been found in the modern streams of this watershed except in reaches where the stream sediments are derived from areas underlain by the Castle Rock Conglomerate.

PLACER GOLD ANALYSES

Samples from the main channels of modern streams at 12 localities in the Russellville district were processed to obtain gold for electron-microprobe analysis. Samples ranged in size from about 100 to 200 pounds and were initially concentrated with a "gold saver." (The gold saver that was used consists basically of a rotating trommel underlain by a mechanically agitated riffle, in which the heavy minerals are concentrated. The entire unit operates under hydraulic conditions.) Heavy minerals (specific gravity >3.0) constituted less than 2 percent by weight of the samples. Concentrates were

[1] U.S. Geological Survey.
[2] Stanford University.

U.S. GEOL. SURVEY PROF. PAPER 700-D, PAGES D134-D139

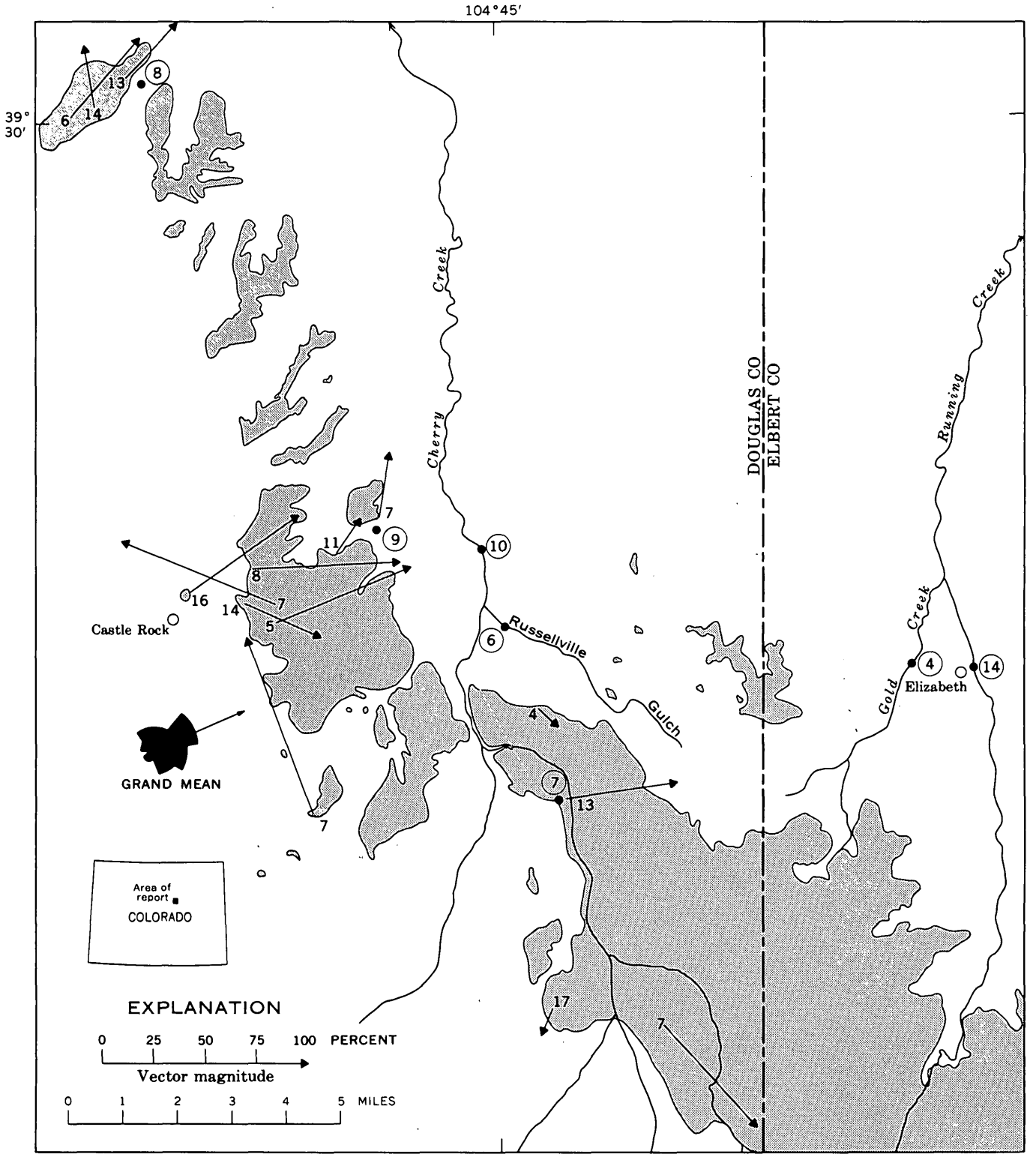

FIGURE 1.—Distribution of Castle Rock Conglomerate (shaded), modified from Richardson (1915). Localities of analyzed gold (table 1) are shown by dots. Vectors show sediment transport direction at each crossbedding locality. Vector length is proportional to magnitude; number at vector origin is number of observations at each locality. Rose diagram is the aggregate of the crossbedding-locality averages, and the arrow shows the grand mean (average transport direction) with a magnitude of 51.5 percent—on a scale of 0–100 percent wherein 0 percent represents completely random distribution of directions measured and 100 percent requires that all directions measured lie within the same azimuth group (Curray, 1956).

panned, and gold particles were individually picked out with the aid of a stereomicroscope. Most of the gold particles that were recovered are flakes, but some are equidimensional and round and some are cylindrical. A few of the grains from the main Russellville placer are filmed with gold-silver amalgam, which is believed to represent contamination from early gold recovery operations.

Forty grains of gold that represented seven localities were analyzed for their silver and copper content by means of the electron microprobe. Homogeneous standards of the following compositions were used (all in percent by weight): Au_{100}, $Au_{98.35}Ag_{0.66}Cu_{0.99}$, $Au_{94.35}Ag_{3.40}Cu_{1.15}Sb_{0.75}$, $Au_{94.26}Ag_{5.74}$, $Au_{88.39}Ag_{1.71}Cu_{9.90}$, $Au_{68.92}Ag_{14.37}Cu_{16.71}$, $Au_{73.25}Ag_{26.75}$, and $Au_{54.90}Ag_{45.10}$. The three Au-Ag alloys were provided by Paul B. Barton, Jr. The other standard alloys were prepared from pure metals. Weighed amounts were sealed in silica tubes (evacuated to about 0.005 mmHg pressure), melted, and then homogenized as solids at 900° for 12 hours. The tubes were quenched in water from 900°C to maintain homogeneity. The beads were examined with a mineragraphic microscope and checked in the electron microscope for homogeneity. The intensity of the following spectral peaks of the standards and the samples was measured with the indicated analyzing crystals: Ag$L\alpha$-*ADP*, Cu$K\alpha$-LiF, and Au$L\alpha$-LiF. The homogeneity of the standards limits the accuracy of analytical results to about ±0.3 percent by weight Ag between $Ag_{0.66}$ and $Ag_{5.74}$, and ±0.2 percent by weight Cu between $Cu_{0.99}$ and $Cu_{1.51}$. The precision of the microprobe, using a fixed-beam current count and a sample current of 2×10^{-8} amperes on Au_{100}, is better than the accuracy of the standard alloys. Detection limits of silver and copper in gold appear to be better than 0.1 percent by weight with these standards.

The results of the electron-microprobe study are reported in table 1. Silver is present in the interior part of gold grains in amounts ranging from <0.1 to 4.9 percent. Some of the amalgamated gold grains from locality 6 (fig. 1) have high-silver rims, which indicates that the rims acquired additional silver in amalgamation. These amalgamated grains were heated to 600°C to remove mercury prior to microprobe analysis. The reported silver values represent one analysis at the apparent center of the polished grain, and the range of four determinations on the rim of the grain at points 90° apart. This method was used in an effort to assess the purity of the gold and also the relative extent to which silver has been depleted on the outer portion of the grains. Copper was not detected in any of the gold grains.

TABLE 1.—*Silver content of selected gold grains from the Castle Rock area*

[<0.1, detected, but less than 0.1 percent; 0, not detected]

Locality No. (fig. 1)	Grain size[1] (mm)	Silver (weight percent)[2]	
		Center	Rim range
4	0.320	<0.1	<0.1
	.270	2.8	0–0.4
	.130	.4	0–0.6
	.480	<.1	<.1
	.380	.9	0.2–2.6
	.235	<.1	0–0.2
	.160	.1	0–1.2
	.245	.5	0.1–0.5
	.147	<.1	0–0.3
6	.107	<.1	<.1
	.262	<.1	0–0.3
[3]6	.112	1.9	0–0.4
	.212	.8	0.2–9.2
	.237	1.5	0–0.7
	.237	1.3	0–22.4
	.150	0	0
7	.312	.4	0
	.175	2.1	0–2.1
	.225	4.5	0.2–3.2
	.150	<.1	<.1
8	.280	.2	0.1–0.9
	.177	<.1	0–2.2
	.185	<.1	0–3.0
9	.445	.4	0–0.3
	.392	<.1	0–0.5
	.407	.9	0–0.8
	.530	.3	0–0.1
10	.377	1.5	0–0.3
	.325	.3	0–1.3
	.355	1.3	0–1.2
	.837	.3	0.4–1.0
	.450	.3	0
	.500	<.1	0–1.9
	.375	.1	0
	.300	<.1	0
	.700	<.1	0–0.6
	.427	<.1	0–4.3
14	.205	2.1	0.1–2.9
	.090	4.9	0.4–5.6
	.115	.2	0–0.8
Average (excluding heated amalgam)	0.31	0.75	

[1] Grain size refers to measured maximum, plus minimum dimensions in polished surface divided by 2.
[2] Precision: 0–0.2±0.05; 0.2–1.0±0.1; 1.0–3.0±0.2; 3.0–6.50±0.3; 6.5–17.0±0.4; 17–25±1.0.
[3] Amalgam heated to 600°C.

Subsequently, we analyzed 126 grains of gold (not tabulated individually here) from six additional localities in the Cherry Creek drainage that have an average silver content for the interior of grains of 0.5 percent by weight with a standard deviation from the mean of 0.5 percent. In this set of samples, four separate analyses were made in the interior of each gold grain to improve precision; the silver-depleted rim was avoided.

The cores of over 80 percent of the 166 gold grains analyzed from the Castle Rock area con-

tained less than 1 percent by weight silver; those of 65 percent contained less than 0.5 percent by weight silver; all the grains contained less than 5 percent by weight silver. Briefly, the gold from the Russellville area is more than 990 fine; this quality is due to the unique purity of the gold of the lode source.

SEARCH FOR PRIMARY SOURCE OF THE GOLD

Previous investigators concerned with the gold of the Russellville placers (Gabriel, 1933; Lovering and Goddard, 1950, p. 41; Malin, 1957) concluded that the Castle Rock Conglomerate and its contained gold were derived from the northwest, in essence from the Clear Creek drainage area west of Denver. They cited evidence of: (1) Precambrian rock types, and (2) paleovalley patterns inferred from the thickness of remnants of Castle Rock Conglomerate. In our study, two separate lines of inquiry force the conclusions that both the source of sediments and the primary source of the gold lie to the west or southwest.

First, the gold of the modern Clear Creek drainage area contains 15–20 times as much silver as that of the Russellville placers. The compositions determined by electron-microprobe methods on the cores of gold grains from seven Clear Creek localities (Desborough and others, 1970) show that 90 percent of the grains contain more than 11 percent silver. No gold source in the Clear Creek drainage area is known that is of sufficient purity to supply the Russellville placers. In fact, the gold in all the known ore deposits of the Front Range mineral belt contains more than 5 percent silver; thus, these deposits are not the source of the Russellville placer gold.

Second, a northeastward transport direction for the Russellville gold is indicated by studies of the crossbedding in the Castle Rock Conglomerate (fig. 1). One hundred forty-nine measurements of the downdip directions of foreset beds were made in each recognizable sedimentation unit at 14 localities. The procedures were those of Potter and Pettijohn (1963). The vectors at each locality and the rose diagram for all localities (fig. 1) summarize the data and indicate the general direction of sediment transport. This evidence shows that the streams from which the Castle Rock Conglomerate was deposited flowed generally northeasterly.

To search for the primary source of the Russellville placers, we turned, thus, to the southwest and sampled both modern stream gravels and Tertiary gravels in the mountains of the Front Range.

Tertiary deposits of boulder alluvium and finer clastics on the mountain highland between Florissant and Woodland Park (fig. 2) were derived from part of a main Tertiary drainage system identified as one of the ancestral courses of the South Platte River by G. R. Scott and R. B. Taylor (oral commun., 1970). Scott and Taylor suggest that the deposits are of probable Miocene and Pliocene age and that the barrier of the Rampart Range, which seemingly would have prohibited flow from the west, was not raised tectonically until the late Pliocene. We extracted two grains of gold from this Tertiary boulder gravel from a channel cut into the Pikes Peak Granite on Bald Mountain (fig. 2). Electron-microprobe analyses of the cores of these grains indicate that the gold contains 0.1 to 0.25 percent by weight silver and no copper. These analyses show a fineness equivalent to that of the Russellville placer gold. Attempts to trace this unusual gold farther upstream were unsuccessful. Gold grains from the modern stream near Florissant (fig. 2) contain 9.3 to 18 percent by weight silver, and are most like placer gold from Tarryall Creek (Desborough and others, 1970).

The telluride ores at Cripple Creek (fig. 2) contain much silver and very little native gold. No gold placers have been found in the streams draining this district, and the nature of the telluride gold mineralization seems to rule out this area as the lode source of the Russellville placers.

CONCLUSIONS

The Russellville placer gold is more than 990 fine. The present placers were formed by secondary concentration of gold from the Castle Rock Conglomerate, and consequently the primary gold mineralization is of Oligocene or older age. The lode source of the placer gold has not been located, but it lies west of the Rampart Range, and the previously suggested origin from lodes in the Clear Creek drainage is untenable.

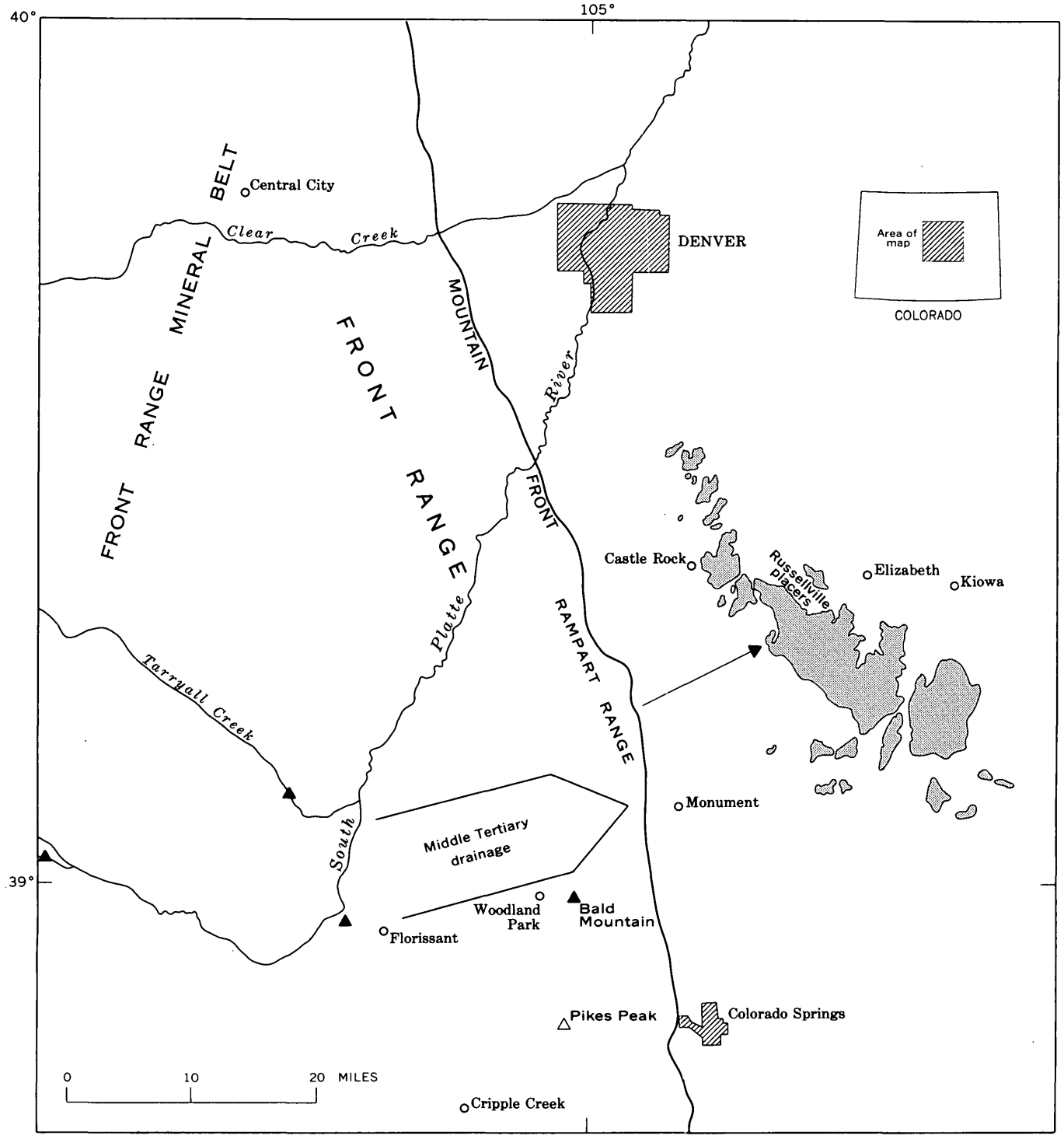

FIGURE 2.—Map showing the relationships of the Castle Rock Conglomerate (shaded) to the Rampart Range, Cripple Creek, middle Tertiary drainage, and the present major drainage. Arrow indicates direction of transport of Castle Rock Conglomerate in study area. Solid triangles show selected gold placer sample localities. Base map is modified from the geologic map of Colorado (Burbank and others, 1935).

REFERENCES

Burbank, W. S., Lovering, T. S., Goddard, E. N., and Eckel, E. B., 1935, Geologic map of Colorado: U.S. Geol. Survey.

Curray, J. R., 1956, The analyses of two-dimensional orientation data: Jour. Geology, v. 64, no. 2, p. 117–131.

Desborough, G. A., Raymond, W. H., and Iagmin, P. J., 1970, Distribution of silver and copper in placer gold derived from the northeastern part of the Colorado Mineral Belt: Econ. Geology. [In press]

Gabriel, V. G., 1933, The Castle Rock Conglomerate and associated gold placer deposits: Colorado School Mines, unpub. Ph. D. dissert.

Lovering, T. S., and Goddard, E. N., 1950, Geology and ore deposits of the Front Range, Colorado: U.S. Geol. Survey Prof. Paper 223, 319 p. [1951]

Malin, E. R., 1957, A study of the Castle Rock Conglomerate (Basal Oligocene), Colorado Piedmont: Nebraska Univ., unpub. Master's thesis.

Potter, P. E., and Pettijohn, F. J., 1963, Paleocurrents and basin analysis: New York, Academic Press, Inc., 296 p.

Richardson, G. B., 1915, Description of the Castle Rock quadrangle, Colorado: U.S. Geol. Survey Geol. Atlas. Folio 198, 13 p.

POTASH IN HALITIC EVAPORITES, SALT RANGE, WEST PAKISTAN

By C. L. JONES, Menlo Park, Calif.

Abstract.—Evaporites in the Salt Range, West Pakistan, are predominantly halitic but include lenticular to stratiform deposits of potassic rocks rich in kainite and langbeinite. The deposits appear to offer considerable promise for commercial development and can supply potassium chloride, potassium sulfate, magnesia, and other substances to agriculture and industry in West Pakistan.

Perennial shortages of grains and other vital foodstuffs in Pakistan have stimulated efforts to find and exploit indigenous sources of potash to provide a greatly needed fertilizer. One source of potash that appears to offer considerable commercial promise consists of kainitic and langbeinitic evaporite deposits underlying a wide section of West Pakistan. These deposits have recently been reconnoitered by the Geological Survey of Pakistan and the U.S. Geological Survey (Jones and Asrarullah, 1968) as part of the U.S. Agency for International Development mineral resource appraisal program in Pakistan. Some additional results from this reconnaissance are presented here.

Interest in the development of evaporite potash resources has centered on the eastern part of the Salt Range in the Rawalpindi Administrative Division of West Pakistan (fig. 1), where deposits of potassic rocks in the Salt Range Formation of late Precambrian or Early Cambrian age are relatively accessible. The area is favorably situated geographically, particularly with respect to the availability of labor, power, water, and proximity to extensive farming districts. It already supports mines for salt, coal, and limestone, and it has the nucleus of an evaporite-based chemical industry in the manufacture of soda ash at Khewra.

The eastern Salt Range is part of a spectacular mountain range, about 150 miles long, which sweeps in a great sinuous arc from the Indus River south and eastward across the region almost to the sharp bend of the Jhelum River at the Indian border. For much of its length, the range forms a scalloped escarpment with many ledgy slopes and bold ridges projecting sharply 2,000 to 2,500 feet above the monotonous low plains that flank its southern slopes. Most ridges have strong scarps toward the south but slope gently northward into the rolling, moderately dissected tableland of the Potwar Plateau.

LATE PRECAMBRIAN TO CAMBRIAN SEQUENCE

The bedrock forming the lower southern slopes of the Salt Range comprises a thick, well-stratified sequence of chemical precipitates and fine-grained clastic rocks containing fossils of Early Cambrian age. The sequence contains five lithologically distinct rock units, first defined and mapped by Wynne (1878) and Gee (1934, 1945) and more recently studied by Schindewolf and Seilacher (1955) and by Asrarullah (1963). Its units crop out mainly in parallel, east-trending belts in which the rocks are successively younger from south to north toward the crest of the range, but there are some fault-bounded plugs and other diapirlike masses of salt and related rocks cutting sharply through Tertiary strata in the Potwar Plateau. The top of the sequence is truncated by a major unconformity, and its base is concealed. The sequence is at least 4,000 feet thick and may be as much as twice this thick. The entire sequence is conformable, with vague transitional boundaries between individual units and with no significant breaks in the sedimentary record. Schindewolf and Seilacher (1955) relate the whole sequence to a single sedimentary cycle. The Committee for the Stratigraphic Code of Pakistan has proposed a late Precambrian to Early Cambrian age for the sequence.

The stratigraphy of the sequence is summarized below in descending order; the names of the units are those proposed by Noetling (1894) and subsequently adopted by the Committee for the Stratigraphic Code of Pakistan.

U.S. GEOL. SURVEY PROF. PAPER 700-D, PAGES D140-D145

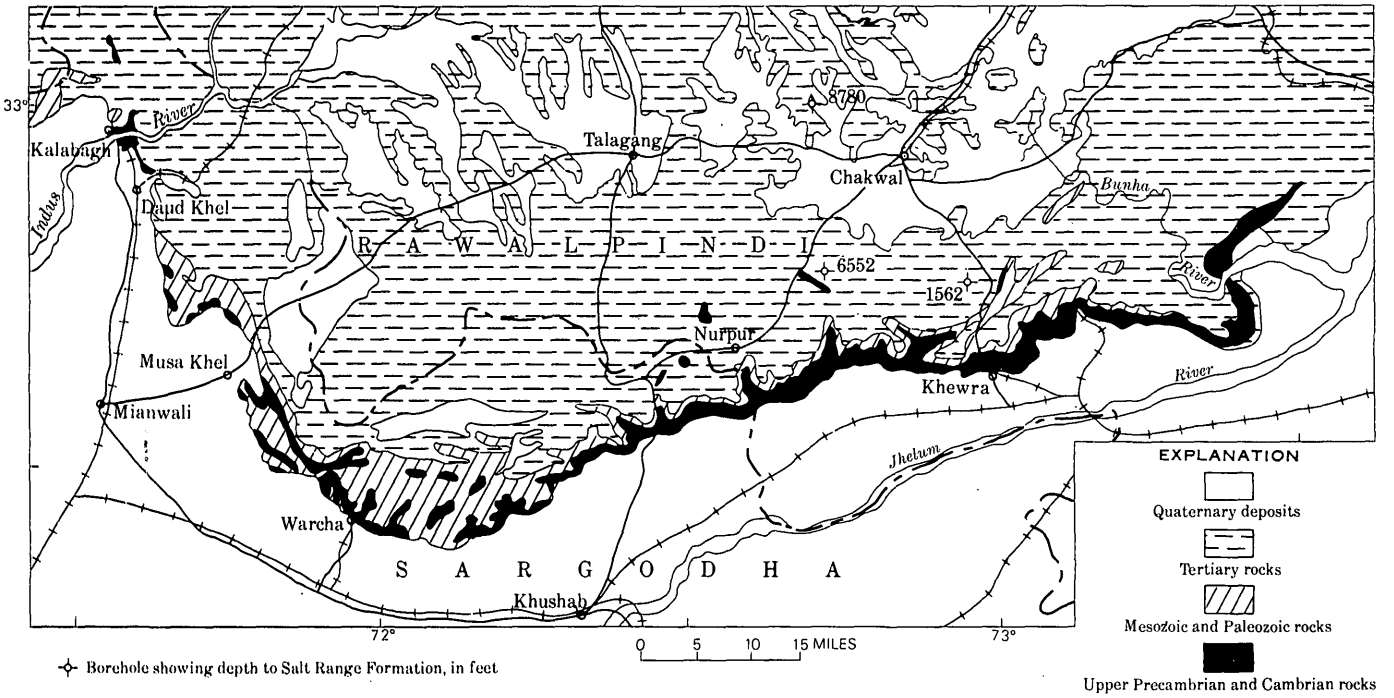

FIGURE 1.—Generalized geologic map of Salt Range area, Rawalpindi and Sargodha Administrative Divisions, West Pakistan. Modified from Gee (1945).

Stratigraphic units in the lower slopes of the Salt Range

Unit and description	Approximate thickness (feet)
5. Baghanwala Formation: Red to reddish-brown shale and siltstone; irregularly bleached greenish-gray in streaky and splotchy masses and seams. Some bedding surfaces are crowded with hopper-shaped salt casts; other show ripple marks	300+
4. Jutana Dolomite: Cream to buff moderately fossiliferous, granular to well crystallized dolomite, in thick, massive beds forming prominent ledges and cliffs. Some beds are oolitic; others are laminated, arenaceous, and intercalated with fine-grained sandstone	240
3. Kussack Shale: Purplish-gray to dark-gray, richly fossiliferous, pyritic shale, intercalated with greenish-gray, glauconitic sandstone and pisolitic dolomite. Characterized by *Neobolus* but contains many other brachiopods as well as some trilobites	100
2. Khewra Sandstone: Thick-bedded, maroon and dull-red to buff sandstone. Becomes thin bedded toward base and contains intercalations of maroon shale. Current bedding is common, and many bedding surfaces show ripple marks, mud cracks, and salt casts	450
1. Salt Range Formation: Colorless to gray, pink, and red rock salt with subordinate maroon shale and siltstone and white to gray anhydrite and dolomite. Contains potassic rocks rich in magnesium sulfate and has a well-developed "cap rock" or "gossan" of unconsolidated gypsiferous marl, a product of evaporite solution and removal	3,000+

SALT RANGE FORMATION

The Salt Range Formation is primarily a subsurface unit, and very little is known about its extent and distribution. Available data suggest that the formation is regionally extensive, occupying much of the foreland slope and stretching from the broad Precambrian shield area of Peninsular India into the great Baluchistan geosyncline of Trans-Indus Pakistan (fig. 2). The formation persists the entire length of the Salt Range, and it underlies most, if not all, of the Potwar Plateau to the north of the range and much of the lowland plains of the Indus River region to the south. From the Indus plains, the formation extends southeastward across the Indian border and presumably merges with evaporite-rich parts of the Upper Vindhyan series in central Rajasthan, India. The Salt Range Formation continues west of the Indus River and may be the source of the salt that forms scattered small plugs and other discordant masses breaching Tertiary rocks south of Kohat.

As shown by exploratory boreholes for petroleum at Dhariala, Karampur, and elsewhere (Day, 1963; Rahman, 1963), the Salt Range Formation is the oldest member of the sedimentary sequence on the foreland slope and rests on Precambrian metamorphic and granitic basement rocks of the region. Its age is considered to be late Precambrian or

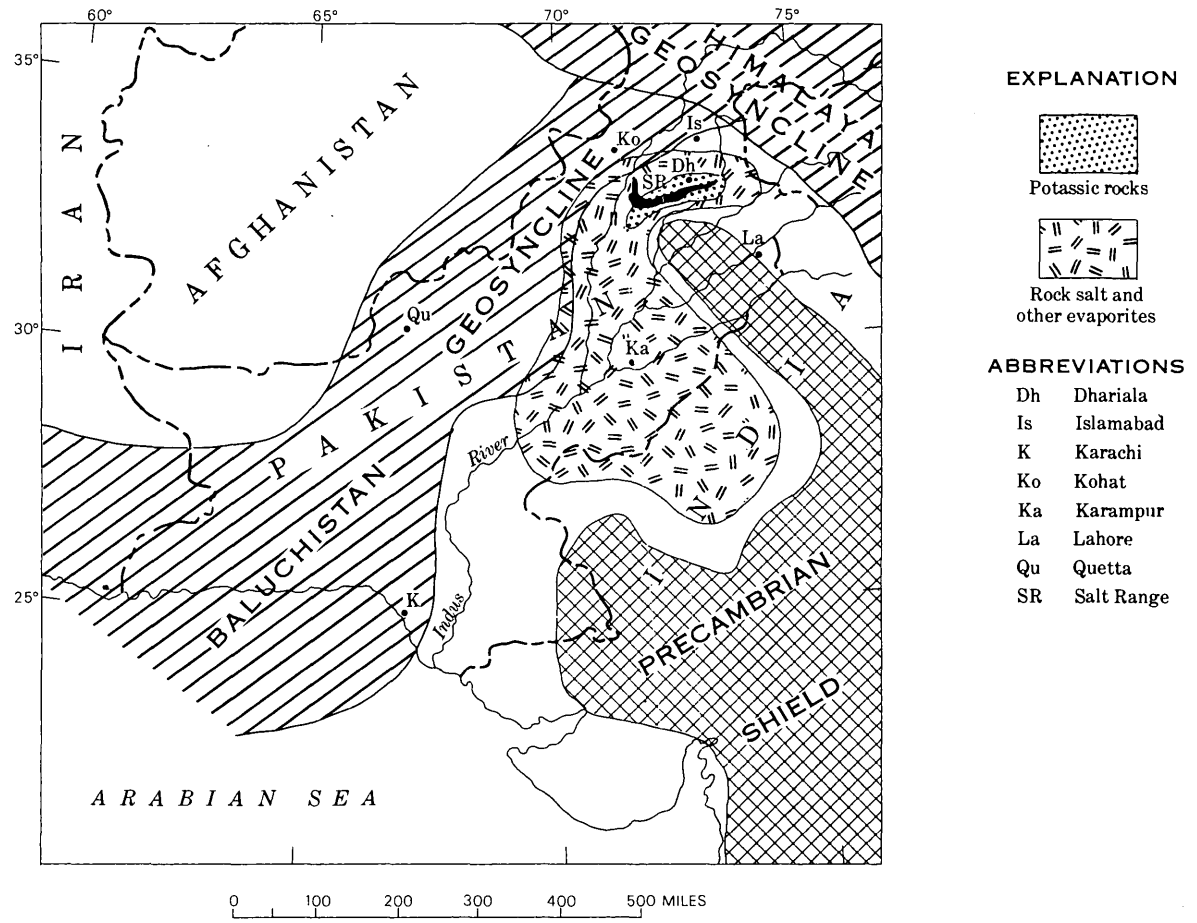

FIGURE 2.—Probable distribution of potassic rocks and other evaporites of the Salt Range Formation in the Indus region, West Pakistan.

Early Cambrian. Lithologically, the formation represents a fairly typical example of the normal marine class of salt-rich evaporites, characterized by the occurrence of magnesium sulfate as simple and complex double salts. The principal parts of the formation are thick units of well-stratified rock salt and highly saliferous shale and siltstone in beds a few feet to more than a hundred feet thick. Some anhydrite beds and subordinate dolomite layers are scattered through the formation at irregular intervals, and there is at least one major potash zone containing a number of discrete seams or deposits rich in kainite and other potassium-magnesium minerals. Intercalated between beds of dolomite and rock salt in the upper part of the formation are volcanic beds, 10–15 feet thick, consisting of bentonitic tuff and potassium-rich trachytic lava (Mosebach, 1956). The volcanic rocks form the principal and virtually the only stratigraphic marker that can be identified with confidence both in the subsurface and in the outcrop.

The Salt Range Formation is weakly resistant to erosion and underlies debris-strewn slopes and valleys; the few poor exposures are deceptive as to the precise nature of the formation. Solution of halite and other evaporites by meteoric waters has been extensive, and virtually the entire area of outcrop is one colossal "cap rock" or "gossan" of clayey residue consisting of unconsolidated maroon to reddish-brown clays and silts, with some vague, discontinuous zones impregnated with small, broken, and corroded fragments of gypsum and dolomite. The residue is massive and conspicuously free of bedding. Information on the number or the composition, structure, and thickness of individual salt beds and other evaporites cannot be obtained from the argillaceous residue, and there is no way to piece together a meaningful stratigraphic section.

POTASH

Potash occurrences in the Salt Range Formation of the eastern Salt Range comprise (1) deposits of

potassic rocks, (2) high-density magnesium chloride brines containing potassium, calcium, and sodium in significant quantities, and (3) sparse disseminations of polyhalite in rock salt. The deposits of potassic rocks are by far the richest in potassium, and they appear to offer the greatest promise of exploitation because of their potassium content and their similarity to productive deposits in other regions. The high-density magnesium chloride brines are relict mother liquors of a type found in virtually all salt formations that contain deposits of potassic rocks, and presumably they are no more susceptible to exploitation than those found in other salt formations. The disseminations of polyhalite lack sufficient potassium to be of economic importance, and they are chiefly of mineralogic and petrographic interest.

Deposits of potassic rocks in the Salt Range Formation have been known since 1873 (Wynne, 1878, p. 80), but they were not studied until after 1910. In the following 9 years, Christie (1914) and Stuart (1919) examined the mineralogy of the deposits, their potash content, and their distribution in salt mines at Khewra, Nurpur, and Warcha to ascertain their economic value. Beyond this, no exploratory drilling or other investigations with a view to developing the deposits have been undertaken.

The potash occurrences in the mines at Khewra and elsewhere are parts of a "potassium" evaporite province of some importance. The full extent of the province is unknown, but it covers a great part of the Salt Range and extends into the Potwar Plateau and the Indus plains. The province contains at least 10 discrete deposits or zones of potassic rocks which are scattered at irregular intervals through several hundred feet of interstratified rock salt and shale in the Salt Range Formation (fig. 3). The deposits are as much as 12 feet thick in places, and they are all of one well-defined type characterized by a lenticular to tabular form and a sizable accumulation of magnesium sulfate with the potassium (Jones and Asrarullah, 1968). In this and other respects they resemble the magnesium sulfate-rich deposits of langbeinitic and kainitic rocks mined in the Carlsbad district of the Southwestern United States, in the sub-Carpathian region of western Russia and northeastern Rumania, and in the Caltanisseta field of central Sicily, and there is every reason to expect them to be as productive as the deposits in these American and European districts have been.

All the deposits of potassic rocks in the Salt Range Formation are mineralogically complex and

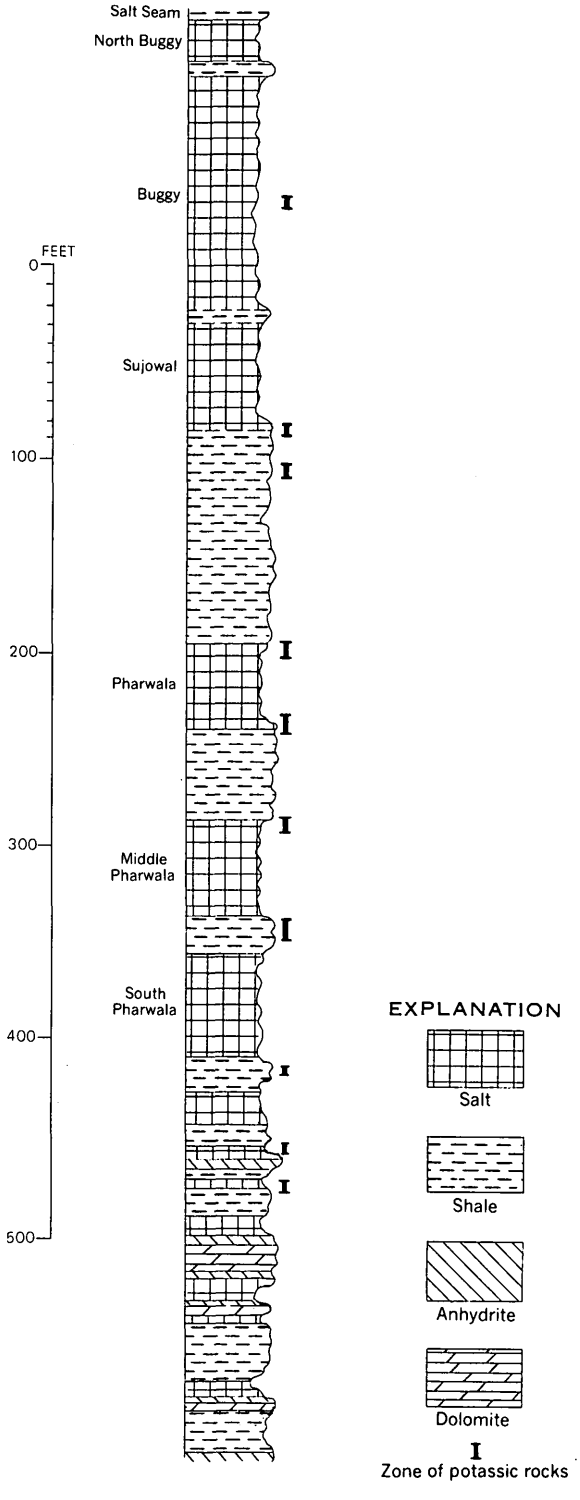

FIGURE 3.—Columnar section showing zones of potassic rocks in salt seams and shale beds of the Salt Range Formation at the Khewra salt mine, eastern Salt Range, West Pakistan. Includes borehole data from Lamb (1947); nomenclature of salt seams from Asrarullah (1963).

TABLE 1.—*Evaporite minerals found in potassic rocks of the Salt Range Formation, eastern Salt Range, West Pakistan*

Mineral	Formula	Constituents (weight percent)						
		K	Mg	Ca	Na	SO_4	Cl	H_2O
Kainite	$KCl \cdot MgSO_4 \cdot 3H_2O$	15.7	9.8	----	----	38.6	14.2	21.7
Langbeinite	$2MgK_2(SO_4)_3$	18.8	11.7	----	----	69.4	----	----
Sylvite	KCl	52.4	----	----	----	----	47.6	----
Polyhalite	$2CaMgK_2(SO_4)_4 \cdot 2H_2O$	13.0	4.0	13.3	----	63.7	----	6.0
Kieserite	$MgSO_4 \cdot H_2O$	----	17.6	----	----	69.4	----	13.0
Halite	NaCl	----	----	----	39.3	----	60.7	----

consist mainly of halite, langbeinite, kainite, kieserite, sylvite, and polyhalite, with small amounts of shale (table 1). Of these, langbeinite and kainite probably represent as much as 80 percent of the potassic material; most of the remainder of the potassium occurs as sylvite. Less than 1 percent of the potassic accumulation is polyhalite. Large amounts of sodium chloride occur as halite, and magnesium sulfate is contained in langbeinite, kainite, and kieserite. The shaly impurities are distinctly clay-rich and include chlorite, illite, and a mixed-layer clay mineral, with abundant quartz and subordinate feldspar, magnesite, and hematite.

The chemistry of the potassic rocks in the Salt Range Formation is imperfectly known. Nevertheless, the high magnesium sulfate content indicated by the presence of kainite and langbeinite in substantial quantities is borne out by the few chemical analyses published by Christie (1914). The data on three of the most completely analyzed rocks from deposits in salt seams in the mines at Khewra and Nurpur are listed in table 2, together with their calculated mineral composition. The chemistry and computed mineralogy of the three rocks are similar, if not identical, to that of the kainitic and langbeinitic rocks mined at various places in the sub-Carpathian region of western Russia and northeastern Rumania.

The potassic rocks from the deposits at Khewra and Nurpur (table 2) contain 10–14 percent K_2O, 24–42 percent $MgSO_4$, and 23–55 percent NaCl. Just how closely or extensively these analyses reflect the tenor of the average or "run-of-mine" ore is unknown, but such material can be treated to yield a variety of products. Run-of-mine ores derived from rocks of this general composition can be readily upgraded by fairly rudimentary beneficiation processes to yield a "kali-mag" concentrate rich in kainite and poor in sodium chloride. In areas where magnesium deficiencies exist in the soil, a concentrate of this sort has value for application as a combined fertilizer and soil conditioner.

Apart from its value as a fertilizer and soil conditioner, a "kali-mag" concentrate of the kainite-rich type obtainable from potassic rocks of the Salt Range Formation can be processed to yield a variety of potassium salts and other substances of agricultural or industrial importance. By using a multistage chlorination-evaporation process, for example, the processing of a kainitic concentrate can incorporate the production of potassium chloride (KCl) and gypsum ($CaSO_4 \cdot 2H_2O$) into a highly useful procedure for disposing of the waste calcium chloride liquor formed in the manufacture of soda ash at Khewra. The process consists of treating the kainitic concentrate with calcium chloride liquor to form gypsum and a sulfate-free potassium magnesium chloride mother liquor. The gypsum is separated from the mother liquor, and the liquor is then evaporated to form carnallite ($MgCl_2 \cdot KCl \cdot 6H_2O$). The carnallite is digested in hot brine, at which

TABLE 2.—*Composition of potassic rocks from salt seams at Kehewra and Nurpur, eastern Salt Range, West Pakistan*

[The names "Buggy" and "Sujowal-Pharwala" refer to units shown on the columnar section, figure 3. Chemical analyses from Christie (1914, p. 248)]

	Khewra		Nurpur
	Buggy	Sujowal-Pharwala	
Chemical analyses			
K	11.9	8.0	11.3
Mg	8.9	4.8	9.0
Na (calculated)	10.0	21.5	9.2
SO_4	39.3	22.9	39.5
Cl	23.3	37.5	21.4
H_2O	7.1	4.9	9.3
Total	100.5	99.6	99.7
Mineral composition (calculated)			
Kainite	49.5	19.5	48.9
Langbeinite	17.9	17.0	17.0
Sylvite	1.4	3.3	0.8
Kieserite	5.8	5.2	9.8
Halite	25.7	54.7	23.2
Total	100.3	99.7	99.7

point potassium chloride crystallizes. The potassium chloride is separated from the liquor, which is rich in magnesium and can be used to manufacture either refractory grade magnesia (MgO) and hydrochloric acid or metallic magnesium and chlorine. The multistage process may be represented in a simplified form by the following equations in which the concentrate is shown as kainite:

$$MgSO_4 \cdot KCl \cdot 3H_2O + CaCl_2 + 5H_2O \rightarrow MgCl_2 \cdot KCl \cdot 6H_2O + CaSO_4 \cdot 2H_2O$$

$$MgCl_2 \cdot KCl \cdot 6H_2O \rightarrow MgCl_2 \cdot 6H_2O + KCl$$

$$MgCl_2 \cdot 6H_2O \rightarrow MgO + 2HCl \text{ in } 5H_2O$$

In accordance with the reactions outlined above, a ton of kainitic concentrate requires the use of only 0.45 ton of calcium chloride to produce 0.69 ton of gypsum, 0.30 ton of potassium chloride, 0.16 ton of magnesia, and 0.66 ton of hydrochloric acid.

Another substance of value that can be produced from the versatile kainitic concentrate is potassium sulfate. The production of this substance involves reactions between brine and solids in the reciprocal salt-pair system magnesium sulfate-potassium chloride-water, and it can be accomplished by employing a two-stage base-exchange process such as that used by the Italian potash industry to exploit kainitic ores from the Caltanisseta deposits in central Sicily. The process consists of treating a kainitic concentrate with magnesium sulfate liquor to form picromerite ($K_2SO_4 \cdot MgSO_4 \cdot 6H_2O$). The picromerite is separated from the magnesium-rich liquor, which can then be used as a source of magnesia and hydrochloric acid. The picromerite is digested in water, at which point potassium sulfate crystallizes. The potassium sulfate is separated, and the magnesium sulfate liquor is used to treat the kainitic concentrate at the start of the process. The process may be represented in a simplified form by the following equations:

$$2MgSO_4 \cdot KCl \cdot 3H_2O \rightarrow K_2SO_4 \cdot MgSO_4 \cdot 6H_2O + MgCl_2$$

$$K_2SO_4 \cdot MgSO_4 \cdot 6H_2O \rightarrow K_2SO_4 + MgSO_4 \text{ in } 6H_2O.$$

With this process, a ton of kainitic concentrate can be expected to yield 0.35 ton of potassium sulfate and sufficient magnesium-rich liquor to produce 0.13 ton of magnesia and 0.55 ton of hydrochloric acid.

CONCLUSIONS

The deposits of potassic rocks found in the Salt Range Formation at Khewra and elsewhere in the eastern Salt Range appear to offer great promise of development. The deposits could become the basis of important new fertilizer and chemical industries greatly needed in Pakistan, but they require study, testing, and sampling to determine whether or not their distribution, grade, composition, and tonnage are sufficient to fulfill all requirements for commercial development.

REFERENCES

Asrarullah, 1963, Rock salt resources of Pakistan, *in* Symposium on industrial rocks and minerals, Lahore, 1962: Central Treaty Organization, Ankara, Turkey, p. 303–313.

Christie, W. A. K., 1914, Notes on the salt deposits of the Cis-Indus Salt Range: India Geol. Survey Recs., v. 44, pt. 4, p. 241–264.

Day, A. E., 1963, Case histories of the Dhulian and Balkassar oil fields, West Pakistan, *in* Case histories of oil and gas fields in Asia and the Far East: United Nations Econ. Comm. for Asia and the Far East, Mineral Resources Devel. Ser., no. 20, p. 83–93.

Gee, E. R., 1934, Recent observations on the Cambrian sequence of the Punjab Salt Range: India Geol. Survey Recs., v. 68, pt. 1, p. 115–120.

——— 1945, The age of the Saline Series of the Punjab and of Kohat, *in* Symposium on the age of the Saline Series in the Salt Range of the Punjab: Indian Natl. Acad. Sci. Proc., v. 14, sec. B, p. 269–311.

Jones, C. L., and Asrarullah, 1968, Potential for potash and other evaporite mineral resources in West Pakistan: U.S. Geol. Survey open-file rept., 18 p., 2 figs.

Lamb, B. S., 1947, Note on cores from a borehole in the Mayo salt mine, Khewra, *in* Second symposium on the age of the Saline Series in the Salt Range of the Punjab: India Natl. Acad. Sci. Proc., v. 16, sec. B, p. 29–36.

Mosebach, Rudolf, 1956, Khewrait vom Khewra Gorge, Pakistan, ein neuer Typus kalireicher Effusivgesteine: Neues Jahrb. Mineralogie Abh., v. 89, p. 182–209.

Noetling, Fritz, 1894, On the Cambrian formations of the eastern Salt Range: India Geol. Survey Recs., v. 27, p. 71–86.

Rahman, Habibur, 1963, Geology of petroleum in Pakistan [with discussion]: World Petroleum Cong., 6th, Frankfurt am Main, Proc., sec. 1, p. 659–683. [1964]

Schindewolf, O. H., and Seilacher, Adolf, 1955, Beitrage zur Kenntnis des Kambriums in der Salt Range (Pakistan): Akad. Wiss. Mainz Abh., Math.-Naturw. Kl., no. 10, p. 261–446.

Stuart, Murray, 1919, The potash salts of the Punjab Salt Range and Kohat: India Geol. Survey Recs., v. 50, pt. 1, p. 28–56.

Wynne, A. B., 1878, On the geology of the Salt Range in the Punjab: India Geol. Survey Mems., v. 14, 313 p., illus.

GOLD RESOURCE POTENTIAL OF THE DENALI BENCH GRAVELS, VALDEZ CREEK MINING DISTRICT, ALASKA

By THOMAS E. SMITH[1], Reno, Nev.

Abstract.—Recent investigations of the bench gravels near Denali, Alaska, including seismic refraction measurements, have defined a deposit of more than 35 million cubic yards of auriferous gravel. More than three-fourths square mile in area and at least 45 feet thick, it extends north and south of Valdez Creek. The sample data that are available indicate that the gravel contains from 50 cents to $1.20 of gold per cubic yard (at $35 per ounce) and that gold is distributed throughout the deposit. Although mining has been confined largely to rich pockets in bedrock depressions or incised channels, gold disseminated through the gravels constitutes the primary economic potential of the district. Potential resource value at 50 cents per cubic yard is in excess of $17 million.

The Valdez Creek placer deposits were discovered in 1903 and have been mined and explored intermittently up to the present. Gold production until 1936 was estimated at $1,250,000 (at $35 per ounce), nearly all of which came from placers (Tuck, 1938, p. 113).

The area was reexamined in 1968–69; this report describes only the placer deposits near the abandoned town of Denali and integrates earlier published information with new seismic refraction data to give resource estimates for the gold-bearing gravels.

The Denali placer area is approximately midway between the towns of Paxson and Cantwell, in east-central Alaska, near the confluence of Valdez Creek with the Susitna River. An unimproved road extends into the area and joins the Denali Highway 5 miles to the south, near milepost 77. Two unimproved airstrips in the area are also accessible to light aircraft (fig. 1).

GEOLOGY

The Denali bench gravels (fig. 1) are underlain by metamorphic rocks that grade from dark-gray argillite and greenish graywackes at the south end of the area to dark lineated phyllites north of Denali. Locally, interbed shearing and minor folding have produced slaty cleavage within both phyllites and higher grade argillites. In the extreme northern end of the area, the phyllites are distinctly spotted with clots of poikiloblastic biotite. The gradational bedrock sequence lies in the lower grade part of a regional metamorphic terrane. Bedding and foliation dip gently northward across the area, but are complicated locally by small folds and numerous faults. The metamorphic zonation is important to the present study because suballuvial seismic velocities vary with the degree of recrystallization. Slight velocity differences along profiles may also in part reflect variations in foliation attitude.

The Denali bench gravels, as referred to informally in this report, include both the auriferous alluvium on the bedrock bench adjacent to Valdez Creek and local channel fillings deposited in a canyon deeply incised within the bench. The deposits are distributed in a broadly curved belt extending northeast and southwest of Valdez Creek (fig. 1). The alluvium on the bedrock bench is a broad blanketlike deposit consisting of well-bedded auriferous gravels. It has been mined for gold intermittently since 1940, in the south wall of Valdez Creek across from Denali (fig. 2) and near Peters Creek.

Early mining in the gravels surrounding Denali was mainly concentrated along a deeply incised bedrock canyon cut by the ancestral Valdez Creek. (For detailed discussion see Moffit, 1912; Ross, 1933; and Tuck, 1938.) This buried canyon—the Tammany channel—and its downstream extension —the Dry Creek cut—were filled by beds of moderately sorted fluvial gravel, much of which has been removed by hydraulic mining. Subrounded boulders are locally concentrated near the channel bottom,

[1] Mackay School of Mines, University of Nevada, Reno, Nev. 89507.

U.S. GEOL. SURVEY PROF. PAPER 700–D, PAGES D146–D152

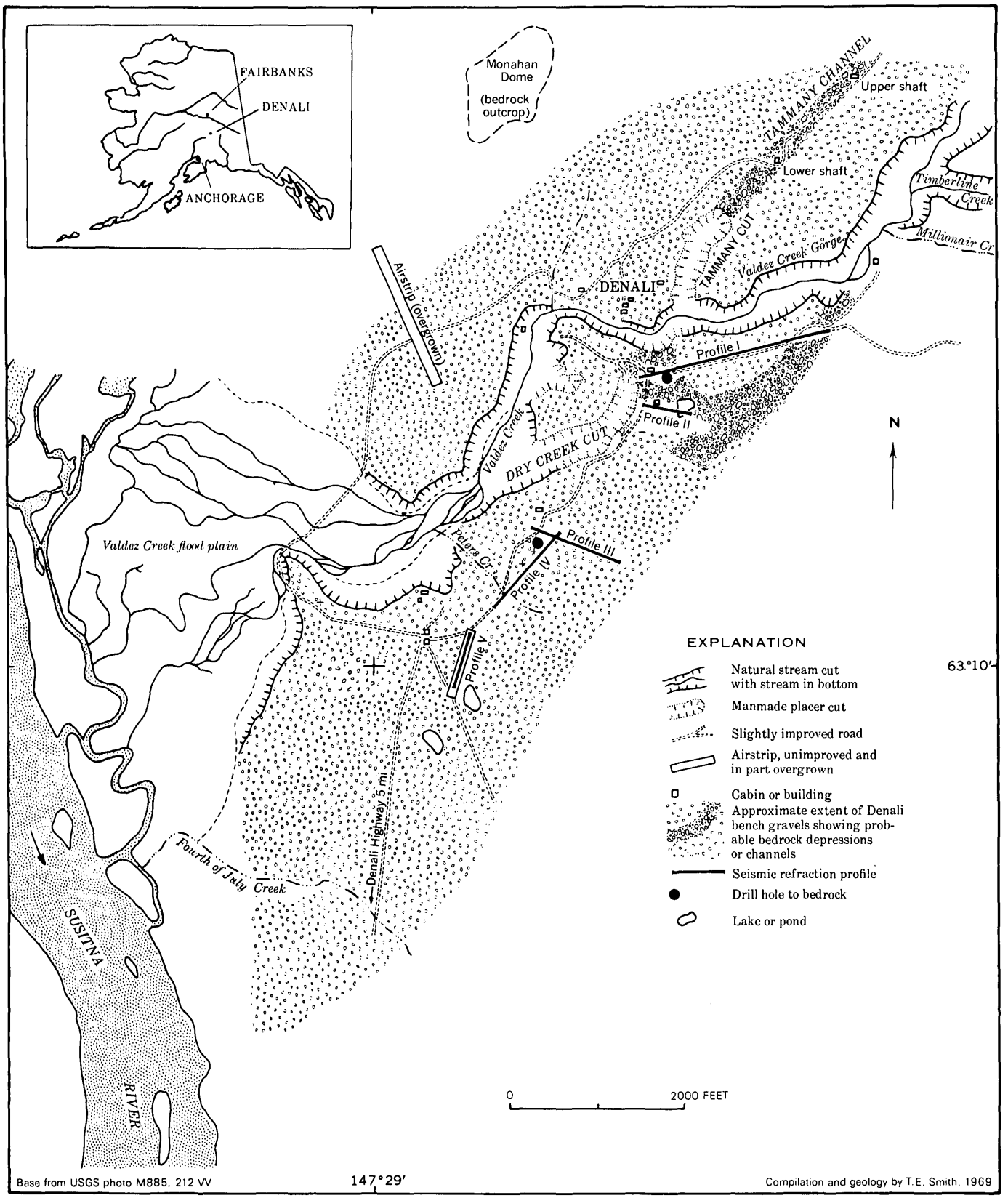

FIGURE 1.—Denali placer area, northwestern part of the Healy A-1 quadrangle (1:63,360), Alaska.

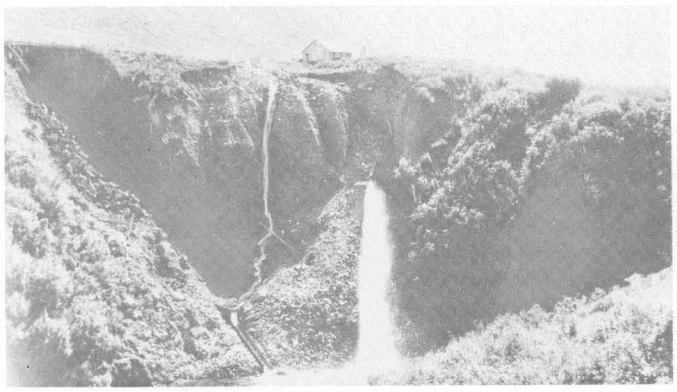

FIGURE 2.—Placer cut in bench gravels across Valdez Creek from Denali. (Photograph taken in 1946, courtesy of L. B. Kercher.) View south.

and quartz diorite, schist, and argillite represent the most abundant lithologies in the gravels. In underground workings along the channel bottom north of the Tammany cut, a thin layer of decomposed phyllite and slate bedrock yielded most of the gold recovered (J. Herman, oral commun., 1969), although all the fill reportedly contained fine gold (Ross, 1933, p. 450). Scour-and-fill structures are prevalent in the lower part of the channel but give way to evenly bedded material near the top. Numerous discontinuous layers of rounded or subrounded cobbles are present throughout the gravels. All detritus appears to be derived from the Valdez Creek drainage; there are no exotic lithologies to suggest that glacial debris from other drainages has been incorporated in the deposits.

The V-shaped cross section and large rounded boulders in the buried channel record a period of vigorous erosion, perhaps during an early Pleistocene interglacial stage. Downcutting during this time was to a base level near the present floor of the Susitna valley. A subsequent local rise in base level, probably due to an advance of the Susitna glacier, initiated a long period of aggradation during which the canyons were filled and surrounding benches covered by bedded fluvial gravels. Within the gravels, such characteristics as a general absence of scour-and-fill structures except in the deeper channels, presence of distinct bedding and dips lower than 2°, and lack of bedding relation to the irregular bedrock surface all suggest moderate-energy deposition on a gentle alluvial plain. In view of their areal configuration parallel to the Valdez Creek valley and their internal character, the gravels are interpreted as a broad proglacial outwash deposit or valley train that formed below the stationary or retreating terminus of the Valdez Creek glacier. The western side of the aggradational outwash plain was apparently bounded and obstructed by the Susitna glacier, deflecting the proglacial deposits southward along the mountain front.

A final advance and rapid retreat of the Valdez Creek glacier mantled the outwash plain with a thin, irregular ground moraine containing abundant angular boulders of lithologies indigenous to the Valdez Creek basin. The moraine is rarely more than 10 feet thick, although locally its surface is undulatory and marked by numerous low ridges and potholes, whose vertical relief also is on the order of 10 feet. This heterogeneous unit, which makes up the present surface, is the greatest source of difficulty in obtaining seismic records from the area.

Valdez Creek, rejuvenated by a drop in base level when the Susitna glacier withdrew, began cutting the deep gorge through which it now flows—approximately 20 feet lower than the floor of the ancestral creek, exposed in the Tammany cut.

SEISMIC REFRACTION STUDIES

Methods of data collection

Shallow seismic refraction measurements were made to aid in estimating the total volume of gravel on the Denali bench and to determine whether other buried channels, comparable to the Tammany, are incised into the bench nearer the mountains. The locations of the profiles are shown on figure 1.

An Electro-Tech 12-channel portable refraction unit was used. The PRA-2-12 amplifier bank, SDW-100 oscillograph, and power supply were mounted on an enclosed, tracked vehicle, providing off-road capability in locating the profiles. Twelve 4.5-cps geophones (EUS-8) were placed at 50-foot intervals along all spreads.

In order to minimize near-surface velocity variations in thawed swamps and morainal debris, the data were recorded in late May, before active-zone ground ice had thawed below a few inches. Almost all the geophones were emplaced directly in the frozen surface layer. A satisfactory acoustic coupling was obtained by similarly placing all shots in holes dug into the frozen layer or in shallow ponds on the frozen surface. One to eight sticks of standard 40-percent dynamite were used, depending on record quality and offset distance to the spread. All profiles were reversed and, with the exception of profile V, were shot at least twice in the same direction from different offsets; this technique provided

the necessary redundancy for establishing bedrock velocities and local departures from linear time-distance curves.

Wherever possible, as at the west end of profiles I and II, shots were placed directly on bedrock in old placer cuts, thus allowing a direct comparison of computed and actual thicknesses. Two drill holes (fig. 1) provide additional control on interpretations.

Interpretation

Time-distance curves and geologic sections inferred from the curves are shown in figures 3 to 6. On all reversed profiles permitting a good estimate of suballuvial velocities, the standard time-intercept method (discussed by Dobrin, 1960, p. 82) was applied to establish the planar bedrock model shown. Only the innermost data between shotpoints were utilized in these computations; redundant data from greater offsets were used merely to check suballuvial velocities and local variations from the linear model. After the data were corrected for surface topography (plotted only on inner data actually used), all departures from a linear traveltime curve were interpreted as variations of the bedrock surface. These are shown as undulations in the basic planar models.

On profile II and the end spreads of profile I, the data do not permit a good choice of traveltime slope. These spreads were interpreted using the method of differences (Jakosky, 1961, p. 725), corrected for appropriate critical propagation angles. The solutions so obtained accord well with the adjacent planar solutions.

Seismic velocities in unfrozen parts of the gravel blanket ranged from 3,000 to 3,800 feet per second

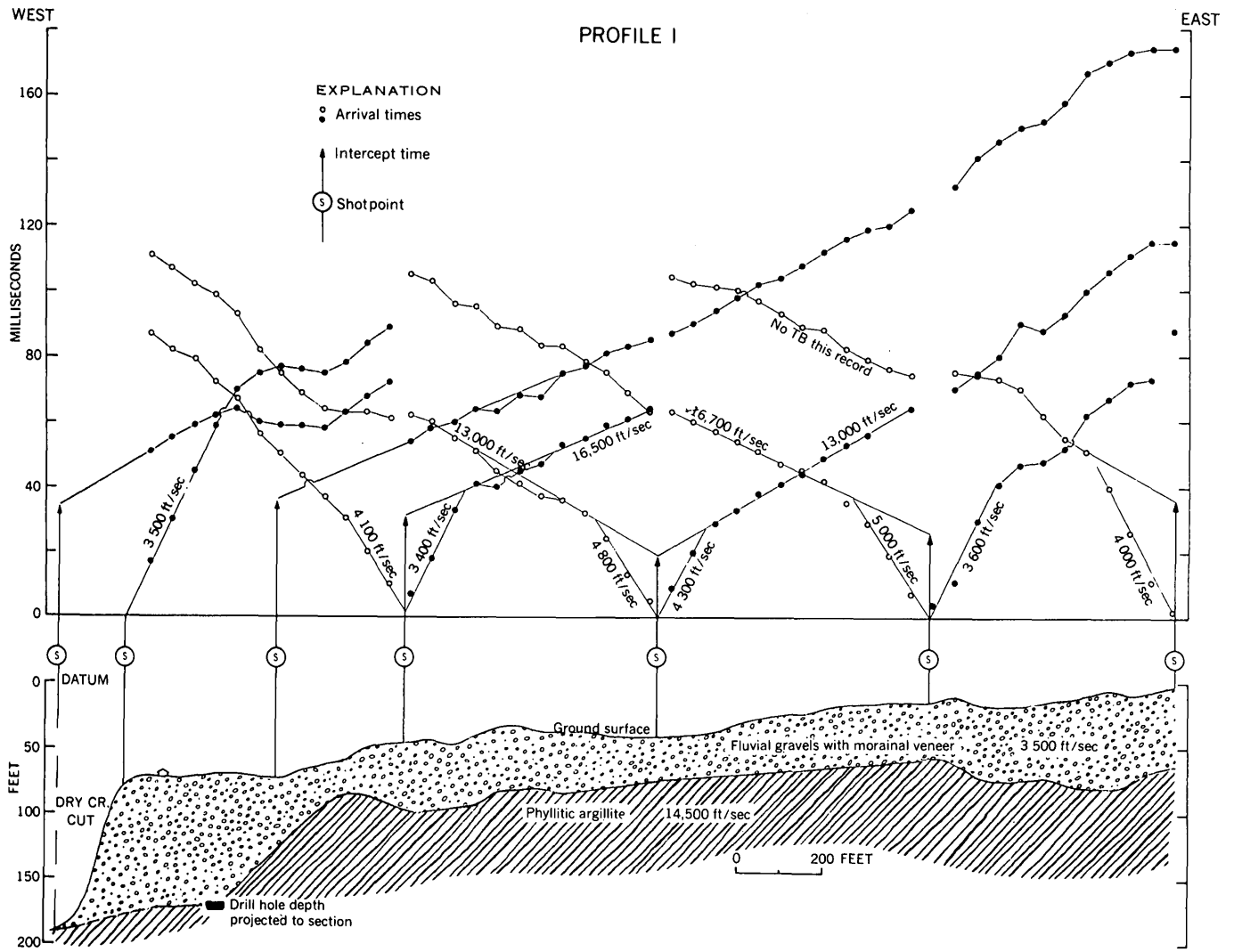

FIGURE 3.—Time-distance curves and geologic section, profile I. TB, time break (instant of shot detonation).

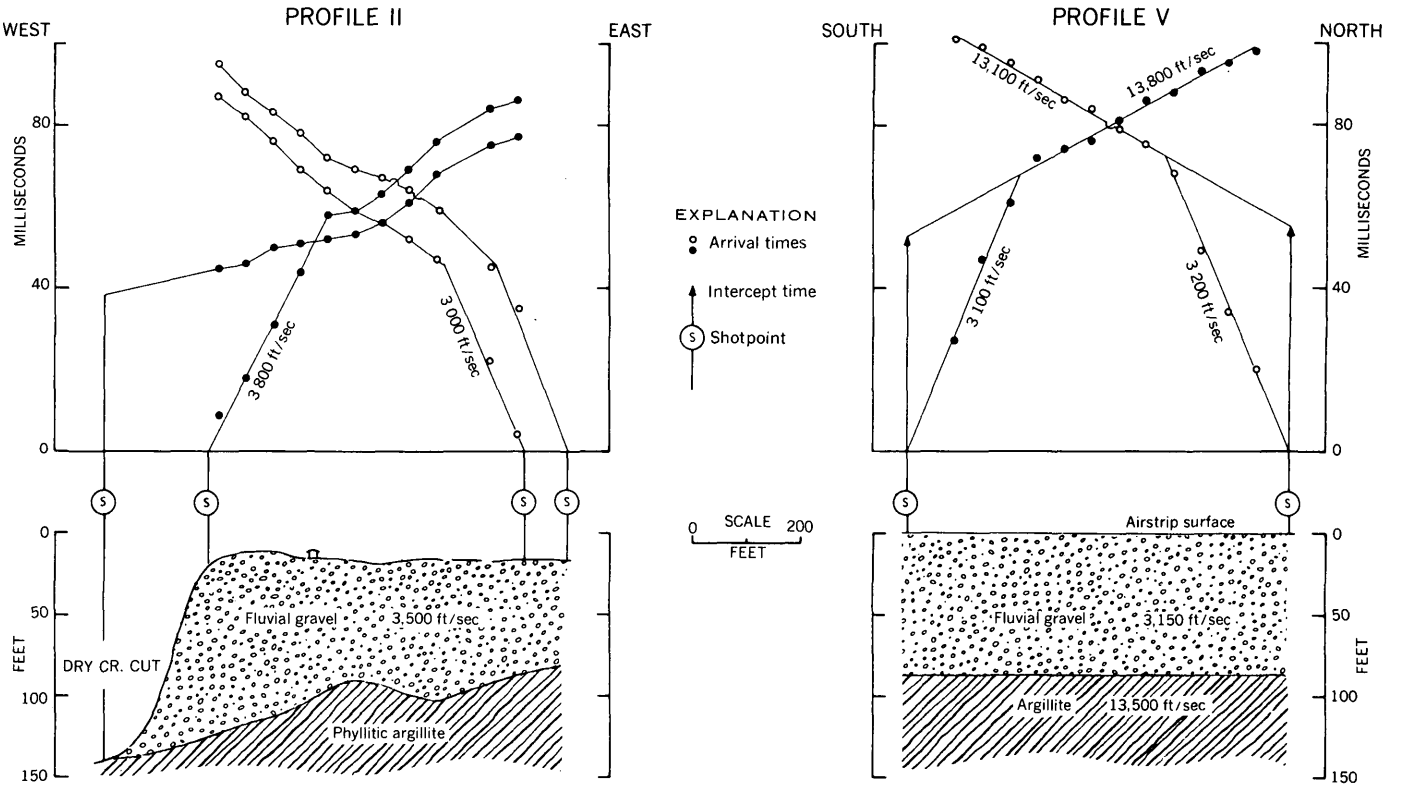

FIGURE 4.—Time-distance curves and geologic sections, profiles II and V.

The presence of a thin frozen layer complicates to some extent the choice of a representative velocity for the gravels and creates a corresponding element of ambiguity in the interpretations. In water-saturated swamp material, the first energy arrived at a velocity characteristic of the frozen surface—6,300 fps in the center of profile III. However, in the better drained areas, as along profile I, the frozen layer velocities ranged from 3,500 to 5,000 fps, depending on content of ground ice. An average lower velocity of 3,500 fps was observed along all profiles except in well-drained areas in the extreme south; this is interpreted as characteristic of the thawed ground. Computational models based on this velocity are in reasonable agreement with drill-hole data (M. J. Wall, written commun., 1969; L. B. Kercher, oral commun., 1969) and with bedrock exposed in the cuts.

The ambiguity arises in the center of profile III, where the velocities in the frozen surface cannot be distinguished from those that permafrost would produce. If the gravels were entirely frozen, the solution would require the bedrock to be deeper than shown in order to satisfy the higher velocity, thus doubling the total amount of gravel estimated for this part of the bench. However, several lines of evidence suggest that permafrost is not present here: (1) solutions which use the high apparent surface velocity place bedrock much deeper than drill-hole data indicate, (2) no time differential occurs between the area of possible permafrost and the thawed material (velocity 3,500 fps) near the west end of profile III, (3) similarly, no change of bedrock velocity is observed between the area in question and the thawed region, and (4) the center of the profile is relatively dry between rainfalls in late summer, but a permafrost lens would probably contribute melt water throughout the dry season. In view of these observations, interpretations in the center of profile III are based on a gravel velocity of 3,500 fps.

Any further attempts to apply seismic methods to the bench gravels, as for example in support of an exploration program, should include a comprehensive evaluation of surface velocities. This could be done with a portable seismic unit in late summer, after seasonal ground ice has melted. With the resulting velocity control at hand, a very accurate compilation of bedrock configuration might be obtained by using the techniques and timing of this investigation.

The inferred geologic sections show that the

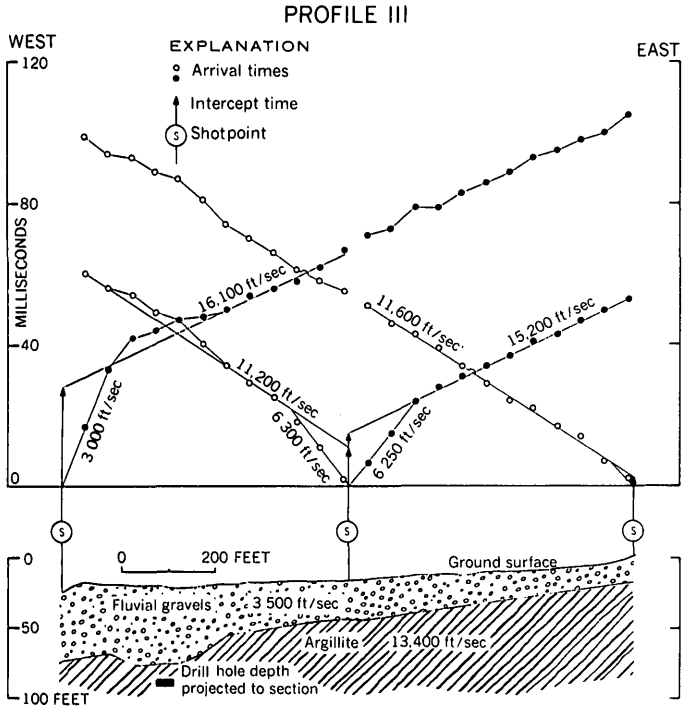

FIGURE 5.—Time-distance curves and geologic section, profile III.

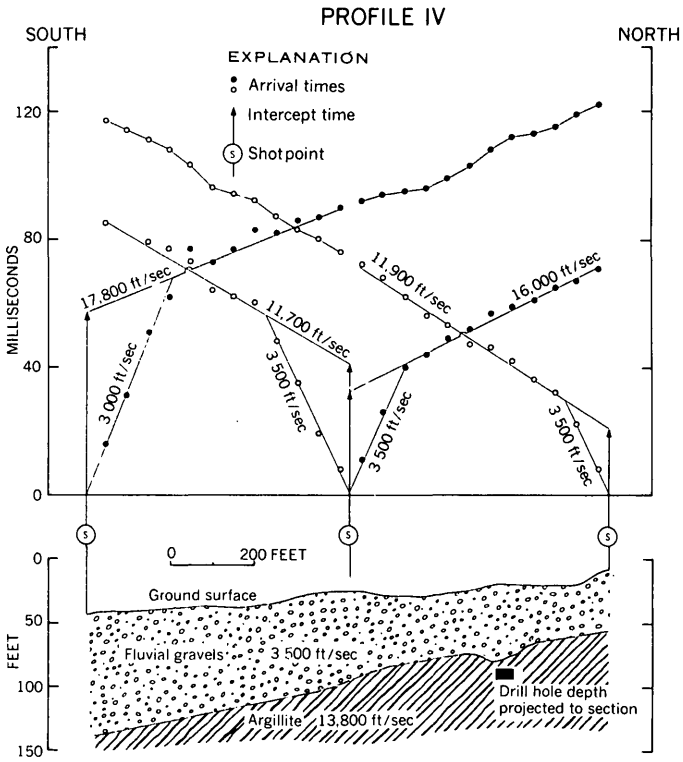

FIGURE 6.—Time-distance curves and geologic section, profile IV.

Denali bench is a relatively smooth bedrock surface. Its relief is characterized by gentle undulations and shallow depressions, rather than deeply incised channels such as the Tammany. Deposits are thickest along the Dry Creek cut. Profiles I and II reveal that mining operations in the cut did not extend to the edge of the buried channel; a considerable volume of channel fill still remains at this location. The seismic data indicate that elsewhere on the bench the thickness of the gravel blanket ranges from 45 feet in the north to nearly 75 feet in the south. These figures are in good agreement with thicknesses observed along the Valdez Creek gorge and with data from the drill holes.

POTENTIAL RESOURCE VALUE

In describing the older workings, Ross (1933, p. 451) reported that by 1931 placer operations in the Tammany channel had processed approximately 500,000 cubic yards of material, yielding some 6,750 ounces of gold ($236,000 at $35 per ounce). The average value for all gravel, including the bedrock concentration, was about $1.10 per cubic yard (at $35 per ounce). Ross also reported that on the south side of Valdez Creek, downstream from Denali, 100,000 cubic yards of bench material yielded 2,850 ounces of gold, excluding that in the sluice boxes at the time of his examination. His estimate of bulk value, recomputed at $35 per ounce, is near $1.20 per cubic yard.

More recent estimates have been made for the gravels near Peters Creek (see fig. 1). There, complete panning of a vertical channel sample, totaling about 16 cubic yards, gave an average value of 50 cents per cubic yard, with little variation throughout the blanket (L. B. Kercher, oral commun., 1969).

Data from a drill hole to bedrock near profile III suggested also that gold is distributed uniformly in the gravels and averages about $1.27 per cubic yard, although some allowance should be made for inadvertent "salting" in the open hole (M. J. Wall, written commun., 1969; L. B. Kercher, oral commun., 1969).

During the present investigation, numerous small samples were panned from various vertical cutbanks in the gravels. Small amounts of gold, visible to the eye, were found in all these samples except those taken at the very top of the gravel blanket. However, the samples were too small to enable an estimate of bulk value. They do, however, verify the extensive distribution of gold throughout the gravels.

A conservative estimate of total value may be extended to the entire blanket by using the lowest bulk value mentioned above and the minimum indicated dimensions of the gravel deposit. Figure 1 shows that the blanket covers an area of at least 3,000 by 7,000 feet, about three-fourths square mile or more, and seismic measurements suggest a minimum thickness of 45 feet. Thus, at least 35 million cubic yards of auriferous detritus may cover the Denali bench. At 50 cents per cubic yard, the Denali bench gravels would have a resource value of more than $17 million. This figure, based on physical measurements and sample data from a small area near previous placer mining, must be considered an estimate of potential value. Further exploration is needed to verify that the bulk values reported here are representative of the entire gravel deposit.

REFERENCES

Dobrin, M. B., 1960, Introduction to geophysical prospecting: New York, McGraw-Hill Book Co., 446 p.

Jakosky, J. J., 1961, Exploration geophysics: Newport Beach, Calif., Trija Publishing Co., 1,195 p.

Moffit, F. H., 1912, Headwater regions of Gulkana and Susitna Rivers, Alaska: U.S. Geol. Survey Bull. 498, 81 p.

Ross, C. P., 1933, The Valdez Creek mining district, Alaska: U.S. Geol. Survey Bull. 849–H, p. 435–467.

Tuck, Ralph, 1938, The Valdez Creek mining district, Alaska, in 1936: U.S. Geol. Survey Bull. 897–B, p. 109–131.

PEAT RESOURCES OF THE UNGLACIATED UPLANDS ALONG THE ALLEGHENY STRUCTURAL FRONT IN WEST VIRGINIA, MARYLAND, AND PENNSYLVANIA

By CORNELIA C. CAMERON, Washington, D.C.

Abstract.—An estimated 634,000 short tons of commercial quality air-dried peat, an amount slightly exceeding half the national annual consumption, was located in the unglaciated uplands along the Allegheny structural front in West Virginia, Maryland, and Pennsylvania. The largest deposits are in Canaan Valley, W.Va. Peat deposits of the filled-basin type, restricted to terraces, divides, or interfluves in large structurally controlled valleys, are potential resources. The classification standard based on geologic parameters developed and adopted by the American Society of Testing and Materials in 1969 is used in evaluating peat quality. Classification factors such as percentage of ash and percentage of fibers longer than 0.15 mm determine usefulness of peat types as soil conditioners and horticultural materials.

Peat has been burned as a low-rank fuel throughout historic time, but recently it has been recognized as a soil conditioner and horticultural material. Use for these latter purposes has increased significantly during the past decade because of the explosive growth of suburbia. In 1964, the total output of the Appalachian peat industry, which is centered in the glaciated part of Pennsylvania, was 99,000 short tons of air-dried peat. This total represented 15.2 percent of the national production and 14.7 percent of the national value.

The last nationwide study of the occurrence and use of peat was by Soper and Osbon in 1922; emphasis was on use as potential fuel, and deposits were not appraised with the restrictive criteria designed for present uses. Moreover, since 1922 many peat deposits have been destroyed, and many new areas probably containing much peat have been made accessible by modern roads.

In 1968, a reconnaissance of peat resources in the Appalachian region (Cameron, 1968) called attention to the nonfuel importance of peat in the area of this report and stressed the need for developing exploration techniques based on stratigraphic and geomorphic concepts.

Acknowledgments.—Data on the physical properties of the peat—moisture, ash, and organic content, water holding capacity, fiber content, and acidity—were obtained by Caroll L. Burton under the direction of Irving May. Radiocarbon age determinations were made by Meyer Rubin and Elliott Spiker. The author was ably assisted in the field by David E. Schieck, a graduate student at the University of Michigan.

PEAT STRATIGRAPHY

In the unglaciated uplands along the Allegheny structural front, beds of reed-sedge and sphagnum moss peat of commercial potential fill basins beneath bogs containing *Sphagnum* moss, marshes containing a reed-sedge type of vegetation, and swamps containing spruce, pine, and maple forests. The normal sequence in these deposits of the filled-basin type comprises a basal clay grading upward to organic clay containing diatoms and algal debris, overlain by peaty clay, clayey peat, and finally reed-sedge peat that may have a top cover of sphagnum moss peat or peat containing stumps and logs. This stratigraphy records a history of changing environments during which the pond, receiving only inorganic clay at first, continues to fill with floating weeds and clay until the water becomes shallow enough to support marsh grass, reeds, and sedges. The cycle of peat development may continue above the level of the original pond. For example, growth of *Sphagnum* moss may produce a climbing bog type of peat deposit on the surface of the filled-basin deposit, or instead, soil may develop which permits a needle-leaved forest growth and subsequent formation of woody peat. Continued accumu-

lation of soil on this forest floor may permit broad-leaved trees to supplant other vegetation in the final stage of a single-cycle peat deposit.

Boundaries are gradational between stratigraphic units belonging to the same cycle. Discontinuities mark the interruption of one cycle and the beginning of another. The discontinuities are recognized by: (1) reed-sedge-peat, representing a marsh environment, resting on woody peat formed on a swamp forest floor; (2) algal or clayey peat, formed in a pond, resting on reed-sedge woody peat formed in a marsh or forest; (3) humus and buried soils or paleosols within the deposit which represent episodes of weathering between episodes of vegetative accumulation; (4) deposits of clastic debris and beds of peat with clay, sand, or silt between beds of peat with much lower ash content; the clastic debris represents episodes of ponding or flooding; and (5) charcoal within the peat deposit, representing peat destruction by ancient forest or bog fires.

Recognition of the various terrane environments of peat formation and the various kinds of discontinuties within the deposit is important in judging both the quality of the deposit and the rate of accumulation. One deposit of a given thickness and very low ash content may form rapidly during one stage of one cycle, whereas another deposit of the same thickness and very high ash content may be the residuum of numerous cycles involving a very long period of time. Recognition of the terrane environments in which units of a given peat deposit formed is also important in interpreting radiocarbon dates obtained in the deposit. Some peat units, such as reed-sedge peat beds, transgress time lines, because they record an environment that typically migrates from the margin of the deposit toward the center as the pond becomes filled. Other peat units, such as moss peat, are generally synchronous in a given deposit.

CRITERIA FOR JUDGING COMMERCIAL QUALITY AND QUANTITY

Organic content (the reciprocal of ash content) and water-holding capacity (the ability to hold water like a sponge) are primary factors in determining a peat's usefulness as a soil conditioner for horticulture. Ash content can be measured directly in percent, and water-holding capacity is largely controlled by kind and size of fibers, which also can be determined quantitatively. Fibers are stems, leaves, or fragments of bog plants 0.15 mm to 12.7 mm in size. Percentages of fiber are based on oven-dried weight at 105°C.

Ash content and the kind, size, and amount of fibers are the basis for the classification standard, ASTM D2607–69 adopted in 1969 by the American Society for Testing and Materials. According to this standard, all commercial peat must have not more than 25 percent ash content and must belong to one of five major types: (1) sphagnum moss peat, which must contain a minimum of 66⅔ percent sphagnum moss fiber; (2) hypnum moss peat, which must contain a minimum of 33⅓ percent fiber composed of at least 50 percent hypnum; (3) reed-sedge peat, which must contain a minimum of 33⅓ percent fiber composed of at least 50 percent reed-sedge and other nonmoss fibers; (4) peat humus, which contains less than 33⅓ percent fiber; and (5) other peat, which contains all other forms of peat not classified above.

The minimum size of a peat deposit worth exploiting varies from place to place. In glaciated areas north of the present study area, where peat is fairly abundant, peat deposits now exploited are at least 10 acres in areal extent and have at least a 5-foot thickness of commercial-quality peat. In the present study area, smaller quantities must be considered. Exploitation of deposits, regardless of areal extent, that have less than a 2-foot thickness of commercial-quality peat does not seem likely. Tonnage in peat deposits is calculated on the basis of 200 tons of air-dried peat per acre-foot.

GEOLOGIC AND PHYSIOGRAPHIC FACTORS THAT CONTROL QUALITY AND QUANTITY

The quantity and quality of a peat deposit are dependent upon constant factors such as size, shape, and composition of the depression containing the deposit, and upon varying factors such as climate, and surface- and ground-water drainage. Studies to the north in the glaciated parts of Pennsylvania and New York (Cameron, 1970a, b) demonstrated relationship of these factors to resource potential of peat deposits of the filled-basin type. Significant relationships are as follows:

1. Peat deposits within or partly within bedrock tend to have a higher precentage of fibers larger than 0.15 mm than those deposits completely surrounded by unconsolidated material. Relationship of quality to kind of material composing the immediate area of the peat deposit and the walls of the depression in which accumulation of peat took place involves several aspects such as water-transmitting characteristics, solubility, resistance to erosion, and weathering products.

2. Within unconsolidated material, peat deposits larger than several acres in areal extent tend to have lower ash content and a higher percentage of fibers larger than 0.15 mm than similar smaller deposits.

3. Peat deposits in depressions with high steep walls tend to be thicker than deposits in depressions with low gently sloping walls. Steep walls favor rapid build-up of marsh-type vegetation above the original pond-surface level and at the same time delay development, along the margins of the depression, of soil conditions that initiate transgression of forest which slows and eventually stops peat formation.

4. Peat deposits accumulated in depressions with high steep stable walls are apt to have lower ash content than deposits in similar depressions with unstable walls.

5. Peat deposits in depressions with small drainage basins tend to have less clay, sand, and silt brought into the depression while peat is accumulating than deposits in larger basins. The ratio of effective drainage area to area of peat accumulation in more than 100 examples in northeastern Pennsylvania showed that if the sediment-producing area is more than 10 times the size of the area of peat accumulation, the ash content is apt to be greater than 25 percent.

6. Peat deposits accumulating in a cool, moist climate are thicker and have lower ash content than deposits accumulating in a cool, dry climate. Humidity is the controlling factor in growth of peat-producing plants and preservation of plant structures.

7. Peat deposits protected topographically from stream flooding are apt to have lower ash content than deposits subject to flooding. Two common causes of flooding are increased precipitation and ponding resulting from landslides or beaver activity.

8. Peat deposits subject to ground-water fluctuation caused by (a) artificial drainage, (b) drainage caused by breaching of dams on adjacent streams, or (c) lumbering operations and extensive forest fires which extinguish springs and seeps, have higher ash content and a lower percentage of fibers greater than 0.15 mm than deposits not subject to ground-water fluctuation. This is because a deposit saturated with ground water is relatively free from aerobic bacterial activity which decays vegetable matter; when the ground-water table falls, permitting oxygen to enter the deposit, decay increases ash content by destroying plant fibers.

SCOPE AND STUDY TECHNIQUES

This report presents a study of 11 areas containing swamps and marshes near the Allegheny structural front (See index map, fig. 1). Most of the undrained areas south of the glacial border are in the uplands of West Virginia, Maryland, and Pennsylvania. All the areas in this study are unexploited except Castleman Basin, Md., where peat mines, opened in 1963, are operated by the Garrett County Processing and Packaging Corp.

In these areas, 30 deposits were selected for field study. These deposits are delineated as peat and muck or Atkins silt loam on county soil maps and as swamps and marshes on topographic maps at scale 1:24,000. Sixteen are on valley or basin floors near present stream level, and 14 are on terraces, divides, and interfluves at least 10 feet above modern flood plains.

Samples were obtained along traverses across each deposit to ascertain the local stratigraphy as well as the configuration of the depression or basin of accumulation. On reconnaissance traverses a Davis peat sampler was used to recover samples of the unconsolidated and water-saturated material. Cores were taken at frequent intervals to determine sites for obtaining very detailed representative cores and to determine the character of representative samples of organic and inorganic material. After traverses with the Davis sampler were completed, very detailed cores were obtained with a MacAlley peat auger.

Selected representative samples of peat, clayey peat, peaty clay, and clay from a MacAlley core in each deposit were submitted to the laboratories of the U.S. Geological Survey for several kinds of analyses. Values for moisture, ash, and organic content, water-holding capacity, fiber content exceeding 0.15 mm, and acidity were obtained from the organic samples. Radiocarbon ages of samples collected from deposits in Canaan Valley and Castleman Basin were determined.

PEAT DEPOSITS IN UPLANDS SOUTH OF THE GLACIAL BORDER

The 30 peat deposits discussed in this paper are restricted to the unglaciated part of the Allegheny structural front. The climate in the region above and near the high steep escarpment that curves southwestward through Pennsylvania, Maryland, and West Virginia favors accumulation of peat, because rains and fogs sweep over the uplands throughout cool summers and help maintain high humidity and the flow of cold springs.

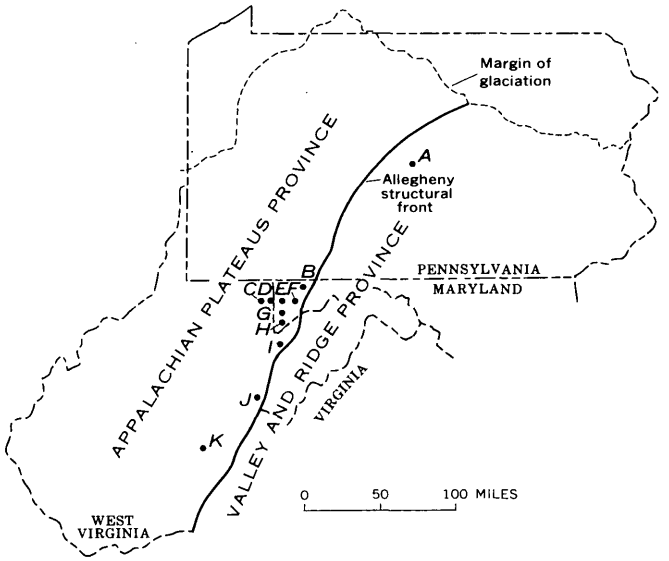

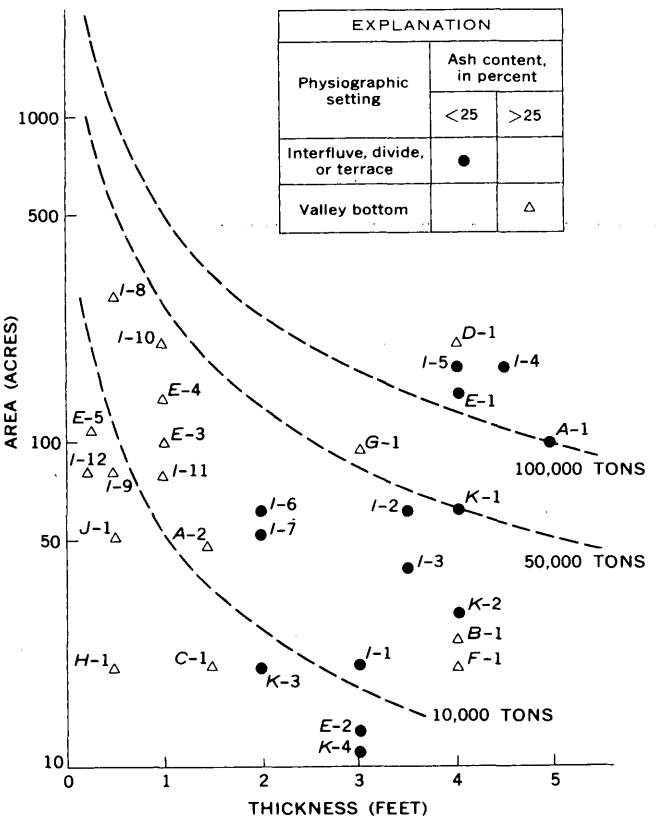

FIGURE 1.—Area, average thickness, ash content, and physiographic setting of peat deposits in 11 areas in the unglaciated uplands of Pennsylvania, Maryland, and West Virginia; estimated tonnage curves based on 200 tons of air-dried peat per acre-foot. Index map shows geographic location of deposits in the following areas:

Area	*Number of deposits*	*Name of location*
A	2	Bear Meadows Natural Area, Centre County, Pa.
B	1	Wolf Swamp, Avilton quadrangle, Garrett County, Md.
C	1	Swamp at head of Cupp Run, Cuzzart quadrangle, Preston County, W. Va.
D	1	Cranesville Swamp Natural Area, Preston County, W. Va.
E	5	Castleman Basin, Garrett County, Md.
F	1	Pine Swamp, Barton quadrangle, Garrett County, Md.
G	1	Hammel Glade, Deer Park quadrangle, Garrett County, Md.
H	1	Swamp at head of Spring Branch of Laurel Run, Gorman quadrangle, Garrett County, Md.
I	12	Canaan Valley–Cabin Mountain, Tucker County, W. Va.
J	1	Blister Swamp, Pocahontas County, W. Va.
K	4	Cranberry Glades Botanical Area, Pocahontas County, W. Va.

The topography in the region is controlled by post-Paleozoic differential erosion. Easily eroded beds follow regional structure rather faithfully. Fourteen deposits containing commercial-quality peat in beds at least 2 feet thick are on terraces, divides, or interfluves within broad valleys with trenched streams (fig. 1). These valleys are generally in areas of almost horizontal beds near the noses of gently plunging anticlines and in troughs of synclines, or on monoclines where dip of beds locally flattens. The depressions filled with peat on these terraces, divides, or interfluves are former stream channels closed by alluvium. Their saucer-shaped bottoms are lined with gray pond clay so impermeable that peat is preserved in a state of saturation.

The remaining 16 deposits, all without commercial potential, have peat beds less than 2 feet thick and ash content greater than 25 percent. These deposits occur in valley bottoms either along or at the heads of streams, where they are subject to flooding or to severe fluctuation of the water table.

The conditions for accumulation and preservation of peat with commercial potential are illustrated in

four areas; Canaan Valley (area *I*, fig. 1) and Cranberry Glades (area *K*) in West Virginia, Castleman Basin (area *E*) in Maryland, and Bear Meadows (area *A*) in Pennsylvania. These areas contain most of the unexploited reserves of peat (peat that is suitable for use as a soil conditioner and horticultural material) that are to be found in the unglaciated uplands of Maryland, Pennsylvania, and West Virginia. The total of 634,000 tons of air-dried peat is little more than half the national annual consumption. In Maryland, deposits of mostly reed-sedge peat are rapidly being mined by one company. In Pennsylvania, deposits of mostly reed-sedge peat, estimated at about 100,000 tons, are in protected areas, but in West Virginia, most of the 470,000 tons of reed-sedge and sphagnum peat are in Canaan Valley where exploitation would be feasible. About 83,000 tons are in Cranberry Glades, a protected botanical area.

Canaan Valley–Cabin Mountain, W. Va.

Canaan Valley (area *I*, fig. 1) just east of Davis, W. Va., is a large, breached, double-plunging anticlinal valley between Canaan and Brown Mountains on the west and Cabin Mountain on the east. Small streams tributary to the Blackwater River have cut shallow valleys floored with alluvium. The alluvium is interspersed with marsh deposits containing muck and peat without commercial potential. Peat is thin, and ash content exceeds 25 percent.

The terraces that compose most of Canaan Valley are about 10 feet above the modern streams and are underlain by shale, shaly sandstone, and limestone of the Greenbrier Limestone, veneered in most places with peat, muck, clay, silt, and sand. Terraces are especially broad in the noses of the Blackwater anticline. The peat deposits of commercial potential are restricted to these broad terraces where they are in bedrock depressions closed by alluvial silt and sand. Shape and thickness of the peat deposits, which are resting on inorganic sediments, are shown in figure 2. Maximum thickness is 5 to 9 feet over gray basal pond clay.

Profile *A–A′* (fig. 3) shows stratigraphy of deposit *I–4*. This deposit is typical of deposits on terraces at the northeast end of the sandstone ridge of the Pocono Formation in central Canaan Valley and between the sides of the northern end of Canaan Valley. These sides are formed of sandstone and shale of the Mauch Chunk and Pottsville Formations. In deposit *I–4*, gray pond clay at the bottom of a former stream channel in the Greenbrier Limestone is covered on the north side by an alluvial sandy silt which may have spilled into the pond or which may represent an erosional remnant of thicker alluvium. The overlying peaty clay, clayey peat, and reed-sedge and sphagnum peat are shown in detailed section in figure 3. The earliest available date, obtained for the base of the reed-sedge peat, is 5,250±250 years B.P. (Meyer Rubin, written commun., May 1969; U.S. Geol. Survey sample W2255). Ash content of less than 25 percent in this dated peat and in the overlying peat indicates that streams were trenched deeply enough to prevent flooding of the terrace ponds and marshes at least as long ago as 5,000 years. The present blanket of living sphagnum moss covering the terrace lies on a surface produced by forest fires several decades ago when peat was burned to a depth of about 3 feet.

Percentage of organic matter, percentage of fibers greater than 0.15 mm, and percentage of water-holding capacity decrease downward from the surface of the peat deposit to the base of the clayey peat layer which is not of commercial quality. The deposit becomes increasingly acidic with depth, which is the reverse of the usual in peat deposits. This probably reflects calcium carbonate derived from Greenbrier Limestone brought by ground water into the deposit above the pond clay aquiclude.

On Cabin Mountain, sphagnum moss and some reed-sedge vegetation are presently growing in valleys along modern streams and in small bedrock basins at the heads of streams, but accumulations of peat of commercial quality have been destroyed as the result of forest fires and lumbering operations. Existing peat deposits are too thin and too high in ash content for commercial use.

Cranberry Glades, W. Va.

Cranberry Glades, west of Marlington, W. Va., is in a steep-walled valley ¼ mile to 1 mile wide in

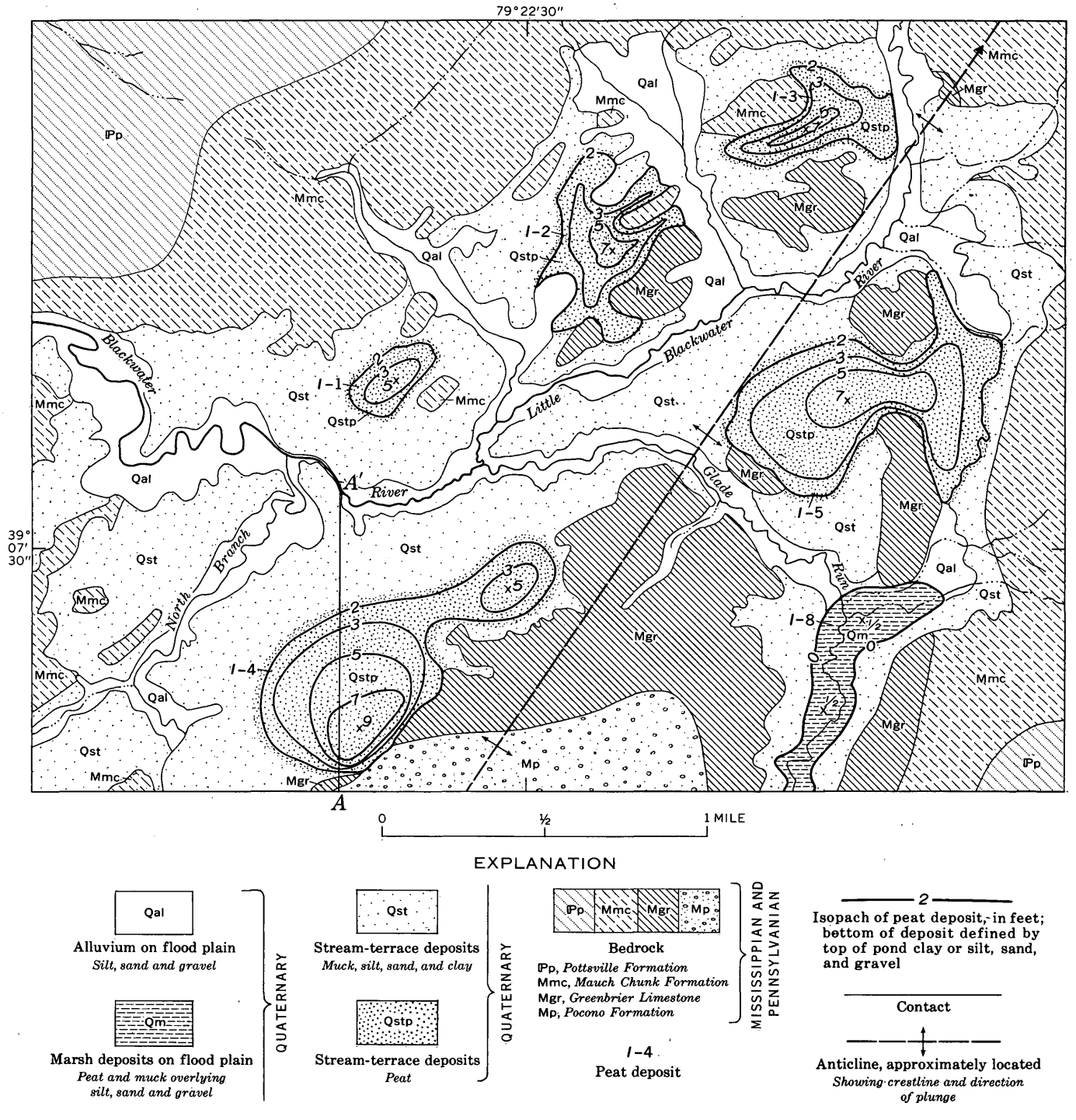

FIGURE 2.—Sketch map of the northern part of Canaan Valley, showing relation of peat deposits to modern streams. Deposits *I–1* through *I–5* on terraces contain peat with commercial potential. Deposit *I–8* on a modern flood plain does not. (Modified from Losche and Beverage, 1967, air photo sheets 15, 16, 22, and 23.)

limestone, sandstone, and shale at the place on a northwest-dipping monocline where the dip sharply decreases. The area is drained down the dip by the Cranberry River and its tributaries. Although the surface of the area appears to be level, it drops 45 feet in 3 miles.

Darlington (1943) studied the relation of the several glades, which are sphagnum bogs, to their physiographic settings. He concluded that

* * * sideward cutting by the Cranberry River system, temporarily at grade in the Mauch Chunk shales, produced the level floored basin near the head of Cranberry River drain-

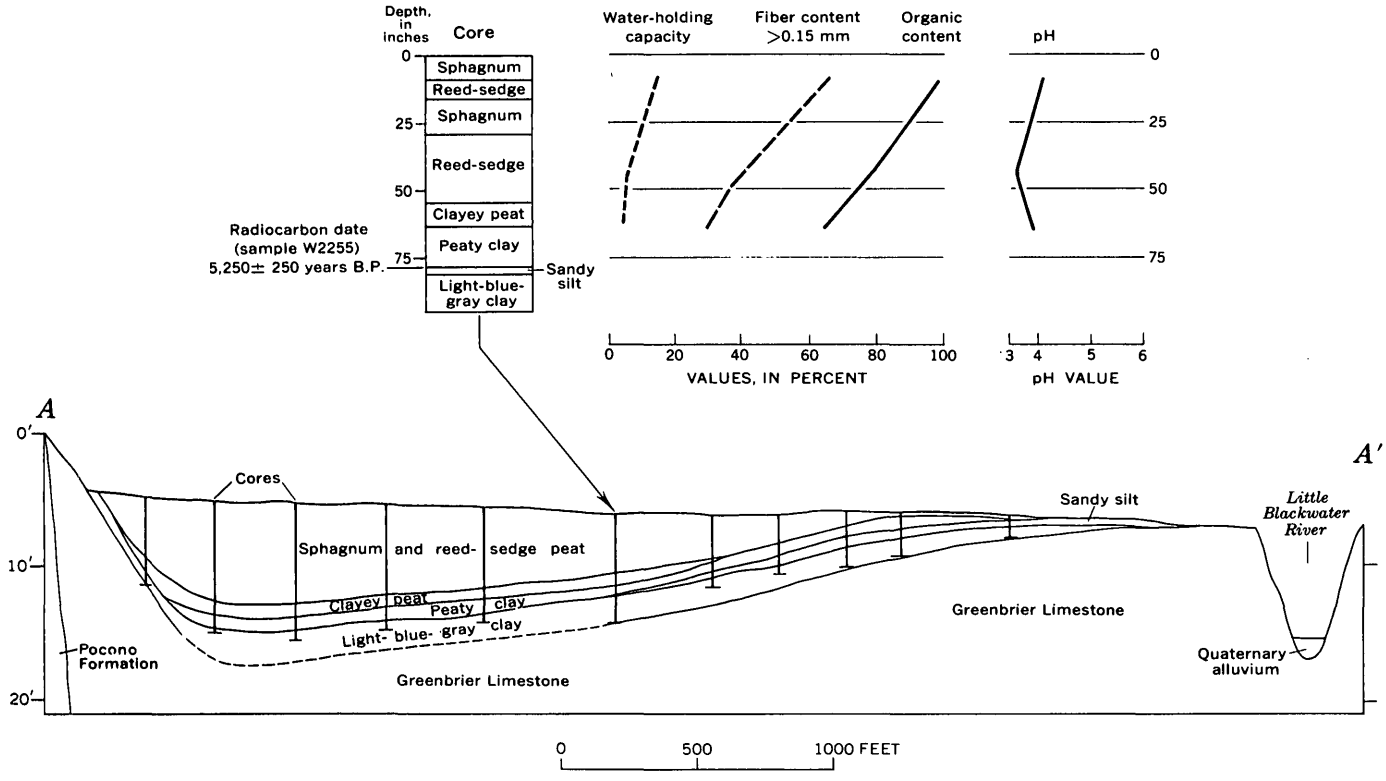

FIGURE 3.—Profile along core traverse *A–A'* (fig. 2) across deposit *I–4* on a terrace near the axis of Blackwater anticline in Canaan Valley. Quality characteristics vary with material and depth, as shown by analyses of core samples collected in sequence.

age. Abandoned stream channels and depressions behind natural levees, at first occupied by ponds, became sites of peat accumulation upon which the present *Sphagnum* bogs developed. As the Cranberry River and its tributaries became intrenched, these bogs were abandoned on the interfluves.

Within the past 15 years, the forest margin has noticeably encroached onto the glades, suggesting a drop in the general water table accompanying downcutting of the hard layers just downstream from the glades.

Cores of the peat deposits made during the present study show the following sequence of beds from the bottom upward: alluvial silt, light-blue-gray pond clay, peaty clay, clayey peat, reed-sedge peat containing wood in its upper part, and, finally, sphagnum moss peat covered with the living moss. The reed-sedge and sphagnum moss peats are 2 to 4 feet thick and of commercial quality. Tonnages in the four deposits range from less than 10,000 to 50,000 tons of air-dried peat.

Castleman Basin, Md.

Castleman Basin in the Maryland panhandle is a large synclinal valley between Meadow and Negro Mountains. Principal drainage is northeast by Castleman River in the direction of axial plunge. The much smaller Cherry Creek breaches the southwest end of the synclinal trough. The largest peat deposit (*E–1*) is in the wind gap between the two drainage systems. A much smaller deposit (*E–2*) is on an interfluve of Cherry Creek drainage. Both deposits are being mined for good-quality peat. The Castleman Basin deposits are similar in origin and stratigraphy to those in Canaan Valley and Cranberry Glades.

The three other peat deposits in Castleman Basin do not have commercial potential. Deposits *E–3* and *E–4* are on valley floors of Cherry Creek, and deposit *E–5*, in Cunningham Swamp, is on a valley bottom of the Castleman Basin drainage system. All three deposits, formed after the dissection of the Castleman Basin floor, began their accumulation much later than did deposits *E–1* and *E–2*. They are also much more subject to contamination by silt during periods of flood.

Bear Meadows, Pa.

Bear Meadows, near State College, Pa., is a State monument and takes its name from a level open marsh meadow through which Sinking Creek meanders. Peat deposit *A–2*, which underlies this marsh

on the flood plain of Sinking Creek, contains little more than 10,000 tons of very poor grade peat. The adjacent broad terrace, about 10 feet above Sinking Creek, is covered with a swamp supporting a dominantly spruce-pine forest. Peat deposit *A–1*, which underlies this forest, contains approximately 100,000 tons of commercial-quality peat. The terrace and the meadow are in a U-shaped basin developed by differential erosion in the nose of a pitching anticline. Sinking Creek heads in this basin and discharges through a narrow steep-sided outlet that, during the Pleistocene Epoch, may have been the site of landslides which from time to time caused ponding in the U-shaped basin as postulated by Kovar (1965). The lowest part of the basal clay may have been deposited in a pond caused by landslides.

Cores through the forested terrace along traverses show sand and gravel overlain by a saucer-shaped bed of light-blue-gray underclay similar in shape to that laid down in ponds in parts of abandoned stream channels and behind alluvial deposits on terraces and interfluves in West Virginia and Maryland. In Bear Meadows, the section near the center of the terrace above the basal clay consists, in ascending order, of 10 inches of peaty clay, 10 inches of clayey peat, 100 inches of reed-sedge peat containing wood in the upper part, and finally 50 inches of muck containing wood layers. Water-holding capacity, organic content, and fiber content are very low in the muck, very high in the reed-sedge peat, and very low in the clayey peat.

A discontinuity separates this clayey peat from the underlying peaty clay as shown by Stingelin (1965, p. 67–70) who interpreted sphagnum moss fibers in the peaty clay as the remnant of a peat bog developed on the erosional surface of light-gray basal pond clay. Westerfield (1961, p. 5) dates this peaty clay at 10,320±230 years B.P. This date is close to the oldest date for the last substage of the Pleistocene, placed by Frye, Willman, Rubin, and Black (1968) as closing between 10,000 and 5,000 years B.P. The pollen grains associated with the moss fibers suggest a pine-spruce (instead of the present oak) forest on the uplands. These evergreens are characteristic of a climate more moist and cool than that of today. Another discontinuity is suggested by the decomposed (low percentage) fiber in the clayey peat layer above the peaty clay. The clayey peat may represent a paleosol marking a period of weathering and vegetal decay before onset of marsh conditions favoring accumulation of the reed-sedge peat. The alternating layers of weathered and less weathered material composing the upper 50 inches of the section, as shown by variations in percentage fiber content, is consistent with a fluctuating water table. Also, charcoal associated with layers having the lowest fiber content suggests temporary levels of low water table during which ancient forest fires destroyed peat. Twice within the past century beaver dams have caused rises of the water table in the meadow plain of Sinking Creek, as is indicated by dead trees. Each time the beavers were trapped, their dams destroyed, and normal water level restored.

AGE AND RATE OF PEAT ACCUMULATION

The structurally controlled bedrock valleys and basins were formed by differential erosion in post-Paleozoic time. The depressions containing commercial peat deposits were developed within these valleys and basins in pre-Holocene time. A date of 13,620±600 years B.P. was obtained near the base of the peaty clay layer in deposit *E–1* in Castleman Basin (Meyer Rubin, written commun., May 1969, U.S. Geol. Survey sample W2253). An estimated date of about 10,000 years is quoted by Darlington (1943) for the base of the peaty clay layer in deposit *K–1* in Cranberry Glades, and a date of 10,320±230 is quoted (Westerfield, 1961) for peaty clay in Bear Meadows.

Any peat deposits of commercial quality formed during the Pleistocene were erased by weathering or erosion, so that the present deposits, all of Holocene age, may lie on truncated remnants of older cycles of peat development. Reed-sedge peat of commercial quality began to form about 5,000 years ago in Canaan Valley. A date of 5,250±250 years B.P. was obtained by Rubin (written commun., May 1969; U.S. Geol. Survey sample W2255) at the base of reed-sedge peat in deposit *I–4*. Peat is presently forming in this deposit. The rate of accumulation, however, during the 5,000-year span cannot be calculated because of the discontinuities during accumulation.

REFERENCES

Cameron, C. C., 1968, Peat, *in* U.S. Geological Survey and U.S. Bureau of Mines, Mineral resources of the Appalachian region: U.S. Geol. Survey Prof. Paper 580, p. 136–145.

——— 1970a, Peat deposits of northeastern Pennsylvania: U.S. Geol. Survey Bull. 1317–A. [In press]

——— 1970b, Peat deposits of southeastern New York: U.S. Geol. Survey Bull. 1317–B. [In press]

Darlington, H. C., 1943, Vegetation and substrate of Cranberry Glades, West Virginia: Bot. Gaz., v. 104, no. 3, p. 371–393.

Frye, J. C., Willman, H. B., Rubin, Meyer, and Black, R. F., 1968, Definition of Wisconsinan Stage: U.S. Geol. Survey Bull. 1274–E, 22 p.

Kovar, A. J., 1965, Pollen analysis of the Bear Meadows bog of central Pennsylvania: Pennsylvania Acad. Sci. Proc., v. 38, no. 2, p. 16–24.

Losche, C. K., and Beverage, W. W., 1967, Soil survey of Tucker County and part of northern Randolph County, West Virginia: Washington, D.C., U.S. Soil Conservation Service, 78 p.

Soper, E. K., and Osbon, C. C., 1922, The occurrence and uses of peat in the United States: U.S. Geol. Survey Bull. 728, 207 p.

Stingelin, R. W., 1965, Late glacial and postglacial vegetation in north-central Appalachian region: State College, Pa., Pennsylvania State Univ., unpub. Ph. D. thesis, 118 p.

Westerfield, W. F., 1961, An annotated list of vascular plants of Centre and Huntingdon Counties, Pennsylvania: Castanea, v. 26, p. 1–80.

A SPHALERITE VEIN AND ASSOCIATED GEOCHEMICAL ANOMALIES IN ST. LAWRENCE COUNTY, NEW YORK

By C. ERVIN BROWN, Washington, D.C.

Abstract.—In the Richville 7½-minute quadrangle, St. Lawrence County, N.Y., a minor replacement vein of sphalerite parallel to layering in marble resembles the major mineralization in the Balmat-Edwards district 13 miles to the southeast. Geochemical sampling of soil in the vicinity of the vein shows a significant anomaly for zinc parallel to the strike of layering and the vein. Mercury as a pathfinder element even more sharply distinguishes the anomalous area. Lead does not show an anomaly; in fact, lead values are very low. Copper values are also low, but the proximity of the highest values to the sphalerite occurrence suggests an association of copper with the zinc mineralization.

In St. Lawrence County, N.Y., lead and zinc deposits occur in two distinct modes. The most important is that of the large zinc ore bodies in the Balmat-Edwards district described by Lea and Dill (1968). These are structurally controlled replacement bodies conformable to the flow layering in the enclosing Precambrian marble. They are believed to be remobilized and metamorphosed early-formed deposits (Brown, 1965, p. 66; Lea and Dill, 1968). The second and less important type is the late vein fillings in steeply dipping fractures mainly in Precambrian gneiss and marble. These are typified by the veins that occur at Rossie, N.Y., west of the Balmat-Edwards district. Nearby at Redwood, a similar vein cuts Upper Cambrian Potsdam Sandstone, indicating a lower Paleozoic or younger age (Buddington, 1934, p. 207).

While doing field mapping in the Richville quadrangle in 1969, the author found a replacement veinlet of sphalerite about 1 inch thick conformable to the flow layering of the marble. Its similarity to the important type of mineralization at Balmat and Edwards, N.Y., 13 miles to the southeast, prompted geochemical sampling of the immediately surrounding area to check whether associated anomalies might justify further exploration.

A few minor veins of the Rossie type had been prospected for lead about 4,000 feet south and southwest of the sphalerite vein. These are along fractures trending N. 70° to 75° W. and consist typically of calcite with a small amount of galena and sphalerite along the vein margins. They bear no resemblance to the sphalerite vein under consideration.

LOCATION AND GEOLOGIC SETTING

The sphalerite vein is in the Richville 7½-minute quadrangle 6 miles north of Gouverneur (fig. 1) and 1½ miles west of an area known locally as North Gouverneur along Rock Island Road. Topographically, the area has low relief, and the terrain is characterized by low elongate hills trending

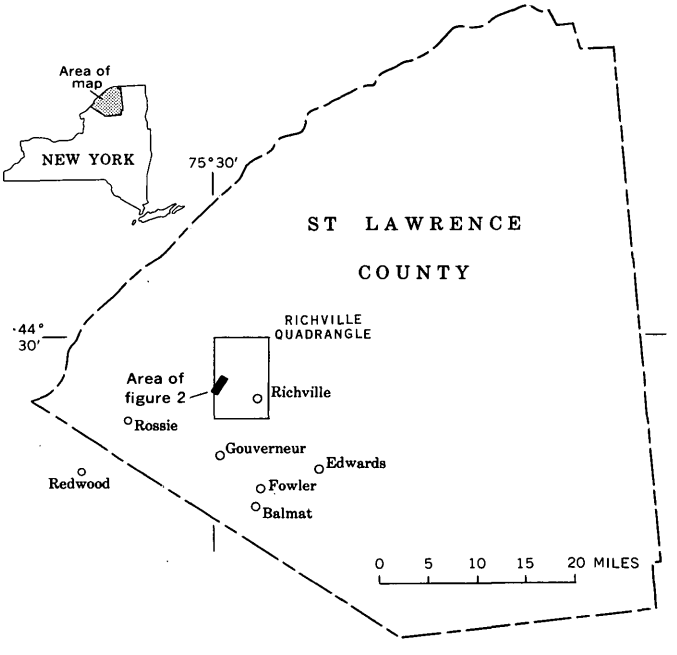

FIGURE 1.—Index map of New York State, showing St. Lawrence County, adjacent area, and the area of this report.

northeast-southwest, parallel with the strike of the bedrock layering. Bedrock is mainly calcitic and dolomitic marble intruded by sheets of gneissic granite (fig. 2). Granite forms tree-covered knobs, and the marble underlies the hayfields and meadows in the lower areas. The occurrence is in an old pasture largely overgrown by prickly-ash, pin cherries, and hawthorn. Marble outcrops are abundant here because the pasture occupies a low divide on which the soil is thin. Marble that underlies most of the nearby low areas is covered by alluvium and loess.

Figure 2 shows the geology of the surrounding area, and figure 3 shows the lithology in the immediate vicinity of the occurrence. The valley immediately northwest of the low ridge on which the sampling was done is cut in silicated dolomite and calcitic marble. The silicated dolomite is believed by the author to locate the axial part of an isoclinal syncline overturned to the southeast. Tops of beds have not been determined, so the structure is called a syncline strictly in a geometric sense. West of this is a large granite sheet that cuts out the remainder of the northwest limb of the fold. According to this interpretation of the geology, the marble at the zinc occurrence is therefore in the normal southeast limb of the overturned fold. The vein occurs in mixed crumbly calcitic and dolomitic marble within a few feet of the contact with quartz-rich calcitic marble.

SPHALERITE VEIN

The 1-inch vein was first found in a float block of crumbly cream-colored dolomitic marble. The block was resting on marble that has disintegrated to loose coarse dolomite sand. Digging through this material revealed the vein in place. The vein is mainly marked by ocher in bedrock and could only be traced for a few feet. It strikes about N. 35° E., parallel to layering in the bedrock. The dip, although not possible to measure accurately, is estimated to be about 30° NW. The vein comprises mottled secondary reddish-brown limonite and white smithsonite splotched with 5-mm black sphalerite grains and some residual dolomite. Boundaries of the vein are fairly distinct, although weathered disseminated grains of sphalerite do occur an inch or so from it. These grains are altered to secondary minerals, and a few show green copper carbonate stain.

SOIL SAMPLING

In order to determine whether this occurrence might have an associated geochemical anomaly, a sampling area roughly 300 by 1,000 feet was laid out with tape and compass. Lines with sample sites every 100 feet were oriented N. 35° E., virtually parallel to the strike of layering (fig. 3). These lines were spaced 50 feet apart. At each site, a sample of soil or weathered crumbly bedrock was collected from at least 1 foot below the surface. Soil is thin but, because the actual bedrock surface is ridged and irregular, pockets of loess, residual soil, and, rarely, glacial drift occur on it. Consequently, samples were of a variety of materials. In all, 50 samples were collected. Samples were analyzed by J. M. Hassemer for copper, lead, and zinc by atomic absorption methods at the U.S. Geological Survey laboratory in Denver, Colo. In addition, trace amounts of mercury were determined by separate chemical analysis by D. G. Murrey. Semiquantitative spectrographic analyses were made at the laboratory by C. L. Forn to detect any unusual concentrations of other elements.

GEOCHEMICAL STUDY

Values for lead, copper, zinc, and mercury were each plotted on the map of the sample grid and contoured (Figs. 4, 5, and 6). Very low values for lead do not show a significant anomaly (fig. 4). Copper, on the other hand (fig. 4), shows a very local anomaly which is mainly influenced by the sample that contained visible weathered vein material at the sphalerite occurrence. Beyond this sample site, copper values drop off abruptly. Zinc (fig. 5) and mercury (fig. 6), however, show an anomaly alined with the layering in the country-rock marble and the trend of the vein.

Semiquantitative spectrographic analyses do not disclose any unusual metal content, except for 1.5 ppm silver and 150 ppm tin in the sample at the vein exposure. Neither silver nor tin were detected in any of the other soil samples. Spectrographic analysis of sphalerite from the vein shows 1 ppm silver and 20 ppm tin—less than that in the soil sample. Perhaps these elements are concentrated in the oxidation products of the vein that are scattered in the soil here.

Cumulative frequency of distribution of analytical data for each element was plotted on probability-graph paper in order to help determine significantly anomalous metal values. This was done according to the methods described by Tennant and White (1959). The small number of samples (50) limits their usefulness somewhat for statistical analysis; however, the cumulative frequency plot (fig. 7) for each metal supports what appears

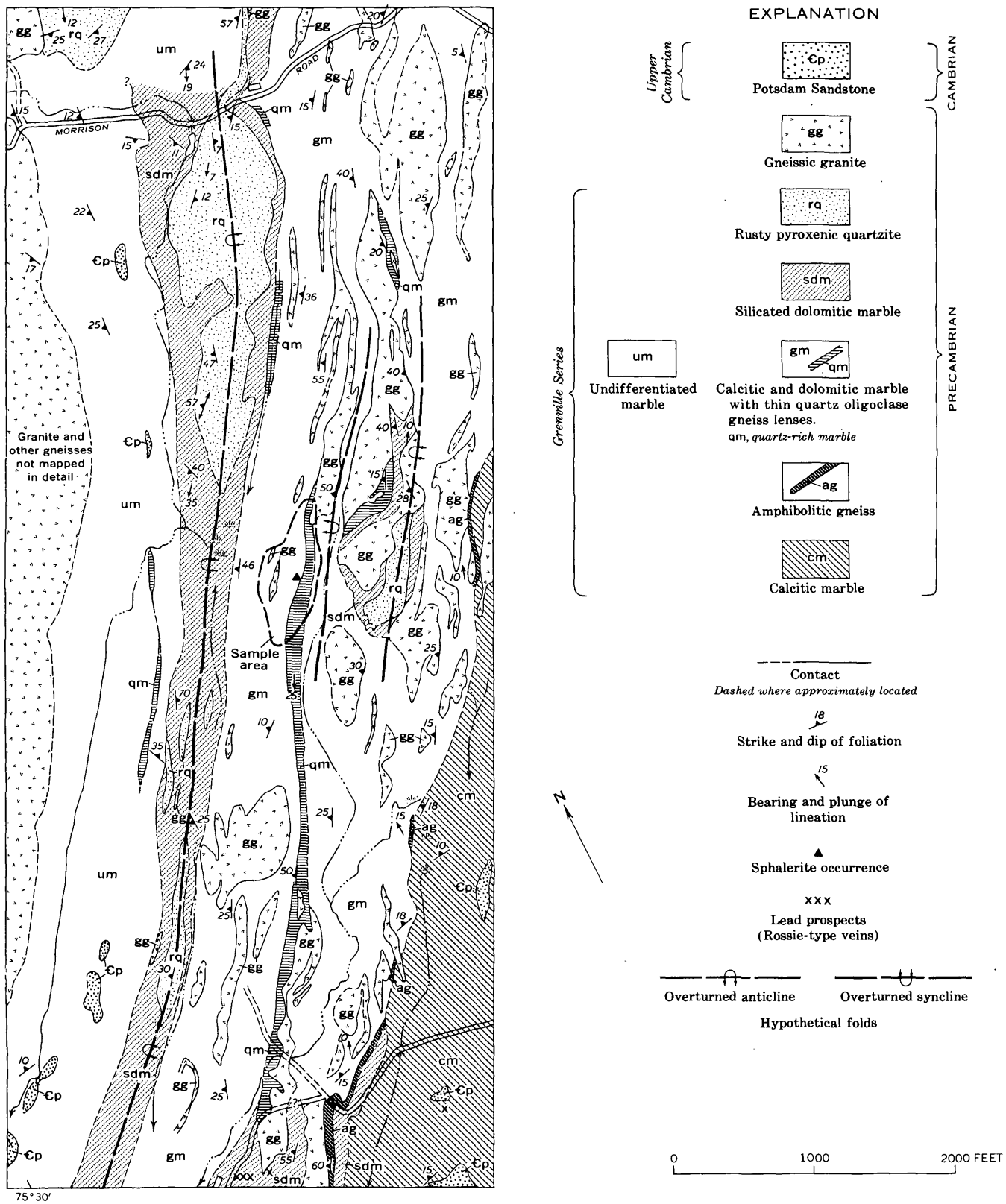

FIGURE 2.—Geologic map of area in vicinity of sphalerite occurrence in the Richville quadrangle, St. Lawrence County, N.Y.

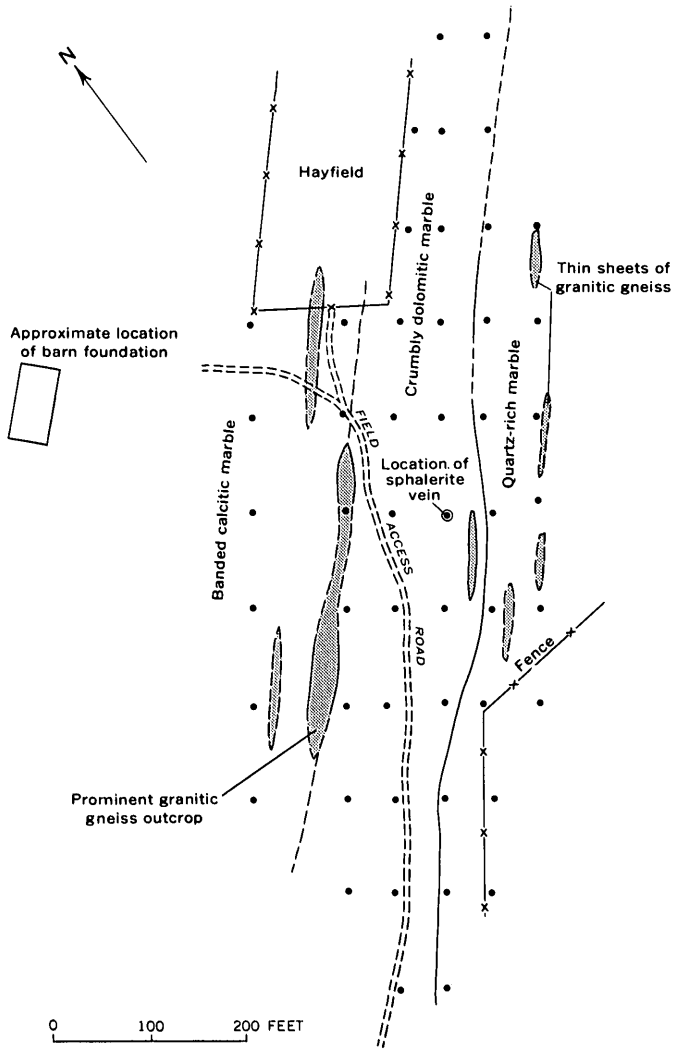

FIGURE 3.—Location map showing lithology and sample sites (black dots).

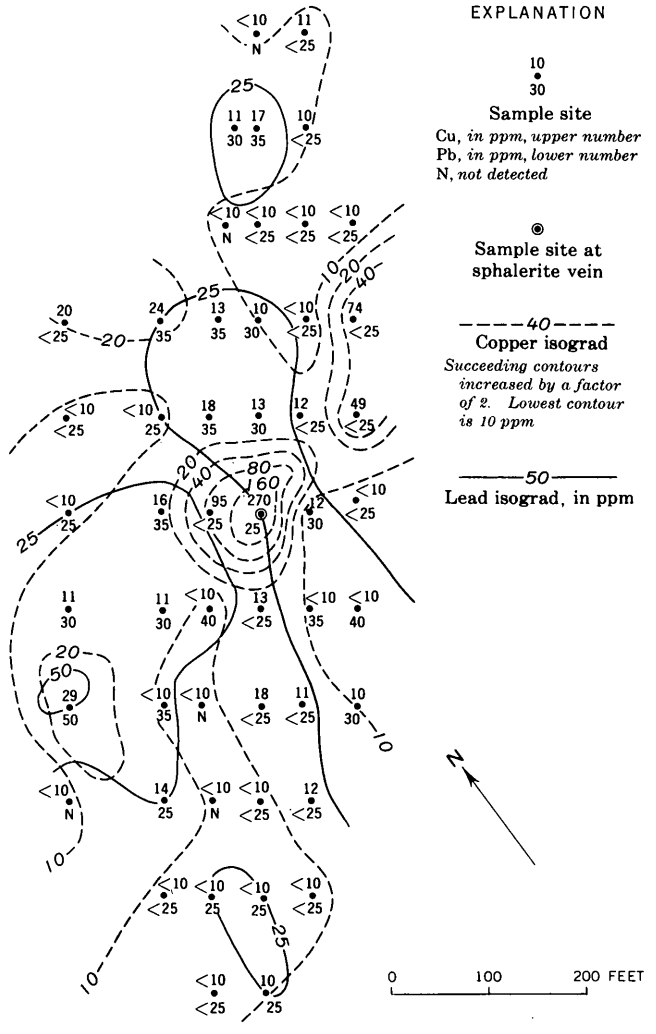

FIGURE 4.—Geochemical contour map showing copper and lead values at sample sites.

obvious by inspection of the contoured values (figs. 4, 5, 6).

Most geochemical data have been found empirically to have log-normal distribution. Cumulative frequency of a single data set plotted on probability-graph paper will produce a straight line. Where analyses represent two populations of data, such as background-metal values and metal values related to ore, the line will show two segments of differing slope or will be S-shaped (Tennant and White, 1959). The threshold value for the set of data that has mineralization significance can be taken at the intersection of the projection of slopes of two distribution curves. Lepeltier (1969) describes a more rigorous statistical approach for determining threshold values when large quantities of data are available. Because of the small number of samples in this study, the author used the cumulative-frequency plot principally to check the validity of the apparent anomalies in the contoured diagrams.

Lead and copper

The distribution plots for lead and copper (fig. 7) are not complete because 42 and 48 percent of the values, respectively, are below the lower detection limits of the analytical method. Therefore, the lower ends of curves are truncated. The remaining analyses for lead do plot as a straight line and thus suggest a log-normal distribution and a single population of data. Because the values are very low, they are assumed to represent only background lead, and the lack of orientation in the contour pattern (fig. 4) supports this conclusion. The distribution curve

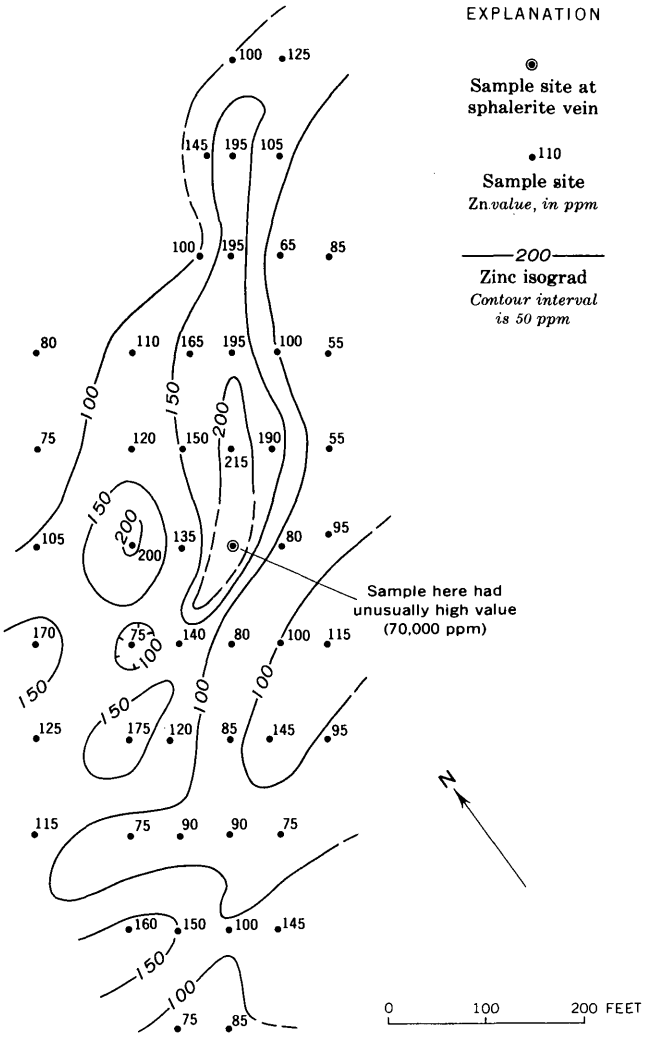

FIGURE 5.—Geochemical contour map showing zinc values at sample sites.

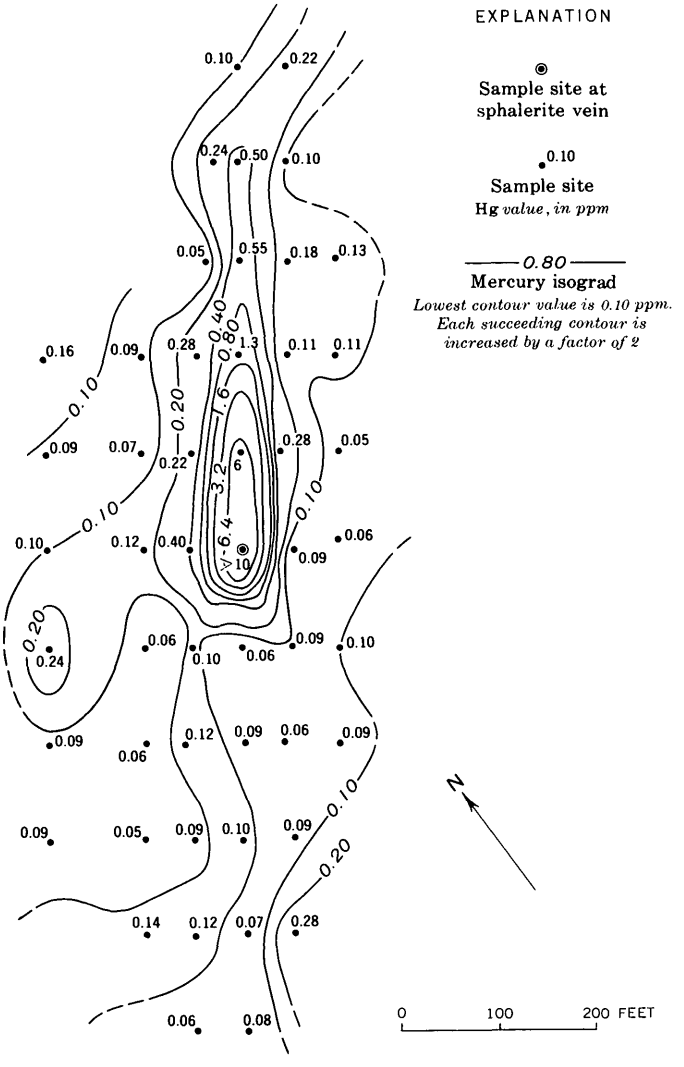

FIGURE 6.—Geochemical contour map showing mercury values at sample sites.

for copper, on the other hand, suggests two populations of data with a threshold value of about 18 ppm at the inflection point on the curve (fig. 7). This fits well with the contoured data on figure 4 which shows an anomalously high value area near the sphalerite vein. The significance of this small anomaly is questionable because it is controlled by very few samples. However, it seems to verify an association between copper and the sphalerite occurrence.

Zinc

The contoured values for zinc (fig. 5) show a low but distinct area of values greater than 150 ppm parallel with the strike of the vein and bedrock layering. This I believe is a significant anomaly. The distribution curve for zinc (fig. 7) shows a break at about 190 ppm. Normally the high values continue the curve at a higher slope, but in this case the slope lessens. Lepeltier (1969, p. 546) interprets such a curve as an expression of an excessive number of low values in virtually log-normal distribution. He says that this can be due to inclusion of a lithologic unit having a low background or to poor sampling. I suspect that the small number of samples is at least part of the problem. The soil sample at the zinc occurrence had an unusually high zinc value (70,000 ppm). It could not be shown in the cumulative-frequency plot, but additional sampling might have yielded a few more high values that would have the effect of increasing the slope of the curve.

Mercury

Mercury-dispersion halos have been shown to have considerable potential as ore guides to base-

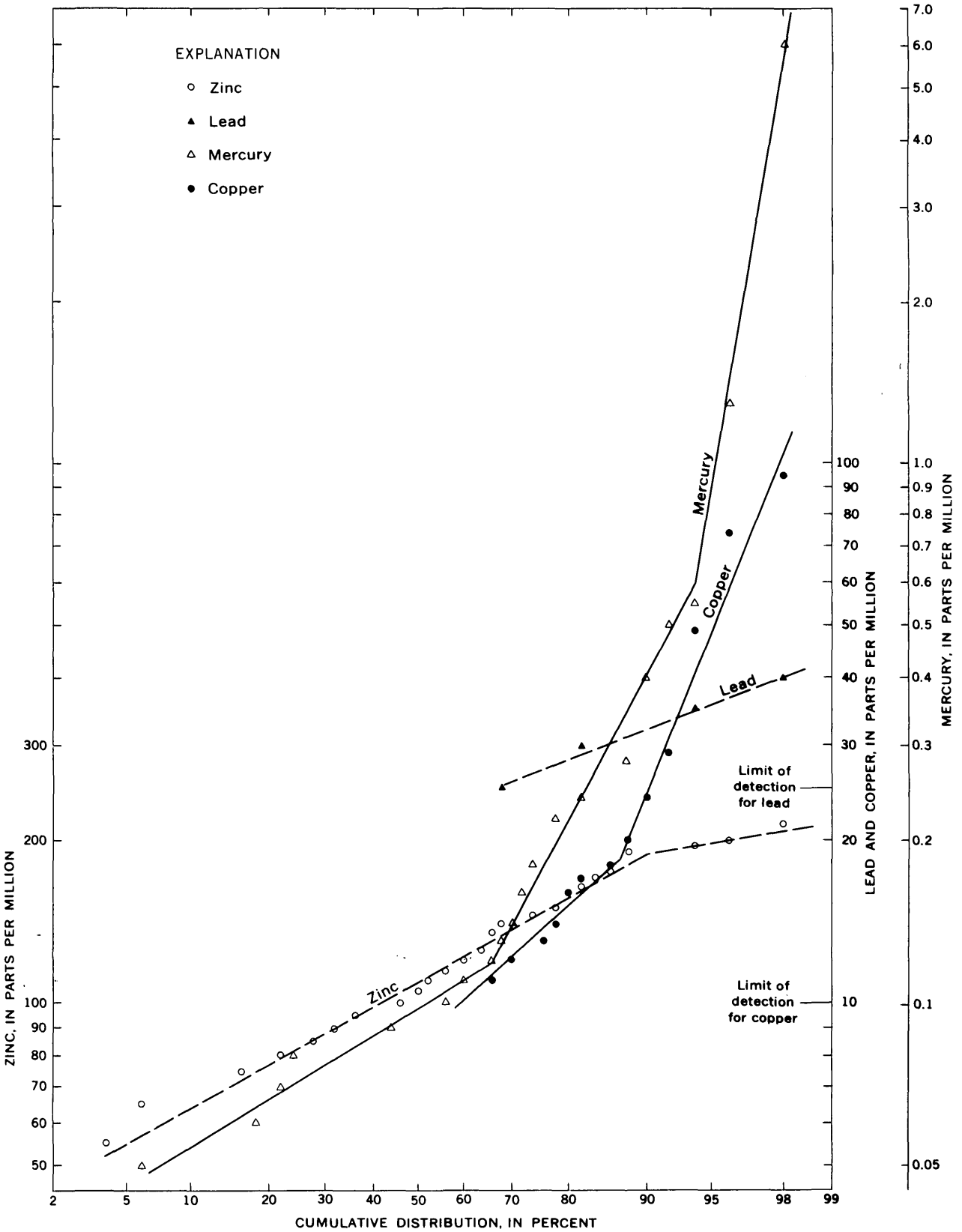

FIGURE 7.—Cumulative frequency distribution for zinc, lead, mercury, and copper.

and precious-metal deposits (Hawkes and Webb, 1962, p. 72). Modern methods of chemical analysis for mercury allow detection of extremely minute quantities; therefore, the soil samples were analyzed for mercury.

Mercury values range from 0.05 ppm to greater than 10 ppm, or at least four orders of magnitude. The geochemical-contour map for mercury (fig. 6) shows a distinct anomaly that is almost directly superimposed on the much less intense zinc anomaly of figure 5. The anomaly, by inspection of figure 6, appears outlined by the 0.2 ppm contour or perhaps more distinctly by the 0.4 ppm contour. Like the zinc anomaly, this one is parallel to both the bedrock layering and the trend of the sphalerite vein.

The cumulative-percentage distribution curve for mercury (fig. 7) shows a 50-percentile or geometric-mean value of 0.1 ppm. This is the mean background value which is also apparent on the contour map. The distribution curve shows a distinct break in slope at 0.12 ppm. A second break in slope occurs at about 0.6 ppm, possibly indicating a mixed population between. Lepeltier (1969, p. 546) in such cases takes the midpoint between inflection points for the threshold value of the mineralization anomaly. In this case the midpoint value is 0.3 ppm, which again fits well with what is apparent as a threshold value on figure 6.

CONCLUSIONS

A zinc anomaly in soil and weathered rock is associated with the sphalerite vein and is alined with layering of the host-rock marble and the trend of the vein. Mercury values likewise show a significant anomaly that is superimposed on the zinc anomaly but strongly accentuated. Copper is associated with the vein, but its anomaly bears little significance to it. Lead values are very low and represent only background.

The host-rock marble dips northwest and appears to be in the southeast normal limb of an overturned isoclinal syncline. This rock continues both to the northeast and southwest and provides a large area of potentially mineralized rock for additional geochemical prospecting, which seems to be warranted by this sphalerite occurrence and its associated anomalies.

REFERENCES

Brown, J. S., 1965, Oceanic lead isotopes and ore genesis: Econ. Geology, v. 60, no. 1, p. 47–68.

Buddington, A. F., 1934, Geology and mineral resources of the Hammond, Antwerp and Lowville quadrangles: New York State Mus. Bull. 296, 251 p.

Hawkes, H. E., and Webb, J. S., 1962, Geochemistry in mineral exploration: New York, Harper and Row, 415 p.

Lea, E. R., and Dill, D. B., Jr., 1968, Zinc deposits of the Balmat-Edwards district, New York, *in* Ore deposits of the United States, 1933–1967 (Graton-Sales volume), v. 1: New York, Am. Inst. Mining Metall. and Petroleum Engineers, p. 20–48.

Lepeltier, Claude, 1969, A simplified statistical treatment of geochemical data by graphical representation: Econ. Geology, v. 64, p. 538–550.

Tennant, C. B., and White, M. L., 1959, Study of the distribution of some geochemical data: Econ. Geology, v. 54, no. 7, p. 1281–1290.

URANIUM-RICH MONAZITES IN THE UNITED STATES

By WILLIAM C. OVERSTREET, AMOS M. WHITE,
and JESSE J. WARR, JR., Denver, Colo.; Washington, D.C.

Abstract.—Uranium-rich monazites in the United States, defined here as being 0.95 percent or more U_3O_8, have thus far been found only in parts of the Inner Piedmont province of North Carolina and South Carolina. The principal sources of these monazites are granitic rocks and pegmatites that range in age from Ordovician to Permian. A posttectonic quartz monzonite of Mississippian(?) to Permian(?) age is the source of the most uranium-rich monazite—2.34 percent U_3O_8—yet reported from the United States. Analyzed monazites from North Carolina and South Carolina have been derived chiefly from stream placers, and they cannot be related positively to their source rocks. A thorough investigation of the geologic factors that influence the distribution of uranium-rich monazite, therefore, will require collection and study of monazite from specific rock units.

Monazite, an anhydrous cerium-earth phosphate used as an ore for the rare-earth elements and thorium, generally contains less than 0.5 percent of U_3O_8. The actual range in percentage of U_3O_8 in monazite from the United States is not reliably known because (1) few analyses made before the late 1940's showed the abundance of U_3O_8, and (2) many of the analyses made thereafter were of monazite mainly from restricted provenance that was investigated for possible economic potential. Of the 550 partial or complete analyses of monazite from the United States that are known to us, 284 analyses show U_3O_8 content which ranges from 0.00 to 2.34 percent (fig. 1). Of these 284 analyses, however, 199 are from North Carolina and South Carolina, 25 are from Idaho, and 16 are from Georgia. The remaining 44 analyses that show uranium in monazite are of samples from 13 States: California, 4; Colorado, 3; Connecticut, 2; Florida, 5; Maine, 1; Michigan, 2; Montana, 2; New Hampshire, 3; New Jersey, 1; New Mexico, 9; Virginia, 2; Washington, 3; and Wyoming, 7.

The monazite that has the highest content of uranium—2.34 percent U_3O_8—found in the United States is from North Carolina. All the monazite from the United States that is known to contain 0.95 percent or more U_3O_8 is from North Carolina and South Carolina. Although this record results partly from the large number of analyses of monazite from North Carolina aand South Carolina compared with the number from the other States, the possibility of geologic control arises because certain abundances of uranium are characteristically associated with monazite from specific regions, as shown in table 1.

The possibility that the differences in mean values for U_3O_8 are related to differences in analytical procedures is effectively eliminated for the Idaho, North Carolina, South Carolina, and Georgia placer monazites. The Idaho monazites (Kline and others, 1950), 9 of the North Carolina monazites, and 12 of the South Carolina monazites were analyzed by the same U.S. Bureau of Mines analysts. The analyses of North Carolina and South Carolina monazites gave results virtually identical with results of analyses of monazites from the same or adjacent placer basins that were made by the U.S. Geological Survey. Chemists in the Survey who analyzed 97 monazites from North Carolina and 75 from South Carolina also analyzed the 16 monazites from Georgia following analytical procedures developed in the U.S. Geological Survey (Grimaldi and others, 1954; Overstreet and others, 1969, p. 65–66). Data for monazites from the rest of the United States are derived from many laboratories and may not be strictly comparable with the data for monazites from Idaho, North Carolina, South Carolina, and Georgia.

URANIUM-RICH MONAZITE

Definition

Uranium-rich monazites are defined here as those in the upper 5 percent of the range in percentage of U_3O_8 found for monazites from the United States. The upper 5 percent of the 284 samples analyzed for U_3O_8 would consist of 14 samples; however, in

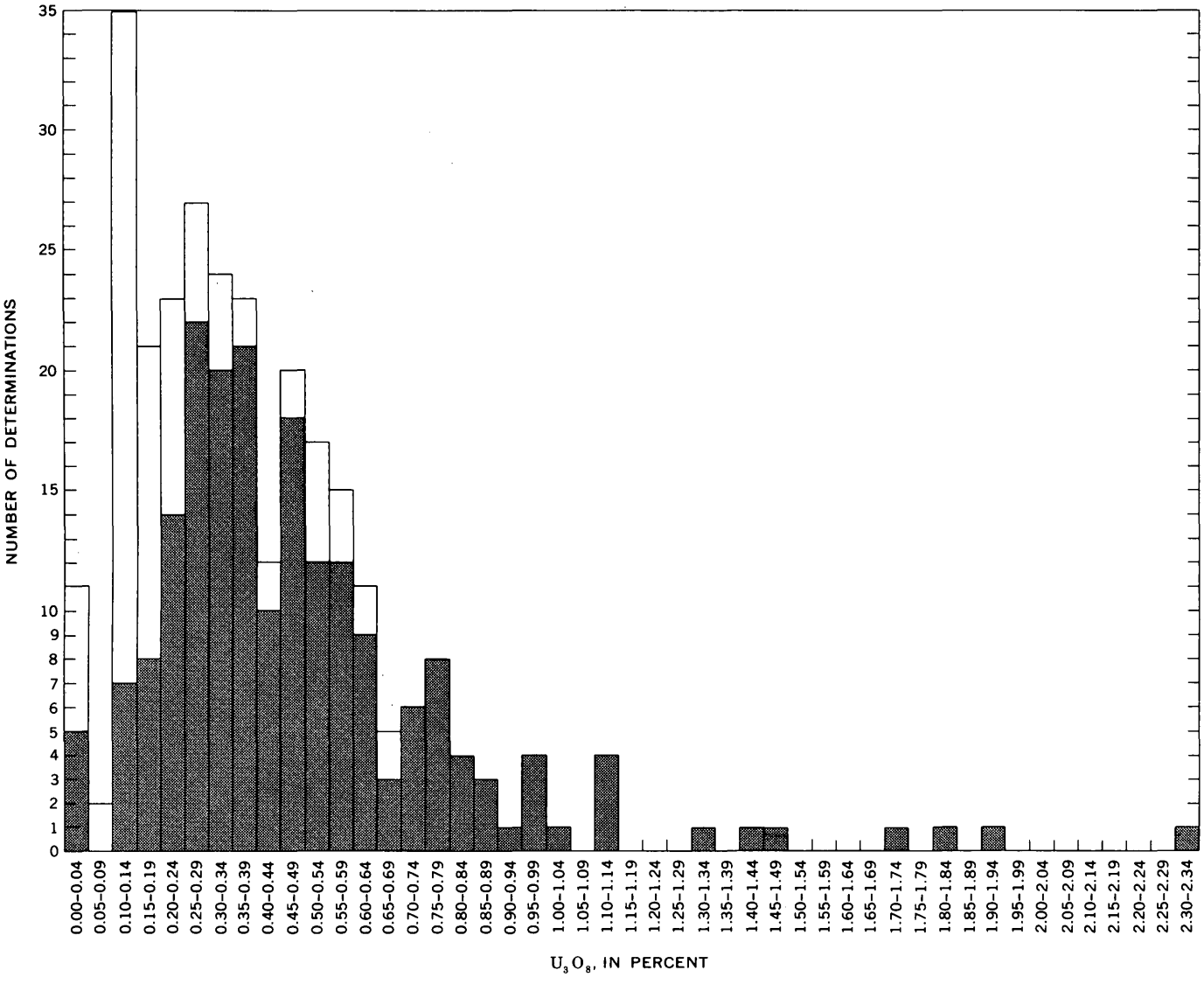

FIGURE 1.—Histogram showing U_3O_8 in monazite. Shaded, samples from North Carolina and South Carolina; white, other States.

figure 1 the group with values between 0.95 and 0.99 percent U_3O_8, where the 14th sample is located, also includes 2 other samples. For the purposes of this paper then, the uranium-rich monazites are taken to include the 16 monazites in the classes of figure 1 beginning with 0.95 percent U_3O_8. The threshold percentage of U_3O_8 for uranium-rich monazites doubtless will be revised as more analyses become available. A review of uranium-rich monazites, thus defined, in the United States devolves into a discussion of uranium-rich monazites from North Carolina and South Carolina. Monazites that are not uranium rich are referred to here as ordinary monazites.

Composition and material analyzed

The 16 known uranium-rich monazites (table 2) were panned and handpicked from 13 localities in North Carolina and South Carolina (fig. 2). Their average U_3O_8 content is 1.3 percent in contrast to an average of 0.41 percent U_3O_8 for all monazites from the United States and 0.49 percent for all monazites from North Carolina and South Carolina.

To insure that these 16 monazites were not mixed with xenotime, two tests were made: (1) a visual examination of the monazites following the method of Murata and Bastron (1956), and (2) determination of the thorium content of the monazites, as shown in table 2. Typically, the uranium content is three to four times as high in xenotime as it is in monazite, but the thorium content is only about one-tenth as much in xenotime as it is in monazite. For example, xenotime from one locality in Rutherford County, N.C., contains a trace of ThO_2 and 4.26 percent U_3O_8 (Palache and others, 1951, p.

TABLE 1.—*Summary of U_3O_8 in analyses of monazite in the United States*

Locality	Source of monazite	Number of analyses	U_3O_8 (percent) Range	Mean
North Carolina	Migmatitic terrane of dominantly upper amphibolite facies and granitic rocks.	112	0.019–2.34	0.49
South Carolina	do	87	0.11–1.8	.48
Georgia	Schist and gneiss of middle and lower amphibolite facies and granitic rocks.	16	0.13–0.67	.39
Idaho	Granitic rocks of Idaho batholith with wallrock schist and gneiss of low to intermediate metamorphic grade.	25	0.003–0.35	.17
Other States	Various	44	0.00–0.65	.20

690), and xenotime from another locality in that county contains 0.2 percent ThO_2 and 1.40 percent U_3O_8 (Griffith and Overstreet, 1953, p. 20). Two samples of xenotime from monazite placers in South Carolina, analyzed by J. J. Warr, Jr., contain 0.49 and 0.45 percent ThO_2 and 1.7 and 1.1 percent U_3O_8. Thus, the analyses for ThO_2 shown in table 2 help insure that the high values for U_3O_8 are from monazite.

Geologic sources

The uranium-rich monazite samples, except samples 5, 8, and 10 (table 2), which are from saprolite, consist of detrital grains separated and concentrated from gravel from the beds of small streams in drainage basins where several kinds of monazite-bearing rocks may be present. In table 2 the dominant rock source is identified where possible, but some monazite may be derived from other rocks. For example, in the part of North Carolina and South Carolina represented by the samples in table 2, monazite may be derived from the following rocks (Overstreet and others, 1963a, table 1):

Rock	*Order of regional abundance*	*Order of abundance of monazite*
Biotite schist	First	Fourth
Sillimanite schist	Second	Third
Syntectonic granitic rocks and associated pegmatites; Ordovician.	Third	Second
Biotite gneiss	Fourth	First
Posttectonic granitic rocks and associated pegmatites; Mississippian(?) to Permian(?).	Fifth	Fifth

The sparse data on source rocks are interpreted here to show that uranium-rich monazites in North Carolina and South Carolina are derived from a narrow segment of possible sources, among which

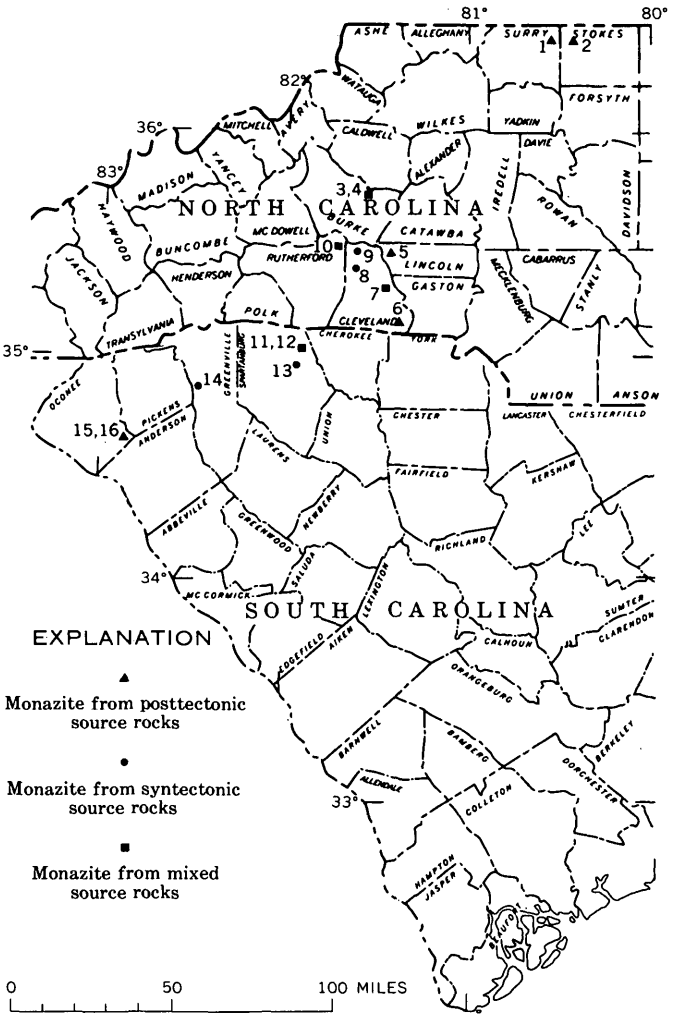

FIGURE 2.—Localities of uranium-rich monazites in North Carolina and South Carolina. Numbers refer to sample numbers listed in table 2.

the posttectonic granitic rocks are far more conspicuous than they are in order of regional abundance and in order of abundance of monazite. The ordinary monazites of these two States are typically associated with sillimanite schist, syntectonic quartz monzonite, and biotite gneiss. However, the geologic distribution of uranium-rich monazites can be fully understood only through a study of monazites taken from their source rocks instead of detrital monazites from streams.

Posttectonic granitic rocks.—In the posttectonic granitic rocks monazite generally is sparse and of local occurrence. Hence, where the posttectonic granitic rocks seem to be the sources for detrital uranium-rich monazite, the other rocks in the basin may have contributed some uranium-lean detrital monazite to dilute the sparse uranium-rich monazite.

Sample 5 (table 2), the monazite with the highest uranium content of any found in the United States,

TABLE 2.—*Locality, source, and partial composition of known uranium-rich monazite in the United States*
[Analyses by J. J. Warr, Jr., unless otherwise specified]

Reference No. used in present report [1]	Sample No.	County	Locality	Inferred source	Composition (percent)		Source of data
					U_3O_8	ThO_2	
North Carolina							
1	52–WE–544A	Surry	Big Creek	Postmetamorphic pluton, possibly granodiorite.	1.7	5.9	This report.
2	52–WE–548A	Stokes	do	Gneiss, schist, and postmetamorphic pluton, possibly mainly granodiorite.	1.9	4.9	Do.
3	52–WE–360A	Burke	Stream 3.8 miles E. of Morganton.	Mixed source, schist and gneiss intruded by quartz monzonite and pegmatite.	.97	5.1	Do.
4	52–WE–360B	do	do	do	1.1	4.9	Do.
5	53–BE–3	Cleveland	Buffalo Creek	Saprolite of Cherryville Quartz Monzonite (posttectonic).	[2]2.34	[3]5.6	Overstreet, Yates, and Griffitts (1963a, tables 4–5), Overstreet and Bell (1965a, p. 110).
6	51–KR–117A	do	Long Branch	Cherryville Quartz Monzonite (posttectonic).	1.4	5.9	This report.
7	45–MT–117	do	Head of Little Hickory Creek, 2¾ miles N. 75° E. of Shelby.	Mixed source, biotite schist permeated by microcline-oligoclase-quartz pegmatite genetically related to Toluca Quartz Monzonite.	[4].98	[4]5.77	Mertie (1953, p. 12), Overstreet, Yates, and Griffitts (1963b).
8	146967	do	Outcrop at bridge over West Fork Brushy Creek, 3.7 miles NNW. of Washburn.	Saprolite of Toluca Quartz Monzonite (syntectonic).	[5]1.1	[3]4.3	Overstreet, Yates, and Griffitts (1963a, tables 4–5).
9	52–CS–753B	do	Upper part of Wards Creek.	Principally Toluca Quartz Monzonite (syntectonic).	1.1	7.2	This report.
10	138543	Rutherford	Quarry 0.5 mile NE. of Hollis.	Saprolite of biotite schist with quartz monzonite dikes.	[5]1.48	[3]4.6	Overstreet, Yates, and Griffitts (1963a, tables 4–5).
South Carolina							
11	52–CS–126A1	Spartanburg	Tributary to Buck Creek.	Mixed source, schist and gneiss intruded by quartz monzonite and pegmatite.	0.99	4.7	This report.
12	52–CS–126B	do	do	do	1.1	5.1	Do.
13	52–CS–315B	do	Tributary to Shoally Creek.	Toluca(?) Quartz Monzonite (syntectonic).	1.0	5.2	Do.
14	52–DC–444B	Greenville	Small tributary to the Saluda River, 3 miles NW. of Greenville.	Quartz monzonite similar to late phase of Toluca Quartz Monzonite (late syntectonic).	1.8	4.3	Do.
15	52–DC–386A	Anderson	Broad Mouth Creek	Unnamed granitic rock that resembles the Yorkville Quartz Monzonite (posttectonic).	1.3	5.3	Do.
16	52–DC–386B	do	do	do	.98	4.8	Do.

[1] Collectors: Samples 1–4, A. M. White; 5, Paul Benson; 6, John Keeler; 7, J. B. Mertie, Jr.; 8, W. R. Griffitts; 9, 10, R. G. Yates; 11–13, N. P. Cuppels; 14–16, D. W. Caldwell.
[2] Analysis by Blanche Ingram.
[3] Analysis by K. J. Murata and H. J. Rose, Jr.
[4] Analysis by F. C. Grimaldi.
[5] Analysis by Carmen Johnson and Blanche Ingram.

and sample 6, a detrital uranium-rich monazite, are derived from the same pluton of posttectonic Cherryville Quartz Monzonite of Mississippian(?) to Permian(?) age (Griffitts and Overstreet, 1952, fig. 1; Keith and Sterrett, 1931, geologic map). The possible range in composition of uranium-rich monazites attributable to the Cherryville Quartz Monzonite is indicated by these two analyses: 1.4–2.34 percent U_3O_8 and 5.6–5.9 percent ThO_2.

Samples 1 and 2 (table 2) are associated with a posttectonic pluton which may be about the same age as the Cherryville Quartz Monzonite (Butler and Dunn, 1968, fig. 8). The tenors in U_3O_8 of these two monazites are well within the range attributed above to monazites of known provenance in the Cherryville. Also, the ThO_2 content of sample 1 is in this range, although in sample 2, which was collected a mile farther east of the pluton, the ThO_2 content is lower than that associated with Cherryville monazites. The interesting possibility exists that sample 2 may be a mixed-source monazite composed of grains of uranium-rich and thorium-rich monazite from the pluton and uranium-poor and thorium-poor monazite from the schist and gneiss. If this is a fact, then some of the monazite from the pluton may contain appreciably more than 1.9 percent U_3O_8. To evaluate this possibility, samples from the pluton and its wallrocks need to be analyzed.

Samples 15 and 16 (table 2) resemble in many respects the late tectonic to posttectonic Yorkville Quartz Monzonite of Permian age that is exposed 75 miles to the northeast. However, monazite is unreported from the Yorkville at its type locality in York County, S.C. Owing to the absence of detailed geologic mapping between Broad Mouth Creek and York County, S.C., no correlation is known to exist between the two rocks (Overstreet and Bell, 1965b).

Syntectonic granitic rocks.—Samples 8 and 9, table 2, are from the syntectonic Toluca Quartz Monzonite of Ordovician age, but some doubt is introduced for sample 9 by the presence of many posttectonic, muscovite-bearing pegmatites in the drainage basin of Wards Creek (Overstreet and others, 1963b). Monazite is in some of these pegmatites, which are genetically related to the Cherryville Quartz Monzonite. Direct sampling of the Toluca Quartz Monzonite in the Wards Creek area is needed to confirm the inference that in this locality it is the source of uranium-rich monazite.

Toluca Quartz Monzonite in the upper parts of Shoally Creek (Overstreet and Bell, 1965b) may be the dominant source for sample 13 which contains nearly the same percentage of U_3O_8 as that from saprolite of the Toluca. A rock similar to the Toluca Quartz Monzonite, but not correlated with it through geologic mapping (Overstreet and Bell, 1965b), may be the main source of sample 14.

Schist and mixed-rock provenance.—Sample 10, table 2, from the saprolite of biotite schist, contains 1.48 percent U_3O_8 and 4.6 percent ThO_2, but the genesis of this monazite is uncertain. It was taken near a quarry where dikes of a late-stage muscovitic Toluca Quartz Monzonite intrude the schist, and are themselves intruded by pegmatite (Overstreet and others, 1963a, pl. 1, tables 4 and 5). Monazite ordinarily is present in both the late-stage Toluca and pegmatite, but one of the dikes of muscovitic Toluca is the only body of Toluca in 96 sampled to lack monazite (Overstreet and others, 1963a, p. F12). The Hollis area is unusual in having less monazite in the quartz monzonite than in schist. Such reversals of the normal distribution of monazite in quartz monzonite and schist were attributed (Overstreet and others, 1963a, p. F12) either to migmatization of the schist and introduction of monazite from the quartz monzonite or to crystallization of monazite in situ owing to thermal rise in the schist in an aureole around the intrusive quartz monzonite.

Monazite from the late-stage Toluca Quartz Monzonite at the Hollis quarry contains 8.4–8.8 percent ThO_2 (Murata and others, 1957, table 2; Overstreet and others, 1963a, table 4) and that from the pegmatite contains 5.4 percent ThO_2 (Overstreet, 1967, table 61), but the percentages of uranium in these monazites are not known. Although the 4.6-percent ThO_2 content in sample 10 is less than the ThO_2 content of monazites from the Toluca and pegmatite it is nearly the same as the 4.8 percent ThO_2 found as the average for 31 monazites from biotite schist in Cleveland and Rutherford Counties (Overstreet and others, 1963a, table 4).

Sample 7, which contains 0.98 percent U_3O_8, is from alluvium derived from pegmatite-impregnated schist similar to that at a locality about 2 miles farther north on Hickory Creek, where the schist contains as much as 1 percent of monazite (Keith and Sterrett, 1931, p. 10), but that monazite contains only 0.33 percent U_3O_8 (Mertie, 1953, p. 12).

The role of pegmatites as sources for uranium-rich monazites in pegmatite-impregnated schist is uncertain, because monazites from pegmatite related to the posttectonic and syntectonic granitic rocks listed in table 2 have not been analyzed for uranium. Five samples of monazite from North Carolina pegmatites, genetically unrelated to the granitic rocks yielding uranium-rich monazite, are reported to contain only 0.019–0.042 percent U_3O_8 (Overstreet, 1967, p. 190, 192). The 21 analyses

available for the United States showing uranium in monazites from pegmatites disclose an average of only 0.09 percent U_3O_8 and a range of 0.00–0.3 percent (Overstreet, 1967; Heinrich and others, 1960, table 2).

The possible tenor of U_3O_8 in monazite from pegmatites genetically related to granitic rocks yielding uranium-rich monazites may be estimated indirectly through analyses of size classes of the detrital monazites. It has been shown (Overstreet and others, 1963a, p. F12–F13) that 28 percent of the grains of monazite in saprolite from pegmatite genetically related to Toluca Quartz Monzonite in Cleveland and Rutherford Counties, N.C., are coarser than 40 mesh. Monazite grains from the Toluca Quartz Monzonite, schist, and gneiss in the same area tend to be finer than 40 mesh, commonly between 100 and 200 mesh. Analyses by sieve fractions of hand-picked, uranium-rich monazite grains from six of the localities listed in table 2 show that the coarse-grained monazites are generally richer in uranium than fine-grained monazites from the same locality, as shown in table 3.

If grain size indicates provenance, then the probability exists that monazites from pegmatites related to the Toluca Quartz Monzonite and Cherryville Quartz Monzonite are not as lean in U_3O_8 as monazite from pegmatites outside the main monazite regions of North Carolina and South Carolina. Thus, such pegmatites may prove to be the source of the uranium-rich monazites in concentrates derived from distributive provinces underlain by schists permeated with pegmatite, and the schists themselves may not be the source rocks of the uranium-rich monazites.

Four monazites, samples 3, 4, 11, 12, table 2, representing two localities between the main plutons of Toluca Quartz Monzonite and Cherryville Quartz Monzonite (Stuckey and Conrad, 1958; Overstreet and Bell, 1965b), are from streams draining schist and gneiss in which dikes and sills of quartz monzonite and pegmatite of several ages are present. These monazites are remarkably similar in their content of U_3O_8 (0.97–1.1 percent) and ThO_2 (4.7–5.1 percent). Possibly they are mixtures of uranium-rich monazites from dikes and sills of the granitic rocks and uranium-lean monazites from other sources, but the likelihood of fortuitous mixtures leading to such similar compositions at two localities seems small. Their percentages of U_3O_8 and ThO_2 most closely resemble those of monazites from the Toluca Quartz Monzonite. This is best seen in the ratio U_3O_8/ThO_2 which ranges from 0.19 to 0.22 and averages 0.21. Uranium-rich Toluca monazites (exclusive of late-stage Toluca) have an average ratio of 0.20. Cherryville monazites have an average ratio of 0.31, curiously close to the ratio of 0.32 for the monazite from schist at Hollis.

TABLE 3.—*Influence of grain size on percentage of* U_3O_8 *in detrital monazites from North Carolina and South Carolina*

[Leaders (---) indicate no data]

Reference No. in table 2	Percentage of U_3O_8 by mesh-size class				
	+40	−40	−40+60	−60+80	−80
3	1.1	0.97	---	---	---
9	1.1	.57	---	---	---
12	1.1	---	0.99	0.88	0.84
13	1.0	.84	---	---	---
14	1.8	.25	---	---	---
16	.98	1.3	---	---	---

The scarcity of uranium-rich monazites attributed in table 2 to schist alone reflects, of course, the decision to identify as "mixed source" those detrital monazites from drainage basins underlain by schists intimately threaded with a variety of granitic sills and pegmatitic dikes but lacking major bodies of granite. Inasmuch as the principal monazite-bearing area in North Carolina and South Carolina is a migmatitic complex, basins uniquely underlain by schist are uncommon and have not been the source of a single uranium-rich monazite. Uranium-rich monazites may actually be absent from schist that is not intruded by granitic rocks.

SUMMARY

The uranium-rich monazites known in the United States are derived dominantly, if not entirely, from granitic rocks and associated pegmatite in a part of the Inner Piedmont of North Carolina and South Carolina, identified as the western monazite belt by Mertie (1953, p. 15). These granitic rocks range in probable geologic age from Ordovician to Permian, with the most common sources being the syntectonic Toluca Quartz Monzonite of Ordovician age and the posttectonic Cherryville Quartz Monzonite of Mississippian(?) to Permian(?) age. The most uranium-rich monazite known in the United States contains 2.34 percent U_3O_8 and is from the Cherryville Quartz Monzonite.

Owing to the use of detrital monazites for study in North Carolina and South Carolina, the geologic controls that effect concentration of uranium in certain monazites could not be clearly investigated. The causes must be sought through study of monazites from rock units.

REFERENCES

Butler, J. R., and Dunn, D. E., 1968, Geology of the Sauratown Mountains anticlinorium and vicinity, *in* Guidebook for field excursions, Geol. Soc. America, Southeastern Sec., Durham, N.C., April 1968: Southeastern Geology Spec. Pub. 1, p. 19–47.

Griffith, R. F., and Overstreet, W. C., 1953, Sandy Run Creek monazite placer, Rutherford County, North Carolina: U.S. Atomic Energy Comm. Rept. RME–3114, 27 p.

Griffitts, W. R., and Overstreet, W. C., 1952, Granitic rocks of the western Carolina Piedmont: Am. Jour. Sci., v. 250, no. 11, p. 777–789.

Grimaldi, F. S., May, Irving, Fletcher, M. H., and Titcomb, Jane, compilers, 1954, Collected papers on methods of analysis for uranium and thorium: U.S. Geol. Survey Bull. 1006, 184 p.

Heinrich, E. W., Borup, R. A., and Levinson, A. A., 1960, Relationships between geology and composition of some pegmatitic monazites: Geochim. et Cosmochim. Acta, v. 19, no. 3, p. 222–231.

Keith, Arthur, and Sterrett, D. B., 1931, Description of the Gaffney and Kings Mountain quadrangles [South Carolina–North Carolina]: U.S. Geol. Survey Geol. Atlas, Folio 222, 13 p.

Kline, M. H., Carlson, E. J., and Griffith, R. F., 1950, Boise Basin monazite placers, Boise County, Idaho: U.S. Atomic Energy Comm. Rept. RME–3129, 37 p.

Mertie, J. B., Jr., 1953, Monazite deposits of the southeastern Atlantic States: U.S. Geol. Survey Circ. 237, 31 p.

Murata, K. J., and Bastron, Harry, 1956, Convenient method for recognizing nonopaque cerium earth minerals: Science, v. 123, no. 3203, p. 888–889.

Murata, K. J., Rose, H. J., Jr., Carron, M. K., and Glass, J. J., 1957, Systematic variation of rare-earth elements in cerium-earth minerals: Geochim. et Cosmochim. Acta, v. 11, no. 3, p. 141–161.

Overstreet, W. C., 1967, The geologic occurrence of monazite: U.S. Geol. Survey Prof. Paper 530, 327 p.

Overstreet, W. C., and Bell, Henry 3d, 1965a, The crystalline rocks of South Carolina: U.S. Geol. Survey Bull. 1183, 126 p.

——— 1965b, Geologic map of the crystalline rocks of South Carolina: U.S. Geol. Survey Misc. Geol. Inv. Map I–413.

Overstreet, W. C., Warr, J. J., Jr., and White, A. M., 1969, Thorium and uranium in detrital monazite from the Georgia Piedmont: Southeastern Geology, v. 10, no. 2, p. 63–76.

Overstreet, W. C., Yates, R. G., and Griffitts, W. R., 1963a, Heavy minerals in the saprolite of the crystalline rocks in the Shelby quadrangle, North Carolina: U.S. Geol. Survey Bull. 1162–F, 31 p.

——— 1963b, Geology of the Shelby quadrangle, North Carolina: U.S. Geol. Survey Misc. Geol. Inv. Map I–384.

Palache, Charles, Berman, Harry, and Frondel, Clifford, 1951, Halides, nitrates, borates, carbonates, sulfates, phosphates, arsenates, tungstates, molybdates, etc., v. 2 *of* The system of mineralogy of James Dwight Dana and Edward Salisbury Dana, Yale University, 1837–1892 [7th ed., revised]: New York, John Wiley and Sons, 1124 p.

Stuckey, J. L., and Conrad, S. G., 1958, Explanatory text for geologic map of North Carolina: North Carolina Div. Mineral Resources Bull. 71, 51 p.

CALCIC SILICEOUS CHABAZITE FROM THE JOHN DAY FORMATION, GRANT COUNTY, OREGON

By RICHARD A. SHEPPARD and ARTHUR J. GUDE 3d,
Denver, Colo.

Abstract.—A calcic, siliceous variety of chabazite makes up about 30–40 percent of an altered vitric tuff in the John Day Formation and is associated with relict siliceous glass, montmorillonite, and opal. Indices of refraction are $\omega = 1.461 \pm 0.001$ and $\varepsilon = 1.465 \pm 0.001$. Hexagonal cell parameters are $a = 13.721 \pm 0.002$ A, $c = 14.795 \pm 0.004$ A, and $V = 2{,}412.4 \pm 0.8$ A^3. Chemical analysis gave a formula of $Ca_{0.45}Mg_{0.04}Na_{0.08}K_{0.11}Al_{1.16}Fe^{+3}_{0.02}Si_{4.82}O_{12} \cdot 4.57H_2O$. Chemical, optical, and X-ray data of other reported chabazites suggest that two chabazite series can be recognized: "normal" chabazites from igneous and metamorphic rocks and "siliceous" chabazites from silicic tuffaceous sedimentary rocks. This calcic chabazite from the John Day Formation is typical of the siliceous series and is characterized by a distinctive X-ray powder diffraction pattern, relatively low indices of refraction, and relatively small cell dimensions.

Chabazite, a common zeolite, occurs in rocks that are diverse in age, lithology, and geologic environment. Most occurrences of chabazite have been reported from amygdales and fracture fillings in basaltic rocks. In recent years, however, chabazite has been recognized as a common rock-forming authigenic constituent in tuffaceous sedimentary rocks. Chabazite from a tuff in the Miocene Barstow Formation of California (Gude and Sheppard, 1966), as shown by chemical analysis, is sodic and is much more siliceous than previously reported chabazites. The chabazite from a tuff in the John Day Formation, described herein, is also siliceous and has physical properties that are similar to those of the Barstow chabazite. Unlike the Barstow chabazite, however, this John Day chabazite is calcic, and thus the known compositional range of chabazite is significantly broadened.

Acknowledgments.—We thank R. V. Fisher and R. E. Wilcox for bringing the John Day chabazite to our attention and for providing samples. We also thank Christel Parker for the chemical analysis.

OCCURRENCE AND PROPERTIES OF THE CHABAZITE

The chabazite-bearing tuff crops out near the North Fork John Day River in the NW¼ SE¼ sec. 2, T. 9 S., R. 27 E., about a mile west of Monument, Grant County, Oreg. The tuff is a gray airfall layer, 2–3 feet thick, located about 60 feet above the base of the upper member of the middle Oligocene to lower Miocene John Day Formation (R. E. Wilcox, oral commun., 1970). The tuff originally consisted chiefly of coarse silicic glass shards, some of which were pumiceous. Those that are still glassy have an index of refraction of $1.497–1.502 \pm 0.001$. Sodic plagioclase and hornblende crystals of presumably pyrogenic origin make up less than 1 percent of the tuff.

In thin section the chabazite makes up about 30–40 percent of the tuff and occurs as aggregates of anhedral to subhedral crystals that cement and in part replace the vitric shards. The crystals range in length from 15 to 200 μm, but most are less than 100 μm long. Much of the chabazite shows undulatory extinction. Minor opal and montmorillonite are locally associated with the chabazite, and their crystallization seems to have preceded that of the chabazite.

The mechanism by which the chabazite formed in the tuff is not understood. Hay (1963) attributed the widespread occurrence of clinoptilolite in tuffs of the John Day Formation to zeolitic diagenesis caused by subsurface water that originated as meteoric water. The presence of a basaltic intrusion (Wilcox and Fisher, 1966) near the chabazite locality, however, suggests that hydrothermal solutions may have been responsible for alteration of the tuff to chabazite at this occurrence.

Chabazite from the John Day Formation is optically positive and is uniaxial or has a very small optic angle. Indices of refraction are: $\omega = 1.461 \pm 0.001$ and $\varepsilon = 1.465 \pm 0.001$. These indices are very similar to those of a siliceous chabazite that occurs in diagenetically altered silicic tuff in the Barstow Formation of California (Gude and Sheppard, 1966), but are lower than the range, 1.470–1.494, reported by Deer, Howie, and Zussman (1963, p. 387) for chabazites from igneous rocks.

X-ray powder diffraction data for the chabazite from the John Day Formation are given in table 1. The *d* values for this chabazite are slightly smaller than those reported for most chabazites and herschelites, but are very close to those of the siliceous chabazite from the Barstow Formation (Gude and Sheppard, 1966). Figure 1 shows diagrammatic X-ray powder diffraction patterns for chabazites from the John Day and Barstow Formations and a chabazite representative of those that occur in igneous rocks.

Cell parameters for the John Day chabazite were obtained by a least-squares refinement of the X-ray powder diffraction data utilizing the U.S. Geological Survey's FORTRAN IV computer program W9214. The resulting hexagonal cell dimensions and volume are $a = 13.721 \pm 0.002$ A, $c = 14.795 \pm 0.004$ A, and $V = 2{,}412.4 \pm 0.8$ A^3. These cell dimensions are smaller than those of chabazites and herschelites from igneous rocks but are similar to those of the siliceous Barstow chabazite. Most chabazites and herschelites from igneous rocks have a cell volume of 2,470–2,490 A^3, but the siliceous chabazites from silicic tuffaceous sedimentary rocks have a cell volume in the range of 2,410–2,430 A^3. The smaller cell of the siliceous chabazites corresponds to 2– to 3–percent reduction in the cell volume.

CHEMICAL COMPOSITION

Chabazite was separated for chemical analysis by first crushing the tuff and then disaggregating it in an ultrasonic bath. The chabazite was then concentrated by repeated centrifuging in a heavy-liquid mixture of bromoform and acetone. The final chabazite concentrate contained about 1 percent glass and montmorillonite impurities.

The chemical analysis and content of the unit cell based on 72 oxygen atoms are given in table 2. The calculated formula for the John Day chabazite is

$$Ca_{0.45}Mg_{0.04}Na_{0.08}K_{0.11}Al_{1.16}Fe^{+3}_{0.02}Si_{4.82}O_{12}\cdot 4.57H_2O.$$

Divalent cations are in excess of monovalent ones, and the Si:Al+Fe^{+3} ratio is 4.09.

TABLE 1.—*X-ray powder diffraction data for chabazite from the John Day Formation*

[Diffractometer, nickel-filtered Cu$K\alpha_1$ radiation, 1° divergence slit, 0.002-inch receiving slit, scanning speed of ½° 2θ per minute, fluorite internal standard]

hkl	*d* (calc.) (A)	*d* (obs.) (A)	*I*
101	9.26	9.27	45
110	6.86	6.86	14
102	6.28	6.28	10
111	6.22	6.24	10
201	5.51	5.51	38
003	4.932	4.929	35
202	4.632	4.631	5
211	4.298	4.298	100
300	3.961	3.964	10
212	3.839	3.839	17
104	3.532	3.532	45
302	3.492	(1)	3
220	3.430	3.428	24
311	3.217	3.213	11
204	3.140	(2)	--
222	3.112	(1)	4
303	3.088	(1)	3
312	3.010	3.007	7
401	2.913	2.911	54
105	2.871	2.871	30
214	2.855	2.855	42
223	2.816	2.815	10
402	2.757	2.758	5
321	2.681	2.680	5
205	2.649	2.648	9
410	2.593	2.594	24
322	2.558	2.559	9
403	2.545	(1)	4
224	2.515	(1)	2
215	2.471	2.473	18
412	2.447	(1)	3
305	2.371	(1)	2
501	2.346	(1)	4
116	2.320	2.320	6
413	2.295	(1)	5
330	2.287	2.286	5
502	2.263	2.265	8
225	2.241	(1)	2
324	2.194	(1)	2
216	2.162	(1)	2
503	2.141	(1)	2
007	2.114	(1)	2
107	2.081	2.079	9
423	2.044	(1)	2
117	2.020	(1)	2
226	2.002	(1)	3
600	1.980	(1)	2
316	1.974	(1)	1
601	1.963	(1)	2
602	1.913	(1)	3
520	1.903	(1)	2
505	1.853	1.853	10
603	1.838	1.837	6

[1] Reflection observed but not accurately measurable.
[2] Reflection obscured by reflection of the fluorite internal standard.

The ideal formulas for chabazite and herschelite are $CaAl_2Si_4O_{12}\cdot 6H_2O$ and $Na_2Al_2Si_4O_{12}\cdot 6H_2O$, respectively, and there are six such formula units per unit cell. Natural chabazites show considerable variation in cation content and Si:Al ratio (Deer and others, 1963, p. 365), explained by replacement of the type

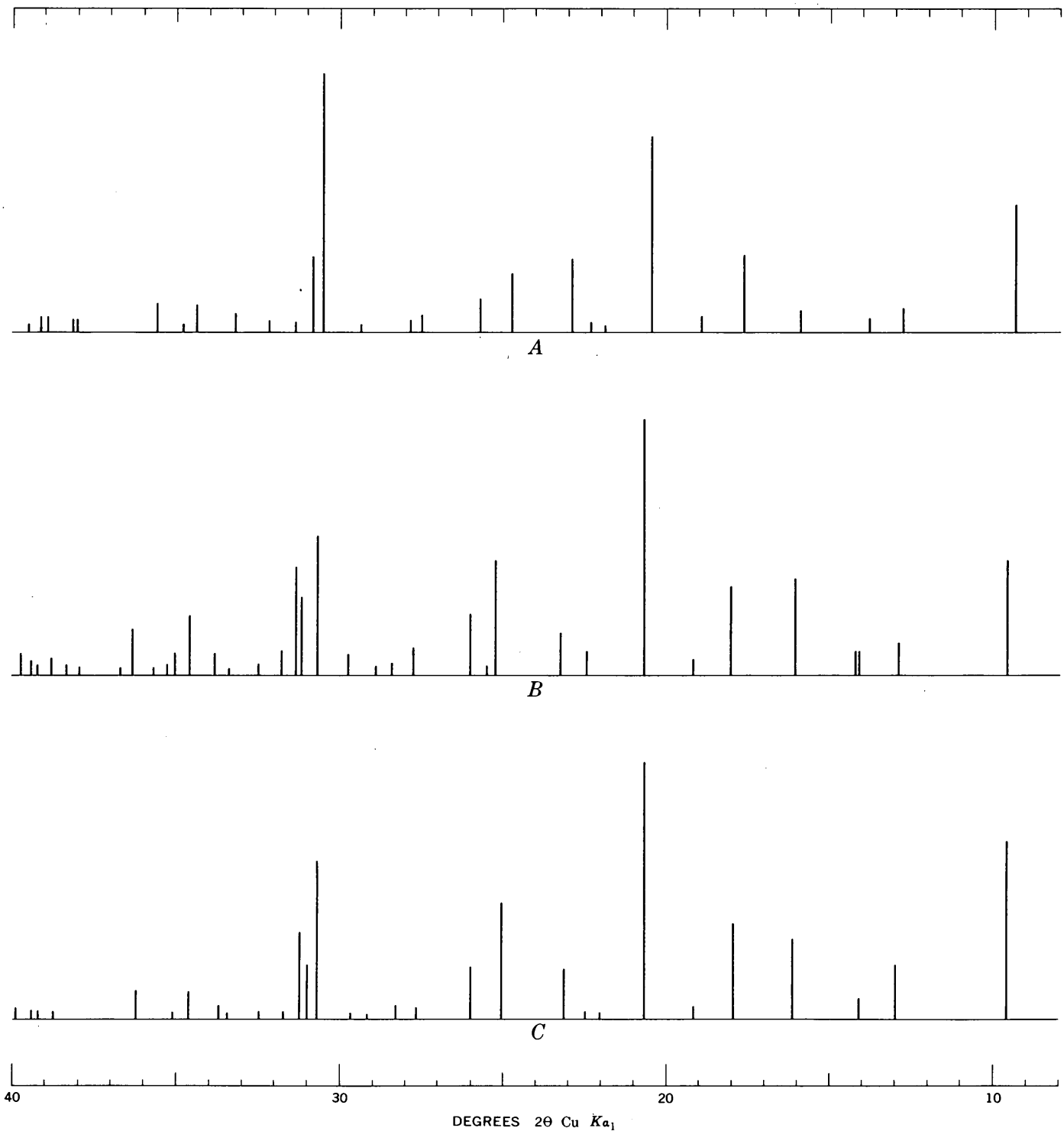

FIGURE 1.—Diagrammatic X-ray powder diffraction patterns for *A*, chabazite from a latite flow at North Table Mountain, Golden, Colo. (Gude and Sheppard, 1966); *B*, siliceous chabazite from the John Day Formation, Oregon; and *C*, siliceous chabazite from the Barstow Formation, California (Gude and Sheppard, 1966). Relative intensities are indicated by height of lines above baseline.

$Na(K)Si \rightleftharpoons Ca(Mg)Al$ and the type $Na_2(K_2) \rightleftharpoons Ca(Mg)$. The chabazite-herschelite series is characterized by $Na_2(K_2)$ replacement of Ca(Mg) (Mason, 1962). The John Day chabazite, however, can be derived from ideal chabazite by about $4.93Na(K)Si$ replacement of $4.93Ca(Mg)Al$ and by about 1.84 $Ca(Mg)$ replacement of $1.84Na_2(K_2)$. The John Day chabazite has only slightly more than half of the

TABLE 2.—*Chemical composition and unit cell contents of chabazite from the John Day Formation*

[Sample collected from NW¼SE¼ sec. 2, T. 9 S., R. 27 E., Grant County, Oreg. Laboratory No. D101151, field No. 59-F-57]

Chemical composition[1] (weight percent)		Unit cell contents[2]	
SiO_2	60.86	Si	28.95
Al_2O_3	12.37	Al	6.93
Fe_2O_3	.39	Fe^{+3}	.14
FeO	.09	Mg	.22
MgO	.31	Ca	2.69
CaO	5.29	Na	.51
Na_2O	.55	K	.66
K_2O	1.09	H_2O+	16.15
H_2O+	10.18	H_2O-	11.25
H_2O-	7.09	O	72.00
TiO_2	.05	$Si+Al+Fe^{+3}$	36.02
P_2O_5	.01	$Si:Al+Fe^{+3}$	4.09
MnO	.01		
CO_2	.01		
Cl	.01		
F	.01		
Total	98.32		

[1] Analyst, Christel Parker.
[2] Atoms per unit cell calculated on the basis of O = 72. Fe^{+2}, Ti, P, and Mn were omitted in the calculation.

cations of ideal chabazite. Charge balance is maintained by the high content of Si, which is greatly in excess of that for ideal chabazite or herschelite.

DISCUSSION

The reported compositions of chabazites are represented in figure 2. Except for the two analyses of the chabazites from the John Day and Barstow Formations, all are from igneous or metamorphic rocks, and their Si: Al + Fe^{+3} ratios are less than 3 and generally near the ideal ratio of 2. The Na+K:Na+K+Ca+Mg ratio ranges from about 0.05 to 0.98, but chabazites with ratios of 0.45–0.65 seem to be absent. Possibly, analyses of specimens from additional occurrences might fill this compositional gap.

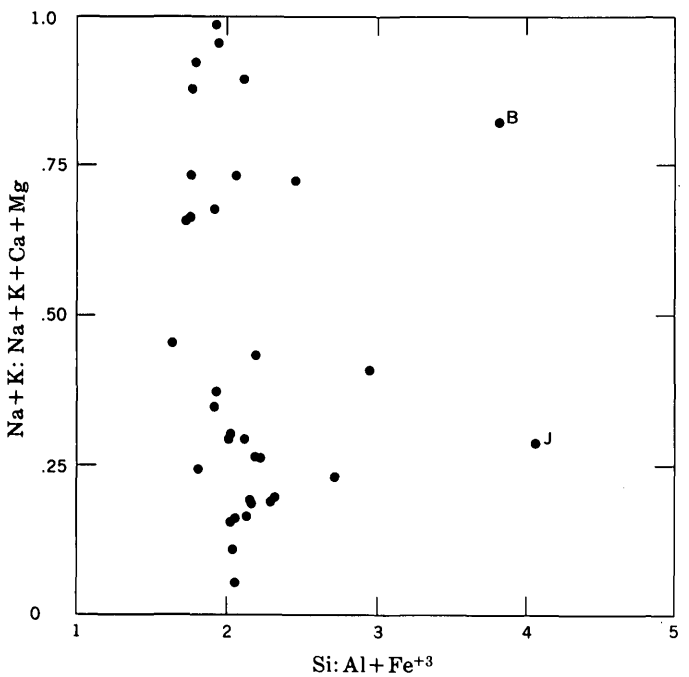

FIGURE 2.—Plot showing the compositional variation of chabazite. Analyses represented by lettered dots are chabazites from B, Barstow Formation (Gude and Sheppard, 1966), and J, John Day Formation (this report).

The present data suggest that two series of chabazites can be distinguished on the bases of Si:Al+Fe^{+3} ratio, indices of refraction, and cell parameters: "normal" chabazites that occur in igneous and metamorphic rocks and "siliceous" chabazites that occur in silicic tuffaceous sedimentary rocks. Most of the analyzed chabazites belong to the normal series and are characterized by a Si:Al+Fe^{+3} ratio less than 3 and generally near the ideal ratio of 2. This normal series includes both sodic members and calcic members; the sodic members are the herschelites of Mason (1962). Indices of refraction for chabazites of the normal series are in the range of 1.470–1.496, wherein the sodic members have relatively low indices and the calcic members have relatively high indices (Mason, 1962, p. 986).

Chabazites of the siliceous series have a Si:Al+Fe^{+3} ratio greater than 3 and, like the normal chabazites, include both sodic and calcic members. Indices of refraction are in the range 1.460–1.474, and sodic members seem to have slightly lower indices than the calcic members. If the Barstow and John Day chabazites are typical members, the cell parameters for this series are significantly smaller than those for normal chabazites.

Since siliceous chabazite in the Barstow Formation of California was reported (Gude and Sheppard, 1966), chabazites that give X-ray powder diffraction patterns similar to those of the Barstow chabazite have been reported from other sedimentary deposits in Arizona (Regis and Sand, 1967; Sheppard, 1969), California (Sheppard and Gude, 1968), Nevada (Hoover, 1968), and Wyoming (Boles, 1968). From Bowie, Ariz., a sodic chabazite with a Si:Al ratio of 3.2 and a calcic chabazite with a Si:Al ratio of about 3.3 were reported, but chemical analyses of these chabazites were not included. The chabazites from the other localities are presumed to be siliceous on the basis of the character of their X-ray powder diffraction patterns, relatively low indices of refraction, and occurrence in silicic vitric tuffs.

REFERENCES

Boles, J. R., 1968, Zeolites and authigenic feldspar along a part of the Beaver Rim, Fremont County, Wyoming: Wyoming Univ., Laramie, unpub. M.S. thesis, 64 p.

Deer, W. A., Howie, R. A., and Zussman, J., 1963, Framework silicates, v. 4 *of* Rock-forming minerals: New York, John Wiley and Sons, Inc., 435 p.

Gude, A. J., 3d, and Sheppard, R. A., 1966, Silica-rich chabazite from the Barstow Formation, San Bernardino County, southern California: Am. Mineralogist, v. 51, p. 909–915.

Hay, R. L., 1963, Stratigraphy and zeolitic diagenesis of the John Day Formation of Oregon: California Univ. Pubs. Geol. Sci., v. 42, no. 5, p. 199–262.

Hoover, D. L., 1968, Genesis of zeolites, Nevada Test Site, *in* Eckel, E. B., ed., Nevada Test Site: Geol. Soc. America Mem. 110, p. 275–284.

Mason, Brian, 1962, Herschelite—a valid species?: Am. Mineralogist, v. 47, nos. 7–8, p. 985–987.

Regis, A. J., and Sand, L. B., 1967, Lateral gradation of chabazite to herschelite in the San Simon basin [abs.], *in* Bailey, S. W., ed., Clays and clay minerals—Clay Minerals Conf., 15th, Pittsburgh, Pa., 1966, Proc.: New York, Pergamon Press (Internat. Ser. Mons. Earth Sci., v. 27), p. 193.

Sheppard, R. A., 1969, Zeolites, *in* Mineral and water resources of Arizona: Arizona Bur. Mines Bull. 180, p. 464–467.

Sheppard, R. A., and Gude, A. J., 3d, 1968, Distribution and genesis of authigenic silicate minerals in tuffs of Pleistocene Lake Tecopa, Inyo County, California: U.S. Geol. Survey Prof. Paper 597, 38 p.

Wilcox, R. E., and Fisher, R. V., 1966, Geologic map of the Monument quadrangle, Grant County, Oregon: U.S. Geol. Survey Geol. Quad. Map GQ–541.

NONOPAQUE HEAVY MINERALS FROM SANDSTONE OF EOCENE AGE IN THE WASHAKIE BASIN, WYOMING

By HENRY W. ROEHLER, Denver, Colo.

Abstract.—Nonopaque heavy minerals were studied from 44 fine-grained sandstones of Eocene age in the Washakie Basin, Wyo. The results indicate that rocks of early Eocene age were derived chiefly from plutonic rocks in nearby mountains, whereas rocks of late Eocene age were derived chiefly from those produced by distant volcanism.

Forty-four fine-grained sandstones of Eocene age were sampled in 1968 for heavy-mineral analysis to determine if their mineral suites were sufficiently diagnostic to be used for the identification and correlation of beds and stratigraphic units in the Washakie Basin. The possibility of establishing petrographic correlations in these rocks had been suggested by the early work of Sinclair (1909) and Johannsen (1914).

STRATIGRAPHY

Eocene rocks in the Washakie Basin are nearly 8,000 feet thick. They consist of lacustrine and fluviatile rocks of the lower and middle Eocene Wasatch and Green River Formations and an unnamed sequence of middle and upper Eocene fluviatile rocks of Bridger and Uinta age. The geographic locations where samples were collected for heavy-mineral study are shown on the geologic map of the southwestern part of the Washakie Basin (fig. 1). Stratigraphic positions of the sample sites are shown on the columnar section (fig. 2).

MINERALOGY

Nonopaque heavy minerals from sandstones of Eocene age in the Washakie Basin clearly are divisible into two distinct suites. One suite was derived from plutonic rocks, and the other suite was derived mainly from volcanic rocks. The heavy minerals of plutonic origin occur chiefly in lower Eocene rocks; those of volcanic origin occur chiefly in middle and upper Eocene rocks. (See table 1.) The plutonic suite (samples 9 through 244) is characterized by abundant garnet and by minor amounts of zircon, rutile, and tourmaline. The volcanic suite (samples 480 through 707) is characterized by augite, oxyhornblende, and green and green-brown hornblende. A transition from the plutonic to the volcanic suite (samples 274 through 467, and the TSB sample) occurs near the early and middle Eocene time boundary (fig. 2 and table 1). The transition interval is characterized by abundant biotite and smaller amounts of garnet as compared with the lower Eocene rocks. The percentages of volcanic and plutonic nonopaque heavy-mineral grains in the various samples are shown in figure 3.

The classification of plutonic and volcanic heavy minerals that is used in this report is based on the work of Sato and Denson (1967), and Denson and Pipiringos (1969). From the limited data available, it is hazardous to assign certain minerals to either the volcanic or the plutonic suite, but rutile and chlorite and possibly staurolite and tourmaline should probably be assigned to the plutonic suite. Augite, oxyhornblende, and brown hornblende almost certainly belong to the volcanic suite and are probably diagnostic of it. (Compare data with those of Sato and Denson, 1967).

LABORATORY METHODS AND ACKNOWLEDGMENTS

Samples of sandstones were crushed and then screened through 50-, 80-, and 100-mesh sieves. Heavy minerals were separated from 200 grams of the minus-100 mesh fraction using bromoform of 2.85 specific gravity. Magnetic grains were removed, and heavy-mineral slides were prepared. The author acknowledges the assistance of E. D. Seals, who made mineral separations and prepared

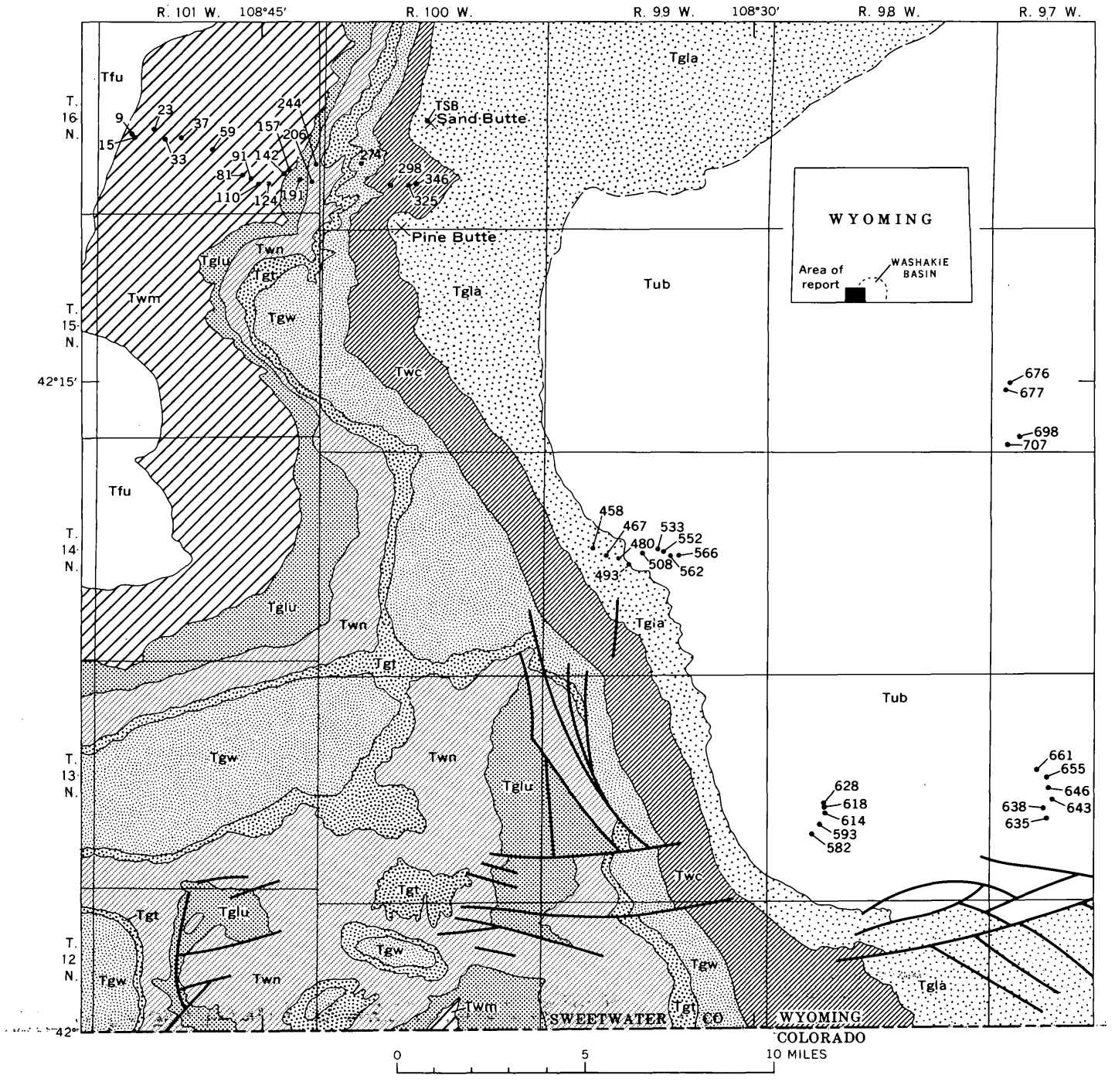

FIGURE 1.—Geologic map of the southwestern part of the Washakie Basin, Sweetwater County, Wyo., showing the localities of heavy-mineral sample sites.

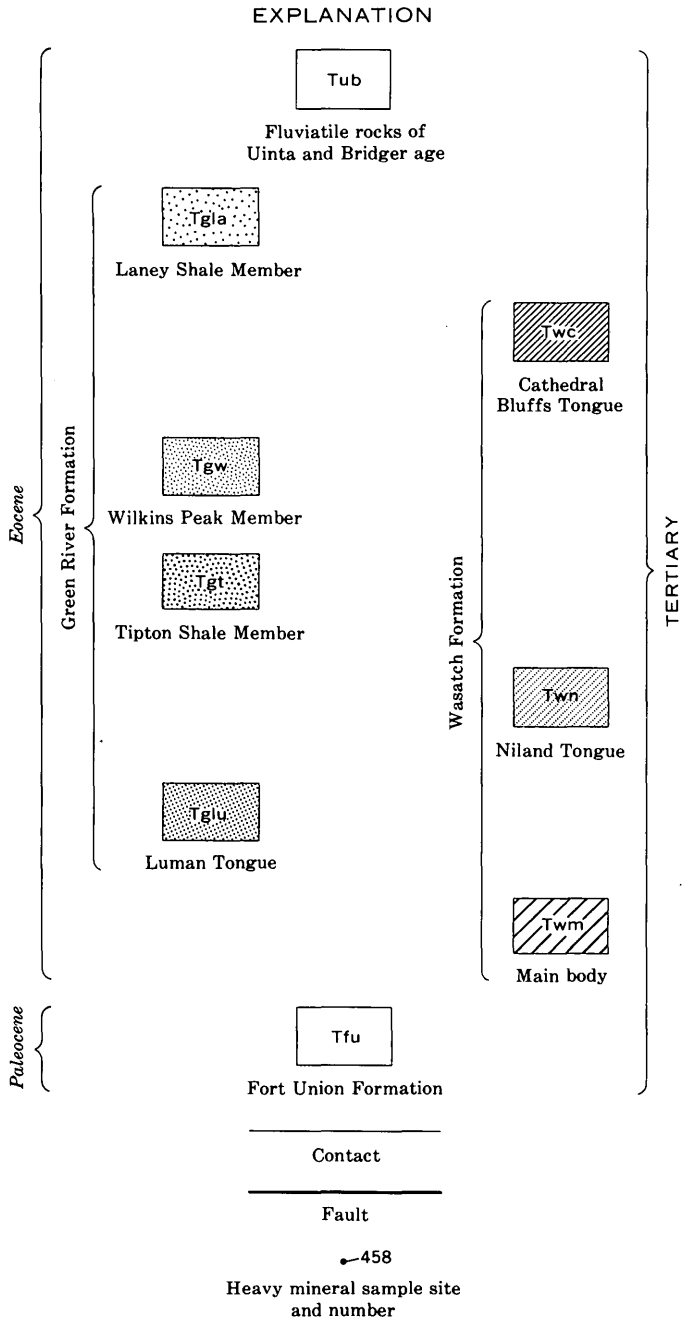
EXPLANATION
Tub
Fluviatile rocks of Uinta and Bridger age
Tgla
Laney Shale Member
Tgw
Wilkins Peak Member
Tgt
Tipton Shale Member
Tglu
Luman Tongue
Twc
Cathedral Bluffs Tongue
Twn
Niland Tongue
Twm
Main body
Tfu
Fort Union Formation
Eocene
Green River Formation
Wasatch Formation
TERTIARY
Paleocene
Contact
Fault
458
Heavy mineral sample site and number

FIGURE 1.

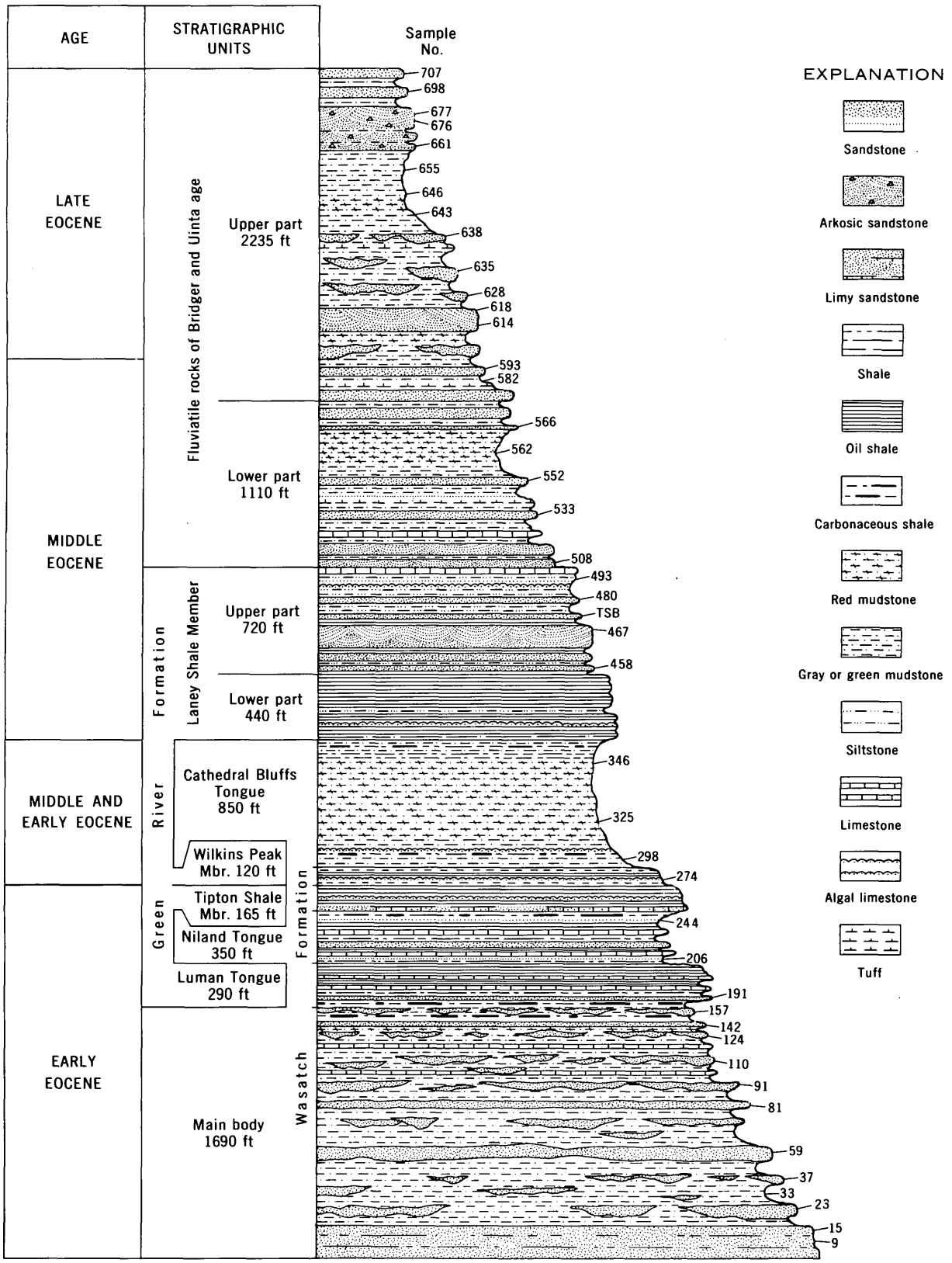

FIGURE. 2.—Composite columnar section of Eocene rocks in the Washakie Basin, showing the stratigraphic positions of fine-grained sandstones sampled for heavy-mineral analysis.

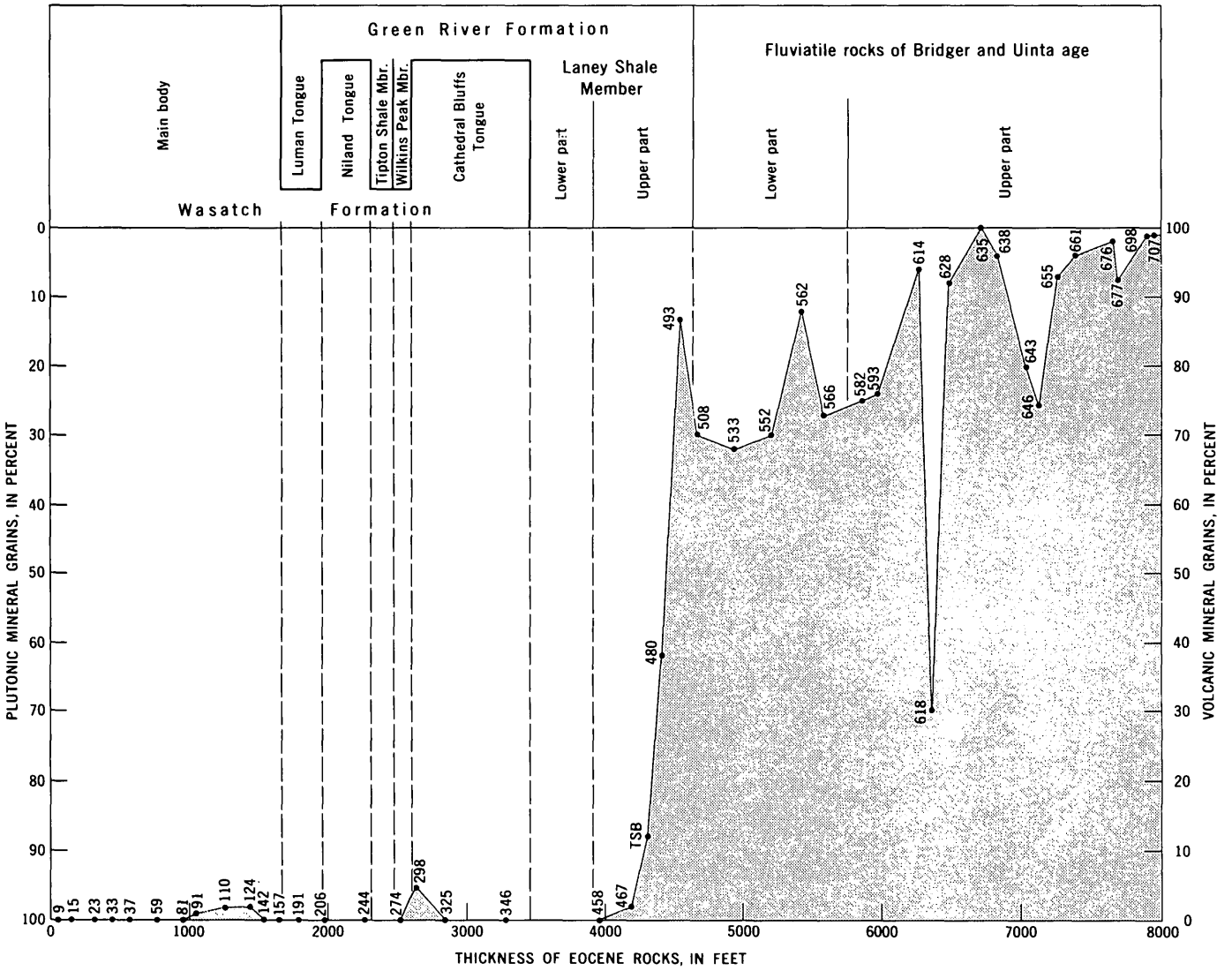

FIGURE 3.—Percentages of volcanic and plutonic nonopaque heavy-mineral grains from 44 samples of fine-grained sandstones of Eocene age in the Washakie Basin. Numbers in diagram are sample numbers.

TABLE 1.—*Distribution of nonopaque heavy minerals from*

[Estimates of the percentage of each mineral were made on 100 grains from each sample. Looked for

Stratigraphic units		Main body, Wasatch Formation												Luman Tongue, Green River Formation	Niland Tongue, Wasatch Formation		Wilkins Peak Member, Green River Formation	Cathedral Bluffs Tongue, Wasatch Formation	
Mineral suite		← Plutonic suite →															←		
Sample No.		9	15	23	33	37	59	81	91	110	124	142	157	191	206	244	274	298	325
1	Augite	--	--	--	--	--	--	--	--	--	--	--	--	--	--	--	--	--	--
2	Oxyhornblende	--	--	--	--	--	--	--	--	--	--	--	--	--	--	--	--	--	--
3	Green, green-brown hornblende	--	--	--	--	--	--	--	1	2	2	--	--	--	--	--	--	5	--
4	Blue-green hornblende	--	--	--	--	--	--	--	--	--	--	--	--	--	--	--	--	--	2
5	Garnet	85	86	92	88	95	83	88	68	89	87	81	90	88	81	83	1	--	76
6	Epidote	--	--	--	--	--	--	--	--	--	1	2	1	--	--	1	--	--	--
7	Zircon	9	11	2	9	4	4	7	10	3	2	10	6	3	14	13	--	--	12
8	Sphene	--	--	--	--	--	--	--	--	--	--	--	--	--	--	--	--	--	--
9	Rutile	4	1	2	2	--	--	1	2	--	1	2	1	--	3	1	--	--	--
10	Tourmaline	--	1	--	--	1	2	--	2	3	3	1	1	--	--	--	--	--	6
11	Staurolite	--	--	1	--	--	--	--	--	--	--	--	--	--	--	--	--	--	--
12	Green-brown biotite	--	--	2	1	--	7	2	4	--	1	2	--	3	--	2	14	34	4
13	Brown biotite	--	--	1	--	--	2	2	13	2	2	2	1	3	1	--	83	58	--
14	Green biotite	--	--	--	--	--	--	--	--	1	1	--	--	--	--	--	1	3	--
15	Red-brown biotite	--	--	--	--	--	--	--	--	--	--	--	--	3	--	--	1	--	--
16	Chlorite	2	1	--	--	--	2	--	--	--	--	--	--	--	1	--	--	--	--

slides. Mineral identifications and estimates of the percentages of the minerals were made by W. A. Chisholm.

CONCLUSIONS

1. Sandstone beds of early Eocene age can be differentiated from those of late Eocene age by their nonopaque heavy-mineral suites.

2. In general, it seems that rocks of early Eocene age in the Washakie Basin were derived from plutonic rocks in nearby mountains, whereas middle and upper Eocene rocks were derived chiefly from unknown, distant volcanic sources.

3. If the amount of volcanic material entering the Washakie Basin during the Eocene Epoch reflects the intensity of Eocene volcanism in the central Rocky Mountain area, then a number of interesting conclusions can be drawn: (a) Volcanism during early Eocene time was minor, but significant eruptions took place at least two times (samples 91, 110, 124, and 298, fig. 3); (b) volcanism of great magnitude began rather abruptly in middle Eocene time (samples 467, TSB, 480, and 493, fig. 3) and continued through late Eocene time (samples 508 through 707, fig. 3); and (c) relatively high percentages of volcanic heavy minerals (samples 493, 562, 614, 635, 676, and 698, fig. 3) may indicate periods of maximum volcanic activity during the middle and late Eocene times.

fine-grained sandstones of Eocene age in the Washakie Basin, Wyo.

but not found: hypersthene, zoisite, sillimanite, kyanite, andaluste, monazite, allanite, diopside and apatite]

Laney Shale Member, Green River Formation						Fluviatile rocks of Bridger and Uinta age																				
Lower part	Upper part					Lower part					Upper part															
Transitional → ← Volcanic Suite →																										
346	458	467	TSB	480	493	508	533	552	562	566	582	593	614	618	628	635	638	643	646	655	661	676	677	698	707	
--	--	--	1	--	43	8	3	1	12	14	9	34	42	8	11	87	79	1	--	35	51	41	38	9	43	1
--	--	1	2	--	2	1	--	--	--	--	1	1	10	--	5	--	1	1	1	2	2	4	6	9	4	2
--	--	1	9	38	42	61	65	69	76	59	65	41	42	22	76	13	16	78	73	56	43	53	48	78	52	3
--	--	--	2	24	10	22	17	26	8	16	13	19	3	4	8	--	2	8	19	5	4	2	6	--	--	4
1	29	55	30	33	2	4	5	2	3	3	8	2	2	58	--	--	1	9	5	2	--	--	2	--	1	5
--	1	1	--	--	--	--	2	--	--	--	--	--	--	--	--	--	--	--	1	--	--	--	--	--	--	6
--	1	1	10	--	--	--	--	1	1	2	1	--	--	4	--	--	1	1	--	--	--	--	--	--	1	--	7
--	--	1	1	1	--	--	--	--	--	--	2	--	--	--	--	--	--	2	1	--	--	--	--	--	--	--	8
--	--	--	--	--	--	--	--	--	--	--	--	--	--	--	--	--	--	--	--	--	--	--	--	--	--	--	9
--	--	--	--	--	--	--	--	--	--	--	--	--	--	1	--	--	--	--	--	--	--	--	--	--	--	--	10
--	--	--	--	--	--	--	--	--	--	--	--	--	--	--	--	--	--	--	--	--	--	--	--	--	--	--	11
57	--	--	11	2	--	--	--	--	--	4	--	--	--	--	--	--	--	--	--	--	--	--	--	--	--	--	12
42	69	39	32	2	1	4	7	1	--	2	1	2	--	3	--	--	--	--	--	--	--	--	--	2	--	13
--	--	--	--	--	--	--	--	--	--	--	--	--	1	--	--	--	--	--	--	--	--	--	--	--	--	--	14
--	--	1	2	--	--	--	1	--	--	--	--	1	--	--	--	--	--	--	--	--	--	--	--	1	--	15
--	--	--	--	--	--	--	--	--	--	--	--	--	--	--	--	--	--	--	--	--	--	--	--	--	--	16

4. Volcanism had a marked effect on the environment of the Washakie Basin area in the middle Eocene. Rocks in the lower part of the Laney Shale Member (fig. 2) are composed mostly of oil shales that were deposited in possibly the largest of the Green River lakes (Lake Gosiute) that inundated the Washakie Basin area. At the beginning of the period of deposition of the upper part of the Laney Shale Member, Lake Gosiute diminished appreciably in size, and by the end of the period of deposition of the upper part of the Laney Shale Member, it had become extinct. The drying-up and withdrawal of Lake Gosiute from the Washakie Basin area were contemporaneous with and probably the direct results of increased volcanism.

REFERENCES

Denson, N. M., and Pipiringos, G. N., 1969, Stratigraphic implications of heavy-mineral studies of Paleocene and Eocene rocks of Wyoming, *in* Wyoming Geol. Assoc. Guidebook 21st Ann. Field Conf., Symposium on Tertiary rocks of Wyoming, 1969: p. 9–18.

Johannsen, Albert, 1914, Petrographic analysis of the Bridger, Washakie and other Eocene formations of the Rocky Mountains: Am. Mus. Nat. History Bull., v. 33, art. 16, p. 209–222.

Sato, Yoshiaki, and Denson, N. M., 1967, Volcanism and tectonism as reflected by the distribution of nonopaque heavy minerals in some Tertiary rocks of Wyoming and adjacent States, *in* Geological Survey Research 1967: U.S. Geol. Survey Prof. Paper 575–C, p. C42–C54.

Sinclair, W. J., 1909, The Washakie, a volcanic ash formation: Am. Mus. Nat. History Bull., v. 26, art. 4, p. 25–27.

OCCURRENCE OF LAUMONTITE IN TERTIARY SANDSTONES OF THE CENTRAL COAST RANGES, CALIFORNIA

By BETH M. MADSEN and K. J. MURATA, Menlo Park, Calif.

Abstract.—Authigenic laumontite occurs sporadically in the Miocene Vaqueros and Briones Sandstones of the central Coast Ranges of California. It replaces clastic plagioclase and is an intergranular cement in the arkosic Vaqueros Sandstone, where it formed mainly through diagenetic alteration of plagioclase. In addition to laumontite of such an origin, the Briones Sandstone, which contains much andesitic debris, has an unusual laumontite-chlorite filling of pores. Laumontite lines the pores and envelops cores of sheaflike aggregates of chlorite, a combination that most likely was produced through interaction of montmorillonite and calcite. Variations in composition and permeability of the sandstones are the major causes of the irregular distribution of laumontite in these small occurrences. A new "staining" technique for laumontite used in this study involves treatment of thin sections or polished slabs with a 10-percent solution of oxalic acid; this selectively deposits finely crystallized calcium oxalate on laumontite.

Among the several zeolites produced through diagenesis of tuffaceous and arkosic sediments, laumontite ($CaAl_2Si_4O_{12}\cdot 4H_2O$) is of special interest because it generally is assumed to form at greater depth and hence under higher temperature and pressure than the others (Deffeyes, 1959; Hay, 1966). The name "laumontite" is used in this paper to include leonhardite ($CaAl_2Si_4O_{12}\cdot 3.5H_2O$), a partially dehydrated variant of laumontite (Coombs, 1952).

Laumontite can often be recognized in the field by a mottling it imparts to sedimentary rocks (fig. 1), a feature of Alaskan laumontized sandstones pointed out to us earlier by J. M. Hoare (Hoare and others, 1964). The lighter areas in figure 1 represent aggregates of sand grains cemented by laumontite. Such aggregates withstand weathering somewhat better than the rest of the rock, and they commonly persist as irregular lumps on weathered surfaces.

In the 28,000-foot Triassic sedimentary section of the Taringatura district in New Zealand, Coombs (1954) found laumontite mostly at depths inferred to have been greater than about 17,000 feet, and heulandite and analcite chiefly at shallower depths. In the Shinjo basin of Japan (Iijima and Utada, 1966), laumontite occurs with authigenic epidote and chlorite at depths inferred to have been 9,100 to 9,800 feet; at deeper levels epidote and chlorite persist, but laumontite and other zeolites do not. Other occurrences of laumontite in thick sedimentary sections have been described from Russia (Zaporozhtseva, 1960), Alaska (Hoare and others, 1964), and Antarctica (Horne, 1968).

Laumontite has been found at shallow depths in geothermal areas of New Zealand (Alfred Steiner *in* Coombs and others, 1959), Kamchatka (Averyev and others, 1961), and Iceland (Sigvaldason, 1963).

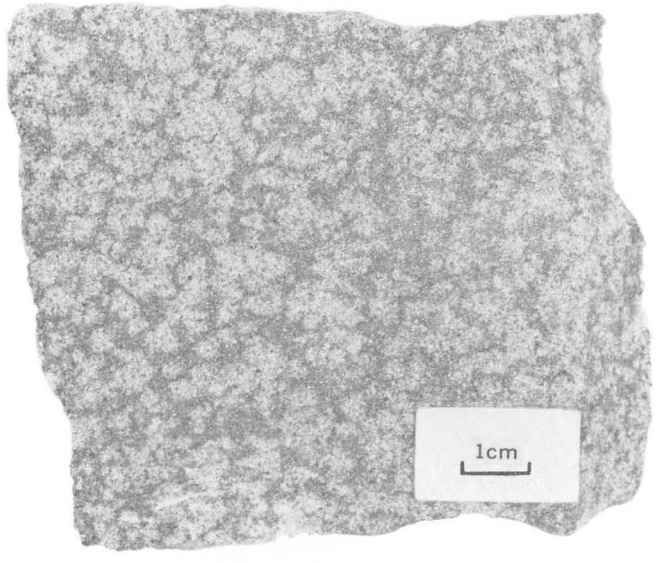

FIGURE 1.—Characteristic mottling of laumontized sandstone. Sample of Briones Sandstone from Penitencia Creek in Santa Clara County, Calif.

U.S. GEOL. SURVEY PROF. PAPER 700-D, PAGES D188–D195

Temperatures ranging between 100° and 240°C characterize the laumontite-bearing zones which, in these abnormally hot areas, are restricted to depths generally less than 3,000 feet. A shallow occurrence of laumontite in Eocene sandstones cut by an intrusive complex in the Spanish Peaks area of Colorado has been interpreted by Vine (1969) to have resulted from hydrothermal alteration induced in the sandstones by the heat of the intrusive.

Laboratory studies (Coombs and others, 1959; Koizumi and Roy, 1960; and Liou, 1968) have not led to the synthesis of laumontite but have indicated an upper temperature limit of 240°–290°C (at water pressures of 0.5 to 3 kilobars) above which the mineral decomposes to wairakite ($CaAl_2Si_4O_{12}\cdot 2H_2O$). Furthermore, laumontite and wairakite appear to be stable only at low partial pressures of CO_2; at high partial pressures of CO_2, both minerals are metastable relative to montmorillonite (or kaolinite) plus calcite (Zen, 1961; Liou, 1968).

Existing data thus suggest that laumontite forms at 100°–240°C. For a normal sedimentary basin with a geothermal gradient of the order of 11°C per 1,000 feet (Birch and others, 1942) and a surface temperature of 20°C, these temperatures would correspond to depths of 7,300 to 20,000 feet. Most regionally developed occurrences of laumontite in geosynclinal sediments do represent depths of this order of magnitude (Hay, 1966). For depth metamorphism of tuffaceous sediments, Coombs, Ellis, Fyfe, and Taylor (1959) have suggested a laumontite stage characterized by temperature and pressure greater than those of the heulandite-analcite stage but less than those of a prehnite-pumpellyite stage.

That factors other than temperature and pressure can control the formation of laumontite has become clear from occurrences of the mineral at unexpectedly shallow depths or in reverse order of depth relative to other metamorphic minerals (Coombs and others, 1959; Dickinson, 1962; Brown and Thayer, 1963; Otálora, 1964). Such deviations seem to arise from differences in the composition of successive beds and from variations in permeability of beds. Several authors (Brown and Thayer, 1963; Horne, 1968; Dickinson and others, 1969) have noted an antipathetic relation between laumontite and calcite cement in tuffaceous sandstones, which is probably due to calcite sealing the sandstones against reactive solutions.

The different modes of occurrence of laumontite, as described from the Triassic beds of New Zealand (Coombs, 1952), have also been observed at many other localities. The mineral replaces (1) glassy shards in tuffaceous beds, (2) heulandite that formed earlier from the shards, (3) detrital K-feldspar or plagioclase, (4) matrix minerals of sandstones (and fills joints and fractures), and (5) calcareous shells of fossils. In sandstones poor in labile volcanic materials, laumontite occurs mostly in modes 3 and 4 and apparently formed through diagenetic alteration of feldspars and clays (Zaporozhtseva, 1960).

CHEMISTRY OF LAUMONTIZATION

Any sedimentary material or combination of materials rich in calcium oxide, alumina, and silica is a potential precursor of authigenic laumontite. The formation of laumontite through an equal-volume replacement of the anorthite component of plagioclase, without any change in the content of albite, has been discussed by Coombs (1954) in terms of the following equation:

$$\underset{\text{276 g, 100 cc}}{\text{anorthite}}\ 0.99\ CaAl_2Si_2O_8 + \underset{\text{35 g}}{\text{water}}\ 1.95\ H_2O \rightarrow \underset{\text{229 g, 100 cc}}{\text{laumontite}}\ 0.49\ CaAl_2Si_4O_{12}\cdot$$

$$\underset{\text{28 g}}{4H_2O} + \underset{\text{52 g}}{0.50\ CaO} + \underset{\text{1 g}}{0.50\ Al_2O_3} + 0.02\ SiO_2. \quad \text{materials removed in solution} \qquad (1)$$

Coombs noted that this reaction not only forms laumontite within grains of plagioclase but also releases substantial amounts of calcium and aluminum for metasomatism elsewhere. He envisioned the released elements reacting with glassy tuffs or with matrix materials of sandstones to form additional laumontite.

Equation 1 also suggests that laumontization and albitization could be coupled reactions. Progressive albitization of plagioclase with increasing depth has been noted in many thick sedimentary sections, in some of which there is a parallel development of laumontite (Coombs, 1954; Dickinson and others, 1969). In other sections, no such relation is found, because laumontite occurs throughout a wide range of depths (Brown and Thayer, 1963; Horne, 1968).

An initial mixture consisting of calcite, kaolinite, and quartz is shown in the following equation (Zen, 1961):

$$\underset{\text{calcite}}{CaCO_3} + \underset{\text{kaolinite}}{Al_2Si_2O_5(OH)_4} + \underset{\text{quartz}}{2SiO_2} + \underset{\text{water}}{2H_2O} \rightarrow$$

$$\underset{\text{laumontite}}{CaAl_2Si_4O_{12}\cdot 4H_2O} + \underset{\text{carbon dioxide}}{CO_2}. \qquad (2)$$

Other clay minerals or reactive aluminosilicate materials could be substituted for kaolinite in the equation. The rare replacement of calcareous shells of fossils by laumontite could also be explained by such a reaction, if migrating solutions carried alumina and silica to the calcite. Equations 1 and 2 satisfactorily account for the different modes of occurrence of laumontite in arkoses, graywackes, and tuffaceous sandstones.

Laumontite is not uncommon in Jurassic and Cretaceous sedimentary rocks of California (Gilbert, 1951; Bailey and others, 1964; Hay, 1966; and Dickinson and others, 1969). In Tertiary rocks of the State, only three occurrences were known hitherto: (1) a Miocene sandstone at a depth of 11,000 feet in an oil well in Kern County (Kaley and Hanson, 1955), (2) Eocene sandstones and shales of the Juncal Formation of Page and others (1951) in the Santa Ynez Range of Santa Barbara County (J. D. Frantz and W. S. Wise, written commun., Nov. 1968), and (3) an Oligocene sandstone in the Sespe Formation of the Santa Monica Mountains of Los Angeles County (R. F. Yerkes, oral commun., Jan. 1970). In the present report, we record two other occurrences of laumontite in Tertiary sedimentary rocks and discuss briefly the diagenetic significance of the mineral.

NEW OCCURRENCES OF LAUMONTITE

The new occurrences of laumontite are in the central Coast Ranges near San Jose (fig. 2). One is in the Diablo Range, to the east of the city, in lithic marine sandstone mapped as the upper Miocene Briones Sandstone by Crittenden (1951). The other occurrence, discussed later, is southwest of San Jose, in the Santa Cruz Mountains. The Briones is a part of a sequence of beds that has been downfolded to form a northwest-southeast trending syncline, which is well exposed in cross section along the canyon of Penitencia Creek. Cursory examination, along the canyon, of the underlying Cretaceous Oakland Conglomerate and Crittenden's Berryessa Formation, of the Miocene Monterey Shale, and of the overlying Pliocene Orinda Formation did not reveal laumontite in these formations. To the north and south of Penitencia Creek, small amounts of laumontite have been detected in the Briones along Felter, Sierra, and Mount Hamilton roads, but these occurrences have not been studied in detail.

Besides grains of quartz, plagioclase, K-feldspar, hornblende, biotite, and chert, the Briones contains abundant (as much as 50 volume percent) fragments of andesite rich in groundmass plagioclase. Occasional andesite fragments enclose large plagioclase phenocrysts, suggesting that some of the plagioclase sand grains were derived from andesite. Fresh plagioclase grains are andesine-oligoclase; turbid altered grains are oligoclase-albite. Calcite, clay minerals, and zeolites cement the sand grains and fill joints and smaller fractures in the sandstone.

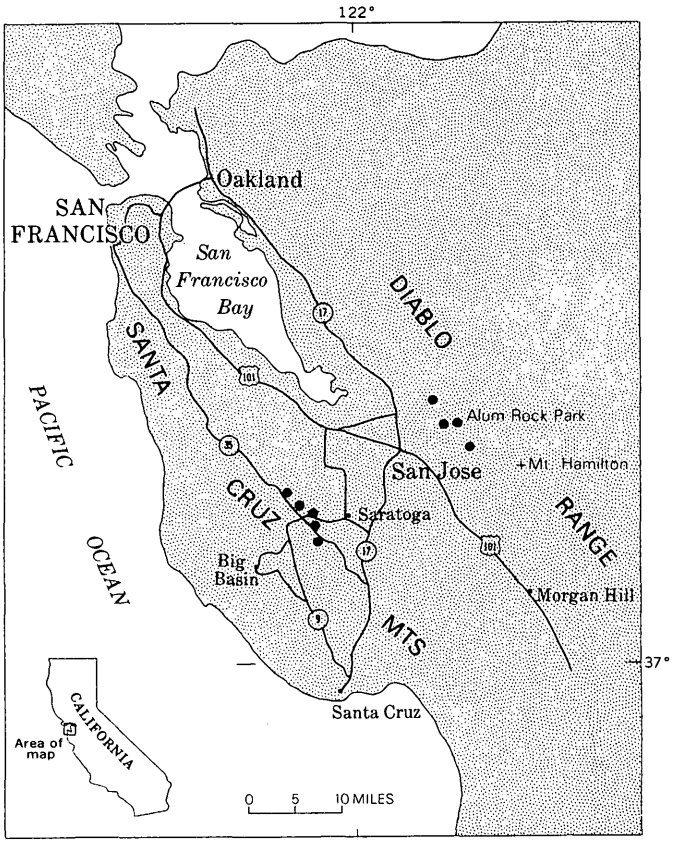

FIGURE 2.—Map showing two laumontite localities (elongate groups of black dots) in the central Coast Ranges of California. The San Andreas fault, a few miles east of State Highway 35 and roughly parallel to it, passes between the two localities.

With regard to the distribution of laumontite along Penitencia Creek the Briones, where it is 3,400 feet thick (Crittenden, 1951), can be divided into three parts. The basal 500 feet is devoid of laumontite and calcite except for minor amounts present as fracture fillings. The main part of the Briones, about 2,400 feet thick, has abundant laumontite as fine-grained intergranular cement along with chlorite, as fracture filling, and as replacement of plagioclase, except in several fossiliferous reefs where the pores of the sandstone are sealed by calcite. The uppermost 500 feet contains minor amounts of interstitial clinoptilolite and, in one place, has thin veins consisting of coarse stilbite, laumontite, and calcite. The overall spatial relations

suggest that there may be a crude vertical zonation of zeolite species in the section, somewhat like that found in New Zealand by Coombs (1954).

The clay minerals of the Briones, identified by X-ray diffraction analysis of glycolated and heated oriented-clay mounts are montmorillonite, chlorite, vermiculite, illite, and interlayered chlorite-vermiculite of the type described by Bradley and Weaver (1956). The basal 500 feet of the formation has sheaflike aggregates of chlorite as a monomineralic filling of pores. The freshest noncalcareous sandstones in the laumontite-rich part have a bimineralic pore filling consisting of chlorite aggregates rimmed by finely crystallized laumontite (fig. 3*C*, *D*). Montmorillonite is minor in these sandstones. On the other hand, montmorillonite is the main clay mineral and chlorite is subordinate in the upper 500 feet of the Briones where clinoptilolite and stilbite are the characteristic zeolites.

Numerous small springs issue from outcrops of

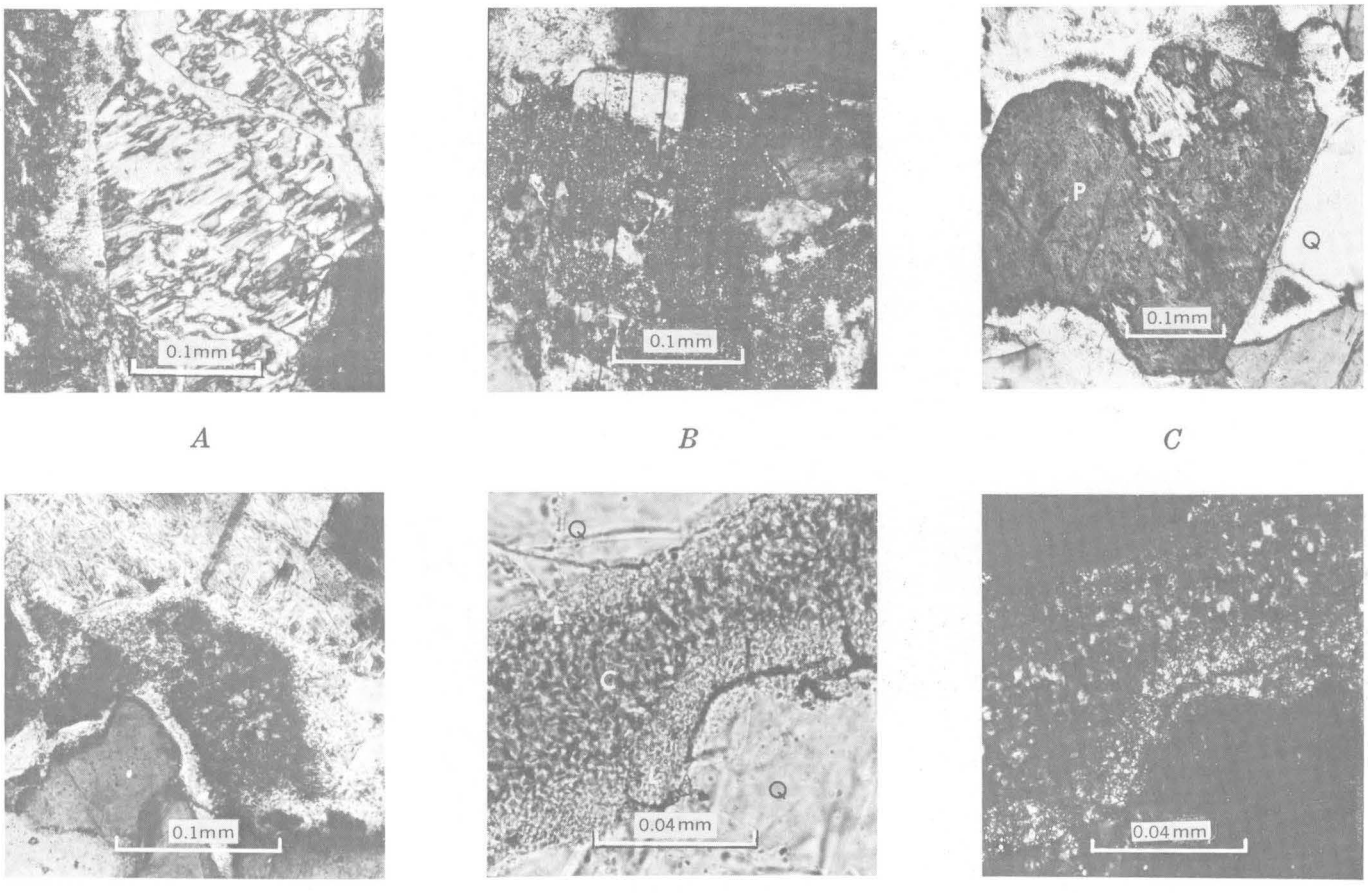

FIGURE 3.—Photomicrographs, at high magnifications, illustrating the modes of occurrence of laumontite in Miocene sandstones.

A, single grain of plagioclase extensively replaced and veined by laumontite (white). A triangular pore filled with laumontite forms the left border of the plagioclase grain. Crossed nicols.

B, grain of plagioclase in a section that was treated with oxalic acid. The laumontized parts are covered by microcrystalline calcium oxalate. Crossed nicols.

C, grain of plagioclase (P) almost at extinction occupies most of the field. Around it are triangular and elongate pores filled with laumontite (white borders) and chlorite (dark granular cores) composite. Q is quartz. Crossed nicols.

D, elongate pore filled with chlorite aggregates (dark weakly birefringent areas) that are surrounded by laumontite (white borders). Crossed nicols.

E, chlorite (C) core and laumontite (L) border of a composite fracture filling in quartz (Q), in a thin section treated with oxalic acid. With the plain light used to obtain this photograph, chlorite was readily recognized by its green color, but the calcium oxalate deposit on laumontite was not distinctive.

F, same view as *E* above, but under crossed nicols, showing the microcrystalline calcium oxalate deposited on laumontite. The oxalate is much finer grained than chlorite.

the Monterey Formation along Penitencia Creek in Alum Rock Park (Waring, 1915). The water is mildly saline (<7,000 ppm total salts), with temperatures (20°–30°C) only slightly above the regional norm, and shows no apparent connection with occurrence of laumontite in the closely associated Briones Sandstone.

The second locality for laumontite is in the Santa Cruz Mountains to the southwest of San Jose (fig. 2), in the upper part of Oligocene(?) and Miocene marine Vaqueros Sandstone, mapped by Brabb (1960), Cummings, Touring, and Brabb (1962), and Dibblee (1966). The mineral occurs sporadically in folded sandstones exposed along State Highways 9 and 35 in secs. 5, 6, 7, and 17, T. 8 S., R. 2 W. The Eocene Butano Sandstone of the region was examined in some detail for laumontite; none was found.

The Vaqueros Sandstone, in the area of our study, differs from the Briones in several respects. It is a purer arkose with minor biotite, contains very few rock fragments, either chert or andesitic debris, and lacks fossiliferous reefs or other high concentrations of calcite. Extensive corrosion of the clasts has caused them to interlock in an intricate manner. The minor clay is mostly vermiculite which probably originated through alteration of biotite.

In certain parts of the Vaqueros, laumontite extensively replaces plagioclase (fig. 3*A*, *B*) and also occurs among the clasts as rather coarsely crystallized intergranular matter. The fine-grained combination of chlorite and laumontite, which so commonly fills the pores of Briones Sandstone, is totally lacking in the Vaqueros. The mineralogic relations broadly suggest that laumontite is primarily a product of alteration of plagioclase in both formations, but significant amounts of laumontite formed additionally in the Briones through alteration of andesitic debris.

CHARACTERIZATION OF LAUMONTITE

In order to facilitate the petrographic study of laumontite-bearing rocks, we have devised a method for making laumontite more conspicuous under the microscope. The method entails immersing the thin section or a finely polished (400-mesh abrasive powder) slab of rock in a tepid (40°C) solution of oxalic acid (about 10 parts of $H_2C_2O_4 \cdot 2H_2O$ in 100 parts of water) for 4 minutes and then thoroughly rinsing the rock with distilled water and drying it.

Oxalic acid liberates calcium from laumontite, either through cation exchange or direct decomposition, but not from plagioclase, clinoptilolite, stilbite, lawsonite, or calcite. The liberated calcium combines with the acid to form an adherent white deposit of finely crystallized calcium oxalate on the surface of laumontite (fig. 3*B*, *F*). Neither the temperature of the acid solution nor the period of immersion of the sample should exceed those stated above because of the danger of softening the balsam of thin sections and of the possibility of other materials like palagonite starting to react with oxalic acid. It is best to treat only a part of a section with the oxalic acid solution. The cover glass should be affixed with care to avoid dislodging the oxalate deposit.

Because coarsely crystallized laumontite is readily recognized by its optical properties, the oxalic acid test is most useful for detecting the fine-grained examples such as the laumontite-chlorite pore filling (fig. 3*E*, *F*) in sandstone from the middle part of the Briones. Small amounts of laumontite within veins of stilbite are very evident in thin sections treated with oxalic acid. The general absence of laumontite within clasts of altered andesite would be more difficult to prove by other techniques.

Results of X-ray examination of laumontite that was separated from sandstone of the Vaqueros Formation are given in tables 1 and 2. The powder diffraction data, obtained with nickel-filtered Cu$K\alpha$ radiation, were indexed and processed to derive cell constants by means of the computer program of Evans, Appleman, and Handwerker (1963). The cell constants of the samples are compared in table 1 with those published by Coombs (1952) and by Lapham (1963) for laumontite and leonhardite. The smallness of the cell indicates that the Vaqueros material is the partially dehydrated variety, leonhardite.

The indexed X-ray powder data of the Vaqueros material are compared in table 2 with powder data of Coombs (1952) and of Lapham (1963). Except for the (110) spacing not included in Coombs' results, the three sets of data are in good agreement.

TABLE 1.—*Unit-cell data for leonhardite and laumontite*

Mineral	Leonhardite	Leonhardite	Laumontite	Leonhardite
Locality	Santa Cruz Mountains Calif.	Hungary		Dillsbury, Pa.
Reference	This paper[1]	Coombs (1952)		Lapham (1963)
System	Monoclinic	Monoclinic	Monoclinic	Monoclinic
Space group	C2	C2	C2	C2
Cell values:				
a (A)	14.72±0.02	14.75±0.03	14.90±0.05	14.75±00.5
b (A)	13.07±0.01	13.10±0.02	13.17±0.02	13.083±0.02
c (A)	7.56±0.01	7.55±0.01	7.55±0.05	7.57±0.05
β	111.9°±0.2°	112.0°±0.2°	111.5°±0.5°	112° appr.
V (A^3)	1,349			

[1] Cell values and the pattern indexing (table 2) were derived using a U.S. Geological Survey least-squares refinement procedure (Evans and others, 1963).

TABLE 2.—*X-ray diffraction data for leonhardite*

hkl	This study			Lapham (1963)		Coombs (1952)	
	d, calculated (angstroms)[1]	*d*, observed (angstroms)[2]	*I*	*d* (angstroms)	*I*	*d* (angstroms)	*I*
110	9.44	9.44	100	9.49	100	--	--
001	7.01	--	--	--	--	--	--
200	6.83	6.83	75	6.86	35	6.88	6
020	6.53	--	--	--	--	--	--
$\bar{1}11$	6.49	--	--	--	--	--	--
$\bar{2}01$	6.18	6.18	10	6.19	2	6.21	2
				5.91	2		
111	5.040	5.040	20	5.052	6	5.07	2
021	4.779	--	--	--	--	--	--
220	4.722	4.724	14	4.731	20	4.75	1
$\bar{2}21$	4.490	4.489	22	4.500	8	4.51	3
$\bar{3}11$	4.427	--	--	--	--	--	--
310	4.300	4.300	1	4.314	2	--	--
201	4.174	--	--	4.156	60	4.18	10
130	4.150	4.149	100				
$\bar{1}31$	3.763	3.767	18	3.768	2	3.77	<1
$\bar{2}02$	3.736	--	--	--	--	--	--
$\bar{4}01$	3.654	3.654	56	3.667	14	3.67	4
$\bar{1}12$	3.603	--	--	--	--	--	--
221	3.518	--	--	3.510	30	3.52	10
002	3.504	3.505	60				
400	3.415	3.407	16	3.411	8	3.42	<1
$\bar{1}31$	3.406						
$\bar{3}12$	3.358	3.358	40	3.367	4	3.36	1
040	3.267	3.267	60	3.272	20	3.28	3
$\bar{2}22$	3.243	--	--	--	--	--	--
311	3.197	--	--	3.205	8	3.21	2
$\bar{3}31$	3.196	3.194	60				
$\bar{4}21$	3.189	--	--				
330	3.148	3.148	32	3.152	16	3.16	1
$\bar{4}02$	3.090	--	--	--	--	3.09	<1
022	3.088	--	--	--	--	--	--
112	3.040	--	--	3.033	25	3.04	4
420	3.027	3.027	40				
041	2.961	2.900	4	2.950	4	2.95	<1
240	2.947						
$\bar{2}41$	2.888	--	--	--	--	--	--
$\bar{5}11$	2.873	2.873	25	2.881	14	2.88	3
$\bar{1}32$	2.841	--	--	--	--	--	--
$\bar{4}22$	2.793	2.790	22	2.798	2	2.80	2
202	2.731	--	--	--	--	2.73	<1
$\bar{3}32$	2.716	--	--	--	--	--	--
401	2.699	--	--	--	--	--	--
510	2.674	--	--	--	--	--	--
$\bar{5}12$	2.642	2.641	4	--	--	2.64	<1
331	2.629	2.628	1	2.629	3	--	--
241	2.573	2.571	30	2.575	14	2.58	3

[1] All calculated interplanar spacings are given down to $d = 2.573$ A. Spacings calculated from the following unit-cell parameters: *a*, 14.72 A; b, 13.07 A; *c*, 7.56 A; $\beta = 111.9°$, space group C2, and using a least-squares refinement procedure (Evans and others, 1963).

[2] Cu$K\alpha$ radiation, Ni filter ($\lambda \pm 1.5418$ A). Pattern taken with North American Philips X-ray diffractometer internally standardized with silicon.

GENESIS OF LAUMONTITE IN THE BRIONES AND VAQUEROS FORMATIONS

The laumontite that replaces plagioclase in both the Briones Sandstone and the Vaqueros Formation and the intergranular laumontite in the Vaqueros seem to be good examples of the mineral having formed through diagenetic alteration of plagioclase (equation 1). Supporting evidence is found in the extensive alteration of plagioclase to albite in laumontite-rich parts of both formations.

The Briones is uniformly rich in clastic plagioclase and in andesitic debris, both potential precursors of laumontite, so the virtual absence of laumontite and the unaltered condition of the pla-

gioclase (andesine-oligoclase) in three separate parts of the formation is of much interest. These three parts are (1) the basal 500 feet, rich in interstitial chlorite and poor in calcite, (2) the calcareous fossiliferous reefs in the middle part, and (3) the uppermost 500 feet marked by interstitial montmorillonite and clinoptilolite and a variable calcite content. The failure of the reaction of equation 1 in these parts of the sandstone may be tentatively ascribed to sealing of the pores by andesite-derived clays in the basal and upper parts and by calcite that excluded solutions necessary for this reaction in the middle part.

Besides having laumontite that is related genetically to plagioclase, the Briones also contains the zeolite in the form of the unusual laumontite-chlorite filling of pores, with laumontite lining the pore and enveloping a central core of chlorite (fig. 3*C*, *D*). The identification of the enveloping mineral as laumontite is based on its optical properties and on its positive reaction with oxalic acid. The close association and regular arrangement of the two minerals suggest that they were produced by one and the same reaction.

The magnesium, iron, aluminum, and silicon needed for chlorite could be derived easily from the andesitic debris abundant in the Briones. If, as seems likely, the starting material were an interstitial montmorillonoid (Lerbekmo, 1957) rather than the original andesite, the calcium content of the system would have to be raised by means of a calcium-rich substance (say, calcite) in order to form much laumontite. We believe that the pore-filling laumontite-chlorite mixture was produced by a diagenetic reaction like that of equation 2. The following equation, in which the symbol "Mg" stands for both magnesium and ferrous iron, describes the postulated reaction:

$$\underset{\text{montmorillonite}}{13.5[Ca_{0.33}(Al_{3.34}Mg_{0.66})Si_8O_{20}(OH_4)]} + \underset{\text{calcite}}{15\,CaCO_3} + \underset{\text{water}}{59\,H_2O} \rightarrow \underset{\text{chlorite}}{[(Al_3Mg_9)(Al_3Si_5)O_{20}(OH)_{16}]} + \underset{\text{laumontite}}{19.5\,[CaAl_2Si_4O_{12}\cdot 4H_2O]} + \underset{\text{quartz}}{25\,SiO_2} + \underset{\text{carbon dioxide}}{15\,CO_2}. \quad (3)$$

The amount of chlorite relative to laumontite would depend in part on the magnesium and iron content of the montmorillonoid, as these two elements enter the structure of chlorite only. The absence of the laumontite-chlorite mixture as pore filler in the Vaqueros could be attributed to the scarcity of both andesitic debris and calcite in that formation. That the mixture is missing in the basal part of Briones may be due to scarcity of calcite.

THE DIFFERENT ROLES OF CALCITE

If sands become impregnated by some cementing material early in their depositional history, they could be protected against later diagenetic effects to the extent that the cement excludes reactive solutions. As previously noted, the antipathetic relation between calcite and laumontite in sandstones has been reported by many authors, and Horne (1968) has attributed the relation to calcite acting as a sealant against migrating solutions that are essential for laumontization. We believe that this explanation accounts for the absence of laumontite from the calcareous reefs in the generally laumontite-rich part of the Briones and from large calcareous concretions that abound in highly laumontized parts of the Juncal Formation of Santa Barbara County.

On the other hand, equations 2 and 3 describe a class of reactions in which calcite is essential to the formation of laumontite. The bimineralic laumontite-chlorite pore fillings in the middle part of the Briones seem to have formed through a reaction of this type, with the numerous fossiliferous reefs of that part providing the necessary calcium to migrating solutions. The gradual dissolution of calcite is indicated at some places by relict pieces of shells that mark zones formerly occupied by calcareous reefs.

In contrast to the regionwide development of laumontite, as in the Triassic section of New Zealand (Coombs, 1954), the occurrences in the Briones and Vaqueros are very sporadic and localized. Effects of large-scale factors, such as depth of burial, are not evident in these small occurrences; this rather emphasizes local variations in chemical composition and permeability of the sediment as controlling factors in the genesis of laumontite.

REFERENCES

Averyev, V. V., Naboko, S. I., and Piip, B. I., 1961, Contemporary hydrothermal metamorphism in regions of active volcanism: Akad. Nauk SSSR Doklady, Earth Sciences Secs., v. 137, no. 2, p. 407–410. English ed., Am. Geol. Inst., Washington, D.C., p. 239–242, 1962.

Bailey, E. H., Irwin, W. P., and Jones, D. L., 1964, Franciscan and related rocks, and their significance in the geology of western California: California Div. Mines and Geology Bull. 183, 177 p.

Birch, Francis, Schairer, J. F., and Spicer, H. C., eds., 1942, Handbook of physical constants: Geol. Soc. America Spec. Paper 36, 325 p.

Brabb, E. E., 1960, Geology of the Big Basin area, Santa Cruz Mountains, California: Stanford Univ., unpub. Ph. D. thesis, 191 p.

Bradley, W. F., and Weaver, C. E., 1956, A regularly interstratified chlorite-vermiculite clay mineral: Am. Mineralogist, v. 41, nos. 5–6, p. 497–504.

Brown, C. E., and Thayer, T. P., 1963, Low-grade mineral facies in the Upper Triassic and Lower Jurassic rocks of the Aldrich Mountains, Oregon: Jour. Sed. Petrology, v. 33, no. 2, p. 411–425.

Coombs, D. S., 1952, Cell size, optical properties, and chemical composition of laumontite and leonhardite: Am. Mineralogist, v. 37, nos. 9–10, p. 812–830.

——— 1954, The nature and alteration of some Triassic sediments from Southland, New Zealand: Royal Soc. New Zealand Trans., v. 82, pt. 1, p. 65–109.

Coombs, D. S., Ellis, J. A., Fyfe, W. S., and Taylor, A. M., 1959, The zeolite facies, with comments on the interpretation of hydrothermal synthesis: Geochim. et Cosmochim. Acta, v. 17, no. 1–2, p. 53–107.

Crittenden, M. D., 1951, Geology of the San Jose–Mount Hamilton area, California: Calif. Dept. Nat. Resources, Div. Mines Bull. 157, 74 p.

Cummings, J. C., Touring, R. M., and Brabb, E. E., 1962, Geology of the northern Santa Cruz Mountains, California, *in* Geologic guide to the gas and oil fields of northern California: California Div. Mines and Geology Bull. 181, p. 179–220.

Deffeyes, K. S., 1959, Zeolites in sedimentary rocks: Jour. Sed. Petrology, v. 29, no. 4, p. 602–609.

Dibblee, T. W., Jr., 1966, Geology of the Palo Alto quadrangle, Santa Clara and San Mateo Counties, California: California Div. Mines and Geology Map Sheet 8.

Dickinson, W. R., 1962, Petrology and diagenesis of Jurassic andesitic strata in central Oregon: Am. Jour. Science, v. 260, no. 7, p. 481–500.

Dickinson, W. R., Ojakangas, R. W., and Stewart, R. J., 1969, Burial metamorphism of the Late Mesozoic Great Valley sequence, Cache Creek, California: Geol. Soc. America Bull., v. 80, no. 3, p. 519–525.

Evans, H. T., Jr., Appleman, D. E., and Handwerker, D. S., 1963, The least squares refinement of crystal unit cells with powder diffraction data by an automatic computer indexing method [abs.]: Am. Cryst. Assoc. Ann. Mtg., Cambridge, Mass., 1963, Program and Abs., no. E–10, p. 42.

Gilbert, C. M., 1951, Laumontite from Anchor Bay, Mendocino County, California [abs.]: Geol. Soc. America Bull., v. 62, no. 12, p. 1517.

Hay, R. L., 1966, Zeolites and zeolitic reactions in sedimentary rocks: Geol. Soc. America Spec. Paper 85, 130 p.

Hoare, J. M., Condon, W. H., and Patton, W. W., Jr., 1964, Occurrence and origin of laumontite in Cretaceous sedimentary rocks in western Alaska, *in* Geological Survey Research 1964; U.S. Geol. Survey Prof. Paper 501–C, p. C74–C78.

Horne, R. R., 1968, Authigenic prehnite, laumontite, and chlorite in the Lower Cretaceous sediments of southeastern Alexander Island: British Antarctic Survey Bull. 18, p. 1–10.

Iijima, Azuma, and Utada, Minoru, 1966, Zeolites in sedimentary rocks, with reference to the depositional environments and zonal distribution: Sedimentology, v. 7, no. 4, p. 327–357.

Kaley, M. E., and Hanson, R. F., 1955, Laumontite and leonhardite cement in Miocene sandstone from a well in San Joaquin Valley, California: Am. Mineralogist, v. 40, nos. 9–10, p. 923–925.

Koizumi, Mitsue, and Roy, Rustum, 1960, Zeolite studies—Pt. 1, Synthesis and stability of the calcium zeolites: Jour. Geology, v. 68, no. 1, p. 41–53.

Lapham, D. M., 1963, Leonhardite and laumontite in diabase from Dillsburg, Pennsylvania: Am. Mineralogist, v. 48, nos. 5–6, p 683–689

Lerbekmo, J. F., 1957, Authigenic montmorillonoid cement in andesitic sandstones of central California: Jour. Sed. Petrology, v. 27, no. 3, p. 298–305.

Liou, Juhn-guang, 1968, Zeolite equilibria in the system $CaO{\cdot}Al_2O_3{\cdot}2SiO_2$–$SiO_2$–$H_2O$–$CO_2$, the stabilities of wairakite and laumontite: Geol. Soc. America Ann. Mtg., Mexico City, 1968, Program with Abstracts, p. 175.

Otálora, G., 1964, Zeolites and related minerals in Cretaceous rocks of east-central Puerto Rico: Am. Jour. Sci., v. 262, no. 6, p. 726–734.

Page, B. M., Marks, J. G., and Walker, G. W., 1951, Stratigraphy and structure of mountains northeast of Santa Barbara, California: Am. Assoc. Petroleum Geologists Bull., v. 35, no. 8, p. 1727–1780.

Sigvaldason, G. E., 1963, Epidote and related minerals in two deep geothermal drill holes. Reykjavik and Hveragerdi, Iceland: Art. 200 *in* U.S. Geol. Survey Prof. Paper 450–E, p. E77–E79.

Vine, J. D., 1969, Authigenic laumontite in arkosic rocks of Eocene age in the Spanish Peaks area, Las Animas County, Colorado, *in* Geological Survey Research 1969: U.S. Geol. Survey Prof. Paper 650–D, p. D80–D83.

Waring, G. A., 1915, Springs of California: U.S. Geol. Survey Water Supply Paper 338, p. 208–212.

Zaporozhtseva, A. S., 1960, On the regional development of laumontite in Cretaceous deposits of Lena Coal Basin: Akad. Nauk SSSR Izv. Ser. Geol., no. 9, English translation, p. 52–59.

Zen, E-an, 1961, The zeolite facies—An interpretation: Am. Jour. Sci., v. 259, no. 6, p. 401–409.

BIOTITES FROM HYBRID GRANITOID ROCKS OF THE SOUTHERN SNAKE RANGE, NEVADA

By DONALD E. LEE and RICHARD E. VAN LOENEN,
Denver, Colo.

Abstract.—Biotite compositions agree with other evidence and indicate distinctly different magmatic affinities for two closely adjacent masses of hybrid granitoid rocks. Within one mass, assimilation of host rocks as chemically distinct as limestone and quartzite has produced a commensurate range of biotite compositions defining a trend in the compositional triangle Fe^{+3}–Fe^{+2}–Mg. When related to the experimentally studied ternary system

$$KFe_3^{+3}AlSi_3O_{12}(H_{-1})–KFe_3^{+2}AlSi_3O_{10}(OH)_2–KMg_3AlSi_3O_{10}(OH)_2$$

and coupled with the estimated positions of biotite solid solutions for different oxygen buffers, the trend suggests that oxygen fugacities in the contaminated magma during biotite crystallization were slightly higher than those defined by the Ni–NiO buffer. The compositional data also indicate that the magma was "buffered" with respect to oxygen by magnetite that coexists with each of the biotites analyzed. Within the second mass, assimilation of argillite has produced a granitoid rock type devoid of iron oxide minerals, in which biotite coexists with large amounts of muscovite. The uniformly low MgO content of these biotites suggests that they were initially equilibrated with respect to the same relatively low oxygen fugacity. Their sharply different Fe_2O_3/FeO values probably are due to postmagmatic processes.

The area of study is in the southern Snake Range of east-central Nevada, about 50 miles southeast of Ely, Nev. (fig. 1). The biotites described were collected from about 20 square miles of granitoid outcrop exposed within the Wheeler Peak quadrangle of Nevada and the Garrison quadrangle of Utah-Nevada. These granitoid rocks are included in an area mapped by Drewes (1958) and by Whitebread, Griggs, Rogers, and Mytton (1962, 1970); the regional setting is shown on the geologic map of White Pine County, Nev., by Hose and Blake (1970).

The chemical petrology of these hybrid granitoid rocks is described by Lee and Van Loenen (1970); the present paper is part of a continuing study of the mineralogy of these rocks, which considers also the allanites and monazites (Lee and Bastron, 1967), the zircons (Lee and others, 1968), and the sphenes (Lee and others, 1969) coexisting with these biotites. In addition, almost all these biotites are described in the companion paper by Lee, Marvin, Stern and Peterman (1970) (p. D92–D102, this chapter). In the present paper, as in previous studies, we relate chemical and mineralogical variables to CaO content of the rock, for reasons given by Lee and Bastron (1967). A given sample number refers both to the rock and to the constituent biotite (and other minerals) recovered from that rock.

GEOLOGIC SETTING

The area is well exposed, and field relations are well known. Jurassic granitoid rocks were intruded into part of a lower Paleozoic miogeosynclinal sequence that is predominantly limestone and quartzite. The sedimentary rocks exposed in intrusive contact with the granitoid rocks are the Precambrian Osceola Argillite (of Misch and Hazzard, 1962) and the Cambrian Prospect Mountain Quartzite, Pioche Shale, and Pole Canyon Limestone. All these granitoid rocks are hybrid, but despite this common genesis these rocks comprise three separate study units, which appear as discrete exposures in the Snake Creek–Williams Canyon, the Pole Canyon–Can Young Canyon, and the Young Canyon-Kious Basin areas. Bases for distinction among these areas (Lee and Van Loenen, 1970) are summarized below.

Influence of host rock type on the chemistry and mineralogy of the granitoid rocks is most obvious in the Snake Creek–Williams Canyon area, where the intrusive is well exposed in contact with quartzite, shale, and limestone host rocks. The CaO content of

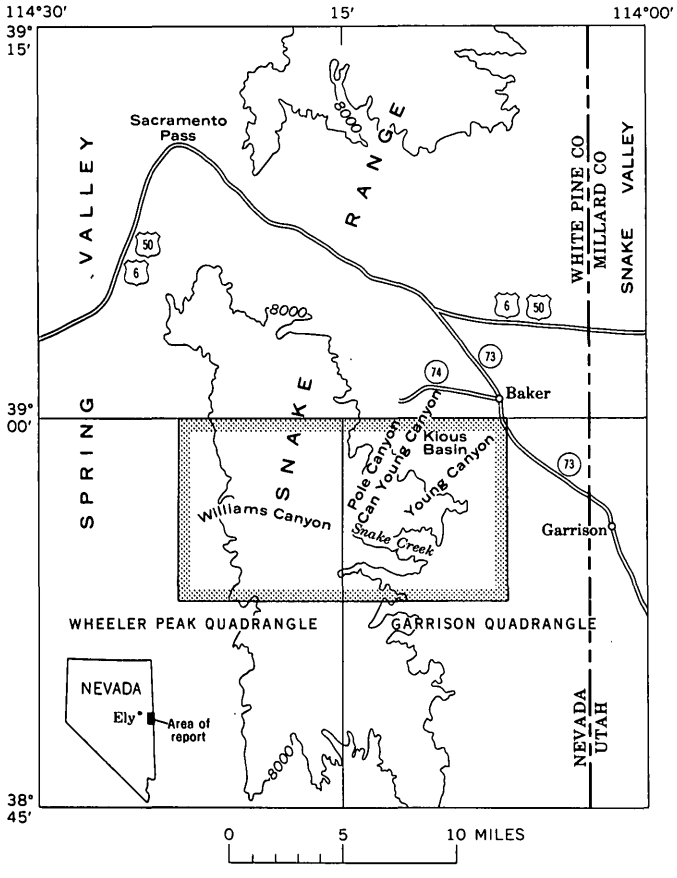

FIGURE 1.—Index map showing location of study area. Hachures indicate area of map in Lee and Van Loenen (1970), on which are shown all sample localities for biotites listed in table 1.

this granitoid rock ranges from 0.5 to 4.5 percent, depending on chemistry of the assimilated host rock. Many corresponding and well-defined chemical and mineralogical differences exist (Lee and Van Loenen, 1970). The complete transition is exposed over a horizontal distance of about 3 miles. Aside from the exceptions noted by Lee and Bastron (1967), the chemistry of these hybrid rocks (including variation of SiO_2 with CaO) is about what one would expect in a series of differentiates.

In the Pole Canyon–Can Young Canyon area, granitoid rock is exposed in contact with quartzite, but it is very different from the intrusive seen in contact with quartzite in the Snake Creek–Williams Canyon area. It is distinguished in part by the presence of large muscovite phenocrysts, many of which contain crystals of biotite, and by an absence of iron oxide minerals. It is also distinguished by an almost complete lack of zircon, except for some tiny acicular crystals included within the accessory apatite present in the rock. We attribute the distinctive nature of this intrusive to assimilation of the Osceola Argillite (750–800 feet thick), even though this argillite is not exposed in contact with the granitoid rock.

The granitoid rock exposed in the Young Canyon–Kious Basin area is significant from the standpoint of the regional geology and tectonics, for part of this outcrop has been cataclastically deformed as a result of movement on the Snake Range décollement. The deformed part of the intrusive is separated from the undeformed part by a fault that probably represents the location of the Pioche Shale before the advent of the intrusive. Above this fault, where the granitoid rock intruded Pole Canyon Limestone, almost all the original biotite has been destroyed by cataclasis. Below the fault the undeformed intrusive is exposed in contact with Prospect Mountain Quartzite. Because of the cataclasis, influence of the country rock on the chemistry of the intrusive has been somewhat obscured, but apparently the chemical petrology of the original, undeformed granitoid rocks was analogous to that of the hybrid rocks so well exposed in the Snake Creek–Williams Canyon area.

OCCURRENCE OF BIOTITE

In the Snake Creek–Williams Canyon area, abundance of biotite is closely related to the chemistry of the rock. As CaO content of the rock rises from about 0.5 percent (76 percent SiO_2; host rock quartzite) to about 4.5 percent (62 percent SiO_2; host rock limestone) modal biotite increases from less than 1 percent to about 25 percent, as illustrated in figure 2, which is based on data for 86 rocks. Microcline-perthite coexists with biotite in all but the most mafic rocks; indeed, the potassium economy of these hybrid rocks is for the most part summarized by the trend for biotite (fig. 2) and an opposite trend for microcline-perthite, as shown in detail by Lee and Van Loenen (1970). Quartz and plagioclase are present in all these rocks.

Magnetite is one of the most abundant accessory minerals in the more mafic parts of the Snake Creek–Williams Canyon intrusive outcrop area, being present in amounts of 0.50 weight percent and more. Magnetite tends to be somewhat less abundant in the more felsic parts of the intrusive. In those rocks having less than about 1.0 percent CaO (74 percent SiO_2), magnetite is either absent or present in amounts of less than 0.05 weight percent. In the most felsic rocks, where magnetite is absent, ilmenite is present. Where CaO content of the rock is between 1.0 and 2.0 percent, ilmenite and magnetite usually coexist; few rocks having

more than 2.0 percent CaO (72 percent SiO_2) contain ilmenite.

Eight biotites from the Snake Creek–Williams Canyon intrusive (table 1) were studied. (The rocks yielding three of them—238–MW–61, 40B–MW–60, and 27–DL–61—were described by Lee and Van Loenen, 1970). In general, none of the eight biotites appears unusual in thin section, and like many other biotites described in the literature they tend to be associated with whatever accessory minerals are present. Biotite in the most felsic rocks is pleochroic from buff to reddish brown and contains inclusions. These inclusions probably are monazite, and each is surrounded by a halo that is dark but not pleochroic. Rocks having more than about 1.1 percent CaO contain biotite that is pleochroic from straw color to dark olive green. Some of this biotite contains inclusions of accessory minerals, mostly apatite, but none of these inclusions is surrounded by a halo.

The undeformed rocks in the Young Canyon–Kious Basin area are, as noted previously, exposed in contact with quartzite. Mineralogically and petrographically they resemble the more felsic parts of the hybrid granitoid rock in the Snake Creek–Williams Canyon area.

Megascopically and petrographically the granitoid rocks of the Pole Canyon–Can Young Canyon area are distinct from all other igneous rocks in the area. Four biotites were studied (table 1). (Rock sample 135–DL–62 is described by Lee and Van Loenen, 1970.) Typically, phenocrysts of muscovite as large as 2 cm across contain small biotite euhedra that are easily visible with a hand lens. It is not uncommon for as many as 20 biotite crystals to be included within a single large grain of muscovite. Petrographically the muscovite and biotite, both of which are very fresh looking, are seen to be associated and often intergrown. They appear to have formed in equilibrium. The muscovite contains no dark inclusions, nor does it present any other evidence that it is secondary after biotite. All the granitoid rocks of the Pole Canyon–Can Young Canyon area contain microcline, plagioclase, and quartz, but they are devoid of magnetite, ilmenite, and sphene, these minerals being undetected not only in thin section but also during systematic mineral separation work on the rocks from which the micas represented in table 1 were recovered.

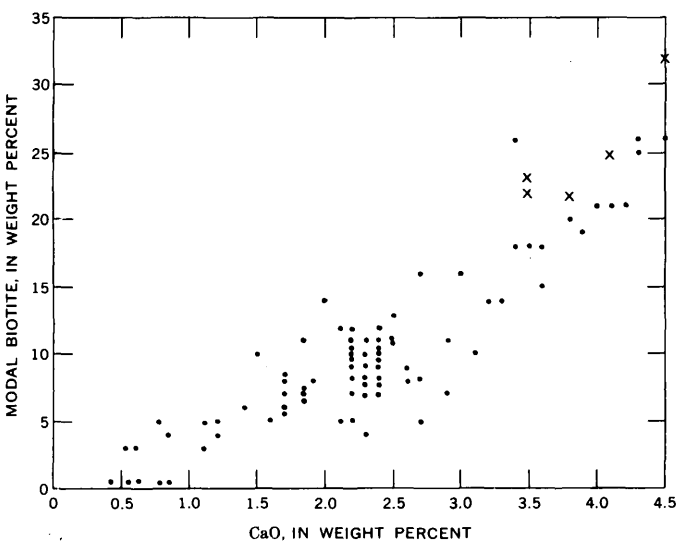

FIGURE 2.—Relation between CaO and modal biotite contents of hybrid granitoid rocks of the Snake Creek–Williams Canyon area. Dot, main intrusive phase; x, xenolith. From Lee and Van Loenen (1970).

BIOTITE ANALYSES AND PHYSICAL PROPERTIES

Method of sample preparation and analysis

The biotite concentrates were ground to −150 mesh (105 microns), and material smaller than about 40 microns was removed by washing in tapwater. The concentrate was then washed with acetone and dried, and final purification was by centrifuging in adjusted mixtures of methylene iodide and bromoform and by repeated passes through the Frantz isodynamic separator. Except for sample 238–MW–61 (table 1), each of the 14 biotites purified for this study made up at least 5 percent of the rock from which it was recovered (see fig. 2). Even though we had fairly large concentrates, purifying these biotites for analysis was rather difficult. Each biotite fractionated over a large specific gravity range, and recovering a homogeneous sample for analysis was difficult—that is, recovering a workable amount of material from within a reasonably narrow specific gravity range (ranges for analyzed biotites are shown in table 1) somewhere near the upper (fresher) part of the overall observed range. Moreover, the large range of specific gravity of the clean biotite grains present in any one rock made it difficult to determine when a biotite fraction was clean enough for analysis. If a mineral fractionates over a narrow specific gravity range, then by centrifuging very carefully at high speeds just on either side of that range the operator can reject most grains containing inclusions that are either lighter or heavier than the candidate for analysis. Nevertheless, we were unable to use this technique effectively during purification of these biotites, and in many instances, after microscopic study indicated a carefully prepared biotite fraction to be

clean enough for analysis, we still could shake loose a startling amount of contaminants by subjecting the "pure" biotite to ultrasonic vibration for about 15 minutes. The contaminants consisted of all the accessory minerals with which the biotite was seen to be closely associated in thin section. Some of the apatite and zircon shaken loose were euhedra about 25 microns long. The ultrasonic treatment must be applied to biotite with care, for it tends to erode away individual grains rather quickly.

Major elements

Biotite analyses (table 1) are grouped according to the three masses, or areas, already discussed. Major elements were determined by chemical methods described by Peck (1964) and calculated on the basis of 24(O, OH, Cl, F) to the general mica formula $X_2Y_{4-6}Z_8O_{20}(OH, F, Cl)_4$, using the computer program described by Jackson, Stevens, and Bowen (1967).

In calculating the structural formulas of these biotites, we have included the small amount of Ca present with the X group of the 12 coordinated large cations. However, whether or not Ca is actually included in the crystal structure of any of the biotites in table 1 is uncertain. The only three of these biotites (151–MW–61, 27–DL–61, and 98–DL–61) that were not subjected to the ultrasonic treatment described above are those biotites showing the largest amounts of CaO (0.22, 0.28, and 0.30 percent, respectively).

Let us consider now the eight biotites from the Snake Creek–Williams Canyon area, arranged in table 1 according to CaO (and SiO_2) contents of rocks from which the constituent biotites were recovered. These rocks were collected over a horizontal distance of about 6 miles. Excluding 190–DL–62, from the west side of the range north of the Williams Creek drainage, the other seven samples are from within a horizontal distance of about 3 miles. The major-element contents of these biotites show a number of trends that relate to the bulk chemistry of these hybrid rocks.

Totals for large cations of the X group fall in the range 1.89–2.02 ions per formula unit, fairly close to the ideal 2.00. The Na_2O contents of these biotites never exceed 0.50 weight percent of individual analyses, but within this restricted range the ratio Na/K+Na shows a trend toward higher values for those biotites from the more felsic rocks (fig. 3). This trend relates to the anorthite contents of the plagioclase feldspars coexisting with these biotites (see table 1). That is, lower activity of albite in the system correlates with less Na_2O in the biotite. Dodge, Smith, and Mays (1969) also found a tendency for Na to increase in biotites with higher Fe/Fe+Mg, that is, biotites from more felsic rocks.

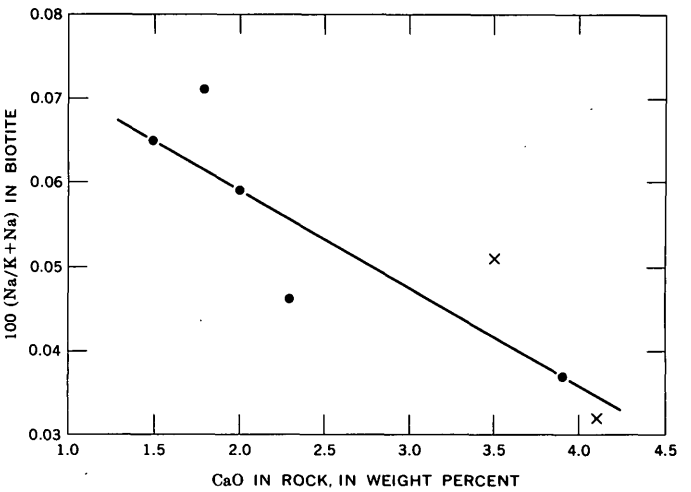

FIGURE 3.—Relation between CaO content of rock and 100 (Na/K+Na) in constituent biotite for hybrid granitoid rocks of the Snake Creek–Williams Canyon area. Data from table 1. Dot, main intrusive phase; x, xenolith.

Octahedral sites occupied by Y group cations are all in the range 5.70–5.77 ions per formula unit, compared with 6.00 in the idealized trioctahedral mica. The Fe^{+2}, Fe^{+3}, and Mg cations in this group are best considered from the standpoint of experimental work on biotite stabilities, and so the well-defined trends involving these cations are discussed in the following section on biotite petrogenesis.

Mn contents are higher in biotites from the more felsic rocks, and the trend is especially marked if we consider only those biotites from the main intrusive phase (excluding xenoliths). Inasmuch as the MnO content of the rock is fairly constant (fig. 4) and most of the MnO is in the biotite, then the MnO content of the biotite is, expectably, inversely related to the amount of biotite in the rock. The dearth of sites available for Mn^{+2} ions in the most Ca-poor rocks is indicated by the presence in these rocks of small amounts of Mn-rich garnets, and, as noted in the following section, Mn-rich ilmenites.

Biotites from rocks of the Snake Creek–Williams Canyon area show a remarkable increase of F with decrease in CaO content of the rock, as shown in figure 5, which includes data for four additional samples (table 2). This striking trend is easily explained by figures 2 and 5 and the same reasoning outlined for MnO. Apatite and muscovite, present in small amounts, are the only other fluorine-bearing minerals in these rocks.

TABLE 1.—*Analytical data for biotites*

[Sampled areas shown roughly on figure 1; exact sample localities shown on geologic map by Lee and Van Loenen (1970). Within each area, samples arranged in order of increasing CaO content and decreasing SiO_2 content for whole rock. Leaders (---), not determined. CaO and SiO analyses by Paul Elmore, Samuel Botts, Gillison Chloe, and Lowell Artis (Lee and Van Loenen, 1970). Specific gravity determined by centrifuging in bromoform-methylene iodide mixtures of known specific gravity. Indices of refraction determined in sodium light by the immersion method; all these biotites are seemingly uniaxial. Anorthite content of coexisting plagioclase from Lee and Van Loenen (1970). Chemical analyses of biotites: samples 238-MW-61, 151-MW-61, 135-DL-62, 122-DL-62, and 120-MW-60 analyzed by Elaine L.

Area	Snake Creek–Williams Canyon					
Sample No.	238-MW-61	147-MW-61	151-MW-61	190-DL-62	8-DL-61	40B-MW-60[1]
CaO content of whole rock (weight percent)	0.78	1.5	1.8	2.0	2.3	3.5
SiO_2 content of whole rock (weight percent)	74.9	73.4	73.2	71.4	70.9	65.8
Anorthite content of coexisting plagioclase	3	18	20	24	25	26
Physical properties of analyzed biotites						
Specific gravity:						
Average	3.08	3.07	3.08	3.09	3.06	3.08
Range	3.04–3.12	3.05–3.09	3.07–3.09	3.07–3.11	3.04–3.08	3.06–3.10
Refractive index:						
β (average)	1.653	1.649	1.653	1.655	1.646	1.652
Chemical analyses of biotites (weight percent)						
SiO_2	35.46	36.49	36.48	35.96	36.57	36.48
Al_2O_3	16.25	15.91	16.01	16.33	16.11	16.26
Fe_2O_3	2.71	2.95	3.09	2.70	3.85	3.69
FeO	18.99	16.69	17.06	17.73	16.38	16.63
MgO	9.42	10.30	9.89	9.62	10.42	9.93
CaO	.00	.00	.22	.00	.02	.08
Na_2O	-----	.45	.48	.41	.29	.34
K_2O	-----	9.60	9.48	9.65	9.58	9.59
H_2O+	-----	2.90	-----	2.93	3.26	3.20
H_2O-	.08	.06	.02	.05	.08	.04
TiO_2	2.84	3.02	2.56	3.26	2.09	2.54
P_2O_5	-----	.01	-----	.01	.02	.04
MnO	-----	.77	-----	.61	.56	.61
Cl	.03	.02	.02	.03	.03	.03
F	1.13	.92	.69	.67	.47	.45
Subtotal		100.09		99.96	99.73	99.91
Less O ≡ Cl, F		.39		.29	.20	.20
Total		99.70		99.67	99.53	99.71
Structural formulas						
Z Si	-----	5.59 | 8.00	-----	5.54 | 8.00	5.59 | 8.00	5.58 | 8.00
Z Al (V)	-----	2.41	-----	2.46	2.41	2.42
Y Al (VI)	-----	.46	-----	.50	.50	.51
Y Fe^{+3}	-----	.34	-----	.32	.44	.43
Y Ti	-----	.35 | 5.74	-----	.38 | 5.77	.24 | 5.73	.29 | 5.70
Y Mg	-----	2.35	-----	2.21	2.38	2.26
Y Fe^{+2}	-----	2.14	-----	2.28	2.10	2.13
Y Mn	-----	.10	-----	.08	.07	.08
X Ca	-----	.00	-----	.00	.00	.01
X Na	-----	.13 | 2.01	-----	.12 | 2.02	.09 | 1.96	.10 | 1.98
X K	-----	1.88	-----	1.90	1.87	1.87
OH	-----	2.96	-----	3.01	3.33	3.26
F	-----	.45 | 3.42	-----	.33 | 3.35	.23 | 3.57	.22 | 3.49
Cl	-----	.01	-----	.01	.01	.01
Atomic ratios						
Fe^{+3}	6.4	7.0	7.4	6.7	8.9	8.9
Fe^{+2}	49.7	44.3	45.5	47.4	42.7	44.2
Mg	43.9	48.7	47.1	45.9	48.4	46.9
100(Fe/Fe + Mg)	56.1	51.3	52.9	54.1	51.6	53.1
100(Na/K + Na)	-----	6.5	7.1	5.9	4.6	5.1
Semiquantitative spectrographic analyses of minor elements (weight percent)						
Ba	0.3	0.5	0.5	0.5	0.5	0.5
Be	.0002	.0002	.0002	0	.0002	.0003
Co	.003	.003	.005	.005	.005	.005
Cr	.007	.01	.01	.007	.01	.0003
Cu	.0015	.0005	.002	.0003	.0015	.001
Ga	.01	.007	.007	.005	.005	.007
Li	.15	.15	.15	.15	.07	.1
Nb	.03	.015	.007	.01	.002	0
Ni	.005	.005	.005	.005	.005	.001
Pb	.002	0	.002	0	0	0
Sc	.015	.01	.01	.007	.003	.003
Sn	.007	.003	.002	.003	0	.001
Sr	0	0	0	0	0	0
V	.05	.05	.07	.05	.07	.07
Zn	0	0	0	0	0	0
Zr	0	0	0	0	0	0

[1] Biotite from xenolith.

from the southern Snake Range, Nevada

Munson; all other samples analyzed by Vertie C. Smith. Semiquantitative spectrographic analyses by R. E. Mays. Results are based on their identity with geometric brackets whose boundaries are 1.2, 0.83, 0.56, 0.38, 0.26, 0.18, 0.12, and so forth, and are reported arbitrarily as midpoints of these brackets: 1., 0.7, 0.5, 0.3, 0.2, 0.15, and 0.1, respectively. The precision of a reported value is approximately plus or minus one bracket at 68-percent confidence, or two brackets at 95-percent confidence. 0, below limit of spectrographic detection]

		Pole Canyon–Can Young Canyon				Young Canyon–Kious Basin	
43-DL-61	27-DL-61[1]	135-DL-62	122-DL-62	120-MW-60	226-MW-60	234-MW-61	98-DL-62[1]
3.9	4.1	0.98	1.1	1.3	1.3	1.6	4.5
66.8	66.2	72.3	73.0	71.6	73.9	72.8	57.4
24	27	----	----	----	----	----	----
Physical properties of analyzed biotites							
3.03	3.03	3.05	3.12	3.10	3.06	3.09	3.06
3.01–3.05	3.01–3.05	3.03–3.07	3.10–3.14	3.08–3.12	3.04–3.08	3.07–3.11	3.05–3.07
1.645	1.642	1.676	1.681	1.680	1.680	1.643	1.653
Chemical analyses of biotites (weight percent)							
36.78	37.22	36.39	36.30	36.42	-----	36.63	37.10
16.78	15.93	17.22	17.57	17.47	-----	16.38	16.29
3.08	2.65	14.94	4.03	11.71	-----	2.90	3.82
15.66	14.58	8.87	19.14	11.21	-----	16.84	15.84
11.67	12.45	6.18	6.03	6.10	-----	9.55	9.63
.00	.28	.13	.03	.10	-----	.04	.30
.24	.19	.33	.64	.57	-----	.35	.40
9.46	9.48	8.77	9.40	8.93	-----	9.76	9.44
3.62	3.43	3.66	2.92	3.41	-----	2.59	3.17
.06	.15	.38	.10	.39	-----	.09	.15
2.03	2.46	2.17	2.46	2.45	-----	2.92	3.03
.00	.02	.03	.05	-----	-----	.07	.10
.25	.38	.39	.67	.69	-----	.82	.45
.03	.04	.01	.01	.02	-----	.02	.02
.33	.37	.71	1.11	.95	-----	1.58	.71
99.99	99.63	100.18	100.46	100.42		100.54	100.45
.14	.17	.30	.47	.40		.67	.30
99.85	99.46	99.88	99.99	100.02		99.87	100.15
Structural formulas							
5.54 } 8.00	5.62 } 8.00	5.47 } 8.00	5.60 } 8.00	5.50 } 8.00	-----	5.61 } 8.00	5.62 } 8.00
2.46	2.38	2.53	2.40	2.50	-----	2.39	2.38
.52	.46	.52	.79	.61	-----	.57	.52
.35	.30	1.69	.47	1.33	-----	.33	.44
.23 } 5.72	.28 } 5.73	.25 } 5.00	.29 } 5.50	.28 } 5.10	-----	.34 } 5.68	.35 } 5.55
2.62	2.80	1.38	1.39	1.37	-----	2.18	2.17
1.97	1.84	1.11	2.47	1.42	-----	2.15	2.10
.03	.05	.05	.09	.09	-----	.11	.06
.00	.05	.02	.01	.02	-----	.01	.05
.07 } 1.89	.06 } 1.94	.10 } 1.80	.19 } 2.05	.17 } 1.91	-----	.10 } 2.02	.12 } 1.99
1.82	1.83	1.68	1.85	1.72	-----	1.91	1.82
3.64	3.45	3.67	3.00	3.44	-----	2.64	3.20
.16 } 3.81	.18 } 3.64	.34 } 4.01	.54 } 3.54	.45 } 3.90	-----	.77 } 3.42	.34 } 3.55
.01	.01	.00	.00	.01	-----	.01	.01
Atomic ratios							
7.1	6.1	40.4	10.9	32.3	-----	7.1	9.5
39.9	37.2	26.6	57.0	34.5	-----	46.1	43.5
53.0	56.7	33.0	32.1	33.2	-----	46.8	47.0
47.0	43.3	67.0	67.9	66.8	-----	53.2	53.0
3.7	3.2	5.6	9.3	9.0	-----	5.0	6.2
Semiquantitative spectrographic analyses of minor elements (weight percent)							
0.5	0.3	0.07	0.07	0.05	0.05	0.15	0.15
0	0	0	.0002	0	.0005	0	0
.005	.003	.0015	0	.0015	.0015	.003	.003
.02	.02	.001	.0007	.001	0	.0015	.0007
.002	.005	.003	.0007	.005	.007	.0015	.002
.005	.005	.007	.015	.007	.005	.007	.007
.07	0	.1	0	.2	.1	.2	.07
0	.002	.005	.005	.01	.01	.015	.003
.01	.015	.001	.0003	.001	.007	.002	.002
0	0	0	0	0	.005	0	0
0	.0015	0	.005	.0015	0	.01	.003
0	0	0	.003	0	0	.007	0
0	0	.003	.005	0	.005	0	.002
.07	.05	.007	.015	.01	.01	.03	.05
0	.05	.1	.1	.1	.15	.1	.07
0	0	.003	.007	.01	.007	.005	0

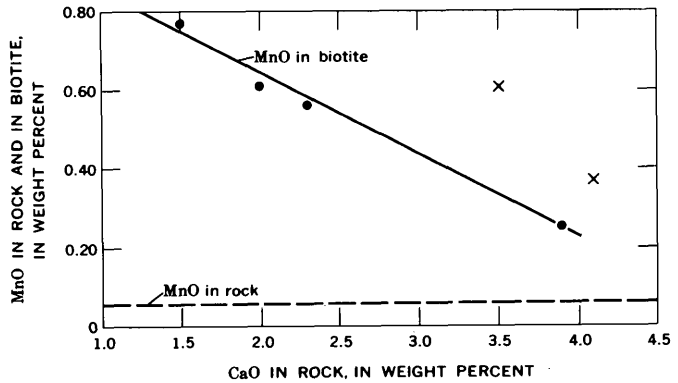

FIGURE 4.—Relation between CaO in rock and MnO in rock and in constituent biotite for samples from the Snake Creek–Williams Canyon area. Dot, main intrusive phase; x, xenolith. Data for biotite from table 1. Trend shown for rocks based on MnO analyses of 87 rocks (Lee and Van Loenen, 1970).

Major-element contents of the biotites from rocks of the Pole Canyon–Can Young Canyon area differ in several respects from those just discussed, as considered below in the section on petrogenesis. The major-element contents of the two biotites from the Young Canyon–Kious Basin area fit rather well into the chemical trends expressed by biotites from the Snake Creek–Williams Canyon area, as one would expect from the geologic setting of the analyzed biotites.

Minor elements

Minor-element contents of biotites (table 1) were semiquantitatively determined by emission spectrography. Despite the relatively low precision of this method (explained in table 1), certain minor-element trends and diffferences among these biotites are well defined.

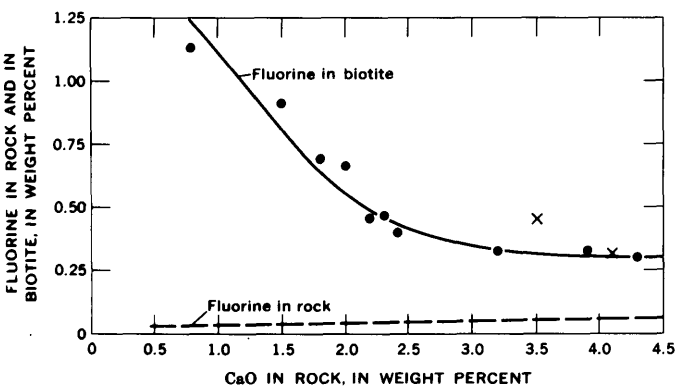

FIGURE 5.—Relation between CaO in rock and fluorine in rock and in constituent biotite for samples from the Snake Creek–Williams Canyon area. Dot, main intrusive phase; x, xenolith. Data for biotite from tables 1 and 2. Trend shown for rocks based on fluorine analyses of 37 rocks (Lee and Van Loenen, 1970).

TABLE 2.—*CaO contents of four rocks from the Snake Creek–Williams Canyon area and F and Cl contents of constituent biotites*

[Analyses, in weight percent, by Vertie S. Smith. Leaders (----), not determined]

Sample No.	Rock CaO	Biotite F	Biotite Cl
14–MW–60	2.2	0.47	0.01
31–DL–61	2.4	.40	.03
152–MW–61	3.2	.33	.02
16–MW–60	4.3	.32	---

If one considers only the Snake Creek–Williams Canyon area, Li, Nb, Sc, and Sn contents are higher in those biotites from the more felsic rocks. None of the minor elements listed shows a very clear tendency to increase in the opposite direction.

As a group, the Snake Creek–Williams Canyon biotites contain more Ba, Co, Cr, Sc, and V, and less Sr, Zn, and Zr than do the biotites of the Pole Canyon–Can Young Canyon area.

The biotites listed in table 1 all contain much more Li than do the 200 samples of biotite studied by Lovering (1969).

X-ray properties

X-ray diffraction work was done on a split of each of the analyzed biotites in table 1, using fluorite as an internal standard. Oriented and disoriented mounts of each sample were scanned from 8° 2θ to 65° 2θ at a speed of ¼° per minute. However, we were unable to refine the measured 2θ values into meaningful cell parameters, even by the method described by Dodge, Smith, and Mays (1969, p. 263).

The d_{060} peak is an apparently reliable measure of b (Wones, 1963). The (060) interplanar spacings of the biotites in table 1 are a constant 1.5413±0.0015 A regardless of composition. These results are in good agreement with those of Dodge, Smith, and Mays, who found the (060) interplanar spacings of the biotites from the Sierra Nevada to be a constant 1.543±0.002 A.

The basal (005) interplanar spacing (table 3) varies rather widely from sample to sample. An increase in F is accompanied by a decrease in d_{005} (fig. 6), a relation also found by Müller (1966) and Dodge, Smith, and Mays (1969).

PETROGENESIS OF BIOTITES

The data in table 1 are of petrologic interest for two main reasons:

1. Relatively large and systematic differences exist in the element contents of biotites from the Snake Creek–Williams Canyon area, a granitoid outcrop area of about 10 square miles.

TABLE 3.—*Basal (005) interplanar spacings of biotites in table 1*

[Internal standard was CaF_2. Margin of error for all spacing measurements is ±0.0002 A]

Sample No.	(005) spacing (angstroms)
238–MW–61	2.0121
147–MW–61	2.0119
151–MW–61	2.0140
190–DL–62	2.0128
8–DL–61	2.0149
40B–MW–60	2.0140
43–DL–61	2.0157
27–DL–61	2.0155
135–DL–62	2.0081
122–DL–62	2.0096
120–MW–60	2.0107
226–MW–60	2.0087
234–MW–61	2.0090
98–DL–61	2.0120

2. Striking compositional differences are present between these biotites as a group and those of the adjoining Pole Canyon–Can Young Canyon area, a distinct granitoid outcrop area of about 3 square miles.

Experimental work by Wones and Eugster (1965) shows the stability of biotites on the phlogopite-annite join in terms of temperature and oxygen fugacity; and the results of this experimental work may be applied to the data in table 1 by assuming that components other than Mg^{+2} have the same effect as Mg^{+2} on the stability of the annite end member, although it should be noted that Rutherford's (1969) data show that Na_2O will lower the stability of very iron rich biotites.

Biotites of the Snake Creek–Williams Canyon and Young Canyon–Kious Basin areas plot within the compositional triangle Fe^{+3}–Fe^{+2}–Mg (fig. 7) along a trend paralleling compositions of "buffered" biotites in the ternary system $KFe_3^{+3}AlSi_3O_{12}(H_{-1})$–$KFe_3^{+2}AlSi_3O_{10}(OH)_2$–$KMg_3AlSi_3O_{10}(OH)_2$ (Wones and Eugster, 1965, p. 1232); oxygen fugacities are thus slightly greater than those of the Ni–NiO buffer.

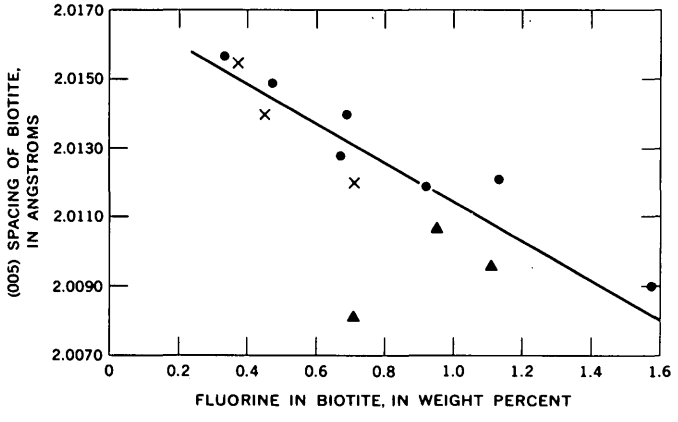

FIGURE 6.—Relation between basal (005) spacings and fluorine contents of biotites in tables 1 and 3. Biotites coexisting with potassium feldspar and magnetite, from Snake Creek–Williams Canyon and Young Canyon–Kious Basin areas: dot, main intrusive phase; x, xenolith. Triangle, biotites coexisting with potassium feldspar; from Pole Canyon–Can Young Canyon area.

Although rock sample 238–MW–61 contains only trace amounts (<0.05 weight percent) of magnetite, all analyzed biotites of the Snake Creek–Williams Canyon area are members of the assemblage potassium feldspar-magnetite-biotite, and the compositional trend of these biotites in figure 7 no doubt reflects the "buffering" effect of magnetite in the crystallizing magma.

Biotites 238–MW–61, 147–MW–61, 151–MW–61, and 190–DL–62 also coexist with 0.05–0.15 weight percent ilmenite, and these same biotites have lower Fe^{+3} contents than most of the biotites coexisting with magnetite alone, indicating crystallization under more reducing conditions. However, we emphasize that these are Mn-rich ilmenites, containing as much as 13 percent MnO (unpub. data), and thus experimental data on f_{O_2}–T stability relations of ilmenite ($FeTiO_3$) (Buddington and Lindsley, 1964) may not be directly applicable.

In the presence of a given buffer, such as the magnetite, oxygen fugacity decreases as temperature decreases. Other conditions being equal, decreasing fugacity of oxygen results in higher

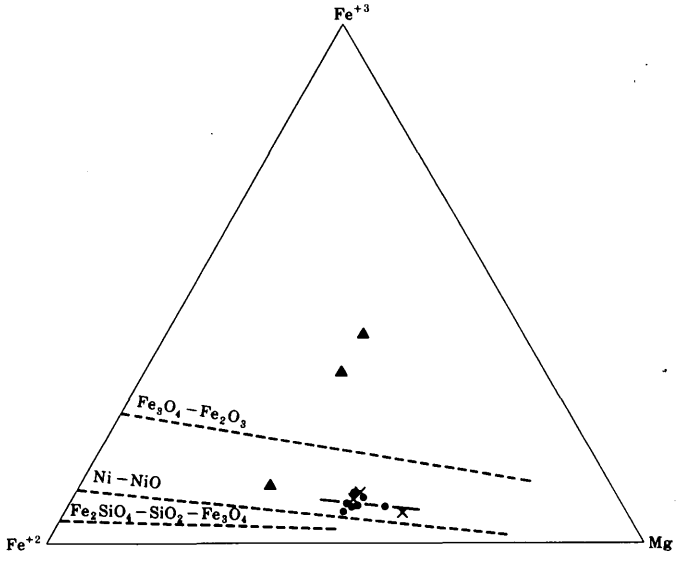

FIGURE 7.—Relation of Fe^{+3}–Fe^{+2}–Mg contents of biotites in table 1. Dashed lines represent compositions of "buffered" biotites in the ternary system $KFe_3^{+3}AlSi_3O_{12}(H_{-1})$–$KFe_3^{+2}AlSi_3O_{10}(OH)_2$–$KMg_3AlSi_3O_{10}(OH)_2$ depicted by Wones and Eugster (1965, fig. 1). Biotites coexisting with potassium feldspar and magnetite; from Snake Creek–Williams Canyon and Young Canyon–Kious Basin areas: dot, main intrusive phase; x, xenolith. Triangle, biotites coexisting with potassium feldspar; from Pole Canyon–Can Young Canyon area.

Fe/Fe+Mg for the biotites that will crystallize from a magma. Relations at 2,070 bars total pressure are shown by Wones and Eugster (1965, fig. 4) and in figure 8, which also indicates the range of compositions of the Snake Creek–Williams Canyon biotites. Dodge, Smith, and Mays (1969) described the range of compositions of 34 biotites recovered from granitoid rocks collected from within an area of about 5,000 square miles of the central Sierra Nevada batholith, California. Although the 100 (Fe/Fe+Mg) values for the Sierra Nevada biotites show the larger range (43.7–72.6), the range of the same ratio for the Snake Creek–Williams Canyon biotites (43.3–56.1) is impressive, inasmuch as a systematic change from lower to higher values occurred over an outcrop area of only a few square miles. The range 43.3–56.1 is consistent with the results of Wones and Eugster's (1965) experimental work and with the observation that the chemistry of these hybrid granitoid rocks, controlled by liquid⇌crystal equilibria, represents the equivalent of a large part (62–76 percent SiO_2; differentiation index 64–92) of the classic differentiation sequence (Lee and Van Loenen, 1970).

In general, the minor-element trends (table 1) correlate well; increase of Sc and Sn with Fe/Fe+Mg was also noted by Dodge, Smith, and Mays (1969), and larger contents of Li in biotites from the more felsic rocks (table 1) are expected. The trend shown for Nb (the opposite of that noted by Dodge and others) might result more from the compositions of the rocks themselves (Lee and Bastron, 1967) and associated minerals than from temperature of formation. Nockolds and Mitchell (1946), Herz and Dutra (1964), and Dodge, Smith, and Mays (1969) all noted increase of Co, Cr, and Ni with temperature. The lack of such trends in our data probably results from the mineralogy and Co, Cr, and Ni contents of the rocks, given by Lee and Van Loenen (1970).

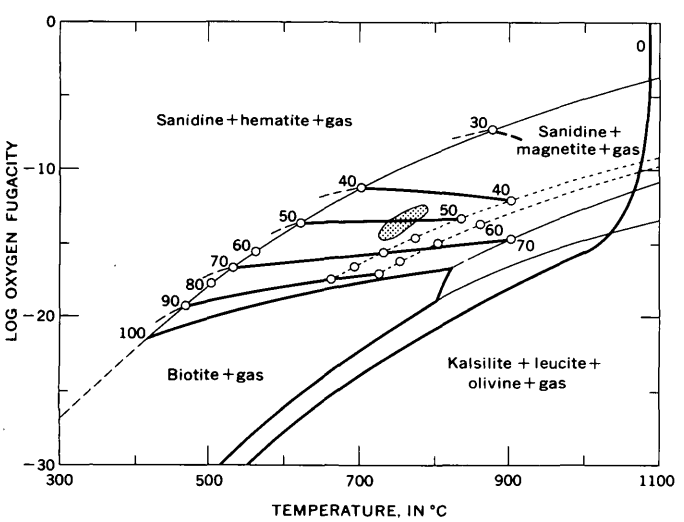

FIGURE 8.—Stability of biotites of specific Fe/Fe+Mg values as a function of log oxygen fugacity and temperature at 2,070 bars total pressure. Thick lines represent contours of constant 100(Fe/Fe+Mg) values. Thin lines and dotted lines depict "buffer" curves. Shaded area represents compositions of Snake Creek–Williams Canyon area biotites along the assumed oxygen fugacity trend of the crystallizing hybrid magma. Compare Dodge, Smith, and Mays (1969, fig. 9). Diagram from Wones and Eugster (1965, fig. 4).

Consider now the large compositional differences between the biotites just discussed and those of the adjacent Pole Canyon–Can Young Canyon area. There coexisting essential minerals are quartz, plagioclase, microcline-perthite, and muscovite; accessory minerals are sparse and include only rather coarse-grained apatite containing tiny acicular zircon and trace amounts of monazite and an allanite-like mineral.

Although MgO contents of the three Pole Canyon–Can Young Canyon biotites are in the range 6.03–6.18 percent, and most other major-element contents are similar from one biotite to another, Fe_2O_3/FeO values differ greatly. The almost identical MgO contents of these biotites would seem to indicate that they were initially equilibrated with respect to the same (relatively low) oxygen fugacity. Localized conditions subsequent to magmatic crystallization may have altered Fe_2O_3/FeO values of the biotites without modifying the overall mineralogy of the rock. The granitoid rocks of this area were pervasively intruded by a late aplitic phase (Lee and Van Loenen, 1970); moreover, biotite 135–DL–62 (14.94 percent Fe_2O_3) comes from an area of the intrusive cut by relatively late shears, and gives an abnormally low radiometric age date, owing to loss of argon (Lee and others, 1970) (p. D92–D102, this chapter).

The differences between minor-element contents of these three biotites and those of the Snake Creek–Williams Canyon area are not obviously related to the chemistry (given by Lee and Van Loenen, 1970) of the rock types undergoing assimilation in the respective areas, nor for the most part can these differences be explained on the basis of the minor-element contents of minerals coexisting with these biotites. One might speculate that there were differences in the minor-element contents of the "source magmas" of the two areas, or significant differences in temperature of formation for the two groups of biotites. Yet neither of these ideas

fits very well with the fact that the rock types containing these micas appear in outcrop separated by a septum of sedimentary rocks a mile long and only about 1,000 feet wide.

SUMMARY AND CONCLUSIONS

Compositions of these biotites support our earlier conclusions based on fieldwork and petrographic and petrochemical work and indicate distinctly different magmatic affinities for rocks from the closely adjacent granitoid outcrops of the Snake Creek–Williams Canyon and Pole Canyon–Can Young Canyon areas.

Within the Snake Creek–Williams Canyon area the large range of biotite compositions found is commensurate with the large range of composition of the hybrid granitoid rocks themselves. This range of granitoid rock composition, resulting from assimilation of such chemically diverse host rocks as limestone and quartzite, represents the equivalent of a large part (62–76 percent SiO_2; differentiation index 64–92) of the classic differentiation sequence, because the end product has resulted from liquid⇄crystal equilibria. For the same reason compositions of the biotites within these rocks resemble those expectable in a series of differentiates. The biotite crystallizing from the Snake Creek–Williams Canyon rocks followed a more iron-rich trend because oxygen fugacity decreased with temperature, owing to the "buffering" action of magnetite (Wones and Eugster, 1965). Some of the minor-element contents of these biotites also relate to temperature of formation; thus Li, Nb, Sc, and Sn contents are higher in biotites from the more felsic rocks. On the other hand, well-defined increase of MnO and F in biotites from more felsic rocks probably is due less to temperature of formation than to lack of available sites for the Mn^{+2} and F^{-1} ions present in the surrounding magma during crystallization.

From the standpoint of the experimental work of Wones and Eugster (1965), biotites from the Pole Canyon–Can Young Canyon area are distinguished mainly by their low and very similar contents of MgO, indicating initial equilibration with respect to a relatively low oxygen fugacity. Sharply different Fe_2O_3/FeO values in these biotites probably are the result of postmagmatic processes.

REFERENCES

Buddington, A. F., and Lindsley, D. H., 1964, Iron-titanium oxide minerals and synthetic equivalents: Jour. Petrology, v. 5, no. 2, p. 310–357.

Dodge, F. C. W., Smith, V. C., and Mays, R. E., 1969, Biotites from granitic rocks of the central Sierra Nevada batholith, California: Jour. Petrology, v. 10, no. 2, p. 250–271.

Drewes, H. D., 1958, Structural geology of the southern Snake Range, Nevada: Geol. Soc. America Bull., v. 69, no. 2, p. 221–239.

Herz, Norman, and Dutra, C. V., 1964, Cobalt, nickel, chromium, scandium and niobium in biotite, and the scandium geological thermometer: Soc. Brasileira Geologia Bol., v. 13, p. 23–42.

Hose, R. K., and Blake, M. C., Jr., 1970, Geologic map of White Pine County, Nevada: U.S. Geol. Survey open-file map, scale 1:150,000.

Jackson, E. D., Stevens, R. E., and Bowen, R. W., 1967, A computer-based procedure for deriving mineral formulas from mineral analyses, *in* Geological Survey Research 1967: U.S. Geol. Survey Prof. Paper 575–C, p. C23–C31.

Lee, D. E., and Bastron, Harry, 1967, Fractionation of rare-earth elements in allanite and monazite as related to geology of the Mt. Wheeler mine area, Nevada: Geochim. et Cosmochim. Acta, v. 31, no. 3, p. 339–356.

Lee, D. E., Marvin, R. F., Stern, T. W., and Peterman, Z. E., 1970, Modification of potassium-argon ages by Tertiary thrusting in the Snake Range, White Pine County, Nevada, *in* Geological Survey Research 1970: U.S. Geol. Survey Prof. Paper 700–D, p. D92–D102.

Lee, D. E., Mays, R. E., Van Loenen, R. E., and Rose, H. J., Jr., 1969, Accessory sphene from hybrid rocks of the Mount Wheeler mine area, Nevada, *in* Geological Survey Research 1969: U.S. Geol. Survey Prof. Paper 650–B, p. B41–B46.

Lee, D. E., Stern, T. W., Mays, R. E., and Van Loenen, R. E., 1968, Accessory zircon from granitoid rocks of the Mount Wheeler mine area, Nevada, *in* Geological Survey Research 1968: U.S. Geol. Survey Prof. Paper 600–D, p. D197–D203.

Lee, D. E., and Van Loenen, R. E., 1970, Hybrid granitoid rocks of the southern Snake Range, Nevada: U.S. Geol. Survey Prof. Paper 668. [In press]

Lovering, T. G., 1969, Distribution of minor elements in samples of biotite from igneous rocks, *in* Geological Survey Research 1969: U.S. Geol. Survey Prof. Paper 650–B, p. B101–B106.

Misch, Peter, and Hazzard, J. C., 1962, Stratigraphy and metamorphism of Late Precambrian rocks in central northeastern Nevada and adjacent Utah: Am. Assoc. Petroleum Geologists Bull., v. 46, no. 3, pt. 1, p. 289–343.

Müller, Georg, 1966, Der Einfluss verschiedener Substitutionen auf die Gitterkonstanten von koexistierenden Biotiten und Muskowiten: Contr. Mineralogy and Petrology, v. 13, no. 1, p. 59–74.

Nockolds, S. R., and Mitchell, R. L., 1946, The geochemistry of some Caledonian plutonic rocks; a study in the relationship between the major and trace elements of igneous rocks and their minerals: Royal Soc. Edinburgh Trans., v. 61, pt. 2, p. 533–575 [1948].

Peck, L. C., 1964, Systematic analysis of silicates: U.S. Geol. Survey Bull. 1170, 89 p.

Rutherford, M. J., 1969, An experimental determination of iron biotite-alkali feldspar equilibria: Jour. Petrology, v. 10, no. 3, p. 381–408.

Whitebread, D. H., Griggs, A. B., Rogers, W. B., and Mytton, J. W., 1962, Preliminary geologic map and sections of the Wheeler Peak quadrangle, White Pine County, Nevada: U.S. Geol. Survey Mineral Inv. Field Studies Map MF–244.

——— 1970, Geologic map of the Wheeler Peak and Garrison quadrangles, White Pine County, Nevada, and Milford County, Utah: U.S. Geol. Survey Misc. Geol. Inv. Map I–578.

Wones, D. R., 1963, Physical properties of synthetic biotites on the join phlogopite-annite: Am. Mineralogist, v. 48, nos. 11–12, p. 1300–1321.

Wones, D. R., and Eugster, H. P., 1965, Stability of biotite —Experiment, theory, and application: Am. Mineralogist, v. 50, no. 9, p. 1228–1272.

INFLUENCE OF GRAIN SIZE ON PERCENTAGES OF ThO_2 AND U_3O_8 IN DETRITAL MONAZITE FROM NORTH CAROLINA AND SOUTH CAROLINA

By WILLIAM C. OVERSTREET, JESSE J. WARR, JR., and AMOS M. WHITE, Denver, Colo., Washington, D.C.

Abstract.—Chemical analyses for ThO_2 and U_3O_8 content in 81 sized fractions of detrital monazite from 33 drainage basins in North Carolina and South Carolina disclosed a strong tendency for the percentage of ThO_2 to vary according to particle sizes of monazite at each locality. Higher percentages of ThO_2 are associated with coarse-grained monazite than with fine-grained monazite. This relation for thorium is thought to result from the tendency of certain grain-size ranges of the detrital monazite to be associated with the origin of the monazite in specific rock units. The role of size in relation to tenor of U_3O_8 was not fully brought out by the study, owing possibly to the use of too small a separation in size of grain. Differences in percentage of U_3O_8 were greater than those that could be attributed to analytical procedure, and more analyses are required to define the trends of these differences. A preparator's tendency to select coarse detrital grains of monazite if a choice lies among grains of diverse size can, therefore, introduce a bias in the reported tenor in ThO_2. However, knowledge that the composition of a detrital mineral may vary with grain size and that grain-size distribution tends to vary by rock type might actually be used to advantage in geochemical exploration.

It is possible that a bias is introduced in the reported chemical composition of monomineralic separates that are made up of individual, handpicked detrital grains from unsized stream-sediment concentrates. The bias would be toward compositions associated with the origin of the minerals in a specific source rock. The bias could be introduced through a combination of two factors: (1) the tendency in the drainage basin for certain ranges in grain size of a mineral to be associated with its origin in specific rock units—even ones of small areal extent, and (2) the preparator's tendency to select coarse grains where a choice lies among individuals of diverse size. Thus, the reported composition of the handpicked mineral might not reflect the average composition of the mineral in the concentrate, and, by extension, the average composition of the mineral in the rocks in the drainage basin.

Evidence for the existence of this bias has come from studies of the abundances of ThO_2 and U_3O_8 in detrital monazite from small streams in the Piedmont province of the Southeastern United States. The first analysis of this problem was based on 15 sized fractions of detrital monazite from six placer concentrates from Georgia. No real differences in the percentages of ThO_2 and U_3O_8 could be related to grain size, because the differences were within the range of laboratory error and the sieved fractions were too few. Selective handpicking of coarse grains had not previously been considered by the authors to be conducive to bias (Overstreet and others, 1969, p. 69, 71). More recently, however, a group of 33 handpicked detrital monazites from small streams in North Carolina and South Carolina was analyzed in sized fractions with results that show higher percentages of ThO_2 in the coarse-grained monazites of a given concentrate. The role of grain size in relation to percentage of U_3O_8 is complex; in general, extreme differences in grain size lead to large differences in the percentage of U_3O_8; this tendency for U_3O_8, however, does not follow uniformly the trend shown by ThO_2.

COMPOSITION BY GRAIN SIZE

Source, preparation, and analysis of monazite

The monazites analyzed in this study were obtained from placer concentrates panned in North Carolina and South Carolina during 1951–52 as part of an investigation of placers undertaken by the U.S. Geological Survey and funded by the U.S.

Atomic Energy Commission (AEC) (Overstreet and others, 1968). Fifty-eight monazite separates were handpicked from these concentrates. These separates were examined under unfiltered ultraviolet light so that xenotime could be identified and removed (Murata and Bastron, 1956).

After this mineralogical check, the 33 heaviest separates—the ones analyzed in this report—were sieved into fractions coarser (+) and finer (−) than 40 mesh. Enough monazite was available in one separate to permit sieving to five sizes: +20, −20+40, −40+60, −60+80, and −80 mesh. Five separates were sieved to four sizes: +40, −40+60, −60+80, and −80 mesh. Two separates were sieved to three sizes: +40, 40–60, and 60–80 mesh. The remaining 25 separates consisted of only enough monazite to permit sieving into two sizes: +40 and −40 mesh.

After the sieving, the whole group of 106 splits, consisting of 25 unsieved and 81 sieved separates, was analyzed by J. J. Warr, Jr. Thorium was determined by the spectrophotometric procedure of Fletcher, Grimaldi, and Jenkins (1957), and nine samples were reanalyzed for thorium by means of the spectrophotometric method of May and Jenkins (1965). Uranium was determined fluorimetrically with a flux containing NaF (Grimaldi and others, 1954).

Two types of controls were run to check the reproducibility of results; these were: (1) replicate analyses of a control sample, and (2) duplicate analyses by a second procedure. A sample of AEC monazite sand No. 7A was run with each batch of separates, under the same condition of small weight of sample. The provisional certificate values for AEC sample 7A are 9.65 percent ThO_2 and 0.38 percent U_3O_8. The mean values obtained by Warr were 9.56 percent ThO_2 and 0.36 percent U_3O_8, with standard deviations of 0.126 percent ThO_2 and 0.0228 percent U_3O_8. Duplicate analyses for ThO_2 were run on nine samples by two procedures: the thoron method of Fletcher, Grimaldi, and Jenkins (1957, p. 963), and the arsenazo method of May and

TABLE 1.—*Content, in percent, of* ThO_2 *and* U_3O_8 *in sized detrital monazite, North Carolina and South Carolina*

[Numbers in parentheses are the mean values of ThO_2 or U_3O_8 in −40+60, −60+80, and −80 mesh monazite. Leaders (----) indicate no determinations made. Sample series CS collected by N. P. Cuppels; DC by D. W. Caldwell PK by P. K. Theobald, Jr.; WE by A. M. White. Analyses by J. J. Warr, Jr.]

Sample No.	ThO_2 (in percent) by sieve size						U_3O_8 (in percent) by sieve size					
	+20	+40	−40	−40 +60	−60 +80	−80	+20	+40	−40	−40 +60	−60 +80	−80
52–CS–43	---	3.6	3.2	---	---	---	---	0.17	0.28	---	---	---
74	---	5.7	5.0	---	---	---	---	.25	.27	---	---	---
114	---	4.8	4.4	---	---	---	---	.62	.59	---	---	---
126	---	5.1	(4.7)	4.7	4.9	4.4	---	1.1	(.90)	0.99	0.88	0.84
315	---	5.2	5.0	---	---	---	---	1.0	.84	---	---	---
408	---	5.0	5.1	---	---	---	---	.35	.30	---	---	---
443	---	5.4	(4.7)	5.1	4.3	---	---	.31	(.39)	.39	.39	---
476	---	5.5	5.5	---	---	---	---	.68	.71	---	---	---
516	---	5.8	4.6	---	---	---	---	.12	.11	---	---	---
753	---	7.2	6.9	---	---	---	---	1.1	.57	---	---	---
785	---	6.1	(6.0)	5.8	6.2	6.1	---	.27	(.32)	.27	.32	.37
52–DC–166	---	4.5	4.7	---	---	---	---	.32	.29	---	---	---
184	---	5.8	5.5	---	---	---	---	.28	.27	---	---	---
367	6.2	6.1	(5.7)	6.0	5.4	5.7	0.65	.49	(.48)	.45	.51	.49
386	---	4.8	5.3	---	---	---	---	.98	1.3	---	---	---
407	---	5.2	5.1	---	---	---	---	.61	.52	---	---	---
444	---	4.3	4.0	---	---	---	---	1.8	.25	---	---	---
671	---	5.8	4.8	---	---	---	---	.62	.48	---	---	---
695	---	6.4	(5.9)	5.8	6.0	5.9	---	.72	(.76)	.59	.83	.86
819	---	5.7	5.5	---	---	---	---	.16	.13	---	---	---
51–PK–63	---	6.0	5.9	---	---	---	---	.28	.33	---	---	---
151	---	4.0	3.9	---	---	---	---	.41	.35	---	---	---
52–PK–83	---	6.2	(6.2)	6.3	6.2	---	---	.21	(.27)	.24	.31	---
52–WE–31	---	5.8	5.5	---	---	---	---	.78	.79	---	---	---
360	---	4.9	5.1	---	---	---	---	1.1	.97	---	---	---
435	---	6.6	6.2	---	---	---	---	.52	.47	---	---	---
619	---	5.7	(5.9)	7.2	5.3	5.2	---	.76	(.80)	.88	.75	.78
638	---	6.8	5.7	---	---	---	---	.66	.70	---	---	---
673	---	6.1	(5.6)	5.9	5.4	5.4	---	.57	(.65)	.62	.62	.72
744	---	5.8	5.2	---	---	---	---	.24	.16	---	---	---
761	---	6.0	6.0	---	---	---	---	.12	.16	---	---	---
847	---	4.9	5.0	---	---	---	---	.38	.50	---	---	---
857	---	5.8	5.0	---	---	---	---	.52	.64	---	---	---

Jenkins (1965); the standard deviation of the duplicate pairs was 0.21 percent ThO_2.

The 95-percentile range of values is equal to plus or minus twice the standard deviation. This is ±0.25 percent ThO_2 for the precision of the thoron procedure on the standard sample and ±0.42 percent ThO_2 for the precision of the thoron versus the arsenazo determinations of ThO_2 on miscellaneous samples. The precision for percentage of U_3O_8 on the standard sample is ±0.045.

Results of analyses

The results of the analyses for thorium and uranium in the 81 sieved separates of monazite (33 concentrates), reported as ThO_2 and U_3O_8, are given in table 1. In these monazites, the ThO_2 ranges in percentage from 3.2 to 7.2, which closely resembles the abundances of ThO_2 reported by Mertie (1953, p. 12) for 53 samples of unsized placer monazite from the same general region in North Carolina and South Carolina. However, the percentages of U_3O_8 for the monazites in table 1, from 0.11 to 1.8, occupy a greater range than the 53 listed by Mertie.

The data in table 1 show that the minimum, median, maximum, and arithmetic average values for percentages of ThO_2 and U_3O_8 are greater for the +40-mesh monazite than for the −40-mesh material:

	+40-mesh monazite		*−40-mesh monazite*	
	ThO_2	U_3O_8	ThO_2	U_3O_8
Minimum	3.6	0.12	3.2	0.11
Median	5.7	.52	5.2	.48
Maximum	7.2	1.8	6.9	1.3
Average	5.5	.56	5.2	.50

Thorium

The results given in table 1 show a strong tendency for higher percentages of ThO_2 to be in the +40-mesh monazite than in the −40-mesh monazite.

An evaluation of the probability that the +40-mesh monazite is richer in ThO_2 than the −40-mesh monazite can be made by applying the Wilcoxon matched-pairs signed-ranks test (Siegel, 1956, p. 75–83), because the data in table 1 give differences in percentage of ThO_2 for sieved pairs from the same concentrate. Under this test, the null hypothesis is that the fine-grained fraction of detrital monazite contains as much ThO_2 as the coarse-grained monazite; the alternative hypothesis is that the coarse-grained detrital monazite tends to be richer in ThO_2 than the fine-grained monazite. Rejection of the null hypothesis is set at a level of significance (α) of 0.01 with a sample size $N=30$ (the total number of pairs of determinations for ThO_2 in table 1, the difference of which is not 0). The differences (d) in percentages of ThO_2 are said to be positive if the percentage is greater in the coarse-grained monazite, and negative if the percentage is greater in fine-grained monazite (table 2). T, the smaller of the sums of the like-signed ranks, is 56. The deviation of the observed values (z) derived from N and T through the formula (Siegel, 1956, p. 81)

$$z = \frac{T - \frac{N(N+1)}{4}}{\sqrt{\frac{N(N+1)(2N+1)}{24}}}$$

is −3.6. Table A of Siegel (1956, p. 247) shows that such an extreme z has a one-tailed probability under the null hypothesis of $p=0.00016$. The value

TABLE 2.—*Differences, in percent, of content of* ThO_2 *in pairs of coarse-grained and fine-grained detrital monazite from North Carolina and South Carolina*

[Leaders (---) indicate not applicable]

Sample No.	ThO_2 (percent) +40 mesh	ThO_2 (percent) −40 mesh	Difference between matched pairs (d)	Rank of d	Rank with less frequent sign
52-CS-43	3.6	3.2	0.4	18	---
74	5.7	5.0	.7	25.5	---
114	4.8	4.4	.4	18	---
126	5.1	4.7	.4	18	---
315	5.2	5.0	.2	9	---
408	5.0	5.1	−.1	−3.5	3.5
443	5.4	4.7	.7	25.5	---
476	5.5	5.5	.0	0	---
516	5.8	4.6	1.2	30	---
753	7.2	6.9	.3	13.5	---
785	6.1	6.0	.1	3.5	---
52-DC-166	4.5	4.7	−.2	−9	9
184	5.8	5.5	.3	13.5	---
367	6.1	5.7	.4	18	---
386	4.8	5.3	−.5	−22	22
407	5.2	5.1	.1	3.5	---
444	4.3	4.0	.3	13.5	---
671	5.8	4.8	1.0	28	---
695	6.4	5.9	.5	22	---
819	5.7	5.5	.2	9	---
51-PK-63	6.0	5.9	.1	3.5	---
151	4.0	3.9	.1	3.5	---
52-PK-83	6.2	6.2	.0	0	---
52-WE-31	5.8	5.5	.3	13.5	---
360	4.9	5.1	−.2	−9	9
435	6.6	6.2	.4	18	---
619	5.7	5.9	−.2	−9	9
638	6.8	5.7	1.1	29	---
673	6.1	5.6	.5	22	---
744	5.8	5.2	.6	24	---
761	6.0	6.0	.0	0	---
847	4.9	5.0	−.1	−3.5	3.5
857	5.8	5.0	.8	27	---
					[1]$T=56$

[1] T, the smaller sum of like-signed ranks (Siegel, 1956, p. 77).

of p is less than the level of significance ($\alpha=0.01$); hence, the null hypothesis is rejected in favor of the alternative hypothesis that states that the coarse-grained detrital monazite tends to be richer in ThO_2 than the fine-grained monazite.

The tendency for higher content of ThO_2 to be in the +40-mesh monazite than in the −40-mesh monazite is also demonstrated by the diagram in figure 1, on which each sample is plotted by the percentages of ThO_2 in the +40-mesh and −40-mesh sizes. In 24 of the 33 samples the percentage of ThO_2 is greater for the +40-mesh monazite than for the −40-mesh monazite. Only three samples contain equal percentages of ThO_2 in the two sizes. Six monazites contain more ThO_2 in the −40-mesh size than in the +40-mesh size.

Figure 2 emphasizes the trend shown in figure 1 by relating the percentages of ThO_2 to the end members by size of each of the eight samples of monazite sieved to three or more sizes. Thus, when the percentage of ThO_2 in the coarsest grains of monazite in a concentrate is compared with the percentage of ThO_2 in the finest grains of monazite in that concentrate, the percentage of ThO_2 is seen to be greater in the coarse grains in six of the eight concentrates. In two samples there is no difference in percentage of ThO_2 that can be related to grain size. None of the fine-grained monazite has a tenor of ThO_2 higher than that of its coarse-grained counterpart.

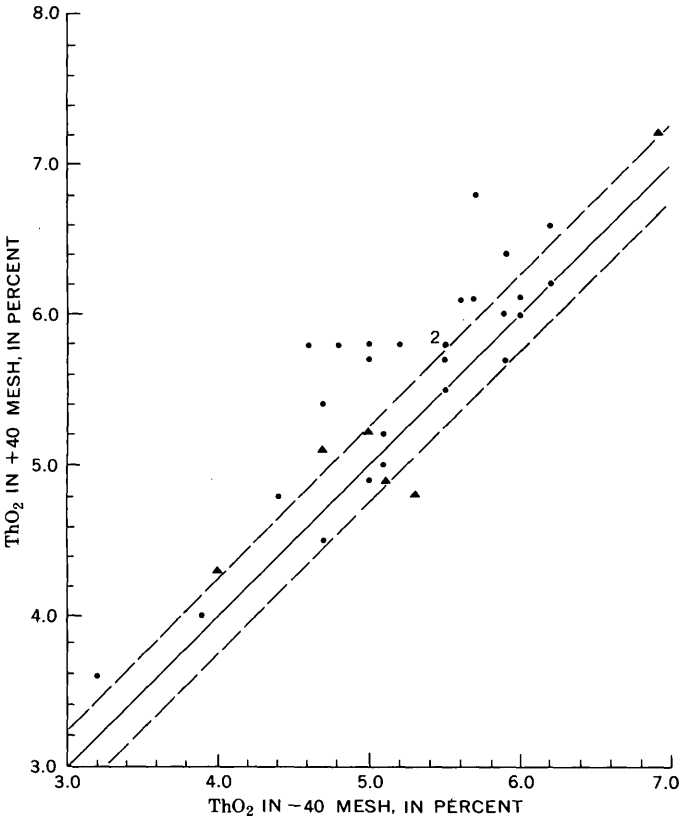

FIGURE 1.—Percentage of ThO_2 by grain size in detrital monazite. Triangle, uranium-rich monazite; dot, ordinary monazite; by +40-mesh and −40-mesh pairs. Dashed lines indicate twice standard deviation 0.126 percent ThO_2 in thoron method of analysis. Number (2) indicates two samples with the same value.

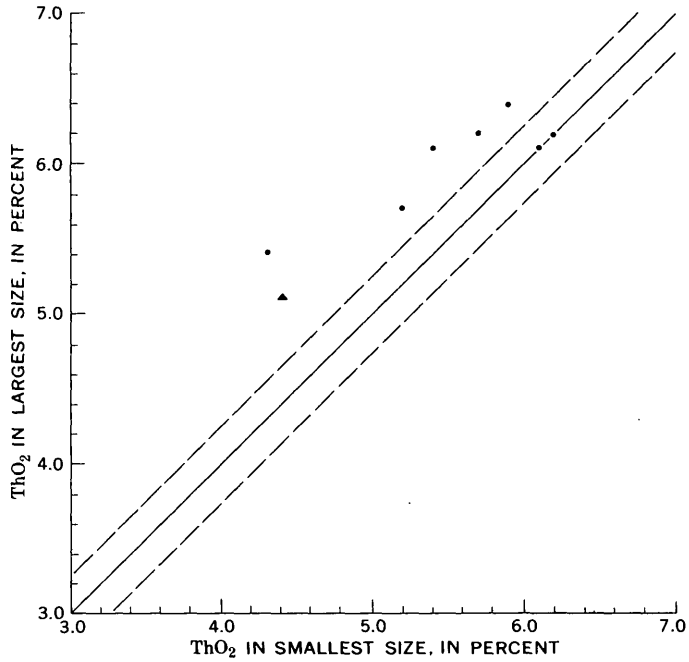

FIGURE 2.—Percentage of ThO_2 related to end members of eight series of sieved fractions of monazite. Triangle, uranium-rich monazite; dot, ordinary monazite; by +40-mesh and −40-mesh pairs. Dashed lines indicate twice standard deviation 0.126 percent ThO_2 in thoron method of analysis.

The tendency for the coarse grains of monazite to be richer in thorium than the fine grains is emphasized when allowance is made for probable laboratory error in the analyses. On figures 1 and 2, dashed lines are drawn at two standard deviations for thoria based on determinations of the whole group of monazites and the standard sample by the thoron method. The standard deviation is shown to be ± 0.126 percent ThO_2; and twice that value, as plotted, is ± 0.25 percent. High percentages of ThO_2 are seen to be associated with coarse-grained monazite in 18 pairs but with fine-grained monazite in only one pair.

These data are interpreted to show that coarse detrital grains of monazite tend to be richer in ThO_2 than fine grains from the same concentrate. A bias toward higher values for ThO_2 in the monazite could be introduced by selectively handpicking coarse grains for analysis.

Uranium

The percentage content of U_3O_8 reported in table 1 shows a tendency toward larger minimum, median, maximum, and average values for coarse-grained monazite than for fine-grained monazite, but these percentages are far from being as strongly defined as are those for ThO_2. Indeed, the differences in minimum and median are within or only slightly greater than two standard deviations in the analytical results for U_3O_8.

The Wilcoxon matched-pairs signed-ranks test (Siegel, 1956, p. 75–83) shows that the +40-mesh monazite is probably not richer in U_3O_8 than the −40-mesh monazite. The deviation of the observed values (z), derived from $N=33$ and $T=258.5$ (table 3) by the formula used above, is −0.3931. This z has a one-tailed probability of $p=0.3472$, much greater than the level of significance set ($\alpha=0.01$); hence, the alternative hypothesis (coarse-grained detrital monazite tends to be richer in U_3O_8 than fine-grained monazite) must be rejected. Rejection of this hypothesis gives rise to questions regarding the correlation (interrelation) of thorium and uranium in monazite that should be investigated further, considering the established use of the ratio U_3O_8:ThO_2 in studies of monazite (Mertie, 1953, p. 12).

A graph of the percentages of U_3O_8, by +40-mesh and −40-mesh pairs, shows that deviations from the 45° line are virtually random for values below 0.95 percent U_3O_8 (fig. 3). Results of the Wilcoxon test of the monazites plotted in figure 3 that contain less than 0.95 percent U_3O_8 show that the differences in composition of the monazite are randomly distributed with respect to size ($N=27$, $T=150.5$, $z=0.93$, and $p=0.18$). The possibility exists, as shown below, that sieving to +40 mesh and −40 mesh results in a size difference too small to affect the analytical results for U_3O_8.

For monazites with more than 0.95 percent U_3O_8 content, identified as uranium-rich monazite (Overstreet and others, 1970, p. D169–D175, this chapter), a possible tendency exists for the +40-mesh grains to be richer in U_3O_8 than the −40-mesh grains. However, from the Wilcoxon test ($N=6$, $T=4$, $p>0.025$) it is seen that, if the tendency

TABLE 3.—*Differences, in percent, of content of* U_3O_8 *in pairs of coarse-grained and fine-grained detrital monazite from North Carolina and South Carolina*

[Leaders (---) indicate not applicable]

Sample No.	U_3O_8 (percent)		Difference between matched pairs (d)	Rank of d	Rank with less frequent sign
	+40-mesh	−40-mesh			
52–CS–43---	0.17	0.28	−0.11	−24	24
74---	.25	.27	−.02	−5	5
114---	.62	.59	.03	7.5	---
126---	1.1	.90	.20	30	---
315---	1.0	.84	.16	29	---
408---	.35	.30	.05	15.5	---
443---	.31	.39	−.08	−21	21
476---	.68	.71	−.03	−7.5	7.5
516---	.12	.11	.01	2.5	---
753---	1.1	.57	.53	32	---
785---	.27	.32	−.05	−15.5	15.5
52–DC–166---	.32	.29	.03	7.5	---
184---	.28	.27	.01	2.5	---
367---	.49	.48	.01	2.5	---
386---	.98	1.3	−.32	−31	31
407---	.61	.52	.09	23	---
444---	1.8	.25	1.55	33	---
671---	.62	.48	.14	28	---
695---	.72	.76	−.04	−11.5	11.5
819---	.16	.13	.03	7.5	---
51–PK–63---	.28	.33	−.05	−15.5	15.5
151---	.41	.35	.06	18.5	---
52–PK–83---	.21	.27	−.06	−18.5	18.5
52–WE–31---	.78	.79	−.01	−2.5	2.5
360---	1.1	.97	.13	27	---
435---	.52	.47	.05	15.5	---
619---	.76	.80	−.04	−11.5	11.5
638---	.66	.70	−.04	−11.5	11.5
673---	.57	.65	−.08	−21	21
744---	.24	.16	.08	21	---
761---	.12	.16	−.04	−11.5	11.5
847---	.38	.50	−.12	−25.5	25.5
857---	.52	.64	−.12	−25.5	25.5
					[1] $T=258.5$

[1] T, the smaller sum of like-signed ranks (Siegel, 1956, p. 77).

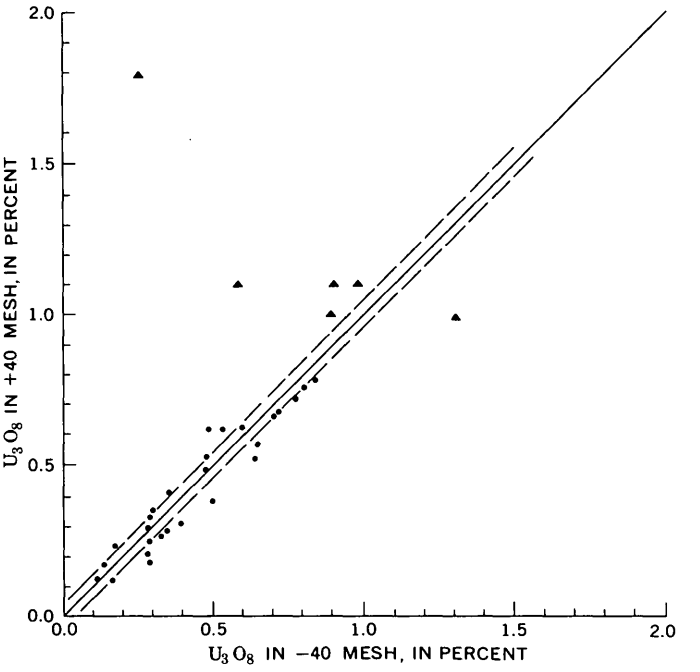

FIGURE 3.—Percentage of U_3O_8 by grain size in detrital monazite. Triangle, uranium-rich monazite; dot, ordinary monazite; by +40-mesh and −40-mesh pairs. Dashed lines indicate twice standard deviation 0.0228 percent U_3O_8.

does exist, more than the six pairs of analyses of uranium-rich monazites are needed to test the strength of the tendency.

The percentages of U_3O_8 in the coarsest and finest sizes of the eight monazites sieved to three or more sizes (table 1) are plotted in figure 4. Those monazites that contain less than 0.95 percent U_3O_8 are seen on figure 4 as tending to have the greater percentages of U_3O_8 associated with the smaller grains. Only one of these seven fails to show this relation, and that one is the single sample in table 1 for which an analysis was made of a +20-mesh fraction. Had the +40-mesh analysis been plotted for this sample instead of the +20-mesh analysis, the result would have fallen on the 45° line in figure 4, slightly strengthening the possibility for existence of a tendency for the percentage of U_3O_8 to be greater in fine-grained than in coarse-grained ordinary detrital monazites. However, use of the +40-mesh analysis for this pair reduces the number of matched pairs ($N=5$, $T=0$) below the limit needed for the Wilcoxon test (Siegel, 1956, table G), and the strength of the tendency cannot be determined. Plotting the +20-mesh analysis in figure 4 places the pair in the field opposite that of the other ordinary monazites; and the Wilcoxon test, now applicable, shows no tendency for the higher percentages of U_3O_8 to be associated with the fine grains ($N=7$, $T=7$, and $p>0.025$). Evidently more samples than the seven pairs used here are needed to test the relation in ordinary monazites. The difference in grain size within the pairs must be greater than the difference between +40-mesh and −40-mesh pairs reported in table 1 to determine if size controls the tenor of U_3O_8 in detrital monazites.

The single uranium-rich monazite plotted on figure 4 follows the trend shown by uranium-rich monazites in figure 3; it has a greater percentage of U_3O_8 in the coarsest grains.

Laboratory variation in the determination of U_3O_8, equal to twice the standard deviation of ±0.0228 percent U_3O_8 and shown by dashed lines on figures 3 and 4, is not a factor in the distributions.

Available data, therefore, are evidence that the differences in percentages of U_3O_8 in detrital monazite by size fractions are greater than the analytical variation, but they do not as yet establish with certainty that these differences are biased. More analyses are needed for U_3O_8 in both ordinary and uranium-rich monazites, and more separation in grain size is necessary for the fractions analyzed to determine if the differences are biased by size.

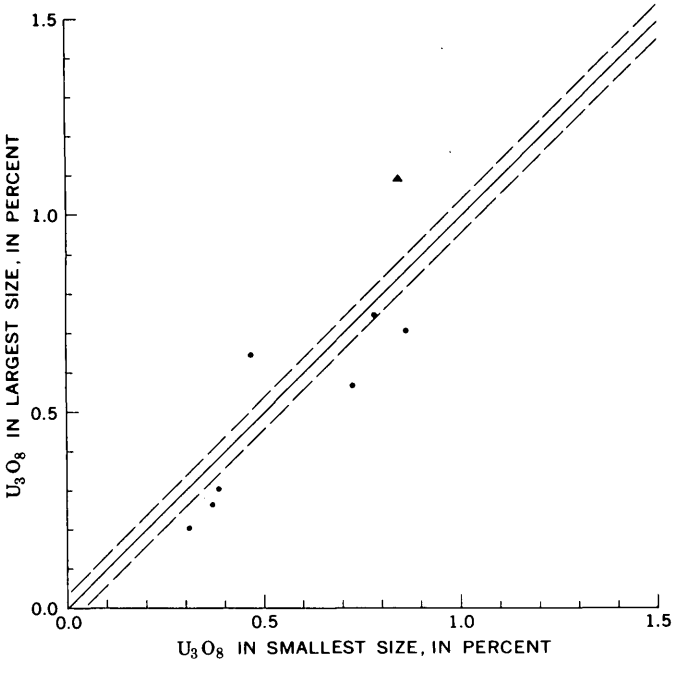

FIGURE 4.—Percentages of U_3O_8 related to end members of eight series of sieved fractions of monazite. Triangle, uranium-rich monazite; dot, ordinary monazite; by +40-mesh and −40-mesh pairs. Dashed lines indicate twice standard deviation 0.0228 percent U_3O_8.

GEOLOGIC CONTROL

Thorium

The tendency for the coarse-grained detrital monazite in a concentrate to contain a higher percentage of ThO_2 than will a fine-grained monazite is here inferred to be related to the origin of the monazites.

Grain-size differences for resistate minerals were observed to be the most obvious of the physical differences among concentrates panned from saprolite of crystalline rocks in the Shelby quadrangle, North Carolina (Overstreet and others, 1963, p. F7). The Shelby area is in the central part of the region of the 33 monazite localities represented by the analyses given here.

The schist and gneiss underlying the Shelby quadrangle are dominant components in the regional lithology; however, several extensive granitic rocks in the northern, eastern, and southern parts of the region covered by the 33 monazite localities are not represented in the Shelby data (table 4). The grain-size differences found for monazite in the Shelby rocks show that the largest percentages of coarse-grained (+45-mesh) monazite are associated with pegmatite and schists impregnated

TABLE 4.—*Percentage of sized monazite grains in saprolite of rock units in the Shelby quadrangle, Cleveland and Rutherford Counties, N. C.*

[Leaders (---), not present; Tr., trace. Recalculated from table 2 of Overstreet, Yates, and Griffitts (1963)]

Sample No.	Percent of monazite by sieve size				
	24	45	100	170	−170
Toluca Quartz Monzonite					
90334	---	Tr.	---	50	50
98942	---	17	42	41	---
109592	---	9	9	41	41
109614	---	---	8	71	22
109615	---	33	22	45	---
114332	---	---	---	20	80
114337	---	---	4	66	30
114362	---	---	---	84	16
114366	---	---	---	73	27
114369	---	---	---	83	17
114372	---	---	---	69	31
Average	---	5	8	58	29
Microcline-oligoclase-quartz pegmatite					
88479	---	17	53	30	---
88501	13	63	13	11	---
90351	---	8	68	20	4
90364	6	48	37	9	---
90367	---	10	35	45	10
90395	Tr.	39	55	6	---
98883	28	60	12	Tr.	---
98935	---	44	49	7	---
114336	---	20	31	49	---
114361	---	---	69	31	---
Average	5	31	42	21	1
Biotite gneiss					
88503	---	---	37	63	---
88529	---	---	55	45	---
114371	---	---	14	78	8
114374	---	---	20	50	30
114380	---	---	Tr.	100	---
114382	---	---	26	59	15
Average	---	---	25	67	8
Biotite schist					
90298	---	16	26	31	27
110848	---	---	50	50	Tr.
88535	---	---	26	74	---
90360	---	---	100	---	---
114334	---	---	27	55	18
114339	---	---	25	75	---
114341	---	---	40	60	---
114352	---	---	Tr.	100	---
114381	---	---	20	60	20
Average	---	1	35	56	8
Biotite schist and pegmatite					
90333	---	Tr.	100	---	---
98868	---	12	43	38	7
Average	---	6	72	19	3
Sillimanite schist					
88480	---	---	29	71	---
114347	---	---	---	50	50
114348	---	---	---	100	---
114364	---	---	20	80	---
114367	---	---	58	18	24
Average	---	---	21	64	15
Sillimanite schist and pegmatite					
98874	---	5	13	69	13
114354	---	52	36	12	---
114356	---	---	30	70	---
114359	---	---	52	48	---
Average	---	14	33	50	3

with pegmatite. (Data on sizes of monazite from saprolite in the Shelby quadrangle were published as 24 mesh, 45 mesh, 100 mesh, and 170 mesh; thus, the sizes are not the same as those used here in table 1. However, a division of the Shelby data into +45 mesh and −45 mesh is sufficiently close to the division into +40 mesh and −40 mesh used in table 1 to permit comparison.) Percentage distributions of monazite by grain size and rock type were as follows:

Rock	*+45 mesh*	*−45 mesh*
Pegmatite	36	64
Sillimanite schist and pegmatite	14	86
Biotite schist and pegmatite	6	94
Toluca Quartz Monzonite	5	95
Biotite schist	1	99
Sillimanite schist	0	100
Biotite gneiss	0	100

The work in the Shelby area also showed that monazite is characteristically present with unequal frequency of occurrence and in different abundances in the several source rocks, that the average percentage of ThO_2 in monazite varies with the source, and that the source rocks are unequally distributed areally (Overstreet and others, 1963, tables 1 and 4, p. F3). These data are summarized in table 5, from which it further can be seen that pegmatitic monazite tends to be richer in ThO_2 than is monazite from areally more common schists. Also, the frequency of occurrence and average abundance of monazite are high in pegmatite compared with the schists.

Monazite from granitic rocks in Georgia has been shown to be notably richer in ThO_2 than monazite from schists, and where the schists resemble those in the Shelby area the contained monazite has percentages of ThO_2 resembling those from schists underlying the Shelby quadrangle (Overstreet and others, 1969, table 3). Data on the sizes of monazite grains associated with individual rock units in the Georgia area and in the parts of North Carolina and South Carolina outside the Shelby quadrangle are lacking; hence, the extent to which the size relations observed for monazite in the Shelby area can be extended to the region as a whole is uncertain. The distribution of particle sizes of the major component minerals in saprolite of the schists in the monazite area was shown to be skewed more strongly toward fine sizes than it is in granitic rocks (Overstreet and others, 1968, p. 29). Possibly the grain-size differences for the minor accessory minerals, including monazite, follow the same distribution. If, indeed, they do, then the grain-size differences found for monazites from rocks in the

TABLE 5.—*Areal relations of monazite to source rocks in the Shelby quadrangle, Cleveland and Rutherford Counties, N. C.*
[Number in parentheses is number of analyses; n.d., no data. Adapted from Overstreet, Yates, and Griffitts (1963, tables 1 and 4, p. F3)]

Rock	Areal distribution (percent of area of quadrangle underlain by rock unit)	Number of concentrates from saprolite	Frequency of occurrence of monazite (percent of concentrates with 1 percent or more of monazite)	Average abundance of monazite (percent of monazite in source rocks)[1]	Average abundance of ThO_2 in monazite (percent)
Toluca Quartz Monzonite	7	96	97	0.004	6.1(23)
Pegmatite		329	88	.006	6.1(43)
Biotite schist	62	198	54	.001	4.8(31)
Biotite schist and pegmatite.		303	75	.004	n.d.
Sillimanite schist	30	150	73	.002	4.8(16)
Sillimanite schist and pegmatite.		106	84	.002	n.d.
Biotite gneiss	1	59	80	.006	5.4(9)

[1] Recalculated to weight percent.

Shelby area possibly are representative of grain-size differences attributable to source rocks in the region as a whole.

The size distribution of heavy minerals in fluvial sediments in the monazite-bearing area between the Savannah and Catawba Rivers in the Inner Piedmont of North Carolina and South Carolina (the source of the monazites in this report) has been described by Caldwell (1962), Cuppels (1962), Theobald (1962), and White (1962). These descriptions show that coarse grains are most common in gravel, and that fine grains, although present in gravel, are typically associated with silt and clay. The range in particle size tends to be least among concentrates from gravel and clay and to be greatest among concentrates from sand and silt. Sand and silt are the most common sediments in the valleys of the monazite area. Coarse-grained monazite is sparse in the source rocks for the alluvium, but it is relatively abundant in gravel in streambeds. The gravel itself contains twice as much monazite per unit volume as the silt and sand, and eight times as much per unit volume as the clay (Overstreet and others, 1968, p. 42). Enormous quantities of source material have been winnowed by the streams to collect coarse grains of monazite in the gravel.

Gravel in the beds of streams is the usual source material for the heavy-mineral concentrates used in prospecting. The natural processes in the streambed have already preferentially retained coarse grains of monazite in the gravel. Panning the gravel to make a concentrate tends to further reduce the fine-grained monazite in proportion to the coarse-grained monazite (Theobald, 1957). Thus, the concentrate made from alluvial gravel tends to emphasize coarse monazite over the average monazite in the drainage basin. When a chemical analysis of this material is made, it will result in reported compositions biased in the direction in which the compositions of coarse grains vary from those of fine grains.

Selective picking of the coarse detrital grains in a concentrate to be prepared for chemical analysis will further bias the recovery of monazite toward individual grains of pegmatitic origin or origin in schists impregnated with pegmatite, and the average tenor of ThO_2 in the handpicked monazite will be further biased toward the high values associated with origin in pegmatite.

Uranium

The data presented here have not demonstrated a significant bias toward percentage of U_3O_8 attributable to grain size in either the ordinary or the uranium-rich monazites. However, the data show that too few analyses are available for the uranium-rich monazites and that too small a size difference was used for the ordinary monazites in the analyses to exclude the possibility of bias in percentage content of U_3O_8 as related to size.

The relation of percentage of uranium in monazite to the source rock of the monazite has received little study. Recent work by the authors has shown that, for the United States as a whole, uranium-rich monazite, that which contains more than 0.95 percent U_3O_8, is restricted to 5 percent of analyzed monazites. Currently known sources for uranium-rich monazites are posttectonic and late syntectonic quartz monzonite and associated pegmatite in the Inner Piedmont of North Carolina and South Carolina, mainly outside the area of the Shelby quadrangle. It remains to be shown from further analyses if the uranium-rich monazites tend to be coarse grained. For ordinary monazite, that which con-

tains less than 0.95 percent U_3O_8, it also remains to be shown, through analysis of more widely separated sizes of monazite, if higher tenors in U_3O_8 are associated with fine-grained monazite such as might be derived from schist (table 4). If these relations can be shown, then the selection of coarse grains of detrital monazite through handpicking could lead to analytical results biased toward higher tenors of U_3O_8 if the source rocks for uranium-rich monazites were in a drainage basin underlain by mixed rocks, or toward lower tenors if the distributive province were mainly schist.

CONCLUSIONS

Differences in the range in grain size of monazite and other resistate accessory minerals in the metamorphic and igneous rocks underlying the Shelby quadrangle, North Carolina, have been shown to reflect petrologic differences in the source rocks (Overstreet and others, 1963, table 2). The percentages of ThO_2 and U_3O_8 in monazite have also been shown to vary according to the kind of source rock (Overstreet and others, 1963, tables 4 and 5; Overstreet, 1967, table 2). Heavy resistate accessory minerals, derived through weathering and erosion of the source rocks, have been shown to be preferentially accumulated in stream sediments in such a way that the coarse and heavy grains are proportionately more abundant in gravel than in sand, silt, or clay (Overstreet and others, 1968, p. 42). Thus, coarse grains of monazite which originated mainly in pegmatites that represent only a small percentage of the volume of rock in a drainage basin tend to be disproportionately concentrated in alluvial gravel.

Such gravel is the medium commonly used as a source for alluvial concentrates in prospecting. During the panning of the concentrate from the gravel, further winnowing by size takes place, and the finest grains of heavy minerals suffer the greatest loss (Theobald, 1957). Hence, the panned concentrate is further enriched in the coarser grains. When, in preparation for chemical analyses, monomineralic fractions of the unsized concentrates are made by handpicking, a still further bias is given to the proportion of coarse grains, owing to the tendency by a preparator to select coarse grains instead of fine ones. The cumulative bias in size seemingly assures that the mineral grains used for analysis represent only a narrow segment, by size and source, of the grains of that mineral in rocks in the distributive province of the sample. The reported composition is not representative of the average composition of grains of the mineral in the concentrate, in the gravel, or in the source rocks.

For monazite, the bias in composition caused by the entry into analysis of a disproportionate amount of coarse grains will have the effect of increasing the reported abundance of thorium with respect to its probable average abundance in the mineral in the distributive province. Further work must be done to learn the relation, if any, between the abundance of uranium and the size of monazite grains. The effect of grain size is certainly different for thorium and uranium, and it may vary for either element if an exotic source coexists with ordinary sources in the distributive province.

Other resistate mineral species in panned concentrates may also display variations in composition because of relations of grain size to origin. Orientation surveys for individual species of heavy minerals to relate composition to source rock may be needed before use is made of the mineral separates as sample media in geochemical exploration. Such surveys should relate the range in composition of the mineral to size classes of the mineral and to the source rocks for the mineral. The results of an orientation survey might allow taking advantage of size-related compositional differences in individual mineral species to emphasize geochemical differences and sharpen the focus of a prospecting program.

Investigations of regional relations of the chemical composition of selected detrital mineral grains to the geology may require particular effort to overcome the bias introduced by grain size. A study to determine the most suitable procedure is needed. Some approaches that are suggested are the analysis of grains of intermediate size, the analyses of predetermined mixtures of two sizes, and the separate analyses of several sizes with the results weighted according to the areal distribution of the source rocks and the relation of size to source. Of these alternatives, only the use of grains of intermediate size and the use of two sizes seem practicable.

A factor not considered above in the discussion of size relations of detrital resistate grains is the probable downstream average decrease in grain size owing to transport and attrition and the resulting effect on the percentages of size-related elements. In streams within the source areas of the particular mineral, fresh supplies of the mineral would continue to enter throughout the drainage system, and the factors influencing size would not be much affected by attrition. In streams leading away from the source area, transport and attrition would probably

have some effect. Tests of this effect need to be made.

A byproduct of the present study is the indirect evidence given by the Wilcoxon matched-pairs signed-ranks tests that the abundance of thorium in monazite is not directly related to the abundance of uranium in monazite. Investigation of the variance of these two elements in monazite is now needed, considering the established use of the ratio U_3O_8–ThO_2 in studies of the regional distribution of monazite in the Southeastern United States (Mertie, 1953, p. 12).

REFERENCES

Caldwell, D. W., 1962, Description, composition, and tenor of unconsolidated sediments in monazite-bearing tributaries to the Savannah and Saluda Rivers in the western Piedmont of South Carolina: U.S. Geol. Survey open-file report, 19 p.

Cuppels, N. P., 1962, Description, composition, and tenor of unconsolidated sediments in monazite-bearing tributaries to the Enoree, Tyger, and Pacolet Rivers in the western Piedmont of South Carolina: U.S. Geol. Survey open-file report, 17 p.

Fletcher, M. H., Grimaldi, F. S., and Jenkins, L. B., 1957, Thoron-mesotartaric acid system for the determination of thorium: Anal. Chemistry, v. 29, no. 6, p. 963–967.

Grimaldi, F. S., May, Irving, Fletcher, M. H., and Titcomb, Jane, 1954, Collected papers on methods of analysis for uranium and thorium: U.S. Geol. Survey Bull. 1006, 184 p.

May, Irving, and Jenkins, L. B., 1965, Use of arsenazo III in determination of thorium in rocks and minerals, *in* Geological Survey Research 1965: U.S. Geol. Survey Prof. Paper 525–D, p. D192–D195.

Mertie, J. B., Jr., 1953, Monazite deposits of the Southeastern Atlantic States: U.S. Geol. Survey Circ. 237, 31 p.

Murata, K. J., and Bastron, Harry, 1956, A convenient method for recognizing nonopaque cerium earth minerals: Science, v. 123, no. 3203, p. 888–889.

Overstreet, W. C., 1967, The geologic occurrence of monazite: U.S. Geol. Survey Prof. Paper 530, 327 p.

Overstreet, W. C., Warr, J. J., Jr., and White, A. M., 1969, Thorium and uranium in detrital monazite from the Georgia Piedmont: Southeastern Geology, v. 10, no. 2, p. 63–76.

Overstreet, W. C., White, A. M., and Warr, J. J., Jr., 1970, Uranium-rich monazites in the United States, *in* Geological Survey Research 1970: U.S. Geol. Survey Prof. Paper 700–D, p. D169–D175.

Overstreet, W. C., White, A. M., Whitlow, J. W., Theobald, P. K., Jr., Caldwell, D. W., and Cuppels, N. P., 1968, Fluvial monazite deposits in the Southeastern United States: U.S. Geol. Survey Prof. Paper 568, 85 p.

Overstreet, W. C., Yates, R. G., and Griffitts, W. R., 1963, Heavy minerals in the saprolite of the crystalline rocks in the Shelby quadrangle, North Carolina: U.S. Geol. Survey Bull. 1162–F, 31 p.

Siegel, Sidney, 1956, Nonparametric statistics for the behavioral sciences: New York, McGraw-Hill Book Co., Inc., 312 p.

Theobald, P. K., Jr., 1957, The gold pan as a quantitative geologic tool: U.S. Geol. Survey Bull. 1071–A, 54 p.

——— 1962, Description, composition, and tenor of unconsolidated sediments in monazite-bearing tributaries to the Broad River in the western Piedmont of South Carolina and North Carolina: U.S. Geol. Survey open-file report, 18 p.

White, A. M., 1962, Description, composition, and tenor of unconsolidated sediments in monazite-bearing tributaries to the Catawba River in the western Piedmont of North Carolina: U.S. Geol. Survey open-file report, 17 p.

DETERMINATION OF ACID-SOLUBLE AND TOTAL MANGANESE IN GEOLOGICAL AND BOTANICAL MATERIALS BY ATOMIC ABSORPTION

By M. A. CHAFFEE, Denver, Colo.

Abstract.—A simple, rapid, sensitive atomic-absorption method for the determination of both acid-soluble and total manganese in geological and botanical materials has been developed. For acid-soluble manganese the sample is digested with hydrochloric or nitric acid, and the supernatant liquid atomized in an atomic-absorption spectrophotometer. For total manganese the sample is first decomposed by means of a hydrofluoric-perchloric-nitric acid digestion, and the resulting residue is then taken up in hydrochloric or nitric acid and atomized as in the acid-soluble procedure. Hydrochloric acid is preferred to nitric as the digesting acid, because it dissolves out more manganese. No interferences have been observed in any routine geochemical samples. The results compare favorably with those obtained from colorimetric or spectrographic methods. A detection limit of 20 ppm has been established, but a lower limit could possibly be obtained after procedural or instrumental modifications.

Although it occurs widely, manganese has not generally been used in geochemical prospecting or in alteration studies related to ore deposits and their discovery. The presence of manganese in the outer zones of base- and precious-metal ore deposits has long been documented. (See, for example, Emmons, 1936.) Recently, Jerome (1966) noted that manganese is present in the outer fringes of porphyry copper deposits. Hewett (1968) has shown that manganese oxide minerals often represent the tops of vein-type mineral deposits that contain deeper zones of various valuable minerals. In a study of wallrock alteration that is associated with precious-metal vein deposits in New Mexico, Bundy (1958) demonstrated that the concentration of manganese decreases through the wallrock toward the vein. Unpublished data obtained by the author in a study of outcrops in the Empire district, Colorado, further indicate that the amount of depletion of manganese in exposures is directly related to the intensity of hydrothermal alteration and economic metalization in the district. Studies of stream sediments in Maine (Canney and others, 1964; Post and Hite, 1964; Post and others, 1967) and in England and Wales (Horsnail and others, 1969) indicate that the manganese-iron coatings on sediments in active streams are an important scavenger of other elements and that the presence or absence of these coatings must be considered in any evaluation of anomalous data obtained in stream-sediment prospecting. The concentration of manganese in plants may be potentially useful as an exploration tool if the roots of plants growing over blind mineral deposits penetrate the overlying material and absorb from the altered or mineralized bedrock manganese which is related spatially to the alteration or mineralization.

The two field methods in current use by the U.S. Geological Survey for determining manganese content semiquantitatively on large numbers of geochemical samples are the six-step direct-current arc emission spectrographic method (Grimes and Marranzino, 1968) and the pyrosulfate fusion–nitric acid colorimetric method. (See, for example, Ward and others, 1963, p. 55–57.) The spectrographic method is generally considered to be equivalent to a total-digestion analysis, whereas the colorimetric method generally determines somewhat less than the total manganese actually present in a sample.

The proposed procedure for determination of acid-soluble manganese content consists of two steps: (1) sample dissolution, accomplished with boiling hydrochloric or nitric acid, and (2) measurement of the dissolved manganese by atomic-absorption spectrophotometry. This acid-soluble procedure is applicable to both geological and botanical materials.

For total-manganese determinations the sample is initially decomposed by means of a hydrofluoric-perchloric-nitric acid digestion, with the resulting residue being taken up in hydrochloric or nitric

U.S. GEOL. SURVEY PROF. PAPER 700-D, PAGES D217–D221

acid. This solution is then analyzed as in step 2 of the procedure for acid-soluble manganese. This method may be used for geological materials, but it is not ordinarily needed for analyzing plants because virtually all the manganese in plant ash is readily extractable by means of the acid-soluble procedure.

REAGENTS AND APPARATUS

Reagents

Manganese standard stock solutions (100 micrograms per milliliter): Dissolve 0.0100 g of electrolytic manganese metal in 10 ml of 6*N* HCl. After the metal has dissolved, allow the solution to cool and transfer it to a 100-ml volumetric flask. Dilute to 100 ml with 6*N* HCl and mix thoroughly. For manganese standards in HNO_3, substitute 8*N* HNO_3 for 6*N* HCl in the above directions, but after dissolution of the manganese metal boil the solution for several minutes to expel any oxides of nitrogen which may have formed. Prepare working solutions from the stock solution by diluting the stock solution with the 1+1 acid that has been selected for use.

Hydrochloric acid, concentrated, reagent grade.

Hydrochloric acid, 6*N* (1+1): Add 500 ml of concentrated HCl to 500 ml of metal-free water.

Nitric acid, concentrated, reagent grade.

Nitric acid, 8*N* (1+1): Add 500 ml of concentrated HNO_3 to 500 ml of metal-free water.

Perchloric acid, concentrated, reagent grade.

Hydrofluoric acid, concentrated, reagent grade.

Apparatus

Hotplate fitted with aluminum heating block drilled to receive 16- ×150-mm test tubes.

Boiling chips, Teflon.

Test tubes, 16- ×150-mm, marked at 10-ml level.

Platinum dishes, 50-ml.

Stirring rod, Teflon.

Centrifuge.

Atomic-absorption spectrophotometer.

Operating parameters:

Wavelengths	2,795 A, 2,798 A, 2,801 A
Source lamp	Hollow cathode
Slit	7 A[1]
Burner	Boling
Air pressure	30 psi
Acetylene pressure	8 psi

[1] Slit opening passes all three listed analytical wavelengths.

PROCEDURE

Acid-soluble manganese

Weigh 0.1 g of pulverized sample into a 16- × 150-mm test tube; add 5 ml of concentrated HCl or HNO_3 and 3–5 Teflon boiling chips. Place the test tube in the aluminum heating block and heat on the hotplate until the solution boils gently. Continue to boil for 30 minutes. Remove the tube from the block, cool slightly, add 5 ml of metal-free water, and mix thoroughly. Reheat the tube and its contents on the hotplate again, just to the boiling point. Remove the tube from the hotplate, allow the contents to cool to room temperature, and adjust the volume to 10 ml by addition of the particular 1+1 acid used. Mix the final solution thoroughly and then centrifuge. Atomize the supernatant liquid into the atomic-absorption instrument, read the percentage absorption, and convert to concentration as directed for the instrument used.

Total manganese

Weigh 0.25 g of pulverized sample into a 50-ml platinum dish. Add about 2 ml of metal-free water and mix to moisten sample. Add, in order: 2 ml of concentrated HNO_3, 2 ml of concentrated $HClO_4$, and about 30 ml of concentrated HF. Mix thoroughly with a Teflon stirring rod and then heat contents of dish slowly on a hotplate for 2–3 hours. After this time has elapsed, increase the heat and take the sample to dryness. Remove the dish from the hotplate, cool, and add 10 ml of 6*N* HCl or 8*N* HNO_3 to the residue. Warm the dish and contents again on the hotplate until the residue has dissolved. Transfer the solution to a 25-ml volumetric flask, dilute it to 25 ml with 6*N* HCl or 8*N* HNO_3, and mix thoroughly. Proceed with atomization of the solution as described above.

DISCUSSION

To evaluate the performance of the proposed method, selected samples of a varied nature were analyzed by this method, by the colorimetric method, and for many of the samples, also by the six-step spectrographic method. Tables 1–6 summarize these data. The atomic-absorption analyses shown in tables 1–5 are all acid-soluble determina-

TABLE 1.—*Comparative analyses, in parts per million, of manganese in plant ash, Vekol Mountains, Pinal County, Ariz.*

[Spectrographic analyst, E. L. Mosier]

Sample No.	Atomic absorption		Colorimetric	6-step spectrographic	Plant type (common name and part)
	HCl	HNO_3			
V–1162I–STM--	100	95	120	100	Ironwood, stems.
1785I–STM--	110	95	75	100	Do.
1817I–STM--	140	120	120	150	Do.
1482P-------	320	270	250	200	Foothill paloverde, stems.
106I–LVS ---	440	400	500	300	Ironwood, leaves.
1212P-------	480	390	380	500	Foothill paloverde, stems.
1200C–LVS--	630	540	750	500	Creosote, leaves.
1387C–LVS--	730	660	750	700	Do.
1521P-------	740	640	750	500	Foothill paloverde, stems.
1683C–LVS--	880	850	750	700	Creosote, leaves.

TABLE 2.—*Comparative analyses, in parts per million, of manganese in rock samples, various localities in Colorado*

[Spectrographic analyst, E. L. Mosier]

Sample No.	Atomic absorption		Colorimetric	6-step spectrographic [1]	Rock description
	HCl	HNO_3			
R2A----	45	35	<50	50	Ferruginous sandstone.
1A----	90	120	75	150	Black, limy shale.
3A----	600	520	380	600	Biotite sillimanite schist.
6A----	740	520	500	700	Granite.
5A----	800	600	700	850	Quartz monzonite porphyry.
4A----	830	440	500	1,500	Hornblende gneiss.
7A----	850	640	700	1,500	Basalt.
8A----	1,600	1,400	1,400	2,000	Dolomite.

[1] Average of two independent analyses.

tions. Table 6 includes, in addition, total-digestion determinations. Colorimetric data were obtained by use of the method of Ward, Lakin, Canney, and others (1963); and the spectrographic data were obtained by use of the method of Grimes and Marranzino (1968). For comparative purposes, data from both hydrochloric and nitric acid digestions are included in all tables. Nearly all the samples digested in hydrochloric acid yield higher values than those digested in nitric acid, regardless of whether an acid-soluble or total-digestion procedure is used. The reason for this difference is not understood; but it may be related to undetermined factors, such as the valence of the manganese atoms during atomization and the interaction effects of other ions in the solutions.

Because hydrochloric acid dissolves a greater amount of manganese, it is the preferred digesting acid; however, digestions using nitric acid may be necessary or expedient, as, for example, when multiple analyses are to be made from a single digestion and some of the elements other than manganese can be determined better in nitric acid. Nitric acid digestions of most routine geochemical samples will still yield usable manganese values that are at least as good as colorimetric values; however, one should realize that these values will generally be lower than those obtained by use of a hydrochloric acid digestion.

In general, if the spread in standard reporting intervals and the precision of the methods are taken into consideration, there is good agreement between the atomic-absorption and colorimetric values for all types of material. For most materials the acid-soluble and the colorimetric values also agree (again within the limits placed on the methods) reasonably well with the six-step spectrographic values. Those few samples that show significantly higher spectrographic than wet chemical values are

TABLE 3.—*Comparative analyses, in parts per million, of manganese in organic-rich soils, Catheart Mountain, Somerset County, Maine*

[Spectrographic analyst, E. L. Mosier. N.d., no determinations made]

Sample No.	Atomic absorption		Colorimetric	6-step spectrographic
	HCl	HNO_3		
CRS-5----	20	<20	<50	50
14----	85	60	100	150
11----	95	50	100	70
4----	100	70	100	100
3----	190	130	100	200
7----	970	800	750	1,000
39----	1,100	1,000	1,100	N.d.
38----	1,500	1,500	1,500	N.d.
10----	1,700	1,600	1,600	2,000
9----	1,700	1,700	1,900	2,000

TABLE 4.—*Comparative analyses, in parts per million, of manganese in different types of samples, Empire district, Colorado*

[Spectrographic analyst, E. L. Mosier]

Sample No.	Atomic absorption		Colorimetric	6-step spectrographic	Sample description
	HCl	HNO_3			
AII-332--	[1]4	[1]4	<50	<10	Pyrite concentrate.
201--	20	20	<50	50	Altered biotite granite.
287--	40	30	<50	30	Do.
277--	150	120	120	150	Do.
257--	310	220	250	700	Do.
279--	410	300	380	700	Do.
327--	420	350	380	300	Impure native sulfur in dump.
281--	1,800	1,400	1,500	2,000	Altered biotite granite.
210--	8,200	6,000	7,000	5,000	Do.

[1] 0.5-g sample used.

TABLE 5.—*Comparative analyses, in parts per million, of manganese in active stream sediments, Pyrite Creek, Somerset County, Maine*

Sample No.	Atomic absorption		Colorimetric
	HCl	HNO_3	
JSD-4----------	1,200	1,000	1,000
5----------	1,200	1,000	1,000
3----------	1,300	1,000	1,000
7----------	1,300	1,000	1,000
8----------	1,300	1,100	1,100
2----------	1,300	1,200	1,100
9----------	1,600	1,300	1,400
6----------	1,900	2,000	1,900
10----------	2,700	2,600	2,800
1----------	5,000	4,300	4,000

TABLE 6.—*Comparison of manganese data, in parts per million, using different analytical methods and techniques, from rock samples, Vekol Mountains, Pinal County, Ariz.*
[Spectrographic analyst, E. L. Mosier]

Sample No.	Acid-soluble digestion–atomic absorption		Standard colorimetric	Total digestion			6-step spectrographic	Rock description
				Atomic absorption		Colorimetric [1]		
	HCl	HNO_3		HCl	HNO_3			
V–1079	280	260	250	250	230	250	200	Quartz latite porphyry.
1084	370	310	380	330	290	250	200	Limonite gossan.
1083	570	400	380	670	630	750	500	Diabase.
1072	980	860	750	2,500	2,200	2,200	1,500	Silicated limestone.
1074	1,100	850	800	1,300	1,300	1,100	1,000	Do.
1081	1,100	1,000	800	1,400	1,200	1,400	1,000	Diabase.
1071	1,200	830	900	1,300	1,200	1,100	700	Do.
1073	1,300	1,100	1,000	3,500	2,900	3,600	2,000	Silicated limestone.
1068	1,600	1,200	1,000	1,900	1,600	1,900	1,500	Cu-Zn sulfide "ore."
1069	9,000	6,500	>6,000	8,900	8,100	8,000	>5,000	Magnetite-rich skarn.

[1] Aliquot taken from total-digestion solution and analyzed by standard method.

generally silicate-rich rocks with a high manganophile (usually mafic) silicate mineral content. (See, for example, table 2, samples R4A and R7A; table 4, samples AII–201, AII–257, and AII–279.) The above data suggest that part of the manganese in these samples is probably tightly held in certain silicate minerals. This part is not put into solution in the acid-soluble method but is released and determined in the spectrographic method. Higher manganese values were obtained by the total-digestion method than were obtained by the acid-soluble digestion method on several of the samples shown in table 6. (See, for example, samples V–1072 and V–1073.) These higher values further substantiate that the acid-soluble technique should not be considered to be a total-extraction technique and that the type of material being analyzed must be considered.

Sensitivity

The proposed atomic-absorption method has a lower limit of detection of about 20 ppm for manganese. This limit can be made lower by using a larger amount of sample or by using more sensitive instrumentation. This detection limit compares very favorably with that of the spectrographic method (10 ppm) and is superior to that of the colorimetric method (about 50 ppm).

Precision

Table 7 summarizes data on the precisions of the proposed method used with both hydrochloric and nitric acids. Precision was established by running determinations on separate 0.1-g portions of the same sample. The relative standard deviation is a measure of the precision of the method. The precision of the method is within acceptable limits for geochemical analyses using either the acid-soluble or the total-digestion method.

Analytical problems

The proposed method has been tested on various types of geological and botanical materials that are normally analyzed in a geochemical exploration laboratory. The values obtained by this method compare favorably with values determined independently by other methods. The tested samples ranged in manganese content from less than 20 ppm to 9,000 ppm. Probably more than 95 percent of all routine field samples in most geochemical surveys would fall in the above concentration range for manganese. No interferences affecting the performance of the atomic-absorption method as compared with the other two methods were noted.

Because high concentrations of manganese are only sparingly soluble in nitric acid, a nitric acid digestion of samples containing more than about 1 percent Mn will not normally extract all the available manganese (G. A. Nowlan, oral commun., 1970); any such samples must be digested with hydrochloric acid or must be analyzed by some other method.

Some of my preliminary work suggests that iron, calcium, magnesium, and other ions, if present in concentrations greater than about 5 percent, may enhance the concentration of manganese somewhat when there is a concentration of less than about 10 ppm of Mn in the solution. Persons desiring to work with very low concentrations of manganese are therefore warned to test for interferences in such samples.

TABLE 7.—*Replicate determinations of manganese in various types of material by atomic absorption*

Sample No.	Description	Acid used	Number of determinations	Mn content (ppm)		Mean with confidence limits at 95-percent level (ppm)	Relative standard deviation (percent)
				Maximum	Minimum		
Acid-soluable manganese							
X-2	Plant ash, creosote.	HCl	10	620	590	610±20	1.6
		HNO_3	10	580	540	560±30	2.5
X-1	---do	HCl	10	470	440	460±20	2.4
		HNO_3	10	400	370	385±20	2.8
R6A	Granite	HCl	10	780	710	740±40	2.6
		HNO_3	10	520	480	510±30	2.7
V-1068	Cu-Zn sulfide "ore."	HCl	10	1,700	1,500	1,570±140	4.3
		HNO_3	10	1,400	1,200	1,270±140	5.3
AII-287	Altered biotite granite.	HCl	10	40	35	38±4	5.6
		HNO_3	9	33	30	31±3	4.0
Total Manganese							
V-1083	Diabase	HCl	10	680	640	670±20	1.7
		HNO_3	10	630	620	626±10	.8

CONCLUSIONS

A new method for the determination of manganese in geological and botanical materials has been developed. This new method is superior to both the existing methods in many respects; it is significantly more rapid than either of the older methods, an important economic factor. The new method has a lower limit of detection (about 20 ppm of Mn or less routinely), which is nearly equal to that of the six-step spectrographic method (10 ppm) but which is more sensitive than the colorimetric method (about 50 ppm). The new method is capable of greater value discrimination than the older methods, because sample values are compared to any point on a calibrated standard curve rather than to only widely spaced standard values. No interferences have been detected in any of a variety of types of geochemical samples analyzed by the proposed method, whereas interferences may present a problem in either or both of the older methods. The new method is suitable for determining either acid-soluble or total manganese.

Unlike the colorimetric method, the solution prepared for the atomic-absorption method can be readily used to determine additional elements with no further preparation except for possible dilution of the sample solution and adjustment of the atomic-absorption spectrophotometer for another element, a relatively simple procedure. This ability to make multiple determinations from a single digestion is an important factor in the growing popularity of atomic-absorption analysis.

REFERENCES

Bundy, W. M., 1958, Wall-rock alteration in the Cochiti mining district, New Mexico: New Mexico Bur. Mines and Mineral Resources, Bull. 59, 71 p.

Canney, F. C., Dennen, W. H., and Post, E. V., 1964, Some observations on the evaluation of stream sediment geochemical data [abs.]: Mining Eng., v. 16, no. 12, p. 92.

Emmons, W. H., 1936, Hypogene zoning in metalliferous lodes: Internat. Geol. Cong., 16th, Washington, D.C., 1933, Rept., v. 1, p. 417–432.

Grimes, D. J., and Marranzino, A. P., 1968, Direct-current arc and alternating-current spark emission spectrographic field methods for the semiquantitative analysis of geologic materials: U.S. Geol. Survey Circ. 591, 6 p.

Hewett, D. F., 1968, Silver in veins of hypogene manganese oxides: U.S. Geol. Survey Circ. 553, 9 p.

Horsnail, R. F., Nichol, Ian, and Webb, J. S., 1969, Influence of variations in secondary environment on the metal content of drainage sediments, *in* Canney, F. C., ed., International geochemical exploration symposium: Colorado School Mines Quart., v. 64, no. 1, p. 307–322.

Jerome, S. E., 1966, Some features pertinent in exploration of porphyry copper deposits, *in* Titley, S. R., and Hicks, C. L., eds., Geology of the porphyry copper deposits, southwestern North America: Arizona Univ. Press, p. 75–85.

Post, E. V., and Hite, J. B., 1964, Heavy metals in stream sediment, west-central Maine [revised ed.]: U.S. Geol. Survey Mineral Inv. Map MF–278.

Post, E. V., Lehmbeck, W. L., Dennen, W. H., and Nowlan, G. A., 1967, Map of southeastern Maine showing heavy metals in stream sediments: U.S. Geol. Survey Mineral Inv. Map MF–301 [1968].

Ward, F. N., Lakin, H. W., Canney, F. C., and others, 1963, Analytical methods used in geochemical exploration by the U.S. Geological Survey: U.S. Geol. Survey Bull. 1152, 100 p.

DETERMINATION OF LEAD IN ROCKS AND MINERALS AFTER EXTRACTION WITH DIETHYLAMMONIUM DIETHYLDITHIOCARBAMATE

By LILLIE B. JENKINS and ROOSEVELT MOORE, Washington, D.C.

Abstract.—A method for determining low concentrations of lead in rocks and minerals is described. Samples are decomposed by attack with mixed acids followed by carbonate and sulfate fusions. Lead is extracted with diethylammonium diethyldithiocarbamate and determined by atomic absorption. Lead can be determined in the parts-per-million range with a standard deviation of 2 to 3 ppm.

Dithizone has been, for many years, the most commonly used reagent for determining trace concentrations of lead. A serious complication arises in applying dithizone methods to determining lead in rocks and in many minerals because of the difficulty in obtaining a clear solution of a 1-g sample at the required pH range of 8 to 11.

The dithiocarbamate class of reagents can be used to extract lead from acid solution. Their use simplifies the problem of maintaining complete solution of a rock sample while extracting lead.

Maynes and McBryde (1957) used diethylammonium diethyldithiocarbamate to separate lead from a number of elements known to interfere in the dithizone procedure. Using successive extractions, they separated the lead and used dithizone to determine its concentration in several minerals.

In the presence of the quantities of iron in a 1-g sample of most rocks, the extraction of lead with diethylammonium diethyldithiocarbamate gives poor recovery. If iron is reduced with ascorbic acid first, lead may be quantitatively extracted from 1.8 to 2.0*N* hydrochloric acid solutions.

A hydrofluoric-nitric acid decomposition, followed by two fusions, one with carbonate then one with sulfate, was found to be the simplest way to insure complete decomposition of most samples.

ANALYTICAL METHOD

Reagents

Water: Redistill water in an all-glass still.

Nitric acid: Redistill nitric acid, reagent ACS, from an all-glass still. Bubble oxygen into the distillation flask to prevent bumping.

Hydrofluoric acid: Purify with strontium chloride (Sandell, 1950, p. 404).

Hydrochloric acid, 6*N*: Glass distill two liters of 1+1 hydrochloric acid. Discard the first 500 ml, and collect 1 liter.

Chloroform, "lead-free", spectraanalyzed, lead 0.01 ppm.

Dithizone, 0.005 percent in chloroform: Use purified dithizone. (Rader and Grimaldi, 1961, p. 1–7).

Sodium carbonate, 20 percent aqueous: Extract with several 10-ml portions of 0.005-percent dithizone. Remove dithizone by shaking with chloroform. Store in plastic bottles.

Potassium sulfate fusion solution: Dissolve 300 g of reagent ACS potassium pyrosulfate in about 800 ml of hot water, cool and add about 200 ml of ammonium hydroxide. Dilute to 3 liters and adjust pH to 9 to 9.6 with ammonium hydroxide. Extract with several small portions of dithizone (0.005 percent). Wash with chloroform, and store in plastic bottles.

L-ascorbic acid, 20 percent: Dissolve 100 g of L-ascorbic acid in 500 ml of hot water. Do not store this solution for more than 1 month because of its instability.

Sulfuric acid, heavy metals as lead less than 1 ppm.

Diethylammonium diethyldithiocarbamate solution: Prepare according to procedure outlined by Strafford, Wyatt, and Kershaw (1945, p. 233). Use undiluted solution.

Standard lead solution (1 ml = 1 mg Pb): Dissolve 1.599 g of lead nitrate ($Pb(NO_3)_2$) in 50 ml of water to which 10 ml of nitric acid has been added. Transfer to a 1-liter flask and make to volume with water.

Standard lead solution (1 ml = 1 mg Pb): Pipet 20 ml of standard solution (1 ml = 1 mg Pb) into a 200-ml volumetric flask containing 10 ml of 1+1 hydrochloric acid and make to volume. Use this solution for making the working standards.

Procedure

All glassware must be cleaned with a dichromate cleaning solution, washed with water, rinsed with nitric acid, and then rinsed with glass-distilled water.

A reagent blank must be carried through the entire procedure for each group of samples.

Weigh 1g of finely ground sample (–200 mesh) into a 75- to 100-ml platinum dish. Disperse in a little water, add 10 ml of nitric acid and digest on

U.S. GEOL. SURVEY PROF. PAPER 700-D, PAGES D222–D224

the steam bath 5 to 10 minutes. Add 30 to 50 ml of hydrofluoric acid and evaporate to dryness. Break up the fluorides by evaporating with three 2-ml portions of nitric acid.

Add 5 to 10 ml of water to the platinum dish, and transfer the sample to a 150-ml beaker containing 32 ml of 6*N* hydrochloric acid. The total volume should be no more than 60 ml.

Bring the sample to a rapid boil, add a small amount of paper pulp and filter through a medium-pore 9-cm filter into the original platinum dish. Return the sample solution to the beaker; transfer the filter paper to the platinum dish and carefully ash the paper. Cool.

Add 5 ml of sodium carbonate solution to the dish, carefully evaporate to dryness under a heating lamp, fuse the sample and cool. Add a few milliliters of water to the dish, then carefully add 15 to 20 ml of the sample solution. Cover and heat gently just short of boiling. Add a little paper pulp and filter through a medium-pore 9-cm filter into the beaker containing the sample solution. Wash with water; the total volume should not exceed 70 to 80 ml after washing. Transfer the filter paper to the platinum dish and carefully ash the paper. Add 5 ml of 1+1 hydrochloric acid to the sample solution and reserve.

To the platinum dish, add 10 ml of potassium sulfate solution. Evaporate to dryness under a heating lamp, add 0.1 ml of sulfuric acid and fuse. Transfer about 20 ml of the sample solution to the platinum dish, heat just short of boiling, then return to the original beaker and bring to a vigorous boil. Cool. The total volume should be 95 ml.

Reduce iron by adding 5 ml of ascorbic acid to the solution, then transfer to a 125-ml separatory funnel containing 15 ml of diethylammonium diethyldithiocarbamate solution. Shake for 5 minutes. Transfer the carbamate layer to the original beaker, washing the funnel with 2 to 3 ml of chloroform. Repeat the extraction with two more 15-ml portions of diethylammonium diethyldithiocarbamate. Cover the beaker with a ribbed watch glass, place in a hood under a heating lamp and carefully evaporate to dryness.

Keeping the beaker covered, add about 3 ml of water, then cautiously add 3 ml of nitric acid to the residue. Evaporate on the steam bath. Add 2 ml of (1+1) hydrochloric acid and evaporate to dryness.

To the dry residue, add 5 ml of (1+1) hydrochloric acid and about 2 ml of water. Cover and heat just short of boiling. Transfer to a 25-ml volumetric flask and make to volume. This solution is now ready for the determination of lead by atomic absorption.

Prepare 10-percent hydrochloric acid solutions of standards ranging from 0 to 100 μg in a series of 25-ml volumetric flasks. Set the atomic absorption spectrophotometer for determining lead as described in the instrument manual.

Atomize the sample alternately between a standard of higher and of lower lead concentration. Calculate parts per million of lead.

DISCUSSION AND RESULTS

It is important to maintain a blank consistently low in lead content, as the concentration of lead in some rocks is below 10 ppm. Reagent ACS potassium pyrosulfate used in the decomposition procedure may contain 10 ppm of heavy metals such as lead. The lead was removed from a solution of the potassium pyrosulfate at a pH of 9 to 10, by extracting with dithizone.

The lead content of the reagent blank was reduced an average of 6 μg when laboratory-prepared diethylammonium diethyldithiocarbamate was used instead of the reagent obtained from one chemical company. The reagent blanks run routinely as controls with samples give a mean value for lead of 6.7 μg (chemist 1) and 6.1 μg (chemist 2) and a standard deviation of 2.1 μg (chemist 1) and 2.0 μg (chemist 2).

Duplicate analyses of more than 400 samples were made by two chemists in this laboratory. The results obtained for standards analyzed routinely with the samples (table 1) are indicative of the reproducibility of the technique.

TABLE 1.—*Comparison of results obtained for lead, in parts per million, in standard samples*

[Chemist 1, L. B. Jenkins; chemist 2, Roosevelt Moore]

	Chemist 1			Chemist 2		
Sample	Number of determinations	Mean	Standard deviation	Number of determinations	Mean	Standard deviation
G-1	16	49.0	2.3	32	50.6	2.9
G-2	16	28.4	3.2	23	30.8	2.4
W-1	16	9.1	2.6	10	7.7	0.6

REFERENCES

Maynes, A. D., and McBryde, W. A. E., 1957, Determination of traces of lead in igneous minerals: Anal. Chemistry, v. 29, no. 9, p. 1259–1263.

Rader, L. F., and Grimaldi, F. S., 1961, Chemical analyses for selected minor elements in Pierre Shale: U.S. Geol. Survey Prof. Paper 391–A, 45 p.

Sandell, E. B., 1950, Colorimetric determination of traces of metals, 2d ed.: New York-London, Interscience, 642 p.

Strafford, N., Wyatt, P. F., and Kershaw, F. G., 1945, A scheme for the photometric determination of minute amounts of arsenic, copper, lead, zinc, and iron (with certain other metals) in organic compounds, e.g., medicinal: Analyst, v. 70, p. 232–246.

A PYROCATECHOL VIOLET SPECTROPHOTOMETRIC PROCEDURE FOR THE DIRECT MICRODETERMINATION OF ALUMINUM IN SILICATE MINERALS

By ROBERT MEYROWITZ, Washington, D.C.

Abstract.—The Al_2O_3 content of 3–5-mg samples of common silicate minerals is determined spectrophotometrically by a direct pyrocatechol violet procedure. The sample is decomposed by sodium hydroxide fusion in a gold crucible, and a hydrochloric acid solution of the melt is used for the determination at a pH of 6.0. Of the common rock-forming elements likely to be present in most silicate minerals, only iron, titanium, and fluorine interfere; however, fluorine in concentrations most likely to be found in most minerals does not interfere. Titanium and iron interference is overcome by adding the titanium and iron contents of the sample to the standard aluminum solutions used for the standard aluminum curve. The absorbance is measured at 580 mμ. Beer's law is obeyed within the range of 0.2–0.8 ppm Al_2O_3. The tolerances of 48 elements were determined. The sensitivity is 0.00045 μg Al/cm². The suitability of the recommended procedure was tested using nine standard silicate minerals and rocks.

This paper is the fourth in a series describing micro- and semimicro-procedures being developed by the author (Meyrowitz, 1963, 1964, 1969) for the direct determination of the common rock-forming elements as part of a scheme for the complete analysis of small samples of silicate minerals. This paper describes the use of pyrocatechol violet for the microdetermination of aluminum in silicate minerals. The procedure is based on extensive studies of the relevant parameters and possible interfering elements. Anton (1960) used pyrocatechol violet for the rapid estimation of aluminum in the presence of magnesium and zinc. Wilson and Sergeant (1963) proposed its use for the "rapid evaluation of aluminum in milligram samples of minerals." Tanaka and Yamayosi (1964) investigated the parameters for the use of the reagent for the determination of aluminum but gave no application. It has been used for determining aluminum in steel, iron alloys, bronze, brass, and special alloys (Mustafin and others, 1967), and in solid solutions of lanthanum aluminate and calcium titanate (Molot and others, 1968).

REAGENTS AND APPARATUS

Reagents

Mercaptoacetic acid, 4 percent (v/v): Prepare fresh daily.

Pyrocatechol violet, 0.03 percent (w/v): Prepare 500 ml, filter through a slow paper, and store in glass. Discard after 5 days. Obtained from J. T. Baker Chemical Co.

Ammonium acetate, 50 percent (w/v): Prepare 1,000 ml, filter through a fast paper, and store in glass.

U.S. National Bureau of Standards standard soda feldspar 99a or equivalent.

Iron solution (1,000 ppm Fe_2O_3; 0.12*N* HCl): Dissolve 4.91 g ferrous ammonium sulfate hexahydrate in distilled water, add 20.0 ml of 6*N* HCl, and dilute to 1 liter.

Titanium solution (1,000 ppm TiO_2): Prepare from U.S. National Bureau of Standards standard titanium oxide 154a. Follow directions in "Procedure for Use as a Standard in Colorimetry" on the certificate of analysis provided with the standard.

Apparatus

Absorbance scanning was made with a Beckman DU spectrophotometer equipped with a Warren Spectrocord recording attachment. Absorbance measurements at a fixed wavelength were made with a Beckman Model B spectrophotometer.

PROCEDURE

Preparation of sample solution

Follow procedure previously described by the author (Meyrowitz, 1969, p. B137), using 3- to 5-mg samples and 3.5- to 4.5-mg portions of the standard feldspar.

Determination of Al_2O_3

Blank, standard, and unknown solutions are run simultaneously in duplicate. The volumetric flasks should be cleansed with 1+1 HCl and rinsed well with water. The neck of each flask is rinsed down

with water, and the contents of the flask are mixed well after the addition of each solution and reagent.

Transfer duplicate 5.00-ml aliquots of 0.06*N* HCl solutions of standard feldspar and sample to each of two 100-ml volumetric flasks. The final concentration of Al_2O_3 is 0.2 to 0.8 ppm. Add the amounts of titanium and iron solutions to the standard feldspar solutions to match the sample. Add 4.5 ml of 0.12*N* $HClO_4$ to the flasks containing the unknown solutions. If the amount of acid present in the flasks containing the standard feldspar solutions is less than the equivalent of 7.0 ml of 0.12*N* H^{+1}, add sufficient 0.12*N* $HClO_4$ to reach this acidity. Add 5.0 ml mercaptoacetic acid solution. Allow to stand for 10 minutes. Add 10.00 ml pyrocatechol violet solution with a transfer pipet. Allow to stand for 10 minutes. Dilute with water to approximately 80 ml. Add 10.0 ml ammonium acetate solution while swirling the flask. Dilute to mark, mix, and let stand for 60 minutes. Determine the absorbances at 580 mμ, using a 1-cm cell path with water as reference solution. Plot a standard Al_2O_3 curve from the data of the standard feldspar solutions. Calculate the Al_2O_3 content of the unknowns from the standard Al_2O_3 curve.

RESULTS

Absorption spectra.—Figure 1 shows the absorption spectra of the reagent blank and of solutions containing aluminum, iron, and titanium developed by the recommended procedure and measured against a distilled water blank; the peak of the aluminum complex occurs at 580 mμ.

Effect of pH.—Figure 2 shows the absorption spectra of solutions containing aluminum at different pH values together with the absorption spectra of the corresponding reagent blanks. The recommended procedure was followed for pH 6.0. For pH 5.7, the equivalent of 25.0 ml of 0.12*N* H^{+1} was present before the addition of the reagents. For pH 6.2, the 10.0 ml of 50-percent ammonium acetate was replaced by 40.0 ml of 25-percent sodium acetate plus 2.5 ml of 0.2*N* NaOH. For pH 6.4, the 10.0 ml of 50-percent ammonium acetate was replaced by 40.0 ml of 25-percent sodium acetate plus 7.5 ml of 0.2N NaOH. The absorbance peak is 580 mμ for pH 5.7 to 6.4.

Adherence to Beer's law and sensitivity.—The system conforms to Beer's law over the range 0.2–0.8 ppm Al_2O_3 using a 1-cm cell path for pure

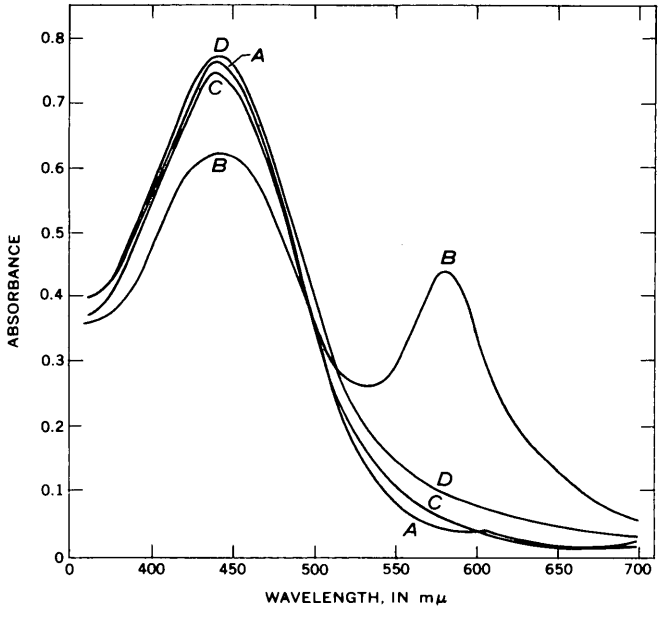

FIGURE 1.—Absorption spectra curves. *A*, reagent blank; *B*, 0.40 ppm Al_2O_3; *C*, 1.00 ppm Fe_2O_3; *D*, 0.25 ppm TiO_2. Reference solution, water; cell path, 1 cm; pH, 6.0.

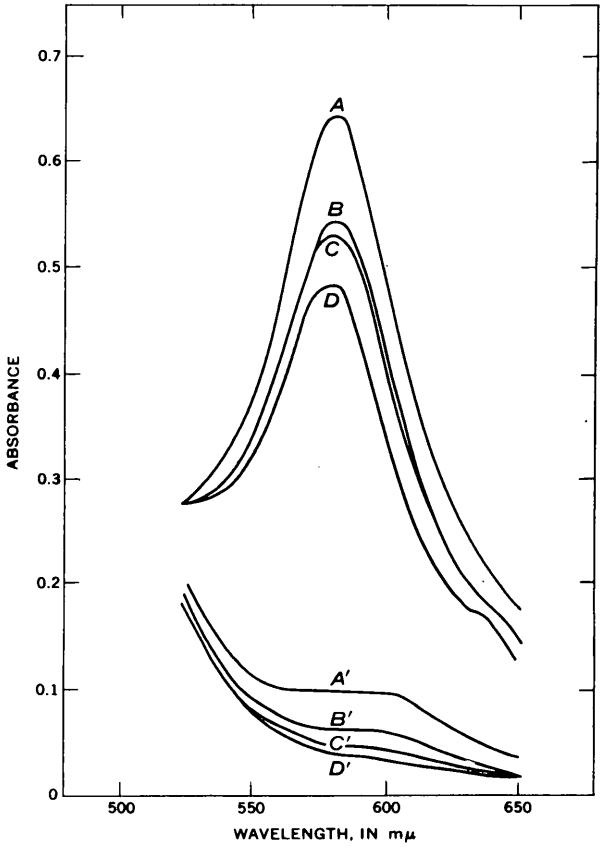

FIGURE 2.—Variation of absorption spectra curves of solutions with different pH. *A*, 0.40 ppm Al_2O_3, pH 6.4; *A'*, reagent blank, pH 6.4; *B*, 0.40 ppm Al_2O_3, pH 6.2; *B'*, reagent blank, pH 6.2; *C*, 0.40 ppm Al_2O_3, pH 6.0; *C'*, reagent blank, pH 6.0; *D*, 0.40 ppm Al_2O_3, pH 5.7; *D'*, reagent blank, pH 5.7. Reference solution, water; cell path, 1 cm.

aluminum solutions. The sensitivity by Sandell's definition (1959, p. 83) is 0.00045 μg Al/cm^2 at 580 mμ.

Effect of development time.—The absorbance of a 0.4-ppm Al_2O_3 solution was measured at 30-minute intervals for 2 hours with distilled water as reference solution. The average increase in absorbance was 0.010 after each 30-minute interval.

Effect of reagent concentration.—Figure 3 shows the effect at constant pH of the concentration of pyrocatechol violet on the increase in absorbance due to the aluminum complex. (10.0 ml of 0.03-percent pyrocatechol violet = final concentration of 30×10^{-4} percent pyrocatechol violet.)

Effect of diverse ions.—Table 1 shows the maximum concentrations ($\leqq$ 1.00 ppm) of some 45 elements, calculated as oxides, tested for effect on absorbance. The tolerance limit of deviation between test solution and blank was held at $\pm$0.003 absorbance unit.

Effect of fluoride.—Table 2 shows the effect of fluoride on absorbance of aluminum solutions at different concentrations.

For an aliquot of sample solution equivalent to 0.25 mg, the factor for converting parts per million of oxide and fluoride in the final solution to percentages of oxide and fluoride in the sample is 40.

Comparative analytical results.—Table 3 gives the results obtained using the recommended procedure in the microdetermination of aluminum in nine standard minerals and rocks. To reduce the sampling error in the analysis of the rock standards, sample sizes larger than the recommended 3 to 5 mg were used. The results obtained are compared with those generally accepted as the "best" values (table 3).

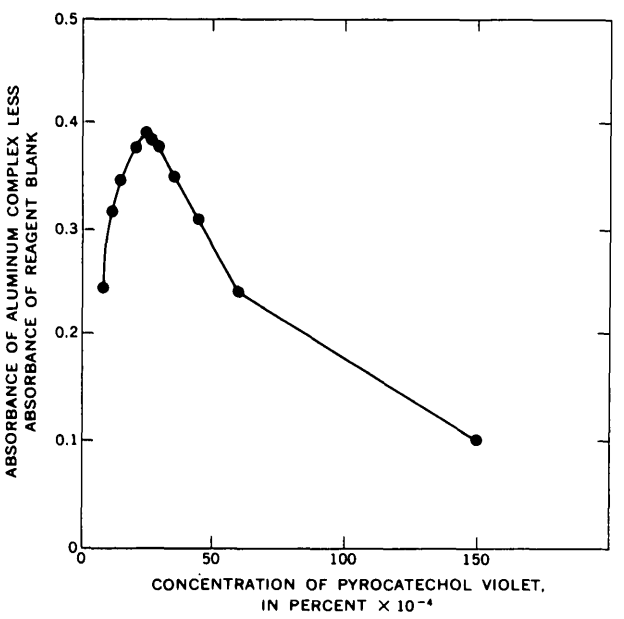

FIGURE 3.—Effect of concentration of pyrocatechol violet on absorbance spectra. Reference solution, water; wavelength, 580 mμ; cell path, 1 cm; concentration of aluminum, 0.40-ppm Al_2O_3; pH, 6.0.

TABLE 1.—*Effect of diverse elements on absorbance*

[maximum concentration of elements tested calculated as oxides, $\leqq$ 1.00 ppm. Limiting tolerance of measured absorbance of test solution versus blank, $\pm$0.003 absorbance unit ($\approx$0.0025 ppm Al_2O_3]

Oxide	Maximum concentration (ppm)	Oxide	Maximum concentration (ppm)	Oxide	Maximum concentration (ppm)
BeO	1.00	Ho_2O_3	1.00	CoO	0.30
MgO	1.00	Er_2O_3	1.00	NiO	1.00
CaO	1.00	Tm_2O_3	1.00	CuO	1.00
SrO	1.00	Yb_2O_3	1.00	ZnO	1.00
BaO	1.00	Lu_2O_3	1.00	CdO	1.00
Sc_2O_3	1.00	TiO_2	(1)	B_2O_3	[2]1.00
Y_2O_3	1.00	ZrO_2	.08	Ga_2O_3	1.00
La_2O_3	1.00	V_2O_5	.08	In_2O_3	1.00
Ce_2O_3	1.00	V_2O_4	.15	Tl_2O_3	1.00
Pr_2O_3	1.00	Nb_2O_5	.08	SnO_2	1.00
Nd_2O_3	1.00	Ta_2O_5	.14	PbO	1.00
Sm_2O_3	1.00	Cr_2O_3	[3].20	P_2O_5	1.00
Eu_2O_3	1.00	MoO_3	1.00	As_2O_5	1.00
Gd_2O_3	1.00	WO_3	.20	ThO_2	.50
Tb_2O_3	1.00	MnO	1.00	UO_3	1.00
Dy_2O_3	1.00	Fe_2O_3	(1)		

[1] TiO_2 and Fe_2O_3 are added to the standard solutions.
[2] No interference in the presence or absence of 0.20 ppm Al_2O_3.
[3] As Cr^{+3} and Cr^{+6}.

TABLE 2.—*Effect of fluoride on absorbance of aluminum solutions*

[Results obtained by subtracting absorbance values of fluoride-containing aluminum solutions from absorbance values of pure aluminum solutions]

Aluminum concentration [1] (ppm)	Fluoride concentration (parts per million)						
	0.0125	0.025	0.050	0.075	0.10	0.15	0.20
0.20	−0.001	—	−0.001	—	0.000	−0.004	−0.005
0.25	—	0.000	−.001	−0.002	—	—	—
0.40	—	+.001	+.001	−.003	−.003	−.008	−.010
0.50	—	+.003	—	—	—	—	—
0.60	—	+.003	.000	—	−.007	—	—

[1] Calculated as Al_2O_3.

DISCUSSION

A pH of 6.0 for the final solution was selected because at this pH there is a relatively large net absorbance. However, the pH of the final solution may range from 5.9 to 6.2, but samples and standards within a set should not differ by more than 0.1 pH unit. If the amount of acid present in the solution contains the equivalent of 7.0 ml of 0.12*N* H^{+1} before the mercaptoacetic acid reagent is added, the pH of all solutions within a set will not differ by

TABLE 3.—*Pyrocatechol violet spectrophotometric microdetermination of aluminum in selected standard silicate minerals and rocks*

Sample	Known concentration of total iron, titanium, and fluorine (weight percent)			Microdetermination, this report				Determination by others	
				Weight of sample (milligrams)		Al_2O_3 values (weight percent)			
	Fe_2O_3	TiO_2	F	Fused	Used	Determined	Mean [1]	Al_2O_3 (weight percent)	Source of data
U.S. National Bureau of Standards standard sample:									
70, feldspar	0.03	0.002	---	6.23	0.312	17.72	17.83	18.03	Certificate of analysis.
				5.31	.266	17.93			
70a, feldspar	.08	.01	---	5.88	.294	17.96	18.03	17.9	Do.
				4.60	.230	18.09			
99, soda feldspar	.07	.02	---	5.46	.273	19.05	19.21	19.06	Do.
				4.13	.207	19.37			
U.S. Geological Survey standards:									
G–1, granite	1.94	.26	0.07	7.29	.365	14.54	14.24	14.04	Fleischer (1969, p. 65, column 3a).
				9.12	.456	14.04		14.08	Ingamells and Suhr (1963, p. 908).
				6.36	.318	14.15		14.20	Mercy and Saunders (1966, p. 178).
W–1, diabase	11.09	1.07	.03	7.34	.367	15.18	15.03	14.85	Fleischer (1969, p. 65, column 3b).
				9.48	.474	14.98		14.94	Ingamells and Suhr (1963, p. 908).
				5.60	.280	14.93		14.98	Mercy and Saunders (1966, p. 178).
G–2, granite	2.76	.53	.13	7.32	.366	15.63	15.41	15.34	Flanagan (1969, p. 109).
				8.52	.426	15.52			
				4.81	.241	15.10			
AGV–1, andesite	6.80	1.08	.04	6.26	.313	17.25	17.04	17.01	Do.
				9.27	.464	16.87			
				4.99	.250	16.99			
GSP–1, granodiorite	4.33	.69	.38	6.90	.345	15.07	14.85	15.11	Do.
				9.99	.500	14.57			
				6.65	.333	14.92			
BCR–1, basalt	13.50	2.23	.05	6.94	.347	13.72	13.42	13.65	Do.
				9.71	.486	13.35			
				6.00	.300	13.20			

[1] Standard deviation, 0.24.

more than 0.1 pH unit. The acid may be either HCl, H_2SO_4, $HClO_4$ or a mixture of them.

Although the absorbance of the final solution increases on standing, experience shows that the recommended procedure is reliable provided that the absorbance of the solutions of the same set is measured in the same order in which they were prepared to insure that the standing time for all solutions is approximately the same.

In the common silicate minerals, only iron, titanium, and fluorine are normally present to affect the determination of aluminum. To overcome the interference of titanium and iron, the same amounts of titanium and iron present in the portion of 0.06*N* HCl solution of the mineral taken for analysis are added to the standard aluminum solutions used to prepare the standard aluminum curve. The amounts of aluminum taken for the standards should bracket or be close to the unknowns. Ordinarily a complete analysis is made so that the titanium and iron data are available for judging the additions. Generally, a 5.00-ml portion of the acid solution of the feldspar is taken for the standard aluminum solution. Therefore, the volumes of titanium and iron solutions added to each standard aluminum solution must not exceed the equivalent of 4.5 ml of 0.12*N* H^{+1}. This limitation must be considered when one prepares the dilute standard titanium and iron solutions to be added. The concentration of fluorine, scandium, zirconium, vanadium, niobium, tantalum, chromium, tungsten, cobalt, and thorium in most common silicate minerals is not sufficient to interfere with the determination of aluminum.

In many analyses where the tolerance level may be exceeded, it is possible to make the determination by taking a smaller portion of the sample, provided that the concentration of the aluminum in the final solution is not less than 0.20 ppm Al_2O_3. Where it is not possible to use a smaller portion of the sample solution, the interference of some elements may be overcome by adding the same amount of interfering element present in the analyzed solution to the feldspar solutions used to prepare the standard aluminum solutions. Similarly, larger portions of the sample solution can be used for the determination of aluminum where the concentration is less than 8 percent Al_2O_3 (less than 0.20 ppm Al_2O_3 in the final solution), provided that the tolerance level of the possible interfering elements is not exceeded. The "spiking" technique may also be used to overcome possible interferences.

The free acid must be maintained at the "equivalent of 7.0 ml of 0.12*N* H^{+1}" mentioned above. If this is exceeded, it can be compensated for by adding sufficient dilute NaOH to neutralize the excess acid. To compensate for the aluminum that might be present in this additional NaOH, the same amount of NaOH is added to the standard aluminum solutions together with the equivalent amount of dilute acid needed to neutralize it.

Wilson and Sergeant (1963) proposed using an acid cupferron–chloroform extraction to overcome the interference of titanium and iron. However, no results of its application to silicate materials were given. Mercy and Saunders (1966, p. 175) tested the cupferron separation procedure of Wilson and Sergeant, and concluded that "The pyrocatechol method serves only to give an approximation of the Al_2O_3 content." This conclusion is not valid for the recommended procedure presented herein because the results obtained by the author in the microanalysis of the standard silicate minerals and rocks compare favorably with those obtained by others using different methods for determining aluminum (table 3).

REFERENCES

Anton, Anthony, 1960, Colorimetric estimation of aluminum with Pyrocatechol Violet: Anal. Chemistry, v. 32, p. 725–726.

Flanagan, F. J., 1969, U.S. Geological Survey standards—[Pt.] 2, First compilation of data for the new U.S.G.S. rocks: Geochim. et Cosmochim. Acta, v. 33, p. 81–120.

Fleischer, Michael, 1969, U.S. Geological Survey standards—[Pt.] 1, Additional data on rocks G–1 and W–1, 1965–1967: Geochim. et Cosmochim. Acta, v. 33, p. 65–79.

Ingamells, C. O., and Suhr, N. H., 1963, Chemical and spectrochemical analysis of standard silicate samples: Geochim. et Cosmochim. Acta, v. 27, p. 897–910.

Mercy, E. L. P., and Saunders, M. J., 1966, Precision and accuracy in the chemical determination of total Fe and Al in silicate rocks: Earth and Planetary Sci. Letters, v. 1, p. 169–182.

Meyrowitz, Robert, 1963, A semimicroprocedure for the determination of ferrous iron in nonrefractory silicate minerals: Am. Mineralogist, v. 48, p. 340–347.

——— 1964, The direct spectrophotometric microdetermination of high-level magnesium in silicate minerals—A Clayton Yellow procedure: Am. Mineralogist, v. 49, p. 769–777.

——— 1969, The direct microdetermination of silicon and aluminum in silicate minerals, *in* Geological Survey Research 1969: U.S. Geol. Survey Prof. Paper 650–B, p. B136–B139.

Molot, L. A., Arkhangel'skaya, A. S., Trusova, M. I., and Mustafin, I. S., 1968, Determination of aluminum in lanthanum aluminate-calcium titanate solid solutions: Zavodskaya Lab., v. 34, p. 408. [In Russian]

Mustafin, I. S., Molot, L. A., and Arkhangel'skaya, A. S., 1967, Polyhydroxytriphenylmethane dyes as reagents for aluminum—Communication 1, Pyrocatechol Violet and its complex with aluminum: Zhur. Anal. Khimii, v. 22, p. 1808–1811. [In Russian]

Sandell, E. B., 1959, Colorimetric determination of traces of metals, 3d ed.: New York, Interscience Publishers, Inc., 1032 p.

Tanaka, Katu, and Yamayosi, Katutosi, 1964, Pyrocatechol Violet as a reagent for colorimetric determination of tin (IV) and aluminum: Bunseki Kagaku, v. 13, p. 540–544.

Wilson, A. D., and Sergeant, G. A., 1963, The colorimetric determination of aluminum in minerals by Pyrocatechol Violet: Analyst (London), v. 88, p. 109–112.

SOME TECHNIQUES FOR PHOTOGRAPHING FOSSILS

By KENJI SAKAMOTO, Menlo Park, Calif.

Abstract.—A newly designed electrically heated spray gun incorporating a variable transformer and using a filtering substance provides a safe and improved method of coating fossils with ammonium chloride sublimate. A photographic technique for producing an initial white background on photographs of megafossils provides a more accurate representation of specimens than do the conventional methods of removing the normal black background by opaquing the negative or trimming the print. This method also permits a significant saving of time over the other methods, particularly opaquing.

Refined techniques of photographing megafossils have been developed as a result of experimentation by the U.S. Geological Survey. These new methods of photographing fossils for scientific publication involve a means of producing an initial white background for specimens and an improved method of coating fossils with ammonium chloride. Incorporation of these techniques with conventional photographic procedures has improved both the quantity and quality of photographs prepared by the Survey's paleontological photographic laboratory.

The purpose of this report is to describe these photographic techniques. The reader is referred to the section on illustration of fossils in Kummel and Raup (1965) for a comprehensive review of techniques of photographing fossils.

WHITENING FOSSILS WITH AMMONIUM CHLORIDE

The purpose of whitening, or coating, fossil specimens prior to photography is to eliminate specular reflection and to minimize spottiness produced by contrasts in surface texture or mottled color. The uniform surface produced by coating also emphasizes fine textural detail (relief) on some kinds of organisms such as the microsculpture on some marine clams. Other techniques of coating fossils are reviewed by Kier, Grant, and Yochelson (1965).

The ammonium chloride coating method is the preferred way to deposit a uniform film of very finely divided sublimate on the surface of a specimen. One technique, here referred to as the wet method, involves the reaction of hydrochloric acid with ammonium hydroxide; another technique, the dry method, involves heating powdered ammonium chloride until it sublimes, at which point the smoke is blown across the specimen to be photographed. A spray gun developed for this purpose is shown in figure 1. It is modified from a device developed by Cooper (1935) and subsequently modified by Teichert (1948) and by Sass (1962). It differs from their apparatus principally in the utilization of a transformer-controlled heating element, in the incorporation of a filtering device, and in certain details of design.

The spray gun (fig. 1) consists of a Pyrex glass tube, one-half inch in diameter by 10 inches in length, one end of which is drawn out and cut off so as to produce a small opening—about one-fifth inch in diameter. The tapered part is about 1½ inches long. The opposite end is closed by a cork stopper that houses a glass tube fitted with a rubber pressure bulb. Powdered ammonium chloride is loaded into the front part of the spray gun; the load is held in place by wads of glass wool. The glass wool at the delivering end of the gun also acts as a filtering device that produces a much finer coating than would be possible without it.

The Pyrex tube is tightly wrapped with a Nichrome wire or a heating tape. The coils should be spaced closer together around the tapered part of the spray gun, as is indicated in figure 1, to prevent cooling and possible clogging of the aperture. It is also important that the tapered portion of the spray gun be relatively short so as to minimize the possibility of clogging. The heating element is wrapped with two or three layers of asbestos cloth. This is secured in place by electrical tape which is also used to fasten a wooden handle to the lower part of the gun.

U.S. GEOL. SURVEY PROF. PAPER 700-D, PAGES D230-D232

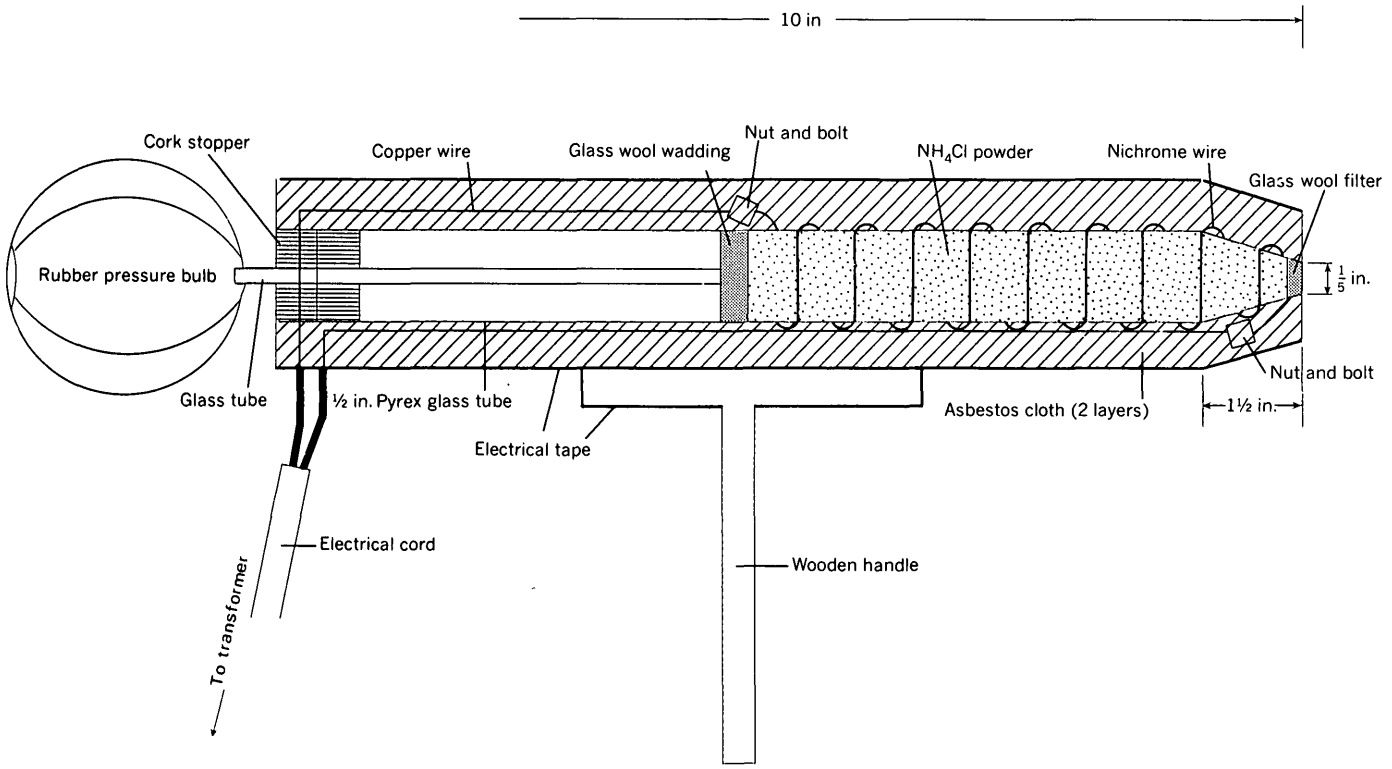

FIGURE 1.—Sketch of electrically heated spray gun (not to scale).

The intensity of heating is controlled by a variable transformer. The amount of heat required for optimal operation of the gun is determined by experience. The electrical current can be reduced or turned off following each application of sublimate, but during a program of continuous fossil photography the gun is usually kept warm so as to reduce the time required to heat it up.

As a safety precaution, the coating procedure should be carried out under a vented hood equipped with an exhaust fan, in order to control the clouds of ammonium chloride smoke generated by the spray gun.

This method of producing an ammonium chloride sublimate has several advantages over the more conventional wet method. It is much safer, is not limited by humidity, and tends to produce a much finer grained sublimate (Cooper, 1935). The use of a variable transformer helps to develop and maintain the optimum temperature for producing the finely divided ammonium chloride sublimate. The heating tape or wire is also safer than an open flame (Teichert, 1948) as a source of heat.

WHITE-BACKGROUND TECHNIQUE

A white background is generally considered best for illustrating megafossils in paleontologic publications (Palmer, 1965, p. 458). Normally, however, the fossils are photographed against a black background. The undesirable black background is removed prior to mounting the photograph either by opaquing the negative or by trimming the print with scissors. Use of scissors to remove the black background is undesirable for photographs of fossils that have irregular or highly ornamented surfaces. Opaquing a negative permits retention of details of a highly ornamented surface, such as delicate spines, but is a very time-consuming procedure and may require considerable artistic skills.

A different, relatively simple technique for producing an initial white background involves the use of a light box for reexposing the specimen against a lighted background. A small light box with a 6-inch-square illuminated surface has proved to be adequate for most megafossil photography. The light source is an internally mounted, transformer-controlled 40-watt bulb; the light box is topped with a pane of frosted glass. A white background for larger specimens, such as vertebrate limbs and giant ammonites, can be achieved by using a portable light table. The procedure is to fix the specimen to a glass plate with a lump of modeling clay. After having been coated with ammonium chloride sublimate, the specimen is centered on top of the light

box, illuminated, and photographed. Next the room is darkened, the light box is switched on, and the dark background surrounding the image on the negative is reexposed. I refer to this procedure as burning the background. An example showing the normal dark background and the white background produced by reexposing the negative is shown in figure 2. Exposure time to obtain the white background depends upon the size of the specimen and the amount of magnification. With professional copy film, the normal exposure time with the aperture set at f/11 is about 20 seconds for natural-size photographs. The length of exposure is greater with higher magnification. The intensity of background illumination can be further controlled by a transformer.

The lighted surface must be only slightly larger than the object to be photographed. If the illuminated area is considerably larger than the fossil, two difficulties may arise: (1) the background may reflect so much additional light into the lens that internal flare will occur in the camera, and (2) the extra light may create disturbing edge reflections around the object being photographed.

The technique of producing an initial white background permits a significant saving of time in preparing fossil plates. Moreover, a much higher degree of accuracy of representation of the fossil specimen can be achieved by producing an initial white background through photographic techniques than can be achieved by trimming with scissors or by opaquing negatives.

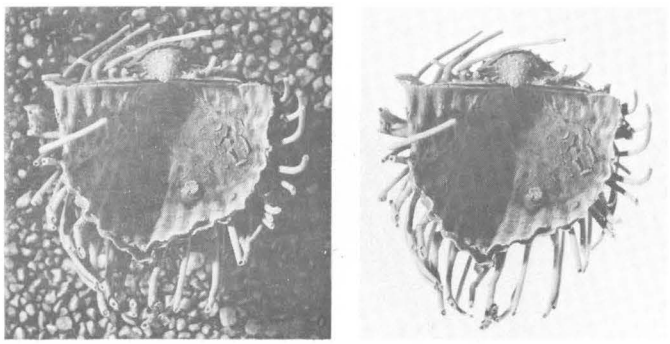

a *b*

FIGURE 2.—Photographs of a spiny brachiopod: *a*, original background; *b*, after reexposing (burning in) the background.

REFERENCES

Cooper, C. L., 1935, Ammonium chloride sublimate apparatus: Jour. Paleontology, v. 9, no. 4, p. 357–359, 2 figs.

Kier, P. M., Grant, R. E., and Yochelson, E. L., 1965, Whitening fossils, *in* Kummel, Bernhard, and Raup, David, eds., Handbook of paleontological techniques: San Francisco, W. H. Freeman & Co., p. 453–456.

Kummel, Bernhard, and Raup, David, 1965, eds., Handbook of paleontological techniques: San Francisco, W. H. Freeman & Co., 852 p.

Palmer, A. R., 1965, Preparation of plates for paleontologic publication, *in* Kummel, Bernhard, and Raup, David, eds., Handbook of paleontological techniques: San Francisco, W. H. Freeman & Co., p. 456–459.

Sass, D. B., 1962, Improved techniques for the photographing of fossils: Jour. Paleontology, v. 36, no. 1, p. 170–176, 1 fig.

Teichert, Curt, 1948, A simple device for coating fossils with ammonium chloride: Jour. Paleontology, v. 22, no. 1, p. 102–104.

BEARING CAPACITY OF LUNAR SURFACE MATERIALS

By GLEN L. MARTIN[1], Bozeman, Mont.

Work done on behalf of the National Aeronautics and Space Administration

Abstract.—Slope stability analysis, applied to failed slopes in lunar craters, suggests that the static mass-bearing capacity of the lunar surface may range from 860 to as much as 9,400 g/cm^2. The analysis includes seismic acceleration as one of the variables. Such accelerations may have a pronounced effect on the stability of lunar slopes.

Several methods have been proposed for indirectly evaluating the bearing capacity of lunar surface materials. One, proposed by Jaffe (1965), applies slope stability analyses to lunar crater walls to estimate the strength parameters of the soil-like material. The resulting strength parameters are then used to evaluate bearing capacity.

Jaffe, working with Ranger 7 photographs, determined a "lower bound for the mass bearing capacity" of lunar surface materials. Although he assumed that the crater slopes selected for analysis had a factor of safety of unity, there was no photographic evidence of slope failure. Jaffe reported that the analyzed slopes had a "soft appearance suggesting substantial dust cover." Such slopes may have reached their configuration by surface erosion rather than failing in accord with the classical "slip circle" assumptions.

In addition, Jaffe assumed that gravity is the only force responsible for the failure of lunar slopes. It is generally accepted that seismic and seepage forces contribute to the failure of terrestrial slopes, and there is no reason to believe that seismic forces are not involved in forming the lunar landscape. Jaffe also did not allow for a "factor of safety" in determining the probable lunar bearing capacity.

[1] Associate Professor of Civil Engineering and Engineering Mechanics, Montana State University, Bozeman, Mont., and Research Civil Engineer, U.S. Geological Survey, Menlo Park, Calif. This work was done under National Aeronautics and Space Administration contract R 66.

The purpose of this paper is to furnish insight into the complexity of indirectly determining lunar bearing capacity by slope-stability techniques, and, also to present what seems to be a rational approach to the problem.

METHODS OF SLOPE STABILITY ANALYSIS

There are many methods of slope stability analysis for determining the factor of safety of a slope against failure. The four more commonly used are: (1) the wedge method, (2) the classical method of slices, (3) Bishop's adaptation to the method of slices, and (4) the finite-element method. In their present form of development, all four assume a linear slope (no curvature normal to the profile of the slope).

The wedge method is valid where a low-strength plane that can be defined controls the failure geometry of the slope. The presence of such a plane in lunar materials has not been established; thus, this method is not applicable.

The method of slices has proven to be an acceptable method of analysis and is presently in a better stage of development than the other three methods mentioned above. It was selected for use in this study.

Bishop's adaptation to the method of slices (Bishop, 1955), which uses effective-stress techniques, yields results which better define the failure state in some terrestrial materials, predominantly those that are cohesive (Schuster, 1967). This more complex method of solution requires much more time and effort, and does not seem justified for lunar near-surface materials because they probably have relatively small values of unit cohesion.

The finite-element method does not yet lend itself

to the determination of strength characteristics, by trial-and-error methods, that can in turn be used in bearing-capacity determinations.

All the aforementioned methods assume a slope with linear contours. However, the contours of slopes of lunar craters tend to be concentric with the rim, and a method for rationally considering the effects of such concave surfaces has not yet been devised. The assumption of a linear slope, when the slope is in reality concave, should result in higher values for the strength parameters than really exist. This results from the fact that the slope concavity itself is a source of "strength."

DEVELOPMENT OF STABILITY CHARTS

Because all the variables that must be known to make unique analyses of the slope stability of lunar near-surface materials are not known, stability charts have been formulated which make multiple analyses a relatively simple task.

The variables involved in a slope stability analysis employing the method of slices are:

1. Surface geometry of the slope.
2. Subsurface geometry of the materials making up the slope.
3. Unit weight of the materials making up the slope.
4. Pore pressures in the materials (pore-liquid or pore-gas pressures).
5. Strength characteristics of the materials (usually expressed in terms of the angle of internal friction and the unit cohesion).
6. Induced seismic forces on the slope.
7. Factor of safety of the slope (defined by Bishop, 1955, p. 7).

A variety of stability charts for the rapid solution of slope stability problems for slopes of isotropic materials have been published. None of these charts, however, incorporate seismic acceleration as a variable. In addition, most charts do not incorporate angles of internal friction greater than 20° or 30°.

Stability charts, with seismic acceleration as a variable, were formulated as follows:

1. A slope geometry, defined by straight lines with the upper boundary horizontal (fig. 1), was assumed. The material making up the slope was assumed to be isotropic, pore pressures were assumed to be nonexistent in the slope, and the circular failure arc was assumed to go through the toe of the slope (because the opposite wall of the crater would prohibit deep-seated failure). The angle that

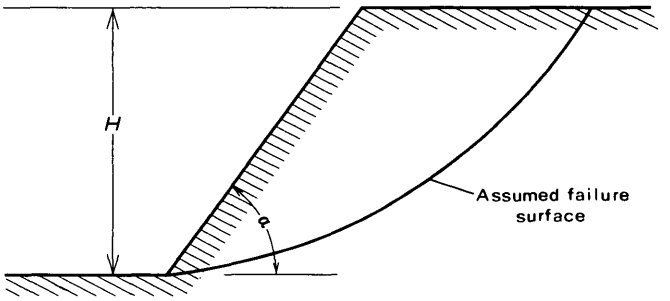

FIGURE 1.—Assumed slope geometry of a hypothetical lunar crater. Symbols are explained in text.

the slope makes with the horizontal was defined as α, and the height of the slope was defined as H.

2. A method-of-slices program on a digital computer was used to determine the minimum factor of safety of the slope by systematically varying

(a) α, the slope angle,
(b) ϕ, the angle of internal friction of the soil material,
(c) A, the horizontal seismic acceleration in terms of the acceleration of gravity (g), and
(d) N_m, stability number, equal to $c/\rho gH$, where
c = cohesion of the soil (dynes/cm^2),
ρ = soil mass density (g/cm^3),
g = acceleration due to gravity (cm/sec^2), and
H = critical height (cm) of an inclined slope that can be maintained by the soil at slope angle α, with horizontal acceleration A.

Typical results of the stability analyses described above are shown in figure 2. The example is for $\alpha=40°$ and $\phi=35°$, with each of the curves representing a different value of horizontal acceleration.

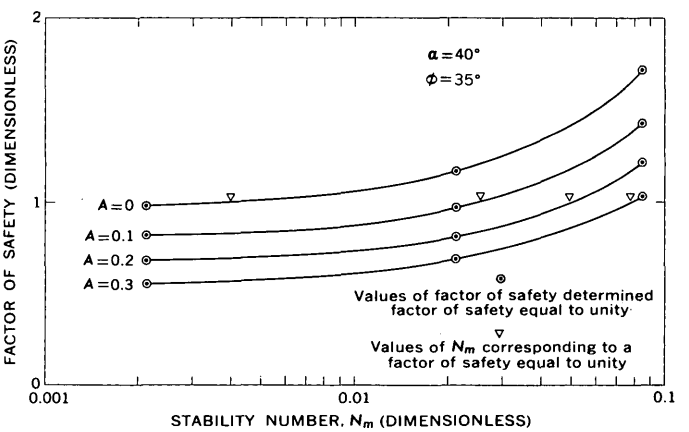

FIGURE 2.—Results of multiple stability analyses with varying parameters for the assumed slope geometry in figure 1. Symbols are explained in text.

3. For each slope angle, α, relationships similar to those shown (fig. 2) were determined for each of several angles of internal friction.

4. The stability number, N_m, corresponding to a factor of safety equal to unity was determined for each of the selected acceleration values. (For a factor of safety equal to unity, the stresses tending to cause slope failure are exactly offset by the strength of the slope.)

5. From the results of 4 above, the relationship between the stability number and seismic acceleration was determined (see fig. 3, which is valid for a slope angle of 40°).

The resulting stability chart (fig. 3) is valid for a single value of slope angle, α, and for a factor of safety equal to unity. The previously stated assumptions with regard to slope geometry, material, pore pressures, and failure surface, are, of course, inherent in the stability chart.

APPLICATION OF STABILITY CHARTS TO THE LUNAR SURFACE

Craters showing evidence of slope failure either by apparent slumping of the crater walls or by apparent concentric tension cracks near the crater rims were observed on Lunar Orbiter II photographs (see fig. 4).

Because the surface bearing capacity is desired, strength characteristics of materials at the surface and at very shallow depths must be approximated. For this reason, small-diameter craters were selected for analysis because the failure of their slopes is limited by their depths. Thus, the analysis applies to near-surface materials.

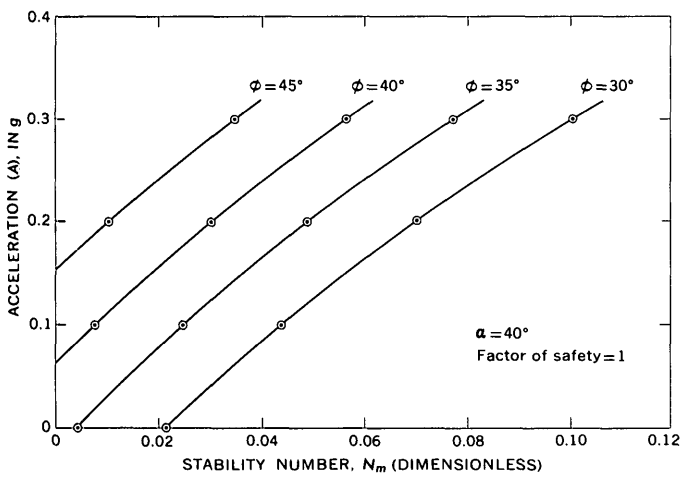

FIGURE 3.—Stability chart for assumed slope geometry (fig. 1) with a slope angle of 40° plotted for four angles of internal friction. Symbols explained in text.

Had craters without the evidence of failure described above been selected, there would be no assurance that the factor of safety would not be considerably greater than unity. Analysis of slopes in such craters could give a very misleading and conservative value for the strength of the soil material.

Very large diameter deep craters would, of course, include deeper, probably more competent materials, and the strength values determined by slope stability techniques would be higher than would actually exist in the near-surface materials.

The limitation imposed by the Lunar Orbiter photographs was that of detection resolution. Had greater detection resolution been available, shallower craters could have been included in the analyses, and the "average" strength characteristics determined would then be more indicative of the near-surface material.

Profiles of selected craters (figs. 4, 5), obtained by means of photoclinometric techniques developed by Glen R. Taylor and J. J. Lambiotte, of Langley Research Center, and by Kenneth Watson (1968), were used to determine slope geometry, the representative slope angle before failure, α, and the slope height, H, for each crater. The results are shown in table 1.

Strength characteristics were then determined as follows: (1) The appropriate chart, selected on the basis of slope geometry, was consulted. (2) The corresponding stability number, N_m, was determined from the chart, with the assumption of a rational value for the angle of internal friction, ϕ, and an assumed seismic acceleration, A.

The corresponding value of unit cohesion was determined by multiplying the stability number, N_m, by the mass density, ρ, the acceleration of gravity, g, and the height of the slope, H. The unit cohesion, c, thus determined would be the minimum required to maintain the stability of the slope under the imposed conditions.

Unit cohesions obtained using the above procedure, with various assumptions for both angle of internal friction, ϕ, and seismic acceleration, A, for selected slopes identified in table 1, are shown in table 2. The density ρ, of the soil-like material is assumed to be 1.5 g/cm^3. Craters with the flatter slopes are excluded because stability charts have not yet been prepared for slopes of less than 25°.

The obverse method of using the example stability chart is to assume a unit cohesion, angle of internal friction, and density. Then, for a slope of a given height and slope angle, the acceleration neces-

sary to cause failure may be found. For example, a slope of 40° (fig. 3) underlain by cohesionless material with an angle of internal friction of 40° would fail if subjected to a horizontal seismic acceleration of 0.06 g.

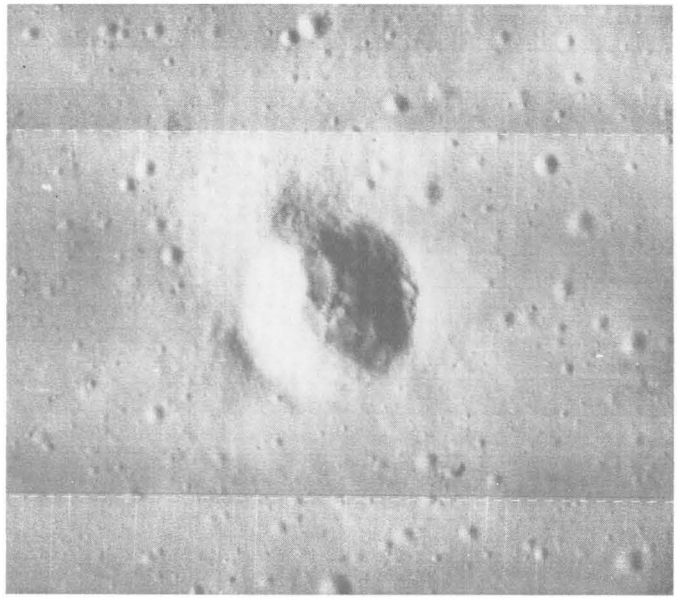

A

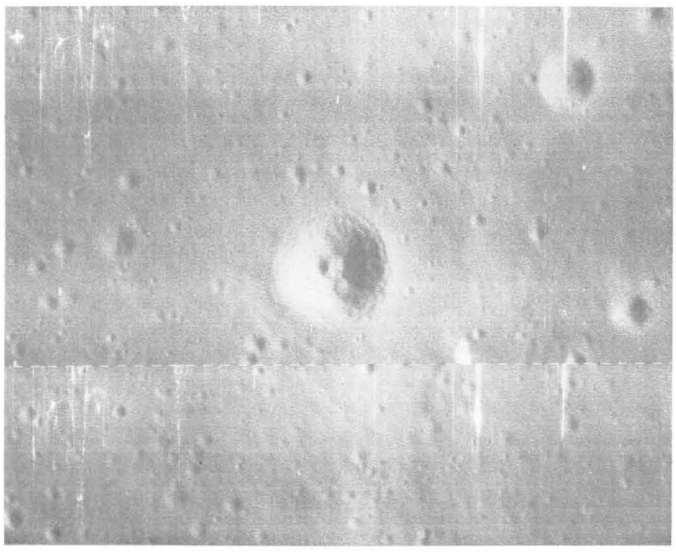

B

FIGURE 4.—Lunar Orbiter photographs showing examples of slope failure. Profiles for these craters are shown in figure 5. *A*, apparent slumping of crater wall (Lunar Orbiter Site II P–2, photograph H–36). *B*, apparent concentric tension crack near crater rim (Lunar Orbiter Site II P–2, photograph H–39).

VALUES OF UNIT COHESION

The value of unit cohesion that is obtained depends greatly on the value of horizontal acceleration that is assumed. A rational value for the horizontal acceleration is not known, but lunar horizon-

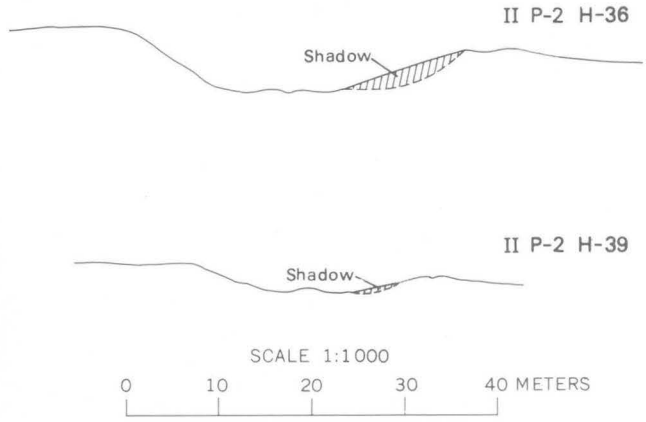

FIGURE 5.—Profiles of craters in figure 4. No vertical exaggeration. Numbers and letters refer to site, photograph, and framelet designations in table 1.

TABLE 1.—*Identification, slope angle, and slope height of selected lunar craters*

Identification			Slope angle, α (degrees)	Slope height, H (meters)
Site	Photograph	Framelet		
II P–2	H–36	142_____35		12.0
II P–2	H–37	223_____25		11.5
II P–2	H–38	425_____25		14.5
II P–2	H–39	483_____20		6.5
II P–2	H–42	913_____30		23.5
II P–6B	H–84	403_____40		14.3
II P–6B	H–87	792_____20		5.0
II P–6B	H–87	796_____20		8.0
II P–11	H–164	884_____30		7.0
II P–11	H–164	924_____45		15.0

TABLE 2.—*Probable values of unit cohesion for lunar surface materials*

[Density, ρ, assumed to be 1.5 g/cm³]

Framelet	Assumed angle of internal friction, Φ (degrees)	Assumed seismic acceleration, A (cm/sec²)	Stability number, N_M	Unit cohesion, c, required for stability (dynes/cm²)
425_____35	35	0.5	0.1030	36,600
	40	.5	.0710	25,200
884_____30	30	.5	.1605	27,600
	35	.5	.1340	23,000
924_____25	25	0	.0470	17,300
	25	.25	.1170	43,000
223_____35	35	.5	.1030	29,000
	40	.5	.0710	20,000
142_____30	30	0	.0073	2,150
	30	.25	.0705	20,800
	35	.25	.0440	13,000
913_____30	30	.5	.1605	92,500
	35	.5	.1340	77,200
403_____30	30	0	.0214	7,500
	30	.2	.0715	25,100
	35	0	.0041	1,440
	35	.2	.0490	17,200

tal accelerations would probably be as great, if not greater, than those experienced on the earth (up to 0.3 g).

Upper and lower bounds for unit cohesion would probably be about 92,000 and 1,000 dynes/cm^2, respectively (table 2). These extremes, along with the listed angles of internal friction, compare favorably with those reported from Surveyor experiments (Scott and others, 1967, p. 61–93; Scott and Roberson, 1968b, p. 121–161, 1968a, p. 171–79; Choate and others, 1968).

DETERMINING EXTREME VALUES OF BEARING CAPACITY

Although many other rational bearing-capacity equations are now in use, the Terzaghi equation, for general shear conditions, best suits the purpose of this study (Scott and O'Keefe, 1967). The use of other equations would give slightly smaller or greater values for bearing capacity, but in consideration of all the previous assumptions it seems doubtful that the selection of another equation would be justified for purposes of accuracy alone. The Terzaghi equation for the ultimate bearing capacity, $q_{ultimate}$, of a surface footing, circular in plan view, is

$$q_{ultimate} = 1.3cN_c + 0.3b\rho gN_\alpha, \quad (1)$$

where c = unit cohesion of the foundation material (dynes/cm^2),

b = diameter of the circular footing (cm),

ρ = mass density of the foundation material (g/cm^3), and

N_c and N_α are dimensionless numbers which are functions of the angle of internal friction of the foundation material.

The ultimate bearing capacity must be divided by an appropriate factor of safety. The appropriate factor of safety is dependent on the assurance of uniform foundation materials and the confidence that the engineer can place in the data used in the analysis. The factor of safety for determining the bearing capacity of terrestrial materials commonly ranges from 1.5 to 3. A factor of safety of 3 seems appropriate in considering lunar materials. The allowable bearing capacity, $q_{allowable}$, would then be $q_{ultimate}/3$, or

$$q_{allowable} = 0.433cN_c + 0.1\, b\rho gN\alpha. \quad (2)$$

The allowable bearing capacity may be expressed as a mass-bearing capacity by dividing each term by the acceleration of gravity, g, or

$$q_{mass\text{-}allowable} = 0.433\frac{cN_c}{g} + 0.1\, b\rho N_\alpha. \quad (3)$$

For the calculation of static mass-bearing capacity on the lunar surface for a structure founded on a circular footing 1 meter in diameter, the allowable mass-bearing capacity would then range from 860 g/cm^2 (ϕ=35°, c=1,440 dynes/cm^2, table 2) to 9,409 g/cm^2 (ϕ=30°, c=92,500 dynes/cm^2, table 2) or 1.4 to 15.3 newtons/cm^2. These values are comparable to those predicted on the basis of Surveyor data (Scott and Roberson, 1968a, p. 171–179; Choate and others, 1968, p. 129–169).

CONCLUSIONS

From the available information, the static mass-bearing capacity on the lunar surface should be at least 860 g/cm^2. The upper limit could conceivably be 9,409 g/cm^2, but is probably less.

Because seismic activity may be influential in forming the lunar landscape, its effects should be ignored when using slope-stability techniques to evaluate lunar bearing capacity.

REFERENCES

Bishop, A. W., 1955, The use of the slip circle in the stability analysis of slopes: Geotechnique, v. 5, p. 7–17.

Choate, R., Battersen, S. A., Christensen, E. M., Hutton, R. E., Jaffe, L. D., Jones, R. H., Ko, H. Y., Scott, R. F., Spencer, R. L., Sperling, F. B., and Sutton, G. H., 1968, Lunar surface mechanical properties, p. 129–170 *in* Surveyor program results: U.S. Natl. Aeronautics and Space Adm. Spec. Pub. SP–184, 423 p.

Jaffe, L. D., 1965, Strength of the lunar dust: Jour. Geophys. Research, v. 70, p. 6139–6146.

Schuster, R. L., 1967, Selection of shear strength parameters for slope stability analysis: 5th Ann. Eng. Geology and Soils Eng. Symposium, Pocatello, Idaho, 1967, Proc., 270 p.

Scott, R. F., and O'Keefe, J. A., 1967, Chondritic meteorites and the lunar surface: Science, v. 158, no. 3805, p. 1174–1176.

Scott, R. F., and Roberson, F. I., 1968a, Soil mechanics surface sampler, p. 171–180 *in* Surveyor program results: U.S. Natl. Aeronautics and Space Adm. Spec. Pub. SP–184, 423 p.

Scott, R. F., and Roberson, F. I., 1968b, Soil mechanics surface sampler, p. 121–162 *in* Surveyor VII, A preliminary report: U.S. Natl. Aeronautics and Space Adm. Spec. Pub. SP–173, 303 p.

Scott, R. F., Roberson, F. I., and Clary, M. C., 1967, Soil mechanics surface sampler—lunar surface tests and results, p. 61–93 *in* Surveyor III, a preliminary report: U.S. Natl. Aeronautics and Space Adm. Spec. Pub. SP–146, 159 p.

Watson, Kenneth, 1968, Photoclinometry from spacecraft images: U.S. Geol. Survey Prof. Paper 599–B, 10 p.

SYNTHESIZING HYDROGRAPHS FOR SMALL SEMIARID DRAINAGE BASINS

By G. S. CRAIG, JR., Cheyenne, Wyo.

Work done in cooperation with the Wyoming State Highway Commission.

Abstract.—Studies of hydrograph shape for 14 small (less than 11 sq mi) drainage basins have led to the development of a possible standard dimensionless hydrograph for semiarid regions. The dimensionless hydrograph, described in detail, is similar to that reported by G. G. Commons in 1942, but was developed with data from small, ephemeral streams in Wyoming. Hydrographs are synthesized from the dimensionless hydrograph by using peak discharge–volume relationships. Only the single-peak event is considered. Synthetic hydrographs produced from the Wyoming dimensionless hydrograph show close agreement with observed hydrographs from Wyoming, New Mexico, and Arizona. The procedure can be used to define a hydrograph for any selected design value of peak frequency.

Many State highway departments are concerned with the design of culverts to handle flood runoff from small drainage basins. The general lack of information on this type of runoff often may result in overdesign in size of culverts. If one considers the number of culverts along any roadway, it becomes apparent that a reduction in size of culverts would result in very large economic savings. More information on magnitude and frequency of runoff events from small basins would permit more realistic design and possibly smaller culverts. One approach that could lead to use of smaller culverts is to utilize any available area on the upstream side of highway embankments to store part of the runoff. This ponded water would drain off naturally as floodflow in the stream receded.

Information on runoff volume and hydrograph shape is necessary for consideration of inflow-storage-outflow studies in culvert design. Most of the highway research projects in the U.S. Geological Survey are directed toward defining the magnitude and frequency of flood peaks from drainage areas of less than 50 sq mi (square miles), but flood-volume studies are not common; consequently, data on peak discharge are fairly plentiful, while data on flood volume and hydrograph shape are very scarce. The variety of shapes a hydrograph can represent for the same volume also poses a problem. In semiarid areas the single-peak event from high-intensity rainfall is probably the most common type and is the only hydrograph shape that can be treated in a general way. The discussion in this paper is restricted to single-peak events.

Investigations of runoff resulting from rainfall on small (less than 11 sq mi) drainage basins in Wyoming indicate that a standard dimensionless hydrograph can be used to produce usable synthetic hydrographs of single-peak runoff events. Studies of hydrograph shape have led to development of mean dimensionless hydrographs for individual drainage basins and ultimately to one composite mean dimensionless hydrograph for 14 drainage basins. The application of this hydrograph is similar to that of the Commons (1942) dimensionless hydrograph, which was based on floods in Texas. The Commons hydrograph has been compared with observed hydrographs of floods in New York, Connecticut, Pennsylvania, and other areas with great success. The Wyoming composite hydrograph has produced synthetic hydrographs that compare well with observed runoff hydrographs from Wyoming, Arizona, and New Mexico. All streams used to develop and test the method are ephemeral.

THE COMPOSITE HYDROGRAPH

The peak discharge in cubic feet per second and the volume of runoff in acre-feet are needed to produce a synthetic hydrograph. Discharge and time-factor constants are determined from the peak discharge and volume of observed events. The constants then are multiplied by increments of discharge and time from the dimensionless hydrograph

to obtain the plotting points of the synthetic hydrograph. The synthetic peak discharge is always the same value as the actual peak; therefore, the peak must be known.

Commons' dimensionless hydrograph, developed by trial and error, had a horizontal (time) scale of 100 units and a vertical (rate-of-flow) scale of 60 units. The area under the curve was 1,196.5 "square units" (time units multiplied by rate-of-flow units). The total floodflow (volume) in acre-feet divided by 1,196.5 gave the value of one "square unit" in acre-feet. Dividing the peak flow in cubic feet per second by 60 gave the value of one unit of flow in cubic feet per second. The rising limb and recession limb of the Commons hydrograph appear characteristic of most streams, large or small, but the long recession is more indicative of large streams that are sustained by flow returning from storage on flood plains or from ground water in the stream banks.

The ephemeral streams in Wyoming do not reflect this large storage effect; consequently, a few changes were employed in developing dimensionless hydrographs in this study. In order to produce a hydrograph shape characteristic of small ephemeral, semiarid streams, an arbitrary value of 1,000 square units was used for the volume, and Commons' value for the peak was retained as 60 flow units. However, unlike the Commons method, where the time scale was fixed, time was allowed to vary as to the actual runoff event. An average time value was determined for each dimensionless hydrograph. The values for volume, peak discharge, and time were used to convert individual observed runoff hydrographs to dimensionless form. For each drainage basin, a minimum of six runoff events, preferably with a wide range in peak discharge, was considered necessary in the development. For many preselected values of flow units the corresponding values of time units on the individual dimensionless hydrographs were averaged to arrive at a mean dimensionless hydrograph for a basin. Planimetered volumes of mean dimensionless hydrographs of 14 drainage basins varied between 915 and 1,035 square units. The rise time of these mean hydrographs varied between 6 and 16 time units, and the average base time varied between 50 and 90 time units. The general similarities of these mean dimensionless hydrographs suggested the possibility that one composite mean hydrograph of the 14 basin mean hydrographs might reasonably describe the characteristic shape of flood volumes on small drainage basins in Wyoming. The composite was developed by averaging time units for preselected flow units. The planimetered volume was 973 square units with a rise time of 12 time units. The average time of the base was 70 time units. This composite hydrograph, shown in figure 1, was then tested using data from stations not used in its development. The hydrograph also has been used to synthesize missing hydrographs on some of the same basins that were used in its development.

DESCRIPTION OF THE METHOD

The composite hydrograph (fig. 1) is used to synthesize a hydrograph, provided that the peak discharge, Q_P, in cfs (cubic feet per second), and the volume, Q_v, in acre-ft (acre-feet), are known. The method consists of two steps. First a discharge constant, Q', a volume constant, V', and a time constant, T', are computed, using the peak (60 flow units) and volume (973 square units) from the composite hydrograph:

$$Q' = \frac{Q_p}{60} = \text{cfs per flow unit} \quad (1)$$

$$V' = \frac{Q_v}{973} = \text{acre-ft per square unit, and} \quad (2)$$

$$T' = 726\frac{V'}{Q'} = \text{min per time unit,} \quad (3)$$

where square units = flow units × time units, and 726 is a combined factor for converting acre-feet to cubic feet and seconds to minutes. (The relation

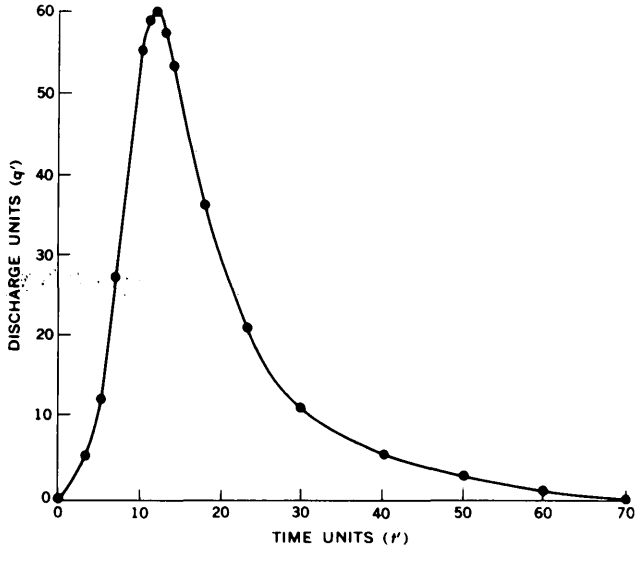

FIGURE 1.—Composite mean dimensionless hydrograph developed from data for 14 small drainage basins in Wyoming. Dots indicate the increments of time and discharge units used in producing a synthetic hydrograph.

between flood peak and flood volume will be developed later in the paper.)

The second step is to compute the actual plotting points, t and q, for the synthetic hydrograph. Sixteen plotting points were selected to define the entire hydrograph as shown in figure 1. The coordinates of these points on the composite hydrograph in figure 1 are designated at t' and q'. Once a set of values of t' and q' has been selected it is used in synthesizing every new hydrograph. For each of the 16 points

$$t = t' T', \text{ and} \quad (4)$$

$$q = q' Q', \quad (5)$$

where

t is time in minutes,

t' is time in units,

q is discharge in cfs,

q' is flow units, and

T' and Q' are as previously defined.

The values of t' and q' are strictly empirical and define the composite hydrograph.

The method can best be shown by developing a synthetic hydrograph for an actual runoff event. On June 10, 1965, a runoff event was recorded on Pritchard Draw near Lance Creek, in eastern Wyoming. The peak discharge was 1,280 cfs, and the volume was computed to be 67.17 acre-ft. From equations (1), (2), and (3), Q', V', and T' were determined as follows:

$$Q' = \frac{1{,}280}{60} = 21.33 \text{ cfs per flow unit,}$$

$$V' = \frac{67.17}{973} = 0.0690 \text{ acre-ft per sq unit, and}$$

$$T' = 726\frac{V'}{Q'} = 726 \times \frac{0.0690}{21.33} =$$

2.35 min per time unit.

Selected increments of time units, t' (in table 1), and corresponding discharge units, q', from the composite mean dimensionless hydrograph are multiplied by constants T' and Q', respectively, to determine the time, t, and corresponding discharge, q, for points on the synthetic hydrograph. The listed values of t' and q' were used in synthesizing all hydrographs shown in this report.

Figure 2 shows the comparison of the synthetic hydrograph with the observed hydrograph for the

TABLE 1.—*Determination of time, t, and corresponding discharge, q, for points on the synthetic hydrograph for Pritchard Draw near Lance Creek, Wyo.*

[$t = t' \times T'$; $q = q' \times Q'$. Symbols explained in text]

t' (time units)	T' (min per time unit)	t (min)	q' (flow units)	Q' (cfs per flow unit)	q (cfs)
0	2.35	0	0	21.33	0
3	2.35	7.1	5.0	21.33	107
5	2.35	12	12	21.33	256
7	2.35	16	27	21.33	576
10	2.35	24	55	21.33	1,173
11	2.35	26	59	21.33	1,258
12	2.35	28	60	21.33	1,280
13	2.35	31	57	21.33	1,216
14	2.35	33	53	21.33	1,130
18	2.35	42	36	21.33	768
23	2.35	54	21	21.33	448
30	2.35	70	11	21.33	235
40	2.35	94	5.3	21.33	113
50	2.35	118	2.4	21.33	51
60	2.35	141	.8	21.33	17
70	2.35	164	0	21.33	0

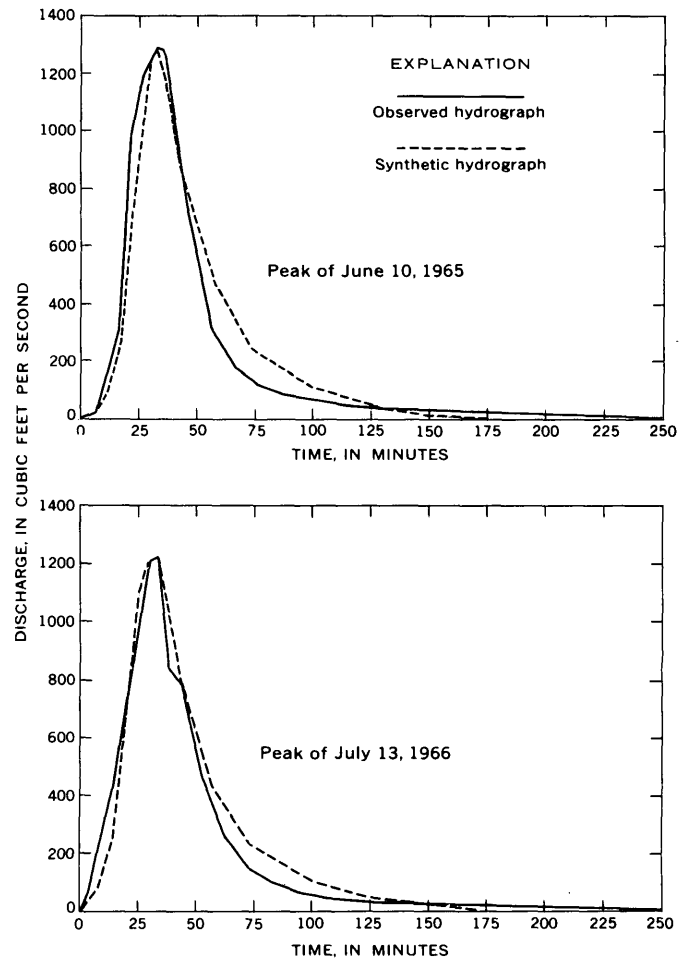

FIGURE 2.—Comparison of observed and synthetic hydrographs for two runoff events on Pritchard Draw near Lance Creek, Wyo.; drainage area 5.12 square miles.

above development and for another peak that occurred July 13, 1966. The time scales of the synthetic hydrographs were adjusted slightly to provide better comparison of the main part of the hydrographs.

SELECTED COMPARISONS

The general similarity of the shape of the hydrographs also was apparent from comparisons in other areas in Wyoming. Figure 3 shows comparisons of observed and synthetic hydrographs in areas independent of the areas used to develop the composite mean dimensionless hydrograph. To test the method in similar areas outside of Wyoming, observed runoff data were also obtained from New Mexico and Arizona. Synthesized hydrographs are shown in comparison with selected observed hydrographs for these areas in figure 4. The consistently close agreement of these and many other comparisons is quite remarkable. Although the concept of a standard hydrograph shape is subject to criticism from a strictly hydrologic point of view, the comparisons to date indicate that the concept is valid for design purposes on small, semiarid, ephemeral streams.

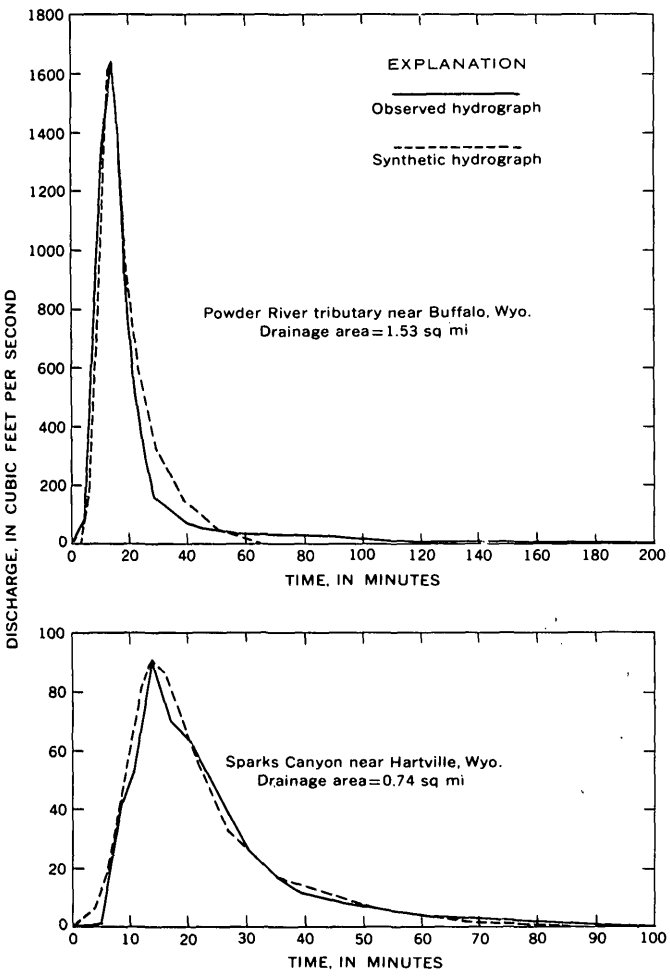

FIGURE 3.—Comparison of observed and synthetic hydrographs for areas in Wyoming not used in the development of the composite dimensionless hydrograph.

USE OF THE METHOD

Peak discharge–volume relations are being developed for individual drainage basins in which hydrograph recorders are in use in Wyoming. Data collected for one basin during the 5-year period 1965–69 are shown in figure 5. The relation is useful for estimating volumes for peak flows not recorded because of damage to, or malfunction of, the recording instrument. The relation also is useful for estimating the single-peak volume associated with a peak discharge for a given design recurrence interval—a 25-year flood, for example. The composite mean dimensionless hydrograph may then be used to produce synthetic hydrographs either for missing peaks or for design peaks, as illustrated in the following example.

A flood occurred on Pritchard Draw near Lance Creek, Wyo., September 3, 1968, damaging the water-level recording instrument to the extent that the flood hydrograph was not recorded. The maximum discharge, as determined by an indirect measurement of the peak flow, was 4,050 cfs. An earlier flood on July 26, 1965, with a peak flow of 2,100 cfs, had not been recorded because of instrument malfunction. Many runoff events occur on Pritchard Draw because it responds readily to the many rainstorms that pass over the area, but the two mentioned above are the highest peak flows in the 5-year period of record.

From figure 5 these two highest peaks were estimated to have volumes of 201 acre-ft and 109 acre-ft, respectively. Computations similar to those described previously were worked out for each event to determine the incremental times and dis-

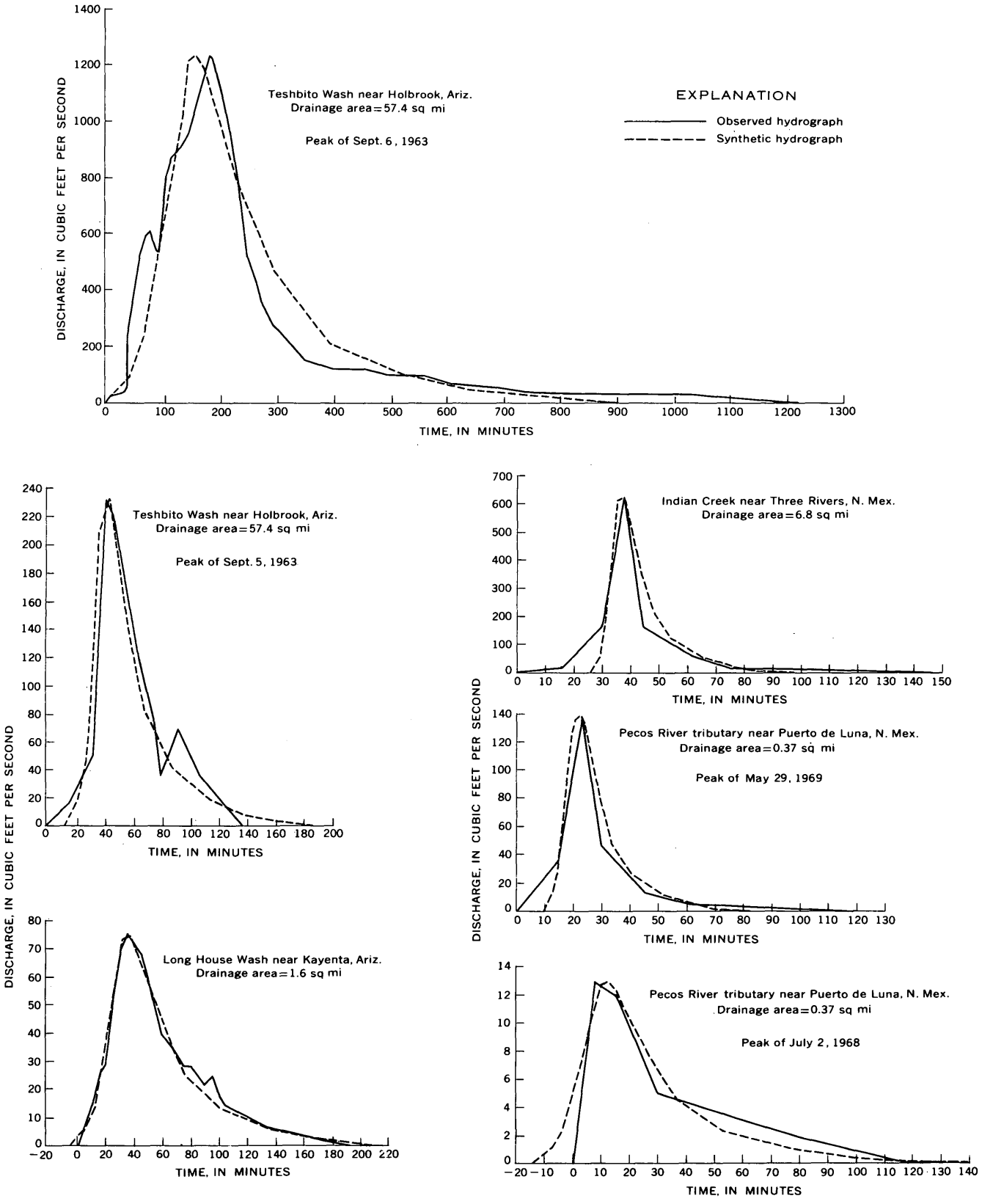

FIGURE 4.—Comparison of observed and synthetic hydrographs for runoff events in Arizona and New Mexico.

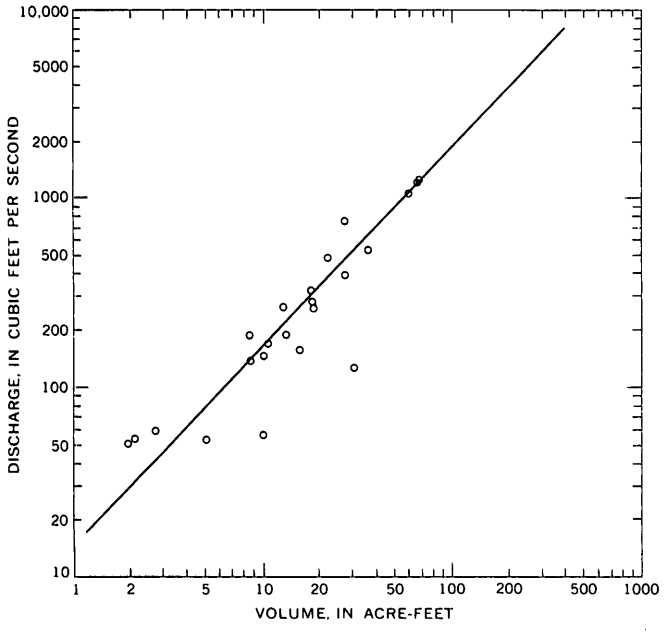

FIGURE 5.—Relation of peak discharge to volume on Pritchard Draw near Lance Creek, Wyo.

charges, which were then plotted. Figure 6 shows the resultant synthetic hydrographs for the two missing flood peaks compared with observed hydrographs of the two highest recorded peaks.

The described procedure can be used to synthesize a hydrograph for any selected design value of peak frequency. Inflow-storage-outflow analysis can then be used to determine the optimum culvert size at the particular site. However, in order to use the procedure at an ungaged site, one must estimate both peak discharge and volume.

REFERENCE

Commons, G. G., 1942, Flood hydrographs: Civil Eng., v. 12, no. 10, p. 571–572.

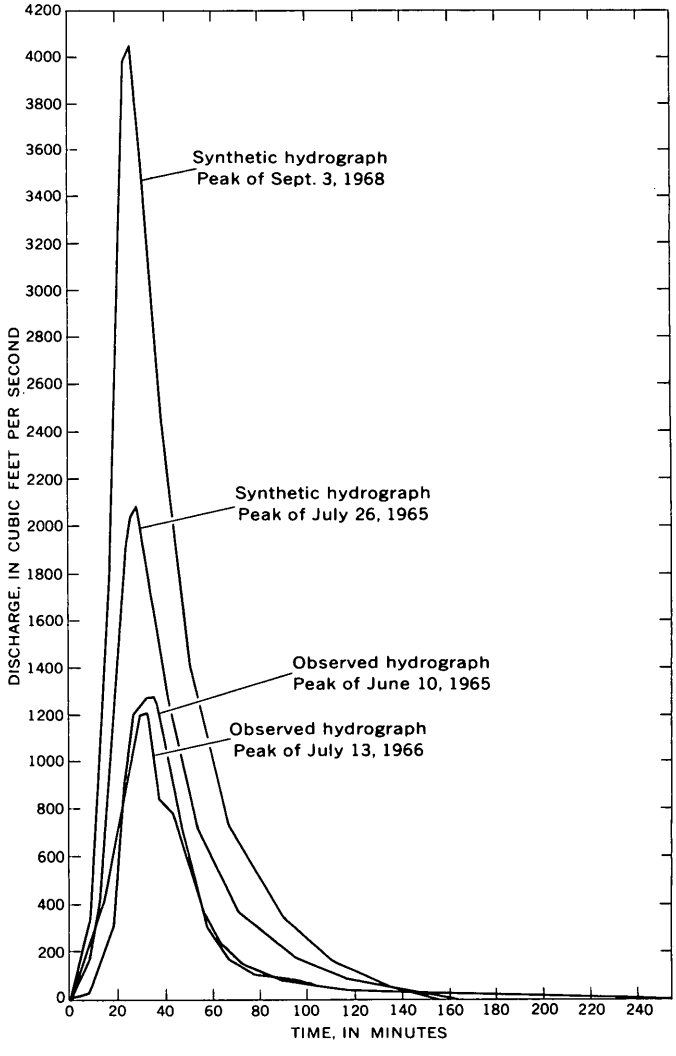

FIGURE 6.—Comparison of observed hydrographs of the highest recorded runoff events with the hydrographs synthesized for two higher nonrecorded runoff events on Pritchard Draw near Lance Creek, Wyo.

EVALUATION OF THE STREAMFLOW DATA PROGRAM FOR ARKANSAS

By JAMES L. PATTERSON, Little Rock, Ark.

Abstract.—An evaluation of the streamflow data available in Arkansas was made to provide guidelines for planning. The basic steps in the evaluation procedure were (1) definition of the long-term goals of the streamflow data program in quantitative form, (2) examination and analysis of available data to determine which goals have already been met, and (3) consideration of alternate programs and techniques to meet the objectives. Since many of the goals could be met by generalization of the data for gaged basins by regression analysis, significant changes could be made in the data program that would allow emphasis to be placed on attaining the goals that have not been met. A streamflow data program based on the guidelines developed in this study is proposed for the future.

The streamflow program of the U.S. Geological Survey in Arkansas has evolved through the years as the Federal and State interests in surface-water resources have increased and as funds for operating the stream-gaging station network have become available. The purpose of this study is to evaluate the streamflow data program and use this evaluation to design a program that will most efficiently produce the types of information needed.

The first records of daily stream discharge were collected in 1903 on the Ouachita River near the site of Remmel hydroelectric dam. Discharge records were collected for short periods at several sites in the State during 1903–26, but it was not until 1927 that the first statewide water-resources program of the Geological Survey in Arkansas was begun, resulting in the establishment of 21 daily-discharge stations during the period 1927–29. The number of stations was reduced to 12 in 1931, and State cooperation was discontinued in 1933. Only a few federally supported streamflow stations were operated from 1933 to 1937.

The disastrous Mississippi River flood of 1937 and the resulting emphasis on flood control brought out the great need for basic streamflow data in the State. During the late 1930's much of the Survey's present network of streamflow stations was established in cooperation with State agencies and the U.S. Army Corps of Engineers. At the end of 1968, records of daily discharge were being collected at 75 sites by the Geological Survey and at 30 sites by the Corps of Engineers.

In 1958 a network of low-flow partial-record sites was established where data were collected to define low-flow characteristics at sites other than those at which daily-discharge records were collected. Now (1969) low-flow data have been collected at about 250 sites throughout the State.

A crest-stage partial record network was begun in 1961. The purpose of this program is to define characteristics of peak flows from small drainage areas. There are now 105 gages in this network, 25 of which are equipped with continuous-stage and rainfall recorders.

CONCEPTS AND PROCEDURES USED IN THIS STUDY

The concepts and procedures used in this study are presented in detail by Carter and Benson (1969), and are summarized only briefly in this report. The basic steps are (1) definition of the long-term objectives of the streamflow data program in quantitative form, (2) examination and analysis of all available data to determine which objectives have already been met, (3) consideration of alternate means of meeting the remaining objectives, and (4) preparation of a proposed program of data collection and analysis to meet the remaining objectives.

The principal concept of this study is that streamflow information may be needed at any point on any stream in Arkansas, and that the program must be designed to accommodate this need. This information can be provided by a combination of data-collection and hydrologic studies that generalize site information.

Another important concept is that the goals of the program, including accuracy goals, should be

U.S. GEOL. SURVEY PROF. PAPER 700–D, PAGES D244–D256

identified in quantitative form. This permits evaluation of existing data to determine which goals have been attained and how the program should be modified.

The procedures used in this study are presented with reference to the design criteria and framework shown in table 1. Streamflow data are classified into four types; (1) data for current use, (2) data for planning and design, (3) data to define long-term trends, and (4) data on the stream environment. For the second type of data, streams are classified as natural or regulated, and each of these classifications is further subdivided into principal or minor, with the separation of the two occurring at a drainage area of 500 square miles.

In the initial phase of the study, program goals were established for each type of data. Available data were then examined and analyzed. This led to a comparison of available information with the goals that had been set and to consideration of the elements that should be included in future programs.

Data for Current Use

Current information on streamflow is needed at many sites for day-to-day decisions on water management, for assessment of current water availabil-

TABLE 1.—*Framework for design of data-collection program*

Type of data	Current use	Planning and design				Long-term trends	Stream environment
		Natural flow		Regulated flow			
		Minor streams	Principal streams	Minor streams	Principal streams		
Goals ------	To provide current data on streamflow needed for day-to-day decisions on water management as required.	To provide information on statistical characteristics of flow at any site on any stream in Arkansas to the specified accuracy.				To provide a long-term data base of homogeneous records on natural-flow streams.	To describe the hydrologic environment of stream channels and drainage basins.
Drainage area limits.	Full range.	Less than 500 sq mi.	Greater than 500 sq mi.	Less than 500 sq mi.	Greater than 500 sq mi.	Full range.	Full range.
Accuracy goal.	As required.	Equivalent to 10 years of record.	Equivalent to 25 years of record.	Equivalent to 10 years of record.	Equivalent to 25 years of record.	Highest obtainable.	As required.
Approach --	Operate gaging stations as required to provide specific information needed.	Relate flow characteristics to drainage basin characteristics using data for gaged basins.	Operate gaging stations to obtain 25 years of record (or the equivalent by correlation) at a network of points on principal streams; interpolate between points.	Develop generalized relations that account for the effect of storage, diversion, or regulation on natural-flow characteristics.	Utilize analytical model of stream system with observed data as input to compute homogeneous records for both natural-flow conditions and present conditions of development.	Operate a few carefully selected gaging stations indefinitely.	Observe and publish information on stream environment.
Evaluation of available data.	Identify stations where data are used currently and code the specific use of data.	Develop relationship for each flow characteristic and compare standard error with accuracy goal. Evaluate sample.	Lay out network of points on principal streams and compare data available at these points with goal.	Appraise type of regulation, data available, and areas where relationships are needed.	Identify stream systems that should be studied using model approach and determine data requirements.	Operate a small network of gaging stations indefinitely for this purpose.	Evaluate information available in relation to goals.
Design of future program.	Identify goals that have not been attained. Consider alternate means of attaining goals. Identify elements of future program.						

ity, for the management of water quality, for the forecast of water hazards, and for the surveillance necessary to comply with legal requirements. Sites at which the needed data are collected are termed "current purpose" streamflow stations.

Data for current use are obtained by operating gaging stations to obtain the data specifically required for water-management systems. Current-purpose data stations are identified separately in this study because (1) justification can be related to specific needs; (2) the data may have little or no transfer value in a hydrologic sense; and (3) the locations of the stations, the accuracy requirements, and the period of operation are specified by the user of the data, who usually provides the financing. Current-purpose stations are not subject to design, but change in response to the needs for data in water management.

More than half of the gaging stations in Arkansas are operated to provide data for current use. It is assumed that the need for this type of data is being met, and that this part of the program can be modified as requirements change.

Data for Plans and Designs

Streamflow records form the principal basis for the planning and design of water-related facilities. Past hydrologic experience, however, is never precisely duplicated in the future; the exact sequence of wet and dry years probably will not occur again. For this reason, designers and planners commonly utilize statistical characteristics of streamflow rather than the records of flow at specific times. It is assumed that the probability of occurrence of a flow of a given magnitude or other statistical parameter in the future can be approximated from the frequency of such occurrence in the past. Typical statistical characteristics are the mean flow, the flood of 50-year recurrence interval, and the standard deviation of annual mean flows.

A long record of streamflow at the specific site is desirable for defining statistical characteristics of streamflow at that site. Although it is not feasible to collect a long continuous streamflow record at every site where it may be needed, a number of such stations are required to provide information that can be transferred to ungaged sites or to sites where little streamflow information is available.

Natural-flow streams

The transfer of information on natural-flow streams is done by relating flow characteristics to basin characteristics, such as drainage area, topography, and climate; by relating a short record to a longer one; or by interpolating between gaged points on a stream channel.

To evaluate the statistical characteristics of streamflow, the streams in Arkansas were categorized as having either natural- or regulated-flow conditions. For the purpose of this study, streams were also defined under each of the above categories as being minor streams (drainage area less than 500 sq mi), or principal streams (drainage area greater than 500 sq mi). The principal-stream network was further defined by first identifying sites with drainage areas of about 500 square miles on the upstream segment of all streams, and then identifying the next and following sites on each stream from the upstream station to the mouth at points where the drainage area has doubled, or more than doubled, owing to large tributaries entering.

Regulated-flow streams

The natural-flow regimen of many streams is altered by the construction of storage reservoirs and the diversion of water for consumptive use. These alterations increase the scope of both the data collection and the analysis that is required to provide information on the flow characteristics.

To be useful in statistical prediction, streamflow data must be homogeneous in time. Frequently, however, it is not possible to obtain a long record under one condition of development before additional changes occur.

Definition of the flow characteristics at any point on any stream is also much more difficult under conditions of regulation. The procedures used for natural streams—regression, correlation, interpolation, and so forth—cannot be applied.

For regulated streams, a systems approach seems to be the most efficient way of providing meaningful information on the statistical characteristics of flow. This approach requires an analytical model of the stream system. Such models are simple in concept and generally consist of water-budget equations and flow-storage equations. However, in many instances the use of the digital computer is required for complex equations, or to handle large volumes of data. A computer program tailored to the individual system can be prepared.

Accuracy goals

In using past hydrologic experience to appraise the probability of future occurrences, some error must be tolerated. Natural streamflow, like other events related to climate, is generally random in occurrence and varies in time and space. Statistical techniques used in the analysis of random events,

therefore, are considered applicable. Measures of the variability with time of annual mean flow and other streamflow characteristics are determined from the historical streamflow data, and the probable errors involved in defining streamflow characteristics can be appraised. The principal measure of the accuracy with which a particular streamflow characteristic can be determined is the statistical measure of error, termed "standard error of estimate," and is expressed in this report as a percentage of the average value of the characteristic. The standard error is the estimated limit above and below the average within which about 67 percent of future values of the characteristics are expected to fall. Conversely, there is only one chance in three that future values will differ from the average by more than one standard error.

In general, the longer the record, the more reliable are the estimates of probable future occurrences. However, even with a long record, say 50–100 years or more, it is not possible to determine with great precision the probability of certain flow characteristics such as floods of a given magnitude, for example. The standard error of various streamflow parameters decreases with the years of available record, but at a decreasing rate; typical examples are shown in figure 1. The incremental economic value of the additional years of record beyond a reasonable limit in the planning and design of projects is under continuing study, but no usable guidelines are available yet.

Accuracy goals for streamflow characteristics are expressed as the accuracy equivalent of an arbitrary number of years of record. For example, see table 2. These goals are the same for natural and regulated flows; that is, accuracy equivalent to that which would be obtained from 10 years of record at the site for minor streams (drainage area, less than 500 sq mi), and accuracy equivalent to that which would be obtained from 25 years of record for principal streams (drainage area, more than 500 sq mi).

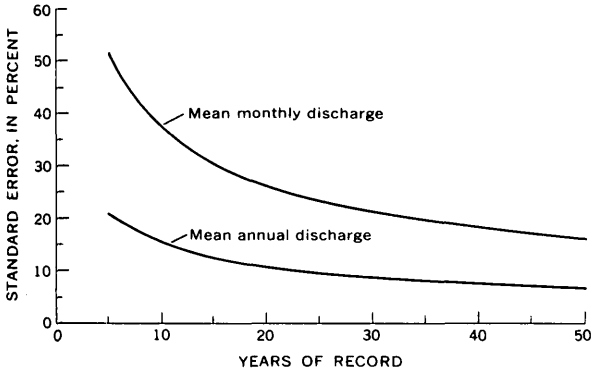

FIGURE 1.—Curves showing relation of standard error to length of record.

TABLE 2.—*Accuracy goals*

Streamflow characteristic	Standard error (percent)	
	10 years	25 years
Mean annual discharge	15	10
Standard deviation of annual discharge	22	14
Mean monthly discharge (average)	37	23
Standard deviation of monthly discharges (average).	22	14
50-year flood	37	23
7-day 2-year low flow	42	25
7-day 20-year low flow	64	37
7-day 50-year high flow	31	20

At sites on natural-flow streams where streamflow records are not available, the desired streamflow characteristics may be defined by means of the relations between a streamflow parameter and the characteristics of the drainage basin. This definition is accomplished by multiple-regression analysis, a statistical method of handling sample data that relates a streamflow characteristic to the topographic and climatic characteristics. This analysis produces regression equations that can be used to compute the flow characteristics at any point on natural streams in Arkansas. The standard error of a regression equation provides a measure of the accuracy of an estimate made from it at an ungaged site. That error may be compared with the error associated with the same characteristic defined from a given number of years of record in order to determine whether the accuracy objective has been met.

In this study on Arkansas streams the goal for this type of data is to define, within the given accuracy, the statistical flow characteristics listed in table 2. This definition applies not only to all streams with natural flow, but also to those streams that are affected by regulation and diversion. The accuracy goals shown for each flow characteristic are equivalent to 10 years of record for minor streams and 25 years of record for principal streams. The standard errors were calculated from a theoretical relation of standard error to index of variability and number of years of record.

Data to Define Long-term Trends

Characteristics of streamflow defined from gaging-station records are used to estimate future flow characteristics, on the assumption that the observed record is a representative sample of the long-term flows of the stream. The goal for this type of data is to operate indefinitely a small network of gaging stations on streams that are expected to be relatively free from manmade changes. One or two stations should be located in each major drainage area

in the State, and stations should be located on streams that differ in physical characteristics.

Data on Stream Environment

Environmental data describe the flow and the stream channel in terms that will be valuable in planning the use of the stream for any purpose such as recreation, waste disposal, conjunctive surface-water–ground-water supply, and in guarding against water hazards. The long-range goals for this type of data in Arkansas are given below.

1. Hydrometric surveys of stream-aquifer systems.
2. Surveys of time of travel of solutes in stream channels.
3. Definition of flood profiles along stream channels.
4. Identification of flood plains of streams for floods of different frequencies.
5. Reconnaissance surveys of streamflow and stream-channel parameters that are related to the use of the stream for recreation, such as velocities, depths, bank vegetation, bed material, water temperature, water quality, and accessibility.

EVALUATION OF THE NATURAL-FLOW SYSTEMS IN ARKANSAS

The purpose of the evaluation is to determine how accurately the statistical characteristics that are listed as goals can be defined by regionalization of the available data.

The most effective known way for defining statistical streamflow characteristics on a broad scale is to relate the streamflow characteristics to basin characteristics in equations developed by use of multiple-regression techniques applied to past data. Once the equation and its constants are defined, streamflow characteristics for a specific site in a given basin can be computed by substituting the appropriate values of the hydrologic variables in the equations.

Records used in the analysis are for 76 streams with 10 or more years of mostly unregulated flow, or flow that can be adjusted to natural conditions. Both minor and principal streams are included. Records were not adjusted to a base period, but a few of the short records were extended by regression methods. Because of some regulation, not all flow characteristics were defined for each record. At some stations, regulation materially affected low flows but insignificantly affected peaks. At a few stations, only mean annual flows, adjusted for storage, were used. No records on very large streams (Arkansas, Red, lower White, and lower Ouachita Rivers) were used because these streams are regulated, and because there are no large ungaged streams in the State to which regression equations could be applied.

Streamflow Characteristics

The following streamflow characteristics defined at gaging stations include the full range of flow and represent that required for planning and design:

1. Low-flow characteristics are the annual minimum 7-day mean flows at 2-year and 20-year recurrence intervals ($M_{7,2}$ and $M_{7,20}$). These were determined from graphical low-flow frequency curves.
2. Flood-peak characteristics are represented by discharges from the annual flood-frequency curve at recurrence intervals of 1.25, 2, 5, 10, 25, and 50 years. In this report, these peak-flow rates are denoted as $Q_{1.25}$, Q_2, and so forth. The frequency curves were prepared as described by the U.S. Water Resources Council (1967).
3. Flood-volume characteristics represent the annual highest average flow for 3-day, 7-day, and 15-day periods at recurrence intervals of 2, 5, 10, 25, and 50 years. These characteristics are noted symbolically in this report as $V_{3,2}$, $V_{3,5}$, $V_{3,10}$, $V_{3,25}$, $V_{3,50}$, $V_{7,2}$, and so forth. They were determined from frequency curves prepared as described by the U.S. Water Resources Council (1967).
4. Mean-flow characteristics are described by the mean of the annual means, Q_a, and by the means of record for each calendar month, q_n, where the subscript refers to the numerical order of the month beginning with January as 1.
5. Flow-variability characteristics are represented by the standard deviations of the annual and monthly means. The symbols used are, respectively, SD_a and SD_n, where the subscript n refers to the numerical order of months with January as 1.

Drainage-basin Characteristics

Drainage-basin characteristics defined for this study are as follows:

1. Drainage area, in square miles, as shown in the latest U.S. Geological Survey streamflow reports.

2. Main-channel length, in miles, from the gaging station to the basin divide, as measured with a template graduated in 0.1-mile units, or as taken from the report by the U.S. Army Corps of Engineers (1954).
3. Main-channel slope, in feet per mile, determined from elevations at points 10 percent and 85 percent of the distance along the channel from the gaging station to the divide. This index was described and used by Benson (1962, 1964).
4. Mean basin elevation, in feet above mean sea level, measured on 1:250,000 Army Map Service maps by laying a grid over the map, determining the elevation at each grid intersection, and averaging those elevations. The grid spacing was selected to give at least 25 intersections within the basin boundary.
5. Forest cover, expressed as the proportional part of the drainage area covered by forests as shown on the topographic map, determined by the grid method.
6. Mean annual precipitation, in inches, determined from an isohyetal map prepared from U.S. Weather Bureau records at 157 sites. The parameter used was mean annual precipitation minus 30.
7. Mean monthly precipitation for each calendar month was computed first as a percentage of the mean annual precipitation for each of 61 long-term precipitation stations. These values for each month were plotted on a map, and isograms of percentages were drawn. Mean monthly precipitation for each basin was then determined by multiplying the mean annual precipitation previously computed for the basin by the percentage of the mean as indicated by the isograms drawn for each month. The parameter used was the computed mean monthly precipitation, in inches, minus 2.
8. Area of lakes and ponds, expressed as percentage of the drainage area, determined by the Arkansas Soil and Water Conservation Commission (1968).
9. The maximum 24-hour rainfall having a recurrence interval of 2 years (24-hour 2-year rainfall), expressed in inches. These values were determined by the U.S. Weather Bureau (1961).

Although values of percentage of lakes and ponds and the maximum 24-hour precipitation were compiled, they were not used in the regression analysis.

Regression Analysis

The next step was to relate each of the streamflow characteristics to basin and climatic characteristics in evaluations developed by using multiple-regression techniques. The equation has the form

$$Y = aA^{b1}S^{b2}P^{b3} \ldots,$$

where Y is a statistical streamflow characteristic; A, S, and P are topographic or climatic characteristics; a is the regression constant; and b_1, b_2, and b_3 are coefficients obtained by regression. This method was described by Benson (1962). In this study, drainage area, main-channel slope, main-channel length, forest cover, and basin elevation were used initially in each regression. Either the mean annual or the mean monthly precipitation was used, depending on whether annual or monthly values were being analyzed. The computer calculated the regression equation, the standard error of estimate, and the significance of each basin parameter. Automatically, then, the computer repeated the calculations, omitting the least significant basin parameter in each calculation until only the most significant parameter remained. After relations for a given streamflow characteristic had all been computed, the entire computation process was repeated using another streamflow characteristic along with the same set of basin characteristics.

The output of the regression analyses of mean annual flow is listed in table 3. On the basis of the regression analyses, the equation for determining mean annual discharge at ungaged sites, including all statistically significant variables, is

$$Q_A = 0.082A^{1.02}P^{0.75}E^{0.06},$$

where Q_A is mean annual discharge, in cubic feet per second; A is drainage area, in square miles; P is mean annual precipitation, in inches (minus 30); and E is the mean elevation of the basin, in feet above mean sea level. By eliminating elevation from the equation, the standard error is increased only 0.5 percent. In this instance, the equation using only drainage area and mean annual precipitation probably would be the most useful, as the use of this equation will eliminate the necessity of computing mean elevation.

Table 4 lists, for each of the 49 streamflow characteristics, the regression constant, the regression coefficient (exponent) for all statistically significant basin parameters, and the standard error of esti-

TABLE 3.—*Summary of regression analyses of mean annual flow*

Dependent variable	Regression coefficients for independent variables						Regression constant	Standard error of estimate	
	Area [1]	Slope	Length	Precipitation [1]	Forest cover	Elevation		Percent	Percent [2] change
Mean annual flow.	0.95	−0.055	0.075	0.81	−0.033	[1]0.14	0.050	11.2	---
	.99	−.075	---	.82	−.021	[1].16	.051	11.2	0
	.99	−.082	---	.80	---	[1].15	.057	11.2	0
	1.02	---	---	.75	---	[3].06	.082	11.8	+.6
	1.01	---	---	.74	---	---	.13	12.3	+.5
	1.00	---	---	---	---	---	1.19	19.4	+7.1

[1] Significant at 1-percent level.
[2] Percent change when least significant variables are dropped, as indicated by dashed line in column.
[3] Significant at 5-percent level.

mate. As the main-channel length was not statistically significant in any of the regression analyses, this parameter was not included in the table.

The standard errors shown in table 4 should be compared with the corresponding values of table 2 to determine whether the accuracy goals have been met. A detailed discussion of this comparison will be deferred to a later section of this report, but it seems that, with the exception of low flows, the regression results generally meet the accuracy goals for minor streams (the equivalent of 10 years of record), but not those of principal streams (the equivalent of 25 years of record).

Principal Streams

The goal for this category can be met only by gaging-station operation, because the accuracy objective, equivalent of 25 years of record, cannot be achieved by techniques of regionalization. The study for this category consisted of the identification of principal-streams network and evaluation of length of record available at these sites.

The principal-streams network for Arkansas includes 29 sites on unregulated streams, with at least 25 years of record at 15 of these sites. At one of the sites, an equivalent of 25 years of record may be obtained by correlating available record with a long-term station.

The principal-streams network is complemented by one gaging station in Oklahoma and four in Louisiana.

EVALUATION OF THE REGULATED-FLOW SYSTEMS

The goals for regulated streams are more difficult to attain because the technique of regionalization does not apply, the characteristics are not necessarily stationary in time, and a meaningful correlation seldom exists between flows at two sites if at least one of the flows is regulated. A systems approach may be used to define the characteristics of regulated streamflow under different patterns of regulation, or under the condition of natural flow. Systems studies for all of the regulated-stream systems in Arkansas will require a major effort. Therefore, the present evaluation is limited to (1) identifying the regulated streams, and (2) describing briefly the approach that would be used.

The stream systems in Arkansas materially affected by regulation are: St. Francis River above Marked Tree, White River above Black River, White River below Black River, Black River above Pocahontas, Little Red River, Petit Jean River, Fourche La Fave River, Little River, Ouachita River, and Little Missouri River. The Arkansas and Red Rivers are major interstate streams with complex regulation patterns; systems studies for these streams should not be limited to the parts in Arkansas.

The approach that might be used in future studies of regulated streams can be described by using Little Red River as an example. This stream was unregulated prior to construction of Geers Ferry Reservoir in 1962. The reservoir is operated by the Corps of Engineers for flood control and hydropower. Streamflow records are available, at a site near the dam, from 1927 to 1968, and since 1939, at sites on streams tributary to the reservoir. Flow characteristics under natural conditions are adequately defined by records from 1927 to 1961, but only about 7 years of records are available for defining the characteristics under the regulated condition. A longer homogeneous record at the gage site, or at any downstream point, could be computed by developing a flow-storage model of the reservoir and the channel. Development of such a model requires information on stage-capacity curves of reservoirs, stage-discharge curves at the outlets, operating-rule curves for the release of water, losses due to evaporation and seepage, the geometry of the stream channel, and records of diversions and return flow. Information on streamflow at some point or points is also needed as input to the model

TABLE 4.—*Summary of regression results*

[Model is $Y = aA^{b1} S^{b2} P^{b3} Pm^{b4} F^{b5} E^{b6}$]

Flow characteristic, Y	Regression constant, a.....	Exponent of basin characteristic						Standard error of estimate (percent)
		Drainage area, A	Main channel slope, S	Mean annual precipitation minus 30, P	Mean monthly precipitation minus 2, Pm	Forest cover, F	Mean basin elevation, E	
Q_a	0.0824	1.02	---	0.75	---	---	0.06	12
SD_a	.147	.93	0.13	.39	---	---	.14	12
q_1	.338	1.00	---	---	0.62	---	.19	25
q_2	.293	.96	−.12	---	1.16	---	.26	16
q_3	.410	.99	---	---	.94	---	.15	11
q_4	.457	1.05	---	---	.87	---	.064	12
q_5	.544	1.03	---	---	1.01	---	---	15
q_6	.00661	1.10	−.31	---	---	---	.72	25
q_7	.0561	1.04	---	---	---	−0.31	.24	38
q_8	.00347	1.14	---	---	---	−.40	.48	59
q_9	.547	.93	−.38	---	1.37	---	---	56
q_{10}	.0541	.91	−.47	---	1.44	---	.42	40
q_{11}	.00217	.81	−.34	---	1.29	−.22	1.03	25
q_{12}	.0374	.99	---	---	7.4	−.19	.45	26
Mean of standard error of regression equations of mean monthly discharges								29
SD_1	2.12	0.95	---	---	0.26	---	---	29
SD_2	.302	.93	−.17	---	.80	---	.29	20
SD_3	.195	.99	---	---	.57	---	.26	26
SD_4	.431	.93	---	---	.65	---	.18	17
SD_5	3.37	.96	---	---	1.27	---	−.29	21
SD_6	.174	1.10	−.20	---	1.90	---	---	32
SD_7	1.18	.86	---	---	---	---	---	45
SD_8	.0149	.99	---	---	---	---	.48	67
SD_9	1.42	.83	−.32	---	1.34	---	---	60
SD_{10}	1.22	.87	−.41	---	2.15	---	---	48
SD_{11}	.0147	.73	−.38	---	1.11	−.20	.89	26
SD_{12}	.370	.91	---	---	.54	−.14	.19	26
Mean of standard error of regression equations of standard deviations of mean monthly discharges								35
$Q_{1.25}$	0.0461	0.71	0.26	1.13	---	---	0.53	35
Q_2	.208	.74	.37	.99	---	---	.46	30
Q_5	1.19	.77	.50	.66	---	---	.36	28
Q_{10}	3.12	.78	.57	.48	---	---	.30	28
Q_{25}	50.8	.85	.80	---	---	---	---	30
Q_{50}	59.6	.84	.82	---	---	---	---	31
$M_{7,2}$	No meaningful equation derived.							
$M_{7,20}$	Do.							
$V_{3,2}$	.152	.86	---	1.11	---	---	.35	26
$V_{3,5}$	.443	.86	---	.76	---	---	.41	27
$V_{3,10}$	.747	.86	---	.59	---	---	.44	28
$V_{3,25}$	1.26	.85	---	.43	---	---	.47	31
$V_{3,50}$	4.97	.85	---	---	---	---	.48	34
$V_{7,2}$	.236	.90	---	1.11	---	---	.17	20
$V_{7,5}$	.703	.90	---	.78	---	---	.21	20
$V_{7,10}$	1.21	.90	---	.62	---	---	.24	22
$V_{7,25}$	1.27	.90	---	.45	---	---	.27	24
$V_{7,50}$	9.10	.89	---	---	---	---	.27	28
$V_{15,2}$	.346	.96	---	1.09	---	---	---	20
$V_{15,5}$	.851	.94	---	.76	---	---	.089	17
$V_{15,10}$	1.37	.93	---	.64	---	---	.11	18
$V_{15,25}$	2.17	.92	---	.52	---	---	.14	19
$V_{15,50}$	2.85	.92	---	.45	---	---	.15	21

and to verify the output. Frequently aquifer characteristics and ground-water pumpage should be considered.

The model and the associated data can be used to derive homogeneous data for both the natural and the regulated conditions. All historical streamflow records for both natural and regulated flows could be used as input to the model. Furthermore, data could also be derived for ungaged sites in the stream system.

DATA TO DEFINE LONG-TERM TRENDS

At present two gaging stations on unregulated streams, Cossatot River near Vandervoort and North Sylamore Creek near Fifty Six, are designated as long-term stations for indefinite operation. No stations on regulated streams are now so designated.

DATA ON STREAM ENVIRONMENT

Many environmental factors were determined for 76 drainage basins for the present study, particu-

larly basin characteristics such as drainage area, extent of forest cover, stream slopes, land elevations, and area of lakes and ponds. Average annual precipitation and rainfall intensity were also determined.

Flood plains have been outlined on 47 topographic quadrangle maps and flood profiles defined for selected streams. Detail channel surveys have been made at the two gaging stations designated as long-term stations. Channel surveys have been made at many sites in connection with indirect determinations of peak flows for unusual floods. Channel geometry has been determined at more than 100 gaging stations.

DISCUSSION OF THE EVALUATION

Of the four data categories used in this study, only one, data for planning and designing of water projects, is clearly subject to design. The requirements for other types of data are established in response to specific needs, or are defined by hydrologic judgment.

The evaluation of available streamflow data by regression analysis was based on data from 76 continuous-record gaging stations. Records from both minor and principal natural-flow streams were included. The conclusions and implications drawn from the results, based on standard errors shown in tables 2 and 4, are:

1. For natural flows, application of the regression equations will provide estimates of mean annual discharge, standard deviation of annual discharge, mean monthly discharge, 50-year flood, and 50-year 7-day high flow at ungaged sites on minor streams within the accuracy objectives, but not on principal streams (those with drainage areas greater than 500 sq mi). Therefore, no additional data are required to define these characteristics on minor streams.
2. Low-flow characteristics at ungaged sites on natural-flow streams, minor and principal, cannot be estimated accurately by regression. Thus, accurate estimates of low-flow characteristics at a site will require a few measurements of low flow correlated with concurrent flows at a suitable continuous-record index station where similar hydrologic conditions prevail.
3. Regression equations are not defined for any of the streamflow characteristics for drainage areas of less than about 50 square miles. Continuous-record or partial-record stations must be operated to define the streamflow characteristics for small drainage areas.
4. The objectives established for identifying the principal-streams network included sites with drainage areas of about 500 square miles on the most upstream segment of the stream and, proceeding downstream, sites where the drainage area is approximately double that of the previous site. The accuracy objective of 25 years of record, or equivalent, has been attained at 8 of the 19 stations on natural-flow principal streams identified solely in this category. To meet the objective of sampling progressively doubled increments of drainage areas on principal streams, three additional stations are needed.

THE PROPOSED PROGRAM

The information developed in different segments of this study has been merged and applied in planning a streamflow-information program that would eventually attain as many of the remaining goals as possible within the limits of available funds. For the optimum program, a balance must be maintained between data collection and data analysis, as continuous interaction between the two is needed, not only to gain a better understanding of the hydrologic system, but also to guide future evaluation of the program in meeting ever-changing needs and in adapting to changing technology.

Data Collection

Data for current use

Operation of the 55 stations, identified as presently meeting the needs for current-purpose data, should be continued. The changing needs will be assessed continuously, and the data-collection network will be modified by adding or discontinuing stations as needs change for current-purpose data. Also the needs for this type of data will be examined for each site, and a determination made as to whether a continuous record of daily discharge is required or whether measurement of specific flow characteristics, such as peak flow or instantaneous flow, would suffice.

Data for plans and designs

Some of the objectives have been attained; however, continued operation of certain stations to obtain either continuous-record or partial-record data is indicated.

Low-flow characteristics at ungaged sites cannot be estimated by regression methods. However,

information on low-flow characteristics has been collected at about 250 sites throughout the State, and this, together with such information available from the regular stream-gaging network, provides a data base from which, by interpolation, reasonable estimates of low-flow characteristics can be made at most ungaged sites. Low-flow characteristics may be defined at ungaged sites, where reasonable estimates cannot be made, by correlating a few low-flow measurements at the site with concurrent flow data at a suitable continuous-record index station where similar hydrologic conditions prevail. No additional index stations are needed in Arkansas, but low-flow measurements must be obtained as the need develops, or as anticipated at specific ungaged sites.

Flood-peak characteristics at recurrence intervals of 100 years are often estimated for project design. Although the objective includes only 50-year flood, it would be desirable to continue collecting flood-peak data at selected sites indefinitely. For each streamflow station subject to discontinuance, consideration will be given to the continued collection of peak-flow data. The needed data can thus be obtained at little cost by operating a partial-record station.

Natural-flow, minor streams.—Application of the regression equations for all flow characteristics except low flow will give results within the accuracy goals for minor streams. Therefore, 13 stations in the present network identified solely with this category of data are not recommended for inclusion in the future program.

Regression equations are not defined for any streamflow characteristic for areas of less than about 50 square miles. Four continuous-record stations, not included in this study because of insufficient length of record, will provide data for this lack of definition. To improve the definition of flood-peak characteristics for the smaller drainage areas, a program was begun in 1961 to establish a peak-flow partial-record station network. The 105 stations now operated should be continued in operation. The records obtained from these stations provide a sample from drainage areas ranging from a fraction of a square mile to about 50 square miles.

Natural-flow, principal streams.—The accuracy objective of 25 years of record, or equivalent, has been attained at 8 of the 19 stations identified solely in this category of data, and those 8 stations are not recommended for inclusion in the future program. Ten other stations identified under this category of data, 8 of which have 25 or more years of record, also are identified as current-purpose stations, and must be continued in operation to meet those specific needs for data. Three new stations should be added to the principal-streams network to sample specified increments of drainage area on the streams.

Regulated-flow, minor streams.—No streams in Arkansas were identified with this category of data; therefore, no data collection on streams in this category is proposed at this time. The program must be adjusted when minor streams are significantly regulated.

Regulated-flow, principal streams.—For purposes of the study, consideration of this category of data was limited only to identifying the regulated-streams systems. In Arkansas these are: St. Francis River above Marked Tree, White River above Black River, White River below Black River, Black River above Pocahontas, Little Red River, Arkansas River, Petit Jean River, Fourche La Fave River, Red River, Little River, Ouachita River, and Little Missouri River.

The proposed programs should include provisions to continue the collection of records of inflow, outflow, reservoir contents, diversions, operation schedules, and other pertinent hydrologic data at the major reservoirs in the regulated-streams systems.

Data to define long-term trends in streamflow

The two stations operated for a short time for defining long-term trends in streamflow in the current program should be continued in operation indefinitely. As a part of this study, nine additional stations in the present network have been designated as long-term-trend stations and should be operated indefinitely to meet the needs for this type of data. The additional stations were selected to provide a long-term sample reflecting areal coverage of the State, a range of drainage-area size, and a variety of climatic and physiographic characteristics.

Summary

The data-collection phase of the proposed program is summarized in table 5. The table includes all streamflow stations now in operation and those to be established for the proposed program. Recommendations are made as to whether the station should be included in the proposed network or whether it has met the objective for which it was operated and could be discontinued. Each station is identified as to type of data. Data collected at most

TABLE 5.—*Streamflow stations in operation (1970) and those needed for proposed network*

Station number and name		Recommendations		Types of data			
		Include in network	Not recommended for inclusion	Current purpose	Planning and design: Minor streams	Planning and design: Principal streams	Long-term trend
7–0320	Mississippi River at Memphis, Tenn.	X	--	X	--	X	--
7–0401	St. Francis River at St. Francis	--	X	--	--	--	--
7–0404.5	St. Francis River at Lake City	--	X	--	--	--	--
7–0466	Right Hand Chute Little River at Rivervale	X	--	--	--	X	--
7–0470	St. Francis River floodway near Marked Tree	--	X	--	--	--	--
7–0475	St. Francis River at Marked Tree	--	X	--	--	--	--
7–0476	Tyronza River near Tyronza	--	X	--	--	--	--
7–0478	St. Francis River at Parkin	X	--	X	--	X	--
7–0479	St. Francis Bay at Riverfront	X	--	X	--	X	--
7–0479.4	L'ANGUILLE RIVER near Wynne [1]	X	--	--	--	X	--
7–0479.5	L'Anguille River at Palestine	X	--	--	--	X	--
7–0479.7	Mississippi River at Helena	X	--	X	--	X	--
7–0480	West Fork White River at Greenland	--	X	--	--	--	--
7–0486	White River near Fayetteville	X	--	X	--	X	--
7–0490	War Eagle Creek near Hindsville	--	X	--	--	--	--
7–0496.91	White River below Beaver Reservoir	X	--	X	--	X	--
7–0505	Kings River near Berryville	X	--	X	--	X	--
7–0550	White River near Flippin	X	--	X	--	X	--
7–0560	Buffalo River near St. Joe	X	--	--	--	X	X
7–0570	Buffalo River near Rush	--	X	--	--	--	--
7–0600	North Fork River at Norfolk Dam	X	--	X	--	X	--
7–0605	White River at Calico Rock	X	--	X	--	X	--
7–0607.1	North Sylamore Creek near Fifty Six	X	--	--	X	--	X
7–0640	Black River near Corning	--	X	--	--	--	--
7–0688.9	Fourche Creek above Pocahontas	--	X	--	--	--	--
7–0690	Black River at Pocahontas	--	X	--	--	--	--
	SPRING RIVER above Hardy [1]	X	--	--	--	X	--
7–0695	Spring River at Imboden	X	--	--	--	X	X
7–0720	Eleven Point River near Ravenden Springs	--	X	--	--	--	--
7–0725	Black River at Black Rock	X	--	X	--	X	--
7–0730	Strawberry River near Evening Shade	--	X	--	--	--	--
7–0735	Piney Fork at Evening Shade	--	X	--	--	--	--
7–0740	Strawberry River near Poughkeepsie	--	X	--	--	--	--
7–0745	White River at Newport	X	--	X	--	X	--
7–0750	Middle Fork Little Red River at Shirley	X	--	--	X	--	X
7–0753	South Fork Little Red River at Clinton	X	--	X	X	--	--
7–0760	Little Red River near Heber Springs	X	--	X	--	X	--
7–0768.5	Cypress Bayou near Beebe	X	--	--	--	X	--
7–0770	White River at DeValls Bluff	--	X	--	--	--	--
7–0773.8	Cache River near Egypt	X	--	--	--	X	--
7–0775	Cache River at Patterson	X	--	--	--	X	X
7–0777	Bayou DeView at Morton	--	X	--	--	--	--
7–0778	White River at Clarendon	X	--	X	--	X	--
7–0779.3	Big Creek near Moro [2]	X	--	--	--	X	--
7–1950	Osage Creek near Elm Springs	X	--	X	X	--	--
7–1958	Flint Creek at Springtown	X	--	--	X	--	--
7–1969	Barren Fork at Dutch Mills	X	--	X	X	--	--
7–2470	Poteau River at Cauthron	X	--	X	X	--	--
7–2494	James Fork near Hackett	X	--	X	X	--	--
7–2495	Cove Creek near Lee Creek	--	X	--	--	--	--
7–2500	Lee Creek near Van Buren	X	--	X	X	--	--
7–2505	Arkansas River at Van Buren	X	--	X	--	X	--
7–2515	Frog Bayou at Rudy	--	X	--	--	--	--
7–2520	Mulberry River near Mulberry	X	--	--	--	X	X
7–2525	Sixmile Creek subwatershed 6 near Chismville	X	--	X	X	--	--
7–2530	Sixmile Creek at Chismville	X	--	X	X	--	--
7–2535	Sixmile Creek near Branch	X	--	X	X	--	--
7–2540	Sixmile Creek subwatershed 5 near Chismville	X	--	X	X	--	--
7–2545	Sixmile Creek subwatershed 2 near Caulksville	X	--	X	X	--	--
7–2550	Sixmile Creek at Caulksville	X	--	X	X	--	--
7–2551	Sixmile Creek subwatershed 23 near Branch	X	--	X	X	--	--
7–2555	Hurricane Creek near Branch	X	--	X	X	--	--
7–2560	Hurricane Creek near Caulksville	X	--	X	X	--	--
7–2565	Spadra Creek at Clarksville	--	X	--	--	--	--
7–2570	Piney Creek near Dover	X	--	--	--	X	--
7–2575	Illinois Bayou near Scottsville	--	X	--	--	--	--
7–2580	Arkansas River at Dardanelle	X	--	X	--	X	--
7–2585	Petit Jean River near Booneville	X	--	X	X	--	--
7–2595	Petit Jean River near Waveland	X	--	X	--	X	--
7–2600	Dutch Creek at Waltreak	--	X	--	--	--	--
7–2605	Petit Jean River at Danville	X	--	--	--	X	X
7–2610	Cadron Creek near Guy	X	--	--	--	X	--

TABLE 5.—*Streamflow stations in operation (1970) and those needed for proposed network*—(continued)

Station number and name		Recommendations		Types of data			
		Include in network	Not recommended for inclusion	Current purpose	Planning and design: Minor streams	Planning and design: Principal streams	Long-term trend
7–2615	Fourche La Fave River near Gravelly	X	--	X	--	X	--
7–2625	Fourche La Fave River near Nimrod	X	--	X	--	X	--
7–2630	South Fourche La Fave River near Hollis	X	--	X	X	--	--
7–2635	Arkansas River at Little Rock	X	--	X	--	X	--
7–2640	Bayou Meto near Lonoke	X	--	--	--	X	--
7–2654.5	Mississippi River at Arkansas City	X	--	X	--	X	--
7–3370	Red River at Index	X	--	X	--	X	--
7–3395	Rolling Fork near DeQueen	X	--	X	X	--	--
7–3400	Little River near Horatio	X	--	X	--	X	--
7–3403	Cossatot River near Vandervoort	X	--	--	X	--	X
7–3405	Cossatot River near DeQueen	--	X	--	--	--	--
7–3410	Saline River near Dierks	X	--	X	X	--	--
7–3412	Saline River near Lockesburg	X	--	X	--	X	--
7–3413.01	Little River near Ashdown	X	--	X	--	X	--
7–3415	Red River at Fulton	X	--	X	--	X	--
7–3494.3	Bodcau Creek at Stamps	--	X	--	--	--	--
7–3560	Ouachita River near Mount Ida	X	--	X	--	X	--
7–3565	South Fork Ouachita River at Mount Ida	--	X	--	--	--	--
7–3575.01	Ouachita River below Blakely Mountain Dam	X	--	X	--	X	--
7–3595	Ouachita River near Malvern	X	--	X	--	X	--
7–3598	Caddo River near Alpine	X	--	X	X	--	--
7–3600	Ouachita River at Arkadelphia	X	--	--	--	X	--
7–3605.01	Little Missouri River below Narrows Dam	X	--	X	X	--	--
7–3610	Little Missouri River near Murfreesboro	--	X	--	--	X	--
7–3612	Ozan Creek near McCaskill	--	X	--	X	--	--
7–3615	Antoine River at Antoine	X	--	--	X	--	X
7–3616	Little Missouri River near Boughton	X	--	--	--	X	--
7–3620	Ouachita River at Camden	X	--	X	--	X	--
7–3621	Smackover Creek near Smackover [3]	X	--	X	--	X	--
7–3625	Moro Creek near Fordyce	X	--	--	--	X	--
7–3630	Saline River near Benton	X	--	--	--	X	--
7–3632	SALINE RIVER near Sheridan [1]	X	--	--	--	X	--
7–3633	Hurricane Creek near Sheridan	X	--	X	X	--	--
7–3635	Saline River near Rye	X	--	--	--	X	X
7–3641.5	Bayou Bartholomew near McGehee	X	--	--	--	X	--
7–3658	Cornie Bayou near Three Creeks	X	--	--	X	--	X
7–3659	Three Creek near Three Creeks	X	--	X	X	--	--

[1] Gaging station to be established.
[2] Gaging station to be moved downstream to include larger drainage area.
[3] Gaging station to be moved downstream below the point of principal pollution.

current-purpose gaging stations may also be used for planning and design.

Data Analysis

The streamflow-data network operated through the years supplies a base for analyses and reports thereon which should be started as soon as the proposed streamflow data program can be implemented. Some aspects of data analyses are of a continuing nature, with the data-collection effort continuing, reoriented as necessary to fill gaps or eliminate deficiencies, and provide data for continuing future analyses.

The proposed program of data analyses for Arkansas streams may be classed in two phases—those based on data collected to date, and those for which additional data will be required.

Data analyses and appropriate reports should be scheduled for completion during the next 2 years on the following:

1. Magnitude and frequency of peak flows—an updating of the Patterson (1961) report, "Floods in Arkansas, magnitude and frequency," prepared in 1960 using discharge records through 1958. When sufficient length of record has been obtained at the 105 peak-flow partial-record stations for areas less then 50 square miles, these data should be merged with those for larger drainage areas for analysis.
2. Flood-volume frequency based on analysis of annual maximum average flows for selected periods of time.
3. Statistics of mean annual and mean monthly flows.
4. Low-flow characteristics of Arkansas streams —an updating of the previous low-flow frequency and flow-duration analysis, expanded to include an inventory of quantity and quality of spring flow and definition of the perennial-stream system in Arkansas.

Utilizing available data to the extent possible, but depending primarily on the collection of additional data specifically required, the following studies

should be initiated as a part of the proposed streamflow data program:

1. Time of travel and dispersion of solutes in selected streams in Arkansas, giving first priority to the reach of the Arkansas River in the State.
2. Regulated-streams systems, giving first priority to the White River basin.
3. The White River stream-aquifer flow system.
4. Areas inundated by floodwaters and flood profiles on principal streams in the State.
5. Gains and losses of flow of selected streams.
6. Frequency of floods in urban and suburban areas.
7. The effects of small reservoirs and ponds on streamflow characteristics.

These are only a few of the data analyses and hydrologic studies that could be made in Arkansas. Changing needs for streamflow information and changes in technology in water-related fields must be continuously evaluated in light of the data analyses that should be generated under the streamflow data program for Arkansas.

REFERENCES

Arkansas Soil and Water Conservation Commission, 1968, Lakes of Arkansas: Arkansas Soil and Water Conserv. Comm. pub., 30 p.

Benson, M. A., 1962, Factors influencing the occurrence of floods in a humid region of diverse terrain: U.S. Geol. Survey Water-Supply Paper 1580–B, 64 p.

——— 1964, Factors affecting the occurrence of floods in the Southwest: U.S. Geol. Survey Water-Supply Paper 1580–D, 70 p.

Carter, R. W., and Benson, M. A., 1969, Concepts for the design of streamflow data programs: U.S. Geol. Survey open-file rept., 33 p.

Patterson, J. L., 1961, Floods in Arkansas, magnitude and frequency: U.S. Geol. Survey open-file rept., 128 p.

U.S. Army Corps of Engineers, 1954, Drainage area data, Arkansas, White, and Red River basins: U.S. Army Corps of Engineers pub., 200 p.

U.S. Water Resources Council, 1967, A uniform technique for determining flood flow frequencies: U.S. Water Resources Council Bull. 15, 15 p.

U.S. Weather Bureau, 1961, Rainfall frequency atlas of the United States: U.S. Weather Bureau Tech. Paper 40, 115 p.

THE PRE-QUATERNARY SURFACE IN THE JORDAN VALLEY, UTAH

By TED ARNOW[1], RICHARD VAN HORN[2], and REED LaPRAY[1],

[1] Salt Lake City, Utah, [2] Denver, Colo.

Work done in cooperation with the Utah Department of Natural Resources, Division of Water Rights

Abstract.—The altitude of the base of the Quaternary deposits in the Jordan Valley, Utah, was determined by interpretation of drillers' logs of water wells supplemented with some geological and geophysical data. The pre-Quaternary surface of the valley generally was similar to the present land surface but had considerably more relief. A map showing contours of the base of the Quaternary deposits can be used as a general guide for water-well drilling and for preliminary determination of the depth to firmest foundation materials.

As part of investigations of the water resources of Salt Lake County and the engineering geology of the Salt Lake City area, the U.S. Geological Survey determined the altitude of the base of the Quaternary deposits in the Jordan Valley, Utah. This work was done as an aid in calculating the amount of fresh water in storage in the valley fill that could be withdrawn by wells and to provide an indication of the approximate depth to firmer foundation material underlying the unconsolidated Quaternary deposits.

The valley fill consists mostly of deposits of Tertiary and Quaternary age. The Tertiary deposits are semiconsolidated or consolidated, and where the older Tertiary deposits crop out at the margins of the valley they include moderately to strongly cemented conglomerate, limestone, tuffaceous mudstone, volcanic rocks, and—at a few places—poorly consolidated lakebeds. Within the valley, however, well logs indicate that a large proportion of the Tertiary deposits are semiconsolidated clay, sand, and gravel which are interspersed with lava and cemented layers of sand and gravel. The Tertiary deposits within the valley are similar in texture to the Tertiary beds described by Hunt, Varnes, and Thomas (1953, p. 13) from exposures in the Jordan Narrows at the south end of the valley.

Neither the Tertiary deposits nor the pre-Tertiary bedrock are known to yield large quantities of water to wells in the report area. Records available for 18 wells that obtain water from Tertiary deposits in the Jordan Valley show an average specific capacity of less than 5 gallons per minute per foot of drawdown. Half of these wells also obtain some water from the overlying Quaternary deposits; the water-yielding capacity of the Tertiary deposits therefore is even less than that indicated by the specific-capacity data. In some parts of the report area the low water-yielding capacity of Tertiary deposits and pre-Tertiary bedrock was used to help differentiate these units from overlying Quaternary deposits of higher water yield.

Quaternary deposits unconformably overlie either Tertiary deposits or pre-Tertiary bedrock. The Quaternary deposits are unconsolidated and consist mostly of materials ranging in size from clay to sand, though they do contain layers of gravel or boulders. Throughout much of the valley these deposits are saturated with water, and where they are fine grained they do not have high bearing strength. Most of the manmade structures in the valley are founded on Quaternary deposits. Some Quaternary deposits are very porous and permeable and yield large quantities of water to wells. Records available for 73 wells that obtain water from Quaternary deposits in the valley show an average specific capacity of 60 gallons per minute per foot of drawdown. The Quaternary deposits constitute the principal ground-water reservoir in the valley.

Soils formed in arid regions, such as the Jordan

U.S. GEOL. SURVEY PROF. PAPER 700–D, PAGES D257–D261

Valley, generally have calcium carbonate accumulations in the lower part of the soil (Soil Survey Staff, 1951, p. 242). Eventually the calcium carbonate accumulation may harden and form a cement-like pan, which has been called by such names as caliche, hardened caliche, or hardpan. Calcium carbonate accumulations that form cemented layers in the lower parts of Pleistocene soil horizons are exposed at several places in the Jordan Valley. Such cemented zones in Pleistocene deposits are generally less than 3 feet thick. Similar zones were probably formed during Tertiary time, and these may account for some of the cemented layers noted in well logs.

METHODS

The base of the Quaternary deposits was determined for most of the valley from information obtained from drillers' logs of water wells. This was supplemented by stratigraphic information from a few logs by geologists and by determination by Arnow and Mattick (1968) of the base of the Quaternary deposits along a seismic-refraction profile in the northern part of the Jordan Valley. The use of drillers' logs is somewhat unsatisfactory in that different drillers may describe the same rock unit with different terms, or drillers may not note conditions that are geologically significant. Despite these drawbacks, drillers' logs were used because no more satisfactory information was available for the entire valley. Gamma-ray logs were available for many wells, but it was not possible to differentiate the Quaternary deposits from underlying Tertiary deposits in these logs.

Approximately 200 drillers' logs of wells mostly more than 500 feet deep were inspected. Contacts between the Quaternary deposits and the underlying pre-Tertiary bedrock were determined in 13 logs and between the Quaternary deposits and the underlying Tertiary deposits in 96 logs. It was not possible to determine the Quaternary-Tertiary contact from the drillers' logs for the remaining wells, none of which were reported to have reached bedrock. The base of the Quaternary deposits was determined for 16 other well sites by means of geological or geophysical data, thus giving a total of 125 subsurface control points for drawing contours of the base of the Quaternary deposits in figure 1. About 60 percent of the control points are east of the Jordan River; in a few large areas west of the river, control points are widely spaced. Additional guidance for the construction of the contours was obtained from rock outcrops and excavations, from gravity data (Cook and Berg, 1961), and from depth-to-bedrock interpretations of Mattick (1970).

Determination of the contact between the Quaternary deposits and the underlying pre-Tertiary bedrock from drillers' logs was fairly simple. The contact was placed at the point where the log stated that the well entered a consolidated rock such as limestone, shale, sandstone, or "bedrock." Drilling generally was stopped after the well had penetrated a few feet into the consolidated rock. The determination made from a driller's log may differ from the actual position of the Quaternary bedrock contact by several feet because it was not possible to recognize weathered bedrock from the description in the driller's log. A discrepancy of several feet is not considered significant, however, considering the 500-foot contour interval used in figure 1.

Determination of the contact between the Quaternary deposits and the underlying Tertiary deposits was more difficult. Drillers make no distinction between the two deposits; and they report similar types of materials such as clay, silt, sand, or gravel for both. Although the Tertiary deposits are semiconsolidated, this is not noted in logs. The top of the Tertiary deposits generally was selected in drillers' logs at the first reported beds of lava, conglomerate, hardpan, or various types of cemented or hard materials that were more than 3 feet thick. No lava of Quaternary age is known in the Jordan Valley or in nearby areas; thus, the report of lava in a driller's log was assumed to be an indication of Tertiary deposits. A report of the other types of hard materials, even if underlain by uncemented material, was also taken as an indication of Tertiary deposits because such materials, where exposed in the Jordan Valley, are characteristic of Tertiary rather than of Quaternary deposits.

It is possible, of course, that the first reported hard bed actually may be a few tens of feet below the top of the Tertiary deposits, because those overlying Tertiary deposits could not be differentiated in the driller's log. For the most part, however, we believe that the first reported thick hard layer does represent the top of the Tertiary deposits. The transition between Tertiary and Quaternary time in the Jordan Valley must have been marked by a period when the Tertiary surface was exposed and a soil was being formed. The calcium carbonate-cemented zone of this soil would be most readily preserved and would mark the top of the Tertiary deposits at places within the valley. In many drillers' logs for the Jordan Valley only one hard layer was reported in the entire log. Although drillers called this layer

Base map prepared from U.S. Geological Survey topographic maps

EXPLANATION

4500

Contour showing altitude of the base of Quaternary deposits
Dashed where approximately located. Contour interval 500 feet. Datum is mean sea level

Driller's log

Geological or geophysical data

Approximate boundary of Quaternary rocks modified from Marsell and Threet (1960), Tooker and Roberts (1961), and Marine and Price (1964)
Hachures are on pre-Quaternary rocks

Excavation exposing pre-Quaternary rocks

FIGURE 1.—Contours of the base of the Quaternary deposits in the Jordan Valley, Utah.

by various names—such as hardpan, conglomerate, hard sand, hard layer—they all are correlated with the residual hard layer at the top of the Tertiary deposits that may have formed in the lower part of the ancient soil zone.

This method of determining the top of the Tertiary deposits was not entirely satisfactory in some parts of the valley, particularly in the area near the mouths of Big and Little Cottonwood Canyons on the east side of the valley. Massive deltas were built by the two Cottonwood Creeks in this area during Quaternary time. Drillers' logs of wells in the Cottonwoods delta area report many hard layers, some very close to the present land surface. The land quite probably was exposed periodically during the formation of the deltas; and soils, including a lower cemented layer, were formed at each exposure, particularly in those localities where the water table was close to the land surface. Because of the inconsistent depth of hard layers in the Cottonwoods delta area, reports of hard layers in drillers' logs generally were discounted as indicators of Tertiary deposits. In that area the full thickness of permeable water-bearing deposits, as reported in well records or indicated by depth of perforations of well casing in successful wells, was used as a guide to indicate the minimum thickness of Quaternary deposits.

RESULTS

The contours in figure 1 indicate that the pre-Quaternary surface in the southern and central parts of the valley was generally similar to the present land surface. The pre-Quaternary surface sloped toward the central part of the valley, and the valley sloped northward toward Great Salt Lake. As many of the present drainageways are reflected in the pre-Quaternary surface, it is likely that the drainage pattern has not changed appreciably since the beginning of the Quaternary Period. The greatest changes probably have been in the lower reaches of the two Cottonwood Creeks.

The contours in the northern part of the valley indicate a marked difference between the present land surface and the pre-Quaternary surface. The present land surface is virtually flat, with slight gradients toward the Jordan River and Great Salt Lake. Between the river and the lake the pre-Quaternary surface had a major divide with a relief of more than 1,000 feet. North of the tailings pond at Magna this divide was cut by a shallow, northeast-trending trough or valley that terminated in the deep valley of the Jordan River. The lowest area on the pre-Quaternary surface was near the Jordan River, at an altitude less than 2,000 feet above sea level. This area corresponds to the area of a low-gravity anomaly reported by Cook and Berg (1961, pl. 13).

The Quaternary deposits are thickest in the northern part of the valley. The maximum thickness is near the Jordan River northwest of Salt Lake City, where the deposits exceed 2,200 feet. The deposits thin gradually toward the west; in a distance of about 11 miles, near the shore of Great Salt Lake, they are about 1,200 feet thick. The Quaternary deposits thin more rapidly toward the south, and about 11 miles away, near Murray, are only about 300 feet thick. The deposits thicken again southeast of Murray, east of the Jordan River; the contours in figure 1 suggest a local maximum thickness of about 800 feet east of Sandy. The area of thickening is indicated by the bulge toward the east in the 4,000-foot contour in figure 1 near the mouths of Big and Little Cottonwood Canyons. Presumably the discharge from the two Cottonwood Creeks was great enough to markedly erode the area opposite the canyon mouths during Tertiary or Quaternary time, and the eroded area subsequently filled with deltaic deposits during Quaternary time.

The Quaternary deposits are thinnest adjacent to the mountain fronts and in the area west of Kearns, where they generally are less than 200 feet thick.

The pre-Quaternary surface of the valley had considerable relief, and the main effect of Quaternary deposition was to reduce this relief by filling topographic lows and forming the overall gradual slopes of the present surface.

CONCLUSIONS

The contours of the base of the Quaternary deposits in figure 1 provide a guide to the maximum depth from which large quantities of water of good chemical quality can be obtained from wells and also provide an indication of the maximum depth to firmer foundation material underlying the unconsolidated Quaternary deposits.

Few existing wells in the valley are known to obtain large quantities of good quality water from deposits at greater depth than that indicated by the contours. The contours are necessarily generalized, however, because of the local sparsity of control and the methods used to establish the control. This, together with the large contour interval, suggests that the contours be used with caution as a rough guide for future well drilling.

Most structures in Salt Lake County are founded on coarse materials or thin cemented zones in the Quaternary deposits. Settling of foundations has been a minor problem; but as heavier structures are built, settling problems will become more critical. The contours in figure 1 can be used as a general guide to indicate the depth to the firmest foundation materials, which underlie the Quaternary deposits.

REFERENCES

Arnow, Ted, and Mattick, R. E., 1968, Thickness of valley fill in the Jordan Valley east of the Great Salt Lake, Utah, *in* Geological Survey Research 1968: U.S. Geol. Survey Prof. Paper 600–B, p. B79–B82.

Cook, K. L., and Berg, J. W., Jr., 1961, Regional gravity survey along the central and southern Wasatch Front, Utah: U.S. Geol. Survey Prof. Paper 316–E, p. 75–89.

Hunt, C. B., Varnes, H. D., and Thomas, H. E., 1953, Lake Bonneville: Geology of northern Utah Valley, Utah: U.S. Geol. Survey Prof. Paper 257–A, 99 p.

Marine, I. W., and Price, Don, 1964, Geology and groundwater resources of the Jordan Valley, Utah: Utah Geol. and Mineralog. Survey Water-Resources Bull. 7, 67 p.

Marsell, R. E., and Threet, R. L., 1960, Geologic map of Salt Lake County, Utah: Utah Geol. and Mineralog. Survey R. S. 83 (supp. to Bull. 69).

Mattick, R. E., 1970, Thickness of unconsolidated to semiconsolidated sediments in Jordan Valley, Utah, *in* Geological Survey Research 1970: U.S. Geol. Survey Prof. Paper 700–C, p. C119–C124.

Soil Survey Staff, 1951, Soil survey manual: U.S. Dept. Agriculture Handb. 18, 503 p.

Tooker, E. W., and Roberts, R. J., 1961, Preliminary geologic map and sections of the north end of the Oquirrh Range (Mills Junction, Garfield, and Magna 7½-minute quadrangles), Tooele and Salt Lake Counties, Utah: U.S. Geol. Survey Mineral Inv. Field Studies Map MF–240.

THE EFFECT OF STREAM DISCHARGE ON STREAMBED LEAKAGE TO A GLACIAL OUTWASH AQUIFER

By STANLEY E. NORRIS, Columbus, Ohio

Work done in cooperation with the U.S. Atomic Energy Commission

Abstract.—Five controlled pumping tests of a glacial outwash aquifer, made in a comparatively small area in the Scioto River valley near Piketon, Ohio, showed ranges in aquifer transmissivity from 165,000 to 300,000 gallons per day per foot and in the rate of streambed leakage from 0.21 to 1.15 million gallons per day per acre for each foot of head difference between the stream and the underlying aquifer. The rate of streambed leakage varies with stream discharge and velocity, suggesting that higher flows progressively clean the streambed and increase its permeability. The relation of discharge to streambed leakage is important not only in the design of local ground-water supply facilities, but also because it may be applicable to a large part of the watercourse aquifer system in the lower Scioto River valley.

In 1963 and 1969 at the request of the U.S. Atomic Energy Commission the U.S. Geological Survey made aquifer tests in the Scioto River valley near the village of Piketon, in south-central Ohio, to determine the feasibility of developing ground-water supplies from wells drilled in sand and gravel outwash adjacent to the Scioto River.

In October 1963, at a time of very low streamflow, a well 83 feet deep, drilled on the flood plain 450 feet from the river (site *A* on the location map, fig. 1) was pumped for 9 days at the rate of 1,000 gallons per minute, and the response of the hydrologic system was determined by measuring the water level in an array of deep and shallow observation wells and in eight drive-point wells installed in the bed of the river. The calculated values of aquifer transmissivity, 215,000 gallons per day per foot, and streambed leakage factor, 0.235 million gallons per day per acre per foot, were used as criteria for the design of four supply wells, which were drilled in 1965 in the immediate area of the test site. These supply wells presently furnish about 10 million gallons per day to the Atomic Energy Commission (AEC) facility from induced stream infiltration.

In 1969 the AEC, considering whether to expand its ground-water supply system, investigated three additional sites along the Scioto River, designated as *B*, *C*, and *D* on figure 1. This investigation provided the opportunity to compare results of aquifer tests made in the same aquifer within a comparatively small area and, more importantly, to determine the effects of changes in stream discharge on the permeability of the streambed.

The Scioto River at Piketon has a drainage area of 5,836 square miles, most of which is in the glaciated area of central Ohio. In the lower 100 miles of its course, from Columbus to its confluence with the Ohio River at Portsmouth, the river flows

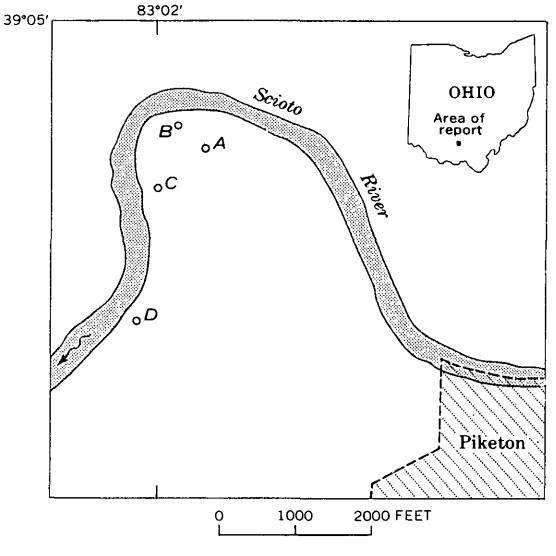

FIGURE 1.—Location of aquifer-test sites.

almost due south in a wide, flat-bottomed, and generally steep-sided bedrock valley, which is partially filled with outwash sand and gravel. These permeable deposits and the associated river constitute one of the State's potentially most productive watercourse aquifer systems. Wells sustained by induced infiltration of streamflow are the principal source of industrial and municipal water supply, not only at Piketon, but also at Circleville, Chillicothe, and other cities on the lower course of the river. The same source is presently being considered for an additional water supply at Columbus.

Piketon is about 20 miles beyond the southern limit of glaciation, and the outwash deposits are relatively homogeneous. They contain no interbedded lenses or layers of till, such as typically occur in outwash deposits within the glaciated region. In the area of the test sites the outwash deposits consist chiefly of sand and medium-size gravel, with lesser quantities of silt, and include scattered, localized bodies of clay. This generally permeable sequence underlies 10 to 15 feet of more recent river alluvium and extends downward to the shale bedrock at depths of about 75 to 85 feet. The water table ranges from about 10 to 15 feet below the surface, and the saturated thickness of the aquifer averages about 60 to 65 feet.

Two controlled pumping tests were made at site B, one test at a time of low flow and the other at a time of relatively high flow. Tests at sites C and D were made during periods of moderately high and moderately low flow, respectively. Except that the wells at sites B, C, and D were pumped for 3 days, rather than for 9 days as at site A, the aquifer-test methods and techniques of analysis were the same as described for the earlier test by Norris and Fidler (1969). Briefly, the procedure involved drilling and pumping a 12-inch-diameter well at each site and observing water-level changes in the aquifer in a series of 2-inch-diameter drive-point wells, including several shallow wells installed in the bed of the river. Located at distances ranging from 150 to 200 feet from the river, the pumped wells ranged in depth from 71 to 76 feet and bottomed at or near the bedrock. Paired shallow and deep observation wells were located on two lines, one line extending through the pumped well toward the river and the other extending through the pumped well approximately parallel with the river. Pumping rates for the 72-hour tests were 700 gpm at site C and 1,000 gpm at sites B and D. Average drawdown values, after being corrected for dewatering, were substituted into equilibrium equations developed by Rorabaugh (1956, p. 120–122) to determine "line-source distance" and aquifer transmissivity. Transmissivity values determined for sites B, C, and D are, respectively, 300,000 gpd per ft, 165,000 gpd per ft, and 210,000 gpd per ft. The relatively low value determined at site C resulted from the presence of a clay bed, 20 feet thick, that occurred immediately above the screen in the pumped well and locally reduced the thickness of the aquifer.

RATE OF STREAMBED LEAKAGE

The quantity of water derived from the river source was determined from an equation by Theis (1941, p. 735) and related to the streambed area to obtain the infiltration rate, expressed in million gallons per day per acre. The infiltration rate was further related to head loss under the river by dividing by an integrated drawdown value determined from observed drawdowns in the riverbed wells. The result is referred to here as the streambed leakage factor, expressed in million gallons per day per acre per foot. As the aquifer tests were made under widely differing river temperatures, the values are adjusted to a temperature of 11.7°C, approximately the same as the ground-water temperature. The values tabulated for the tests are shown in table 1.

TABLE 1.—*Data from aquifer tests made in the Scioto River valley near Piketon, Ohio*

Site	Date of test	Discharge of Scioto River (cubic feet per second)	Average velocity (feet per second)	Infiltration rate (mgd per acre)	Streambed leakage factor (mgd per acre per foot)	Temperature of Scioto River (°C)	Temperature factor	Streambed leakage factor adjusted to 11.7°C (mgd per acre per foot)
A----	Oct. 1963	342	0.59	0.10	0.23	15.6	0.90	0.21
B----	Feb. 1969	3,980	1.98	.71	.89	4.4	1.24	1.07
	Oct. 1969	733	.86	.94	.69	12.8	.97	.67
C----	Jan. 1969	2,100	1.45	.12	.82	1.1	1.38	1.15
D----	Oct. 1969	1,010	1.02	.11	.46	10.0	1.05	.48

RELATION OF STREAMBED LEAKAGE TO STREAM DISCHARGE

Within the observed range of data the streambed leakage factor varies exponentially with stream discharge. The relation is shown on a graph in which the adjusted values are plotted against stream discharge and velocity (fig. 2). The plots are based on mean velocity values picked from the graph in figure 3, which shows the relation of velocity, width, and depth of the Scioto River to discharge in the aquifer test area. The discharges were measured at different places, and there is considerable scatter of points, but, nevertheless, these graphs express closely the relation between the discharge and mean values of velocity, width, and depth for the typical natural stream section.

As discharge is a function not only of velocity, but also of width and depth, it is obvious that the data points on figure 2 would also bear a relation to the latter parameters somewhat similar in form to that shown for velocity. Velocity, however, is the only discharge variable not used in the calculation of the infiltration rate, and hence is the only one of the three variables for which the observed relation is independent of the calculations. Variations in stream width are compensated for in the calculations as width enters into the determination of the area through which infiltration occurs. Variations in depth are not directly involved in the calculations, as it is not the depth of the stream but the head difference between the stream and the underlying water table that is a factor in the movement of water from the stream into the aquifer. Prior to pumping, the level of the water table in the vicinity of the river was virtually the same as the water surface. In all tests the drawdown beneath the river, caused by pumping, was only a small fraction of the river's total depth.

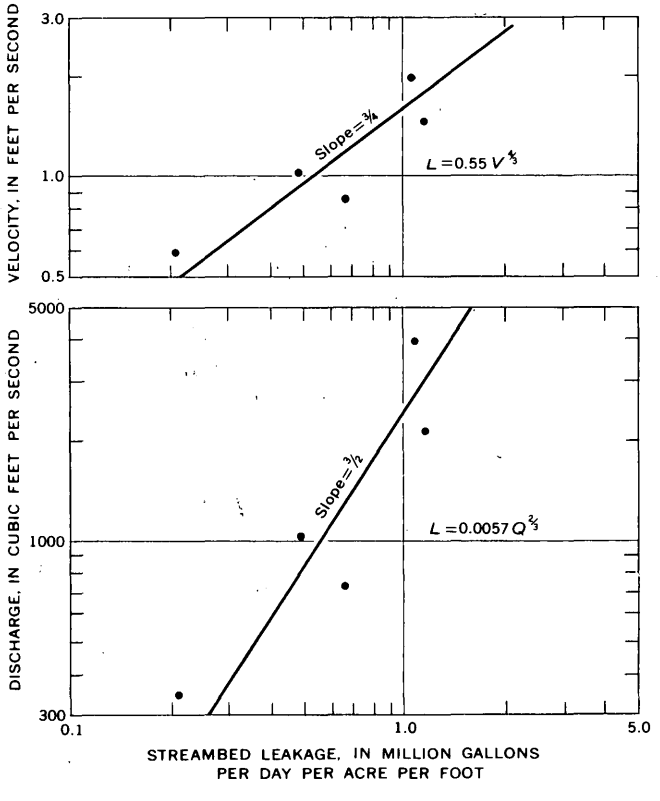

FIGURE 2.—Relation of streambed leakage to stream discharge and velocity.

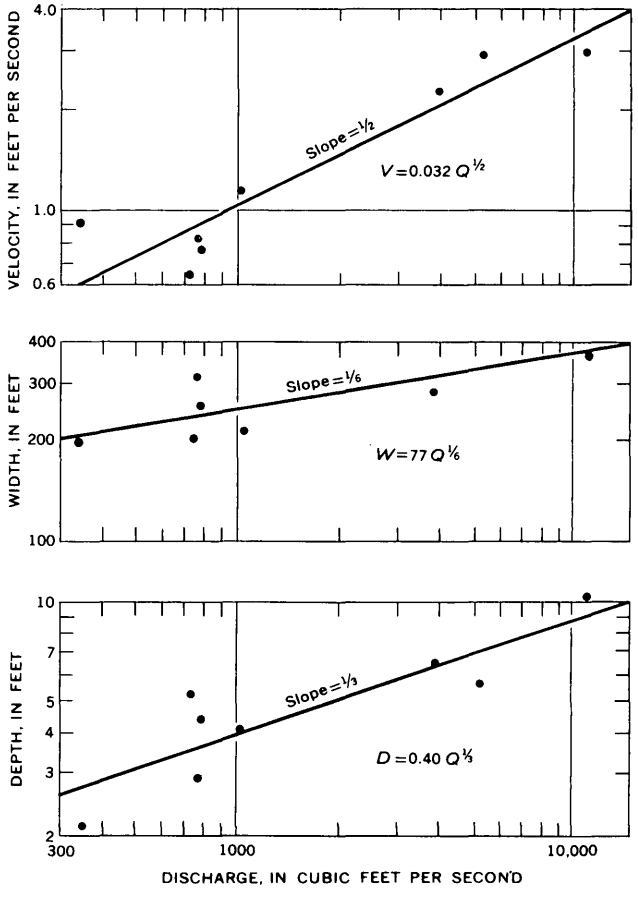

FIGURE 3.—Relation of velocity, width, and depth of the Scioto River to discharge at Piketon, Ohio.

The relation between streambed leakage and velocity suggests that the higher the flow the "cleaner," and hence more permeable, the streambed becomes. This could result from the progressive removal of silt and other fine-grained material, including organic debris, that accumulate in periods of relatively low flow.

Values of the streambed leakage factor, L, in the equations expressed by the graphs in figure 2 are:

for discharge, Q, $L = 0.0057\ Q^{2/3}$; and, for velocity, V, $L = 0.55\ V^{4/3}$, where the discharge is expressed in cubic feet per second and the velocity in feet per second.

The observed relation between the streambed leakage factor and velocity does not apply when the stream overflows its banks. At Piketon this occurs at a discharge of about 15,000 cubic feet per second, above which the width increases rapidly as the flood plain between the river and manmade levees is inundated. The ground through which infiltration occurs changes character because the flood plain is composed of different material than is the streambed, and a totally new relation between the rate of streambed leakage and discharge results. However, discharges in the magnitude of 15,000 cfs occur only about 7 percent of the time at Piketon, and the relation (fig. 2) will prevail the remainder of the time. The estimated discharge equaled or exceeded 90 percent of the time is 510 cfs; the estimated discharge equaled or exceeded 50 percent of the time is 1,830 cfs. The mean annual discharge at Piketon, estimated at 4,900 cfs, is equaled or exceeded about 25 percent of the time.

SIGNIFICANCE

If we assume that streambed permeability consistently varies with velocity, and hence with the discharge of the Scioto River, development in the Piketon area can be based on the rate of streambed leakage associated with a selected discharge.

More importantly, the data developed at Piketon may be applicable to a much larger area. Evidence suggests that the character of the outwash deposits and river conditions, including sediment load and water quality, are virtually uniform in most of the 40-mile long reach extending from Chillicothe to the mouth of the river. If the relation observed at Piketon between streambed leakage and discharge proves generally applicable, the design of groundwater facilities along this entire reach will be simplified, and so also will future water-management decisions which are likely to be necessitated by the continued growth of population and industry in this part of the Scioto River basin.

More work could be done with the Piketon data by collecting and analyzing bed samples and in determining the manner in which velocity acts to change streambed permeability. If permeability is controlled by a relatively thin skin of sediment at the top of the bed, perhaps it could be determined at what discharge the stream velocity is sufficiently high to completely remove this skin. Complete removal from the streambed of a thin layer of poorly permeable material would presumably result in a condition of maximum streambed permeability, controlled by the vertical permeability of the aquifer. This would permit calculation of the maximum value of streambed leakage for use in the design of infiltration water-supply systems.

Judgment obviously is called for in extrapolating the Piketon data into other areas. Especially is this true with respect to the transmissivity values determined at the four test sites. Although all values were high, confirming the already proven suitability of the aquifer for large-scale ground-water development, the fact remains that transmissivity varied over a range of about 82 percent within a relatively small area. This wide variation indicates a need for additional aquifer tests in other areas to determine the range in transmissivity that more generally characterizes the outwash deposits in the lower Scioto River valley.

The Piketon data represent an important step in the quantitative evaluation of one of Ohio's principal aquifers. Such an evaluation is requisite to sound planning related to development, conservation, and future allocation of the State's water resources.

REFERENCES

Norris, S. E., and Fidler, R. E., 1969, Hydrogeology of the Scioto River valley near Piketon, south-central Ohio: U.S. Geol. Survey Water-Supply Paper 1872, 70 p.

Rorabaugh, M. I., 1956, Ground water in northeastern Louisville, Kentucky, with reference to induced infiltration: U.S. Geol. Survey Water-Supply Paper 1360–B, p. 101–169.

Theis, C. V., 1941, The effect of a well on the flow of a nearby stream: Am. Geophys. Union Trans., pt. 3, p. 734–738.

A METHOD FOR RELATING INFILTRATION RATES TO STREAMFLOW RATES IN PERCHED STREAMS

By D. E. BURKHAM, Tucson, Ariz.

Work done in cooperation with the city of Tucson, the U.S. Bureau of Reclamation, and the University of Arizona

Abstract.—A method has been developed for relating infiltration rates (volume per unit time) to streamflow rates for streams that are perched above the water table. The equations derived were based on relations of streamflow rates to width, depth, and velocity and on the assumed relations between infiltration velocity (expressed in depth of water per unit time) and these parameters. The equations were compared to measured streamflow data for a reach of an ephemeral stream entrenched in alluvium. The bed of the stream normally is coated with fine-grained material deposited during periods of low flow. An equation based on the assumption that infiltration velocity is proportional to stream depth seems to correlate closely with infiltration rates during typical short-duration flows. The layer of fine-grained material on the streambed probably is the main control on the infiltration velocity during these flows.

In the arid and semiarid regions of the United States, the proper management of the hydrologic system to obtain maximum benefit from the surface-water and ground-water supplies can be the most important factor affecting the overall economy of an area. Proper management of the system requires a comprehensive knowledge of all the natural characteristics of the system and of the interrelations of its many components, which affect the amount of water available. Infiltration from streamflow—a source of recharge to the ground-water reservoir—is a component of the hydrologic system that has not been adequately defined.

The purpose of this report is to describe a method for relating infiltration rates [1] to streamflow rates for streams that are perched above the water table. The method includes the development of theoretical equations relating infiltration rates to inflow rates and comparisons of the equations with the measured data. The equations were based on the relations of streamflow rates to width, depth, and velocity and on the relations between infiltration velocity [2] and these parameters as hereafter discussed. Although the method is applicable to any perched stream, ephemeral streams entrenched in alluvium were of primary interest in this study.

Infiltration in an alluvial channel is dependent on many factors: (1) surface area and depth of water in the channel; (2) permeability, moisture distribution, and temperature of the subsurface alluvium; (3) physical quality of the water and length of time the water is available at the land surface; (4) chemical quality of the surface and subsurface water; and (5) structural stability of the porous media. In addition, air within the porous media and atmospheric pressure affect the infiltration process. These factors are so variable in time and space that they generally cannot be assigned meaningful quantitative values; however, many of the dominant forces and parameters affecting infiltration also are related directly to the width, depth, and velocity of streamflow. Continuous records of streamflow are available for many places on main and tributary streams. Therefore, data are available to develop equations relating infiltration rates to streamflow rates without detailed quantitative studies of the factors that influence the process of infiltration.

In deriving a useful equation it is necessary to make assumptions and simplifications of the behavior of some of the variables. Infiltration velocity

[1] As used in this report, the term "infiltration rate" is the rate at which infiltration takes place, expressed in volume per unit time.

[2] The term "infiltration velocity" is the rate at which water moves into the streambed, expressed in depth of water per unit time.

and stream discharge are related in several respects and were of primary importance in this study.

Generally, infiltration of water into dry structurally stable porous media takes place rapidly when water is first applied and then gradually decreases as the porous media approach saturation. Under these conditions, the changes in infiltration velocity with time can be depicted either by an exponential function, as described by Horton (1939, 1940), or by an application of Darcy's law, as modified by Stallman (1954, p. 171). These approaches, however, apparently do not describe infiltration accurately for unsteady flows of short duration in channels of movable bed.

One of the factors that govern the movement of water into the porous media is the permeability of the surface layer. The beds of most alluvial channels are not structurally stable; during flow events, some movement and rearrangement of the material occur on the bed, which affect infiltration velocities by changing the permeability. In most alluvial channels the silt and clay fractions of the surface layer are set in motion as the stream velocity increases and settle to the bottom as the stream velocity decreases, leaving stratified layers having the finest material on top. Therefore, the permeability of the surface layer is altered during the fluctuations of streamflow velocity.

The quantitative relation between streambed permeability and streamflow velocity is not known; however, the permeability probably increases at a greater rate than the velocity—up to a limiting value. Flume studies by Matlock (1965) indicated that the infiltration velocity varied with the streamflow velocity because of changes in permeability. The changes in permeability were caused by the movement of fine material, which reduced the pore spaces in the coarse material and also developed a layer of fines. The action of the fines in modifying infiltration is similar to that of a valve.

Matlock (1965, p. 94) stated: "The increase [in infiltration velocity] can continue until the permeability of the bed surface is no longer the limiting factor." Matlock used clear water in the dry bed along Rillito Creek—a typical ephemeral stream in Arizona—in which there were no visible silt deposits; cylinder infiltration tests showed infiltration velocities of hundreds of feet per day for short periods of time and tens of feet per day for longer periods of time. A silt layer only $\frac{1}{8}$ to $\frac{1}{16}$ inch thick reduced infiltration velocities markedly, and a silt layer 3 to 4 inches thick permitted almost no infiltration.

The relation between streamflow velocity and infiltration velocity derived by Matlock (1965) in his flume studies is not likely to be duplicated by nature. For example, a constant depth and width of flow were maintained in the flume, and the velocity of flow was proportional to discharge—a situation that is not likely to occur in an alluvial channel. Because of the increase in sediment size with depth below the streambed and because of the valve effect of the fine material, at some point in the subsurface alluvium the rate of movement of water away from the near-saturated zone—which develops near the channel surface—is equal to the percolation rate within it. That is, beyond some point, the soil permeability times a hydraulic gradient of one (gravity gradient) is equal to or greater than the soil permeability within the near-saturated zone times its hydraulic gradient. Because of the valve effect of the fine material along the channel, the thickness of the near-saturated zone probably is fairly small and constant during some flows.

Upon the arrival of a short-duration flow event, the infiltration velocity probably is small because the fines left on the surface by preceding flows restrict infiltration; however, as the fines begin to move, the infiltration velocity increases during the ascending limb of the flow event and decreases as the fines in suspension settle during the recession of the flow. Hypothetically, then, the curve of infiltration velocity versus time should be similar in shape to the curve of stream depth versus time and (or) stream velocity versus time; the infiltration velocity, I, would tend to be linearly related to the stream depth, D, and (or) stream velocity, V. That is,

$$I \propto D, \text{ or}$$
$$I \propto V, \text{ or}$$
$$I \propto VD.$$

If a long-duration flow event occurs when there are no stratified layers of fine material on the streambed, the infiltration velocity probably is fairly constant during recession of the flow.

DEVELOPMENT OF EQUATIONS

Differential equations for infiltration

The assumption was made that unsteady flow in an incremental stream reach varies as a function of infiltration velocity and stream dimensions. The pertinent variables are shown on figure 1. At any point between L_i and L_o in the stream reach, the stream has width B and depth D. Inflow at the upstream end, L_i, is Q_i. The inflow is depleted by

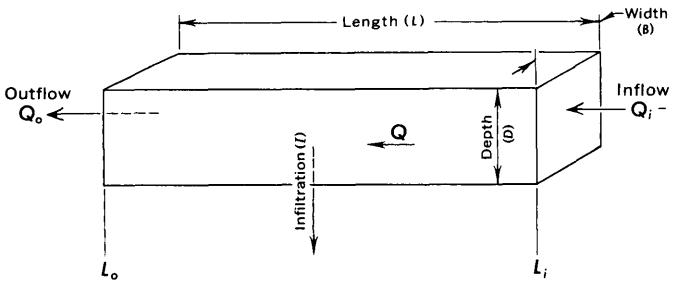

FIGURE 1.—Schema of a stream reach, L_i–L_o, showing nomenclature.

infiltration through the streambed, and downstream at L_o the discharge is Q_o. At any point between L_i and L_o at time t, the variables Q, I, B, and D are related as follows:

$$\frac{\delta Q}{\delta L} + IB = B\frac{\delta D}{\delta t}. \quad (1)$$

The right side of equation 1 refers to temporal variations in Q caused by changing stream depth. To be exact in application, B and D should be treated as variables dependent upon L and t; however, as used in this report, they will be assumed to be a function of Q only. The available data are insufficient to consider both the time and space variations implied in equation 1, and this report is restricted to the definition of spatial changes in discharge. Unfortunately, such a restriction will cause additional scatter in the data points used to develop the relation between streamflow and infiltration.

For steady flow,

$$\frac{\delta D}{\delta t} = 0, \quad (2)$$

and equation 1 may be expressed as an ordinary differential equation:

$$\frac{dQ}{dL} = -IB. \quad (3)$$

Equation 3 can be written in useful terms where traveltimes between specific points along the stream are known. If a given surface area along the stream is known, the steady flow can be described as

$$dQ = -IB\left(\frac{\delta L}{\delta t}\right) dt$$

or

$$dQ = -IBVdt, \quad (4)$$

where dt is the time increment required for an element of surface area to travel an incremental distance dL, and dQ is the change in streamflow over the distance $L - (dL/2)$ to $L + (dL/2)$. Equations relating streamflow and infiltration rates can be derived if the parameters I, B, and V can be related to discharge or can be assumed to be constant.

Hydraulic geometry parameters

The equations, nomenclature, and techniques used by Leopold and Maddock (1953) have been used to describe the hydraulic geometry of streams in alluvial channels in this study. Leopold and Maddock (1953) found that, below bankfull stage, values of stream width, depth, and velocity vary with discharge as a simple power function at a given river cross section. Furthermore, the functions derived for a given cross section and among different cross sections along alluvial channels differ only in numerical values of coefficients and exponents.

The basic equation defining the relations among stream discharge, width, depth, and velocity is

$$Q = BDV, \quad (5)$$

where

$$B = aQ^b, D = cQ^f, \text{ and } V = kQ^m. \quad (6)$$

Substitution of equation 6 into equation 5 yields:

$$Q = a \cdot c \cdot k \cdot Q^b \cdot Q^f \cdot Q^m \quad (7)$$

from which it is evident that

$$a \cdot c \cdot k = 1, \text{ and } b + f + m = 1. \quad (8)$$

Theoretical equations relating surface inflow and infiltration

Equations that relate infiltration within a reach to the streamflow at the upper end can be derived by combining (1) one of the flow equations [eqs. 3 or 4], (2) selected relations between streamflow and stream geometry [eq. 6], and (3) an assumed form of the relation between infiltration and stream geometry. For example, by assuming $\frac{I}{D} = C_1$, a constant, equation 4 is resolved to

$$-C_1 dt = \frac{dQ}{BDV}$$

or

$$-C_1 dt = \frac{dQ}{Q}. \quad (9)$$

If we assume that the relation $\frac{I}{D} = C_1$ is applicable

for steady inflow in all incremental reaches and integrate for a given traveltime, T, of discharge within a reach, equation 9 becomes

$$-C_1\int_0^T dt = \int_{Q_i}^{Q_o} Q^{-1}dQ$$

or

$$\frac{Q_i}{Q_o} = e^{C_1 T}$$

and

$$Q_o = Q_i e^{-C_1 T}. \qquad (10)$$

Therefore,

$$Q_f = Q_i(1 - e^{-C_1 T}), \qquad (11)$$

where

$$Q_f = Q_i - Q_o.$$

In applying equation 11 to the flow in a given length of channel the traveltime, T, is a variable, T_1. The variable time T_1 is the elapsed time necessary to translate a definable area of streamflow through a given length of channel. The traveltime is a function of streamflow rate and infiltration rate. Data adequate for solving equation 11 are generally not available.

If we assume that the relation $\frac{I}{D} = C_1$ is applicable for steady inflow in all incremental reaches, equation 3 can be resolved to describe streamflow depletion as follows:

$$Q_f = Q_i - (Q_i^m - macC_1L)^{1/m}. \qquad (12)$$

Other equations were developed from equation 3 using procedures similar to those used in developing equation 11. The assumed relations and the resultant equations are as follows:

Assumed relation	*Equation*	*No.*
$\frac{I}{D} = C_1$	$V_f = mC_1L,$	(13)

in which, $V_f = V_i - V_o$, and V_i and V_o are the stream velocities at the upstream and downstream ends of the reach, respectively.

$\frac{I}{V} = C_2$	$Q_f = Q_i - (Q_i^f - kaf\,C_2L)^{1/f}.$	(14)
$\frac{I}{VD} = C_3$	$Q_f = Q_i(1 - e^{-C_3 L}).$	(15)
I is constant (I_c)	$Q_f = Q_i - [Q_i^{1-b} - (1-b)(aI_cL)]^{1/1-b}.$	(16)

COMPARISONS OF EQUATIONS WITH MEASURED DATA

Streamflow data from a reach of the ephemeral Santa Cruz River in the Tucson basin, Arizona, were analyzed in order to test the algebraic forms derived for relating streamflow to infiltration. The reach extends downstream from the gaging station at Continental, Ariz., to the gaging station at Tucson (fig. 2).

Hydrologic characteristics of the study reach

The Santa Cruz River is a continuous channel from Continental to Tucson, Ariz. The channel is

FIGURE 2.—Index map of Arizona, showing study reach of the Santa Cruz River.

entrenched in stream alluvium to depths of from 5 to 30 feet. The channel is less than 300 feet wide at bankfull stage and, except in a few places, is sufficiently large to contain most floodflows. The river is a losing stream throughout the 28.5-mile study reach. The particle size of the stream alluvium underlying the channel ranges from clay to gravel as much as 50 millimeters in diameter. During periods of no flow, the surface of the bed generally is coated with clay and silt layers. The depth to the water table ranges from 20 to 100 feet below the surface of the channel. About 85 percent of the inflow to the reach occurs from July through October in a series of short-duration flow pulses resulting from erratically distributed thunderstorms. A flow pulse usually lasts less than one day and contains large concentrations of clay and silt.

The coefficients and exponents in equation 6, which represent the hydraulic geometry of the stream, were computed using streamflow and cross-section data collected in and near the study reach. The data are from long-term gaging-station records and miscellaneous discharge measurements for 1940–43 and 1965–66. In periods of low flow, the discharge measurements were made by wading, or if wading was impossible, the measurements were made from bridges. The bridge measurements may not represent natural conditions because the width of flow often was constricted by the bridge abutment. Therefore, the data obtained from wading measurements were given more weight than the data obtained from bridge measurements. The miscellaneous discharge measurements were used as though they were made at a given cross section in the channel.

The variables a, b, k, and m in equation 6 were derived from graphical plots and the slope-intercept formula. The coefficients and exponents from the many data sets were averaged to obtain an equation relating discharge to velocity and another equation relating discharge to width. The equations derived from the miscellaneous measurements agreed closely with those derived from gaging-station records. The average relation between discharge and depth was obtained by evaluating the coefficient c and exponent f in the identities $a \cdot c \cdot k = b + f + m = 1$, using the known values for the other variables.

The main features of the equations describing the hydraulic geometry of the Continental-Tucson reach of the Santa Cruz River are as follows:

Coefficients	*Exponents*
$a = 5.8$	$b = 0.5$
$c = 0.24$	$f = 0.2$
$k = 0.73$	$m = 0.3$

Inflow–infiltration-rate relations

The coefficients and exponents, which describe the main features of the equations for the hydraulic geometry of the reach, can be inserted into equations 12, 13, 14, 15, and 16 to give the following:

Assumed relation	*Equation*	*No.*
$\frac{I}{D} = C_1$	$Q_f = Q_i - (Q_i^{0.3} - 0.42C_1L)^{3.33}$,	(17)
	and	
	$V_f = 0.3C_1L$,	(18)
$\frac{I}{V} = C_2$	$Q_f = Q_i - (Q_i^{0.2} - 0.85C_2L)^5$,	(19)
$\frac{I}{VD} = C_3$	$Q_f = Q_i(1-e^{-C_3L})$,	(15, 20)
I is constant (I_c)	$Q_f = Q_i - (Q_i^{0.5} - 2.9I_cL)^2$.	(21)

In this paper, comparisons between measured and computed data and the equations are limited to equations 15, 17, 19, and 21. Two types of streamflow data were available for use in the comparisons —measured streamflow and computed infiltration rates for flows of short duration and for flows of long duration. The inflow and outflow data were for periods when there was no known tributary inflow. The computations were based on the premise that streamflow depletion was totally by infiltration.

The average inflow and infiltration rates were computed for short-duration flow events by dividing (1) the inflow volume and (2) the inflow volume minus the outflow volume (equals infiltration), respectively, by the duration of inflow. The duration of inflow was the total time the inflow rate was 10 cfs (cubic feet per second) or greater; thus, part of the inflow time was eliminated for flows that were totally depleted in transit. By averaging the flow rates for the duration of the flow event, channel-storage effects were minimized.

Infiltration rates were computed as the difference between corresponding instantaneous rates of inflow and outflow for fairly constant long-duration flow events. The instantaneous outflow rates were determined by correcting the time of occurrence of a particular inflow rate by the estimated traveltime through the reach. For fairly constant inflow rates, the effects of channel storage on outflow rates were small; thus, it was not necessary to determine the traveltime precisely.

The streamflow and infiltration data obtained from the flow events may contain a serial or time relation between sets of data and a spurious relation between measured inflow rates and computed infiltration rates. During some flow events, the infiltration rates may be dependent on the amount of infiltration during a previous flow event—thus, the possible serial relation. The infiltration rates were not determined independently from the inflow rates—thus, the possible spurious relation.

For the study reach, 143 sets of inflow- and infiltration-rate data were available; 82 were for short-duration flows (averaging about 1-day duration), and 61 were for fairly constant flows of long duration. The inflow rates at Continental and the infiltration rates—computed as the difference between inflow at Continental and outflow at Tucson—for the 28.5-mile reach are shown in figure 3. Although several equations were developed for relating infiltration to inflow (see eqs. 14 to 21), figure 3 indicates that the relation may be represented adequately by the equation

$$Q_f = 1.6(Q_i)^{0.8}. \qquad (22)$$

The coefficient and exponent in equation 22 were determined using the method of least squares. During some flow events in which the average inflow rate was as much as 150 cfs, the total flow was depleted in transit by infiltration; the part of the study reach in which the infiltration took place is unknown. Only 107 sets of data having inflow rates greater than 150 cfs were used in the comparisons.

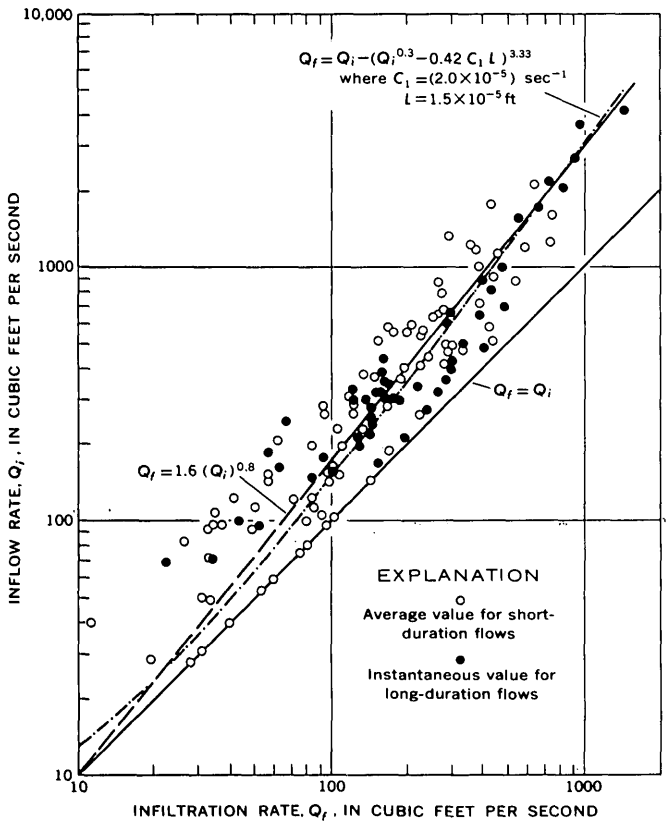

FIGURE 3.—Relation between inflow rate and infiltration rate for the 28.5-mile reach of the Santa Cruz River from Continental to Tucson, Ariz.

The infiltration rates computed from the streamflow data were compared with the rates derived from equations 15, 17, 19, and 21, in which the coefficients C_3, C_1, C_2, and I_c, respectively, were varied until the best possible correlation between the computed and derived infiltration rates was obtained. Substituting a value of $(2.0\times10^{-5})\,\text{sec}^{-1}$ for the coefficient C_1 in equation 17 gave the best results (fig. 3) when an unadjusted (uncorrected for possible serial and spurious effects) standard error of estimate of about 0.15 was obtained. The coefficient C_1 of $(2.0\times10^{-5})\,\text{sec}^{-1}$ is equivalent to an infiltration velocity of 1.7 feet per day when the stream depth is 1 foot.

In a previous study the author (Burkham, 1970) used the equation $Q_f = 1.6\ (Q_i)^{0.8}$ to estimate infiltration rates for streamflow of more than 10 cfs entering the reach at Continental. Because of the close agreement between equations 17 and 22 for flow rates of between 20 and 3,000 cfs, either equation may be used for estimating infiltration in the total study reach (fig. 3). If, however, estimates of infiltration are desired for reaches having different lengths than that of the study reach, equation 17 probably is the most suitable.

REFERENCES

Burkham, D. E., 1970, Depletion of streamflow by infiltration in the main channels of the Tucson basin, Arizona: U.S. Geol. Survey Water-Supply Paper 1939–B. [In press]

Horton, R. E., 1939, Analysis of runoff-plat experiments with varying infiltration-capacity: Am. Geophys. Union Trans., pt. 4, p. 693–711.

——— 1940, An approach toward a physical interpretation of infiltration capacity: Soil Sci. Soc. America Proc., v. 5, p. 399–417.

Leopold, L. B., and Maddock, Thomas, Jr., 1953, The hydraulic geometry of stream channels and some physiographic implications: U.S. Geol. Survey Prof. Paper 252, 57 p.

Matlock, W. G., 1965, The effect of silt-laden water on infiltration in alluvial channels: Univ. Arizona, Tucson, unpub. doctoral thesis, 102 p.

Stallman, R. W., 1954, Discussion of "The effect of surface head on infiltration rates based on the performance of ring infiltrometers and ponds," by Leonard Schiff: Am. Geophys. Union Trans., v. 35, no. 1, p. 171–173.

SPECIFIC CONDUCTANCE AS A MEANS OF ESTIMATING IONIC STRENGTH

By CAROL J. LIND, Menlo Park, Calif.

Abstract.—In an aqueous solution each cation-anion combination has its own characteristic curve on a plot, made on a log-log scale, of ionic strength versus conductance. If the major ionic combinations are known for a particular salt solution or natural-water source, ionic strength can be estimated from such a plot of these major cation-anion combinations. If, on the basis of previous periodic analyses, the ionic composition has only dilution as the main variable, then a characteristic plot may be made for that salt solution or natural-water source and used for future estimations of its ionic strength.

For an understanding of exact thermodynamic relationships, accurate values of activity coefficients are required. The activity coefficients for aqueous systems are normally obtained by means of the Debye-Hückel equation, the use of which requires knowledge of ionic strength. A means of estimating ionic strength that does not require the determination of the molality of each ion present in the solution in question is often desirable and is presented in this report. The same variable used here, specific conductance, was also used by Langmuir (1969) to calculate ionic strength in a study of geochemistry of ground water in New Jersey.

THEORETICAL BASIS

Ionic strength, a term originally proposed by Lewis and Randall (1921), gives the strength of the electrostatic field in an aqueous solution and is defined as the summation

$$I = \tfrac{1}{2}\Sigma m_i Z_i^2, \qquad (1)$$

where I is the ionic strength, m_i is the molality, and Z_i is the charge of each ionic species. The accepted method of determining ionic strength is by a complete chemical analysis, because ionic strength is a function of the summation of the molalities of the individual ionic species present in a system.

A simplification of the Debye-Hückel expression for single-ion activity coefficients is

$$-\log\gamma_i = \frac{AZ_i^2\sqrt{I}}{1 + a_i^\circ B\sqrt{I}} \qquad (2)$$

where γ_i is the activity coefficient. A and B are constants characteristic of the solvent at a specified temperature and pressure, and a_i° is dependent on the "effective diameter" of the ion in solution. The activity coefficient of an ion multiplied by its molality, m_i, gives the value of the activity, a_i, of an ionic species

$$\gamma_i m_i = a_i. \qquad (3)$$

A relationship between specific conductance and ionic strength for a solution of a single salt can be derived theoretically.

The specific conductance, k, of a solution is defined by the equation

$$k = \frac{\Lambda N \text{ ohms}^{-1}\text{ cm}^{-1}}{1{,}000}, \qquad (4)$$

where Λ is the equivalent conductance of a given solute, and N (normality) is the gram-equivalent of that solute per liter. In this report, specific conductance is expressed in terms of micromhos, (μmhos), the unit normally used by the U.S. Geological Survey, and is obtained in these units by multiplying equation 4 by 10^6, giving

$$k = 1{,}000\ \Lambda N\ \mu\text{mhos cm}^{-1}. \qquad (4a)$$

The equivalent conductance of an electrolyte is related to the equivalent conductance at infinite dilution, $\Lambda_\circ$, by the properties of the solvent described by the constants C and D, the temperature, and the gram-equivalents per liter, N, of the solute by the abbreviated form of the Onsager equation,

$$\Lambda = \Lambda_\circ - (C + D\Lambda_\circ)\sqrt{N}\ . \qquad (5)$$

For water at 25°C and a uni-univalent electrolyte, C is 60.2 and D is 0.229. A modification of this form of the Onsager equation is necessary for solutions of electrolytes that are not completely ionized. The degree of dissociation, α, is inserted to give

$$\Lambda = \alpha[\Lambda_\circ - (C + D\Lambda_\circ)\sqrt{\alpha N}]. \quad (6)$$

This modification is particularly applicable to ions of high valence. For very weak electrolytes, the term $(A + B\Lambda_\circ)\sqrt{\alpha N}$ becomes negligible, and then

$$\Lambda = \alpha\Lambda_\circ. \quad (7)$$

Divalent ions such as sulfate are intermediate between strong and weak electrolytes. A substitution of equation 6 into equation 4a,

$$k = 1{,}000\,\alpha N[\Lambda_\circ - (60.2 + 0.229\,\Lambda_\circ)\sqrt{\alpha N}], \quad (8)$$

provides a basis for calculating specific conductance of an electrolyte at a particular concentration.

A value of $\Lambda_\circ$ can be obtained by summing values which are obtainable in the literature for the equivalent conductances, λ, of the ionic components of the salt in question,

$$\Lambda_\circ = \lambda \text{ cation} + \lambda \text{ anion}. \quad (9)$$

Table 1 lists the equivalent conductance at infinite dilution at 25°C for the ionic species in this report, and table 2 lists the sums of the equivalent conductance at infinite dilution at 25°C of the cation-anion pairs in this report.

TABLE 1.—*Equivalent conductance at infinite dilution at 25°C of ionic species in this report*

Ion	Conductance (mhos)	Reference
Na^{+1}	50.10	Shedlovsky (1932), Benson and Gordon (1945b).
Ca^{+2}	59.50	Shedlovsky and Brown (1934), Benson and Gordon (1945a).
Mg^{+2}	53.0	Shedlovsky and Brown (1934).
Cl^{-1}	76.35	Benson and Gordon (1945b), Owen and Zeldes (1950).
HCO_3^{-1}	44.5	Shedlovsky and MacInnes (1935).
SO_4^{-2}	80.0	Jenkins and Monk (1950).

TABLE 2.—*Equivalent conductance at infinite dilution at 25°C of cation-anion pairs in this report*

Cation-anion pair	Conductance (mhos)
NaCl	126.45
$NaHCO_3$	94.60
$Ca(HCO_3)_2$	104.00
Na_2SO_4	130.10
$CaSO_4$	139.50
$MgSO_4$	133.0

Equation 8 may be simplified for dilute solutions after considering the results of conversion to logarithmic form, substituting the value for $\Lambda_\circ$ given in table 2, and entering the values $N = 0.03$ and $N = 0.0003$ for NaCl. (The latter values cover, for the most part, the concentration range over which this presentation was tested, and at these values of N, $\alpha = 1$ for NaCl.)

For $N = 0.03$,

$$\log k = 3 - 1.5229 + 0 + \log[126.45 - (60.2 + 0.229\times126.45)\sqrt{1\times0.03}] = 1.4771 + \log[111.05] = 1.4771 + 2.046.$$

For N = 0.0003,

$$\log k = 3 - 3.5229 + 0 + \log[126.45 - (60.2+0.229\times126.45)\sqrt{1\times0.0003}] = -0.5229 + \log[124.9] = -0.5229 + 2.097.$$

These calculations show how the factor $\Lambda_\circ - (C + D\Lambda_\circ)\sqrt{\alpha N}$ is altered by 0.05 log units across this one-hundredfold range of N values. For approximate work the change in this factor may be considered negligible and the factor considered constant, and the form $\log k = \log N +$ constant may be applied.

Ionic strength can be related to specific conductance by combining equation 1 with equation 8, because normality, N, is defined as molarity, M, times the charge, Z, on the ion in question, ($N = MZ$). (In very dilute solutions molality and molarity are almost equal. The approximate densities for the most concentrated solutions of each cation-anion combination measured in this report (except for $Ca(HCO_3)_2$) were found in the literature and a conversion from molarity to molality made. The difference in the two values when applied to the proposed method was less than could be positively detected. Thus in this report, molarity and molality are used interchangeably.) Table 3 gives the conversion factors necessary for each salt to be considered. The proposed equations obtained by substituting I for N are given in table 4. (From table 3 it can be seen that the relationship for NaCl is similar to that of $NaHCO_3$, that of Na_2SO_4 to that of $Ca(HCO_3)_2$, and

TABLE 3.—*Conversion factor for* N *to* I *conversion of salts in this report*

Salt type	Modified equation	N (equivalent)
NaCl, $NaHCO_3$	$I = \frac{1}{2}(N\times1^2 + N\times1^2) = N$	I
Na_2SO_4, $Ca(HCO_3)_2$	$I = \frac{1}{2}(N\times1^2 + N/2\times2^2) = 3/2N$	$\frac{2}{3}I$
$CaSO_4$, $MgSO_4$	$I = \frac{1}{2}(N/2\times2^2 + N/2\times2^2) = 2N$	$\frac{1}{2}I$

TABLE 4.—*Equations relating* k *to* I

Salt type	Substituted equation	Simplification
NaCl	$\text{Log } k = \log I + \text{constant}$	$\text{Log } k = \log I + \text{constant.}$
$Ca(HCO_3)_2$	$\text{Log } k = \log \frac{2}{3} I + \text{constant}$	$\text{Log } k = \log I + \text{constant}'.$
$CaSO_4$	$\text{Log } k = \log \frac{1}{2} I + \text{constant}$	$\text{Log } k = \log I + \text{constant}''.$

that of $CaSO_4$ to that of $MgSO_4$.) As I approaches zero and when α equals one, a plot of k versus I for different salts on a log-log scale should yield straight lines with characteristic slopes and spacing dependent on the nature of the salts. As the concentration increases, the value of α decreases, owing to incomplete dissociation which may be because of complexing, incomplete ionization, or ion pairing; then the suggested plot is no longer linear. In regard to the ionic combinations considered in this report, this nonlinearity is exhibited most strongly by calcium and magnesium sulfates.

EXPERIMENTAL DATA

Values were determined for ionic strength and specific conductance of many samples of natural water and of prepared dilute solutions of known concentration of the major ionic constituents of the salts in these samples. The conductance values for the natural-water samples were taken from published U.S. Geological Survey reports. The published reports give specific conductance at 25°C. The ionic strength was computed from the total analysis reported in milligrams per liter. Pure salt solutions were prepared in the laboratory and their specific conductance measured by standard methods and equipment (Rainwater and Thatcher, 1960). (Rainwater and Thatcher recommend that the methods and equipment they describe be used for the determination of specific conductances ranging from about 25 to 3,500 μmhos. Consequently, measurements far in excess of these limits have been avoided in this report.) The pure salt solutions were prepared from analytical reagents, dried at the temperature listed in table 5, and were made up to the molarity desired by dilution with demineralized water.

TABLE 5.—*Specifications of the salts and their prepared solutions used in this report*

Original salt	Temperature of heating (°C)	Duration of heating (hours)	Dried salt formula (assumed)	Molarity of prepared solution	Molarity of strongest solution plotted
$CaSO_4 \cdot 2H_2O$	163	16	$CaSO_4$	0.0500	0.00996
Na_2SO_4	100	16	Na_2SO_4	.0700	.0700
$NaHCO_3$	No heat	0	$NaHCO_3$	.714	.0714
$MgSO_4 \cdot 7H_2O$	200	60	$MgSO_4$	.100	.0500
NaCl	100	16	NaCl	.100	.0500

The salt $Ca(HCO_3)_2$ does not exist, but Ca^{+2} and HCO_3^{-1} are often the main ionic constituents in natural water. The most concentrated solution of Ca^{+2} and HCO_3^{-1} was prepared by dissolving a known amount of CaO, analytical reagent, in demineralized water. This solution was kept at a pressure of approximately 1 atmosphere CO_2 by rapidly bubbling CO_2 gas into an almost closed system. (It was assumed that the barometric pressure during the preparation was 1 atmosphere.) A sample of this solution was withdrawn with a syringe, with the system closed to the air as much as possible, and the conductance was quickly measured. This process was repeated until the conductance remained constant, suggesting an equilibrium condition. The concentration of Ca^{+2} was 4.66×10^{-3} M. To simulate a hypothetical $Ca(HCO_3)_2$ solution, the concentration of (HCO_3^{-1}) should be 9.32×10^{-3} M if α equaled 1. The instability of the solution, when removed from the approximated 1 atmosphere CO_2 condition, necessitated hurried dilutions and conductivity measurements. As a result the pH was not observed closely, but it was noted to be between 5 and 6, indicating that HCO_3^{-1} was the predominant anion present. Application of the H_2CO_3 equilibrium equations 10 and 11 shows that the desired (HCO_3^{-1}) value is bracketed by these pH's. In the equilibrium equation, [ ] stands for activity, ( ) stands for molality, γ for activity coefficient, P for pressure, and K for equilibrium constant.

$$\frac{[H_2CO_3]}{P_{CO_2}} = K_{CO_2} = 10^{-1.47} \qquad (10)$$

$P_{CO_2} = 1$ atm, so $[H_2CO_3] = 10^{-1.47}$.

$$\frac{[H^{+1}]\,[HCO_3^{-1}]}{[H_2CO_3]} = K_{H_2CO_3} = 10^{-6.4}. \qquad (11)$$

For pH 6.0,

$$[HCO_3^{-1}] = 10^{-6.4} \times 10^{-1.47} \times 10^{6} = 10^{-1.87}.$$

The approximate $I = 4.66 \times 10^{-3}\, m \times 3 = 1.4 \times 10^{-2}$, and then

$$\gamma_{HCO_3^{-1}} = 0.88 = 10^{-0.05}.$$

$$(HCO_3^{-1}) = 10^{-1.87} \times 10^{+0.05} = 10^{-1.82} = 1.5 \times 10^{-2}\, m.$$

For pH 5.0,

$$(HCO_3^{-1}) = 10^{-2.82} = 1.5 \times 10^{-3}\, m.$$

From these observations, and from the close agreement of the plot of the specific conductance and ionic strength values for dilutions of this solution with that of the values for $Ca(HCO_3)_2$-rich natural waters, as shown later in figure 3, it may be safely

concluded that the hypothetical Ca $(HCO_3)_2$ salt solution had been prepared. The more dilute solutions were prepared by rapidly mixing measured (by burette) amounts of demineralized water and the Ca $(HCO_3)_2$ prepared solution and quickly reading the conductance.

With the assumption $\alpha = 1$, a comparison is made in table 6 of the values of specific conductance obtained by the application of the empirical equation 8 with values reported in the literature and with estimated values. The estimated values were obtained from a plot on a log-log scale of specific conductance versus ionic strength by using the measurements made on the prepared pure salt solutions described above. (See figure 1.) There is good agreement of all three values for both of the concentrations listed for NaCl and for the more dilute solutions of Na_2SO_4. There is also good agreement between the estimated value for Na_2SO_4 and the reported value for the more concentrated solutions. However, it is obvious that the assumption that $\alpha = 1$ leads to considerable error for the more concentrated solution of Na_2SO_4 and for both of the concentrations of solutions listed for $MgSO_4$. Thus, unless one is quite confident of the value of α, the application of equation 8 is limited to indicating that there is a simple relation between ionic strength and specific conductance.

The relation of specific conductance and ionic strength to the major cation-anion combinations in natural water is shown by a comparison of the plot on a log-log scale of specific conductance versus ionic strength for water analyses in figures 2, 3, and 4 with plots for measured pure salt solutions in the same figures. Detailed descriptions of the natural-water samples considered are given in table 7. In table 7 the contribution of each of the major ionic constituents is expressed in terms of the percentage of the total ionic milligram equivalents per liter present in the water. In figures 2, 3, and 4 the natural-water samples are represented by open circles

TABLE 6.—*Specific conductances at 25°C, in micromhos, determined by different means*

Salt	Normality	Specific Conductance (k)		
		Calculated	Estimated	Reported [1]
NaCl	0.01	1.18×10^3	1.18×10^3	1.1851×10^3
Na_2SO_4	.01	1.21×10^3	1.13×10^3	1.1244×10^3
$MgSO_4$	.01	1.23×10^3	$.80 \times 10^3$	
NaCl	.001	1.26×10^2	1.25×10^2	1.2374×10^2
Na_2SO_4	.001	1.27×10^2	1.26×10^2	1.2415×10^2
$MgSO_4$	.001	1.30×10^2	1.07×10^2	

[1] The values for NaCl were reported by Shedlovsky, Brown, and MacInnes (1934) and by Gunning and Gordon (1942), and those for Na_2SO_4 quoted by MacInnes (1939) as reported by Shedlovsky and Longsworth.

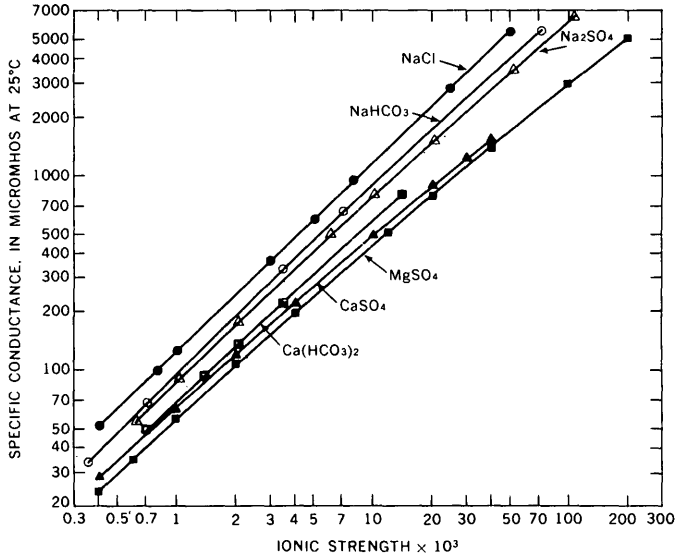

FIGURE 1.—Plots on a log-log scale of specific conductance against ionic strength of pure salt solutions.

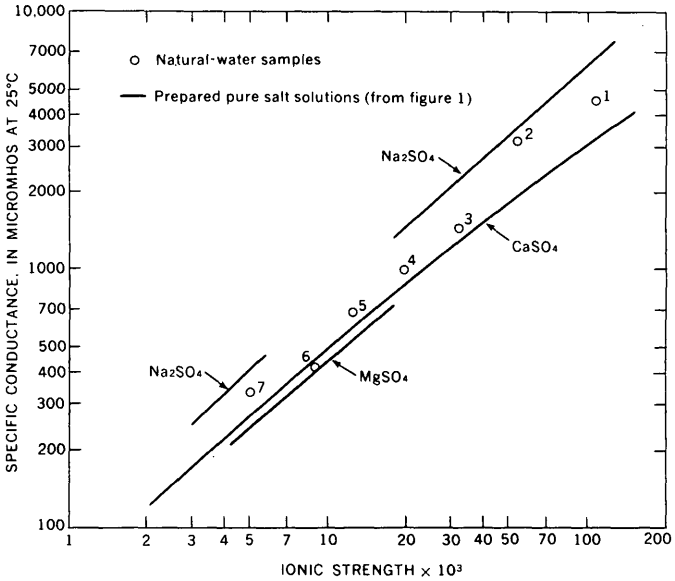

FIGURE 2.—Plot on a log-log scale of specific conductance against ionic strength of pure salt solutions compared with a similar plot of natural-water samples (numbers are samples listed in table 7). Principal anion is sulfate.

and the measured pure salt solutions by lines. In the water samples plotted in figure 2, the principal anion is sulfate; the dominant cation in sample 2 is sodium, and the dominant cation in samples 3–5 is calcium. Concentrations of cations are more nearly equal in samples 1, 6, and 7. All the points fall within the lines from measured data for the pure sulfate salt solutions. In figure 3, the water samples contain mostly calcium and bicarbonate and line up very well on the curve for the prepared pure solutions of Ca^{+2} and HCO_3^{-1}. In figure 4, the water samples contain mostly sodium and bicarbonate.

TABLE 7.—*Description of natural-water samples plotted in figures 2, 3, and 4*

Sample No. (this report)	Figure No.	Information source	Location and description of water	Date collected	Percent of total milligram equivalents per liter of the major ionic species							k (micromhos)	$I \times 10^3$
					Ca^{+2}	Mg^{+2}	Na^{+1}	HCO_3^{-1}	SO_4^{-2}	Cl^{-1}	Other ion		
1	2	Scott and Barker (1962, p. 23, III).	Well, 7 miles northeast of Monticello, Drew County, Ark. Depth, 22 ft. Water-bearing formation, Jackson Group (shale, sand, and marl).	12/13/55	18.3	13.0	15.5	---	41.3	8.9	---	4,570	107.6
2	2	Water-Supply Paper 1162 (U.S. Geol. Survey, 1954, p. 457).	Moreau River at Bixby, S. Dak. Composite of 2 daily samples; mean discharge, 1.7 cfs.	7/2–3/49	2.7	5.4	41.3	10.0	36.9	.7	---	3,140	53.63
3	2	Hem (1959, p. 64)	Drainage of collar, drill hole 89, 7th level Mather A iron mine, Ishpeming, Mich. Temp., 15.1°C.	1/30/52	38.3	3.8	6.5	2.8	44.3	1.9	---	1,460	32.15
4	2	Hem (1959, p. 83)	Oasis flowing well, SW¼ sec. 15, T. 11 S. R. 25 E. Chaves County, N. Mex. Depth, 843 ft., flow, over 9,000 gpm when drilled. Water-bearing formation, San Andres (limestone and dolomitic limestone with minor amounts sandstone, gypsum, and anhydrite).	3/11/52	30.7	15.1	4.0	17.2	27.7	4.7	---	997	19.73
5	2	Hem (1959, p. 77)	Industrial well, Willimansett, Mass. Depth, 120 ft. Water-bearing formation, Portland Arkose. Temp., 12.2°C.	12/8/54	33.6	10.8	5.5	15.1	29.8	4.8	---	690	12.47
6	2	Hem (1959, p. 114)	Peace Creek at State Hwy. 17 bridge, Salfa Springs, Fla. Mean discharge, 140 cfs.	5/19/52	22.1	15.3	12.7	10.4	23.8	3.6	(PO_4^{-3}) 9.5	413	8.97
7	2	Water-Supply Paper 1951 (U.S. Geol. Survey, 1966, p. 71).	Little Sandy Creek above Eden, Wyo., gaging station 9 miles upstream from Pacific Creek, 11 miles NE. of Farson, and 14 miles NE. of Eden, Sweetwater County. Drainage area, approximately 170 sq mi.	4/3/63	23.7	6.6	18.7	19.8	28.3	1.7	---	334	5.01
8	3	Hem (1959, p. 64)	Well 3, Nelson Rd., Water Works, Columbus, Ohio. Depth, 117 ft. Water from glacial outwash. Temp., 13.3°C.	5/28/52	30.1	16.9	.3	34.3	14.1	.1	---	885	16.48
9	3	Scott and Barker (1962, p. 59).	City well at Bushton, Rice County, Kansas. Depth, 99 ft. Water-bearing formation, Dakota Sandstone.	6/6/54	37.6	5.0	7.2	44.6	1.2	3.1	---	543	8.40
10	3	Scott and Barker (1962, p. 19).	Big Spring, Huntsville, Ala. Water-bearing formation, Tuscumbia Limestone. Temp., 16.1°C.	3/28/52	42.4	6.4	1.1	44.3	1.9	2.3	---	250	4.00
11	3	Water-Supply Paper 1948 (U.S. Geol. Survey, 1965 p. 297).	Partridge River near Aurora, Minn. Composite sample. Mean discharge, 30.8 cfs.	10/1–31/62	22.8	16.2	10.2	27.9	15.1	4.6	---	188	3.04
12	3	Hem (1959, p. 77)	Cumberland River at Smithland, Ky. Discharge, 17,100 cfs.	5/19/52	34.5	8.76	5.66	40.7	6.78	1.69	---	172	2.66
13	3	Hem (1959, p. 83)	Wisconsin River at Muscoda, Grant County, Wis. Flows through area of magnesian limestone.	5/21/52	26.4	19.9	2.9	42.2	5.6	1.2	---	165	2.59
14	3	Hem (1959, p. 55)	Well at Valdese General Hospital, Rutherford College, Burke County, N.C. Depth, 400 ft. Water from micaschist. Temp., 15.0°C.	3/22/52	33.5	5.3	12.4	42.8	4.7	1.6	---	130	1.85
15	3	Water-Supply Paper 1951 (U.S. Geol. Survey, 1966, p. 647).	Yakima River near Parker, Wash.	5/17/63–6/3/63	25.3	12.7	9.6	44.9	3.5	1.7	---	81	1.16
16	3	Water-Supply Paper 1951 (U.S. Geol. Survey, 1966, p. 605).	Green River near Auburn, Wash.	12/6/62	26.9	8.0	12.6	38.7	8.1	4.5	---	46	.665
17	3	Water-Supply Paper 1951 (U.S. Geol. Survey, 1966, p. 610).	Snohomish River at Snohomish, Wash.	1/3/63	31.9	7.0	9.4	34.9	9.8	3.0	---	24	.346
18	4	Torrey and Kohout (1956, p. 44).	Well, SE¼NE¼ sec. 2, T. 22 N., R. 59 E. Richland County, Mont. Depth, 500 ft. Water-bearing formation, Ft. Union (sandstone and shale).	10/3/49	.2	.1	49.6	44.3	.0	2.6	---	2,960	39.69
19	4	Unpublished data, U.S. Geological Survey files.	Wagon Wheel Gap hot spring, Mineral County, Colo. Discharge, 20 gpm; temp., 62.2°C. Associated with vein of Wagon Wheel Gap.	8/31/58	6.5	2.0	40.7	32.1	6.7	11.3	---	2,430	29.27
20	4	Hem (1959, p. 88)	Well at Raleigh-Durham Airport, Wake County, N.C. Depth, 184 ft. Water-bearing formation, Coastal Plain sediments.	6/3/52	.7	1.0	48.6	41.3	.0	1.6	(CO_3^{-2}) 6.1	718	9.01
21	4	Scott and Barker (1962, p. 63; 101).	Well 79: 8–50 Public Supply, Memphis, Tenn. Depth, 1,310 ft. Water from sand of the Wilcox Formation. Temp., 22.2°C.	3/8/52	3.3	4.1	39.4	41.9	2.9	3.4	---	162	2.34

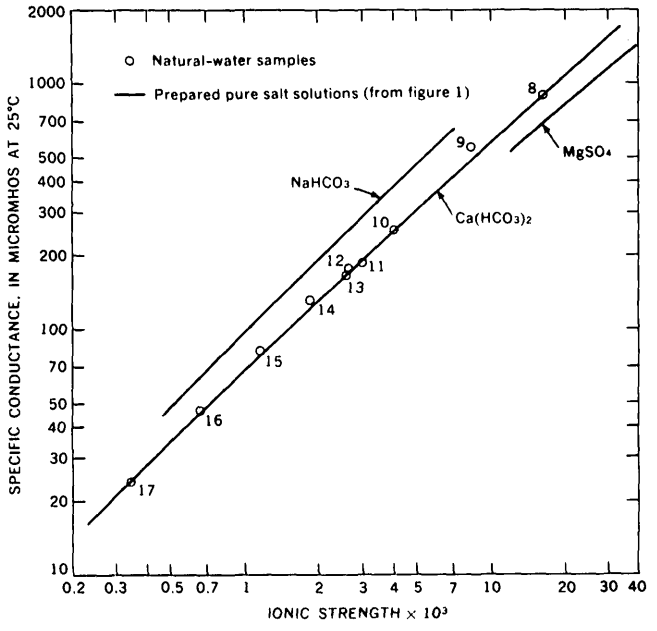

FIGURE 3.—Plot on a log-log scale of specific conductance against ionic strength of pure salt solutions compared with a similar plot of natural-water samples (numbers are samples listed in table 7). Mostly $Ca(HCO_3)_2$.

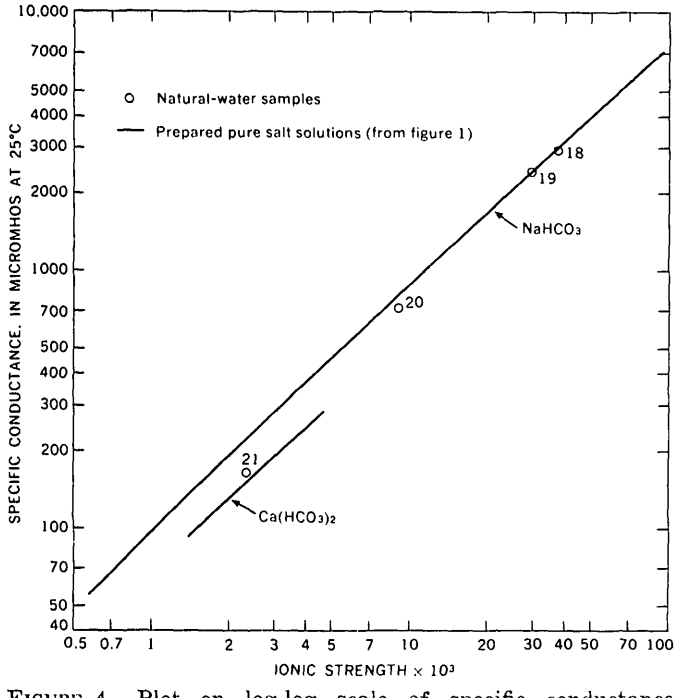

FIGURE 4.—Plot on log-log scale of specific conductance against ionic strength of pure salt solutions compared with a similar plot of natural-water samples (numbers are samples listed in table 7). Mostly $NaHCO_3$.

In many natural streams the ionic composition remains nearly constant, although concentrations change owing to dilution. This is more likely to be true of water with few ionic constituents. Figures 5*A* and *B* show seven different water samples where dilution is the main factor for change in conductance. Here the points fall on relatively straight lines. In figure 6*A*, *B*, *C*, and *D*, the ionic composition varies from time to time, probably because there are so many ions involved and the sources which deliver them are variable. There is some scatter of the points about the curves, but still there is a definite relationship of specific conductance to ionic strength. The analyses of the natural-water samples considered in figures 5 and 6 are given in table 8.

APPLICATIONS

Ionic strength may be estimated from specific conductance if, on the basis of previous periodic analyses, the ionic composition of a natural-water source has only dilution as the main variable or if the major ionic combinations are known for a particular dilute salt solution or natural-water source.

The relationship between specific conductance and ionic strength for water from a particular stream can be established by preparing a graph of the specific conductance versus the ionic strength on a log-log scale from data obtained from previous analyses. (In this report, the range of specific conductance which was compared with ionic strength was 25 to 3,500 micromhos.) It is recommended that the suggested plot for a particular stream be within these limits and that it cover the entire scope of specific conductances this stream may normally have. The chief source of error involved is related to the accuracy with which the described plot can be made and read.

If the predominant dissolved ionic species are known, plots are made on a log-log scale of the specific conductance versus the ionic strength for pure salt solutions. (These salts correspond to the cation-anion combinations possible for the major ionic species present in the dilute salt solution or natural water in question.) The specific conductance of the salt solution or natural water in question is determined and the ionic strength estimated from the plots. The accuracy improves as the percentage

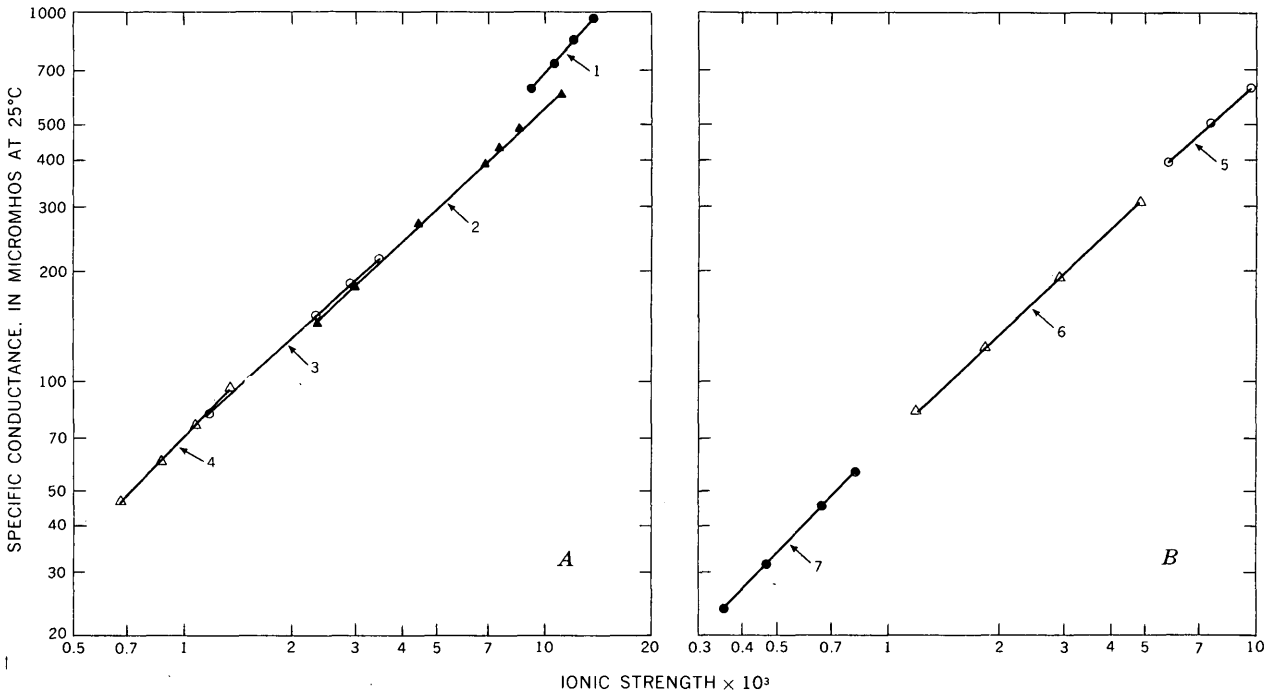

FIGURE 5.—Plots on a log-log scale of specific conductance against ionic strength of natural-water samples, plotted over a specific conductance range (numbers are samples listed in table 8). Few major ionic components.

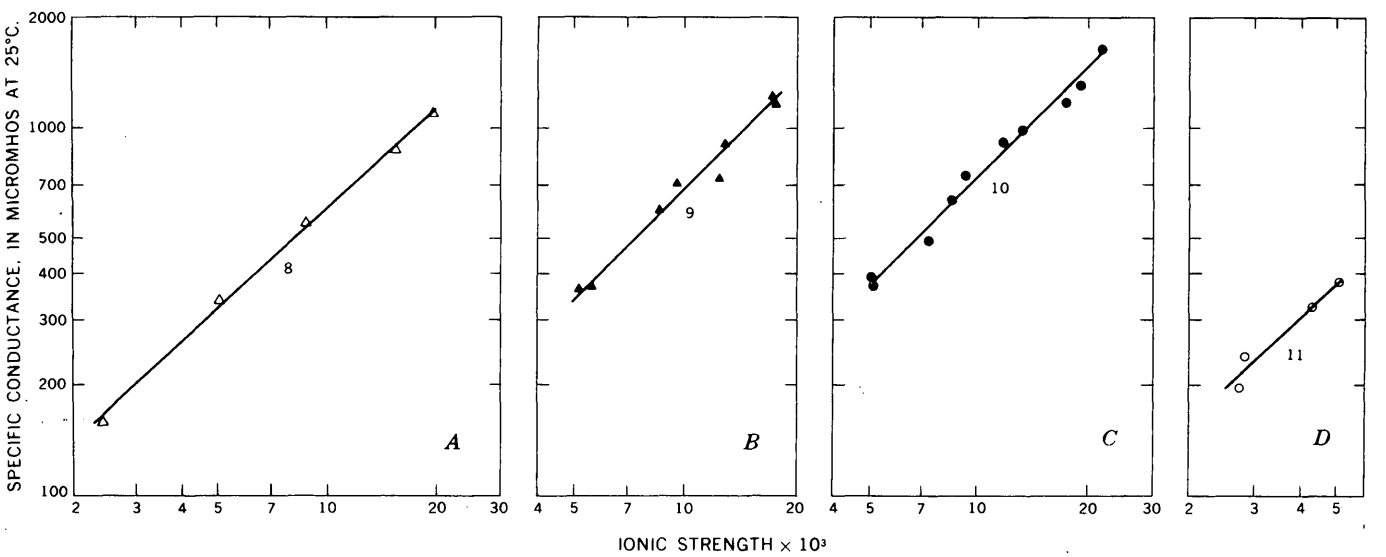

FIGURE 6.—Plots on a log-log scale of specific conductance against ionic strength of natural-water samples, plotted over a specific conductance range (numbers are samples listed in table 8). Several major components.

TABLE 8.—*Description of natural-water samples plotted in figures 5 and 6*

Sample No. (this report)	Figure No.	Information source	Location and description of water	Date collected	Individual ion contribution to ionic strength							k (micro-mhos)	$I \times 10^3$
					Ca^{+2}	Mg^{+2}	Na^{+1}	HCO_3^{-1}	SO_4^{-2}	Cl^{-1}	Other ion		
1	5A	Water-Supply Paper 1951 (U.S. Geol. Survey, 1966, p. 637).	Crab Creek near Smyrna, Wash.	10/24/62	2.0	2.06	2.35	2.68	2.38	0.61	---	841	12.3
											(PO_4^{-3})		
				2/28/63	2.3	2.14	2.83	2.92	3.04	.07	0.26	969	13.8
				6/25/63	1.65	1.65	1.57	1.93	1.86	.40	---	614	9.21
				9/26/63	1.85	1.81	1.96	2.29	2.15	.52	---	726	10.8
2	5A	(p. 65–66)	Green River at Warren Bridge near Daniel, Wyo.	10/1–12/62	3.05	1.07	.07	.94	2.31	---	---	411	7.47
				12/1–31/62	4.65	1.56	.12	1.29	3.73	.01	---	599	11.39
				1/1–31/63	3.55	1.56	.10	1.79	1.50	.02	---	486	8.55
				5/10–18/63	2.95	.99	.08	1.16	1.61	---	---	387	6.82
				5/19–31/63	2.00	.62	.04	.93	.83	.01	---	264	4.45
				6/24–28/63	1.25	.47	.05	.60	.58	.01	---	179	2.97
				7/4–12/63	1.00	.32	.03	.47	.48	.01	---	141	2.32
				9/1–15/63	1.90	.58	.06	.62	1.27	.01	---	264	4.45
3	5A	(p. 633)	Spokane River at Long Lake, Wash.	11/20/62	1.1	.60	.08	.76	.25	.03	---	177	2.87
				5/22/63	.48	.19	.04	.30	.16	.01	---	80	1.19
				7/22/63	.80	.58	.06	.61	.18	.03	---	145	2.31
				9/20/63	1.2	.91	.09	.93	.23	.06	---	215	3.48
4	5A	(p. 605)	Green River near Auburn, Wash.	12/6/62	.25	.074	.059	.180	.075	.021	---	46	.665
				3/6/63	.35	.091	.074	.246	.083	.025	---	60	.88
				7/9/63	.40	.165	.081	.303	.096	.021	---	75	1.08
				9/3/63	.50	.222	.107	.385	.100	.042	---	95	1.37
5	5B	(p. 245)	Humboldt River at Palisade, Nev.	1/1–23/63	3.05	1.40	1.18	2.64	1.00	.31	---	631	9.73
				2/1–28/63	2.35	.91	.91	1.96	.90	.27	---	507	7.45
				5/22–31/63	2.05	.69	.65	1.65	.52	.14	---	384	5.79
6	5B	(p. 646)	Yakima River near Parker, Wash.	11/1–18/62	.90	.58	.26	.83	.18	.06	---	189	2.87
				11/29–30/62	1.35	1.07	.39	1.02	.75	.16	---	311	4.85
				2/12/63–3/4/63	.60	.37	.14	.55	.096	.025	---	122	1.81
				5/17/63–6/3/63	.425	.214	.081	.377	.058	.014	---	81	1.16
7	5B	(p. 610)	Snohomish River at Snohomish, Wash.	10/10/62	.275	.066	.046	.180	.062	.021	---	46	.656
				1/3/63	.150	.033	.022	.082	.046	.007	---	24	.346
				6/12/63	.200	.033	.028	.131	.038	.014	---	32	.455
				9/3/63	.300	.132	.054	.221	.067	.021	---	57	.803
8	6A	(p. 71)	Little Sandy Creek above Eden, Wyo.	10/4/62	2.55	.82	.98	.89	3.42	.07	---	546	8.76
				2/6/63	5.00	1.89	2.51	1.53	8.60	.17	---	1,090	19.77
				4/3/63	1.50	.42	.59	.62	1.79	.05	---	334	5.01
				7/3/63	.85	.19	.22	.33	.79	.02	---	159	2.41
				8/7/63	3.90	1.73	1.68	.85	7.18	.06	---	862	15.45
9	6B	(p. 287)	Alameda Creek near Niles, Calif.	10/13–15/62	1.30	.91	.65	.95	.77	.44	---	363	5.19
				10/16–31/62	2.20	1.81	1.44	1.58	1.17	1.28	---	710	9.59
				12/1–10/62	3.05	2.22	1.87	2.05	1.81	1.72	---	903	12.80
				1/1–12/63	3.80	3.29	2.72	2.66	2.07	2.38	---	1,220	17.18
				2/13–18/63	1.60	1.15	.52	1.31	.73	.31	---	373	5.71
				2/19–28/63	2.80	3.47	1.26	2.12	1.90	.82	---	744	12.47
				5/11–26/63	3.60	4.20	2.18	2.79	2.87	1.75	---	1,150	17.50
				8/1–10/63	2.20	1.89	.96	1.65	.92	.80	---	597	8.15
											(NO_3^{-})		
10	6C	(p. 285)	Arroyo de la Laguna at Verona, Calif.	10/13–15/62	1.35	.91	.61	.98	.77	.40	0.06	376	5.18
				10/16–31/62	2.00	1.81	1.50	1.44	1.12	1.49	.05	730	9.48
				1/1–12/63	3.55	5.27	3.78	2.99	1.98	3.82	.30	1,630	21.92
				1/13–18/63	2.35	1.98	2.18	1.59	1.48	2.09	.08	906	11.82
				2/3–5/63	1.50	1.15	.48	1.22	.71	.04	.04	362	5.19
				2/23–28/63	3.35	3.79	2.44	2.75	3.06	1.86	.07	1,150	17.41
				3/1–12/63	2.60	2.30	2.44	1.61	2.11	2.12	.12	994	13.24
				4/7–20/63	1.95	1.65	.72	1.67	1.00	.37	.04	482	7.44
				5/9–25/63	3.75	4.12	2.85	2.80	3.19	2.19	.12	1,290	19.12
				6/21–30/63	1.90	1.73	1.22	1.34	1.13	1.09	.06	626	8.52
11	6D	Water-Supply Paper 1947 (U.S. Geol. Survey, 1967, p. 62).	Passaic River at Little Falls, N.J.	11/27/62	.850	.461	.196	.262	.771	.169	---	196	2.78
				3/6/63	.750	.338	.413	.262	.624	.367	---	237	2.82
				7/30/63	1.15	.62	.61	.62	.81	.44	---	322	4.32
				9/24/63	1.20	.72	.78	.66	1.10	.42	---	377	5.06

of the total ionic composition approaches 100 percent of a single cation-anion combination. When there is more than one cation-anion combination, the accuracy also depends on which ions are present in sufficient concentration to influence the conductance reading. (It has already been shown that α plays an important part in the value of the conductance measured and that it varies with the particular salt considered and its concentration.) Thus no single term for the estimation of error can be applied for all the salts and concentrations of interest in this report. If the composition is unknown, figure 1 suggests the ionic strength of a solution whose conductance is 1,000 micromhos might range from 0.85×10^{-2} to 2.7×10^{-2}, a rather broad range.

REFERENCES

Benson, G. C., and Gordon, A. R., 1945a, The conductance of aqueous solutions of calcium chloride at temperatures from 15° to 45°C: Jour. Chem. Physics, v. 13, p. 470–472.

——— 1945b, A reinvestigation of conductance of aqueous solutions of potassium chloride, sodium chloride and potassium bromide at temperatures from 15° to 45°C: Jour. Chem. Physics, v. 13, p. 473–474.

Gunning, H. E., and Gordon, A. R., 1942, The conductance and ionic mobilities for aqueous solutions of potassium and sodium chlorides at temperatures from 15°–45°C: Jour. Chem. Physics, v. 10, p. 126–131.

Hem, J. D., 1959, Study and interpretation of the chemical characteristics of natural water: U.S. Geol. Survey Water-Supply Paper 1473, 269 p.

Jenkins, I. L., and Monk, C. B., 1950, The conductances of sodium, potassium and lanthanum sulfates at 25°: Am. Chem. Soc. Jour., v. 72, p. 2695–2698.

Langmuir, Donald, 1969, Geochemistry of iron in a coastal-plain ground water of the Camden, New Jersey area, *in* Geological Survey Research 1969: U.S. Geol. Survey Prof. Paper 650–C, p. C224–C235.

Lewis, G. M., and Randall, Merle, 1921, The activity coefficients of strong electrolytes: Am. Chem. Soc. Jour., v. 43, p. 1112–1154.

MacInnes, D. A., 1939, The principles of electrochemistry: New York, Reinhold Publishing Corp., 478 p.

Owen, B. B., and Zeldes, H., 1950, The conductance of potassium chloride, potassium bromide, and potassium iodide in aqueous solutions from 5° to 55°: Jour. Chem. Physics, v. 18, p. 1083–1085.

Rainwater, F. H., and Thatcher, L. L., 1960, Methods for collection and analysis of water samples: U.S. Geol. Survey Water-Supply Paper 1454, 301 p.

Scott, R. C., and Barker, F. B., 1962, Data on uranium and radium in ground water in the United States 1954 to 1957: U.S. Geol. Survey Prof. Paper 426, 115 p.

Shedlovsky, Theodore, 1932, The electrolytic conductivity of some uni-univalent electrolytes in water at 25°: Am. Chem. Soc. Jour., v. 54, p. 1411–1428.

Shedlovsky, Theodore, and Brown, A. S., 1934, The electrolytic conductivity of alkaline earth chlorides in water at 25°: Am. Chem. Soc. Jour., v. 56, p. 1066–1071.

Shedlovsky, Theodore, Brown, A. S., and MacInnes, D. A., 1934, Conductance of aqueous electrolytes: Electrochem. Soc. Trans., v. 66, p. 165–178.

Shedlovsky, Theodore, and MacInnes, D. A., 1935, The first ionization constant of carbonic acid, 0° to 38°, from conductance measurements: Am. Chem. Soc. Jour., v. 57, p. 1705–1710.

Torrey, A. E., and Kohout, F. A., 1956, Geology and ground-water resources of the lower Yellowstone River valley, between Glendive and Sidney, Montana: U.S. Geol. Survey Water-Supply Paper 1355, 92 p.

U.S. Geological Survey, 1954, Quality of surface waters of the United States: U.S. Geol. Survey Water-Supply Paper 1162, 662 p.

——— 1965, Quality of surface waters of the United States, 1963—Parts 3 and 4, Ohio River basin and St. Lawrence River basin: U.S. Geol. Survey Water-Supply Paper 1948, 390 p.

——— 1966, Quality of surface waters of the United States, 1963—Parts 9–14, Colorado River basin to Pacific slope basins in Oregon and Lower Columbia River basin: U.S. Geol. Survey Water-Supply Paper 1951, 781 p.

——— 1967, Quality of surface waters of the United States, 1963—Parts 1 and 2, North Atlantic slope basins and South Atlantic slope and eastern Gulf of Mexico basins: U.S. Geol. Survey Water-Supply Paper 1947, 472 p.

STATUS OF SALT-WATER ENCROACHMENT IN 1969 IN SOUTHERN NASSAU AND SOUTHEASTERN QUEENS COUNTIES, LONG ISLAND, NEW YORK

By PHILIP COHEN and G. E. KIMMEL, Mineola, N.Y.

Work done in cooperation with the Nassau County Department of Public Works and the New York State Department of Conservation, Division of Water Resources

Abstract.—Chloride data obtained from "outpost" wells and other wells in southern Nassau and southeastern Queens Counties, Long Island, N.Y., indicate that landward movement of a deep wedge of salty ground water in the area has been minimal from 1960 to 1969. Significant changes in chloride content were noted in only 3 of 30 outpost wells. Chloride content of water from a well in southeastern Queens County increased from 34 mg/l in 1960 to 112 mg/l in 1969, as a result of intensive ground-water withdrawals in that county; chloride content in two wells in Nassau County increased from 8,520 to 11,000 mg/l and from 2,000 to 8,110 mg/l during the same period. These increases resulted from local heavy pumping near the zone of diffusion. No increase in chloride content was noted in water from the Lloyd aquifer, except where leaky casings permitted downward flow of salty water.

Salty ground water on Long Island, N.Y., especially in southeastern Queens and southern Nassau Counties (fig. 1), has been studied intensively for several decades. Among the more recent studies pertinent to the subject are those reported on by Lusczynski (1961a, b), Lusczynski and Swarzenski (1960, 1962, 1966), Perlmutter and Crandell (1959), Perlmutter and Geraghty (1963), Perlmutter, Geraghty, and Upson (1959), Soren (1970), and Swarzenski (1959). As a byproduct of much of this work, a network of so-called outpost wells was established to monitor the rate and extent of the landward movement of salty ground water (commonly referred to as salt-water encroachment) in the area.

The most recent report on salt-water encroachment in southeastern Queens and southern Nassau Counties (Lusczynski and Swarzenski, 1966) includes data from the outpost wells up to 1960–62. The major purpose of this paper is to review the chloride data obtained from 1960 to 1969 from the outpost wells and from other selected wells, and to consider the significance of these data, especially with regard to possible salt-water encroachment. Because salt-water encroachment into the deeper artesian aquifers is of primary concern to the Long Island water managers, the occurrence and movement of salty water in these aquifers are emphasized in this paper.

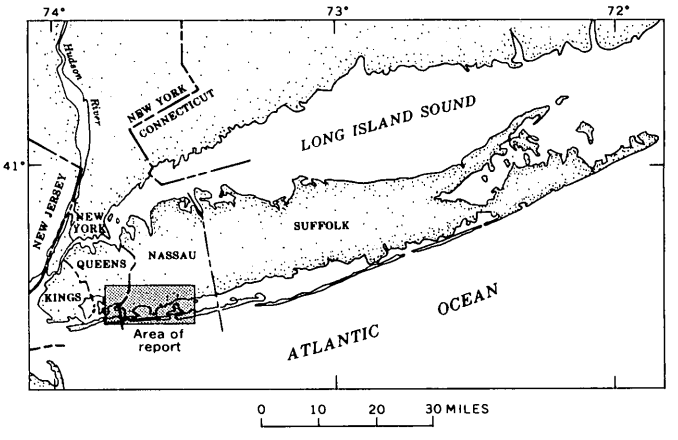

FIGURE 1.—Index map of Long Island, N.Y., showing area of report.

Acknowledgments.—Many individuals and agencies supplied much of the basic data given in this report. The authors are especially grateful to the

Nassau County Department of Health, the Nassau County Department of Public Works, and the New York State Department of Conservation, Division of Water Resources.

HYDROGEOLOGIC SETTING

The major hydrogeologic units beneath southeastern Queens and southern Nassau Counties and pertinent characteristics of these units are listed in table 1.

Under natural conditions, precipitation on Long Island was the source of all the fresh ground water beneath the study area (the shaded area in fig. 1). Ground water was discharged naturally by seepage to streams, which in turn flowed into the south-shore bays; by subsurface outflow to the bays and probably the Atlantic Ocean; and to a small extent by evapotranspiration near the shorelines.

At present (1969) ground-water recharge in the study area results mainly from (1) infiltration of precipitation through areas of bare soil, (2) subsurface inflow from upgradient areas, (3) infiltration of storm runoff through recharge basins, (4) injection of water used for industrial purposes into recharge wells, and (5) discharge of waste water into cesspools, septic tanks, and disposal basins (especially in the eastern part of the area). All the natural mechanisms of ground-water discharge are still operative in the area. In addition, a substantial quantity (several tens of millions of gallons per day) of ground water is artificially discharged by pumping and by the subsequent disposal of the pumped water to the sea by way of sewage-treatment plants.

TABLE 1.—*Major hydrogeologic units in southern Nassau and southeastern Queens Counties, Long Island, N.Y.*

Hydrogeologic unit [1]	Approximate maximum thickness in study area (feet)	Description
Upper glacial aquifer	100	Mainly sand and gravel of high hydraulic conductivity; some thin beds of clayey material of low hydraulic conductivity.
Gardiners Clay	100	Clay, silty clay, and a little fine sand of low to very low hydraulic conductivity.
Jameco aquifer	200	Mainly medium to coarse sand of moderate to high hydraulic conductivity.
Magothy aquifer	800	Mainly very fine sand, silt, and clay of low to very low hydraulic conductivity; some coarse to fine sand of moderate hydraulic conductivity; locally contains gravel of high hydraulic conductivity.
Raritan clay	200	Clay of very low hydraulic conductivity; some silt and fine sand of low hydraulic conductivity.
Lloyd aquifer	300	Sand and gravel of moderate hydraulic conductivity; some clayey material of low hydraulic conductivity.
Bedrock	---	Crystalline rock of very low interstitial hydraulic conductivity.

[1] Nomenclature after Cohen, Franke, and Foxworthy (1968).

Gross ground-water pumpage data for the period 1960–68 in selected subareas of Nassau and Queens Counties are listed in table 2.

TABLE 2.—*Gross pumpage in selected subareas of Long Island, N.Y., 1960–68*

[Data from the New York State Department of Conservation, Division of Water Resources]

Year	Pumpage (million gallons per day)				
	Nassau County	Queens County	Study area (fig. 1)	Mill Road well field	Long Beach
1960	146	67	35	4.9	5.6
1961	153	71	35	5.0	6.2
1962	172	74	40	5.1	7.1
1963	180	77	42	5.2	6.4
1964	194	78	46	5.6	6.8
1965	209	78	45	5.1	7.2
1966	215	75	47	5.0	7.6
1967	181	73	45	4.5	7.2
1968	208	78	50	5.0	8.0

Four bodies of salty ground water are found near and beneath parts of the study area—a shallow body in the upper glacial aquifer, an "intermediate wedge" that extends downward from the Gardiners Clay through the Jameco aquifer and into the upper part of the Magothy aquifer, a "deep wedge" that locally is in the Jameco aquifer but mainly is in the lower and middle parts of the Magothy aquifer, and a wedge in the Lloyd aquifer (Lusczynski and Swarzenski, 1966, p. F1 and pl. 3).

The shallow salty ground water is associated with, and is more or less freely connected with, the salty bays and estuaries and with the Atlantic Ocean. The intermediate and deep wedges thicken appreciably and ultimately merge in a seaward direction. Little is known about the wedge of salty ground water in the Lloyd aquifer except that it is believed to be seaward of the barrier beaches in the study area (see below). The three deepest wedges are moderately to highly confined (the salty ground water is under artesian pressure), and are, in one manner or another, hydraulically connected with the sea.

The landward extent of the intermediate and deep wedges of salty ground water, as mapped by Lusczynski and Swarzenski in 1961 (1966, fig. 5), is shown in figure 2. Sufficient data were not available in 1961 and are not presently available to map the landward limits of the other bodies of salty ground water accurately.

Mixtures of fresh and salty water form so-called zones of diffusion that separate the fresh and highly salty ground water in the study area. According to Perlmutter and Geraghty (1963, p. A92), the chloride content of the zones of diffusion on Long Island ranges from 10 to 40 mg/l (milligrams per liter) on the fresh-water sides to about 18,000 mg/l on the salt-water sides. Lusczynski and Swarzenski (1966, p. F19–F20) state that the chloride content of fresh ground water on Long Island is about 10 mg/l or less and that, "***a chloride concentration of more than 40 ppm [mg/l] in shoreline areas is assumed to indicate contamination by salty water."

CHLORIDE CONTENT OF WATER FROM WELLS

The chloride content of water from the outpost wells from 1960 through 1969 is listed in table 3. Significant trend-indicating changes in chloride content were noted in only 3 of the 30 wells—wells N6581, N6701, and Q1237.

Well N6581 is screened in the zone of diffusion near the leading edge of the deep wedge of salty ground water (fig. 2). The well is near the southern margin of the Mill Road well field, where pumpage during the past decade (table 2) has averaged about 5 mgd (million gallons per day). The moderately intensive local pumpage, a continual increase in regional pumpage, regional effects of a severe drought in 1962–66 (Cohen and others, 1969), decreased recharge resulting from urban development, and perhaps to some extent the effects of sewering in the area (Franke, 1968) have resulted in a decline in the water level in the well of about 2

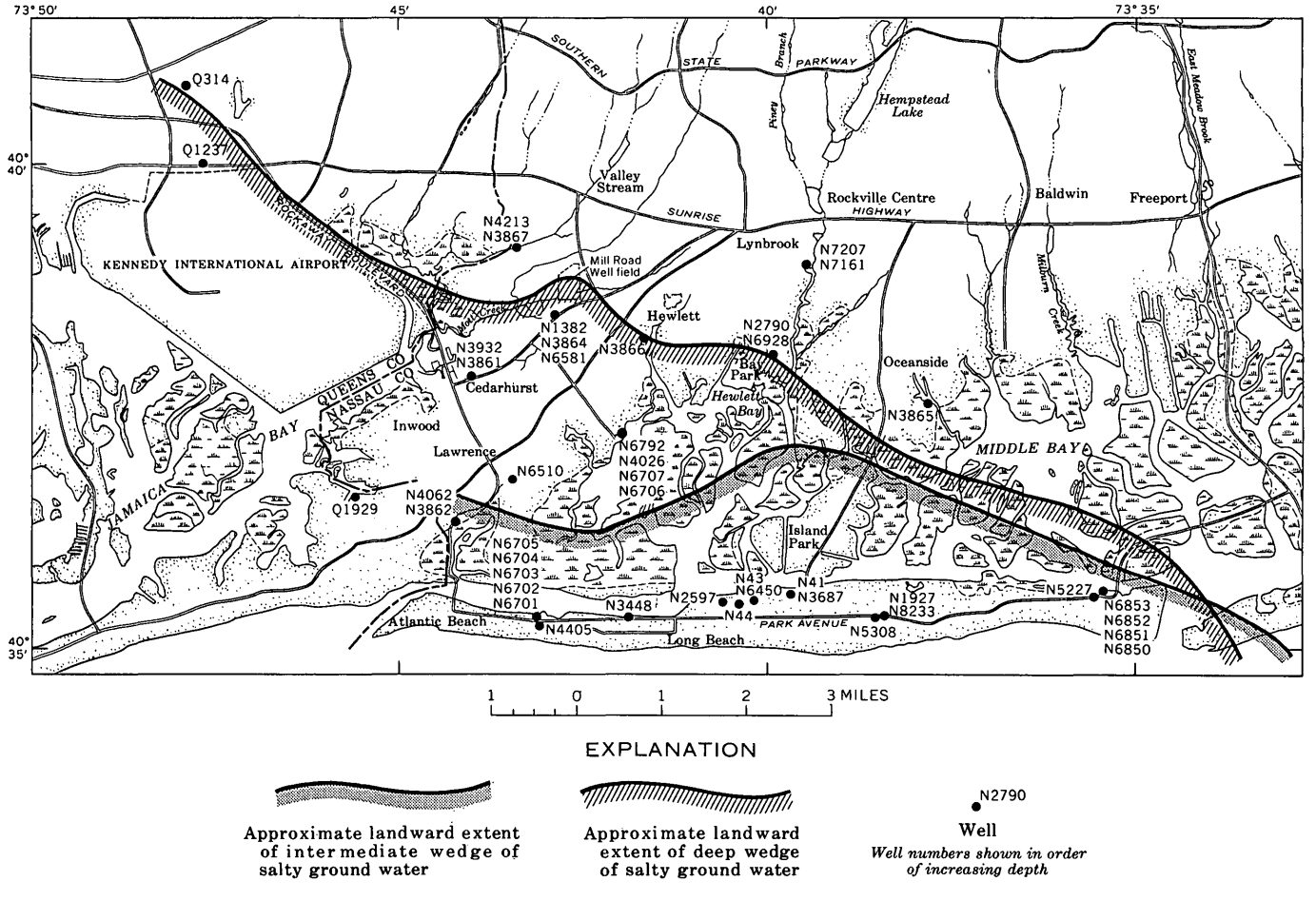

FIGURE 2.—Location of selected wells and the landward extent of the intermediate and deep wedges of salty ground water in southern Nassau and southeastern Queens Counties, Long Island, N.Y. Position of deep and intermediate wedges of salty ground water after Lusczynski and Swarzenski (1966, fig. 5).

TABLE 3.—*Chloride content of water from outpost wells in southern Nassau and southeastern Queens Counties, Long Island, N.Y.*

[Hydrogeologic units: Qug, upper glacial aquifer; Qg, Gardiners Clay; Qj, Jameco aquifer; Km, Magothy aquifer; Krc, Raritan clay. Analyses by several agencies. Rounding of data and use of decimals partly reflect the policy of the reporting agency]

Well No.	Hydrogeologic unit tapped	Depth of screen below sea level (feet)	Chloride (milligrams per liter)						
			1960	1961	1962	1963	1965	1967	1969
N1382	Qj	168–188	---	---	---	5	7	3.5	---
N2790	Km	535–557	3	4	4.5	5	5	3.3	3.0
N3861	Km	515–526	15,500	---	16,500	---	15,600	15,000	15,500
N3862	Km	289–299	---	---	---	2,200	2,030	2,000	2,000
N3864	Km	455–466	---	---	---	5.0	---	2.8	3.5
N3865	Km	548–558	4	---	---	5	---	4.1	5.5
N3866	Km	395–405	4	---	---	---	---	---	4.6
N3867	Km	499–509	5	---	---	5	6	3.8	4.0
N3932	Qj	165–169	5	---	---	5	5	3.7	3.8
N4026	Km	144–148	5.8	---	---	5	5	2.4	4.1
N4062	Qg	130–135	40	---	33	26	24	24	25
N4213	Qj	125–129	4	---	---	5	---	6.8	5.7
N6510	Km	447–452	14,500	---	14,600	14,200	11,840	---	---
N6581	Km	565–575	8,520	8,710	9,100	9,100	9,640	9,720	11,000
N6701	Krc	811–821	2,000	3,800	4,600	4,500	5,320	7,800	8,110
N6702	Km	656–666	15,800	15,900	16,000	15,000	14,700	16,000	16,000
N6703	Km	457–467	4,830	6,000	6,100	6,300	5,280	5,600	5,870
N6704	Km	273–283	9	8	7	8	6.0	7.0	6.6
N6705	Qj	136–146	12,200	12,500	11,900	11,000	10,800	12,200	12,400
N6706	Km	618–623	15,000	15,000	15,100	15,200	14,200	15,500	---
N6707	Km	487–497	1,150	1,400	1,700	1,600	1,420	1,400	1,580
N6792	Qug	42–44	---	---	6	7	---	6.1	7.9
N6850	Km	891–902	106	111	109	102	121	110	111
N6851	Km	544–549	3.6	6	6	6	---	4.0	4.0
N6852	Km	251–256	8,900	9,200	8,600	8,300	8,000	8,700	8,600
N6853	Km	120–125	4	4	4.5	5	---	3.6	3.4
N6928	Krc	710–720	13	---	11	12	---	13	12
N7161	Km	654–659	---	5	---	5	8	4	3.8
N7207	Km	87–90	---	---	4.5	6	5	4.3	3.7
Q1237	Qj	178–202	34	---	---	54	68	---	112

feet [1] since 1960. Accompanying the decline in water level, the chloride content of water in the well increased from 8,520 mg/l in 1960 to 11,000 mg/l in 1969.

Well Q1237, which is screened in the Jameco aquifer, taps the zone of diffusion near the upper part of the deep wedge of salty ground water. The water level in the well declined about 3 feet since 1960, to a point about 3 feet below sea level in 1969. During the same period the chloride content increased from 34 mg/l to 112 mg/l (table 3).

The chloride content of water from well N6701, which also taps the zone of diffusion, increased from 2,000 mg/l in 1960 to 8,110 mg/l in 1969. The well is screened near the bottom of the Raritan clay, very close to the base of the deep wedge of salty ground water (Lusczynski and Swarzenski, 1966, pl. 2, sec. *A–A'*). Since 1960, the water level in this well declined about 4 feet, to a point about 8 feet above sea level in 1969. To some extent, all the regional factors that affected the water level in well N6581 probably also affected the water level in this well. However, local pumpage from the Lloyd aquifer, which is only about 10–20 feet beneath the screen of well N6701, probably was the major cause of the decline.

The chloride content of water from selected public-supply, industrial, and private wells is listed in table 4. The first group of 12 wells listed, wells N41–N8233, are public-supply or abandoned public-supply wells on Long Beach, the barrier beach along the south shore of western and central Nassau County, and all tap the Lloyd aquifer. Most of the water in the upper glacial and Magothy aquifers beneath Long Beach is salty. However, water in the underlying Lloyd aquifer is fresh and, therefore, that aquifer is the sole source of fresh water for the communities on Long Beach. Pump-

[1] All water levels and changes in water levels in wells described in this report are expressed in terms of equivalent fresh-water heads (Lusczynski and Swarzenski, 1966, p. F41).

age on Long Beach increased from 5.6 mgd in 1960 to 8.0 mgd in 1968 (table 2).

The chloride content of water from 10 of the 12 wells in the group has been less than 15 mg/l since 1960, and the chloride content of the water from the 10 wells showed no particular upward or downward trend during the period 1960–69. Prior to 1960, the chloride content of water from well N41 was as high as 80 mg/l, but since 1960 it has decreased steadily to 5.6 mg/l in 1968. The casing of the well reportedly had failed (presumably because of rusting), and salty water was entering the well from one of the shallower aquifers. The ruptured casing was repaired in 1962. Nonetheless, the well was abandoned that same year, and since then has been pumped infrequently only to obtain samples for chemical analyses.

Well N1927 also was abandoned because a ruptured casing allowed salty ground water from the shallower aquifers to enter. Well N8233, which is about 100 feet from abandoned well N1927, was constructed as a replacement well; the chloride content of water from this well is only 4.4 mg/l.

Well Q314 is of particular interest because Perlmutter and Geraghty (1963, pl. 5) and Lusczynski and Swarzenski (1966, pl. 5) showed the leading edge of the deep wedge of salty ground water to be at or near the well in 1961. In 1940, the chloride content of water from the well was about 5 mg/l, and it increased at a fairly steady rate to about 20 mg/l in the late 1950's. Since 1960, it has fluctuated by about 1–3 mg/l, and in 1969 it reportedly was 2 mg/l greater than in 1960 (table 4). This slight increase in chloride content obviously cannot be considered to be indicative of significant landward movement of the wedge of salty ground water in the vicinity of the well since 1960.

A marked rise in chloride content, from 17 mg/l in 1961 to 1,300 mg/l in 1969, was noted in well Q1929 (table 4). The shallower aquifers in the vicinity of the well largely contain salty ground water. Down-hole photographic equipment was used to determine if a ruptured casing was allowing salty ground water to leak downward into the Lloyd aquifer. No break was found in the casing; however, a recent detailed chemical analysis indicates that the salty ground water pumped from the well apparently contains a small amount of detergent constituents (0.17 mg/l), which is probably characteristic of much of the shallow ground water in the area. Detergent constituents are not found in water from the Lloyd aquifer where that aquifer is more than several hundred feet below the water table, except in the vicinity of wells that are known or suspected to have ruptured casings. Accordingly, despite the negative evidence furnished by photographs, the increase in the chloride content of water from well Q1929 is believed to be related largely or entirely to leaks in the casing rather than more widespread salt-water encroachment into the Lloyd aquifer.

CONCLUSIONS

Increases in the chloride content of water from outpost wells Q1237 and N6581 from 1960 to 1969 are believed to have been caused by the landward movement of parts of the deep wedge of salty ground water beneath southern Nassau and southeastern Queens Counties. The heads in both wells

TABLE 4.—*Chloride content of water from selected production wells on Long Island, N.Y.*

[Hydrogeologic units: Qj, Jameco aquifer; Krl, Lloyd aquifer. Data largely from Nassau County Health Department. Rounding of data and use of decimals partly reflect the policy of the reporting agency]

Well	Hydrogeologic unit tapped	Depth of screen below sea level (feet)	Chloride (milligrams per liter)									
			1960	1961	1962	1963	1964	1965	1966	1967	1968	1969
N41	Krl	1,190–1,250	24.8	19.2	16.8	---	12.0	7.4	8.0	6.2	5.6	---
N43	Krl	1,188–1,259	5.8	2.4	5.6	6.8	6.0	5.8	---	---	---	---
N44	Krl	1,184–1,254	9.8	6.2	8.0	8.8	8.4	7.5	6.2	7.2	7.2	8.2
N1927	Krl	1,149–1,209	2.0	---	---	12.4	11.8	41.0	---	---	---	---
N2597	Krl	1,169–2,129	6.0	3.8	7.2	6.4	7.4	7.6	7.4	6.6	6.0	6.2
N3448	Krl	1,187–1,227	9.0	---	9.0	7.8	8.6	9.0	8.2	10.4	8.6	8.4
N3687	Krl	1,190–1,240	4.8	3.6	5.4	4.8	---	5.0	6.2	5.0	4.6	5.2
N4405	Krl	991–1,061	10.2	---	11.4	9.4	11.8	11.0	10.4	12.8	11.0	12.6
N5227	Krl	1,190–1,250	2.0	2.6	---	3.2	2.6	3.6	3.6	2.2	2.0	3.2
N5308	Krl	1,150–1,210	3.4	---	4.8	2.8	3.2	2.9	3.0	3.0	4.2	6.8
N6450	Krl	1,210–1,270	5.0	---	6.2	5.8	5.6	6.4	5.6	6.0	4.8	5.8
N8233	Krl	1,170–1,220	---	---	---	---	---	---	---	---	---	4.4
Q314	Qj	209– 269	19	19	18	18	19	18	18	20	20	21
Q1929	Krl	961–1,012	---	17	16	18	---	65	180	---	215	1,300

declined from 1960 to 1969. In well Q1237, the decline in head is probably related to a widespread cone of depression, more than 10 square miles of which is below sea level, in southern Queens County. The landward encroachment of salty ground water in the area is thought to be fairly widespread (Soren, 1970). A much smaller cone of depression exists near well N6581, which partly reflects intensive pumping at the Mill Road well field. The salt-water encroachment seems to be limited to a small tongue of salty ground water in the immediate vicinity of the well field.

The increased chloride content in outpost well N6701 is mainly related to intensive pumping on Long Beach, which in turn is causing salty ground water in the Raritan clay to move downward toward the underlying Lloyd aquifer. To date, no firm evidence is available to conclude that salty ground water has invaded the Lloyd aquifer beneath Long Beach (either laterally or by downward leakage from the Raritan clay), except locally by downward flow through several abandoned wells having ruptured casings.

The positions of the landward limits of the intermediate and deep wedges of salty ground water as shown in figure 2 are those given by Lusczynski and Swarzenski (1966, pl.5, and fig. 12), and none of the presently available data can be used as a basis for shifting these positions either landward or seaward. In other words, if the toes of the wedges have moved landward since 1960, as they probably have locally (for example, in the vicinities of wells Q1237 and N6581), the coarseness of the network of available sampling points presently precludes a more exact delineation of the positions of the toes of the wedges and a clear recognition of movement of the wedges since 1960.

Finally, the data obtained since 1960 do not contradict the conclusions of Lusczynski and Swarzenski (1966, p. F56 and F71–72) that: (1) "The present (1961) occurrence, position, alignment, and even the sizable thickness and width of the zone of diffusion of the deep wedge of salt water as well as the intermediate wedge, therefore, are phenomena attributable mainly to natural conditions that prevailed long before the start of ground-water development in the report area;" (2) regionally, the deep wedge of salty ground water, "***is apparently moving no faster than 10 feet a year;" and (3) the intermediate wedge of salty ground water, "***is apparently moving landward at less than 10 to 20 feet a year."

REFERENCES

Cohen, Philip, Franke, O. L., and Foxworthy, B. L., 1968, An atlas of Long Island's water resources: New York Water Resources Comm. Bull. 62, 117 p.

Cohen, Philip, Franke, O. L., and McClymonds, N. E., 1969, Hydrologic effects of the 1962–66 drought on Long Island, New York: U.S. Geol. Survey Water-Supply Paper 1879–F, 18 p.

Franke, O. L., 1968, Double-mass-curve analysis of the effects of sewering on ground-water levels on Long Island, New York *in* Geological Survey Research 1968: U.S. Geol. Survey Prof. Paper 600–B, p. B205–B209.

Lusczynski, N. J., 1961a, Filter-press method of extracting water samples for chloride analysis: U.S. Geol. Survey Water-Supply Paper 1544–A, 8 p.

——— 1961b, Head and flow of ground water of variable density: Jour. Geophys. Research, v. 66, no. 12, p. 4247–4256.

Lusczynski, N. J., and Swarzenski, W. V., 1960, Position of the salt-water body in the Magothy(?) Formation in the Cedarhurst-Woodmere area of southwestern Nassau County, Long Island, N.Y.: Econ. Geology, v. 55, no. 8, p. 1739–1750.

——— 1962, Fresh and salty ground water in Long Island, New York: Am. Soc. Civil Engineers Proc. v. 88, no. 3207, p. 173–194.

——— 1966, Salt-water encroachment in southern Nassau and southeastern Queens Counties, Long Island, New York: U.S. Geol. Survey Water-Supply Paper 1613–F, 76 p.

Perlmutter, N. M., and Crandell, H. C., 1959, Geology and ground-water supplies of the southshore beaches of Long Island, N.Y.: New York Acad. Sci. Annals. v. 80, art. 4, p. 1060–1076.

Perlmutter, N. M., and Geraghty, J. J., 1963, Geology and ground-water conditions in southern Nassau and southeastern Queens Counties, Long Island, N.Y.: U.S. Geol. Survey Water-Supply Paper 1613–A, 205 p.

Perlmutter, N. M., Geraghty, J. J., and Upson, J. E., 1959, The relation between fresh and salty ground water in southern Nassau and southeastern Queens Counties, Long Island, New York: Econ. Geology, v. 54, no. 3, p. 416–435.

Soren, Julian, 1970, Ground-water and geohydrologic conditions in Queens County, Long Island, New York: U.S. Geol. Survey Water-Supply Paper 2001–A. [In press]

Swarzenski, W. V., 1959, Determination of chloride in water from core samples: Am. Assoc. Petroleum Geologists Bull., v. 43, no. 8, p. 1995–1998.

VERTICAL MOLECULAR DIFFUSION OF XENON-133 GAS AFTER INJECTION UNDERGROUND

By JOHN B. ROBERTSON, Idaho Falls, Idaho

Work done in cooperation with the U.S. Atomic Energy Commission

Abstract.—Nine hundred and eighty-seven curies of radioactive Xe^{133} gas mixed with 2.83×10^4 m^3 of air was injected rapidly into permeable basalt strata at the National Reactor Testing Station, Idaho. A capping layer of fine-grained playa sediments confined the gas underground. The subsurface Xe^{133} was monitored by Geiger-Müller (GM) detectors and by air samples from observation wells surrounding the injection well. Underground distribution patterns after injection pressures had dissipated were evaluated by materials-balance analyses. Most of the Xe^{133} apparently remained underground and decayed radioactively. Molecular diffusion rates of Xe^{133} from the ground were estimated using a simplified mathematical model. A maximum flux rate of 2,560 $\mu c/hr$ from a ground-atmosphere interface area of 2.67×10^5 m^2 was calculated for the first day after injection. The estimated rates indicated a total diffusion loss of 0.37 c for the total area during the 26-day observation period. The calculated rates had fairly good agreement with the measured flux rates at the ground surface. Erratic variations in the measured flux rates were attributed to other influences such as barometric-pressure changes.

The Division of Reactor Development and Technology (RDT) of the U.S. Atomic Energy Commission (AEC) is currently investigating the concept of disposing of radioactive gaseous wastes by injecting them underground. Such a process would provide a certain amount of indirect, natural treatment of wastes by allowing radioactive decay and reactions with the earth materials to proceed during confinement underground. Where feasible, this type of disposal would have some obvious advantages over discharging the wastes directly to the atmosphere.

A large-scale field test was conducted by the AEC in September-October 1967 to evaluate some aspects of this concept of disposal. In this experiment, 987 c (curies) of radioactive Xe^{133} gas mixed with $2.83x10^4$ m^3 STP (standard temperature and pressure) of air was injected underground at the National Reactor Testing Station (NRTS), Idaho. Xe^{133} is a beta-gamma emitting noble-gas isotope which decays with a half-life of 5.27 days to stable Cs^{133}. Among the prime objectives of that test was the determination of the underground distribution and behavior, and the flux rate to the atmosphere, of the gas after injection. As one of the cooperating participants in the test, the U.S. Geological Survey has assisted in the analyses of the test results.

After the pressure effects of injecting the gas dissipated, the principal factors which could have influenced the behavior of the gas underground were molecular diffusion, sorption and solution reactions, and convective mechanisms such as barometric-pressure variations and buoyant effects. Because of the complexities of the system, it is impossible at present to evaluate the quantitative effects of all these influences. However, it is feasible to consider the more significant mechanisms on a simplified, individual basis and estimate some of their possible effects; such estimates can then be related to observed field-test data. The role of molecular diffusion as a vertical-transport mechanism of Xe^{133} from the ground to the atmosphere was estimated in this manner; the results of this analysis are presented in this report. A materials-balance analysis of the subsurface Xe^{133} is also presented as a supporting investigation.

The objectives of the studies in this report are to: (1) evaluate the subsurface Xe^{133} distributions

U.S. GEOL. SURVEY PROF. PAPER 700-D, PAGES D287-D300

(after injection), as interpreted from the radiochemical air-sample and subsurface Geiger-Müller-tube data; (2) estimate the upward diffusion rates of Xe^{133} through the playa sediments during the test period and the total diffusional losses (with the assumption that there are no other losses); and (3) relate estimated diffusion effects to ground-surface flux rates of Xe^{133} measured in the field.

The diffusion study was accomplished by adapting theoretical diffusion concepts to the field conditions and solving the problems by simple mathematical methods. A finite grid system was fitted to the injection site and the diffusion conditions defined at each grid point. Diffusion rates were then calculated at each grid point for various times and then integrated areally and over the time of the test period. The materials-balance inventories utilize a similar grid-system technique.

Acknowledgments.—The injection test was initiated by the Division of Reactor Development and Technology of the U.S. Atomic Energy Commission, Washington, D.C., and was cosponsored by the Advanced Research Projects Administration of the Department of Defense. It was conducted by Mr. Bruce L. Schmalz, Chief, Waste Management Section, Environmental Branch, NRTS Health Services Laboratory with the cooperation and assistance of the U.S. Geological Survey and the Environmental Science Services Administration, Institute of Atmospheric Sciences. Mr. J. T. Barraclough, Research Project Chief, U.S. Geological Survey, NRTS, contributed many valuable interpretations and suggestions in the analysis of this test. The subsurface, interface, and atmospheric gas samples were collected and analyzed by two contracting companies, Isotopes—A Teledyne Co. (Hardaway and others, 1968) and Texas Instruments, Inc. (Bowman and Bennett, 1968). A more comprehensive report summarizing all aspects of the injection test has been compiled by Schmalz (1969). Also, a previous, more comprehensive report by Robertson (1969a) describes some aspects of the test, such as barometric-pressure effects, that are not included in the present report.

FIELD TEST CONDITIONS

The injection test was conducted at the Birch Creek Playa, in the northern part of the NRTS (fig. 1). The playa covers an area of nearly 13 km^2 and is underlain mainly by fine-grained lacustrine sediments. The playa sediments are as much as 18 m thick and are underlain by basalts and interbedded sediments of the Snake River Group (Walker, 1964). In the area of the test, the water table is within the basalt at a depth of about 62.5 m.

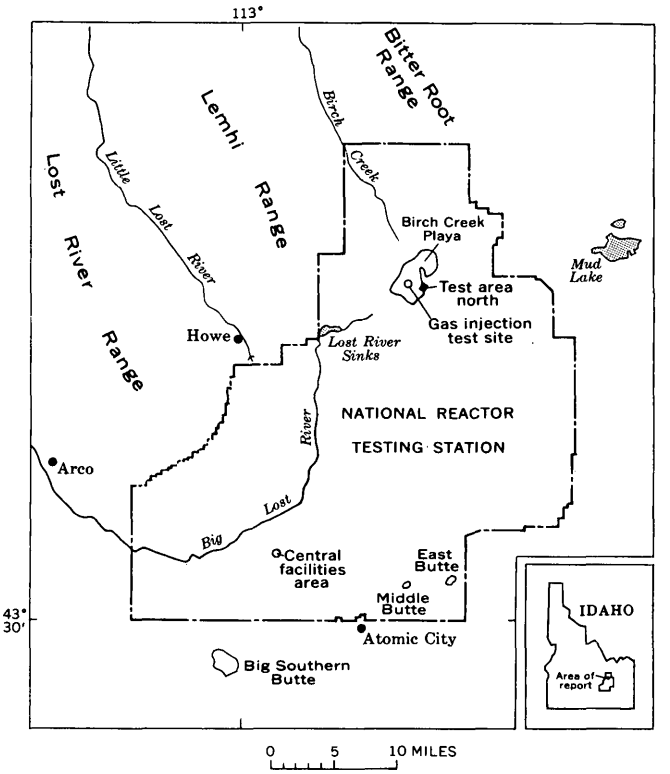

FIGURE 1.—Location map of the gas-injection test site. National Reactor Testing Station, Idaho.

The field test utilized an injection well surrounded by 14 observation wells. The generalized physical setting of the experiment is depicted in figure 2. The locations of the injection and observation wells are shown in figure 3. The injection well

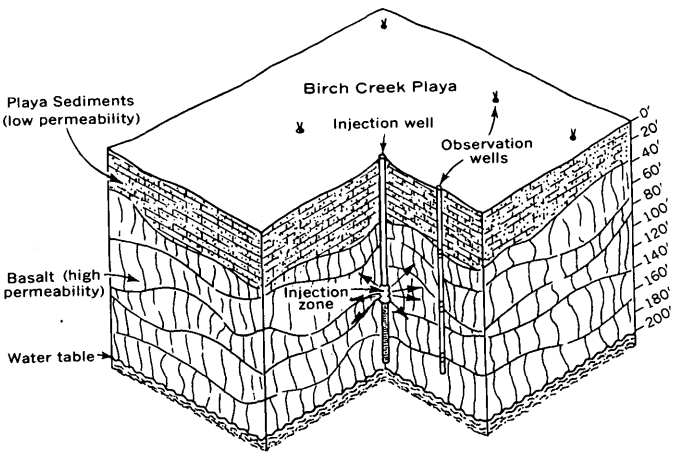

FIGURE 2.—Block diagram showing the generalized physical setting of the gas injection test. Vertical scale approximate.

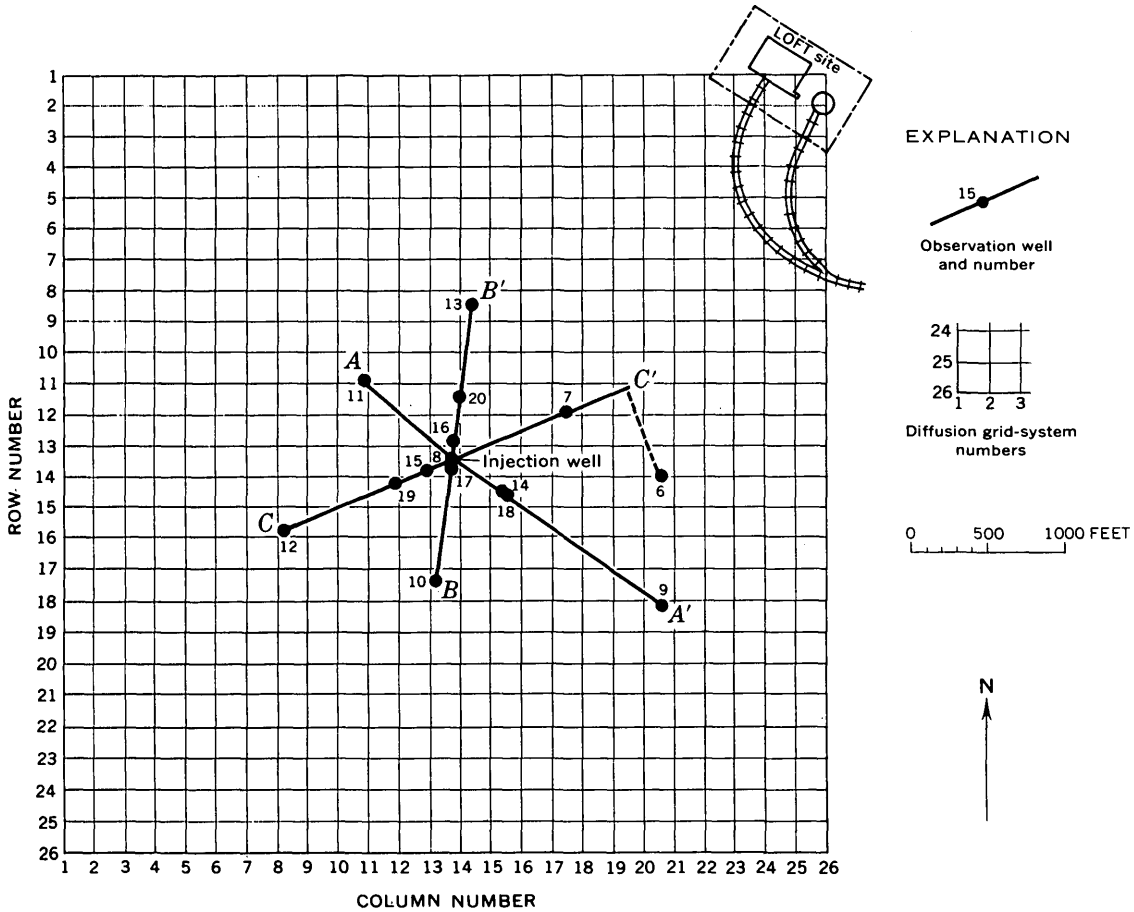

FIGURE 3.—Map of the gas-injection test site, showing locations of the injection well, observation wells, lines of cross section (fig. 4), and the grid system used in the materials-balance and diffusion analyses.

was drilled to a depth of 62 m, and air-injection tests were run on various sections with the aid of packers. The well was then backfilled, cemented to a depth of 37.3 m, and completed so that only the bottom 4 m (33.3 to 37.3 m) was open to the basalt. The injection test indicated this was the most permeable interval of basalt at the well. The 14 monitor wells ranged in depth from 22.5 m to 62 m. Each one was constructed with isolated sampling ports at several depths so that a subsurface gas sample could be withdrawn at the surface from any one of the subsurface ports. Four of the monitor wells (7, 18, 19, and 20) were equipped with calibrated Geiger-Müller (GM) tubes. These tubes were installed at ports at three different depths in each well and were connected by cables to counters and automatic data accumulators.

The injection of the gas underground was accomplished by pumping the air-tracer mixture down the injection well and out into the basalt through the 4-m open zone. Compressors injected 2.83×10^4 m^3 STP (10^6 cubic feet) of air containing 987 c of Xe^{133} at a rate of about 28.3 m^3/min STP on September 30, 1967. The injection zone was very permeable and accepted 28.3 m^3/min with only 0.104 to 0.114 bar wellhead gage pressure. The temperature of the injected gas mixture ranged from 12°C to 26°C and averaged 18°C.

The subsurface distribution of Xe^{133} gas was then monitored by withdrawing air samples from the observation wells for radiochemical Xe^{133} analysis, and by recording the GM-tube outputs. Concentrations of Xe^{133} in the atmosphere directly above the test site and flux rates across the ground-atmosphere interface were measured periodically. Texas Instruments, Inc., collected and analyzed the subsurface air samples while Isotopes—A Teledyne Co. performed the atmospheric sampling and analysis. Both made independent Xe^{133} flux measurements at the ground surface. The sampling and observation period lasted 26 days (approximately five Xe^{133} half-lives) after injection.

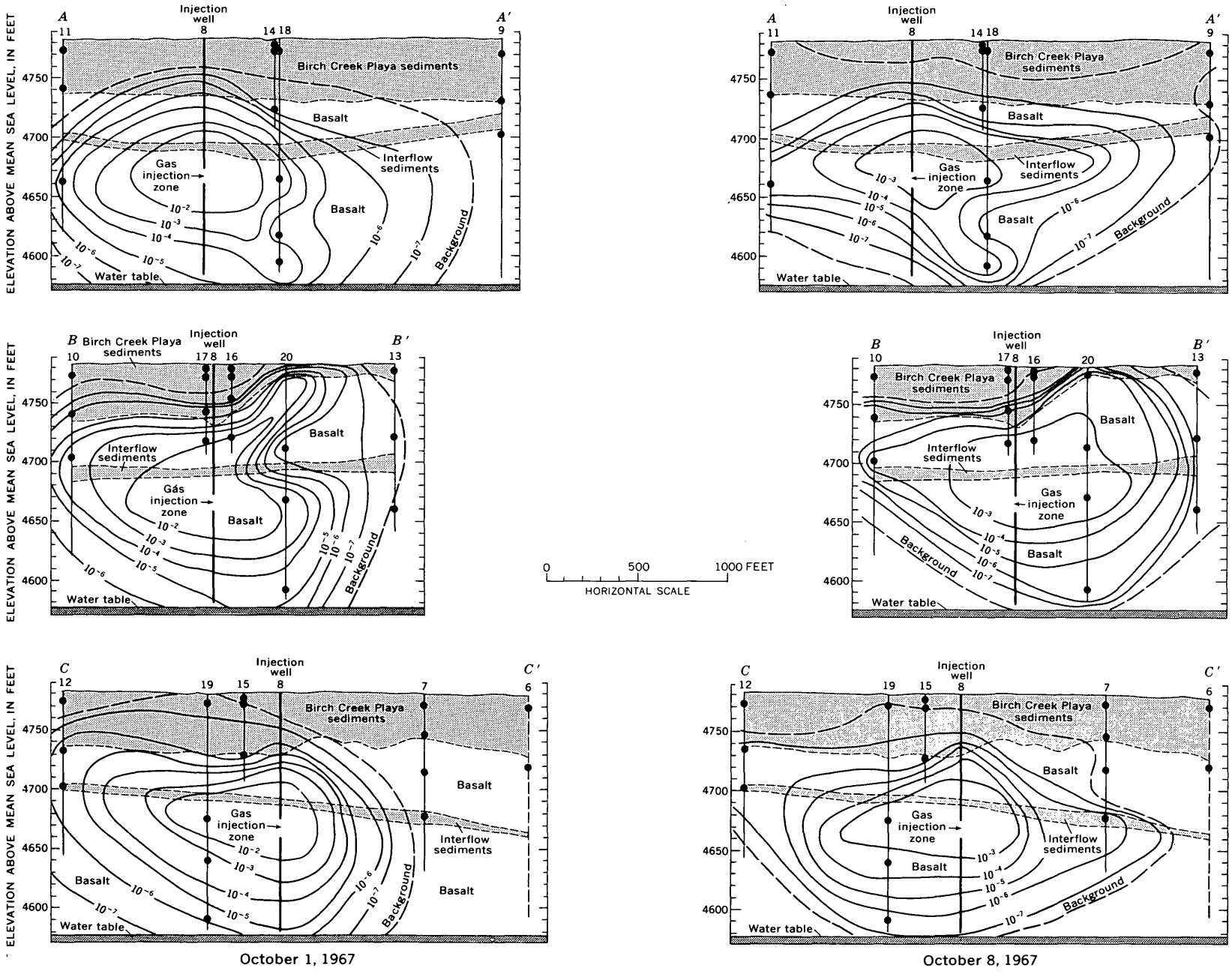
ELEVATION ABOVE MEAN SEA LEVEL, IN FEET
4750
4700
4650
4600
A
A′
Injection well
11
8
14 18
9
Birch Creek Playa sediments
Basalt
Interflow sediments
Gas injection zone
Basalt
Background
Water table
B
B′
10
17 8
16
20
13
C
C′
12
19
15
8
7
6
0
500
1000 FEET
HORIZONTAL SCALE
October 1, 1967
October 8, 1967

FIGURE 4.

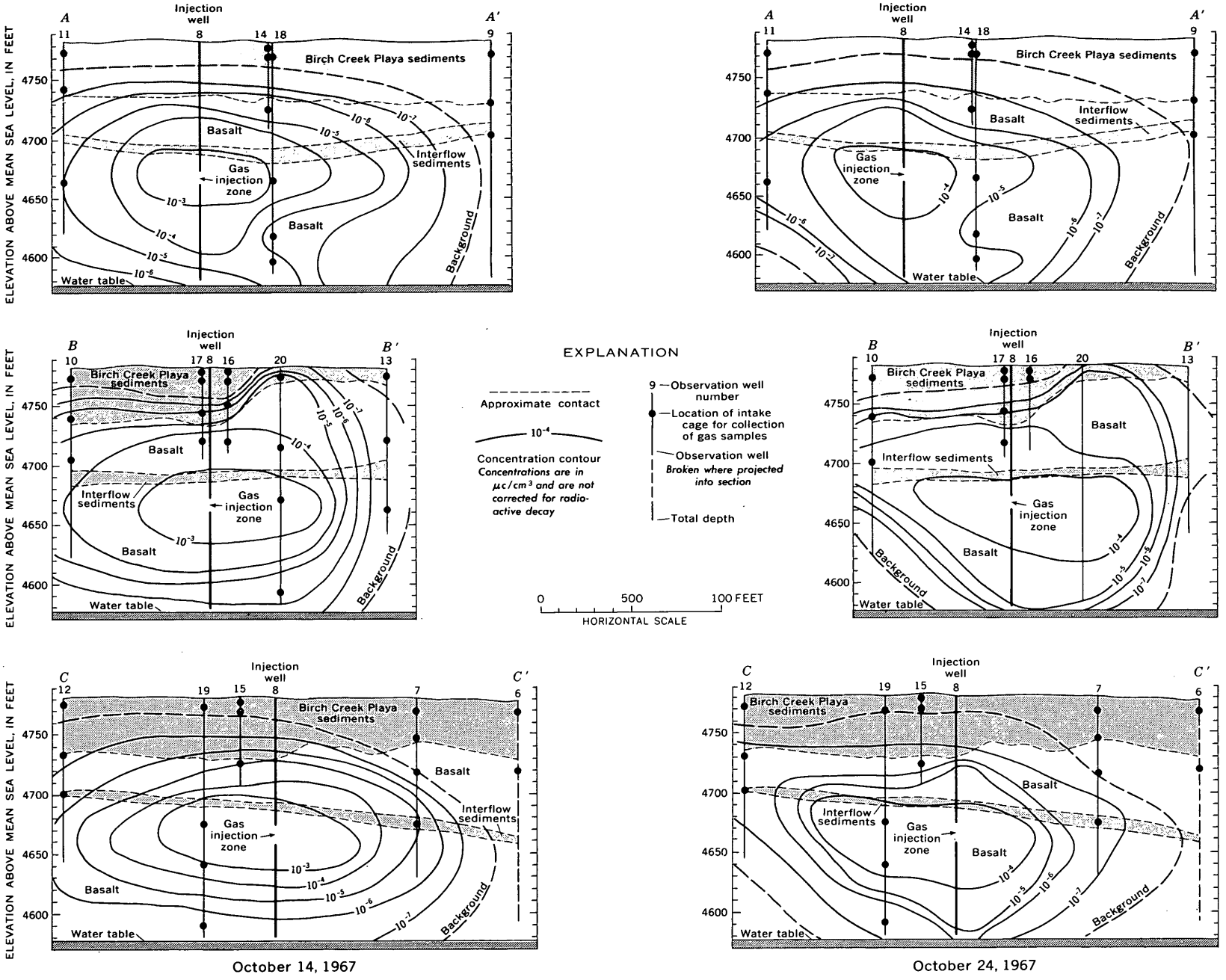

FIGURE 4.—Cross sections through the gas-injection site, showing the contoured concentration distribution of Xe^{133} as interpreted from adjusted sample analyses and GM-tube data, October 1967. The general geology and well construction are shown also.

SUBSURFACE Xe^{133} DATA

The distribution of the Xe^{133} tracer underground could be defined only approximately at various times during the 26 days. The GM-tube data were collected at frequent time intervals throughout the experiment, but the spatial distribution of these data was limited to only four wells. The radiochemical air-sample data were collected from all the observation wells but were poorly distributed in time because of limitations in numbers of samples that could be collected and analyzed during the test period. Because of the very low concentrations and unique analytical procedures involved, the results of radiochemical sample analysis had relatively poor accuracy. They were therefore adjusted to fit the subsurface GM-tube data. The combined GM-tube and adjusted sample-analysis data were then used to interpret the subsurface Xe^{133} distribution at various times during the observation period.

The concentration data for October 1, 8, 14, and 24 were selected as the best representatives of the subsurface Xe^{133} distribution during the observation period. Three geologic cross sections, whose locations are shown on figure 3, were selected for plotting and interpreting the Xe^{133} concentration data. The cross sections were located so as to best represent the subsurface data points. The cross sections show the general stratigraphy of the site and the locations of the subsurface sampling ports and GM tubes. The generalized distribution of the Xe^{133} for the 4 days is contoured on the cross sections in figure 4. The concentrations are not corrected for radioactive decay because the actual quantities present at each time were of greater interest. The Xe^{133} concentration patterns shown on these figures represent the distribution interpreted from the GM-tube data and from the adjusted subsurface-sample data. The distribution patterns of Xe^{133} appear fairly uniform. The most notable anomaly is the high concentration "bulge" toward the upper part of well 20 (cross section *B–B′*). Apparently, a zone of higher permeability in the basalt extended to that region. Also, the thinnest zone in the capping playa sediments is in the vicinity of well 20; therefore, that area provided the least confinement.

MATERIALS BALANCE OF SUBSURFACE Xe^{133}

Appraisals of the quantity of Xe^{133} remaining underground at various times during the test period were calculated, using the interpretive distribution patterns shown in fig 4. The underground inventories of Xe^{133} were estimated for each of the 4 days, October 1, 8, 14, and 24. The estimates were made by dividing the basalt volume between the ground surface and water table at the site into small blocks of variable height and calculating the volume and average Xe^{133} concentration in each block. The quantity of Xe^{133} in the surface playa sediments was negligible and was ignored. The products of the volume times the average concentration for each block were summed for the total subsurface quantity of Xe^{133}. A 61-m square grid system shown on figure 3 served as the basis for the finite-block subdivision. Each grid point represents a vertical column with a 61-m square base, which can be divided into a vertical stack of blocks having variable heights and representing different concentration ranges. Generally, each concentration zone was selected to represent a concentration range of one order of magnitude; in some cases, more precise subdivisions were made. For example, each block within the column representing c_1 (a concentration range) is determined for each grid point (see fig. 5) and then the heights are summed, multiplied by the area of the grid square (3,710 m^2) and multiplied by the concentration. The same procedure is followed for the other concentration ranges, c_2, c_3, and so forth. The final sum must then be multiplied by

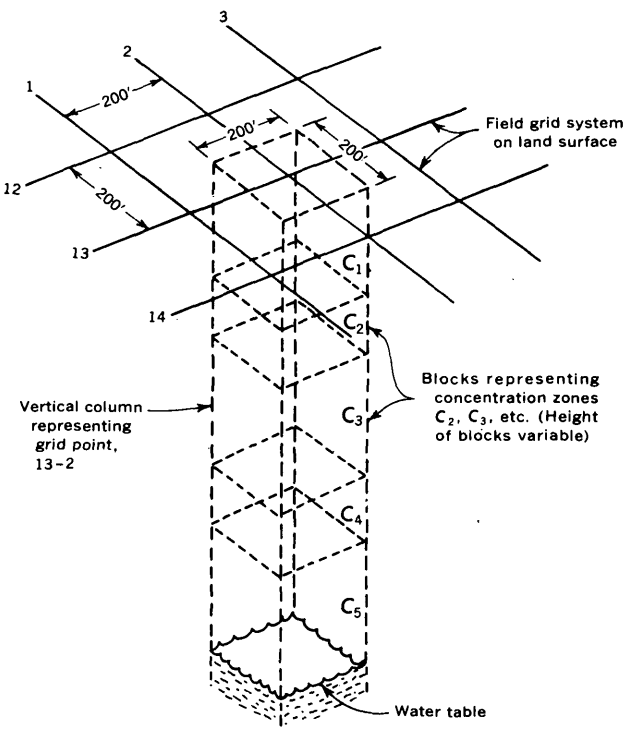

FIGURE 5.—Schematic diagram showing how the gas injection site was subdivided into finite blocks to make the subsurface Xe^{133} inventory calculations.

the effective porosity of the medium, to subtract the portion of the subsurface column occupied by solid or liquid material (rock and water).

The effective porosity of the medium is that part of porosity that can be utilized in the transmission as well as the containment of gas; in other words, to be effective the pores must be interconnected. In some rocks nearly all the pores are effective, while in others, many of the pores may be sealed, too small, or occupied by water. G. H. Chase (written commun., 1966) stated that much of the pore space in basalt is in the form of intercrystalline spaces (very small) and fine-to-coarse vesicles. Such spaces are not effectively interconnected; however, according to Chase, much of the effective porosity is in the form of fractures.

The total porosity can be measured from core samples, but average effective porosity is more difficult to determine; however the approximate range can be estimated by other means. Nace, Stewart, Walton, and others (1959) reported a figure of 3.5 percent as a probable average effective porosity for water-saturated basalt at the NRTS. According to Chase (written commun., 1966) an average total porosity of 17.7 percent was obtained from analyses of 100 basalt samples from the NRTS region. He concluded that an average of 3 to 4 percent would be a reasonable value for the effective porosity. In the south-central part of the NRTS, a value of 6 to 8 percent appears to be reasonable from a previous study (Barraclough and others, 1967). All indications are that the effective porosity should be in the range of 2 to 10 percent for the transmission of water.

The effective porosity for a gas would probably be somewhat higher than that for water; gas can more readily permeate small pores than water can. In order to make some quantitative comparison of the basalts from the gas-injection site to the basalts sampled by Chase, the porosity was calculated from the cores obtained from observation well 6. Core was recovered from 42 m of the well. The weight and volume of the dried core were measured and the bulk density ρ_b, calculated. The total porosity, θ, was then determined by using the density of the mineral constituents, ρ_m, of the basalt so that $\theta = \frac{\rho_m - \rho_b}{\rho_m} \times 100$. A total porosity of 18.5 percent was obtained from this analysis, which agrees with Chase's average value of 17.7 percent. The effective porosity was then estimated to be 5 percent on the basis of all the available evidence from the NRTS. One reason for selecting this low value was that the cores from wells 6 and 7 indicated that many of the larger and more effective (to water) porosity features, such as joints, were filled with fine-grained sediments which had filtered downward from the overlying playa deposits. Furthermore, some of the pore space in the subsurface basalts was undoubtedly occupied by moisture.

By using an estimated porosity of 5 percent and the procedure outlined above, the quantities of Xe^{133} remaining in the ground were calculated for October 1, 8, 14, and 24 and are shown in the left-hand column of table 1. The amount, in curies, of Xe^{133} that should be present if no significant quantities had escaped the ground is shown in the right-hand column.

TABLE 1.—*Inventories of Xe^{133} remaining underground, on the basis of concentration data shown on figure 4, compared with radioactive decay of the actual 987 curies injected*

Date (1967)	Estimated curies of Xe^{133} underground, based on figure 4 and 5-percent porosity	Curies of Xe^{133} which should be present in the basalt after radioactive decay, if there is no other loss
October 1	940	900
8	250	340
14	160	155
24	26	40

These values are also shown graphically on figure 6. The materials-balance curves on figure 6 match fairly well, indicating that the distribution patterns on figure 4 and the 5-percent porosity are reasona-

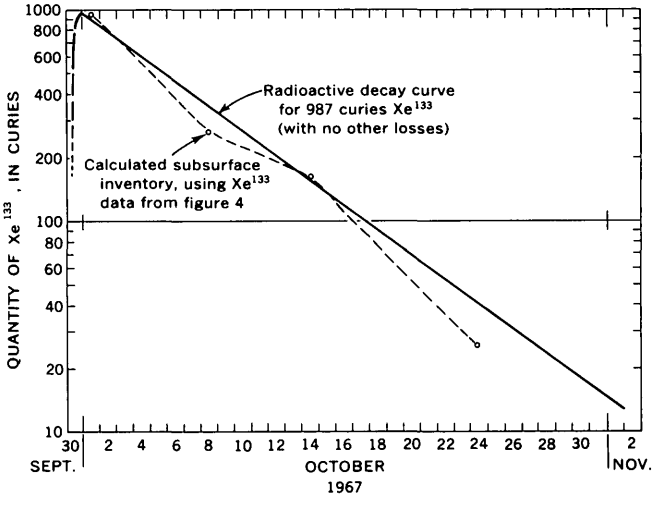

FIGURE 6.—Graph showing the four calculated subsurface Xe^{133} inventories (Oct. 1, 8, 14, and 24, 1967) based on the subsurface GM and sample data (dashed line). The solid line represents the inventory as it should appear if the 987 curies injected remained underground and dissipated by radioactive decay.

ble. The results also suggest that nearly all 987 c in the gas remained underground and decayed radioactively during the 26 days of observation. On the basis of the above evidence, the Xe^{133} distribution patterns on figure 4 were accepted as valid for use in the molecular diffusion analysis which follows.

BASIC DIFFUSION THEORY

Molecular diffusion obeys the principles of potential flow so that flow occurs parallel to the direction of a potential gradient (in an isotropic medium). The parameter of potential in diffusion is the concentration of the diffusing material. A diffusion rate in a particular system is therefore proportional to the concentration gradient. This concept is expressed mathematically as Fick's first law,

$$Q = -D\frac{\delta c}{\delta x}, \qquad (1)$$

where Q is the diffusion rate, D is the diffusion coefficient which is constant for the particular system, c is the concentration of diffusing material, x is the distance in the direction of flow, and $\frac{\delta c}{\delta x}$ is the concentration gradient. If the concentration of a diffusing material decreases from c_1 to c_2 over the distance δx, the concentration gradient at that point is given by $\frac{c_1 - c_2}{\delta x} = \frac{-\delta c}{\delta x}$. The particular system has a diffusion coefficient of D so that the diffusion rate, Q, can be calculated as

$$Q = D\left(\frac{c_1 - c_2}{\delta x}\right). \qquad (2)$$

If the length units are in centimeters, time in hours, and concentration in microcuries per cubic centimeter ($\mu c/cm^3$), the diffusion coefficient, D, will be in cm^2/hr and the unit-area diffusion rate, Q, will be in $(\mu c/hr)/cm^2$. The units of the concentration gradient are therefore $(\mu c/cm^3)/cm$ or $\mu c/cm^4$. The general diffusion coefficient, D, represents the diffusion rate per unit concentration gradient for the particular system. It is therefore expressed as $D = \frac{-Q}{\delta c/\delta x}$ or $\frac{(\mu c/hr)/cm^2}{(\mu c/cm^3)/cm}$, which reduces to cm^2/hr.

The diffusion coefficient is a function of the type of diffusing gas, the type of gas into which the diffusion occurs, the pressure and temperature of the gases and the nature of the porous medium. In a porous medium, the diffusion coefficient, D, is influenced by porosity and tortuosity effects which attenuate the diffusion rate. For the special case of a completely open gaseous medium with no solid matrix (100-percent porosity), the diffusion coefficient will be referred to as D_0 in this report. The diffusion coefficient will always be lower in a porous medium than in an open medium for the same gas conditions. The amount of the attenuation depends on the porosity, geometry, and moisture content of the medium.

FIELD DIFFUSION CONDITIONS

The basic physical system consists of the basalt layers above the water table (62.5 m deep) and the playa sediments above the basalt, as shown schematically on figure 2. The basalt sequence is a highly permeable horizontal layer, about 46 m thick, between an impermeable (to gas) water surface at the bottom and a blanket of fine-grained sediments of low permeability at the top. When the gas was injected into the basalt, it moved out horizontally and remained semiconfined between the water table and the playa sediments. If one assumes that the Xe^{133} is not soluble and does not diffuse into the water, the problem becomes one of vertical diffusion of Xe^{133} through the playa sediments from the basalt to the atmosphere. There undoubtedly were some horizontal components of diffusion in the system also, which would gradually change the Xe^{133} concentration distribution in the sediments as well as in the basalt. However these changes were slow and can be accounted for approximately by analyzing the distributions in discrete time steps. The horizontal diffusion rates are not of particular interest in the present study, which is concerned mainly with vertical Xe^{133} losses to the atmosphere. The horizontal concentration gradients and corresponding diffusion rates are considerably lower than the vertical values and were assumed to have negligible effects on the vertical diffusion rates. If the Xe^{133}concentration at the base of the playa sediments is known and the concentration at the top is near zero, a vertical concentration gradient can be calculated provided the sediment thickness, H, is also known:

$$\frac{\delta c}{\delta x} = \frac{c}{H}. \qquad (3)$$

The instantaneous diffusion rate can then be calculated for that point if the diffusion coefficient is known, using equation 2 so that

$$Q = D\left(\frac{c}{H}\right). \qquad (4)$$

The concentrations at the base of the playa sediments and the thickness of the sediments vary from place to place so that the diffusion conditions are not constant in space. The concentrations and therefore the diffusion rates also change with time, so that the system varies both spatially and temporally.

MATHEMATICAL MODEL OF THE FIELD CONDITIONS

Because of the complex geometry and the time variations, the field-diffusion conditions would be impractical to model exactly by rigorous mathematics that would require relatively sophisticated computer techniques. However, with some simplifications, an approximate analytical model can be formulated. This can be done conveniently, in this case, by dividing the system into many finite blocks and analyzing each block separately as a uniform element. The individual analyses can then be integrated over the complete test system. The time period can also be broken down and analyzed in discrete time steps.

The geometrical subdivision of the test site was accomplished by superimposing the grid system of 61-m squares over the area (fig. 3) as was done in the materials-balance analysis. Each grid point is then assumed to represent a 3,710-m^2 area surrounding it. This size grid was found to be adequate for the accuracy desired in this analysis and is compatible with the accuracy of the other variables in the system. Therefore, if values for playa-sediment thickness, diffusion coefficient, and Xe^{133} concentration at the base of the sediments can be assigned for a grid point, a diffusion rate can be calculated, by using equation 4, for any particular time. This calculation assumes that a constant diffusion coefficient over the area and depth represented by the point, a linear concentration gradient from the bottom to the top of the sediments, and negligible horizontal-diffusion effects exist. When the concentration gradient changes with time, diffusion calculations can be made in short time increments so that each calculation assumes constant conditions for the duration of the increment. A more rigorous multidimensional analysis could probably be applied to this test if sufficient justification develops in the future; however, for the present requirements, the one-dimensional flow model appears sufficient and compatible with the accuracy of other aspects of the test.

If the Xe^{133} concentration distribution at the base of the playa sediments can be mapped for a particular point in time, the total diffusion rate over the test area can be approximated for that time. This is accomplished by calculating the diffusion rate at each grid point within the test area (with equation 4), then summing all the rates and multiplying by the area that each point represents $3.71\times10^7 cm^2$. Thus,

$$Q_s = 3.71\times10^7 \sum_{i=1}^{n} D_i \frac{c_i}{H_i}, \qquad (5)$$

where Q_s is the total diffusion rate over the test area in $\mu c/hr$, n is the number of grid points used, and the subscript, i, represents each grid-point identification number. If the subsurface Xe^{133} distribution is mapped for several different times during the test period, the total quantity diffused can be approximated by multiplying each areal diffusion rate, Q_s, times the time increment it represents and then summing these products, so that

$$S = \sum_{t=0}^{T} (Q_s)_t \Delta t, \qquad (6)$$

and substituting equation 5,

$$S = \sum_{t=0}^{T} \left(3.71\times10^7 \sum_{i=1}^{n} D_i \frac{c_i}{H_i} \right)_t \Delta t, \qquad (7)$$

where t is the time or number of Δt increments after injection, T is the total time period of the test or number of time units (Δt's) used, and S is the amount of Xe^{133}, in microcuries, which diffused out of the ground during the test period T.

APPLICATION OF THE MATHEMATICAL MODEL TO THE FIELD TEST

The procedure described above can be applied to the field test by determining values for D, H, and c for each grid point at several different times during the test period.

The areal distribution of the playa-sediment thickness, H, was determined by drilling 79 auger holes to the top of the basalt over the entire test area. By superimposing the grid system (fig. 3) on an isopachous sediment-thickness map (determined from the drilling), an H value was assigned to each grid point of interest.

The diffusion coefficient, D, cannot be defined so readily at each point because it could not easily be measured in the field. However, Millington (1959) presented a method for calculating D if the porosity and moisture content of the porous medium are

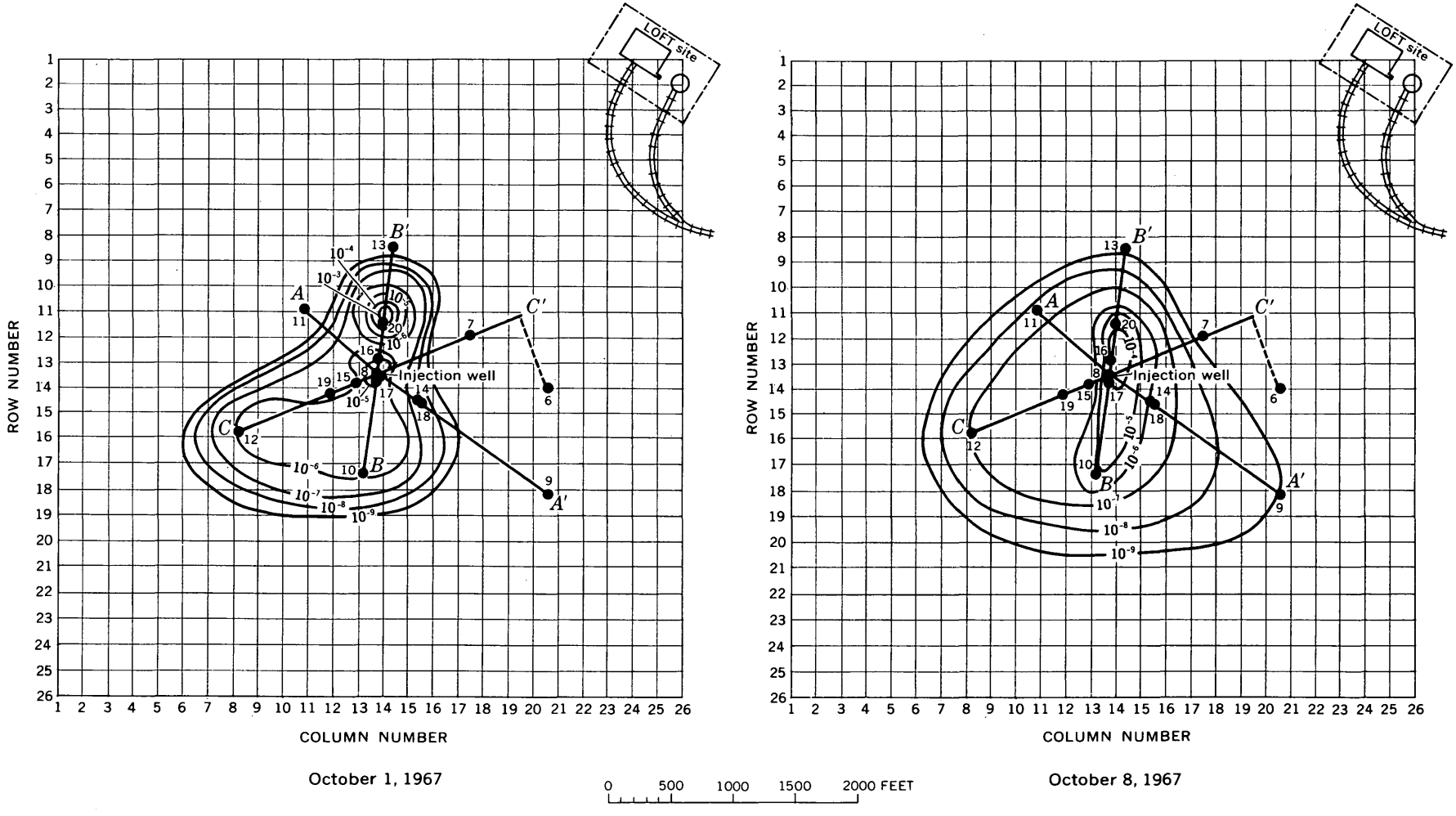
LOFT site
Injection well
ROW NUMBER
COLUMN NUMBER
October 1, 1967
October 8, 1967
0 500 1000 1500 2000 FEET

FIGURE 7.

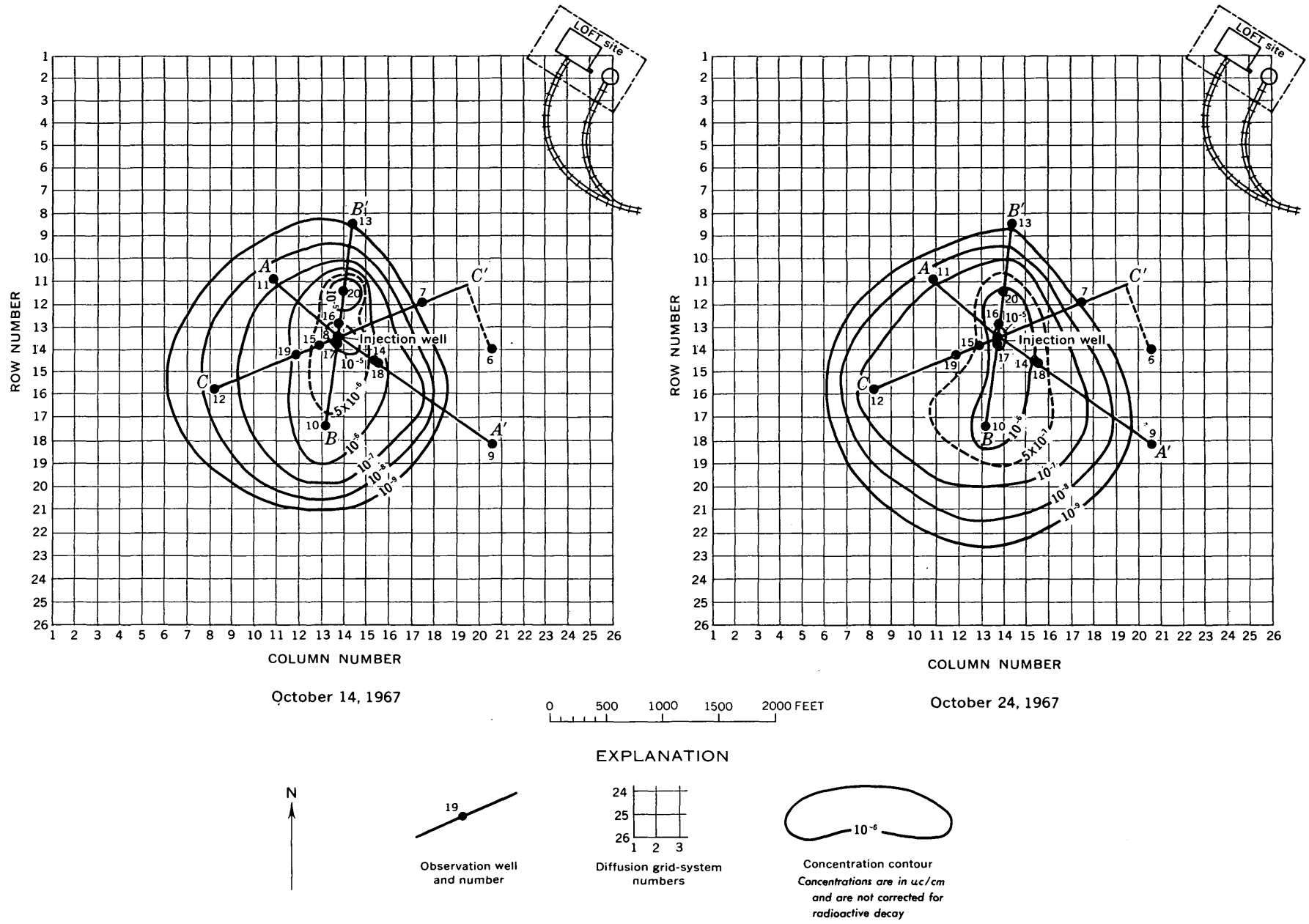

FIGURE 7.—Contoured distribution patterns of Xe^{133} at the base of the playa sediments, based on adjusted sample analysis and GM-tube data, October 1967.

known. He related D to the open-medium binary diffusion coefficient, D_0, of the gases so that

$$\frac{D}{D_o} = \left(\frac{n}{m}\right)^2 (\theta_1)^{4/3}, \quad (8)$$

where θ_1 is the gas-filled porosity of a moist sample and n/m is the ratio of gas-filled pore volume to total pore volume. This method yielded satisfactory results for a previous diffusion study in the Birch Creek playa sediments (Robertson, 1969b).

D_0 for Xe^{133} in air has been calculated to be 0.125 cm^2/sec at 1.013 bar and 26.6°C (Bolch and others, 1967). The average subsurface field temperature and pressure were 12°C and 0.868 bar, respectively. The Lennard-Jones equation (Bolch and others, 1967) was used to correct the D_0 value to 0.138 cm^2/sec for field temperature and pressure. Porosity and moisture-content data obtained on 17 drive-core samples from the test site were used for the data needed in equation 8. The samples ranged from 0.7 to 8.8 m deep and were analyzed in the laboratory of the U.S. Geological Survey, Denver, Colo. The average total porosity of the samples was 39.1 percent (ranging from 29.3 to 44.7 percent), and the average moisture content was 16.5 percent (ranging from 12.0 to 21.5 percent) on a volume basis. For equation 8, n/m would be $(39.1-16.5)/39.1=0.578$ and $\theta_1=0.391-0.165=0.226$. The ratio $D/D_0=(0.578)^2\ (0.226)^{4/3}=0.046$ and therefore,

$D=0.046\ D_0=(0.046(0.138)=0.00635\ cm^2/sec.$

This value of D is assumed to apply everywhere. If more detailed information in the future shows this to be an unacceptable assumption, appropriate variations in D can be assigned to the proper grid points. However, for the present analysis the assumption of a uniform D appears satisfactory.

The subsurface Xe^{133} distributions, shown in cross section on figure 4, were used to interpret the Xe^{133} -concentration distribution at the base of the playa sediments for the four different days. Those distributions are mapped on figure 7. From these maps, it is possible to select a Xe^{133} concentration value, c, for each grid point on each of the 4 days. Thus, with values for thickness, diffusion coefficient, and base concentration, equation 4 can be applied to each grid and the diffusion analysis carried out as outlined previously.

CALCULATIONS AND RESULTS

To facilitate the analysis, a computer program was written in FORTRAN 63 to make the calculations on a Control Data 1604 computer. A punched data card was set up for each grid point to contain the following information: the grid location (row and column number); playa-sediment thickness at the grid point, H; date and time; and Xe^{133} concentration, c. Using the data for each grid location, the computer then evaluated equation 5 for each of the 4 days. The computer output included the total areal-diffusion rate, Q_s, for each of the 4 days; the point-diffusion rate, Q, for each of the grid points; the point which had the highest diffusion rate; and the average point-diffusion rate, Q_a, over the area occupied by Xe^{133} (as indicated on figure 7). These results are summarized in table 2.

The total areal-diffusion rates, Q_s, for the 4 days are plotted in figure 8. The plotted data form the type of curve that should be expected. The slope of the diffusion-rate curve approaches the slope of the radioactive-decay curve for Xe^{133} after the first week. The total amount of Xe^{133} which diffused from September 30 through October 25 was calculated from this curve by calculating and summing totals in 1-day increments. This total is $3.7\times10^5\mu c$ (0.37c) for the 26 days. When this total is corrected for radioactive decay, it becomes $9.3\times10^5\mu c$ (0.93 c). In other words, if the subsurface Xe^{133} concentration had not declined by radioactive decay, 0.93 c would have diffused to the atmosphere under the assumed conditions. By the end of October 25, the original 987 c had decayed to 33 c so that 96.7 percent of the original Xe^{133} was lost by decay. The diffusion calculations indicate that only about 0.37 c could have been lost by diffusion—a rather small part of the total injected.

Table 2 also indicates the location of the zone which had the maximum calculated diffusion rate. On all 4 days, the maximum calculated rate was in the same area, near observation well 20. In that area, the playa sediments are thinnest (2.5 to 3.5 m) and the subsurface Xe^{133} concentrations rela-

TABLE 2.—*Diffusion rates calculated for the test area within the outer iso-concentration contour shown on figure 7 for four different days*

[The average rate, Q_a, is the average of all the point rates, Q, in the area. The total areal rate, Q_s, represents the average point rate, Q_a, integrated over the entire area]

Date (1967)	Average point diffusion rate, Q_a ($\mu c/cm^2$)/hr	Point of maximum diffusion: Grid point having maximum diffusion rate, Row	Point of maximum diffusion: Grid point having maximum diffusion rate, Column	Diffusion rate at maximum point ($\mu c/cm^2$)/hr	Total diffusion rate, over test area, Q_s (μc/hr)
October 1	9.58×10^{-7}	11	14	6.61×10^{-5}	2,560
8	1.47×10^{-7}	12	14	8.20×10^{-6}	655
14	6.77×10^{-8}	11	14	2.64×10^{-6}	275
24	1.31×10^{-8}	12	14	1.64×10^{-7}	65

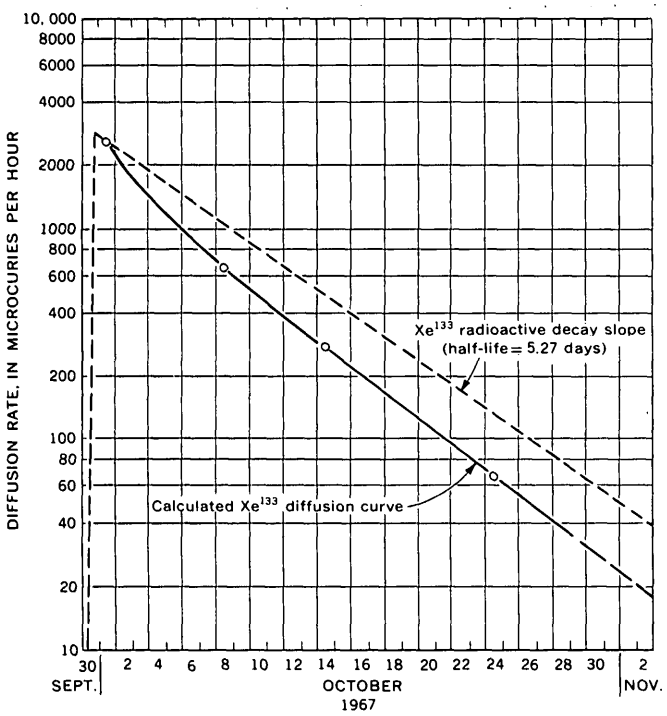

FIGURE 8.—Graph showing calculated total areal-diffusion rates, Q_s, (table 2) plotted against time, as compared with the radioactive decay slope of Xe^{133}.

tively high. This agrees with results of field-measured flux rates discussed below.

COMPARISON OF DIFFUSION ESTIMATES WITH MEASURED FLUX RATES

The calculated diffusion rates compare fairly well, in a general sense, with the ground-to-air flux rates measured in the field by the two contractors.

Texas Instruments, Inc., completed 129 flux measurements during the test period at 24 different locations over the test site (Bowman and Bennett, 1968). Ninety-six (75 percent) of their values agree well with the diffusion calculations. However, most of the agreement was among the values that showed little or no flux. Texas Instruments, Inc., detected Xe^{133} in only 10 of the 129 measurements; the ten positive values were obtained at 4 different locations (near the following grid row-column locations: 11–14, 14–14, 10–15, 8–14). Of those 10, only 2 agree well with calculated rates; 3 were high by factors of 10 to 100, and 5 were low by a factor of approximately 10. The diffusion calculations indicate that 3 of the 10 positive values should have shown no flux. The remaining 119 samples indicated no measurable Xe^{133} flux. However, according to the diffusion estimates, 25 of those negative results should have shown measurable flux, if there were no other flow influences. Of the 4 locations at which Texas Instruments, Inc., found a measurable flux, only 2 of them should have had some, according to the diffusion analysis; and of the other 20 sample sites at which they found no measurable flux, 4 theoretically should have had some.

The calculated diffusion rates were also compared with 90 flux measurements made by Isotopes—A Teledyne Co. at 50 different field locations (Hardaway and others, 1968). Forty-two (47 percent) of their values agreed reasonably well with calculated diffusion rates; that is, they were within factors of 0.5 to 5 of the diffusion estimates. Sixty-eight (76 percent) of the samples were within one order of magnitude of the calculated rates. The remaining 22 values deviated from the diffusion calculations in the following manner: 14 were high by an approximate factor of 100; four were low by a factor of 100; three were 1,000 times too high and one was 1,000 times too low.

The wide range of deviations of flux rates measured by both companies may be due to factors such as barometric-pressure variations (Robertson, 1969a) that influenced the actual flux rates. However, the measurements generally were near the same magnitude as the calculated values. Most of the deviations in the Texas Instruments, Inc., data were to the low side of the calculated rates, while most of Isotopes—A Teledyne Co. flux-rate deviations were on the high side. The apparent variation in the values calculated by the two companies may be the result of analytical or calculational errors. It should be emphasized that, although the deviations in the flux-measurement data for both companies were relatively large, the amounts of Xe^{133} involved were very small. The equipment detected extremely small quantities of Xe^{133}, so that orders-of-magnitude differences were still very small amounts. The measured flux rates therefore support the implied conclusions of the calculated diffusion rates: that the ground-to-atmosphere flux rates were extremely low (although measurable in some cases) in comparison with the quantity of Xe^{133} injected, and that only a small portion of the gas (less than 0.1 percent) escaped to the atmosphere.

Isotopes—A Teledyne Co. detected positive Xe^{133} flux rates in 52 samples, whereas Texas Instruments, Inc., had only 10 positive readings. This difference is partly the result of the more sensitive (lower) detection limit of Isotopes' equipment, and the differences in the locations of the sampling points. Also more of Isotopes' flux-sampling points

were concentrated in the areas of higher potential flux rates.

SUMMARY AND CONCLUSIONS

Results of these studies show that from the standpoint of the applicability of this technique of gas disposal, the injection test was generally successful. During injection, gas moved out laterally through the permeable basalt (above the water table) in a fairly uniform pattern, while the playa sediments, capping the basalt, served as a semiconfining upper boundary. Materials-balance calculations on the Xe^{133} support the conclusions that underground Xe^{133} distribution patterns, interpreted from the subsurface GM and air-sample analysis data, were within acceptable tolerances and that almost all the Xe^{133} remained underground within the test area after injection.

From the analyses of molecular diffusion of the subsurface gas, it is concluded that there were probably no appreciable Xe^{133} losses by this process during the test period. This agrees with the conclusion from the materials-balance calculations that nearly all the injected Xe^{133} remained underground and decayed to stable Cs^{133}. Molecular diffusion could have produced detectable ground-to-air Xe^{133} flux rates of the same magnitude as the actual rates measured onsite. Although the field-measured ground-to-air flux rates were more erratic, they are generally compatible with calculated diffusion rates. Other influences, such as barometric-pressure fluctuations could adequately account for the variations in measured flux rates. In any case, the amounts of radioactive Xe^{133} that escaped to the atmosphere were very small, certainly less than 5 c and probably less than 1 c.

The diffusion calculations, based on the theoretical model, are admittedly approximate and subject to some error. However, it is not likely that the overall error is more than one order of magnitude. Even if the theoretical estimates were low by a factor of 10, the total diffusion loss would still have been only 3.7 c, or less than 1 percent of the 987 c injected. In conclusion, therefore, it appears that molecular diffusion produced measurable flow rates of Xe^{133} from the ground to the atmosphere, but that these rates were too low to account for a significant loss in the total injected quantity of Xe^{133}.

Additional analysis of data will be necessary to evaluate fully the effects of barometric-pressure changes; however, the results at this stage indicate that the disposal of certain waste gases by underground injection apparently is feasible where there is a geological environment similar to the one described here, that is, a highly permeable zone above the water table and beneath a capping stratum of low permeability. Methods and techniques used in the materials-balance and diffusion investigations for this test appear to be suitable for other gas-injection sites, regardless of the geological environment.

REFERENCES

Barraclough, J. T., Teasdale, W. E., Robertson, J. B., and Jensen, R. G., 1967, Hydrology of the National Reactor Testing Station, Idaho, 1966: U.S. Geol. Survey open-file report, p. 60–64 *and* U.S. Atomic Energy Comm., Idaho Operations Office, Idaho Falls, Idaho, IDO 22049.

Bolch, W. E., Selleck, R. E., and Kaufman, W. J., 1967, Gas dispersion in porous media—Peclet-Reynolds number correlations: Sanitary Engineering Research Laboratory Report no. 67–10, Univ. California, Berkeley, p. 23, 79.

Bowman, C. R., and Bennett, Richard, 1968, Tracer studies at the Loss of Fluid Test (LOFT): Dallas, Tex., Texas Instruments, Inc., Science Services Div., 43 p.

Hardaway, J. E., Barrientos, C. S., Kalin, E. G., Reed, W. E., and Sigalove, J. J., 1968, Gas injection experiment NRTS, Idaho—measurement of xenon-133 flux and surface-level air concentrations: Westwood, N.J., Isotopes —A Teledyne Co., 90 p.

Millington, R. J., 1959, Gas diffusion in porous media: Science, v. 130, p. 100–102.

Nace, R. L., Stewart, J. W., Walton, W. C., and others, 1959, Geography, geology, and water resources of the National Reactor Testing Station, Idaho—Pt. 3. Hydrology and water resources: U.S. Geol. Survey open-file report, 253 p.

Robertson, J. B., 1969a, Behavior of xenon-133 gas after injection underground—Molecular diffusion, materials balance, and barometric pressure effects: U.S. Geol. Survey open-file report, 37 p.

——— 1969b, Diffusion from a gaseous source in a porous medium—A field and theoretical comparison, *in* Geological Survey Research 1969: U.S. Geol. Survey Prof. Paper 650–D, p. D265–D273.

Schmalz, B. L., 1969, Injection of gas into the lithosphere at the National Reactor Testing Station: U.S. Atomic Energy Comm., Idaho Operations Office, Idaho Falls, Idaho, IDO–12069, 166 p.

Walker, E. H., 1964, Subsurface geology of the National Reactor Testing Station, Idaho: U.S. Geol. Survey Bull. 1133–E, 22 p.

RETENTION TIME AND CIRCULATION STUDY IN A SEWAGE STABILIZATION LAGOON

By WILLIAM G. STAMPER, Raleigh, N.C.

Work done in cooperation with the North Carolina Department of Water and Air Resources

Abstract.—Two sewage stabilization lagoons used by the town of Benson, N.C., were suspected of having an average retention time much less than the designed 30 days. A short circuit in the flow pattern was suspected to be the cause. During the summer of 1969, fluorescent dye was injected into the two lagoons in studies designed to determine the average retention time and the flow pattern of each sewage lagoon. The retention times were found to be considerably less than 30 days, and a definite short circuit in the flow pattern was shown to exist.

Sewage stabilization lagoons are shallow basins designed to retain untreated sewage for a certain period of time to allow a biological breakdown of the organic materials by photosynthesis, a process which keeps the dissolved oxygen at a high level. This breakdown is accomplished by letting the sewage slowly circulate in flow patterns inside the lagoon for a number of days before being discharged at the lower end (Fair and Geyer, 1956, p. 853). Even though the movement of the sewage in the lagoon is by gravity flow, the net movement toward the outlet is not readily apparent in a properly designed lagoon.

During the summer of 1969, the Municipal Waste Section of the North Carolina Department of Water and Air Resources collected routine samples from the effluent of two sewage stabilization lagoons used by the town of Benson, N.C., about 30 miles south of Raleigh. The samples had a very low content of dissolved oxygen, indicating a low degree of biological decomposition of the sewage in the effluent. A short circuit in the flow pattern, resulting in a retention time much less than the 30-day design retention time, was suspected.

DETERMINATION OF RETENTION TIME

A dye study was begun on July 14, 1969, to determine the retention time of the two sewage lagoons. Each lagoon was dosed at the inflow pipe with 1 liter of 40-percent rhodamine BA dye solution. Daily samples were collected from the effluent of each lagoon until September 1, 1969, at which time dye concentrations had returned to the approximate background concentration observed before dye was injected.

The concentration-versus-time curve for a time-of-travel study in a lined canal has almost a normal distribution owing to nearly uniform velocity and the lack of dead water areas. In contrast, the curves in figure 1, which show dye concentration versus days after dye injection in the sewage lagoons, are extremely skewed, indicating a great variation in the velocity pattern of the lagoon caused by short circuiting.

Typically the center of mass is used to compute traveltime when the concentration-versus-time curves have a definite skew. To determine the center of mass, each curve was integrated, and the total area under the curve was divided into two equal parts. The vertical lines in figure 1 separating these parts indicate the mean traveltime from the inflow to the outfall, or the mean retention time of the lagoon.

The mean retention time, found to be 7 days for lagoon 1 and 9 days for lagoon 2, was the time necessary for half the dye to be flushed from the lagoon. Thus, on the average, 50 percent of the sewage effluent will be composed of sewage that has

U.S. GEOL. SURVEY PROF. PAPER 700-D, PAGES D301-D304

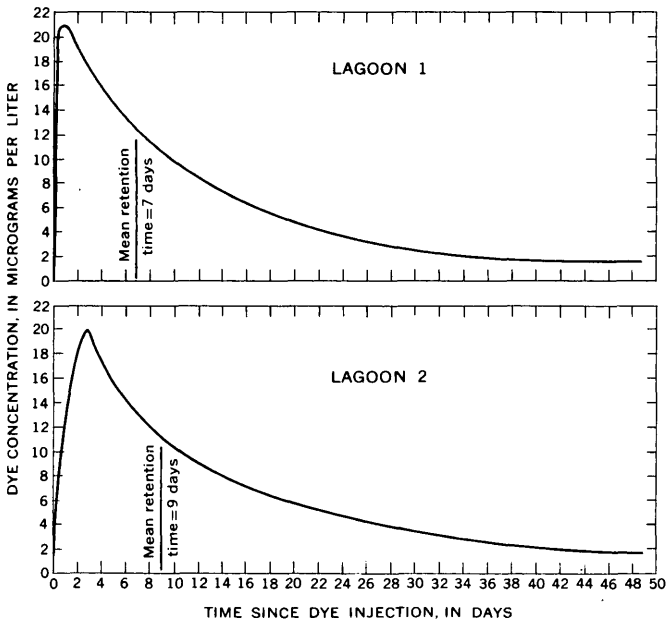

FIGURE 1.—Curves showing dye concentration, in micrograms per liter, versus time since dye injection, in days, for lagoons 1 and 2.

been retained in lagoon 1 for 7 days or less and in lagoon 2 for 9 days or less.

Sewage should be held for 3 to 4 weeks in the basin to obtain a satisfactory reduction in biochemical oxygen demand and produce a high dissolved-oxygen level (Fair and Geyer, 1956, p. 853). This condition was not achieved by either of the two lagoons, as shown by the percentages of sewage effluent of various ages found in the lagoons (fig. 2). Almost 90 percent of the sewage effluent from lagoon 1 had been retained less than the minimum time suggested. Likewise, about 83 percent of the sewage effluent from lagoon 2 was released too soon. This premature release of the sewage from both lagoons, shown by the dye study, confirmed suspicions that a short circuit existed in the flow patterns of the lagoon. In other words, the sewage moved from the inflow with some noticeable velocity directly toward the outfall instead of indirectly with undetectable movement. This situation is probably caused by a combination of factors—inflow pipes being too close to the outfalls, and absence of baffles in the lagoons.

FLOW PATTERNS IN THE LAGOONS

If a solution of dye were injected into a basin of stagnant water, the dye cloud would spread out by molecular diffusion in equal distances from the center in all directions. The action of the dye cloud

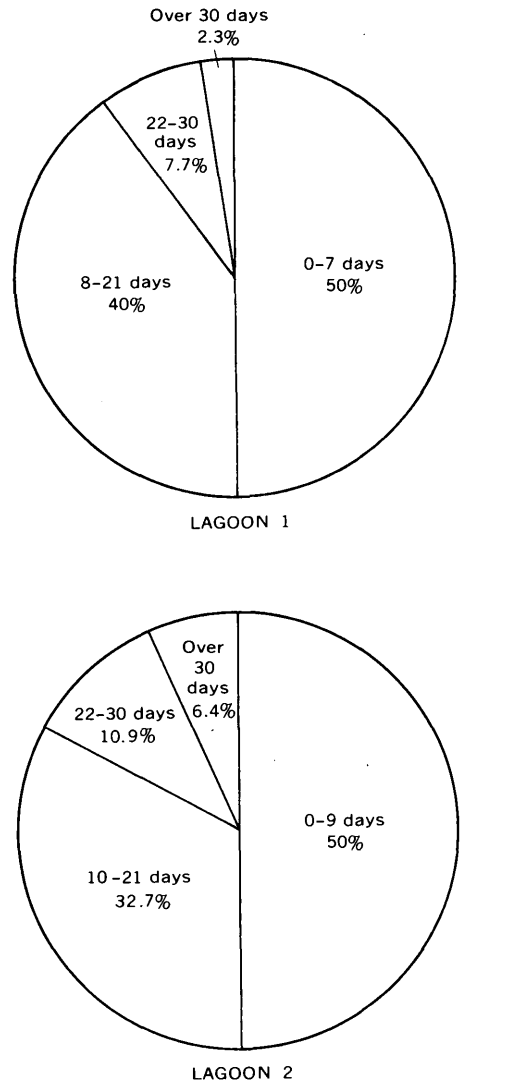

FIGURE 2.—Pie diagrams showing percentage of effluent, by age, discharged from lagoons 1 and 2.

could be compared to the concentric waves caused by a rock thrown into still water. However, the dye cloud would become elongated in the direction of any distinct flow.

A second injection of rhodamine BA dye was made on September 5, 1969, in an attempt to determine the flow patterns in the two lagoons. Two hours after the injection, samples were collected across predetermined cross sections in the lagoons. Lagoon 1 was resampled 4½ hours after the injection because the shape of the dye cloud had visually changed by that time. Figure 3 shows the resulting concentrations.

Examination of the dye clouds does not enable one to determine numerical values of width and

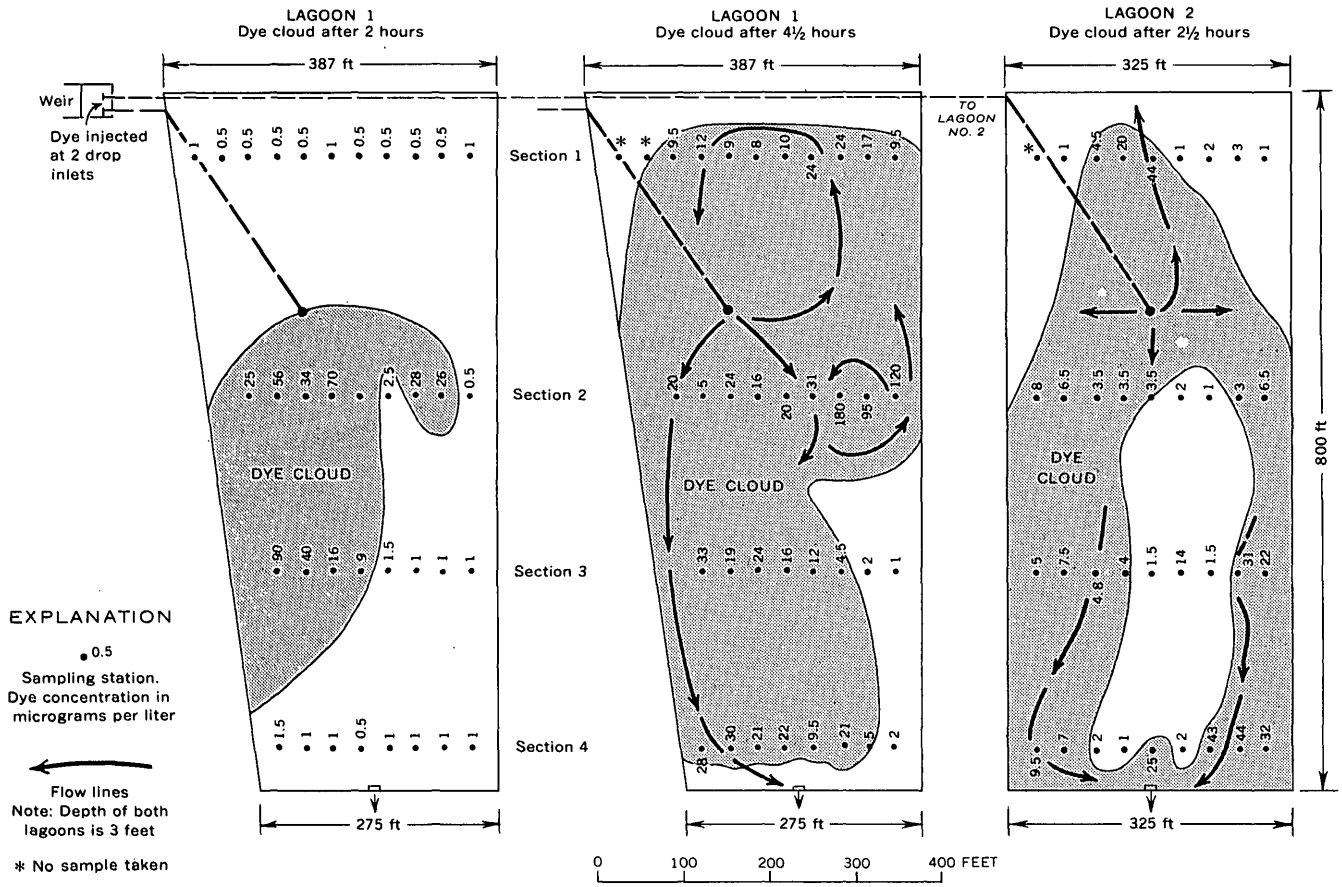

FIGURE 3.—Diagrams showing the position of the dye cloud in lagoons 1 and 2 at a given number of hours after the dye injection.

velocity of threads of flow through the lagoons, but their shape and the variation of concentrations within the clouds do indicate that such threads exist, and several useful conclusions about the performance of the lagoons can be drawn.

After 2 hours the dye cloud in lagoon 1 had concentrated mostly along the right side (looking from entrance to outfall) and below the inflow point. The dye cloud was found to have widened toward the middle and to be just approaching the outfall after 4½ hours.

The flow lines shown on the second sketch for lagoon 1 are deduced from both sets of data, the first set collected 2 hours and the other set 4½ hours after injection. The dye clouds observed at both times indicated a tendency for some localization of flow along the right side. The shape of the cloud after 2 hours and the high concentration near the left end of section 3 after 4½ hours indicated that a relatively large slug of sewage effluent moved toward that point and then split (and possibly eddied) with threads of flow moving off in two directions, as shown.

In lagoon 2, the dye cloud followed a somewhat different pattern and reached the outfall after 2½ hours. Dye concentrations indicated a rather uniform movement in all directions from the inflow point. Above section 2, however, the flow split into at least two threads, with strips of relatively dead water in between, possibly owing to some nonuniformity of depth across the section.

An arbitrary background concentration of 4μg/l (micrograms per liter) was assumed to correct for some dispersion of the dye caused by movement of the sampling boat. Therefore, any concentration much greater than about 4μg/l at a point indicated some movement of the dye cloud to the point. The shape of the dye cloud as well as localized threads of relatively large flows were verified by field observations. Streamers of color were noticed outward from the inflow points shortly after the dye injection.

CONCLUSIONS

Studies involving fluorescent tracer dyes have become increasingly more widespread and varied in

application in the last few years. Results of the study indicate that fluorescent dye can be used successfully to trace the flow patterns in sewage lagoons under field conditions.

REFERENCE

Fair, G. M., and Geyer, J. C., 1956, Water supply and waste water disposal: New York, John Wiley, 973 p.

AN EVALUATION OF ANALOG TECHNIQUES FOR IMAGE REGISTRATION

By ROBERT B. McEWEN, Washington, D.C.

Abstract.—Registration of multispectral images of the earth transmitted by three Return Beam Vidicon (RBV) television cameras carried in a 960-km polar orbit in 1972 by the first Earth Resources Technology Satellite (ERTS-A) will require careful calibration of distortion parameters. The parameters, the expected distortions, and the desired calibration accuracies are listed. Four analog techniques considered and evaluated are (1) optical projection and rectification, (2) line-scan modulation, (3) orthophoto image correlation, and (4) analytically controlled transformations of incremental areas. The last offers the best approach for analog image registration.

The purpose of this paper is to review some of the problems involved in registering multispectral imagery and to examine possible analog solutions. In the immediate context is the 1972 launch of the first Earth Resources Technology Satellite (ERTS-A) which will place three Return Beam Vidicon (RBV) television cameras into a 960-km polar orbit. In a larger context the registration of multispectral imagery is common to many applications of remote sensing.

Multispectral images will be received in three spectral bands and the earth scene will be viewed many times during the year of satellite life. Some of the relatively high resolution triplets will require registration for multispectral analysis and for cartographic referencing of photomaps.

Registration may be either relative or geometric. The former removes distortions from one image until it overlies a second image. While satisfactory for certain interpretations and color reproductions, relative registration is not suitable for cartographic products. Geometric registration removes image distortions according to a theoretical geometric model, usually a central perspective. Interpretations, color reproductions, and cartographic photomaps can be prepared. Both types of registration will require considerable effort. Geometric registration is a more desirable goal.

Geometric registration requires careful evaluation and calibration of all distortion parameters. Included herein is a table of expected distortion parameters of the RBV and the calibration accuracy required. All parameters will require calibration because manufacturing tolerances are inadequate for 10-μm geometric registration.

Analog-registration techniques, mechanical, electronic, optical, or a combination of these, will certainly require digital computation of supporting parameters. However, the image tones are transferred and geometrically positioned by analog-processing techniques. These techniques are evaluated for application to the RBV system.

BASIC CONCEPTS OF ANALOG REGISTRATION

Four basic concepts set the ground rules for analog registration:

1. A suitable analog technique is characteristically an efficient method of solving a given problem where the parameters vary predictably over a small range of values.
2. An analog-registration technique may be mechanical, electronic, or optical. It most likely will require the digital computation of supporting parameters. Most important for the RBV system or any system involving a video link is the absence of an analog-to-digital conversion of the video signal for the purpose of manipulating the geometric location of each pixel.
3. The equipment employed in analog registration should be amenable to parallel data flow. There should be no constriction where one piece of expensive specialized equipment controls the data flow rate. Increased production should be possible with additional equipment operated in parallel.

U.S. GEOL. SURVEY PROF. PAPER 700-D, PAGES D305–D311

4. The analog-registration technique must allow for an adequate treatment of calibration data. Thus the range of applicable parameters must be sufficiently flexible.

GOAL OF ANALOG REGISTRATION

The goal of any registration technique is to remove the positional distortions in the image. Such a statement is, however, much too broad, and several refinements are in order. The first distinction is between relative registration and geometric registration.

Relative registration involves the correction of the image positions on one photograph to the corresponding images on a second photograph. The second photograph may or may not have appreciable distortions. When completed, relative registration allows the corrected images of photograph 1 to overlay the corresponding images on photograph 2. It is not necessary that relative registration be accomplished simultaneously over the entire image format. Various stereoscopic viewers or multiprojector viewers allow relative registration of small parts of a format even when considerable distortion exists. The area of registration and the tolerable distortion are dependent on the accuracy required by the user.

Geometric registration, in contrast with relative registration, involves the correction of the image positions on one photograph to some previously defined geometric model. Commonly the model would be a central perspective. Obviously, geometric registration requires that the distortions from the model to the image be calibrated. If several photographs are corrected to the same geometric model, the corresponding images of all photographs will overlay one another. The products obtained from geometrically registered overlays (often a color product) will be very similar in appearance to overlays which have only relative registration. The two concepts involved are very different however. The utility of the two types of products, relatively registered versus geometrically registered, can vary considerably.

For cartographic purposes geometric registration is essential. Before any photomaps or thematic maps can be prepared, the imagery on the photograph must conform to an acceptable geometric model. Likewise before any corrections are applied for external geometric effects such as tilt or earth curvature, the photograph must be geometrically correct.

Many applications of remote-sensing techniques will require the data to be displayed on a map. The discipline-oriented data of geology, water resources, or agriculture, to mention but a few, will be considerably degraded if the cartographic location of the data is unreliable. Although the interpretation of multispectral or sequential imagery can be accomplished with relative registration, the cartographic referencing of the interpretation may be impossible. With geometric registration both the interpretation and the cartographic referencing are possible.

It is possible to conceive of a relative registration which also performs a geometric registration. The only necessary condition is that photograph 2 in the example of relative registration be in the format of a defined geometric model. Many plans for rectifying panoramic as well as television pictures are based on this concept. While the concept is theoretically excellent, the lack of a suitable geometric photograph causes many practical problems.

The second refinement of the registration goals is to specify the tolerable lack of registration. The absolute maximum displacement of one image from the corresponding image on another photograph can be specified, and the useful format over which the maximum displacement shall not be exceeded can be specified. If geometric registration is performed, then the final image displacement from the position in the theoretical geometric model should be specified. All these specifications must relate closely to the resolution of the imaging system.

Finally, the registration goals must be compatible with the calibration and stability of the system. All the distortions must be calibrated to a common order of accuracy. This is especially true for geometric registration.

At the present time it is desirable to separate in concept the task of registration from the task of a cartographic referencing. Cartographic referencing logically follows geometric registration. It includes the scaling and gridding of the product according to a suitable cartographic map projection. Ultimately it may be possible to combine several steps, but before that time arrives the separate problems must be much better defined.

It seems necessary to mention that there is considerable uncertainty in estimating either the relative registration or geometric registration requirements for a system such as ERTS. Very likely some triplets will have only slight interpretive value and therefore will not require any type of registration. Cloud cover, for example, will preclude the use of some photographs for acquiring earth-surface data.

Other interpretive data can be acquired with sufficient quality without registration. For many users the desirability of registration will only be evident after initial examination. The requirement for geometric registration will pertain very likely to a small selected number of photographs. Thus it appears very necessary to consider several types of product with sufficient flexibility for the user to select and order the product most useful for his needs.

The remainder of this paper is focused on the problems of geometric registration by analog techniques. If only relative registration is required, then the task should be pursued with relaxed specifications—the format area of required registration should be small, and the maximum allowable displacement should be large. The considerable effort required for any type of registration which will approach the resolution of the system should be directed toward geometric registration. For cartographic purposes, only geometric registration is adequate. For sequential images of time-variant features, geometric registration will be of greater value than relative registration.

DISTORTIONS

Specific examples of some distortions expected in the RBV system on ERTS-A that emphasize the importance of system calibration are shown in table 1. The content of the table purposely goes beyond the present topic of geometric registration and considers the distortion parameters which will affect cartographic referencing. The reason for considering both topics is found in the close relationship between them. When calibration specifications are developed, common accuracy must be maintained throughout the system. This is true even when registration is considered a separate task from cartographic referencing. A single large uncalibrated distortion source can reduce other calibrations to wasted effort.

The values in table 1 were developed with the assumption that the width of a single TV line of the RBV is 6 μm. The desirable geometric registration which should be attained with some confidence is about 10 μm at the original RBV scale of 1:7,000,000. The 10 μm represents 70 meters on the ground, which is at least two times the resolution of the system for high-contrast ratios of natural objects. Although ground objects of 70 meters could not normally be resolved by the RBV (200-meters resolution is more realistic for normal contrast ratios of natural objects), the contribution of geometric registration errors to the total cartographic error would be about 70 meters. This is a reasonable order-of-magnitude contribution if the final photomaps are prepared at 1:1,000,000 scale, at which National Map Accuracy Standards allow 500 meters. The geometric registration would be in proportion to the other sources of geometric error in the system.

Table 1 is separated into several categories of distortion parameters which should be calibrated. The expected system accuracies of these parameters have been derived from several sources, some of them of an interim status. The system accuracy values for several of the parameters, therefore, are subject to change. The system accuracy is the expected distortion from uncalibrated manufactured components. The calibration accuracy values, on the other hand, present a consistent set for 10-μm geometric registration and 1:1,000,000-scale cartographically referenced photomaps. All parameters will require calibration, since the normal system accuracy of the manufactured components is inadequate for the geometric registration requirements.

The first set of parameters relates to the internal geometry of the RBV system including the video transmission and hard-copy presentation. The second set of parameters relates to the relative geometry of the three cameras with respect to each other and to the spacecraft. The third set relates to absolute geometric orientation of the cameras with an object-space coordinate system.

All the internal geometric parameters together with the relative orientation between the three cameras affect registration. The remaining parameters are concerned with cartographic referencing. It is believed that if geometric registration to 10 μm is achieved, then the parameters affecting cartographic referencing can be calibrated and controlled to the accuracy required for 1:1,000,000-scale maps.

CALIBRATION OF DISTORTION PARAMETERS

It appears realistic to achieve the calibration accuracy for the reseau coordinates and the lens parameters as shown in table 1. The actual calibration procedure has not been clearly established in all cases, but there do not appear to be any unsolvable problems.

The electronic distortions include a number of separate distortions, some of which may be nonlinear. The electronic effects are considered to be the largest distortion source and the one about which the least is known. Present indications are that the

electronic distortions will have large systematic components that remain stable for appreciable periods of time (weeks or months). Thus, it will be profitable to calibrate the systematic electronic distortions. If 75 percent of the 750 μm of electronic distortion is considered systematic, then about 190 μm of random distortion remains. Even 90 percent of the systematic distortion (a reasonable figure by some tests) will leave a 75-μm random component. While there may be uncertainty on the form and magnitude of electronic distortion, it does appear clear that measurements of the reseau are the best available source of correction data. Moreover, with the distinct possibility of random electronic distortions greater than 10 μm, at least some reseau measurements must be performed on every photograph to be geometrically registered. It will also be logical to expect nonlinear parameters which require small areas of the photograph to be corrected individually from one another.

TABLE 1.—*Parameters of distortions expected in RBV imagery from ERTS–A*

	Distortion parameters	System accuracy	Calibration accuracy
Internal geometry	Reseau coordinates	± 10 μm	± 3 μm
	Lens:		
	Focal length	$+270$ μm, -980 μm	± 20 μm
	Principal point	± 65 μm	± 5 μm
	Radial distortion	± 30 μm	± 5 μm
	Electronic effects	± 750 μm (about 125 TV lines of 6 μm each)	± 5 μm
Relative geometry	Orientation between cameras.	$\pm 7.0 \times 10^{-4}$ radians (about 2.4 minutes of arc)	$\pm 1.5 \times 10^{-5}$ radians (about 3 arc seconds)
	Camera orientation to attitude determination system.	?	$\pm 1.0 \times 10^{-3}$ radians (about 3.5 minutes)
Absolute geometry	Ephemeris position	800 m	(See note 1)
	Attitude reference	(See note 2)	$\pm 1.0 \times 10^{-3}$ radians (about 3.5 minutes)
	Attitude auxiliary data	$\pm 1.7 \times 10^{-3}$ radians (about 6 minutes)	$\pm 1.0 \times 10^{-3}$ radians (about 3.5 minutes)
	Earth curvature	(See note 3)	$\pm 1.7 \times 10^{-3}$ radians (about 6 minutes of tilt in the final image)
	Topography	(See note 4)	---
	Map projection	± 50 m	(See note 5)

NOTES

1. An ephemeris position of better than 350 meters is necessary in order to scale and position the photograph correctly for a cartographic quality photomap. However, at the same time, the final attitude accuracy would have to improve to better than 4.0×10^{-4} radians (about 1.3 minutes). Attainment of such attitude accuracy is doubtful. Therefore, it will be more realistic to seek attitude accuracies of 1.7×10^{-3} radians (about 6 minutes), which will allow the satisfactory reduction of earth-curvature distortions (see note 3) to acceptable values for the RBV resolution. The ephemeris position accuracy of 800 meters is then satisfactory. It should be realized that these conclusions lead to a condition wherein the distortions due to tilt can be removed with the aid of auxiliary data, but the cartographic referencing of the photomap must be accomplished with ground control points.
2. It is presently believed that a horizon scanner will be used for attitude reference. This method is less accurate than a star tracker. The system accuracy of a horizon-scanning reference may approach 1.7×10^{-3} radians (6 minutes), but the system is often less accurate because of variable atmospheric conditions.
3. The effect of earth curvature can amount to several hundred meters of positional error. It can be reduced to about 50 meters [1] by rectifying the tilt to $\pm 1.7 \times 10^{-3}$ radians (6 minutes or 0.1°) and, at the same time, scaling the image to an optimum secant plane. It is believed that the rectification can be accomplished with auxiliary data if the system is properly calibrated. The scaling must be accomplished with ground control.
4. Relief of 1,000 meters near the corner of a photograph can cause positional errors of about 165 meters. Such a distortion is undesirable, but it cannot easily be corrected in the absence of a stereomodel. The cautious use of photographs with such relief will be necessary.
5. Preliminary analysis indicates that there will be less than 50 meters of distortion between a properly rectified and scaled photograph and the map projection.

[1] All the values quoted in notes 3, 4, and 5 are taken from Colvocoresses (1970).

ANALOG REGISTRATION METHODS

There appear to be four general analog methods, described below, by which the registration goal of removing distortions might be achieved and the resulting photograph transformed to a geometric model. All four have some merit, but only the last is believed applicable to RBV imagery. The following discussion omits considerable detail concerning the construction and operating characteristics of various pieces of equipment. These details may be found in other literature. Only pertinent conclusions are developed here.

Optical projection and rectification

The principles of optical projection and rectification are relatively well developed and straightforward, and their application provides an excellent method for removing tilt and for changing scale. With some modification the method can be used for affine rectification. However, optical rectifiers basically operate with linear parameters which are constant for the entire format and may be severely limited for removing distortions caused by nonlinear electronic parameters.

The real value of optical projection and rectification for RBV imagery appears in two applications, neither of which is a complete solution. First it should be possible to develop an inexpensive optical viewer or projector which could be used by individuals to examine small parts of imagery in pairs or triplets. This device should have sufficient flexibility to correct the major distortions over small areas. It would obviously be a relative registration device. Several types of equipment already designed or on the market will perform this task.

The second application of optical rectification is for the removal of tilt and an accompanying scale change. This will clearly be a required operation in cartographic referencing and the production of photomaps. One possibly might compute the rectifier tilt settings from satellite auxiliary data, but the scaling and positioning data will be derived from ground control.

Line-scan modulation

The RBV video signal received at a data center will be printed in photographic form on a high-resolution line-scan printer. This may be of the Laser Beam Recorder (LBR) or Electron Beam Recorder (EBR) design. Both devices have resolution equivalent to that of the RBV, with the LBR being of greater stability and the EBR having greater flexibility.

In theory scan modulation of the recorder may be possible so that most of the distortions are removed. This would require that scan lines be stretched or contracted and the spacing from scan to scan be varied. The data upon which to base the modulation function would come either from auxiliary data telemetered with the video signal or from measurements performed on a preliminary printing of the photograph.

There appear to be three primary difficulties with the scan modulation concept. The first is the basic difficulty in providing sufficient modulation on a printing device which, for high resolution, needs to be very stable. The LBR has high mechanical inertia, and only a limited stretching or shortening of the scan lines is possible. It is almost impossible to modulate the scan spacing successfully. The EBR has a very low inertia, and in principle it may be possible to modulate it with geometric correction parameters. At present the EBR is in the research and development stage, and more time is needed to evaluate its potential.

The second difficulty lies with the undesirable scan gaps and overlaps which are inherent in any scan modulation technique. When scan lines are moved, there will be a gap between scans (or an overlap) unless the scan width is also adjusted. This problem is not amenable to an easy solution, and most likely the gaps and overlaps would always remain.

The final difficulty is the limited number of modulation parameters which can be successfully incorporated into a line-scan recorder. Line stretching can produce an affine rectification, and simple scale changes are easily possible. However the effort required for the inclusion of other parameters may not be worthwhile. Perhaps the best role for line-scan modulation will be to remove, during initial printing, the larger components of scale variation which may occur on a regular basis.

Orthophoto image correlation

The existence of several types of automatic or semiautomatic image correlators with their accompanying orthophoto printers appears at first glance as a readymade solution to image registration. These instruments recognize corresponding images on a stereopair of photographs and simultaneously transform and print one of the images in an orthographic projection. Several different types of equipment are available; classifications based on electronic or optical image transfer, analytical or mechanical functions, manual or automatic correlation, and on-line or off-line orthophoto operation are

possible. Most of the different classifications are relatively unimportant here. What seems important is the virtual impossibility of any of these devices achieving geometric registration when both images are distorted. They all are designed for use with geometric photographs, usually a central perspective in a frame format. Thus, unless at least one photograph of the pair has geometric fidelity, the general result will only be relative registration.

Even relative registration may be somewhat difficult to achieve. Like all analog devices, the orthophoto image correlators were designed for a specific set of parameters. The primary variable is the x parallax between the stereopair of photographs, which is then directly related to an object space z coordinate. Any y parallax between the stereopair is removed with the usual five relative orientation parameters. For registration of RBV imagery, these particular parameters will probably prove inappropriate and inadequate. Primarily, of course, the RBV images do not represent a stereopair. The x and y parallax cannot be expected to fit the z coordinate and orientation-parameter model except in some approximate nonpredictable manner. Recent experiments have shown that two similar photographs, misregistered by a small tilt, can be registered through an orthophoto device. However the tilt introduced represents only one parameter upon which the analog device is designed to operate very easily. As far as is known, the more complicated types of expected distortions have not been simulated. In any event the final result would still be only a relative registration.

A further negative argument can be directed against the automatic correlation devices. All are designed to scan small incremental areas on stereopairs. The image tones and patterns are expected to be approximately the same in the two scanned areas, subject to small amounts of parallax and sometimes terrain slope. However, in multispectral imagery the principal value of the imagery lies in the nonsimilar tones. Often there may be many tone reversals from object to object within the spectral bands. Thus, the automatic correlation function will frequently have difficulty and will require constant human assistance. Automatic correlation circuits will probably be completely unsuitable for the registration tasks.

The present outlook for the adaptation of orthophoto correlation devices is not particularly promising. They do not provide an adequate solution to the problems of geometric registration. However some of the technology already developed in these devices can be utilized in the approach presented in the following section.

Analytically controlled transformations of incremental areas

This fourth analog approach to geometric registration offers the best chance of success. Apparently, it has not been attempted, although various steps in the process are used in other applications.

The basic concept involves the transformation (rectification) of small incremental areas of a photograph under the control of external analytical parameters. Each small area would be moved and shaped from an incorrect position and shape to a corrected position and shape. The shaping of the incremental area is necessary to eliminate gaps and overlaps.

The entire process can be conceived in four sequential steps. These are (1) initial printing on a stable base, (2) mensuration, (3) analytical computation of parameters, and (4) incremental area transformation. These four steps represent a sequence quite similar to many analytical photogrammetric processes.

Initial printing on stable-base material.—The first step is the conversion of the analog video tape for each of the three RBV cameras into three photographs on dimensionally stable material. The main goal is to print the photographs with as much resolution as possible together with a minimum of distortions due to the printer. These photographs (either diapositive or negative) would become the master plates for subsequent processing. They could also be used for preparing unregistered quick-look photo products.

Mensuration.—The master plates would proceed to a mensuration phase. Here all or some of the reseau coordinates would be measured with a standard type of x-y measuring engine. It may be possible to automate some of the mensuration with a device like the Bolsey image correlator. The reseau marks have a generally predictable size, tone, and position. The correlator could be automatically driven into approximate position after which automatic lock-on and measurement would be performed.

In addition to the reseau points, the location of identifiable ground points should be marked and measured. The measurement of ground points would be manual. The ground-point coordinates would allow the computation of the RBV camera position and orientation, which are necessary for subsequent cartographic referencing. Ground points may not be

clearly identifiable in all photographs, in which case the orbital position and attitude would carry greater weight in the cartographic referencing computations.

Analytical computation of parameters.—This third step would utilize as input data the measured reseau and ground coordinates of step two, all available calibration data (geometric and photometric), and whatever auxiliary orbital position and attitude data are available. A relatively high-speed scientific digital computer of moderate capacity would be required. The computational algorithms would be based on a geometric model of central perspective. The results of the computations would be the corrections to be applied to each incremental area of the photograph. The positional translation would remove the distortions and restore the photograph to a geometric central perspective, and the shaping parameters of each area would permit a smooth edge match between incremental areas.

Incremental area transformation.—The final step involves a scan and print of incremental areas. In principle it would be possible to develop an optical-mechanical device for this function. However, there seems to be a very desirable flexibility in an electronic line scan. Primarily, the area shaping would be difficult with a mechanical device, whereas it has been done very easily on electronic scanners.

The electonic scanner traces out a raster scan over a small rectangular area at some given position on the master plate. The image density represented in the analog scan is corrected according to the photometric calibration data. The size and shape of the scan are corrected according to the shaping parameters. Finally the incremental area is printed at a corrected position on a new plate of dimensionally stable material. The process then moves under analytical parameter control to the next incremental area.

Most of the hardware and electronic circuitry for such a scan-print device has already been developed in one form or another, and much of it has been used on the various automatic-correlation orthophoto-compilation instruments mentioned previously. However a special instrument would have to be built for the particular task of geometric registration. Most important would be the software development, which should be reasonably flexible and accessible. An optimum series of geometric and photometric corrections could be incorporated as required.

CONCLUSIONS AND RECOMMENDATIONS

The four conclusions of this report all fall within the context of recommendations for the ERTS/RBV system.

1. Geometric registration is a more desirable goal than relative registration. The considerable effort and equipment for either type of registration should be directed toward geometric registration.

2. Geometric registration is a necessary first step before any cartographic referencing. It will also be helpful, if not essential, to many types of remote-sensing analysis.

3. Geometric registration requires an adequate calibration of the RBV camera system. The calibration accuracy is higher than the expected system accuracy. The various distortion parameters affecting geometric registration and cartographic referencing must be calibrated to comparable orders of accuracy. The present studies of calibration methods should continue.

4. An analog method of geometric registration is possible. It will, however, require new instrumentation so that analytical parameters can be used to control the scanning, transformation, and printing of incremental areas on a photograph. Studies affecting the design of such an instrument should be commenced.

REFERENCE

Colvocoresses, A. P., 1970, ERTS-A satellite imagery: Photogramm. Eng., v. 36, no. 6, p. 555–561.

SUBJECT INDEX

[For major headings such as "Economic geology," "Geochemistry," "Ground water," see under State names or refer to table of contents]

SUBJECT INDEX

AUTHOR INDEX

☆ U.S. GOVERNMENT PRINTING OFFICE: 1971 O—398-875